University of Alberta

NMR investigation into the therapeutic potential of troponin

by

Ian Michael Robertson

A thesis submitted to the Faculty of Graduate Studies and Research
in partial fulfillment of the requirements for the degree of

Doctor of Philosophy

Department of Biochemistry

The man who comes back through the Door in the Wall will never be quite the same as the man who went out. He will be wiser but less cocksure, happier but less self-satisfied, humbler in acknowledging his ignorance yet better equipped to understand the relationship of words to things, of systematic reasoning to the unfathomable Mystery which it tries, forever vainly, to comprehend.

Aldous Huxley, Doors of Perception

Abstract

The pumping of the heart is controlled at the molecular level by the calcium dependent interaction between troponin C (cTnC) and troponin I (cTnI). The central role this protein-protein interaction plays in the muscle contraction cascade makes it a prime target for the development of drugs for the treatment of heart disease.

In Chapters 2 and 3, we show that the natural products, EGCg and resveratrol, bind preferentially to the C-terminal domain of cTnC (cCTnC). NMR structures reveal that EGCg binds to the surface of the hydrophobic pocket of cCTnC, whereas resveratrol binds deeper in the protein, akin to the Ca^{2+}-sensitizer, EMD 57033. The comparisons between the two structures highlight specific interactions between the compounds and cCTnC that define differences in their binding poses.

The next section (Chapters 4, 5, and 6) is devoted to understanding the mechanism of drugs that target the N-terminal domain of cTnC (cNTnC). Specifically, the modulation of cTnI binding to cNTnC is entertained as the mechanism by which molecules that bind to cNTnC modulate contraction. In Chapter 4 some pharmacophores are identified and an ideal cNTnC-cTnI construct for the design of drugs is described. Chapter 5 explores the structure and function of a novel Ca^{2+}-sensitizer, dfbp-o. We find that dfbp-o enhances cTnI binding *in vitro* and increases contractility *in situ*. This enhanced cTnI binding is postulated to originate

from an electrostatic attraction between R147 of cTnI and the carboxylate moiety of dfbp-o. In Chapter 6 the synthesis and activity of some novel analogs of the inhibitor, W7, is outlined. The results support the electrostatic mechanism outlined in Chapter 5.

In Chapters 7 and 8 we investigate how one can modify calcium sensitivity by changing residues on either cNTnC or cTnI. We show that the mutation L48Q stabilizes the open state of cNTnC thereby enhancing cTnI binding and contractiltity. A specific histidine on skeletal TnI has been shown to increase the calcium sensitivity of a myofilament when compared to cTnI, at low pH. In Chapter 8, we show that under acidic conditions, this histidine is protonated and its binding to cNTnC is enhanced by the appearance of an electrostatic interaction with E19 of cNTnC.

Acknowledgements

These past six years have been truly amazing, and there are so many people I would like to thank. The first person I would like to thank is my supervisor, Professor Brian Sykes; I couldn't have hoped for a better mentor, colleague, and friend. We have shared so many great memories, including exploring interesting scientific questions, golfing (especially the times at Long Beach and the Cairns Golf and Country Club), sharing (a) bottle(s) of wine in Boston or really, wherever, and curling at the JP and annual lab tournament. I would like to thank Brian for encouraging my meandering mind and providing me with an environment that allowed me to explore new avenues of research. The years spent in Brian's lab have been very special to me, and while I will miss the times we had, I look forward to the new memories and discoveries we will share in the future.

I would like to extend a special thanks to my lab mate and good friend, Dr. Olivier Julien, and his wife Dr. Sue Ann Mok and William. You have been like a second family to Ashley and I. Thank you for your friendship and kind support over all these years. I have two final things to say to OJ: 1) I don't care what you say, yellow cheese is the greatest cheese!, and 2) "Je suis un pamplemousse". To Dr. Monica Li, I would like to thank for all her support and making me feel welcome in Brian's lab. Monica has been my rock: regardless of her schedule she would always find time for me. In addition to her moral support, she nurtured me scientifically: showing me how to prepare samples, run spectra, perform titrations, and be a careful scientist.

There are many past members of the lab I'd like to thank. Dr. Xu Wang, Dr. Darrin Lindhout, Dr. Tharin Blumenshein, Dr. Steffen Graether, Gerry McQuaid, and Dr. Eric Saude. Darrin's kind words about Brian when I first joined the department were part of the reason why I decided to come to Brian's lab. Without the pioneering work done by Xu on the troponin C-drug complex structures, many of my projects would have taken much longer than they did. Dr.

Tharin Blumenshein and I have enjoyed many Brazilian barbeques together; I'm indebted to her insights into the magic of papaya. No more "meat sweats" for me!

My early Ph.D. overlapped with a number of people who had a significant impact on me, and I would like to individually thank them. I would like to thank Dr. Jan Rainey for all the fun nights we had at Biophysics. Jan's successful academic career has been a source of encouragement for me to continue on in science. I would like to thank Dr. Olga Baryshnikova for all her criticism. There have only been a few people that have pushed me as hard as her. Finally, Dr. Ryan Hoffman for the conversations we had, from Spinoza to the definition of ethnicity, it was always a pleasure. To Dr. Marta Oleszczuk for all the fun we had together - I'm thinking of that time in Boston, Martusia! I would like to thank her for opening my eyes to the diversity of European cultures and to what defines a good movie.

Other past lab members I would like to thank include: Dr. Xingang Zhao (Gump) for his patience in teaching me quantum chemistry and how to derive the Schrodinger equation; Dr. Subhrangsu Chatterjee and his delectable meals and endearing laugh; Dr. Sam Szeto for opening my eyes to the abounding options for scientists outside academia; Jeff DeVries and Nick Shaw for maintaining the spectrometers. Jeff was probably the only *true cowboy* I met while I was in Alberta. Nick Shaw for his technical assistance and challenging views; to Angela Thiessen, Elia Fong, and Melissa Crane, I would like to thank for their technical support, I am truly indebted to them all.

To current lab members: Peter Holmes for his endless enthusiasm for science. On the days when I was feeling overwhelmed he always managed to give me the motivation to get back to the bench. To Brian Lee, a.k.a. Lee-szczuk – I will never forget our week together in Baltimore; to Dr. Pascal "no mercy" Mercier, I would like to give my thanks for not only his help in structure determination and software help, but also for the conversations we had on science, politics, and football. To Robert Boyko, R-B-O, for the many times we spent playing darts, curling, discussing finance, and of course, for his endless patience dealing with my computer incompetence; Stacey Reinke for bugging OJ

I would like to thank my parents for bestowing in me the attitude that I could accomplish anything. I know that I was not always the easiest child, and I would like to thank them for all their unconditional love and support. I would like to thank my little sis', Susan, for always being there for me. Even though she is younger than me, I will forever look up to her. Finally, I would like to thank my wife, Ashley. This document and degree is as much hers as it is mine. Without her tireless support and understanding, I'm certain that I would not be here today. Our life together is only beginning and while we already have so much to be grateful for, I am even more excited about the future unfolding before us.

Table of Contents

Appendices

List of Tables

List of Figures

and cNTnC•cTnI$_{147-163}$•bepridil

Gd^{3+} bound to cNTnC-cTnI

List of Abbreviations

1D, 2D, 3D	one, two, three dimensional
ADP	adenosine diphosphate
ATP	adenosine triphosphate
CDZ	Calmidazolium
cAMP	cyclic adenosine monophosphate
CSA	chemical shift anisotropy
(c,s)Tn	(cardiac, skeletal) troponin
(c,s)TnC	(cardiac, skeletal) troponin C
(c,s)CTnC	C-domain (cardiac, skeletal) troponin C
(c,s)NTnC	N-domain (cardiac, skeletal) troponin C
cIp	inhibitory peptide (residues 129-147)
cSp	switch peptide (residues (147-163)
CSP	chemical shift perturbation
(c,s,ss)TnI	(cardiac, skeletal, slow skeletal) troponin I
(c,s)TnT	(cardiac, skeletal) troponin T
CVD	cardiovascular disease
DCM	dilated cardiomyopathy
DFT	density functional theory
DMPC	dimyristoylphosphatidylcholine
DMSO	dimethylsulfoxide
DSS	2,2-dimethyl-2-silapentane-5-sulfonate sodium salt
DTT	dithiothreitol
EGCg	(-)-epigallocatechin gallate
ESI	electrospray ionization
FHC	familial hypertrophic cardiomyopathy
FRET	Förster resonance energy transfer
FT	Fourier Transform
GIAO	gauge including atomic orbitals

HCM	hypertrophic cardiomyopathy
HF	heart failure
HF	Hartree-Fock
HMQC	heteronuclear multiple quantum coherence
HOESY	heteronuclear overhauser effect spectroscopy
HSQC	heteronuclear single quantum correlation
IR spectroscopy	infrared spectroscopy
MALDI	matrix-assisted laser desorption/ionization
MD	molecular dynamics
MS	mass spectrometry
NMR	nuclear magnetic resonance
NMR spectroscopy	nuclear magnetic resonance spectroscopy
NOE	nuclear Overhauser effect
NOESY	nuclear Overhauser effect spectroscopy
PCS	pseudocontact shift
PDE III	phosphodiesterase III
PKA	protein kinase A
PPM	parts per million
PRE	paramagnetic relaxation enhancement
ROESY	rotating frame Overhauser effect spectroscopy
SSE	sum of squared error
TCEP	tris(2-carboxyethyl) phosphine
TFP	trifluoperazine
TFA	trifluoroacetic acid
THF	tetrahydrofuran
Tm	tropomyosin
TnC	troponin C
TOCSY	total correlation spectroscopy

Chapter 1

The heart: regulation and enhancement of its function*

> *It is instantly produced inside the lungs by a mixture of inhaled air and subtle blood, while it is elaborated and communicated from the heart's right ventricle to the left one. This communication is not mediated via the median septum of the heart, as it is habitually thought; on the contrary, the subtle blood is transferred from the right ventricle, in an brilliant way, by following a long circuit through the lungs, which submits it into a transformation, in order for the blood to come out coloured yellow: the arterial vein [pulmonary artery] transports it into the venous artery [pulmonary vein]. From that moment on, the blood is mixed in that very same venous artery with the inhaled air in order to become re-purified from all fuliginous materials, during this expiration. In this way, the entirety of this mixture is finally attracted by the left ventricle of the heart, during the diastole, to serve as a base for the vital spirit.*
>
> *Michael Servetus (1)*

*A section of this chapter has been adapted from: Li, MX, Robertson, IM, and Sykes, BD. (2008) Interaction of cardiac troponin with cardiotonic drugs: a structural perspective. *Biochem. Biophys. Res. Commun.* 369, 88-99.

A brief history of the heart and its function

The heart is the driving force behind human life. It tirelessly propels blood throughout our body; beating an average of 2.5 billion times over the course of a person's life. It is surprising then, that given its vital importance, the notion of the heart as a muscle that pumps blood was not widely accepted until the 17th century.

The ancient Greeks were aware of the heart and blood vessels, and many theories about the function of the heart had been already considered by 300 BCE. In the *History of Animals,* Aristotle (384-322 BCE) (Figure 1-1) rejected the commonly held notion that the brain was the source of the veins, instead he concluded that all blood vessels stemmed from the heart (*2*). He considered the heart as a type of container that served as a resting point for blood on its voyage between the aorta and the *vena cava*. In addition to his misunderstanding of the heart's purpose, Aristotle thought that there were only three cavities of the heart: the left atrium, left ventricle, and the right ventricle (*2*) - it is believed that Aristotle mistook the right atrium as being part of the *vena cava* (*3*). Herophilos (335-280 BCE) had differentiated between the arteries and veins by the thickness of their walls. He also determined that veins carried only blood, and not a mixture of blood and air (*2*).

The role of the heart put forth by Aristotle and Herophilos survived for almost 500 years, until the Roman physician, Galen (ca. 130 – 200 CE) (Figure 1-2). Galen built upon Herophilos's theories to conclude that the arteries too, contained only blood. Galen also set straight the number of chambers in the heart, from three to four, for which he chastised Aristotle: "*What wonder that Aristotle, among his many anatomical errors, thinks that the heart in large animals has three cavities?*" (*2*). Galen discerned that the heart controls its own pulsations and he noted the muscular nature of the heart; however, he failed to make the connection that the heart functioned as a muscle to drive blood, instead he thought that it
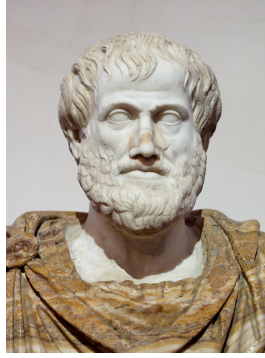
Figure 1-1. Roman marble copy of the bust of Aristotle, originally done in bronze, by the Greek sculptor, Lysippos, of the 4th century BC (Location: National Museum of Rome).

dilated to draw in blood (*4*). Like his predecessors, Galen thought that the venous and arterial systems were separate: the venous blood carried nutrients and originated in the liver; the arterial blood transmitted the "vital spirit" from the lungs to the rest of the body through the heart (Figure 1-2). Galen likened the heart to a furnace, providing heat for the body and as such, produced a sooty waste. The soot was cleansed by blood coming from the lungs, which mixed with venous blood through tiny pores in the septum between the left and right ventricles (*2, 4*).

Not much changed in the theory of the function of the heart until several independent observations were made 1000-1400 years later. The physician, Ibn Al-Nafis (1213-1288 CE), while working in Cairo, was the first person to publically renounce Galen's postulate that blood from the right ventricle mixed with blood from the left ventricle through the septum. The lack of pores between the ventricles led him to conclude that blood comingled in the lungs, and then returned to the left ventricle of the heart, making this the first rudimentary description of pulmonary circulation (*2, 5*).

A few centuries later, the anatomist, Andreas Vesalius (1514-1564 CE), criticized Galen's knowledge of anatomy. Although a great admirer of his, he corrected approximately 200 errors made by Galen, including noting that the septum did not contain pores (*2*). The first European to describe of pulmonary circulation was the Spanish-born theologian and physician, Michael Servetus (1511-1553 CE). Servetus published his conclusions (see chapter quote) in a pamphlet entitled, *The restoration of Christianity* (1). In *The restoration of Christianity*, Servetus also criticized the Trinity, which led to the destruction of most of the copies of the manuscript and his burning at the stake (*2, 6*). Pulmonary circulation was again described by Servetus's contemporary, Realdo Colombo (ca. 1510-1559 CE). Colombo worked at the University of Padua as a dissectionist under Vesalius. Colombo again denied the presence of pores in the septum of the heart and defined the pulmonary circuit. It is likely, however, that Colombo knew of Servetus' work, but did not explicitly reference
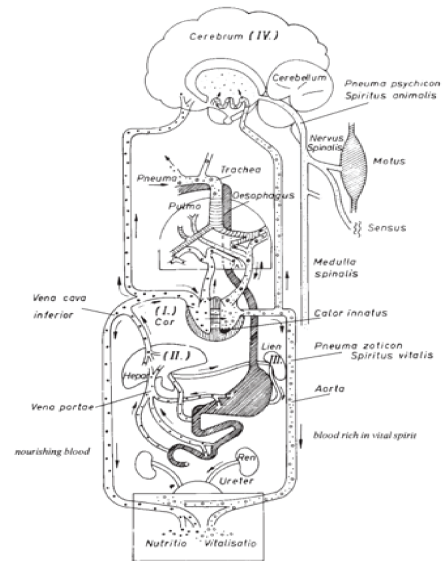
Figure 1-2. Illustration of Galen and his version of the circulatory system. Illustration of Galen was done by the 16th century French surgeon, Ambroise Paré (c. 1510 – 20 December 1590). Note the two separate pathways of blood flow in Galen's circulatory system (7).

Servetus for fear of persecution by the Inquisition (*6*). Colombo also disagreed with Galen's idea that the heart functioned as a furnace producing fuliginous waste and he was the first person to state that the heart 'set the blood in motion' (*2*).

Hieronymus Fabricius (1537-1619 CE) also worked at the University of Padua and noted the presence of valves in veins, astonishingly not discovered until him! However, physicians would not be completely free of the shackles of Galenism until discoveries made by Fabricus's student, the English physician, William Harvey (1578-1657 CE). Harvey described the systemic circulation of blood, a notion he supported from the fact that the amount of blood far exceeds the quantity that could be made by the liver from food. Harvey also noted that all the valves in the veins point towards the main veins and heart, and therefore their function was to prevent the flow of blood away from the heart, towards the smaller veins (Figure 1-3). Instead of thinking of the heart as a way station or a dilator that draws blood into it, Harvey described the heart as a pump that drove blood around one large circuit of the body (*2, 7*). Harvey's monumental discovery of circulation and of the heart's role as a pump changed the way the heart was viewed. In his writing, *On the movements of animals*, Giovanni Borelli (1608-1679 CE) made the claim: "*The immediate cause of the heart's movement is the same as that which moves limb muscles.*" (*2*).

The contemporary view of the heart and circulation has only slightly changed since Harvey's findings. Briefly, the heart drives blood through the pulmonary and systemic circuits. Blood freshly fuelled with oxygen at the lungs travels to the heart *via* the pulmonary veins into the left atrium, and on the left ventricle. The left ventricle is tasked with propelling blood throughout the entire body, starting at the aorta and spreading outward by a network of arteries. Following the transfer of nutrients and oxygen through capillaries, blood returns to the right side of the heart by the superior and inferior vena cava. It is then pumped from the right ventricle
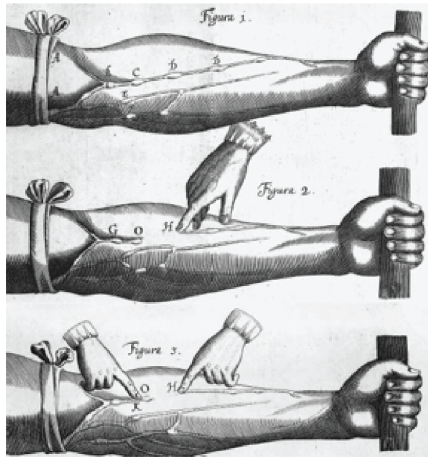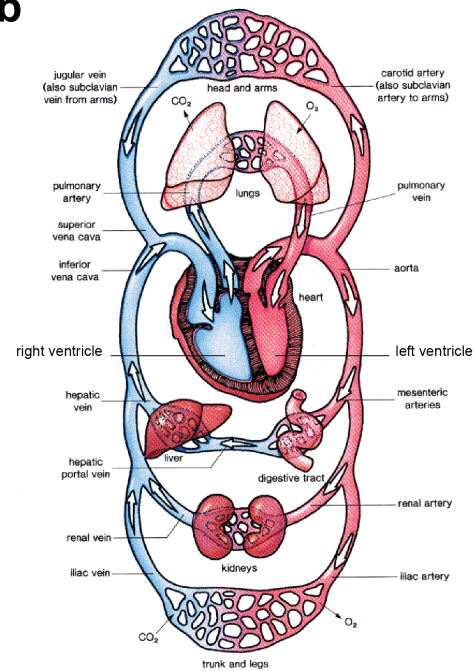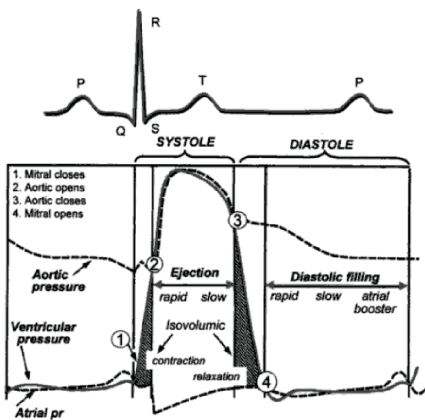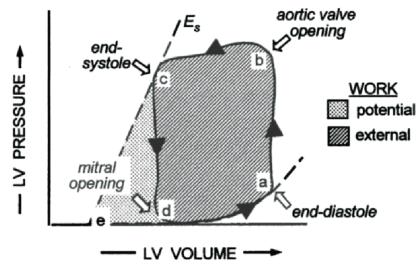
Figure 1-3. **a.** William Harvey's proof that the valves of veins prevent the backflow of blood (*2*). **b.** Modern view of circulation. Red blood is rich in oxygen and blue blood is low in oxygen. Arrows indicate the path of blood flow (http://faculty.plattsburgh.edu/david.curry/NUR464/Circul2.gif). **c.** A simplified cardiac cycle (Wiggers diagram) depicting the electrocardiogram (note the PQRST phases), aortic, ventricular and atrial pressures as a function of time (x axis). **d.** Pressure-volume loop of the left ventricle. See text for a detailed description of the different phases depicted. **c.** and **d.** are adapted from (*8*).

to the pulmonary arteries and on to the lungs, thereby completing its full circuit of the body (Figure 1-3) (*8*). Equipped with the understanding of the heart as a pump to propel blood, we will next review how the heart achieves this purpose. The action of the heart is commonly describe in terms of the cardiac cycle, which is summarized by the Wiggers diagram (Figure 1-3) (*9*). In relation to ventricular function, the Wiggers diagram plots (left or right) ventricular pressure, (left or right) atrial pressure, ventricle volume, and electrical changes caused by heart muscle depolarization (electrocardiogram) as a function of time. Sometimes heart sounds or arterial flow are also included (*8*).

During ventricular systole (contraction phase, from the Greek, *systole,* meaning contraction), depolarization of ventricular muscle cell membranes opens the L-type calcium channels. The influx of calcium into the cytosol induces contraction of heart muscle through its interaction with proteins on the muscle filament (see the following section for the molecular basis of this). Muscle contraction results in a surge of pressure in the left and right ventricles beyond that of the atria, resulting in the closing of the valves that connect these chambers (the tricuspid and mitral). Once the pressure in the left and right ventricles has increased enough, the pulmonary and aortic valves open and blood is ejected from the ventricles.

Following ejection, the cytosolic calcium levels drop (by entering the sarcoplasmic reticulum *via* the sarco(endo)plasmic Ca^{2+}-ATPase (SERCA) pump), and the heart muscle begins to relax (diastole – from the Greek for send and apart). As ventricle pressure declines, the residual pressures in the pulmonary artery and aorta cause the pulmonary and aortic valves to close. There is a brief period when both the mitral and aortic valves of the left ventricle (tricuspid and pulmonary, on the right side of the heart) are shut, then the mitral and tricuspid valves open as atrial pressures increase beyond the ventricle's and ventricular filling begins (*8*).

As detailed in the above section, pressure is a convenient way to describe ventricular function. Another useful description is the cardiac work (work done to move fluid is volume x pressure). Cardiac work can be determined by integrating pressure-volume area (the product of systolic pressure and stroke volume) from the pressure-volume diagram (Figure 1-3). The appearance of the pressure-volume diagram can provide valuable information about the performance of the heart and may be used to assess whether a heart is suffering from heart failure (*8*). The pressure-volume diagram contains a lot of the same information that can be found in Wiggers diagram and it is therefore useful to look at them in tandem (*8*).

In the pressure-volume diagram the full cardiac cycle can be followed (Figure 1-3d depicts the pressure-volume diagram for the left ventricle). As the ventricle contracts, pressure builds up (a ➔ b); but since the aortic valve remains closed, the volume remains unchanged. At b, the aortic valve opens and blood is ejected into the aorta. The slight increase in ventricular pressure following b is because the ventricle must overcome the pressure in the aorta. From b ➔ c the volume decreases commensurate with the ejection of blood into the aorta. Ventricle muscle relaxation following ejection at end-systole causes ventricle pressure to dramatically drop (c ➔ d). As the pressure drops below atrial pressure the mitral valve is opened, d, and ventricle filling follows (d ➔ a), thus completing the cardiac cycle (*8*). Now that we have an understanding of how the heart functions as an organ to drive circulation, we will next review muscle regulation at the molecular level.

The molecular mechanism of contraction and the role of troponin

Hugh Huxley and Andrew Huxley published two independent studies in 1954 where they describe muscle contraction as the sliding of thin filaments past thick filaments (Figure 1-4) (*10, 11*). Although Ringer observed that Ca^{2+} had an impact on heart function in 1883 (*12*), the
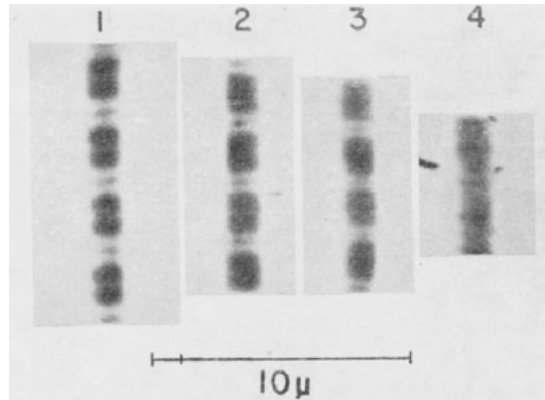
Figure 1-4. The shortening of the sarcomere during contraction. The same four sarcomeres of one myofibril photographed during contraction induced by ATP from rest length (1) down to 50 per cent rest length (4). Figure and legend adapted from (*11*).
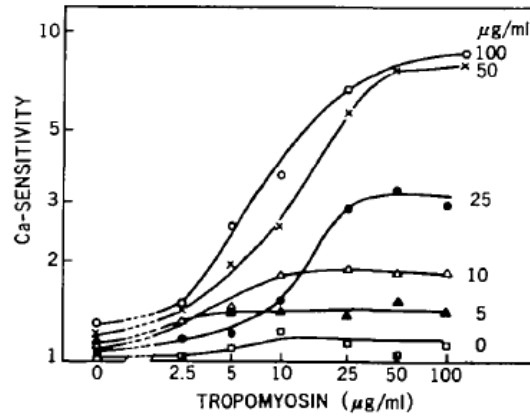
Figure 1-5. Effect of varying concentrations of troponin and tropomyosin on the Ca^{2+}-sensitivity of synthetic actomyosin. Concentrations of troponin are shown on the right of the curves. As troponin concentration increases, so does the Ca^{2+}-sensitivity of contraction. Figure and legend adapted from (*13*).

this effect were not identified until the 1960s, when Ebashi identified troponin as the Ca^{2+} sensing molecule that regulates contraction (Figure 1-5) (*13*). Since these pioneering discoveries, our understanding of muscle contraction has grown dramatically. The following sections provide an overview of the structure of a muscle fiber and the molecular regulation of contraction. Refer to references (*8, 14-19*) for more detailed descriptions on the structure and function of muscle.

Anatomy of the muscle cell

Striated muscle tissue is comprised of a distinct class of cells known as muscle fibers. Muscle fibers are elongated and multinucleated, and contain threadlike myofibrils that extend the length of the cell (Figure 1-6). Each myofibril contains a bundle of even smaller filamentous structures called myofilaments. Myofilaments are made up of the actin-rich thin filament (actin comes from the Latin, *actus*, meaning "motion" or "doing") and the myosin-rich thick filament (Latin, *myosin*, meaning "within muscle").

The actin and myosin filaments are arranged in repeating functional units, known as sarcomeres (Figure 1-7). The sarcomere is made up of an organization of thin and thick filaments such that a hexagonal arrangement of thin filaments exists around each thick filament (Figure 1-7b). The light bands (I-bands) of the sarcomere are solely composed of actin thin filaments and the dark bands (A-bands) contain both myosin and actin. The regions of the A-band where both the thin and thick filaments are located are darker than the thin filament-free central region (H-zone; for *helle* from the German word meaning "bright"). Each sarcomere is defined by Z-lines, which run down the center of the I-bands.

When a muscle fiber contracts, sliding of the thin and thick filaments past one another shortens the sarcomere. The effect of the shortening of the sarcomere is a movement of the Z-lines towards the M-line (at the center of the H-zone); the I-bands and the H-zone also get
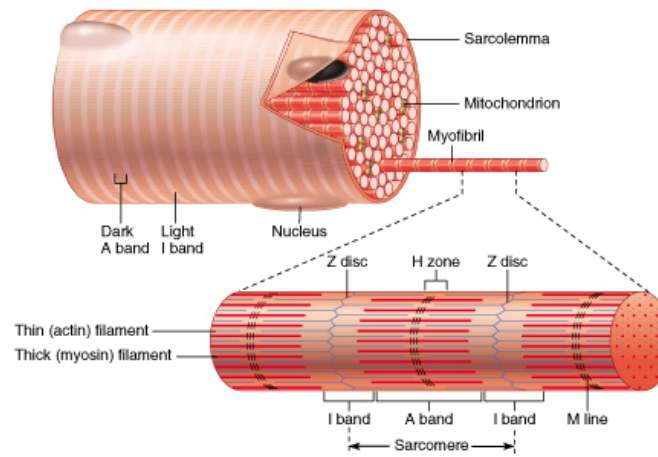
Figure 1-6. The muscle fiber to the sarcomere. The figure is adapted from (*175*).
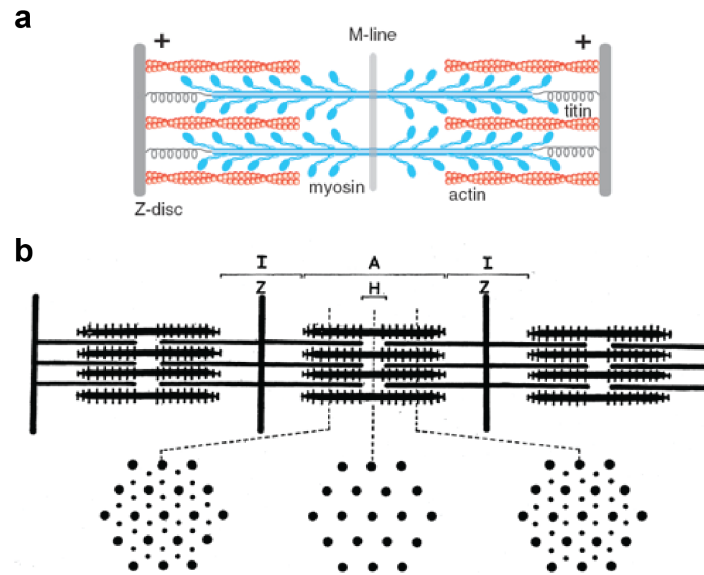
Figure 1-7. The **a.** cartoon (*176*) and **b.** diagrammatic representations of the sarcomere (*177*).

shorter as the thin filaments are pulled deeper into the A-band. Filament sliding is caused by cross-bridges formed between actin and myosin. The formation of these *actomyosin* cross-bridges is modulated by the interaction of Ca^{2+} with the thin filament protein troponin.

The thin filament

The thin filament (Figure 1-8) is composed of three proteins: actin, tropomyosin, and troponin. Actin monomers spontaneously polymerize to form filamentous actin, F-actin, the backbone of the thin filament. F-actin has a double-stranded helical structure and is intimately associated with another filamentous protein, tropomyosin. Tropomyosin is a ~42 nm long molecule that exists as a dimer of two α-helical chains stabilized as a coiled coil. Tropomyosin is bound to F-actin and runs the length of the thin filament by overlapping with neighboring molecules in a head-to-tail fashion. The location of tropomyosin on F-actin establishes whether contraction is inhibited or not and is precisely controlled by troponin (Figure 1-8).

Troponin is a heterotrimeric protein made up of troponin C (TnC), troponin I (TnI), and troponin T (TnT). The exact arrangement of the subunits is dependent on Ca^{2+} and determines the contractile fate of the myofilament. TnC is the calcium binding subunit; it is a bi-lobed protein that has two high-affinity metal binding sites in its C-terminal domain (CTnC) and two low-affinity Ca^{2+} binding sites in the N-terminal domain (NTnC). A crucial difference between the cardiac and skeletal isoforms of TnC is that in the cardiac isoform, site I of the N-terminal domain is unable to bind Ca^{2+}. TnI is the inhibitory subunit of troponin, and it interacts with TnC, TnT, and actin. The interaction between the N-terminal region, H1 or the 'anchoring region', of TnI and CTnC is thought to be important in tethering the complex to the thin filament and requires that both metal binding sites are occupied with either Mg^{2+} of Ca^{2+}. The interaction between the 'switch region' (H3) of TnI and NTnC is the regulatory step,
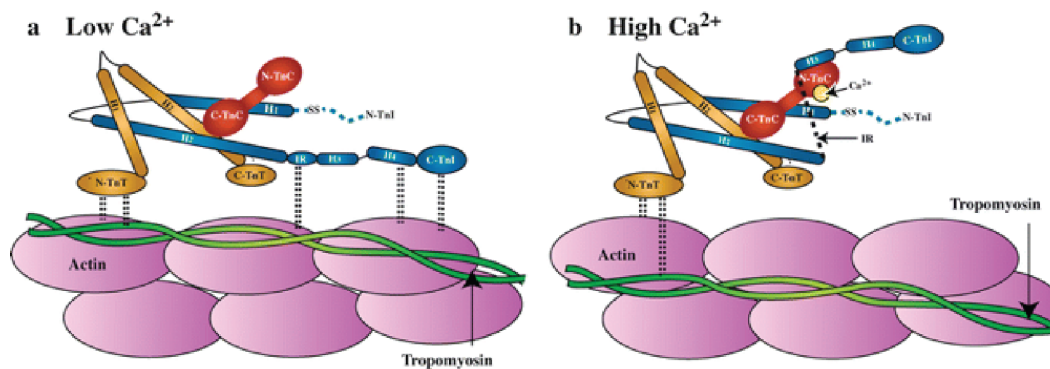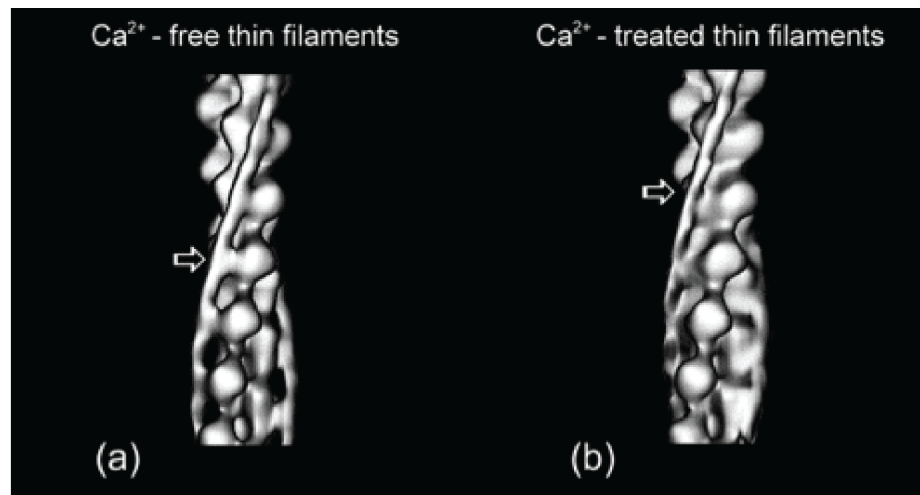
Figure 1-8. The thin filament at low and high Ca^{2+} levels. (top) EM single-particle reconstitution of the thin filament (*178*). (bottom) The cartoon depiction of the arrangement of the thin filament components (*179*).

and occurs only when Ca^{2+} is bound to NTnC. When sarcoplasmic Ca^{2+} levels are low, Ca^{2+} and the switch region of TnI dissociate from NTnC. The release of TnI from NTnC leads to the interaction of the 'inhibitory' and C-terminal domains of TnI with actin. The interaction between of TnI with actin inhibits contraction by positioning tropomyosin on the thin filament so that the myosin binding sites are blocked. When Ca^{2+} levels are high, the switch region of TnI drags the inhibitory and C-terminal domains of TnI off actin, tropomyosin moves towards the actin double helical groove, and the actomyosin cross-bridges form. TnT interacts with TnI and tropomyosin, connecting the troponin complex to the thin filament at every seventh actin monomer.

The thick filament

The thick Filament is composed mainly of myosin. Myosin is made up of four light chains: two regulatory light chains and two essential light chains, and two heavy chains. The heavy chains are connected by an elongated coiled-coil interaction (myosin rod). Each heavy chain has a globular N-terminal domain, termed the myosin head (or S1). The thick filament is made by the staggering of the myosin rods that interact with each other *via* charge-charge interactions, thereby arranging the myosin heads along the filament at regular intervals. At the M-line in the center of the thick filament, the myosin rods align in a tail-to-tail manner, thus giving the thick filament its bipolar configuration (Figure 1-7).

The cross-bridge cycle and muscle contraction

At sub-micromolar Ca^{2+} concentrations, the troponin-tropomyosin complex blocks the formation of strong, force producing cross-bridges between actin and myosin. At micromolar concentrations, Ca^{2+} binds to the regulatory domain of TnC, resulting in a cascade of structural changes in troponin and the movement of tropomyosin deeper into the groove of the actin strand, thus revealing actin binding sites for myosin attachment

(discussed above). Adenosine diphosphate (ADP) and inorganic phosphate (Pi) associated myosin heads bind weakly to actin. The release of Pi results in a strongly actin-bound ADP-Myosin state and is the force generation step (the power stroke). ADP is then released, and subsequent adenosine triphosphate (ATP) binding to myosin causes the myosin heads to detach from actin. ATPase activity of the free myosin head primes the ADP + Pi bound form of myosin, and the heads again bind to actin, thus perpetuating the contractile cycle (Figure 1-9). Contraction continues in this fashion until Ca^{2+} dissociates from troponin. *The function of troponin propagates the regulatory signal along the thin filament and therefore acts as a Ca^{2+}-sensitive molecular switch of contraction.* In order to further understand the structural basis for troponin's activity we will next review the various high-resolution structures that have been solved.

Structural insights into the function of troponin

The first three-dimensional structure of skeletal TnC (sTnC) was solved by X-ray crystallography in 1985 (*20, 21*). In this structure, the N-terminal domain (sNTnC) Ca^{2+}-binding sites were unoccupied, while the C-terminal domain (sCTnC) was in a two Ca^{2+}-bound state. By comparing the crystal structure of the apo N-domain with its homologous Ca^{2+}-bound C-domain, Herzberg et al. (*22*) proposed a model for the Ca^{2+}-induced conformational change in sNTnC that involved a 'closed-to-open' transition accompanied by the exposure of the hydrophobic pocket. The first direct structural evidence describing the Ca^{2+}-induced conformational change in sNTnC came in 1995 when the NMR solution structures of sTnC in $4Ca^{2+}$ state (*23*) and of sNTnC in apo and $2Ca^{2+}$ states (*24*) were determined. Subsequently, the X-ray structures of sNTnC•$2Ca^{2+}$ (*25*) and sTnC•$4Ca^{2+}$ (*26*) were reported. The main difference between the X-ray and solution structures of sTnC is in the central linker that connects the N- and C-terminal domains; in the crystal form it is α-helical, whereas in solution it is
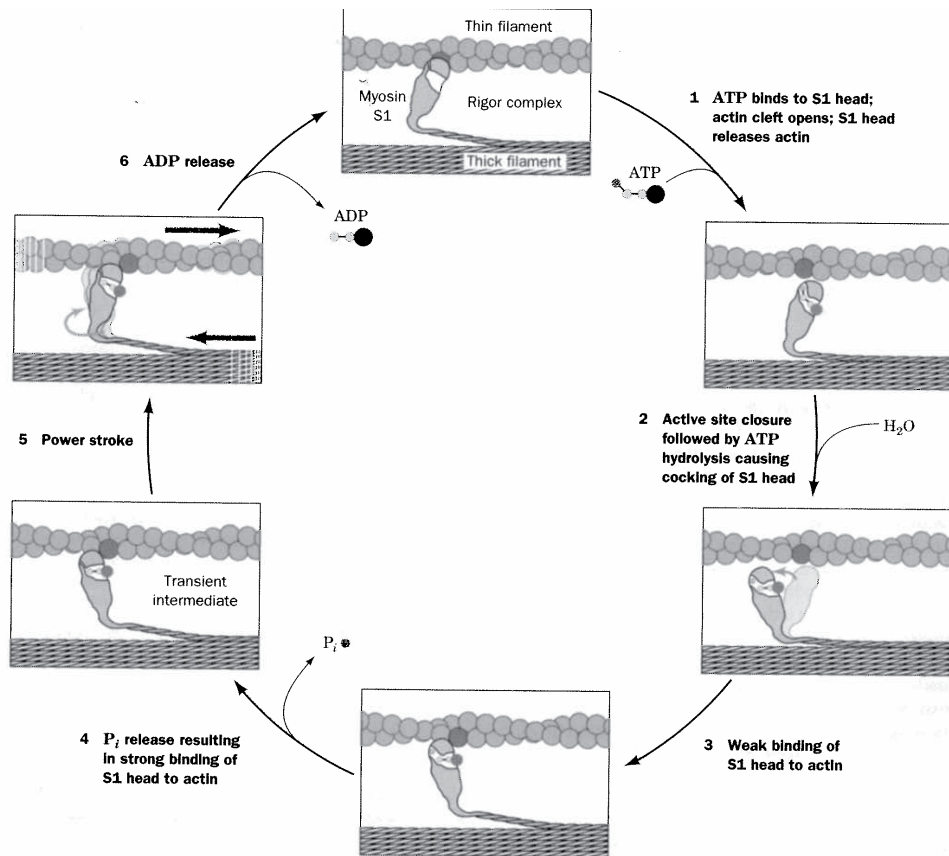
Figure 1-9. The myosin cross-bridge cycle. Figure and legend adapted from (*180*).

flexible. The response of cardiac TnC (cTnC) to Ca^{2+}-binding was unknown until the determination of the NMR solution structures of cTnC•$3Ca^{2+}$ (*27*) and the regulatory domain of cTnC (cNTnC) in both the apo and Ca^{2+}-bound states (*28*). Strikingly, cNTnC remains essentially 'closed' in the Ca^{2+} state, unlike sNTnC, a consequence of the defunct site. The significant reduction in the hydrophobic surface of cNTnC suggested that the mode of interaction between cTnC-cTnI may be different than that between sTnC-sTnI. However, both the regulatory domains of sTnC and cTnC assume similar 'open' conformations when bound to switch regions of sTnI and cTnI regions (sTnI$_{115-131}$ and cTnI$_{147-163}$), respectively (*29, 30*). This indicates that the pathways involved in initiating skeletal and cardiac muscle contraction are structurally very similar; however, the kinetics and thermodynamics of the pathways must differ for the two systems to account for the different physiological behavior of the two muscle types (*31*). A structural comparison of the isoform dependent responses to Ca^{2+} and TnI is given in Figure 1-10.

NMR studies of TnC with various TnI peptides have yielded detailed information on the structure of TnC when bound to TnI (*32-35*), on the structure of TnI inhibitory peptide (*36, 37*), and on the overall topology of TnC-TnI arrangement (*38-48*). There are a number of high-resolution structures of TnC-TnI available: the X-ray structure of sTnC•$2Ca^{2+}$•sTnI$_{1-47}$ (*49*); the NMR structures of cNTnC•Ca^{2+}•cTnI$_{147-163}$ (*29*), sNTnC(rhodamine)•$2Ca^{2+}$•sTnI$_{115-131}$ (*30*), and cCTnC•$2Ca^{2+}$•cTnI$_{128-147}$ (*50*); the X-ray structure of the core domain cardiac troponin complex, cTnC•$3Ca^{2+}$•cTnI$_{34-210}$•cTnT2$_{182-288}$ (*51*); and the X-ray structures of the core skeletal troponin complex in both the apo and Ca^{2+}-state, sTnC(apo)•sTnI$_{1-182}$•sTnT$_{156-262}$ and sTnC•$4Ca^{2+}$•sTnI$_{1-182}$•sTnT$_{156-262}$ (*52*). In the structure of sTnC•$2Ca^{2+}$•sTnI$_{1-47}$, the 31-residue long sTnI α-helix (residues 3-33) stretches on the surface of the sTnC and stabilizes its compact conformation by multiple contacts with both TnC domains (*49*). The corresponding region of cTnI (cTnI$_{34-71}$) was found to bind to the
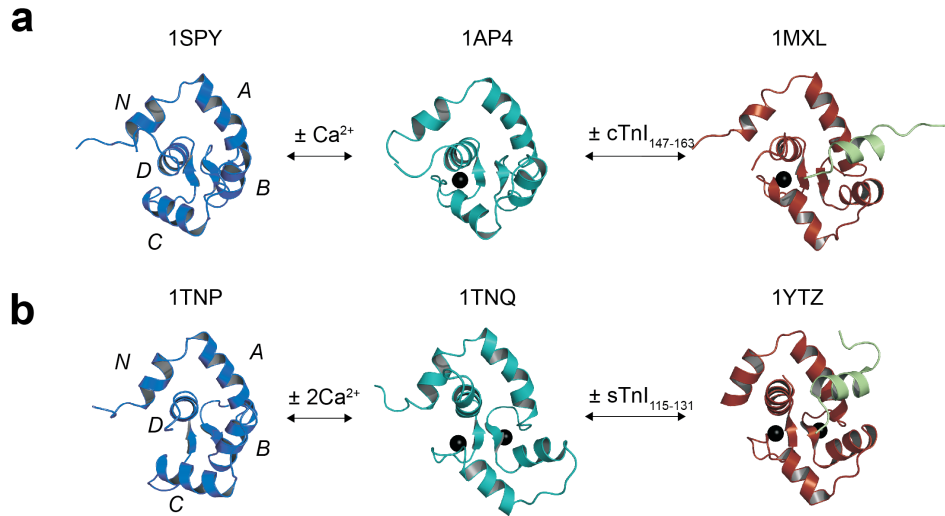
Figure 1-10. Open-to-closed transition differences between **a**. cardiac and **b**. skeletal TnC. The structure of cNTnC remains relatively unchanged when Ca^{2+} binds, whereas in sNTnC, two Ca^{2+} ions fully stabilize the open state. Note the AB-helix interface differences. When troponin I binds to cNTnC the open state is stabilized.

hydrophobic cleft of the C-domain of cTnC (*35*) and had a similar conformation and orientation as observed in the structure of cTnC•3Ca^{2+}•cTnI$_{34-210}$•cTnT$_{182-288}$ (*51*). In the structure of cNTnC•Ca^{2+}•cTnI$_{147-163}$, the bound cTnI$_{147-163}$ peptide adopts an α-helical conformation spanning residues 150–159 in the 17-residue peptide. The α-helical region interacts with the AB helical interface to stabilize the open conformation of cNTnC•Ca^{2+} (Figure 1-10). The corresponding sTnI$_{115-131}$ peptide adopts a similar structure and a similar mode of interaction with sNTnC as observed in the structure of sNTnC(rhodamine)•2Ca^{2+}•sTnI$_{115-131}$ (*30*). In the structure of cCTnC•2Ca^{2+}•cTnI$_{128-147}$, residues L134-K139 of cTnI form an α-helix and residues R140-R147 adopt an extended conformation. With the helical region interacting with the E and H helices of cCTnC•2Ca^{2+}, the highly basic R140-R147 region containing R140, R144, R145, and R147 makes potential electrostatic contacts with the acidic residues present on the linker region (beginning of the E-helix) including E94, E95, and E96. The conformation and orientation of cTnI$_{128-147}$ in this structure is similar to those reported from an electron spin labeling work which shows that a section of the inhibitory region (cTnI$_{129-137}$) displays a helical profile, with the C-terminal residues 139-145 displaying no discernible secondary structure characteristics (*53*).

In the X-ray structure of cTnC•3Ca^{2+}•cTnI$_{34-210}$•cTnT$_{182-288}$ most of the inhibitory region of cTnI is not visualized; however, the conformation and orientation of the N-terminal and switch regions of cTnI are in good agreement with those observed from the binary complexes. The overall core domain structure (Figure 1-11) is dominated by α-helical elements and can be divided into structurally distinct subdomains, denoted as the regulatory head (consisting of the N-domain of cTnC and the switch region of cTnI) and the IT arm (consisting of the C-domain of cTnC, cTnI$_{42-136}$ and cTnT$_{203-271}$). These subdomains are connected by flexible linkers, including the one connecting the two domains of cTnC, as well as the inhibitory region of cTnI. The arrangement of cTnC and cTnI in this
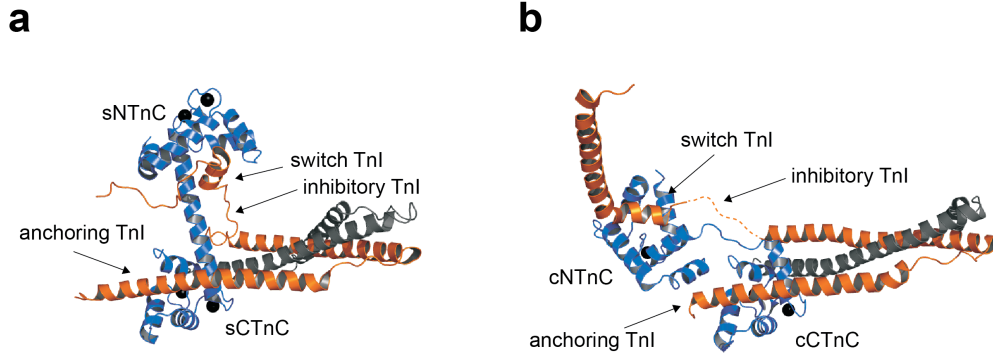
Figure 1-11. Cartoon representations of the X-ray crystal structures of the core **a** skeletal (sTnC•4Ca^{2+}•sTnI$_{1-182}$•sTnT$_{156-262}$) and **b** cardiac (cTnC•3Ca^{2+}•cTnI$_{34-210}$•cTnT$_{182-288}$) troponin complexes. In both structures, TnC is colored in slate, TnI in orange, and TnT in grey. Some of the domains of TnC and TnI are highlighted. The inhibitory region of TnI in cardiac X-ray structure was not observed, and therefore is indicated by a dashed line.

structure is antiparallel, with the N-terminal domain of TnI interacting with the C-terminal domain of TnC and *vice versa*. This agrees with the earlier proposal that emerged from integrating various biochemical and biophysical data (for a review, see (*54*)). Two other α-helices of cTnI are observed in this structure, $cTnI_{164-188}$ and $cTnI_{90-136}$. While $cTnI_{164-188}$ is free of contact with cTnC and cTnT, $cTnI_{90-136}$ forms a coiled-coil with a portion of the T2 fragment of cTnT, $cTnT_{226-271}$, as predicted previously (*55*). Upstream from the coiled-coil, $cTnT_{204-220}$ forms another α-helix. The N-terminal extension of cTnI is not present in the core domain structure. The overall orientation of the cTnI in this complex would direct the cardiac specific region to extend upwards toward the N-domain of cTnC. Direct interaction of this region of cTnI with cNTnC has been demonstrated (*44, 48, 56-58*). This interaction has been reported to influence conformational exchange in the regulatory domain by shifting the equilibrium to favor an open conformation that exposes the hydrophobic cleft. These contacts are disrupted by protein kinase A (PKA) phosphorylation of S22 and S23, and loss of these interactions shifts the conformational equilibrium in cNTnC towards a more closed state. A recent study has shown that bisphosphorylation extends and stabilizes the C-terminal helix region of $cTnI_{1-32}$, weakening the interaction with $cNTnC \cdot Ca^{2+}$ and bends over so its N-terminal acidic residues make electrostatic contacts with the inhibitory region of cTnI (*59*).

The recently published 3.0 Å X-ray structure of skeletal troponin complex in the Ca^{2+}-activated state (Figure 1-11), $sTnC \cdot 4Ca^{2+} \cdot sTnI_{1-182} \cdot sTnT_{156-262}$, and a 7.0 Å structure in the Ca^{2+}-free state, $sTnC \cdot apo \cdot sTnI_{1-182} \cdot sTnT_{156-262}$ (*52*), have provided mechanistic features that are not found in the cardiac troponin structure. The main difference between the cardiac troponin complex and the skeletal troponin complex resides in the fact that the central helix is preserved in the skeletal version in Ca^{2+} bound state which plays a key role in stabilizing the inhibitory region of sTnI. Loss of Ca^{2+} causes the rigid central helix of sTnC to

collapse and to release the inhibitory region of sTnI (*60*). A recent study has shown that $sTnI_{139-182}$ in the sTnC•sTnI•sTnT2 ternary complex constitutes a mobile actin-binding domain that tumbles independently of the core domain and that this tumbling is more restricted through the closer contact with the core domain at high Ca^{2+} concentrations (*61*). This study also proposed a structure for the mobile domain that consists of two helices connected by a β-bulge (*61*).

Based on the cardiac core domain structure, Takeda et al (*51*) proposed a "drag and release" model for cTnC-cTnI interaction. In this model, the movement of the switch region of TnI towards the hydrophobic cleft of N-domain of TnC drags the adjoining inhibitory region from actin causing its release from actin, and the C-terminus of cTnI is carried along with this motion. As such, the C-terminal half of cTnI toggles between cNTnC and actin-tropomyosin during the relaxation and contraction cycle and this movement is controlled by the C-domain of cTnC together with the N-domain of cTnI and the IT arm. A similar model based on the structure of skeletal troponin in both the apo and Ca^{2+}-saturated states is also proposed (*52*). Robinson *et al.* (*62*) further propose that as cTnI is released from actin-tropomyosin, residues within the inhibitory region switch from a β-turn/coil to an extended quasi-α-helical conformation and the switch region remains α-helical. This is based on FRET measurements of the Ca^{2+}-dependent distance change between the inhibitory and the switch regions of cTnI in a cardiac troponin complex reconstituted in the presence of tropomyosin, actin, and myosin subfragment-1 (S1). An alternative mechanism based on NMR relaxation data for sTnI in the Tn complex (*63*) proposes that any structure in the C-terminal regions of sTnI ($sTnI_{131-182}$) is nascent, and only stabilized upon binding to actin (*64*). Furthermore, NMR relaxation data and MD simulations point to the absent of any structure in the C-terminal domain of TnI (*65*). These data point a "fly-casting" mechanism (*66*) of contraction regulation, in which the C-terminus and inhibitory regions of TnI are intrinsically disordered when

bound to TnC. Once Ca^{2+} dissociates from NTnC, these disordered regions of TnI could serve to speed up binding to actin.

The high-resolution structures of troponin have helped to assemble a global picture of the control of contraction by troponin. The structures have pointed to several crucial TnC-TnI interactions that are involved in the transmission of the Ca^{2+} signal to the other thin filament proteins. In order to develop the idea of troponin as a therapeutic target, we will outline the significance of cardiovascular disease and introduce some commonly used treatments.

Positive inotropic therapy of cardiovascular disease

Cardiovascular disease is the leading cause of death worldwide. The World Health Organization reported that 17.1 million people, or 29% of all global deaths, were caused by cardiovascular disease in 2004, and by 2030 this number is expected to increase to 23.6 million (*67*). In the United States, roughly 1 in 9 deaths were caused by heart failure in 2007 (almost 300 000) (*68*). Approximately 6-10 in 100 people over the age of 65 have heart failure and 30-40% of patients die within the first year of diagnosis (*69*) and ~50% will die within 5 years (*68, 70*).

Heart failure may be caused by a number of illnesses and is broadly defined as a decline in cardiac output. Katz defines heart failure as: "*a clinical syndrome in which heart disease reduces cardiac output, increases venous pressures, and is accompanied by molecular abnormalities that cause progressive deterioration of the failing heart and myocardial cell death*" (*71*). Heart failure can be split into two classifications: systolic and diastolic heart failure. In systolic heart failure, the heart's ability to contract is impaired, and in diastolic heart failure ventricular filling during diastole is hindered. Most pharmaceutical therapies for heart failure involve decreasing venous pressures through the use of diuretics and improving cardiac output by decreasing afterload

with antihypertensive agents. For diastolic failure, these are currently the only available and effective pharmacologic agents. For systolic heart failure, an additional decrease in mortality can be gained through the use of 'beta blockers', angiotensin inhibitors, and aldosterone antagonists (*71-74*). In the following section, we will discuss the use of inotropes as another therapeutic option for heart failure.

The first treatment for heart failure was the cardiac glycoside, digitalis. The beneficial effect digitalis had on the heart was first outlined in detail by William Withering (1741-1799), in a 1785 publication: *An account of the foxglove and some of its medical uses; with practical remarks on the dropsy, and some other diseases*. Digitalis comes from the plant, *Digitalis purpurea* (commonly known as foxglove (Figure 1-12). In his publication, Withering noted that digitalis had "*a power over the motion of the heart*" (*4, 71*). The digitalis cardiac glycosides, digoxin and digitoxin, exert a positive inotropic effect (increase in myocardial contractility) through inhibition of the Na^+/K^+ ATPase. The blocking of Na^+/K^+ ATPase leads to an increase in sarcoplasmic Na^+, which in-turn prevents the Na^+/Ca^{2+} exchanger from pumping Ca^{2+} out of the cell and an increase in the force of contraction (Figure 1-13). For a recent review on the mode of action of Digitalis see Schwinger *et al*. (*75*).

A more recently explored inotropic therapy increases contraction by altering cAMP levels. Dobutamine specifically activates the beta-adrenergic receptor subtype β1 and is referred to as a 'beta agonist'. Activation of the β1 adrenergic receptor results in the stimulation of adenylyl cyclase, the enzyme that converts ATP to cAMP (Figure 1-13). Milrinone and amrinone are examples of another group of inotropic agents that likewise increase intracellular cAMP. They inhibit phosphodiesterase III (PDE III) which prevents the conversion of cAMP to 5'-AMP (Figure 1-13). The rise in cAMP caused by PDE III inhibitors or beta agonists, subsequently activates protein kinase A (PKA), which has a number of intracellular targets, such as: phospholamban, whose phosphorylation
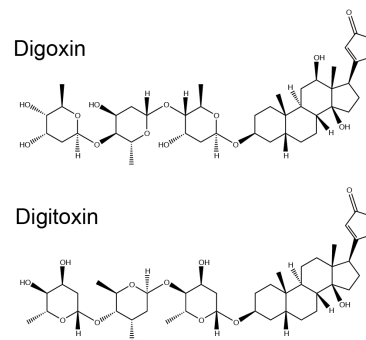
Figure 1-12. Foxglove and Digitalis. Illustration of foxglove by Franz Köhler from Medizinal-Pflantzen (1887). Chemical structures of two medically relevant cardiac glycosides from *Digitalis purpurea*.

leads to an increase in Ca^{2+} sequestration by the sarco(endo)plasmic Ca^{2+}-ATPase (SERCA) during diastole; ryanodine-sensitive Ca^{2+} channels, whose phosphorylation leads to an increase in Ca^{2+} release during systole; troponin I, whose phosphorylation leads to a decrease in the Ca^{2+}-sensitivity of the myofilament. The net result of all these changes is an increase in contractility during systole and an increase in the rate of relaxation during diastole (*76-78*).

A disadvantage of using the cardiac glycosides, beta agonists, or PDE III inhibitors is the potential for Ca^{2+} overload and arrhythmia. Moreover, the increase in Ca^{2+} transport leads to a rise in the energy demand of the cell, making contraction less efficient (*76, 79*). To circumvent these drawbacks, a different type of inotropic therapy has been explored. Instead of modulating Ca^{2+} levels to increase contraction, small molecules that enhance the myofilament's response to normal Ca^{2+} levels may prove to be a safe alternative (Figure 1-13). Energy consumption is not dramatically altered because extra ATP consumption occurs at the force step, not at the secondary steps of increasing Ca^{2+} transport (*76*). One potential limitation of Ca^{2+}-sensitizers is the risk that they may impair relaxation; however, many Ca^{2+} sensitizing agents have been shown to have secondary effects that counteract sustained contraction. For example levosimendan not only acts as a Ca^{2+} sensitizer, but also has limited PDE III inhibition and vasodilatory effects through activation of the K^{+}-ATP channels (*80*). It has also been suggested that since levosimendan dissociates from troponin C at low Ca^{2+} levels, it may not significantly impede relaxation (*81*). More studies need to be done to assess this possible drawback of Ca^{2+}-sensitizers.

There are a number of different proteins in the myofilament that represent viable sites for the development of inotropes. The screening of compounds that activate cardiac myosin ATPase led to the discovery of a novel positive inotrope, omecamtiv mecarbil (*82, 83*). Omecamtiv mecarbil is a myosin activator that stimulates contraction by enhancing the
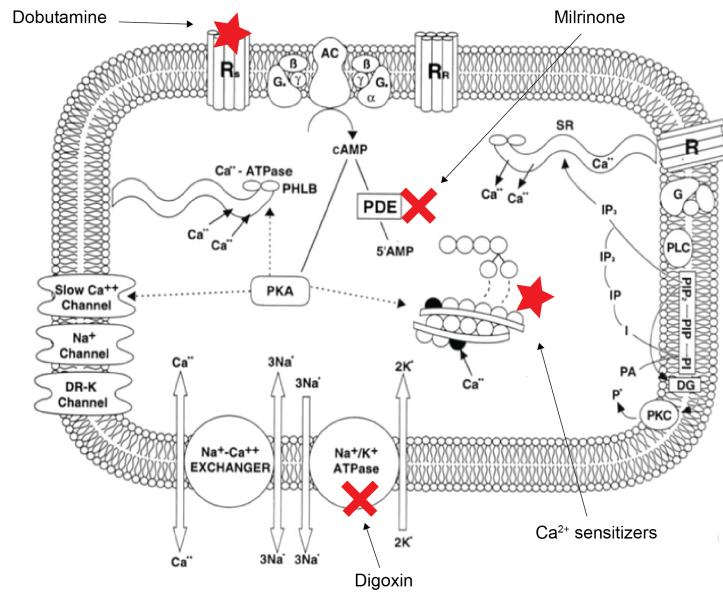
Figure 1-13. Mode of action of inotropic agents (stars indicate activation and crosses indicate inhibition). Milrinone inhibits PDE III, dobutamine stimulates the stimulatory adrenergic receptors; both therapies result in an increase in cAMP and thus an increase in PKA activity. Digoxin inhibits the Na^+/K^+ ATPase and Ca^{2+} sensitizers specifically target the contractile proteins to enhance their response to Ca^{2+}. Figure adapted from (*181*).

transition rate from weakly bound to strongly bound myosin heads (*84*). The binding site is predicted to be at a cleft formed by the relay helix and the converter domain of myosin (*84*). Although omecamtiv mecarbil enhanced ATP turnover, it did not increase energy consumption (*85*). The Ca^{2+}-sensitizer, EMD 57033, may also regulate the thick-thin filament interactions; it was shown that in the absence of tropomyosin and troponin, EMD 57033 increased the actomyosin interactions (*86*). CGP 48506 is another Ca^{2+}-sensitizer that may elicit its function by targeting actin-myosin cross-bridges (*87, 88*). The troponin C-Ca^{2+}-troponin I regulatory pathway has also received a lot of attention for the development of novel inotropes as well. Molecules that target troponin C can act as Ca^{2+} sensitizers by either directly enhancing its affinity for Ca^{2+}, modulating the troponin C – troponin I interaction, or by a combination of both mechanisms. The literature surrounding the development of troponin-targeting inotropes is vast, and therefore will be reviewed in the following separate section.

Troponin as a drug target

The TnC-TnI interaction plays a critical role in transmitting the Ca^{2+}-signal to the other myofilament proteins in heart muscle contraction, and the TnC-TnI interface constitutes a potential target for the development of cardiotonic agents that modulate the Ca^{2+}-sensitivity of the myofilaments in diseased hearts (*76, 89, 90*). In addition to the large amount of *in vivo* and *in situ* evidence for troponin-targeting inotropes, recent structural studies have provided insights into the molecular mode of action of many of these small molecules. In the following section, we will review some of these discoveries. We first present the seven compounds (bepridil, trifluoperazine, calmidazolium, levosimendan, pimobendan, anapoe, and W7) that bind to the N-terminal domain, followed by EMD 57033 and two

Figure 1-14. Chemical structures of agents that target troponin C.
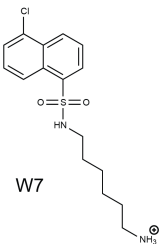
natural compounds, resveratrol and epigallocatechin gallate (Figure 1-14), which may function by targeting the C-terminal domain of cTnC.

Bepridil: Bepridil is a Ca^{2+} channel blocker and a calmodulin (CaM) antagonist. Early evidence indicated that it was able to enter cardiomyocytes and bind to the thin filament (*91*). Studies have demonstrated direct binding of bepridil to cTnC•$3Ca^{2+}$ with a K_D of ~10 µM and found that it enhances Ca^{2+} binding to the regulatory site of cTnC both free in solution and in skinned fiber bundles (*92*). Using stopped flow fluorescence techniques, MacLachlan *et al.* showed that bepridil slows the Ca^{2+} release from the N-domain of cTnC (*93*). An NMR study, using signals from methionine methyls, identified three bepridil binding sites in cTnC (*94*), which was later confirmed by the X-ray structure of cTnC•$3Ca^{2+}$•3bepridil (*95*). In the structure, two bepridil molecules pull the N- and C-domains together to result in a compact cTnC structure while a third bepridil appears to stabilize an open cNTnC conformation by binding to the center of the hydrophobic pocket (Figure 1-15), much like the switch region $cTnI_{147-163}$. Interpretation of the structural data in relation to the biochemical and functional data suggested that the bepridil molecules located in the hydrophobic cavity between the C- and N- domains would be replaced by cTnI, which was later confirmed by an NMR study that detected only one binding site of bepridil (K_D = ~140 µM) when cTnI was in complex with the N-domain of cTnC (*96*). Thus, the two binding site of bepridil that are blocked by cTnI may not be functionally relevant. As is the case with cTnI binding to cNTnC, bepridil binding requires the domain be Ca^{2+} bound. The proposed mode of action of bepridil is that it impedes the closure of the N-domain hydrophobic pocket, slowing Ca^{2+} release from site II, in so doing increasing the Ca^{2+}-sensitivity of the myofilament.

An ideal Ca^{2+}-sensitizer would not only increase the affinity of Ca^{2+} for cNTnC, but also not hinder cTnI binding to cNTnC (*97*). NMR spectroscopy was used to examine the effect bepridil had on cTnI binding,
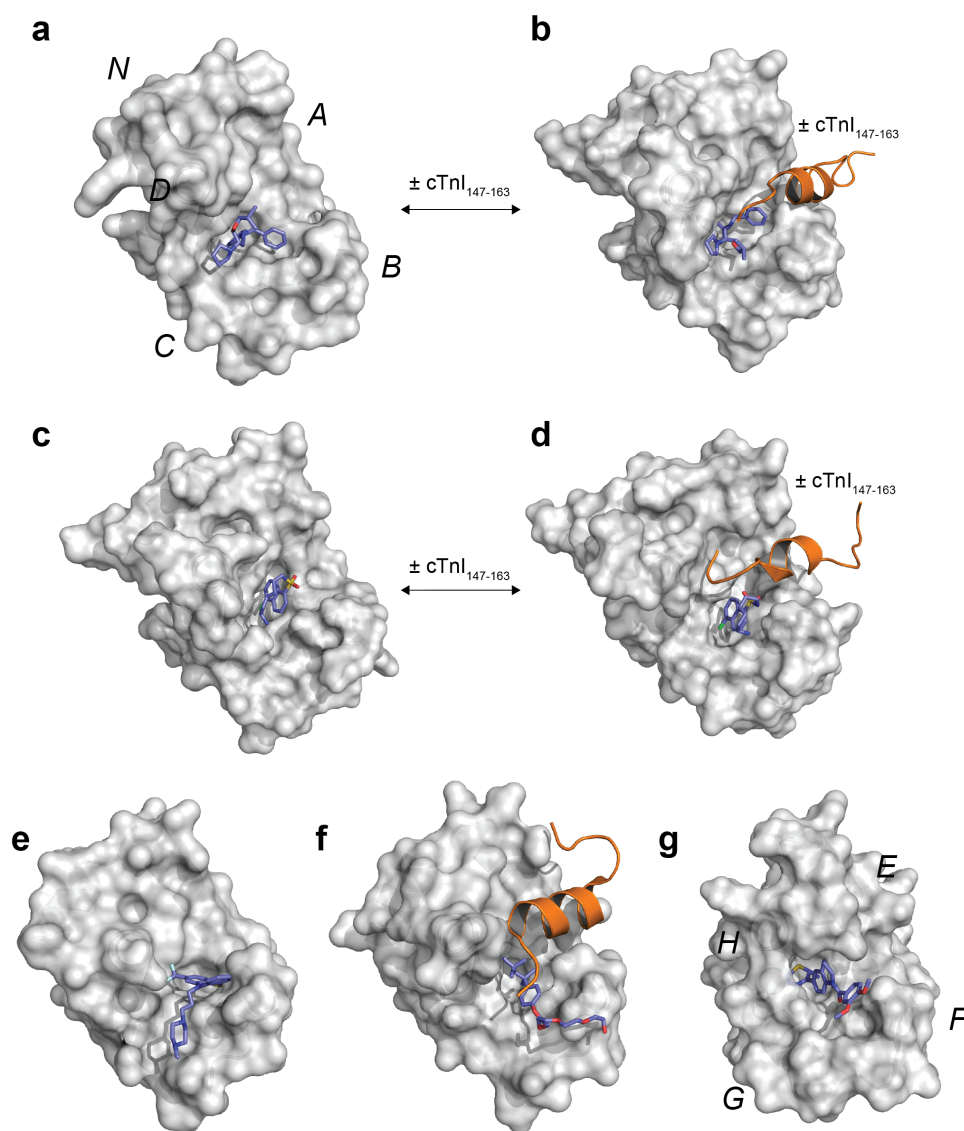
Figure 1-15. NMR and X-ray structures of cardiotonic agents bound to TnC and a TnC-TnI complex. Looking towards the hydrophobic core of the (**a-f**) N- and **g** C-terminal domains of TnC (locations of the helices are identified in **a** and **g**). Bepridil bound to **a** cNTnC (pdb: 1DTL) and **b** cNTnC-cTnI$_{147-163}$ (pdb: 1LXF); W7 bound to **c** cNTnC (pdb: 2KFX) and **d** cNTnC-cTnI$_{147-163}$ (pdb: 2KRD); **e** TFP bound to cNTnC (pdb: 1WRK); **f** anapoe bound to sNTnC-sTnI$_{115-131}$ (pdb: 1YTZ); **g** EMD 57033 bound to cCTnC (pdb: 1IH0). For all structures TnC is shown in transparent surface representation (light grey), TnI is in cartoon representation (orange), and cardiotonic agents in stick from (colored by atom type: carbon, slate; oxygen, red; nitrogen, blue; sulfur, yellow; chlorine, green; and fluorine, cyan).

by measuring the affinity of bepridil to cNTnC•Ca^{2+} in the absence and presence of cTnI$_{147-163}$ and the affinity of cTnI$_{147-163}$ to cNTnC•Ca^{2+} in the absence and presence of bepridil. The results showed that bepridil and cTnI$_{147-163}$ bind to cNTnC•Ca^{2+} simultaneously but the affinity of cTnI$_{147-163}$ for cNTnC•Ca^{2+} is reduced ~3.5 fold by bepridil and *vice versa* (*98*). This was consistent with the study by the result of Abusamhadneh, E. *et al*, in which bepridil bound the cTnC-cTnI complex weaker than to isolated cTnC (*96*). The negative cooperativity between bepridil and cTnI for cTnC suggests that the positive inotropic effect of bepridil may result from a combination of many integrated effects within the myofibrillar lattice. The NMR structure of the cNTnC•Ca^{2+}•cTnI$_{147-163}$•bepridil ternary complex reveals a binding site for cTnI$_{147-163}$ primarily located on the AB interhelical interface and a binding site for bepridil in the hydrophobic core of cNTnC•Ca^{2+} (Figure 1-15). The structure also provides clues for the negative cooperativity between bepridil and cTnI. The N-terminus of the peptide clashes with part of the bepridil molecule due to both the steric hindrance and repelling force between the positively charged side chain of R147 of cTnI$_{147-163}$ and the partial positive charge of the pyrrolidine group of bepridil (*98*). In accord with the experimental results mentioned above, a computational study predicted that bepridil competes with cTnI for binding to cNTnC and cTnI binding to full-length cTnC (*99*).

This study has important implications with respect to the design of Ca^{2+}-sensitizers. Ca^{2+} binding to cNTnC induces little structural changes but sets the stage for cTnI$_{147-163}$ binding. A large closed-to-open conformational transition occurs in cNTnC upon binding bepridil or cTnI$_{147-163}$. Despite the simultaneous presence of the two ligands that are capable of inducing the opening of cNTnC, the domain is, in fact, more closed than if either one of the ligands was complexed to cNTnC alone (*98*). This is the result of the steric clash between the two ligands. Ideally, a Ca^{2+}-sensitizer would increase the Ca^{2+}-binding affinity of cTnC and enhance the cTnC-cTnI interaction. The high-resolution structures of the

cTnC•3Ca^{2+}•3bepridil and cNTnC•Ca^{2+}•bepridil•cTnI$_{147-163}$ together with the detailed binding mechanism not only contribute to the understanding of the mode of action of bepridil in cardiac troponin but also provide useful information for the design of cardiotonic drugs in general.

Trifluoperazine (TFP): The antipsychotic phenothiazine derivative, TFP, is a CaM antagonist that has been documented to have Ca^{2+}-sensitizing ability. TFP was shown to bind TnC in a Ca^{2+} specific manner (*100*) and its affinity ranges from 10 - 30 µM (*101, 102*). TFP has been shown to increase the Ca^{2+} affinity of TnC and the Ca^{2+} sensitivity of muscle preparation (*103*). Using NMR spectroscopy and chemical shift mapping, three-four TFP binding sites were identified in cTnC•3Ca^{2+} (*94*). This study suggested that there are two drug binding sites in the N-domain hydrophobic pocket, with one site (demarked by M45, M60, and M80) conferring Ca^{2+}-sensitizing effects, and the other site (containing M47, M81, and M85) also being capable of coordinating ligand, but being capable of inhibiting the association of cTnC with cTnI or cTnI peptides. This finding is verified in the X-ray structures of cNTnC•Ca^{2+}•2TFP in two different crystal forms (pdb code: 1WRK and 1WRL) (*104*). The structure is a dimer with four TFP molecules shared between two cNTnC•Ca^{2+} domains. One of the TFP molecules fits in the hydrophobic pocket of cNTnC•Ca^{2+} domain with its –CF$_3$ group pointed inwards, towards the hydrophobic cleft (Figure 1-15). The second TFP binds at the AB helical interface, where cTnI$_{147-163}$ binds in both the NMR and X-ray structures (*105, 106*). Therefore, it is likely that one of the TFP molecules would be completely replaced by the cTnI$_{147-163}$ peptide, as was the case for the bepridil-cTnC complex. TFP was shown to increase Ca^{2+}-sensitivity at low concentrations (10-30 µM); however, at higher concentrations it decreased the maximal force (100-300 µM) (*101*). This might be due to the competition of TFP with cTnI at higher concentrations, which would actually remove TnC from the myofilament. In fact, TnC can be extracted

from muscle fibers in the presence of 500 µM TFP (*107*). It is possible that TFP has one high-affinity binding site that does not compete with cTnI (Figure 1-15), and then two-three other low-affinity sites: one in the N-domain that competes with the switch region of cTnI at the AB interface and one or two that compete with the anchoring region of cTnI in the C-domain of cTnC.

Calmidazolium (CDZ): CDZ is another calmodulin antagonist, that has also been shown to increase the Ca^{2+} sensitivity of cardiac myofibril ATPase activity (*103*). El-Saleh and Solaro showed that at low concentrations, CDZ increased cardiac ATPase activity by specifically targeting the regulatory lobe of cTnC (*108*). Interestingly, at concentrations above 20 µM, ATPase activity was inhibited by CDZ, which may be the result of CDZ washing cTnC off the myofilament (like TFP) (*108*). CDZ induced a leftward shift in the pCa curve of both cardiac and skeletal myofilaments (*108, 109*). *In vitro* fluorescence measurements indicated that CDZ increases cTnC affinity for Ca^{2+} (*108*). Reid *et al.* used ^{1}H-NMR to investigate CDZ binding to isolated sTnC (*110*). The effect of CDZ on sTnC was also seen by fluorescence spectroscopy and it is possible that CDZ increases the affinity of sTnC for Ca^{2+} by slowing Ca^{2+} dissociation (*111*). CDZ had different stimulatory effects on the ATPase activity of cardiac myofibrils in adult and neonatal muscle. Since neonatal hearts have a different TnI isoform than adults, CDZ may specifically modulating the Ca^{2+}-sensitive response of the TnC-TnI interaction (*112*).

Levosimendan: Levosimendan, a pyridazinone derivative, is the most widely studied Ca^{2+}-sensitizer to date. This drug has been proven to be a well-tolerated and effective treatment for patients with severe decompensated heart failure (*97*). Levosimendan treatment enhances cardiac efficiency without an increase in oxygen demand associated with enhanced contractility induced by other agents, such as dobutamine,

currently in clinical use (see review by Endoh (*89*)). Levosimendan increases myofilament Ca^{2+} sensitivity by a molecular mechanism that appears to involve direct binding to the N-domain of Ca^{2+}-saturated cTnC (*113, 114*), although this was challenged by a study showing that levosimendan did not bind to cTnC or a cTnC/cTnI complex (*115*). A later report has shown that the inability to observe levosimendan binding to cTnC was in part due to sample degradation and the use of a recombinant cTnC having C35 and C84 mutated to serines (*114*). It appears that C84 is necessary for the interaction of levosimendan and cTnC. Furthermore, this report shows that levosimendan is capable of binding to both domains of cTnC. The exact location of the binding site of this drug on cTnC remains unclear due to the lack of a high-resolution structure of the cTnC•levosimendan complex.

Sorsa *et al.* used NMR chemical shift mapping to demonstrate levosimendan binding to the N-domain of cTnC in the presence of the cTnI peptides, $cTnI_{32-79}$ and $cTnI_{128-180}$, corresponding to the N-terminal and the inhibitory-switch regions of cTnI (*116*). In the presence of these peptides, no significant levosimendan-induced chemical shift changes were detected in the C-domain of cTnC, indicating that levosimendan does not bind to the C-domain when cTnI is present. Levosimendan induced amide chemical shift changes were detected throughout the N-domain of cTnC in the presence of the cTnI peptides. A number of N-domain resonances were either broadened beyond detection or exhibited multiple chemical shifts. A large number of both polar and non-polar residues that exhibit chemical shift changes upon levosimendan binding precluded identification of the levosimendan-binding site on cNTnC. Sorsa *et al.* attributed the numerous N-domain chemical shift changes to levosimendan altering either the dynamic equilibrium or the rate of exchange between open and closed N-domain conformations by partially stabilizing defunct Ca^{2+}-site I in $cNTnC•Ca^{2+}$. The authors estimate that the dissociation constant of levosimendan binding to $cTnC•3Ca^{2+}•cTnI_{32-}$

$_{79}$•cTnI$_{128-180}$ is ≥ 200 µM. In order to understand the exact location and effect of the pharmacophores of levosimendan on cTnC, a detailed structure-to-activity relationship (SAR) analysis of a group of levosimendan analogs has shown that both the hydrogen-bond donor and acceptor groups (=N-NH-, -CO) on the pyridazinone ring or on the mesoxalonitrile hydrazone moieties of the molecule are important for stabilizing the Ca^{2+}-saturated conformation of cNTnC (117).

Pimobendan: Pimobendan is similar in structure to levosimendan; and is the only other Ca^{2+}-sensitizer commercially available. Pimobendan has been shown to bind to isolated cTnC (118). Like levosimendan, pimobendan also has some PDE III inhibitory activity (119, 120). It has also been shown that pimobendan increases the Ca^{2+}-sensitivity of canine skinned cardiac fibers (121-123). Both isomers of pimobendan increase contractility, although the l-isomer is more potent (124). The Ca^{2+}-sensitizing ability of pimobendan appears to originate from its interaction with cNTnC and subsequent increase in Ca^{2+} affinity; however, an enhanced cTnI-cNTnC interaction may also be responsible (121). The fact that both levosimendan and pimobendan have pyridazinone moieties makes it tempting to conclude that both molecules target cNTnC in a similar manner; however, no structural evidence exists to confirm this.

Anapoe: Anapoe is a detergent that was used to optimize the crystal quality of the sTnC•4Ca^{2+}•sTnI$_{1-182}$•sTnT$_{156-262}$ complex (52). In the structure, anapoe binds at the interface formed by sTnI and sNTnC and interacts with hydrophobic side chains residues from sNTnC and sTnI. The polar tail of the detergent molecule extends out of the hydrophobic cavity and may form hydrogen bonds with Q50 of sTnC (Figure 1-15). This network of interactions contribute to the stabilization of the N-domain hydrophobic pocket, corresponding to the facilitation of the binding of Ca^{2+} to the regulatory sites and the observed enhancement of the contractile

force of muscle fibers (*52*). The binding site of anapoe on sNTnC is similar to that of bepridil on cNTnC in the cNTnC•Ca^{2+}•cTnI$_{147-163}$•bepridil complex (Figure 1-15). In both cases, the small molecule fits into the hydrophobic pocket together with the switch region of TnI. The affinity of anapoe for sTnC•4Ca^{2+}•sTnI$_{1-182}$•sTnT$_{156-262}$ (K$_D$ = ~ 0.64 mM) is weaker than that of bepridil for cNTnC•Ca^{2+}•cTnI$_{147-163}$ (K$_D$ = ~ 80 μM). This may be the result of more extensive hydrophobic contacts made by bepridil (two aromatic rings) to cNTnC than anapoe (one aromatic ring) to sNTnC. In the case of the bepridil-bound structure, cTnI$_{147-163}$ was pushed out of the hydrophobic pocket when compared with the cNTnC•Ca^{2+}•cTnI$_{147-163}$ structure (*125*). In contrast, the position of the switch region of sTnI appears unperturbed by the presence of anapoe, when compared with the X-ray structure of cTnC•3Ca^{2+}•cTnI$_{34-210}$•cTnT$_{182-288}$ or with the NMR structure of cNTnC•Ca^{2+}•cTnI$_{147-163}$. The smaller hydrophobic surface of anapoe and its lack of a positive moiety may explain why it does not compete with sTnI for binding to sTnC. The relatively high affinity of anapoe for sTnC•4Ca^{2+}•sTnI$_{1-182}$•sTnT$_{156-262}$ is not ideal; however, its chemical structure could be optimized to improve its affinity for sNTnC without competing with sTnI.

W7: Like the other CaM antagonists, bepridil, TFP, and CDZ; W7 binds TnC. However, contrary to the other CaM antagonists, W7 inhibits the maximum cardiac and skeletal ATPase activity and tension development (*103, 126*). W7 has been shown to bind TnC with an affinity of 25 μM *in vitro* (*127*). Hoffman *et al.* used 2D ^{1}H,^{15}N- and ^{1}H,^{13}C-HSQC NMR spectroscopy to monitor W7 binding to cTnC (*128*). They found that consistent with bepridil and TFP (*94*), W7 bound to both domains of cTnC (*128*). In the titration of cCTnC•2Ca^{2+}, the spectral peaks originating from a subset of residues changed nonuniformly, and could not be described as single-site binding. A global fit of the cCTnC•2Ca^{2+} titration data to a two-site, sequential binding model yielded a dissociation constant (K$_D$) of 0.85-

0.91 mM for the singly bound state, with the second dissociation constant fit to 3.40-3.65 mM. The titration data for cNTnC•Ca^{2+} was globally fit to single-site binding model with a K_D of 0.15-0.30 mM (*128*). Titration of cTnC•3Ca^{2+} with W7 shows that residues throughout the sequence, including the N- and C-domains and the central linker, are affected (*129*). Analysis of the binding stoichiometry and the trajectories of chemical shift changes indicate that W7 binding occurs at multiple sites. To address the issue of whether multiple binding is relevant within the troponin complex, W7 was titrated to a cTnC-cTnI complex (TnC•3Ca^{2+}•cTnI$_{34-71}$•cTnI$_{128-163}$) (*129*). In the presence of the N-terminal (residues ~34-71), the inhibitory (residues ~128-147), and the switch (residues ~147-163) regions of cTnI, W7 induces chemical shift changes only in the N-domain and not in the C-domain or the central linker of cTnC. The affinity of W7 for the cTnC-cTnI complex was ~0.5 mM. The drop in affinity of W7 for the cTnC-cTnI complex when compared to binding the isolated domain (K_D from 0.15-0.3 mM to 0.5 mM) is consistent with a competition between cTnI and W7 for cTnC and correlates with the functional data (*103, 126*).

Following these results, the structures of W7 bound to cNTnC•Ca^{2+} (*130*) and cNTnC•Ca^{2+}•cTnI$_{147-163}$ (*131*) were determined by NMR spectroscopy (Figure 1-15). As was the case for TFP and bepridil, W7 bound to the hydrophobic pocket of cNTnC. The positively charged primary amine of W7 was pointed towards the exterior of the protein. In cNTnC•Ca^{2+}•cTnI$_{147-163}$, the position of W7 was relatively unperturbed by the binding of cTnI$_{147-163}$. On the other hand, cTnI$_{147-163}$ was shifted away from the core of cNTnC. Moreover, the affinity of cTnI$_{147-163}$ was decreased by ~10-fold by the presence of W7. As was the case for bepridil, the strong competition between W7 and cTnI$_{147-163}$ is caused by a steric clash between molecules as well as an electrostatic repulsion between the positively charged amino of W7 and the side chain of R147 from cTnI$_{147-163}$.

The negative inotropic, or Ca^{2+}-desensitizing, effects of W7 may represent a novel treatment of hypertrophic cardiomyopathy (HCM). Mutations in the sarcomere that have been linked to HCM have been found to increase Ca^{2+}-sensitivity and impair relaxation (*132*). Reversal of these phenomena by the desensitization of the sarcomere to Ca^{2+} may represent a novel treatment of HCM (*132*). The myosin inhibitors, blebbistatin (*133*) and pentabromopseudilin (*134*) have been shown to bind to myosin at two different allosteric sites to inhibit function (*134, 135*). Blebbistatin was shown to decrease the risk of arrhythmias in hypertrophic causing, thin-filament mutations (*136*). Desensitizing agents appear to have a therapeutic promise, and should be investigated further.

EMD 57033: EMD 57033 is a thiadiazinone derivative. It has been found to increase the Ca^{2+}-sensitivity of both myofibrillar ATPase and force development by skinned muscle fibers (*137, 138*). *In vivo* studies have also demonstrated that EMD 57033 enhances cardiac contractile function without affecting Ca^{2+}-homeostasis (*139-143*). The myofibrillar Ca^{2+}-sensitizing effect of EMD 57033 is stereospecific. EMD 57033 is the (+)-enantiomer of a racemate. The (-)-enantiomer, EMD 57439, exhibits no Ca^{2+}-sensitizing activity but acts as a pure phosphodiesterase III inhibitor (*137, 138*). The drawback in the development of EMD 57033 as a Ca^{2+}-sensitizer is from observations that treatment with EMD 57033 resulted in not only positive inotropic effects but also impaired relaxation in some heart muscle preparations (*138, 144*). However, Tsutsui *et al* showed that EMD 57033 increased contractility of isolated myocytes, studied at 37˚C, from hearts of control dogs and dogs with induced heart failure with no effect on diastolic cell length or mechanical dynamics (*143*). Studies in conscious dogs with and without induced heart failure showed a dramatic effect of EMD 57033 on contractility in both control and failed hearts with improvement of mechanical efficiency and without compromise of diastolic function (*140*). Furthermore, studies with open chest pig hearts stressed

by a stunning protocol, also demonstrated an improvement of contractility with improved mechanical efficiency (*145*). A related study has shown that EMD 57033 is effective in restoring systolic function in a mouse model harboring a proteolytic truncation of cTnI, $cTnI_{1-193}$, associated with myocardial stunning (*146*). Taken together, these studies indicate that the potentially undesirable effects of EMD 57033, such as diastolic abnormalities and impaired relaxation, may not be a problem *in vivo*.

Recently, several key studies have provided new insights in the understanding of the molecular mechanism underlining the Ca^{2+}-sensitizing effects of EMD 57033. Evidence that EMD 57033 binds to the C-domain of cTnC has come from both direct binding measurements (*147*) and NMR chemical shift changes (*115, 148*). This indicates that EMD 57033 has a unique mechanism from other troponin-targeting ligands. EMD 57033 also enhances muscle contractility in the absence of cTnC, and therefore may also function by the actin-myosin interaction (*86*). With EMD 57033, there appears to be an amplification of the hydrophobic surface in the C-domain of cTnC that modifies the interaction of cTnC with cTnI rather than an increase in Ca^{2+}-binding to the regulatory domain of cTnC. Measurement of the NMR spectra in the presence of cTnI peptide indicates a competition between $cTnI_{34-71}$ and EMD 57033, whereas the inhibitory region $cTnI_{128-147}$ did not share a common binding site with EMD 57033 (*149*). Thus a straightforward mechanism for the Ca^{2+}-sensitizing effect of EMD 57033 is that this drug disrupts and therefore weakens the interaction of $cTnI_{34-71}$ with cCTnC in the myofilaments, and consequently, enhances binding of the C-terminal region of cTnI to cTnC. Since this interaction is Ca^{2+}-dependent, the apparent Ca^{2+}-sensitivity of the contractile system would be enhanced. This hypothesis is supported by a study showing that EMD 57033 can restore the Ca^{2+}-sensitivity of myofilaments containing pseuodophosphorylated cTnI, cTnI-S41E-S43E and a familiar hypertrophic cardiomyopathy (FHC) mutant α-tropomyosin (E180G); both of the modifications surround the C-domain of cTnC (*150*).

In the high-resolution structure of cCTnC•2Ca^{2+}•EMD 57033 (Figure 1-15), the drug molecule is orientated such that the chiral group of EMD 57033 is deep in the hydrophobic pocket and makes several key contacts with the protein (*149*). This stereospecific interaction explains why the (-)-enantiomer of EMD 57033 is inactive. Since the methyl group attached to the chiral carbon of EMD 57033 makes extensive contacts with methyl groups of I112, L117, and I148, located on the β-sheet connecting the two Ca^{2+} binding sites, these contacts would be weakened or lost if the stereo-specificity of the chiral carbon were changed. In support of this the (-)-enantiomer, EMD 57439, induces no chemical shift changes of cCTnC•2Ca^{2+}, suggesting a lack of interaction between the two (Wang and Sykes, unpublished data).

Natural Compounds: The beneficial effects of consuming food and drink high in polyphenols are well established (*151, 152*). The health improvement from these molecules is thought to be in-part from their antioxidant and free-radical scavenging capabilities (*153*). In addition to these broad-spectrum effects, there is a growing body of work that suggests that polyphenol compounds also have specific targets in the body. Two compounds that have been the target of intense investigation are (-)-epigallocatechin gallate (EGCg) and resveratrol.

Green tea (*Camellia sinensis*) is the second most consumed beverages in the world (water being the first), and several epidemiological studies have linked the consumption of tea with the decrease in cardiovascular disease (*154, 155*). EGCg is a polyphenol abundant in unfermented teas, and has been identified as a modulator of heart contraction through its interaction with the C-domain of cTnC (*156-158*). EGCg decreases the Ca^{2+}-sensitivity of skinned cardiac myofilaments (*159*) and it binds to the C-terminal domain of cCTnC *in vitro (156)*. It is possible that EGCg decreases myofilament Ca^{2+} sensitivity by enhancing the affinity of cTnI$_{34-71}$ for cCTnC (*159*).

Resveratrol has a variety of reported physiological effects such as antiplatelet aggregation, anti-inflammatory, and antioxidant activity linked to longevity (*160, 161*); cancer chemoprevention (*162, 163*); and cardioprotection (*164*). Amongst its cardioprotective effects, resveratrol improves ventricular function recovery following ischemia reperfusion injury (*165*). It was demonstrated that resveratrol modulates the contractile function of guinea-pig myocytes. In the cells where it induced contraction, its relation with the Ca^{2+} transients was quantitatively determined indicating an increase in myofilament Ca^{2+}-sensitivity (*166*). Preliminary evidence suggests that the natural compound, propyl gallate, also acts as a Ca^{2+}-sensitizer (*167*). These data point to a common mechanism by which polyphenols may target the sarcomere to modulate contractility.

Setting the field

Despite much progress in modern medicine, cardiovascular disease remains a grave global health concern. The search for novel approaches to attenuate heart disease has received a long overdue boost in recent years. The developments of cardiotonic agents that enhance cardiac contractility without increasing levels of intracellular Ca^{2+} (*e.g.* omecamtiv mecarbil and levosimendan) represent an exciting alternative treatment. Experiments on muscle fibers have pointed to cTnC as one of the sarcomere proteins that represents a plausible target for this novel therapy. The structural and functional studies of small molecules that target troponin to elicit a contractile response have laid the foundation for recognizing the critical role the cTnC-cTnI interaction plays in modulating Ca^{2+}-sensitivity. This dissertation builds on this knowledge by several different avenues of investigation.

The targeting of EMD 57033 to the C-domain of cTnC has raised some questions about how this drug functions *in vivo* and whether the C-

domain of cTnC represents a realistic drug target. The C-domain of cTnC is generally thought of as playing a structural role through its interaction with the anchoring region of cTnI. On the other hand, the dilated cardiomyopathy, G159D (*168*), and the hypertrophic cardiomyopathy, D145E (*169*), suggest that this domain does more than to just act as a tether. Furthermore, recent evidence that EGCg targets the C-domain of cTnC to modify contractility implies that this domain is a bona fide regulator of contraction. Chapters 2 and 3 of this thesis employ NMR spectroscopy to study the molecular mechanism by which EGCg and resveratrol bind cCTnC. In combination with the cCTnC•2Ca^{2+}•EMD 57033 structure some common structural elements between the ligands are highlighted and a potential mechanism by which small molecules that target cCTnC may impede with cTnI binding is posited.

Given the regulatory role of cNTnC, a number of drugs have been developed that enhance the Ca^{2+} response of the myofilament by specifically interacting with this domain. Structural investigations have indicated that molecules (bepridil and TFP) may enhance contractility by stabilizing the open state of cNTnC, thus increasing the affinity of cNTnC for Ca^{2+}. The structural and functional data from the negative inotrope, W7, indicate that simply stabilizing the open state of cNTnC is not sufficient to increase contraction. In Chapters 4, 5, and 6, we examine the pharmacophores responsible for determining if a molecule is a Ca^{2+}-sensitizers or desensitizers. Our results indicate that the activity of a small molecule largely hinges on its interaction with cTnI in the troponin complex. In addition to stabilizing the open conformation of cNTnC, an archetypical Ca^{2+}-sensitizer would enhance cTnI binding to cNTnC. The structural and functional studies presented herein point toward a critical electrostatic interaction between an arginine rich region of cTnI and the inotropes.

To address the importance of the cTnC-cTnI interaction in regulating contraction we also looked at a couple of mutations in the

troponin system that have been shown to regulate contractility. Firstly, we look at the mutation of L48 to a glutamine. L48 is involved in stabilizing the AB interface by a series of hydrophobic interactions and mutating it to a glutamine has been shown to have a pronounced Ca^{2+}-sensitizing effect (*170*). In Chapter 7, we investigate the structural and functional implications of this mutation and show that it stabilizes the open state of cNTnC, thereby enhancing its interaction with cTnI. Secondly, it has also been shown that modulation of the cTnC-cTnI interaction by mutating A162 on cTnI to a histidine has a pronounced Ca^{2+}-sensitizing effect at low pH (*171, 172*). In both skeletal and neonatal troponin I this histidine is already present, and these muscle types have been shown to be less sensitive to low pH (*173, 174*). In Chapter 8, we probe the structural role of the histidine on sTnI by NMR spectroscopy. It appears that H130 on sTnI protects against the Ca^{2+}-desensitizing effects of acidosis by enhancing the cNTnC-TnI interaction at low pH by the formation of an electrostatic interaction with E19 of cNTnC.

The common theme underlying this thesis is the vital role the TnC-TnI interaction plays in controlling the Ca^{2+}-sensitivity of muscle; therefore, targeting this interaction has exciting therapeutic possibilities for cardiovascular disease. I have assembled this thesis using primarily published material or manuscripts in progress. Therefore each chapter is designed as an independent piece of work. At the beginning of each chapter I have included a brief description of my contribution to the work. In the final chapter, I bring all the research together to construct a final mechanism. Projects that are auxiliary to the main focus of thesis or that are ongoing have been placed in the Appendices.

References

1.   Servetus, M. (1790) *The restoration of Christianity*, Nuremberg.
2.   Graubard, M. (1964) *Circulation and Respiration, the Evolution of an Idea*, Harcourt, Brace & World.
3.   Shaw, J. R. (1972) Models for cardiac structure and function in Aristotle, *J. Hist. Biol. 5*, 355-388.
4.   Katz, A. M. (1997) Evolving concepts of heart failure: cooling furnace, malfunctioning pump, enlarging muscle--Part I, *J. Card. Fail. 3*, 319-334.
5.   Haddad, S. I., and Khairallah, A. A. (1936) A Forgotten Chapter in the History of the Circulation of the Blood, *Ann. Surg. 104*, 1-8.
6.   Stefanadis, C., Karamanou, M., and Androutsos, G. (2009) Michael Servetus (1511-1553) and the discovery of pulmonary circulation, *Hellenic J. Cardiol. 50*, 373-378.
7.   Schultz, S. G. (2002) William Harvey and the circulation of the blood: the birth of a scientific revolution and modern physiology, *News Physiol. Sci. 17*, 175-180.
8.   Opie, L. H. (2003) *Heart Physiology: From Cell to Circulation*, Fourth ed., Lippincott Williams & Wilkins.
9.   Wiggers, C. (1915) *Modern aspects of circulation in health and disease*, Lea & Febiger, Philadelphia.
10.   Huxley, A. F., and Niedergerke, R. (1954) Structural changes in muscle during contraction; interference microscopy of living muscle fibres, *Nature 173*, 971-973.
11.   Huxley, H., and Hanson, J. (1954) Changes in the cross-striations of muscle during contraction and stretch and their structural interpretation, *Nature 173*, 973-976.
12.   Ringer, S. (1883) A further Contribution regarding the influence of the different Constituents of the Blood on the Contraction of the Heart, *The Journal of physiology 4*, 29-42 23.
13.   Ebashi, S., Kodama, A., and Ebashi, F. (1968) Troponin. I. Preparation and physiological function, *J Biochem 64*, 465-477.
14.   Gordon, A. M., Homsher, E., and Regnier, M. (2000) Regulation of contraction in striated muscle, *Physiol. Rev. 80*, 853-924.
15.   Holmes, K. C., and Geeves, M. A. (2000) The structural basis of muscle contraction, *Philosophical Transactions of the Royal Society of London Series B-Biological Sciences 355*, 419-431.
16.   Kobayashi, T., Jin, L., and de Tombe, P. P. (2008) Cardiac thin filament regulation, *Pflugers Archiv-European Journal of Physiology 457*, 37-46.
17.   Li, M. X., Wang, X., and Sykes, B. D. (2004) Structural based insights into the role of troponin in cardiac muscle pathophysiology, *J. Muscle Res. Cell Motil. 25*, 559-579.

18. Tobacman, L. S. (1996) Thin filament-mediated regulation of cardiac contraction, *Annu. Rev. Physiol. 58*, 447-481.

19. Parmacek, M. S., and Solaro, R. J. (2004) Biology of the troponin complex in cardiac myocytes, *Prog. Cardiovasc. Dis. 47*, 159-176.

20. Herzberg, O., and James, M. N. G. (1985) Structure of the calcium regulatory muscle protein troponin-C at 2.8 A resolution, *Nature 313*, 653-659.

21. Sundaralingam, M., Bergstrom, R., Strasburg, G., Rao, S. T., Roychowdhury, P., Greaser, M., and Wang, B. C. (1985) Molecular structure of troponin C from chicken skeletal muscle at 3-Å resolution, *Science 227*, 945-948.

22. Herzberg, O., Moult, J., and James, M. N. G. (1986) A model for the Ca^{2+}-induced conformational transition of troponin C, *J. Biol. Chem. 261*, 2638-2644.

23. Slupsky, C. M., and Sykes, B. D. (1995) NMR solution structure of calcium-saturated skeletal muscle troponin C, *Biochemistry 34*, 15953-15964.

24. Gagné, S. M., Tsuda, S., Li, M. X., Smillie, L. B., and Sykes, B. D. (1995) Structures of the troponin C regulatory domains in the apo and calcium-saturated states., *Nat. Struct. Biol. 2*, 784-789.

25. Strynadka, N. C. J., Cherney, M., Sielecki, A. R., Li, M. X., Smillie, L. B., and James, M. N. G. (1997) Structural details of a calcium-induced molecular swith: X-ray crystallographic analysis of the calcium-saturated N-terminal domain of troponin C at 1.75 Å resolution, *J. Mol. Biol. 273*, 238-255.

26. Houdusse, A., Love, M. L., Dominguez, R., Grabarek, Z., and Cohen, C. (1997) Structures of four Ca^{2+}-bound troponin C at 2.0 angstrom resolution: further insights into the Ca^{2+}-swith in the calmodulin superfamily, *Structure 5*, 1695-1711.

27. Sia, S. K., Li, M. X., Spyracopoulos, L., Gagné, S. M., Liu, W., Putkey, J. A., and Sykes, B. D. (1997) NMR structure of cardiac troponin C reveals an unexpected closed regulatory domain, *J. Biol. Chem. 272*, 18216-18221.

28. Spyracopoulos, L., Li, M. X., Sia, S. K., Gagné, S. M., Chandra, M., Solaro, R. J., and Sykes, B. D. (1997) Calcium-induced structural transition in the regulatory domain of human cardiac troponin C, *Biochemistry 36*, 12138-12146.

29. Li, M. X., Spyracopoulos, L., and Sykes, B. D. (1999) Binding of cardiac troponin-I 147-163 induces a structural opening in human cardiac troponin-C, *Biochemistry 38*, 8289-8298.

30. Mercier, P., Ferguson, R. E., Corrie, J. E., Trenthem, D. R., and Sykes, B. D. (2003) Structure and dynamics of rhodamine labeled N-domain of skeletal troponin C in complex with with skeletal troponin I 115-131, *Biochemistry 42*, 4333-4348.

31. McKay, R. T., Saltibus, L. F., Li, M. X., and Sykes, B. D. (2000) Energetics of the induced structural change in a Ca2+ regulatory

protein: Ca2+ and troponin I peptide binding to the E41A mutant of the N-domain of skeletal troponin C, *Biochemistry 39*, 12731-12738.

32. McKay, R. T., Tripet, B. P., Hodges, R. S., and Sykes, B. D. (1997) Interaction of the second binding region of troponin I with the regulatory domain of skeletal muscle troponin-C as determined by NMR spectroscopy, *J. Biol. Chem. 272*, 28494-28500.

33. McKay, R. T., Tripet, B. P., Pearlstone, J. R., Smillie, L. B., and Sykes, B. D. (1999) Defining the region of troponin-I that binds to troponin-C, *Biochemistry 38*, 5478-5489.

34. McKay, R. T., Pearlstone, J. R., Corson, D. C., Gagne, S. M., Smillie, L. B., and Sykes, B. D. (1998) Structure and interaction site of the regulatory domain of troponin-C when complexed with the 96-148 region of troponin-I, *Biochemistry 37*, 12419-12430.

35. Gasmi-Seabrook, G. M., Howarth, J. W., Finley, N., Abusamhadneh, E., Gaponenko, V., Brito, R. M., Solaro, R. J., and Rosevear, P. R. (1999) Solution structures of the C-terminal domain of cardiac troponin C free and bound to the N-terminal domain of cardiac troponin I, *Biochemistry 38*, 8313-8322.

36. Campbell, A. P., and Sykes, B. D. (1991) Interaction of troponin I and troponin C: use of the two-dimensional nuclear magnetic resonance transferred nuclear overhauser effect to determine the structure of the inhibitory troponin I peptide when bound to skeletal troponin C, *J. Mol. Biol. 222*, 405-421.

37. Hernandez, G., Blumenthal, D. K., Kennedy, M. A., Unkefer, C. J., and Trewhella, J. (1999) Troponin I inhibitory peptide (96-115) has an extended conformation when bound to skeletal muscle troponin C, *Biochemistry 38*, 6911-6917.

38. Brito, R. M., Putkey, J. A., Strynadka, N. C., James, M. N., and Rosevear, P. R. (1991) Comparative NMR studies on cardiac troponin C and a mutant incapable of binding calcium at site II, *Biochemistry 30*, 10236-10245.

39. Brito, R. M., Krudy, G. A., Negele, J. C., Putkey, J. A., and Rosevear, P. R. (1993) Calcium plays distinctive structural roles in the N- and C-terminal domains of cardiac troponin C, *J Biol Chem 268*, 20966-20973.

40. Krudy, G. A., Brito, R. M., Putkey, J. A., and Rosevear, P. R. (1992) Conformational changes in the metal-binding sites of cardiac troponin C induced by calcium binding, *Biochemistry 31*, 1595-1602.

41. Krudy, G. A., Kleerekoper, Q., Guo, X., Howarth, J. W., Solaro, R. J., and Rosevear, P. R. (1994) NMR studies delineating spatial relationships within the cardiac troponin I-troponin C complex, *J. Biol. Chem. 269*, 23731-23735.

42. Howarth, J. W., Krudy, G. A., Lin, X., Putkey, J. A., and Rosevear, P. R. (1995) An NMR and spin label study of the effects of binding

calcium and troponin I inhibitory peptide to cardiac troponin C, *Protein Sci. 4*, 671-680.

43. Lin, X., Krudy, G. A., Howarth, J., Brito, R. M., Rosevear, P. R., and Putkey, J. A. (1994) Assignment and calcium dependence of methionyl epsilon C and epsilon H resonances in cardiac troponin C, *Biochemistry 33*, 14434-14442.

44. Finley, N., Abbott, M. B., Abusamhadneh, E., Gaponenko, V., Dong, W., Gasmi-Seabrook, G., Howarth, J. W., Rance, M., Solaro, R. J., Cheung, H. C., and Rosevear, P. R. (1999) NMR analysis of cardiac troponin C-troponin I complexes: effects of phosphorylation, *FEBS Lett. 453*, 107-112.

45. Kleerekoper, Q., Howarth, J. W., Guo, X., Solaro, R. J., and Rosevear, P. R. (1995) Cardiac troponin I induced conformational changes in cardiac troponin C as monitored by NMR using site-directed spin and isotope labeling, *Biochemistry 34*, 13343-13352.

46. Abbott, M. B., Gaponenko, V., Abusamhadneh, E., Finley, N., Li, G., Dvoretsky, A., Rance, M., Solaro, R. J., and Rosevear, P. R. (2000) Regulatory domain conformational exchange and linker region flexibility in cardiac troponin C bound to cardiac troponin I, *J. Biol. Chem. 275*, 20610-20617.

47. Abbott, M. B., Dvoretsky, A., Gaponenko, V., and Rosevear, P. R. (2000) Cardiac troponin I inhibitory peptide: location of interaction sites on troponin C, *FEBS Lett. 469*, 168-172.

48. Abbott, M. B., Dong, W. J., Dvoretsky, A., DaGue, B., Caprioli, R. M., Cheung, H. C., and Rosevear, P. R. (2001) Modulation of cardiac troponin C-cardiac troponin I regulatory interactions by the amino-terminus of cardiac troponin I, *Biochemistry 40*, 5992-6001.

49. Vassylyev, D. G., Takeda, S., Wakatsuki, S., Maeda, K., and Maeda, Y. (1998) Crystal structure of troponin C in complex with troponin I fragment at 2.3-A resolution, *Proc. Natl. Acad. Sci. U. S. A. 95*, 4847-4852.

50. Lindhout, D. A., and Sykes, B. D. (2003) Structure and dynamics of the C-domain of human cardiac troponin C in complex with the inhibitory region of human cardiac troponin I, *J. Biol. Chem. 278*, 27024-27034.

51. Takeda, S., Yamashida, A., Maeda, K., and Maeda, Y. (2003) Structure of the core domain of human cardiac troponin in the Ca^{2+}-saturated form, *Nature 424*, 35-41.

52. Vinogradova, M. V., Stone, D. B., Malanina, G. G., Karatzaferi, C., Cooke, R., Mendelson, R. A., and Fletterick, R. J. (2005) Ca^{2+}-regulated structural changes in troponin, *Proc Natl Acad Sci U S A. 102*, 5038-5043.

53. Brown, L. J., Sale, K. L., Hills, R., Rouviere, C., Song, L. K., Zhang, X. J., and Fajer, P. G. (2002) Structure of the inhibitory region of troponin by site directed spin labeling electron paramagnetic resonance, *Proc. Natl. Acad. Sci. U. S. A. 99*, 12765-12770.

54. Farah, C. S., and Reinach, F. C. (1995) The troponin complex and regulation of muscle contraction, *FASEB J. 9*, 755-767.

55. Pearlstone, J. R., and Smillie, L. B. (1985) The interaction of rabit skeletal muscle troponin-T fragments with troponin I, *Can. J. Biochem. Cell Biol. 63*, 212-218.

56. Gaponenko, V., Abusamhadneh, E., Abbott, M. B., Finley, N., Gasmi-Seabrook, G., Solaro, R. J., Rance, M., and Rosevear, P. R. (1999) Effects of troponin I phosphorylation on conformational exchange in the regulatory domain of cardiac troponin C, *J. Biol. Chem. 274*, 16681-16684.

57. Ward, D. G., Brewer, S. M., Comes, M. P., and Trayer, I. P. (2003) A cross-linking study of the N-terminal extension of human cardiac troponin I, *Biochemistry 42*, 10324-10332.

58. Baryshnikova, O. K., Li, M. X., and Sykes, B. D. (2008) Modulation of cardiac troponin C function by the cardiac-specific N-terminus of troponin I: influence of PKA phosphorylation and involvement in cardiomyopathies, *J. Mol. Biol. 375*, 735-751.

59. Howarth, J. W., Meller, J., Solaro, R. J., Trewhella, J., and Rosevear, P. R. (2007) Phosphorylation-dependent conformational transition of the cardiac specific N-extension of troponin I in cardiac troponin, *J. Mol. Biol. in press*.

60. Blumenschein, T. M., Stone, D. B., Fletterick, R. J., Mendelson, R. A., and Sykes, B. D. (2005) Calcium-dependent changes in the flexibility of the regulatory domain of troponin C in the troponin complex, *J. Biol. Chem. 280*, 21924-21932.

61. Murakami, K., Yumoto, F., Ohki, S. Y., Yasunaga, T., Tanokura, M., and Wakabayashi, T. (2005) Structural basis for Ca^{2+}-regulated muscle relaxation at interaction sites of troponin with actin and tropomyosin, *J. Mol. Biol. 352*, 178-201.

62. Robinson, J. M., Dong, W. J., Xing, J., and Cheung, H. C. (2004) Switching of troponin I: Ca^{2+} and myosin-induced activation of heart muscle, *J. Mol. Biol. 340*, 295-305.

63. Blumenschein, T. M., Stone, D. B., Fletterick, R. J., Mendelson, R. A., and Sykes, B. D. (2006) Dynamics of the C-terminal region of TnI in the troponin complex in solution, *Biophys. J. 90*, 2436-2444.

64. Hoffman, R. M. B., Blumenschein, T. M., and Sykes, B. D. (2006) An interplay between protein disorder and structure confers the Ca2+ regulation of striated muscle, *J. Mol. Biol. 361*, 625-633.

65. Julien, O., Mercier, P., Allen, C. N., Fisette, O., Ramos, C. H. I., Lague, P., Blumenschein, T. M. A., and Sykes, B. D. (2011) Is there nascent structure in the intrinsically disordered region of troponin I?, *Proteins-Structure Function and Bioinformatics 79*, 1240-1250.

66. Shoemaker, B. A., Portman, J. J., and Wolynes, P. G. (2000) Speeding molecular recognition by using the folding funnel: the fly-casting mechanism, *Proc. Natl. Acad. Sci. U. S. A. 97*, 8868-8873.

67. WHO. (2011) Cardiovascular diseases (CVDs).

68. Roger, V. L., Go, A. S., Lloyd-Jones, D. M., Adams, R. J., Berry, J. D., Brown, T. M., Carnethon, M. R., Dai, S., de Simone, G., Ford, E. S., Fox, C. S., Fullerton, H. J., Gillespie, C., Greenlund, K. J., Hailpern, S. M., Heit, J. A., Ho, P. M., Howard, V. J., Kissela, B. M., Kittner, S. J., Lackland, D. T., Lichtman, J. H., Lisabeth, L. D., Makuc, D. M., Marcus, G. M., Marelli, A., Matchar, D. B., McDermott, M. M., Meigs, J. B., Moy, C. S., Mozaffarian, D., Mussolino, M. E., Nichol, G., Paynter, N. P., Rosamond, W. D., Sorlie, P. D., Stafford, R. S., Turan, T. N., Turner, M. B., Wong, N. D., Wylie-Rosett, J., American Heart Association Statistics, C., and Stroke Statistics, S. (2011) Heart disease and stroke statistics--2011 update: a report from the American Heart Association, *Circulation 123*, e18-e209.

69. McMurray, J. J., and Pfeffer, M. A. (2005) Heart failure, *Lancet 365*, 1877-1889.

70. Tang, W. H., and Francis, G. S. (2010) The year in heart failure, *J. Am. Coll. Cardiol. 55*, 688-696.

71. Katz, A. M. (2000) *Heart Failure: pathophysiology, molecular biology and clinical management*, Lippincott Williams & Wilkins.

72. Johnston, G. D. (1999) *Fundamentals of Cardiovascular Pharmacology*, John Wiley & Sons.

73. McKinsey, T. A., and Kass, D. A. (2007) Small-molecule therapies for cardiac hypertrophy: moving beneath the cell surface, *Nat. Rev. Drug Discovery 6*, 617-635.

74. Kaye, D. M., and Krum, H. (2007) Drug discovery for heart failure: a new era or the end of the pipeline?, *Nat. Rev. Drug Discov. 6*, 127-139.

75. Schwinger, R. H., Bundgaard, H., Muller-Ehmsen, J., and Kjeldsen, K. (2003) The Na, K-ATPase in the failing human heart, *Cardiovasc. Res. 57*, 913-920.

76. Kass, D. A., and Solaro, R. J. (2006) Mechanisms and use of calcium-sensitizing agents in the failing heart, *Circulation 113*, 305-315.

77. Dorn, G. W., 2nd, and Molkentin, J. D. (2004) Manipulating cardiac contractility in heart failure: data from mice and men, *Circulation 109*, 150-158.

78. Solaro, R. J., and Kobayashi, T. (2011) Protein phosphorylation and signal transduction in cardiac thin filaments, *J. Biol. Chem. 286*, 9935-9940.

79. Endoh, M. (2002) Mechanisms of action of novel cardiotonic agents, *J. Cardiovasc. Pharmacol. 40*, 323-338.

80. Lehtonen, L., and Poder, P. (2007) The utility of levosimendan in the treatment of heart failure, *Ann. Med. 39*, 2-17.

81. Haikala, H., Nissinen, E., Etemadzadeh, E., Levijoki, J., and Linden, I. B. (1995) Troponin C-Mediated Calcium Sensitization Induced by

Levosimendan Does Not Impair Relaxation, *J. Cardiovasc. Pharmacol. 25*, 794-801.

82. Malik, F. I., and Morgan, B. P. (2011) Cardiac myosin activation part 1: From concept to clinic, *J. Mol. Cell. Cardiol.*

83. Morgan, B. P., Muci, A., Lu, P. P., Qian, X. P., Tochimoto, T., Smith, W. W., Garard, M., Kraynack, E., Collibee, S., Suehiro, I., Tomasi, A., Valdez, S. C., Wang, W. Y., Jiang, H., Hartman, J., Rodriguez, H. M., Kawas, R., Sylvester, S., Elias, K. A., Godinez, G., Lee, K., Anderson, R., Sueoka, S., Xu, D. H., Wang, Z. P., Djordjevic, N., Malik, F. I., and Morgans, D. J. (2010) Discovery of Omecamtiv Mecarbil the First, Selective, Small Molecule Activator of Cardiac Myosin, *Acs Medicinal Chemistry Letters 1*, 472-477.

84. Malik, F. I., Hartman, J. J., Elias, K. A., Morgan, B. P., Rodriguez, H., Brejc, K., Anderson, R. L., Sueoka, S. H., Lee, K. H., Finer, J. T., Sakowicz, R., Baliga, R., Cox, D. R., Garard, M., Godinez, G., Kawas, R., Kraynack, E., Lenzi, D., Lu, P. P., Muci, A., Niu, C., Qian, X., Pierce, D. W., Pokrovskii, M., Suehiro, I., Sylvester, S., Tochimoto, T., Valdez, C., Wang, W., Katori, T., Kass, D. A., Shen, Y. T., Vatner, S. F., and Morgans, D. J. (2011) Cardiac myosin activation: a potential therapeutic approach for systolic heart failure, *Science 331*, 1439-1443.

85. Shen, Y. T., Malik, F. I., Zhao, X., Depre, C., Dhar, S. K., Abarzua, P., Morgans, D. J., and Vatner, S. F. (2010) Improvement of cardiac function by a cardiac Myosin activator in conscious dogs with systolic heart failure, *Circ Heart Fail 3*, 522-527.

86. Solaro, R. J., Gambassi, G., Warshaw, D. M., Keller, M. R., Spurgeon, H. A., Beier, N., and Lakatta, E. G. (1993) Stereoselective Actions of Thiadiazinones on Canine Cardiac Myocytes and Myofilaments, *Circ. Res. 73*, 981-990.

87. Palmer, S., Di Bello, S., Davenport, S. L., and Herzig, J. W. (1996) The novel inotropic agent CGP 48506 alters force primarily by Ca(2+)-independent mechanisms in porcine skinned trabeculae, *Cardiovasc. Res. 32*, 411-421.

88. Wolska, B. M., Kitada, Y., Palmiter, K. A., Westfall, M. V., Johnson, M. D., and Solaro, R. J. (1996) CGP-48506 increases contractility of ventricular myocytes and myofilaments by effects on actin-myosin reaction, *Am. J. Physiol. 270*, H24-32.

89. Endoh, M. (2001) Mechanism of action of Ca^{2+}-sensitizers-update 2001, *Cardiovasc. Drug Ther. 15*, 397-403.

90. Endoh, M. (2007) Could Ca^{2+} sensitizers rescue patients from chronic congestive heart failure, *Br. J. Pharmacol. 150*, 826-828.

91. Cramb, G., and Dow, J. W. (1983) Two site binding of bepridil an modulation of adenylate cyclase in cardiac sarcolemmal membranes, *Biochim. Biophys. Acta 736*, 99-108.

92. Solaro, R. J., Bousquet, P., and Johnson, J. D. (1986) Stimulation of cardiac myofilament force, ATPase activity and troponin C Ca^{2+} binding by bepridil, *J. Pharmacol. Exp. Ther. 238*, 502-507.

93. MacLachlan, L. K., Reid, D. G., Mitchell, R. C., Salter, C. J., and Smith, S. J. (1990) Binding of a calcium sensitizer, bepridil, to cardiac troponin C. A fluorescence stopped-flow kinetic, circular dichroism, and proton nuclear magnetic resonance study, *J. Biol. Chem. 265*, 9764-9770.

94. Kleerekoper, Q., Liu, W., Choi, D., and Putkey, J. A. (1998) Identification of binding sites for bepridil and trifluoperazine on cardiac troponin C, *J. Biol. Chem. 273*, 8153-8160.

95. Li, Y., Love, M. L., Putkey, J. A., and Cohen, C. (2000) Bepridil opens the regulatory N-terminal lobe of cardiac troponin C, *Proc. Natl. Acad. Sci. U. S. A. 97*, 5140-5145.

96. Abusamhadneh, E., Abbott, M. B., Dvoretsky, A., Finley, N., Sasi, S., and Rosevear, P. R. (2001) Interaction of bepridil with the cardiac troponin C/troponin I complex, *FEBS Lett. 506*, 51-54.

97. Sorsa, T., Pollesello, P., and Solaro, R. J. (2004) The contractile apparatus as a target for drugs against heart failure: interaction of levosimendan, a calcium sensitizer, with cardiac troponin C, *Mol. Cell Biochem. 266*, 87-107.

98. Wang, X., Li, M. X., and Sykes, B. D. (2002) Structure of the regulatory N-domain of human cardiac troponin C in complex with human cardiac troponin I$_{147-163}$ and bepridil, *J. Biol. Chem. 277*, 31124-31133.

99. Varughese, J. F., Baxley, T., Chalovich, J. M., and Li, Y. (2011) A computational and experimental approach to investigate bepridil binding with cardiac troponin, *J. Phys. Chem. B 115*, 2392-2400.

100. Levin, R. M., and Weiss, B. (1978) Specificity of the binding of trifluoperazine to the calcium-dependent activator of phosphodiesterase and to a series of other calcium-binding proteins, *Biochim. Biophys. Acta. 540*, 197-204.

101. Kurebayashi, N., and Ogawa, Y. (1988) Increase by Trifluoperazine in Calcium Sensitivity of Myofibrils in a Skinned Fiber from Frog Skeletal-Muscle, *Journal of Physiology-London 403*, 407-424.

102. Herzig, J. W., Tkachuk, V. A., Baldenkov, G. N., Feoktistov, I. A., Men'shikov, M., and Quast, U. (1987) Calmodulin and troponin C as targets for drug action, *Biomed. Biochim. Acta 46*, S440-443.

103. Silver, P. J., Pinto, P. B., and Dachiw, J. (1986) Modulation of Vascular and Cardiac Contractile Protein Regulatory Mechanisms by Calmodulin Inhibitors and Related-Compounds, *Biochem. Pharmacol. 35*, 2545-2551.

104. Igarashi, T., Takeda, S., and Mori, H. (2005) Crystal structure of the N-terminal domain of human cardiac troponin C in complex with a calcium-sensitizer; trifluoperazine, *J. Mol. Cell. Cardiol. 39*, 1016-1016.

105. Li, M. X., Spyracopoulos, L., and Sykes, B. D. (1999) Binding of cardiac troponin-I147-163 induces a structural opening in human cardiac troponin-C, *Biochemistry 38*, 8289-8298.

106. Takeda, S., Yamashita, A., Maeda, K., and Maeda, Y. (2003) Structure of the core domain of human cardiac troponin in the Ca(2+)-saturated form, *Nature 424*, 35-41.

107. Metzger, J. M., Greaser, M. L., and Moss, R. L. (1989) Variations in cross-bridge attachment rate and tension with phosphorylation of myosin in mammalian skinned skeletal muscle fibers. Implications for twitch potentiation in intact muscle, *J. Gen. Physiol. 93*, 855-883.

108. Elsaleh, S. C., and Solaro, R. J. (1987) Calmidazolium, a Calmodulin Antagonist, Stimulates Calcium-Troponin C and Calcium-Calmodulin-Dependent Activation of Striated-Muscle Myofilaments, *J. Biol. Chem. 262*, 17240-17246.

109. Regnier, M., Martyn, D. A., and Chase, P. B. (1996) Calmidazolium alters Ca2+ regulation of tension redevelopment rate in skinned skeletal muscle, *Biophys. J. 71*, 2786-2794.

110. Reid, D. G., Maclachlan, L. K., Gajjar, K., Voyle, M., King, R. J., and England, P. J. (1990) A Proton Nuclear-Magnetic-Resonance and Molecular Modeling Study of Calmidazolium (R24571) Binding to Calmodulin and Skeletal-Muscle Troponin-C, *J. Biol. Chem. 265*, 9744-9753.

111. Johnson, J. D., Nakkula, R. J., Vasulka, C., and Smillie, L. B. (1994) Modulation of Ca2+ exchange with the Ca(2+)-specific regulatory sites of troponin C, *J. Biol. Chem. 269*, 8919-8923.

112. Murphy, A. M., and Solaro, R. J. (1990) Developmental difference in the stimulation of cardiac myofibrillar Mg2(+)-ATPase activity by calmidazolium, *Pediatr. Res. 28*, 46-49.

113. Pollesello, P., Ovaska, M., Kaivola, J., Tilgmann, C., Lundstrom, K., Kalkkinen, N., Ulmanen, I., Nissinen, E., and Taskinen, J. (1994) Binding of a new Ca^{2+} sensitizer, levosimendan, to recombinant human cardiac troponin C. A molecular modelling, fluorescence probe, and proton nuclear magnetic resonance study, *J. Biol. Chem. 269*, 28584-28590.

114. Sorsa, T., Heikkinen, S., Abbott, M. B., Abusamhadneh, E., Laakso, T., Tilgmann, C., Serimaa, R., Annila, A., Rosevear, P. R., Drakenberg, T., Pollesello, P., and Kilpelainen, I. (2001) Binding of levosimendan, a calcium sensitizer, to cardiac troponin C, *J. Biol. Chem. 276*, 9337-9343.

115. Kleerekoper, Q., and Putkey, J. A. (1999) Drug binding to cardiac troponin C, *J. Biol. Chem. 274*, 23932-23939.

116. Sorsa, T., Pollesello, P., Permi, P., Drakenberg, T., and Kilpelainen, I. (2003) Interaction of levosimendan with cardiac troponin C in the presence of cardiac troponin I peptides, *J. Mol. Cell Cardiol. 35*, 1055-1061.

117. Levijoki, J., Pollesello, P., Kaivola, J., Tilgmann, C., Sorsa, T., Annila, A., Kilpelainen, I., and Haikala, H. (2000) Further evidence for the cardiac troponin C mediated calcium sensitization by levosimendan: structure-response and binding analysis with analogs of levosimnedan, *J. Mol. Cell Cardiol. 32*, 479-491.

118. Jaquet, K., and Heilmeyer, L. M., Jr. (1987) Influence of association and of positive inotropic drugs on calcium binding to cardiac troponin C, *Biochem. Biophys. Res. Commun. 145*, 1390-1396.

119. Scholz, H., and Meyer, W. (1986) Phosphodiesterase-inhibiting properties of newer inotropic agents, *Circulation 73*, III99-108.

120. Perrone, S. V., and Kaplinsky, E. J. (2005) Calcium sensitizer agents: a new class of inotropic agents in the treatment of decompensated heart failure, *Int. J. Cardiol. 103*, 248-255.

121. Solaro, R. J., Fujino, K., and Sperelakis, N. (1989) The Positive Inotropic Effect of Pimobendan Involves Stereospecific Increases in the Calcium Sensitivity of Cardiac Myofilaments, *J. Cardiovasc. Pharmacol. 14*, S7-S12.

122. Fujino, K., Sperelakis, N., and Solaro, R. J. (1988) Sensitization of Dog and Guinea-Pig Heart Myofilaments to Ca2+ Activation and the Inotropic Effect of Pimobendan - Comparison with Milrinone, *Circ. Res. 63*, 911-922.

123. Ruegg, J. C., Pfitzer, G., Eubler, D., and Zeugner, C. (1984) Effect on contractility of skinned fibres from mammalian heart and smooth muscle by a new benzimidazole derivative, 4,5-dihydro-6-[2-(4-methoxyphenyl)-1H-benzimidazol-5-yl]-5-methy l-3(2H)-pyridazinone, *Arzneimittelforschung. 34*, 1736-1738.

124. Fujino, K., Sperelakis, N., and Solaro, R. J. (1988) Differential-Effects of D-Pimobendan and I-Pimobendan on Cardiac Myofilament Calcium Sensitivity, *J. Pharmacol. Exp. Ther. 247*, 519-523.

125. Wang, X., Li, M. X., and Sykes, B. D. (2002) Structure of the regulatory N-domain of human cardiac troponin C in complex with human cardiac troponin I147-163 and bepridil, *J. Biol. Chem. 277*, 31124-31133.

126. Adhikari, B. B., and Wang, K. (2004) Interplay of troponin- and myosin-based pathways of calcium activation in skeletal and cardiac muscle: the use of W7 as an inhibitor of thin filament activation, *Biophys. J. 86*, 359-370.

127. Hidaka, H., Yamaki, T., Naka, M., Tanaka, T., Hayashi, H., and Kobayashi, R. (1980) Calcium-regulated modulator protein interacting agents inhibit smooth muscle calcium-stimulated protein kinase and ATPase, *Mol. Pharmacol. 17*, 66-72.

128. Hoffman, R. M. B., Li, M. X., and Sykes, B. D. (2005) The binding of W7, an inhibitor of striated muscle contraction, to cardiac troponin C, *Biochemistry 44*, 15750-15759.

129. Li, M. X., Hoffman, R. M. B., and Sykes, B. D. (2006) Interaction of cardiac troponin C with calmodulin antagonist W7 in the presence of three functional regions of cardiac troponin I, *Biochemistry 45*, 9833-9840.

130. Hoffman, R. M. B., and Sykes, B. D. (2009) Structure of the Inhibitor W7 Bound to the Regulatory Domain of Cardiac Troponin C, *Biochemistry 48*, 5541-5552.

131. Oleszczuk, M., Robertson, I. M., Li, M. X., and Sykes, B. D. (2010) Solution structure of the regulatory domain of human cardiac troponin C in complex with the switch region of cardiac troponin I and W7: The basis of W7 as an inhibitor of cardiac muscle contraction, *J. Mol. Cell. Cardiol. 48*, 925-933.

132. Ashrafian, H., McKenna, W. J., and Watkins, H. Disease pathways and novel therapeutic targets in hypertrophic cardiomyopathy, *Circ. Res. 109*, 86-96.

133. Straight, A. F., Cheung, A., Limouze, J., Chen, I., Westwood, N. J., Sellers, J. R., and Mitchison, T. J. (2003) Dissecting temporal and spatial control of cytokinesis with a myosin II Inhibitor, *Science 299*, 1743-1747.

134. Fedorov, R., Bohl, M., Tsiavaliaris, G., Hartmann, F. K., Taft, M. H., Baruch, P., Brenner, B., Martin, R., Knolker, H. J., Gutzeit, H. O., and Manstein, D. J. (2009) The mechanism of pentabromopseudilin inhibition of myosin motor activity, *Nat. Struct. Mol. Biol. 16*, 80-88.

135. Allingham, J. S., Smith, R., and Rayment, I. (2005) The structural basis of blebbistatin inhibition and specificity for myosin II, *Nat. Struct. Mol. Biol. 12*, 378-379.

136. Baudenbacher, F., Schober, T., Pinto, J. R., Sidorov, V. Y., Hilliard, F., Solaro, R. J., Potter, J. D., and Knollmann, B. C. (2008) Myofilament Ca2+ sensitization causes susceptibility to cardiac arrhythmia in mice, *J. Clin. Invest. 118*, 3893-3903.

137. Lues, I., Beier, N., Jonas, R., Klockow, M., and Haeusler, G. (1993) The two mechanisms of action of racemic cardiotonic EMD 53998, calcium sensitization and phosphodiesterase inhibition, reside in different enantiomers, *J. Cardiovasc. Pharmacol. 21*, 883-892.

138. Solaro, R. J., Gambassi, G., Warshaw, D. M., Keller, M. R., Spurgeon, H. A., Beier, N., and Lakatta, E. G. (1993) Stereoselective actions of thiadiazinones on canine cardiac myocytes and myofilaments, *Circ. Res. 73*, 981-990.

139. Haeusler, G., Jonas, R., Minck, K. O., Schliep, H. J., Schelling, P., Weygandt, H., and Lues, I. (1997) *In vivo* evidence of positive inotropism of EMD 57033 through calcium sensitization, *J. Cardiovasc. Pharmacol. 29*, 647-655.

140. Senzaki, H., Isoda, T., Paolocci, N., Ekelund, U., Hare, J. M., and Kass, D. A. (2000) Improved mechanoenergetics and cardiac rest and reserve function of *in vivo* failing heart by calcium sensitizer EMD 57033, *Circulation 101*, 1040-1048.

141. de Zeeuw, S., Trines, S. A., Krams, R., Duncker, D. J., and Verdouw, P. D. (2000) In vivo evidence that EMD 57033 restores myocardial responsiveness to intracoronary Ca^{2+} in stunned myocardium, *Eur. J. Pharmacol. 403*, 99-109.

142. de Zeeuw, S., Trines, S. A., Krams, R., Verdouw, P. D., and Duncker, D. J. (2000) Cardiovascular profile of the calcium sensitizer EMD 57033 in open- chest anaesthetized pigs with regionally stunned myocardium, *Br. J. Pharmacol. 129*, 1413-1422.

143. Tsutsui, H., Kinugawa, S., Ide, T., Hayashidani, S., Suematsu, N., Satoh, S., Nakamura, R., Egashira, K., and Takeshita, A. (2001) Positive inotropic effects of calcium sensitizers on normal and failing cardiac myocytes, *J. Cardiovasc. Pharmacol. 37*, 16-24.

144. Slinker, B. K., Wu, Y., Green, H. W. I., Kirkpatrick, R. D., and Campbell, K. B. (2000) Overall cardiac functional effect of positive inotropic drugs with differing effects on relaxation, *J. Cardiovasc. Pharmacol. 36*, 1-13.

145. Trines, S. A., Smits, C. A., van der Moer, J., Slager, C. J., Verdouw, P. D., and Krams, R. (2002) Calcium sensitizer EMD 57033, but not the beta1-adrenoreceptor agonist dobutamine, increases mechanical efficiency in stunned myocardium, *J. Cardiovasc. Pharmacol. 39*, 61-72.

146. Soergel, D. G., Georgakopoulos, D., Stull, L. B., Kass, D. A., and Murphy, A. M. (2004) Augmented systolic response to the calcium sensitizer EMD 57033 in a transgenic model with troponin I truncation, *Am. J. Physiol. Heart Circ. Physiol. 286*, H1785-1792.

147. Pan, B.-S., and Johnson, J., R. G. (1996) Interaction of cardiotonic thiadiazinone derivatives with cardiac troponin C, *J. Biol. Chem. 271*, 817-823.

148. Li, M. X., Spyracopoulos, L., Beier, N., Putkey, J. A., and Sykes, B. D. (2000) Interaction of cardiac troponin C with Ca2+ sensitizer EMD 57033 and cardiac troponin I inhibitory peptide, *Biochemistry 39*, 8782-8790.

149. Wang, X., Li, M. X., Spyracopoulos, L., Beier, N., Chandra, M., Solaro, R. J., and Sykes, B. D. (2001) Structure of the C-domain of human cardiac troponin C in complex with the Ca^{2+} sensitizing drug EMD 57033, *J. Biol. Chem. 276*, 25456-25466.

150. Burkart, E. M., Arteaga, G. M., Sumandea, M. P., Prabhakar, R., Wieczorek, D. F., and Solaro, R. J. (2003) Altered signaling surrounding the C-lobe of cardiac troponin C in myofilaments containing an alpha tropomyosin mutation linked to familial hypertrophic cardiomyopathy, *J. Mol. Cell Cardiol. 35*, 1285-1293.

151. Khan, N., and Mukhtar, H. (2007) Tea polyphenols for health promotion, *Life Sci. 81*, 519-533.

152. Bertelli, A. A., and Das, D. K. (2009) Grapes, wines, resveratrol, and heart health, *J. Cardiovasc. Pharmacol. 54*, 468-476.

153. Yao, L. H., Jiang, Y. M., Shi, J., Tomas-Barberan, F. A., Datta, N., Singanusong, R., and Chen, S. S. (2004) Flavonoids in food and their health benefits, *Plant Foods Hum. Nutr. 59*, 113-122.

154. Hertog, M. G., Feskens, E. J., Hollman, P. C., Katan, M. B., and Kromhout, D. (1993) Dietary antioxidant flavonoids and risk of coronary heart disease: the Zutphen Elderly Study, *Lancet 342*, 1007-1011.

155. Keli, S. O., Hertog, M. G., Feskens, E. J., and Kromhout, D. (1996) Dietary flavonoids, antioxidant vitamins, and incidence of stroke: the Zutphen study, *Arch. Intern. Med. 156*, 637-642.

156. Liou, Y. M., Kuo, S. C., and Hsieh, S. R. (2008) Differential effects of a green tea-derived polyphenol (-)-epigallocatechin-3-gallate on the acidosis-induced decrease in the Ca(2+) sensitivity of cardiac and skeletal muscle, *Pflugers Arch. 456*, 787-800.

157. Hotta, Y., Huang, L., Muto, T., Yajima, M., Miyazeki, K., Ishikawa, N., Fukuzawa, Y., Wakida, Y., Tushima, H., Ando, H., and Nonogaki, T. (2006) Positive inotropic effect of purified green tea catechin derivative in guinea pig hearts: The measurements of cellular Ca2+ and nitric oxide release, *Eur. J. Pharmacol. 552*, 123-130.

158. Tadano, N., Yumoto, F., Tanokura, M., Ohtsuki, I., and Morimoto, S. (2005) EGCg, a major polyphenol in green tea, binds to the C-lobe of cardiac troponin and desensitizes cardiac muscle contraction to Ca2+, *Biophys. J. 88*, 314a-314a.

159. Tadano, N., Du, C. K., Yumoto, F., Morimoto, S., Ohta, M., Xie, M. F., Nagata, K., Zhan, D. Y., Lu, Q. W., Miwa, Y., Takahashi-Yanaga, F., Tanokura, M., Ohtsuki, I., and Sasaguri, T. (2010) Biological actions of green tea catechins on cardiac troponin C, *Br. J. Pharmacol. 161*, 1034-1043.

160. Das, D. K., Mukherjee, S., and Ray, D. (2010) Resveratrol and red wine, healthy heart and longevity, *Heart Failure Reviews 15*, 467-477.

161. Lekli, I., Ray, D., and Das, D. K. (2010) Longevity nutrients resveratrol, wines and grapes, *Genes and Nutrition 5*, 55-60.

162. Jang, M. S., Cai, E. N., Udeani, G. O., Slowing, K. V., Thomas, C. F., Beecher, C. W. W., Fong, H. H. S., Farnsworth, N. R., Kinghorn, A. D., Mehta, R. G., Moon, R. C., and Pezzuto, J. M. (1997) Cancer chemopreventive activity of resveratrol, a natural product derived from grapes, *Science 275*, 218-220.

163. Holme, A. L., and Pervaiz, S. (2007) Resveratrol in cell fate decisions, *J. Bioenerg. Biomembr. 39*, 59-63.

164. Das, D. K., and Maulik, N. (2006) Red wine and heart: A cardioprotective journey from grape to resveratrol, *Alcoholism-Clinical and Experimental Research 30*, 84a-84a.

165. Ray, P. S., Maulik, G., Cordis, G. A., Bertelli, A. A. E., Bertelli, A., and Das, D. K. (1999) The red wine antioxidant resveratrol protects

isolated rat hearts from ischemia reperfusion injury, *Free Radical Biology and Medicine 27*, 160-169.

166. Liew, R., Stagg, M. A., MacLeod, K. T., and Collins, P. (2005) The red wine polyphenol, resveratrol, exerts acute direct actions on guinea-pig ventricular myocytes, *Eur. J. Pharmacol. 519*, 1-8.

167. Tadano, N., Morimoto, S., Takahashi-Yanaga, F., Miwa, Y., Ohtsuki, I., and Sasaguri, T. (2009) Propyl Gallate, a Strong Antioxidant, Increases the Ca2+ Sensitivity of Cardiac Myofilament, *J. Pharmacol. Sci. 109*, 456-458.

168. Mirza, M., Marston, S., Willott, R., Ashley, C., Mogensen, J., McKenna, W., Robinson, P., Redwood, C., and Watkins, H. (2005) Dilated cardiomyopathy mutations in three thin filament regulatory proteins result in a common functional phenotype, *J. Biol. Chem. 280*, 28498-28506.

169. Landstrom, A. P., Parvatiyar, M. S., Pinto, J. R., Marquardt, M. L., Bos, J. M., Tester, D. J., Ornmen, S. R., Potter, J. D., and Ackerman, M. J. (2008) Molecular and functional characterization of novel hypertrophic cardiomyopathy susceptibility mutations in TNNC1-encoded troponin C, *J. Mol. Cell. Cardiol. 45*, 281-288.

170. Tikunova, S. B., and Davis, J. P. (2004) Designing calcium-sensitizing mutations in the regulatory domain of cardiac troponin C, *J. Biol. Chem. 279*, 35341-35352.

171. Dargis, R., Pearlstone, J. R., Barrette-Ng, I., Edwards, H., and Smillie, L. B. (2002) Single mutation (A162H) in human cardiac troponin I corrects acid pH sensitivity of Ca2+-regulated actomyosin S1 ATPase, *J. Biol. Chem. 277*, 34662-34665.

172. Day, S. M., Westfall, M. V., Fomicheva, E. V., Hoyer, K., Yasuda, S., La Cross, N. C., D'Alecy, L. G., Ingwall, J. S., and Metzger, J. M. (2006) Histidine button engineered into cardiac troponin I protects the ischemic and failing heart, *Nat. Med. 12*, 181-189.

173. Li, G., Martin, A. F., and Solaro, J. R. (2001) Localization of regions of troponin I important in deactivation of cardiac myofilaments by acidic pH, *J. Mol. Cell. Cardiol. 33*, 1309-1320.

174. Westfall, M. V., Rust, E. M., and Metzger, J. M. (1997) Slow skeletal troponin I gene transfer, expression, and myofilament incorporation enhances adult cardiac myocyte contractile function, *Proc. Natl. Acad. Sci. U. S. A. 94*, 5444-5449.

175. Marieb, E. N. (2001) *Human Anatomy & Physiology*, Vol. 5th, Benjamin Cummings.

176. Gunther, S., and Kruse, K. (2007) Spontaneous waves in muscle fibres, *New Journal of Physics 9*.

177. Huxley, H. E. (1969) Mechanism of Muscular Contraction, *Science 164*, 1356-&.

178. Pirani, A., Xu, C., Hatch, V., Craig, R., Tobacman, L. S., and Lehman, W. (2005) Single particle analysis of relaxed and activated muscle thin filaments, *J. Mol. Biol. 346*, 761-772.

179. Day, S. M., Westfall, M. V., and Metzger, J. M. (2007) Tuning cardiac performance in ischemic heart disease and failure by modulating myofilament function, *J. Mol. Med. (Berl.) 85*, 911-921.

180. Voet, D. V. a. J. G. (1995) *Biochemistry*, 2nd ed., John Wiley & Sons, New York.

181. Feldman, A. M. (1993) Classification of positive inotropic agents, *J. Am. Coll. Cardiol. 22*, 1223-1227.

Chapter 2

The Solution Structure of Human Cardiac Troponin C in Complex with the Green Tea Polyphenol; (-)-Epigallocatechin-3-gallate*

Summary

Heart muscle contraction is regulated by Ca^{2+} binding to the thin filament protein troponin C. In cardiovascular disease, the myofilament response to Ca^{2+} is often altered. Compounds that rectify this perturbation are of considerable interest as therapeutics. Plant flavonoids have been found to provide protection against a variety of human illnesses such as cancer, infection, and heart disease. (-)-epigallocatechin gallate (EGCg), the prevalent flavonoid in green tea, modulates force-generation in isolated guinea pig hearts (Hotta, Y., *et al*. (2006) *Eur J Pharmacol* 552, 123-130) and in skinned cardiac muscle fibers (Liou, Y.M., *et al*. (2008) *Pflugers Arch* 456, 787-800 and Tadano, N., *et al*. (2005) *Biophys J* 88, 314a). In this report we describe the solution structure the Ca^{2+} saturated C-terminal domain of troponin C in complex with EGCg. Moreover, we show that EGCg forms a ternary complex with the C-terminal domain of troponin C and the anchoring region of troponin I. The structural evidence indicates that the binding site of EGCg on the C-terminal domain of troponin C is in the hydrophobic pocket in the absence of troponin I, akin to EMD 57033. Based on chemical shift mapping, the binding of EGCg to the C-terminal domain of troponin C in the presence of troponin I may be to a new site formed by the troponin C- troponin I complex. This interaction of EGCg with the C-terminal domain of troponin C-troponin I complex has not been shown with other cardiotonic molecules and illustrates the potential mechanism by which EGCg modulates heart contraction.

Introduction

Cardiovascular disease (CVD) is the number one cause of morbidity and mortality in western culture. In the United States, approximately 1 in 3 deaths in 2004 were caused by CVD (*1*). In heart failure, the ability of the heart to distribute blood throughout the body is perturbed, and there is a growing interest to develop drugs that directly regulate the response of the myofilament to Ca^{2+}. Regulation of muscle contraction is triggered by Ca^{2+} binding to troponin. The troponin complex is situated at regular intervals along the thin filament, which is made up of two elongated polymers: f-actin and tropomyosin. The backbone of the thin filament is comprised of actin molecules arranged in a double-helix with tropomyosin wound around actin as a coiled-coil. Anchored at every seventh actin molecule is the heterotrimeric troponin complex, which consists of troponin C (TnC), troponin I (TnI), and troponin T (TnT). TnC is the Ca^{2+}-binding subunit of troponin, and has four EF-hand helix-loop-helix motifs. TnI is the inhibitory subunit of troponin. It regulates the actin-myosin cross-bridge formation by flipping between TnC and actin in a Ca^{2+}-dependant manner. At low levels of cytosolic Ca^{2+}, TnI is bound to actin, causing tropomyosin to sterically block the binding of the actomyosin cross-bridges. On the other hand, when Ca^{2+} concentration is high, cTnI translocates from actin to TnC inducing tropomyosin to change its orientation on actin so that the actin-myosin interaction may occur. The subunit TnT tethers the troponin complex to the thin filament by way of its association with TnI (for reviews on contraction see references (*2-5*)).

The large number of structural studies on troponin and the thin filament has helped gain insight into the molecular mechanism of muscle contraction. TnC is a dumbbell-shaped protein that consists of terminal domains connected by an elongated flexible linker, as shown by solution NMR (*6*). The overall folds of the terminal domains of skeletal TnC (sTnC) and cardiac TnC (cTnC) are very similar (*7-9*). The apo state of the N-

domain of sTnC (sNTnC) and cTnC (cNTnC) reveals that the domain is in a "closed" conformation, such that the hydrophobic core of the protein is buried ($8, 10, 11$). In the skeletal system, sNTnC "opens" when two Ca^{2+} ions bind ($8, 10, 11$). Alternatively, cNTnC contains only one functional Ca^{2+} binding site, and its global conformation does not change as significantly as in sNTnC (11). Nonetheless, Ca^{2+}-binding promotes the association of the switch region of cTnI (residues 147-163) with cNTnC. $cTnI_{147-163}$ forms an α-helix when associated with cNTnC, and has been elucidated by NMR in the solution structure of $cNTnC\cdot Ca^{2+}\cdot cTnI_{147-163}$ (12), and by the X-ray crystallography structure of $cTnC\cdot 3Ca^{2+}\cdot cTnI\cdot_{31-210}\cdot cTnT_{183-288}$ (13) The interaction of $cTnI_{147-163}$ with $cNTnC\cdot Ca^{2+}$ is essential to draw the inhibitory ($cTnI_{128-147}$) and C-terminal ($cTnI_{163-210}$) regions of cTnI away from actin. $cTnI_{128-147}$ is not visualized in the cardiac structure, probably due to disorder (13). In the skeletal crystal structure of $sTnC\cdot 4Ca^{2+}\cdot sTnI_{1-182}\cdot sTnT_{156-262}$; however, the inhibitory region of sTnI is visualized, and makes electrostatic contacts with the central helix connecting the N and C terminal lobes of cTnC (14). The C-domain (CTnC) of both sTnC and cTnC has two functional binding sites for Ca^{2+}, and remains largely unstructured without Ca^{2+} bound. The folding of this domain occurs in the presence of Ca^{2+}($15, 16$). Throughout the relaxation-contraction cycle, cCTnC is Ca^{2+} saturated with both Ca^{2+}-binding sites occupied ($cCTnC\cdot 2Ca^{2+}$), and is associated with the anchoring region of cTnI ($cTnI_{34-71}$). The crystal structure of $cTnC\cdot 3Ca^{2+}\cdot cTnI\cdot_{31-210}\cdot cTnT_{183-288}$ shows $cTnI_{34-71}$ is α-helical when bound with $cCTnC\cdot 2Ca^{2+}$(13). The interaction of $cCTnC\cdot 2Ca^{2+}$ with $cTnI_{34-71}$ is the primary site in which cTnC is tethered to the thin filament.

In light of the importance of the Ca^{2+}-dependent cTnI-cTnC interaction in the signaling of muscle contraction, the design of drugs that modulate this interaction would be useful in the treatment of heart disease. Compounds that treat CVD through the modulation of activity of cTnC are called Ca^{2+}-sensitizers, or -desensitizers; depending on whether they

positively or negatively influence the interactions. These drugs are safer than other currently prescribed medicines that alter the cytosolic Ca^{2+} homeostasis (such as milrinone and dobutamine), which may cause arrhythmia or death with prolonged usage.

The potential therapeutic advantage of Ca^{2+}-(de)sensitizers has led to the development of a number of compounds that target cTnC. Compounds have been identified that elicit their activity through binding either cNTnC or cCTnC. Levosimendan and pimobendan are examples of molecules that increase heart muscle contractility through binding to cNTnC. Conversely, the molecule W7 decreases contractility *via* its interaction with cNTnC. For recent reviews on the molecular mechanism of these compounds and others see references (*17-19*). The discovery of small molecules that bind to cCTnC to elicit their Ca^{2+}-sensitizing effects suggests that cCTnC is also a suitable target for the development of therapeutics. The Ca^{2+}-sensitizer, EMD 57033, is approved for the treatment for heart failure in dogs and binds to cCTnC•$2Ca^{2+}$(*20*). In the NMR structure of cCTnC•$2Ca^{2+}$•EMD 57033, EMD 57033 is associated in the hydrophobic cavity of cCTnC•$2Ca^{2+}$ (*21*). The interaction of EMD 57033 with cCTnC is stereospecific for the (+)-enantiomer, and explains why the (-)-enantiomer is inactive (*22*). Since EMD 57033 has been shown to bind cCTnC•$2Ca^{2+}$ concurrently with $cTnI_{128-147}$ but not with $cTnI_{34-71}$ (*23*), one postulate is that EMD 57033 acts as a Ca^{2+}-sensitizer by weakening the interaction of $cTnI_{34-71}$ with cCTnC•$2Ca^{2+}$, thus increasing the propensity of $cTnI_{128-147}$ to bind cCTnC•$2Ca^{2+}$ *in vivo*. The dilated cardiomyopathy (DCM) mutation, G159D, of cCTnC has renewed interest in the role of the C-lobe for regulation in contraction. The mutation has been identified to decrease the sensitivity of the thin filament to Ca^{2+} (*24*). The source of the DCM phenotype of G159D might come from the modulation of the interaction of cCTnC•$2Ca^{2+}$ with $cTnI_{34-71}$ (*25*).

Green tea (*Camellia sinensis*) is one of the most widely consumed beverages in the world, and several epidemiological studies have linked

the consumption of tea with a decrease in CVD (*26, 27*). (-)-Epigallocatechin gallate (EGCg) is a polyphenol that exists abundantly in unfermented teas, and has been identified as a modulator of heart contraction through its interaction with cTnC (*28-30*). In the following report, we use NMR spectroscopy to elucidate the 3D structure of the cCTnC•2Ca^{2+}•EGCg complex. The solution structure reveals that EGCg binds at the hydrophobic core of cCTnC inducing a small structural "opening". We also use 2D NMR spectroscopy to monitor the binding of EGCg to cCTnC•2Ca^{2+} and cCTnC•2Ca^{2+}•cTnI$_{34-71}$. Since EGCg and cTnI$_{34-71}$ can bind cCTnC concurrently, the inotropic effect of EGCg may stem from its modulation of the cTnI$_{34-71}$-cCTnC•2Ca^{2+}interaction. The solution structure of cCTnC•2Ca^{2+}•EGCg provides insight into the mechanism in which EGCg might influence heart contraction. These results taken with previous research on the Ca^{2+}-sensitizer EMD 57033 and the DCM mutation G159D, bring into question the dogma that cNTnC is the exclusive site for regulation of contraction in cTnC.

Experimental Procedures

Sample Preparation: The expression vectors for cCTnC (91-161) and cTnC were designed and the uniformly labeled ^{13}C, ^{15}N cCTnC was isolated from *E. coli* as previously described (*31, 32*). Unlabeled cTnI$_{34-71}$, acetyl-AKKKSKISASRKLQLKTLLLQIAKQELEREAEERRGEK-amide, was synthetically prepared by GL Biochem Ltd. EGCg was purchased from Sigma-Aldrich. All stock solutions of EGCg were prepared in 70-80 mM TCEP in aqueous solution or DMSO-d_6 (Cambridge Isotopes Inc.) at a concentration of ~100 mM. The solvents TCEP and DMSO-*d6* did not influence the interaction of EGCg with cCTnC. The stock solutions were freshly prepared before any experiment was acquired, and during the titrations the stock solutions of EGCg were kept dark to prevent light catalyzed degradation. The 500 μL NMR samples were prepared with ^{15}N-

or ^{13}C, ^{15}N-labeled TnC in 5% D_2O, 2.5 mM DSS (Chenomx standard), pH = 6.7-6.9, 100 mM KCl, 8 mM $CaCl_2$ and 10 mM imidazole as a buffer. Samples of cCTnC•$2Ca^{2+}$•$cTnI_{34-71}$ contained ~1:1 ratio of cCTnC:$cTnI_{34-71}$. All experiments run for the structure calculation contained ^{13}C, ^{15}N-cCTnC-EGCg at a ratio of ~1:4.

Stability of EGCg in aqueous solution: Certain steps had to be taken when working with EGCg, since it is rapidly oxidized in aqueous solution. For most of the experiments, TCEP was used to keep EGCg reduced for the duration of the longer 3D experiments (4-5 days). TCEP has been shown to be an adequate reducer of ascorbic acid (*33*). For some of the shorter experiments, the sample was simply flushed with Ar_2 gas prior to the addition of EGCg. Titrations with EGCg were all initially done with no TCEP present, and then repeated with TCEP. This confirmed that TCEP had no influence on the interaction of EGCg with cCTnC (data not shown). In order to monitor sample stability ^{1}H, ^{15}N-HSQC spectra were acquired before and after each long 3D experiment. In cases where degradation of EGCg was witnessed, the solution first began to change from clear to a brownish hue, and eventually, precipitate started to form at the bottom of the NMR tube. In this stage the ^{1}H, ^{15}N-HSQC spectrum revealed a slight recession of the amide correlation peaks towards the unbound chemical shifts of cCTnC. In addition to the visual cues of EGCg degradation, 1D-^{1}H NMR spectra were used to monitor the transition of EGCg from its reduced form to the oxidized state. When EGCg was oxidized, additional peaks began to appear in the spectrum, and peaks representative of the reduced form of EGCg decreased in intensity (data not shown). Figure 2-3 shows the chemical structure and 1D-^{1}H NMR spectrum of 1.1 mM EGCg in DMSO-*d6*.

Titrations of EGCg to cTnC, cCTnC, and cCTnC-cTnI$_{34-71}$ monitored by NMR spectroscopy: All NMR samples contained 500 µL of aqueous NMR

buffer (see sample preparation section). The protein concentration was determined by amino acid analysis and tyrosine absorption at 280 nm. Protein and EGCg concentrations were corrected for the dilution factor. The stock solutions of EGCg were prepared in DMSO-*d6* or in an aqueous TCEP buffer. TCEP was used to keep EGCg reduced during the titration. The pH was adjusted with NaOH when necessary. EGCg concentration was determined by weight and by comparing EGCg peak heights or integrals with the internal standard DSS in the 1D ^{1}H NMR spectrum. EGCg was titrated into a 0.45 mM ^{15}N-cTnC NMR sample to final EGCg concentrations at each step of 0.10, 0.20, 0.30, 0.40, 0.50, 0.60, 0.79, 0.99, 1.19, 1.57, and 2.53 mM. EGCg was titrated into a 1.13 mM ^{15}N-cCTnC NMR sample to final EGCg concentrations at each step of 0.13, 0.25, 0.37, 0.50, 0.61, 0.86, 1.22, 1.57, 2.38, 3.16, and 4.23 mM. EGCg was titrated into a 0.35 mM ^{15}N-cCTnC•cTnI$_{34-71}$ NMR sample to final EGCg concentrations at each aliquot of 0.18, 0.36, 0.71, 1.42, 2.14, 2.90, and 4.12 mM. EGCg was titrated into a 80 µM ^{15}N-cCTnC NMR sample to final EGCg concentrations at each step of 8, 17, 25, 32, 41, 49, 57, 65, 83, 98, 113, 143, 218, 293, 378, 443, 578, and 713 µM.

NMR Spectroscopy: Most NMR experiments were collected on either a Varian Inova 500-MHz or a Unity 600-MHz spectrometer. All data was collected at 30ºC. Both spectrometers have triple resonance HCN probes, and z-pulsed field gradients. The titration of EGCg to 80 µM ^{15}N-cCTnC was done at 25°C on a Varian Inova 800-MHz equipped with a cryogenic probe.

Data Processing and Peak Calibration: All 2D and 3D NMR data were processed with NMRPipe (*34*). One-dimensional NMR spectra to assign EGCg in DMSO-*d6* and address EGCg degradation were processed using VNMRJ (Varian Inc.) Assignment of chemical shifts was carried out in NMRView (*35*) and backbone assignments were aided with the software

package SmartNotebook (*36*) (http://www.bionmr.ualberta.ca/bds).
Intramolecular NOEs of EGCg measured from 2D NOESY acquired in
D_2O were categorized as strong (1.8-4.0Å), medium (1.8-5.0Å), and weak
(1.8-6.0 Å). Intermolecular NOEs were categorized as strong (1.8-4.0Å),
medium (1.8-5.0Å), and weak (1.8-6.0 Å). Intramolecular NOEs of cCTnC
were calibrated automatically with the CYANA standard procedure, with
upper bounds set to 6 Å. The chemical shifts that were assigned in
NMRView were converted to CYANA nomenclature, for NOE calibration.
After the CYANA refinement, the final restraints were converted to
XPLOR-NIH nomenclature. Since CYANA calculates distances differently
than XPLOR-NIH, NOE restraints were loosened by 1 Å.

Generation of EGCg structure file for structure refinement: The structure
file of EGCg was generated for XPLOR-NIH by the PRODRG2 webserver
(http://davapc1.bioch.dundee.ac.uk/prodrg/) (*37*). This online resource
converts the chemical structure of a small ligand into PDB format.
Following PDB conversion, XPLO2D
(http://xray.bmc.uu.se/usf/xplo2d_man.html#H4) was used to generate
XPLOR-NIH compatible structure files of EGCg.

Structural Calculation: Structures were initially generated using the
program CYANA 2.1 (*38-40*). Unambiguous restraints were assigned
manually and were forced to keep their assignments during the first four
runs of CYANA calculations, after which they were open for automatic
assignment with the "noeassign" command of CYANA (*41*). Distance
restraints were calibrated with CYANA standard procedure using upper
limits of 6 Å. Dihedral angle restraints from TALOS (*42*) were used as well
as 12 distance restraints from X-ray crystallographic data of chelating
oxygen atoms to the two Ca^{2+} ions. CYANA was used to calculate 100
structures, of which the 30 conformers with the lowest target function were
used to further refine the structure. The 30 conformers were averaged in

X-PLOR-NIH, and used as a template structure in the simulated annealing protocol, with 10,000 high temperature steps and 6000 cooling steps. After the structure of cCTnC was well defined, the binary cCTnC•Ca^{2+}•EGCg structure was solved in a similar manner, starting with an extended conformation of cCTnC. The calculations contained 10 intramolecular EGCg NOE restrains and 18 intermolecular NOE restraints. The final ensemble discussed in this article is represented by the 30 lowest energy structures of the 100 calculated (see Table I for statistics). The final refined ensemble has been deposited in the protein data bank (www.rcsb.org) with the accession code of 2kdh.pdb.

Results

2D ^{1}H,^{15}N-HSQC and ^{1}H,^{13}C-HSQC NMR experiments were used to monitor the binding of EGCg to cTnC•3Ca^{2+}, cCTnC•2Ca^{2+}, and cCTnC•2Ca^{2+}•cTnI$_{34-71}$. The HSQC experiment correlates backbone or side chain ^{1}H with^{15}N or ^{13}C nuclei, so that each cross-peak in the spectrum represents an individual ^{1}H-^{15}N (or ^{1}H-^{13}C) from the ^{13}C,^{15}N-labeled protein. Typically, when a ligand binds a labeled protein, the chemical shifts of individual cross-peaks in the spectrum move as a function of the ligand concentration. The changes in chemical shifts can be quantified to derive ligand stoichiometry and affinity, as well as be used to approximate the ligand binding site on the protein; an approach commonly referred to as chemical shift mapping.

The effect of EGCg on cTnC•3Ca^{2+}.

EGCg was titrated into cTnC•3Ca^{2+} to assess its primary binding site. The backbone of EGCg-free cTnC•3Ca^{2+} was assigned by the 3D CBCACONNH and HNCACB NMR experiments, and well resolved amide resonances in the ^{1}H,^{15}N-HSQC spectrum were followed throughout the EGCg titration. EGCg perturbed amide resonances of both the C- and N-

terminal domains; however, it induced the largest chemical shift changes in the C-terminal domain (Figure 2-1). We posit that the amide resonances that are shifted greatly in the C-terminal domain represent direct binding of EGCg, and the smaller shifts in the N-terminal domain of cTnC are from "communication" between the two domains. This indicates that the principal binding site for EGCg is in the C-terminal domain of cTnC. It has also been shown by fluorescence spectroscopy (*28*) and NMR spectroscopy (*30*) that EGCg targets cCTnC. A global fitting approach using the program xcrvfit (www.bionmr.ualberta.ca/bds/software/xcrvfit) was used as described previously (*43*) to determine the dissociation constant K_D which best fit the equation:

$$cTnC \cdot 3Ca^{2+} + EGCg \leftrightarrow cTnC \cdot 3Ca^{2+} \cdot EGCg$$
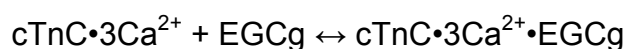
The binding curves that were globally fit are shown in supplementary Figure 2-1. The binding of EGCg to cTnC·$3Ca^{2+}$ was fit to a 1:1 stoichiometry, with a best-fit K_D of 1.12 mM. The K_D was also calculated by averaging the normalized individual chemical shifts as a function of the ligand to protein ratios and fitting using xcrvfit. This approach yielded a K_D of 1.1 ± 0.12 mM. The observation that EGCg targets the C-terminal domain of cTnC focused our subsequent structural analysis to cCTnC.

The effect of EGCg on cCTnC·$2Ca^{2+}$.

The assigned $^1H,^{15}N$-HSQC and $^1H,^{13}C$-HSQC NMR spectrum of cCTnC·$2Ca^{2+}$ were used to observe the binding of EGCg to cCTnC·$2Ca^{2+}$ (Figure 2-2a,b). The $^1H, ^{15}N$-HSQC spectrum of cCTnC·$2Ca^{2+}$ has been previously assigned (*21, 44*), and the $^1H, ^{15}N$-HSQC and $^1H, ^{13}C$-HSQC spectra of the cCTnC·$2Ca^{2+}$·EGCg complex were assigned using 3D CBCACONNH and HNCACB NMR spectra. Since the resonance perturbations of cCTnC are in fast exchange, the chemical shifts could be
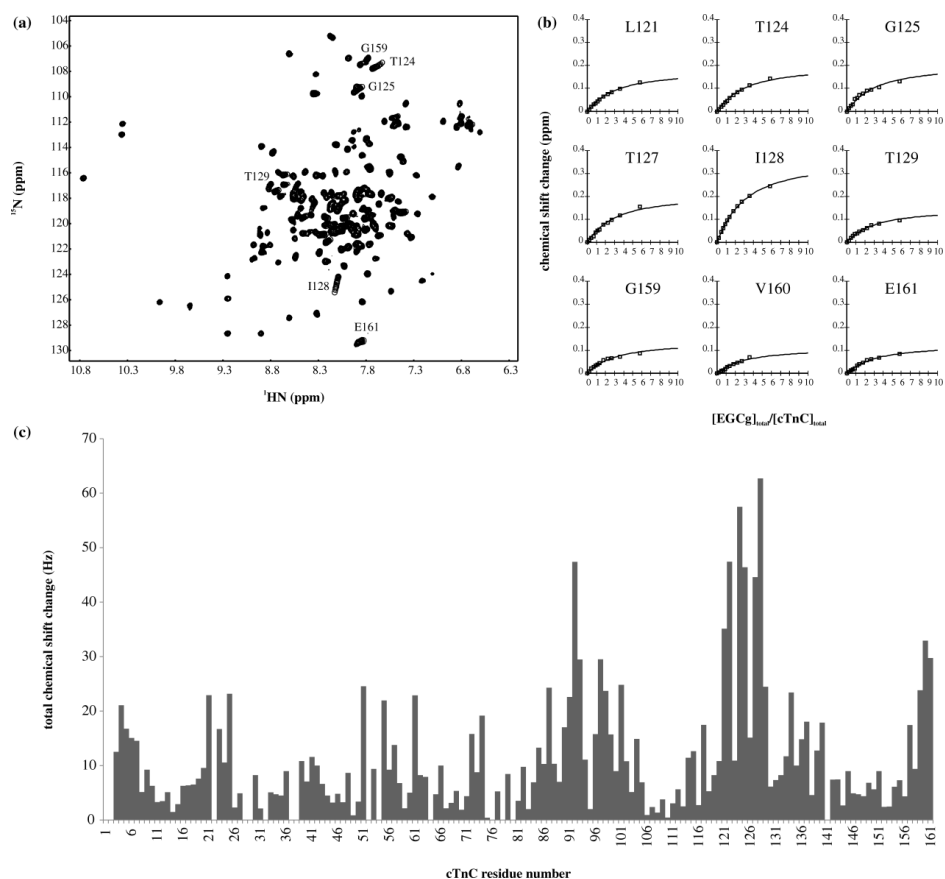
Figure 2-1. Titration of cTnC•3Ca^{2+} with EGCg. 2D ^{1}H, ^{15}N-HSQC (a) spectra arising from backbone and side chain amide groups are overlaid for a series of EGCg additions. Each titration point represents the titration points described in the materials and methods. The titration was made into ^{15}N-labeled cTnC•3Ca^{2+} and ^{1}H, ^{15}N-HSQC spectra were acquired at each titration point. Assignments of some of the cross-peaks are labeled. The multiple contours (●) represent the initial point in the titration, with no EGCg added, and the open contours (○) represent the end point in the titration for a given residue. (b) The curves represent example residues affected by ligand binding, as shown in (a). The curves were fit as a function of total chemical shift perturbation vs. [EGCg]$_{total}$/[cTnC•3Ca^{2+}]$_{total}$. (c) The EGCg induced chemical shift changes of the backbone amides of cTnC•3Ca^{2+}. Total chemical shift change ($\Delta\delta$) is presented in Hz and calculated as follows: $\Delta\delta=[(\Delta\delta_{1H})^2 + (\Delta\delta)^2]^{1/2}$. Since Hz is used instead of parts per million (ppm) a correction factor of 1/5 for the ^{15}N dimension is not used.
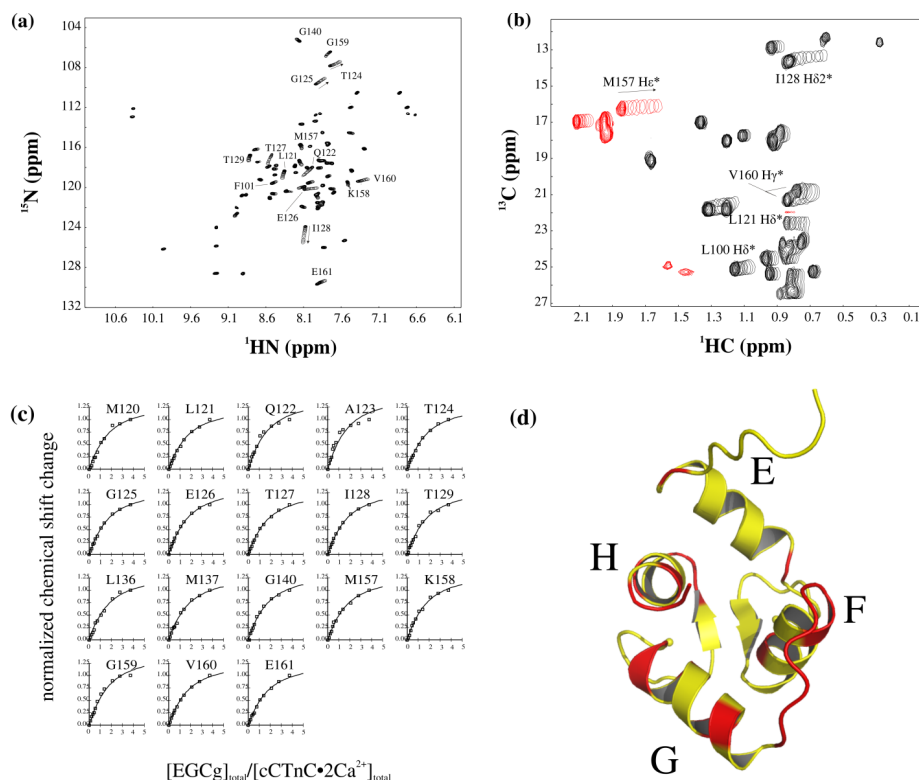
Figure 2-2. Titration of cCTnC•2Ca^{2+} with EGCg. 2D ^{1}H, ^{15}N-HSQC (a) and ^{1}H, ^{13}C-HSQC (b) spectra arising from backbone and side chain amide groups (a) and side chain methyl groups (b) are overlaid for a series of EGCg additions. Each titration point represents the titration points described in the materials and methods. The titration was made into ^{13}C, ^{15}N-labeled cCTnC•2Ca^{2+} and both the ^{1}H, ^{15}N-HSQC and ^{1}H, ^{13}C-HSQC spectra were acquired at each titration point. Assignments of some of the cross-peaks are labeled. The multiple contours (●) represent the initial point in the titration, with no EGCg added, and each open contour (○) represents a specific point in the titration for a given residue. (b) The red contours represent cross-peaks with negative intensity, a feature of the constant-time ^{1}H,^{13}C-HSQC experiment. The direction the peaks shift is indicated with arrows, for example see G125. (c) The curves represent the amide resonances belonging to residues affected by ligand binding, as shown in (a). The curves were fit as a function of normalized total chemical shift perturbation vs. [EGCg]$_{total}$/[cCTnC•2Ca^{2+}]$_{total}$. The total chemical shift changes were calculated in hertz (Hz) as follows: $\Delta\delta = [(\Delta\delta^1H)^2 + (\Delta\delta^{15}N)^2]^{1/2}$. Since hertz is used instead of parts per million (ppm) a correction factor of 1/5 for the ^{15}N dimension is not used. (d) Chemical shift mapping on the structure of cCTnC•2Ca^{2+}.The ribbon representation of cCTnC•2Ca^{2+} is shown in yellow and residues that were perturbed greater than the mean chemical shift change for all backbone amide resonances of cCTnC are colored in red.

easily followed throughout the titration. The chemical shift of each assigned amide peak was recorded for every titration point, and a total chemical shift was normalized for each resonance. A global fitting approach using the program xcrvfit to determine the dissociation constant K_D which best fit the equation:

$$cCTnC \cdot 2Ca^{2+} + EGCg \leftrightarrow cCTnC \cdot 2Ca^{2+} \cdot EGCg$$
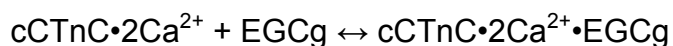
The binding curves that were globally fit are shown in Figure 2-2c. The binding of EGCg to cCTnC·2Ca^{2+} was fit to a 1:1 stoichiometry, with a best-fit K_D of 1.10 mM. The K_D was also calculated by averaging the normalized individual chemical shifts as a function of the ligand to protein ratios and fitting using xcrvfit. This approach gave a K_D of 1.09 ± 0.08 mM. Given EGCg binding to the C-terminal domain of cTnC·3Ca^{2+} and to cCTnC·2Ca^{2+} induced effectively identical chemical shift changes and dissociation constants, we concluded that EGCg binds both the C-terminal domain of cTnC·3Ca^{2+} and cCTnC·2Ca^{2+} in a similar fashion.

The dissociation constant was significantly higher than previous groups reported for EGCg (*28*). In order to investigate whether there were concentration dependent effects of EGCg, such as aromatic stacking, we lowered the protein concentration to 80 µM and repeated the titration. The data gave a best-fit K_D of 385 µM, which indicates that EGCg is undergoing a competing equilibrium in aqueous solution. Therefore, the observed or apparent K_D is an upper limit of the actual dissociation constant. The chemical shift changes were identical in both the low and high concentration titrations, suggesting that the location of the binding site of EGCg is independent on cCTnC concentration.

A number of cCTnC·2Ca^{2+} ^{1}H,^{15}N and ^{1}H,^{13}C cross-peaks underwent significant chemical shift perturbations during the EGCg titration. Chemical shift mapping of the amide peaks was used to identify specific regions of the protein that underwent large perturbations induced

from EGCg binding to localize the binding site of EGCg (Figure 2-2d). The amide resonances of residues on the loop connecting helices F and G (T124-T129) underwent the largest changes in chemical shifts, suggesting a close proximity of the ligand to their backbone and side chain nuclei or a large change of conformation or dynamics in the loop. This may reflect a change in the positions of helices F and G relative to one another upon formation of the EGCg-cCTnC complex. Other residues of cCTnC that had significant backbone chemical shift perturbations were residues M120, L121, Q122, and A123 on helix F, residues L136, G140 and D141 of helix G, and residues M157, K158, G159, V160, and E161 of helix H. Amide and methyl resonances of residues on the β-sheet (Y111, I112, D113, R147, I148, and D149) did not undergo any significant chemical shift. This suggests that the binding of EGCg is near the opening of the hydrophobic cleft of cCTnC, rather than deep within the pocket. In order to obtain a more detailed knowledge of the interaction of cCTnC with EGCg, the solution structure of cCTnC•2Ca^{2+}•EGCg was determined by NMR spectroscopy.

The structure of cCTnC•2Ca^{2+}•EGCg.

The solution structure of cCTnC•2Ca^{2+} bound to EGCg was determined using the NMR experiments listed in Table 2-1 (see references for experiments therein). Dihedral angle restraints were calculated from chemical shifts with the program TALOS (*42*). The chemical shifts corresponding to backbone atoms of cCTnC in the cCTnC•2Ca^{2+}•EGCg complex were assigned using the 2D ^{1}H,^{15}N-HSQC, and the 3D CBCACONNH and HNCACB NMR spectra. The 2D ^{1}H,^{13}C-HSQC and the 3D HCCH-TOCSY, CCONH, and HCCONH NMR spectra were acquired to assign side chain resonances. The ^{15}N-edited HNHA and HNHB experiments were acquired to assign Hα and Hβ resonances. Distance restraints for cCTnC were determined using ^{13}C-NOESYHSQC and the

Table 2-1. NMR Spectra acquired for structure calculation of cCTnC

Experiment name	Nuclei	^{1}H freq (MHz)	nt	x-pts	y-pts	z-pts	x-sw (Hz)	y-sw (Hz)	z-sw (Hz)	Mix (ms)	Ref.
HNHB	^{1}H,^{1}H,^{15}N	500	8	1074	96	96	8400	8400	2030	-	(60)
HNHA	^{1}H,^{1}H,^{15}N	500	8	1074	96	96	8400	8400	2030	-	(61)
CBCA(CO)NNH	^{1}H,^{13}C,^{15}N	500	8	1074	118	64	8400	10060	2030	-	(62)
HNCACB	^{1}H,^{13}C,^{15}N	500	8	1074	118	64	8400	10060	2030	-	(62)
HCCH-TOCSY	^{1}H,^{1}H,^{13}C	500	16	2048	128	96	8400	8400	10060	-	(63)
HCCONH	^{1}H,^{1}H,^{15}N	500	16	1074	128	64	8400	8400	2030	-	(64)
CCONH	^{1}H,^{13}C,^{15}N	500	16	2048	128	64	8400	10060	2030	-	(64)
3D ^{15}N-edited NOESY-HSQC	^{1}H,^{1}H,^{15}N	500	8	1074	256	64	8400	8400	2030	100	(65)
3D ^{13}C-edited NOESY HSQC	^{1}H,^{1}H,^{13}C	600	16	1024	128	128	8400	6000	4525	100	(65)
3D ^{13}C/^{15}N-filtered/edited NOESY	^{1}H(^{14}N/^{12}C),^{1}H,^{13}C	600	16	1024	216	64	8400	8400	6030	200	(66)
2D NOESY (in D$_2$O)	^{1}H,^{1}H	500	32	4096	512	-	8400	8400	-	150	(67)
2D DQF-COSY (in D$_2$O)	^{1}H,^{1}H	500	32	8192	384	-	8400	8400	-	-	(68)

77

^{15}N-NOESYHSQC NMR spectra. Resonances for aromatic residues of cCTnC were assigned using the 2D NOESY NMR spectrum in D_2O.

The 1D ^{1}H spectrum of free EGCg was first assigned in DMSO-d_6; the ^{1}H spectrum of free EGCg in D_2O has been previously assigned (*45*), and the ^{1}H chemical shifts are virtually identical in either solvent. Following assignment of free EGCg, the ^{1}H chemical shifts were assigned for cCTnC•2Ca^{2+} bound EGCg using the 2D NOESY NMR spectrum in D_2O (Figure 2-3). [13]C/^{15}N-edited/filtered experiments (2D and 3D) were run to assign intermolecular NOEs between EGCg and cCTnC to identify the binding site and orientation of EGCg when bound to cCTnC•2Ca^{2+}. 12 Ca^{2+} distance restraints from crystallographic data were incorporated into the structure determination as previously described (*21*). There were in total, 1052 structural restraints used in the structure determination, including 899 intramolecular cCTnC distance restraints, 18 intermolecular distance restraints, 10 intramolecular EGCg distance restraints, 12 Ca^{2+} distance restraints, and 114 dihedral restraints. Table 2-2 contains a list of the structural statistics for cCTnC•2Ca^{2+}•EGCg.

Plots of the intermolecular NOEs between EGCg and cCTnC•2Ca^{2+} are shown in Figure 2-4a. In order to assign the intermolecular NOEs both the 3D and 2D versions of the ^{13}C/^{15}N-edited/filtered experiment were acquired. The 2D experiment was acquired because it provides better a signal-to-noise ratio than the 3D experiment, and the ^{13}C-edited 3D experiment was run to confirm the 2D assignments. The NOE restraints observed between EGCg and cCTnC•2Ca^{2+} are between a number of hydrophobic residues that line the hydrophobic pocket. Residues that have NOEs to EGCg include M157 and V160 on the terminal end of helix H, L121 and M120 on helix F and L136 on helix G, all of which point towards the hydrophobic pocket of cCTnC. The tetrahydropyran ring of EGCg contains four hydrogen atoms (H01, H02, H15 and H33), all of which make significant contacts to cCTnC. The two hydrogen atoms on the benzenediol ring, on the other hand, do not make any NOE contacts to
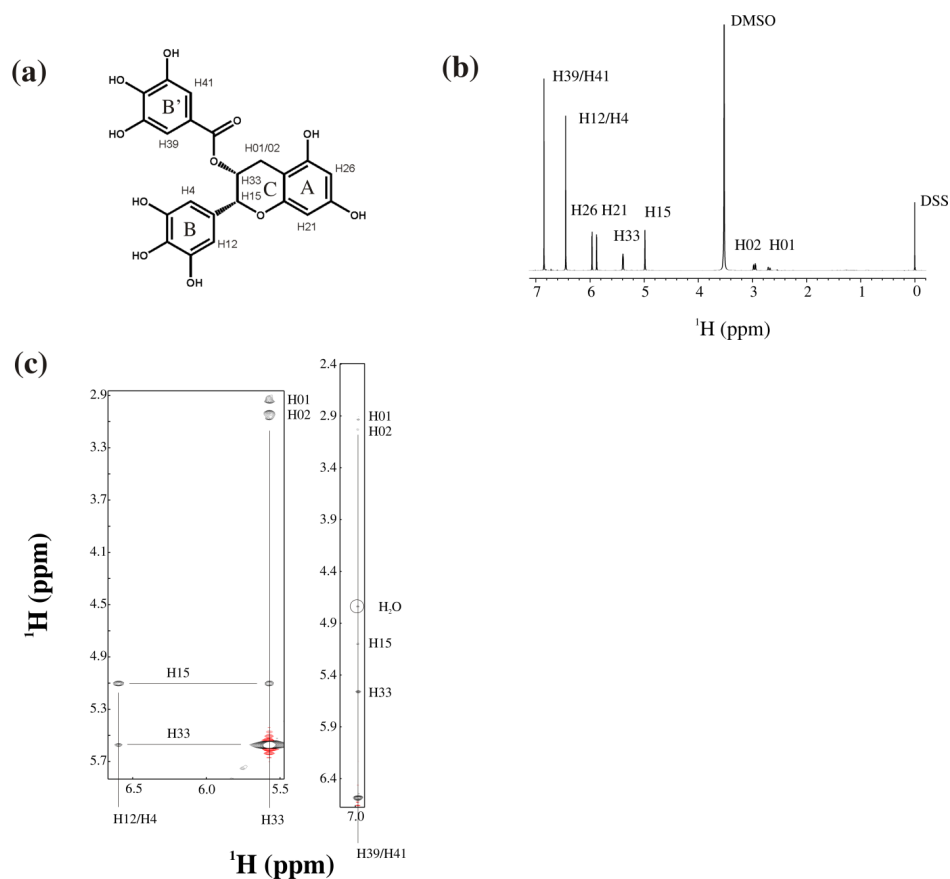
Figure 2-3. Assignment of EGCg. (a) The chemical structure of EGCg. The benzenediol is labeled as ring A, the pyrogallol ring as B, the galloyl moiety as B`, and ring C is the tetrahydropyran moiety. The hydrogen atoms attached to carbon atoms are also labeled. (b) The assigned 1D ^{1}H-NMR spectrum of EGCg in DMSO-d_6. (c) A few strip plots from the 2D NOESY with resonances assigned that belong to EGCg in complex with cCTnC•2Ca^{2+}. The data were acquired in D$_2$O as to remove amide signals that predominate this region of the 2D NOESY spectrum in H$_2$O. Details of the experiment are outlined in Table 2-2.
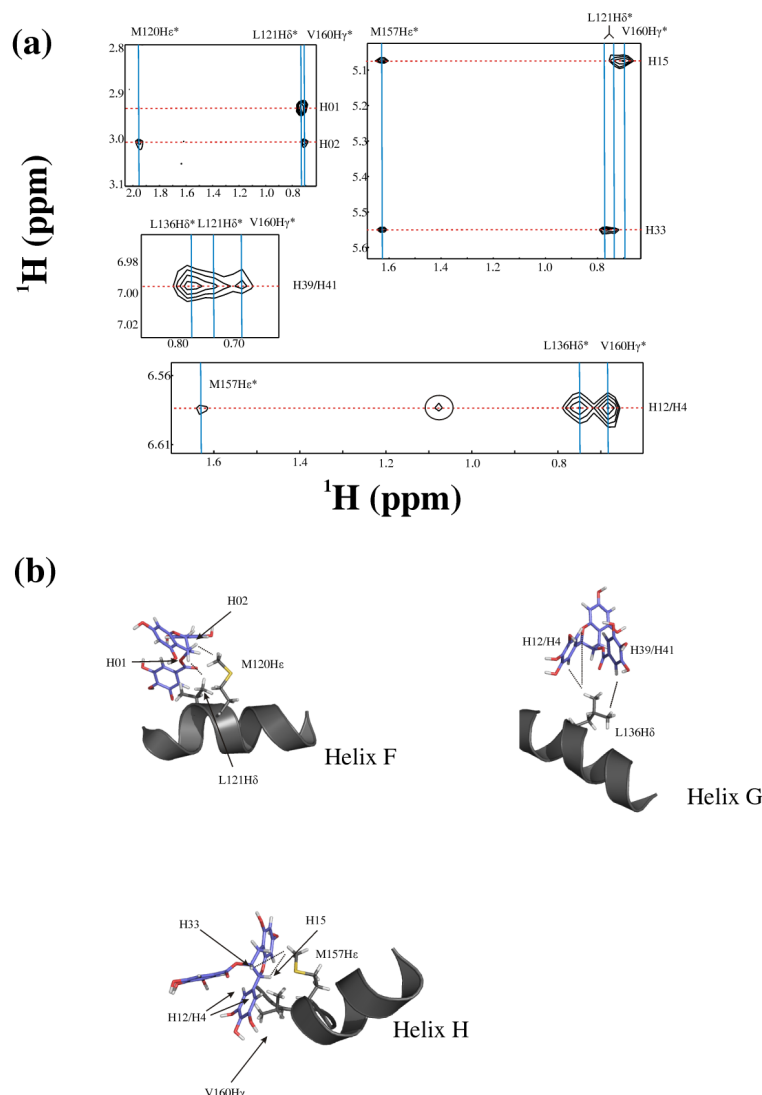
Figure 2-4. Intermolecular NOEs between EGCg and cCTnC•2Ca^{2+}. (a) A series of strip plots assigned from the 2D ^{13}C-edited/filtered NOESY NMR experiment. The ^{1}H resonances that correspond to EGCg are labeled on the right side of the spectra, and the ^{1}H that correspond to ^{15}N,^{13}C-labeled cCTnC•2Ca^{2+} are labeled at the top of the strips plots. The circled peak is an artifact from the intermolecular NOE experiment. (b) The cartoon depiction of several of the NOE contacts assigned in (a). EGCg is shown in stick representation with carbon atoms colored in purple, oxygen atoms color in red, and hydrogen atoms colored in white. cCTnC is depicted in cartoon representation with the residues involved in making NOEs to EGCg shown in stick representation. Carbon atoms for cCTnC are colored in grey, sulfur atoms in yellow, and hydrogen atoms in white. The dotted lines indicate contacts measured by the ^{13}C-edited/filtered NOESY NMR experiment.

Table 2-2. Structural statistics for 30 NMR structures of cCTnC in complex with EGCg.

	Backbone atoms	Heavy Atoms
R.m.s.d. from the average		
Residues (90-161)[a]	1.08 ± 0.14	1.52 ± 0.15
Well-defined residues	0.80 ± 0.14	1.27 ± 0.13
NOE Restraints		
Total	927	
Short range ($|i\text{-}j|$=1)	519	
Medium range (1<$|i\text{-}j|$<5)	201	
Long range ($|i\text{-}j|{\geq}5$)	179	
Intermolecular NOEs	18	
Intramolecular EGCg NOEs	10	
Ca^{2+} distance restraints	12	
Dihedral restraints (ϕ/ψ)	114	
Energies[b]		
E_{total}	208 ± 1	
E_{NOE}	0.28 ± 0.22	
$E_{dihedral}$	0.30 ± 0.20	
NOE violations[c]		
> 0.5 Å	0	
> 0.3 Å	0	
> 0.1 Å	3	
Dihedral Violations (º)	0.0	
ϕ/ψ in core or allowed regions[d]	99.3 %	

[a]Residues 94-121, 132-143 and 145-157 have well-defined backbone atoms

[b]The final K_{NOE} and $K_{dihedral}$ used were 50 kcal/mol and 200 kcal/mol•rad^2

[c]Violations are for the 30 NMR lowest energy structures

[d]As determined by PROCHECK (*58, 59*)

cCTnC, hence its loosely defined orientation. Figure 3b depicts the specific observed NOEs between cCTnC residues and EGCg hydrogen atoms. There were no intermolecular NOEs observed between EGCg and the hydrophobic residues of the β-sheet (I148 or I112), indicating that EGCg is not buried deep in the hydrophobic pocket as is EMD 57033. Also, no NOEs were observed between EGCg and any residues along the loop between helices F and G, even though these residues had the greatest chemical shift perturbation (Figure 2-2). The large perturbations of the loop residues could result from a proximity to the aromatic polyphenol rings of EGCg, or from a change in the conformation or dynamics of the loop upon binding EGCg.

The ensemble of the 30 lowest energy structures of EGCg in complex with cCTnC•2Ca^{2+} is depicted in Figure 2-5a, and b. The ensemble of EGCg is shown in Figure 2-5c and the lowest energy structure of cCTnC•2Ca^{2+}•EGCg is shown in cartoon representation in Figure 2-5d. The overall fold of cCTnC is similar to that which has been previously described for cCTnC. There are four well-defined helices as follows: helices E, F, G, and H. The two Ca^{2+} binding sites (sites III and IV) are between helices E and F and G and H. There is a short twisted anti-parallel β-sheet that joins the two EF-hands. The r.m.s.d. of cCTnC for the backbone atoms of the well-defined residues is 0.80 ± 0.14Å. The well-defined regions (r.m.s.d. < 1 Å) involve residues 94-122, 132-143, and 145-157. These regions include residues from helices E, F, G, and H as well as those of the Ca^{2+}-binding loops and anti-parallel β-sheet. The N- and C- termini as well as the inter-helical F-G loop of cCTnC•2Ca^{2+} had fewer structural restraints, and hence had a larger r.m.s.d. in the ensemble. Given the rotational freedom of EGCg around the galloyl (ring B') and pyrogallol (ring B) moieties, there was significant mobility in the ensemble of EGCg (Figure 2-5c). In addition to the rotational freedom of the trihydroxyphenyl rings, the pairs of hydrogen atoms on the rings (H39/H41 and H12/H4) are chemically equivalent, and so it was not
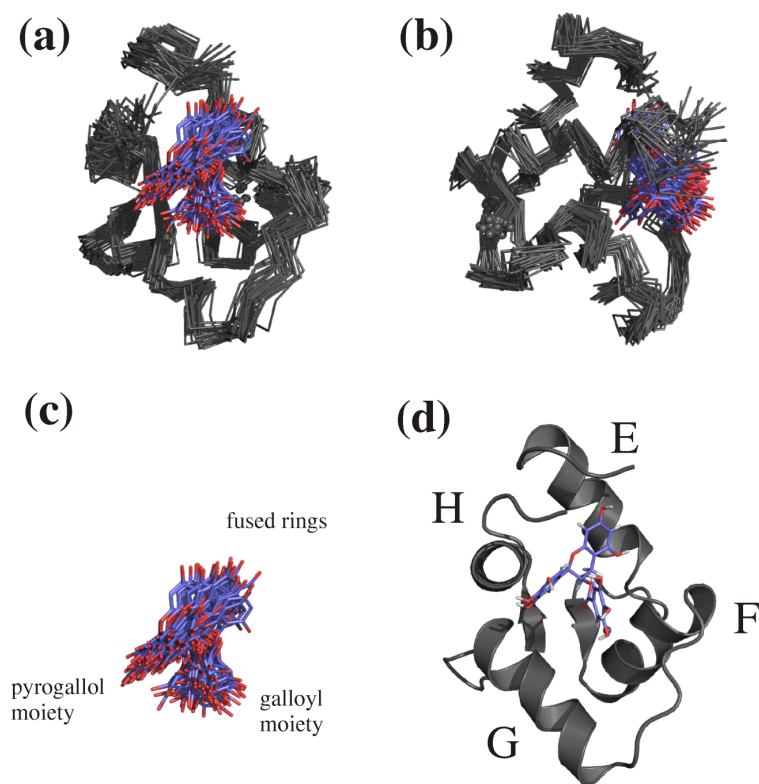
Figure 2-5. Diagram of the solution structure of cCTnC•2Ca^{2+}•EGCg. (a) The ensemble of the 30 lowest energy structures of EGCg in association with cCTnC•2Ca^{2+} is depicted with just the backbone atoms of cCTnC drawn as ribbons, and of EGCg as sticks. The ensemble of cCTnC•2Ca^{2+} is colored in grey, the Ca^{2+} ions are shown as grey spheres, and the ensemble of EGCg is colored with carbon atoms in purple and oxygen atoms in red. (b) a 90° rotation about the y axis. (c) The ensemble of EGCg and the chemical groups of EGCg are labeled. (d) The cartoon representation of the lowest energy structure of the ensemble of cCTnC•2Ca^{2+}•EGCg with the helices labeled and consistent coloring as above. The orientation of cCTnC is the same as in (a).

possible to differentiate NOE contacts within the pairs. Nonetheless, the 10 intramolecular NOEs of the bound EGCg and the 18 intermolecular NOEs between EGCg and cCTnC•2Ca^{2+} positioned the three functional moieties of EGCg with reasonable precision. The galloyl moiety is positioned near the loop connecting helix F and helix G. The large chemical shift perturbations of the F-G loop residues (Figure 2-2) could in-part result from a propinquity to the galloyl trihydroxyphenyl ring. The pyrogallol ring rests near the C-terminus of cCTnC, which explains the large chemical shift perturbations of helix H residues M157-E161 during titration with EGCg (Figure 2-1). The fused tetrahydropyran (ring C) and benzenediol (ring A) rings lie near the surface of helix E that faces the hydrophobic core of cCTnC•2Ca^{2+}.

Comparison of solution structures cCTnC•2Ca^{2+} and cCTnC•2Ca^{2+}•EGCg. The solution structure of cCTnC•2Ca^{2+}•EGCg adopts a similar fold to other structures determined for cCTnC (*6, 13, 21*). The differences in the structures determined for cCTnC are all primarily the result of varying degrees of "openness", in which the helices are spread out from the hydrophobic core of the protein. The degree in which cCTnC is "open" is described by the inter-helical angles between helices E and F, and between helices G and H. The closer the inter-helical angles are to 90°, the more "open" the structure is. Inter-helical angles were calculated using the program interhlx (K. Yap, University of Toronto).

When the structure of cCTnC•2Ca^{2+}•EGCg was overlaid with the NMR structure of cCTnC•2Ca^{2+}(*6*) a minor perturbation in the structure is observed. Between the two structures, an r.m.s.d. of 1.53 Å for backbone atoms of helices E, F, G, and H was observed (Figure 2-6a, b). Notable differences between the structures include helix E, helix G, and helix H are positioned slightly away from the core of the protein when compared with cCTnC•2Ca^{2+}. The E-F inter-helical angle of cCTnC•2Ca^{2+} is 112°, and the G-H angle is 117°. The E-F inter-helical angle of cCTnC•2Ca^{2+}•EGCg is
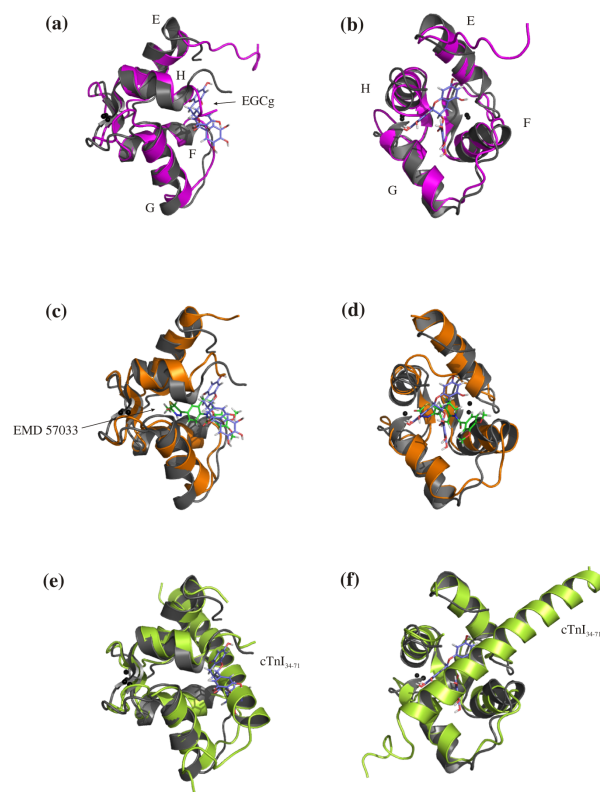
Figure 2-6. A backbone overlay of cCTnC•2Ca^{2+}•EGCg with several structures of cCTnC. In all of the images, cCTnC is depicted in cartoon form and colored in grey. EGCg is shown in stick representation, and carbon atoms are colored in purple, oxygen atoms are colored in red, and hydrogen atoms are shown in white. (a) cCTnC in the cCTnC•2Ca^{2+}•EGCg complex is overlaid with cCTnC in the cCTnC•2Ca^{2+} complex (PDB:3CTN) shown in magenta. (b) a 90° rotation about the y axis. The helices are labeled in two diagrams and EGCg is also labeled. (c) cCTnC in the cCTnC•2Ca^{2+}•EGCg complex is overlaid with cCTnC in the cCTnC•2Ca^{2+}•EMD 57033 complex (PDB:1IH0) shown in orange. EMD 57033 is colored with carbon atoms shown in green, sulfur atoms in yellow, oxygen atoms in red, and hydrogen atoms in white. (d) a 90° rotation about the y axis. EMD 57033 is identified with an arrow. (e) cCTnC in the cCTnC•2Ca^{2+}•EGCg complex is overlaid with cCTnC in the cCTnC•2Ca^{2+}•cTnI$_{34-71}$ complex (PDB:1J1D) shown in lime green. (f) a 90° rotation about the y axis. cTnI$_{34-71}$ is labeled in both representations.

105°, and the G-H inter-helical angle is 113°; revealing that the overall outcome of EGCg binding is a more "open" conformation of cCTnC.

The solution structure of cCTnC•2Ca^{2+} bound to EMD 57033 has also been solved (21). When cCTnC•2Ca^{2+}•EGCg is overlaid with cCTnC•2Ca^{2+}•EMD57033, the backbone r.m.s.d. for the helices is 1.84 Å (Figure 2-6c, d). The inter-helical angles of the E-F and the G-H helices of cCTnC•2Ca^{2+}•EMD57033 are 96° and 118°, respectively. The largest difference between the structures is in the positions of the G and F helices. In the EMD 57033 bound structure, the G helix is shifted nearer to the core of cCTnC (as in the unbound form of cCTnC•2Ca^{2+}). In contrast, helix F is further from the core of cCTnC in the EMD 57033 bound structure when compared to the EGCg bound structure of cCTnC•2Ca^{2+}. The location of the two ligands is similar, with both drugs binding the core of the protein; however, EMD 57033 is buried deep within cCTnC while EGCg remains near the surface of the opening of cCTnC. The methyl on the thiadiazinone ring of EMD 57033 makes several NOE contacts with I148 and I112 of the β-sheet. In the case of EGCg, the ring protons all make contacts exclusively to hydrophobic residues that line the surface of cCTnC.

The region of the crystal structure of the cardiac troponin complex (13) corresponding to cCTnC•2Ca^{2+}•cTnI$_{34-71}$ was also overlaid with cCTnC•2Ca^{2+}•EGCg and gives a r.m.s.d. of 1.45 Å for the backbone atoms of the helix residues (Figure 2-6e, f). In accordance with the good agreement in r.m.s.d.s, the inter-helical angles of cCTnC in the cCTnC•2Ca^{2+}•cTnI$_{34-71}$ complex also resemble the cCTnC in the cCTnC•2Ca^{2+}•EGCg complex; the E-F inter-helical angle is 100°, and the G-H inter-helical angle is 114°. Therefore, EGCg induces a conformational change in cCTnC most closely akin to that caused by cTnI$_{34-71}$. The helices of cCTnC bound to cTnI$_{34-71}$ all align well with the cCTnC-EGCg complex, suggesting an analogous "opening" of cCTnC. Helix G is further from the core of the protein in the EGCg bound structure when compared

to the $cTnI_{34-71}$ bound form of $cCTnC \cdot 2Ca^{2+}$. EGCg and the backbone of $cTnI_{34-71}$ occupy the same surface of cCTnC. In order to test how this steric clash affects EGCg binding, we titrated EGCg into the $cTnI_{34-71}$ saturated $cCTnC \cdot 2Ca^{2+}$ complex.

The effect of EGCg on $cCTnC \cdot 2Ca^{2+} \cdot cTnI_{34-71}$.

The interaction of EGCg with $cCTnC \cdot 2Ca^{2+} \cdot cTnI_{34-71}$ was monitored using the $^1H,^{15}N$-HSQC and $^1H,^{13}C$-HSQC NMR spectra acquired at a series of EGCg-$cCTnC \cdot 2Ca^{2+} \cdot cTnI_{34-71}$ ratios (Figure 2-7a,b). The total chemical shift was normalized for a number of resonances, and a global fitting approach using xcrvfit was used to determine the dissociation constant which best fit the equation:

$$cCTnC \cdot 2Ca^{2+} \cdot cTnI_{34-71} + EGCg \leftrightarrow cCTnC \cdot 2Ca^{2+} \cdot cTnI_{34-71} \cdot EGCg$$
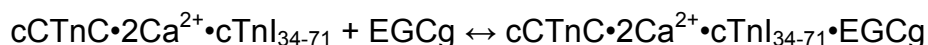
The binding curves that were globally fit are shown in Figure 2-7c. The binding of EGCg to $cCTnC \cdot 2Ca^{2+} \cdot cTnI_{34-71}$ was fit to a 1:1 stoichiometry, with a best-fit K_D of 1.8 mM, about 1.5 fold weaker than the K_D for EGCg binding to $cCTnC \cdot 2Ca^{2+}$ calculated at the higher concentration. The K_D was also calculated by averaging the normalized individual chemical shifts as a function of the ligand to protein ratios and fitting using xcrvfit. This approach gave a K_D of 1.64 ± 0.24 mM.

The perturbation of $^1H,^{15}N$ cross-peaks was less than for binding of EGCg to $cCTnC \cdot 2Ca^{2+}$ alone, and the perturbed residues correspond to several isolated regions of cCTnC. This made chemical shift mapping difficult to interpret, forestalling the localization of the binding surface of EGCg. $^1H,^{13}C$-HSQC NMR spectra of $cCTnC \cdot 2Ca^{2+}$ in the $cCTnC \cdot 2Ca^{2+} \cdot cTnI_{34-71}$ complex were also acquired during the EGCg titration to hone in on the binding surface on $cCTnC \cdot 2Ca^{2+} \cdot cTnI_{34-71}$ complex. The methyl region of the $^1H,^{13}C$-HSQC NMR spectra are shown in Figure 2-7b. Two or three regions of the protein experienced large
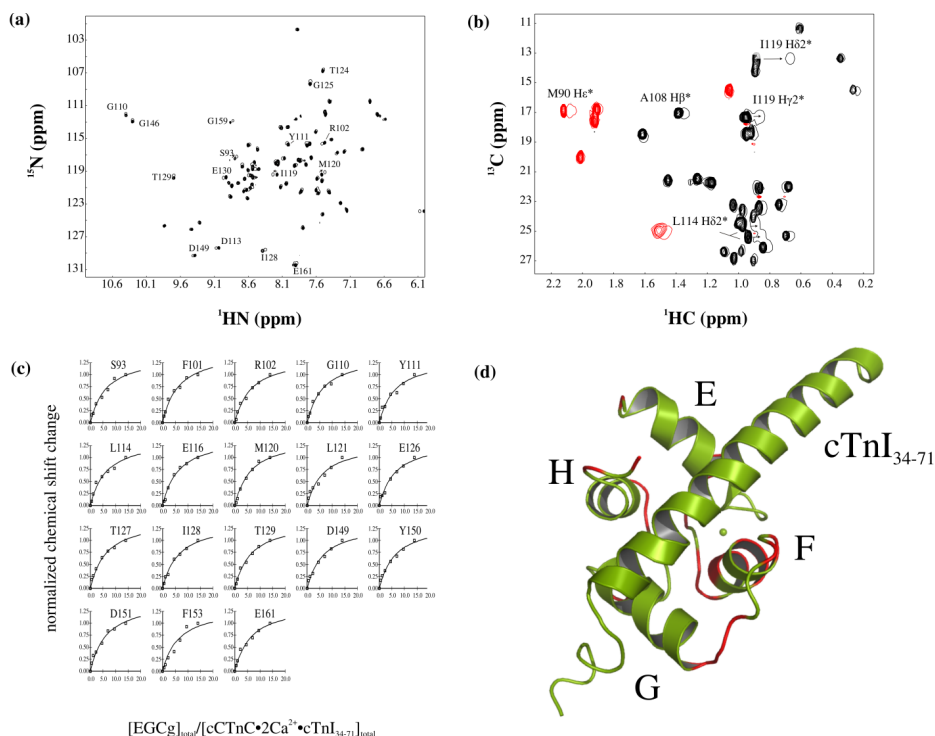
Figure 2-7. Titration of cCTnC•2Ca^{2+}•cTnI$_{34-71}$ with EGCg. 2D ^{1}H, ^{15}N-HSQC (a) and ^{1}H, ^{13}C-HSQC (b) spectra arising from backbone and side chain amide groups (a) and side chain methyl groups (b) are overlaid for a series of EGCg additions. Each titration point represents the titration points described in the materials and methods. The titration was made into ^{13}C, ^{15}N-labeled cCTnC•2Ca^{2+}•cTnI$_{34-71}$ and both the ^{1}H, ^{15}N-HSQC and ^{1}H, ^{13}C-HSQC spectra were acquired at each titration point. Assignments of some of the cross-peaks are labeled. The multiple contours (●) represent the initial point in the titration, with no EGCg added, and the open contours (○) represent the end point in the titration for a given residue. (b) The red contours represent cross-peaks with negative intensity, a feature of the constant-time ^{1}H,^{13}C-HSQC experiment. The direction that the peaks shift is indicated by arrows, for example see M120. (c) The curves represent a number of residues affected by ligand binding, as shown in (a). The curves were fit as a function of normalized total chemical shift perturbation vs. [EGCg]$_{total}$/[cCTnC•2Ca^{2+}•cTnI$_{34-71}$]$_{total}$. (d) The cCTnC•2Ca^{2+}•cTnI$_{34-71}$ complex is shown in lime green with cCTnC•2Ca^{2+} and cTnI$_{34-71}$ shown in cartoon representation. Chemical shift perturbations of the backbone amide resonances induced by EGCg binding to cCTnC•2Ca^{2+}•cTnI$_{34-71}$ are colored in red for residues that shifted greater than the mean shift of all residues of cCTnC. Total chemical shift changes are calculated in hertz (Hz) as follows: $\Delta\delta = [(\Delta\delta^1H)^2 + (\Delta\delta^{15}N)^2]^{1/2}$. Since hertz is used instead of parts per million (ppm) a correction factor of 1/5 for the ^{15}N dimension is not used.

chemical shift changes in the ^{1}H,^{13}C-HSQC NMR spectra: near the E-H helix interface, along the F helix, and E-F loop.

The amide resonances that were most perturbed upon EGCg titration are mapped onto the structure of cCTnC•2Ca^{2+}•cTnI$_{34-71}$ (Figure 2-7d) from the core troponin structure (*13*). It seems that EGCg binds in the proximity of helix F. Further evidence of EGCg binding near helix F is given when the methyl region of the ^{1}H, ^{13}C-HSQC spectrum was monitored during the titration of cCTnC•Ca^{2+}•cTnI$_{34-71}$ with EGCg. The terminal methyls of the F helix residues, L114 and I119, underwent large chemical shift perturbations (Figure 2-7b). It may be that EGCg binds to the interface between cTnI and cCTnC near helix F or simply to the side of the protein near the F-G loop. There were also perturbations of amide resonances near the N-terminus of helix H towards the β-sheet and of residues on the β-sheet. These perturbations may be caused by direct contact with EGCg, or from a conformational change in the structure of cCTnC•2Ca^{2+}•cTnI$_{34-71}$ to lodge EGCg.

Discussion

Common treatment schemes of heart failure modify levels of cytosolic Ca^{2+}. This provides immediate improvement in heart function, but can lead to serious side effects if used for an extended period of time. Drugs that alter the Ca^{2+} sensitivity of the thin filament, rather than the cytosolicCa^{2+} concentration provide a safer alternative. There are compounds that increase or decrease the sensitivity of the thin filament through interacting specifically with troponin. An increase in Ca^{2+} sensitivity would be beneficial for the treatment of heart failure; whereas the use of Ca^{2+} desensitizers may provide protection against the development of hypertrophic cardiomyopathy (HCM). HCM is identified by an enlargement of the heart muscle, and a decrease in chamber volume of the ventricles. Patients with HCM often suffer from shortness of breath and angina, but

may also eventually experience heart failure, arrhythmia and sudden death. The treatment of HCM has been traditionally pursued with the use of negative inotropes that block neurohormones, target pathological load on the heart, or block calcium channels (for reviews on HCM and therapies, see references (*46-49*)). The use of Ca^{2+}-desensitizers would provide another treatment option, since Ca^{2+}-desensitizers do not disrupt the cytosolic Ca^{2+} homeostasis or hormone levels. A compound that has demonstrated the ability to inhibit cardiac muscle activation is W7. In skinned rabbit psoas fibers, W7 was shown to inhibit the striated muscle activation (*50*). Silver *et al.* also indicated that W7 inhibited ATPase activity, and proposed this deactivation occurred through interaction with cTnC (*51*). NMR has been utilized to show that W7 binds both the C- and N-terminal domains of cTnC in the absence of cTnI (*43*); however, in the presence of $cTnI_{34-71}$ and $cTnI_{128-163}$, W7 associates exclusively in the N-terminal domain of cTnC (*52*). Similarly, EGCg has been identified by the preliminary study of Tadano *et al.* (*30*) and by the recent work of Liou and coworkers (*28*) to reduce the Ca^{2+} sensitivity of myofibrillar ATPase activity in cardiac myofibrils. Contrary to W7; however, we illustrate by NMR that EGCg binds to the C-domain of cTnC preferentially. This observation has also been shown by fluorescence and NMR spectroscopy (*28, 30*).

Structural biology has supplemented the understanding of cardiac muscle contraction, and has revealed interesting therapeutic opportunities with cTnC as the primary target. In this paper we used NMR spectroscopy to define the molecular details of the interaction between EGCg and cCTnC. Analogous to other ligands, we found that EGCg binds in the hydrophobic cavity of $cCTnC•2Ca^{2+}$. In addition to the EGCg-cCTnC interaction, we found that EGCg also binds to the $cCTnC•Ca^{2+}•cTnI_{34-71}$ complex. Both of these observations have also been described by others, and it is thought that it is these interactions with the C-domain of cTnC that is responsible for the activity of EGCg (*28, 30*). 2D HSQC NMR spectra

were acquired and chemical shift changes of ^{15}N, ^{13}C labeled cCTnC were followed during the EGCg titration into solutions containing cCTnC•2Ca^{2+} or cCTnC•2Ca^{2+}•cTnI$_{34-71}$. Since 2D HSQC NMR spectroscopy provides information regarding the chemical environment surrounding individual nuclei in the protein, we were able to identify specific residues that were affected by EGCg. This branded residues that are proximal to EGCg in the protein-ligand complex, or that experience conformational changes upon ligand binding. The $^{1}H,^{13}C$-HSQC NMR experiment was utilized to elucidate nearby residues via side chain resonance perturbations, and thus gain insight into the binding location of EGCg to cCTnC.

The solution structure of cCTnC•2Ca^{2+}•EGCg was determined in order to unravel the mode of action of EGCg. It was found that EGCg binds to the hydrophobic pocket of cCTnC•2Ca^{2+} as does other ligands of cCTnC, such as the anchoring region of cTnI (cTnI$_{34-71}$), and the cardiotonic drug (EMD 57033) (*13, 21*). Unlike cTnI$_{34-71}$ and EMD 57033, EGCg binds closer to the surface of the hydrophobic pocket rather than deep within the core of cCTnC. EGCg was shown to "open" the core of cCTnC•2Ca^{2+} in a similar manner as cTnI$_{34-71}$ does. It was also seen that EGCg occupies the same binding site as cTnI$_{34-71}$ (Figure 2-6e, f), which might suggest the mode of action of EGCg. EGCg may compete with cTnI$_{34-71}$. In order to address the possibility that EGCg may compete with cTnI$_{34-71}$ for binding to cCTnC, the interaction of EGCg with cCTnC•2Ca^{2+}•cTnI$_{34-71}$ was measured.

We found that EGCg induced chemical shift perturbations of cCTnC•2Ca^{2+}•cTnI$_{34-71}$; however, the overall magnitude of the perturbations, when compared with cCTnC•2Ca^{2+} appeared smaller and the affinity of EGCg for the complex is decreased. Possible reasons for the lessened affinity of EGCg for cCTnC•2Ca^{2+}•cTnI$_{34-71}$ are EGCg and cTnI$_{34-71}$ compete for the same binding site on cCTnC•2Ca^{2+} or there is a new binding site for EGCg in the cCTnC•2Ca^{2+}•cTnI$_{34-71}$ complex. The chemical shift changes induced by EGCg on the cCTnC•2Ca^{2+}•cTnI$_{34-71}$

complex do not indicate a dissociation of $cTnI_{34-71}$ from $cCTnC \cdot 2Ca^{2+}$, but rather suggest the formation of a 'ternary' complex, $cCTnC \cdot 2Ca^{2+} \cdot cTnI_{34-71} \cdot EGCg$. The smaller chemical shift changes suggest less of a structural perturbation of the troponin C-I complex, than of cCTnC.

The affinity of EGCg for cTnC has been measured by intrinsic tyrosine fluorescence quenching to be 3-4 µM for EGCg to cTnC (*28*). At the higher concentrations typically used for NMR spectroscopy, we found that EGCg bound to cTnC with an K_D of 1.1 ± 0.12 mM, to cCTnC with a K_D of 1.09 ± 0.08 mM, and to $cCTnC \cdot cTnI_{34-71}$ with a K_D of 1.64 ± 0.24 mM. It has been shown that aromatic stacking of EGCg occurs in aqueous solution (*53, 54*), and this additional equilibrium would confound accurate K_D determination. Prompted by these reports, we repeated the titration of EGCg into $cCTnC \cdot 2Ca^{2+}$ at a lower concentration. Our results show that as we decrease the concentration of cCTnC, the apparent K_D was decreased as well (from 1.09 mM to 385 µM). This enhanced affinity supports the notion of EGCg stacking *in vitro*, and explains the weaker affinity we measured when compared with fluorescence spectroscopy.

The perturbation of the $cCTnC-cTnI_{34-71}$ interaction by EGCg could weaken the anchoring of cCTnC to the thin filament and thus decrease the sensitivity of the thin filament for Ca^{2+}. There are compounds that have been identified to bind the N-terminal domain of cTnC, and function by modulating the interaction of cNTnC and cTnI. Levosimendan is expected to work by increasing the affinity of $cTnI_{147-163}$ for cNTnC; thus increase the Ca^{2+}-sensitivity of the thin filament through an indirect mechanism (*55*). There has been renewed interest in the role of the so-called structural domain of cTnC (cCTnC) in regulation of contraction. EMD 57033 is a drug that has been shown to interact exclusively with cCTnC. EMD 57033 may act as a Ca^{2+}-sensitizer by modulating the interaction of cCTnC and $cTnI_{34-71}$. Small compounds that bind to and inhibit, or strengthen the interaction of cCTnC for $cTnI_{34-71}$ may have a pronounced effect on contraction rate or force, and Ca^{2+}-sensitivity.

With the aid of this solution structure it might be possible to design new agents using EGCg as a lead compound. The strategic methylation some of the hydroxyl groups on the polyphenol rings, for example, could potentially increase the potency of EGCg. In fact, it has been shown that catechin and epicatechin are O-methylated in rat small intestine (*56*), the *in vivo* mechanism of EGCg on thin filament activity may include these substituted metabolites. The concept of chemical modification of natural products to improve their effectiveness is common, and there are many examples of pharmaceuticals currently prescribed that are derived from natural products (for a review see Koehn and Carter (*57*)). The potential role of EGCg as a Ca^{2+}-desensitizer is particularly interesting in regards to treatment for HCM, since there is evidence that reactive oxygen species (ROS) may be one of the causes of cardiac hypertrophy (*49*). Since EGCg is a known scavenger of radicals, it may help treat and/or prevent HCM by sequestering ROS as well as by inhibiting ATPase activity.

The data presented in this work provide evidence to support the notion that cTnC is one of the primary targets for EGCg in the myofilament, the effective binding site is in the hydrophobic pocket of cCTnC, and the binding induces an "opening" of the domain. We describe the interaction of EGCg with the $cCTnC \cdot 2Ca^{2+} \cdot cTnI_{34-71}$ complex; indicating a possible mechanism in which EGCg modulates contraction. EGCg may compete with $cTnI_{34-71}$ and weaken the anchoring of cTnC to the thin filament. This has been postulated for the DCM mutation G159D. The G159D mutation is in the cCTnC and has been shown to weaken the affinity of $cTnI_{34-71}$ for cCTnC (*25*). EGCg may work in a similar manner, protecting the heart from the development of hypertrophy.

References

1. Rosamond, W., Flegal, K., Furie, K., Go, A., Greenlund, K., Haase, N., Hailpern, S. M., Ho, M., Howard, V., Kissela, B., Kittner, S., Lloyd-Jones, D., McDermott, M., Meigs, J., Moy, C., Nichol, G., O'Donnell, C., Roger, V., Sorlie, P., Steinberger, J., Thom, T., Wilson, M., and Hong, Y. (2008) Heart disease and stroke statistics - 2008 update - A report from the American Heart Association Statistics Committee and Stroke Statistics Subcommittee, *Circulation 117*, E25-E146.

2. Parmacek, M. S., and Solaro, R. J. (2004) Biology of the troponin complex in cardiac myocytes, *Prog. Cardiovasc. Dis. 47*, 159-176.

3. Li, M. X., Wang, X., and Sykes, B. D. (2004) Structural based insights into the role of troponin in cardiac muscle pathophysiology, *J. Muscle Res. Cell Motil. 25*, 559-579.

4. Tobacman, L. S. (1996) Thin filament-mediated regulation of cardiac contraction, *Annu. Rev. Physiol. 58*, 447-481.

5. Gomes, A. V., Potter, J. D., and Szczesna-Cordary, D. (2002) The role of troponins in muscle contraction, *IUBMB Life 54*, 323-333.

6. Sia, S. K., Li, M. X., Spyracopoulos, L., Gagne, S. M., Liu, W., Putkey, J. A., and Sykes, B. D. (1997) Structure of cardiac muscle troponin C unexpectedly reveals a closed regulatory domain, *J. Biol. Chem. 272*, 18216-18221.

7. Houdusse, A., Love, M. L., Dominguez, R., Grabarek, Z., and Cohen, C. (1997) Structures of four Ca2+-bound troponin C at 2.0 A resolution: further insights into the Ca2+-switch in the calmodulin superfamily, *Structure 5*, 1695-1711.

8. Herzberg, O., and James, M. N. (1988) Refined crystal structure of troponin C from turkey skeletal muscle at 2.0 A resolution, *J. Mol. Biol. 203*, 761-779.

9. Satyshur, K. A., Rao, S. T., Pyzalska, D., Drendel, W., Greaser, M., and Sundaralingam, M. (1988) Refined structure of chicken skeletal muscle troponin C in the two-calcium state at 2-A resolution, *J. Biol. Chem. 263*, 1628-1647.

10. Gagne, S. M., Tsuda, S., Li, M. X., Smillie, L. B., and Sykes, B. D. (1995) Structures of the troponin C regulatory domains in the apo and calcium-saturated states, *Nat. Struct. Biol. 2*, 784-789.

11. Spyracopoulos, L., Li, M. X., Sia, S. K., Gagne, S. M., Chandra, M., Solaro, R. J., and Sykes, B. D. (1997) Calcium-induced structural transition in the regulatory domain of human cardiac troponin C, *Biochemistry 36*, 12138-12146.

12. Li, M. X., Spyracopoulos, L., and Sykes, B. D. (1999) Binding of cardiac troponin-I147-163 induces a structural opening in human cardiac troponin-C, *Biochemistry 38*, 8289-8298.

13. Takeda, S., Yamashita, A., Maeda, K., and Maeda, Y. (2003) Structure of the core domain of human cardiac troponin in the Ca(2+)-saturated form, *Nature 424*, 35-41.

14. Vinogradova, M. V., Stone, D. B., Malanina, G. G., Karatzaferi, C., Cooke, R., Mendelson, R. A., and Fletterick, R. J. (2005) Ca(2+)-regulated structural changes in troponin, *Proc. Natl. Acad. Sci. U. S. A. 102*, 5038-5043.

15. Mercier, P., Li, M. X., and Sykes, B. D. (2000) Role of the structural domain of troponin C in muscle regulation: NMR studies of Ca2+ binding and subsequent interactions with regions 1-40 and 96-115 of troponin I, *Biochemistry 39*, 2902-2911.

16. Gasmi-Seabrook, G. M., Howarth, J. W., Finley, N., Abusamhadneh, E., Gaponenko, V., Brito, R. M., Solaro, R. J., and Rosevear, P. R. (1999) Solution structures of the C-terminal domain of cardiac troponin C free and bound to the N-terminal domain of cardiac troponin I, *Biochemistry 38*, 8313-8322.

17. Li, M. X., Robertson, I. M., and Sykes, B. D. (2008) Interaction of cardiac troponin with cardiotonic drugs: a structural perspective, *Biochem. Biophys. Res. Commun. 369*, 88-99.

18. Endoh, M. (2001) Mechanism of action of Ca2+ sensitizers--update 2001, *Cardiovasc. Drugs Ther. 15*, 397-403.

19. Kass, D. A., and Solaro, R. J. (2006) Mechanisms and use of calcium-sensitizing agents in the failing heart, *Circulation 113*, 305-315.

20. Pan, B. S., and Johnson, R. G. (1996) Interaction of cardiotonic thiadiazinone derivatives with cardiac troponin C, *J. Biol. Chem. 271*, 817-823.

21. Wang, X., Li, M. X., Spyracopoulos, L., Beier, N., Chandra, M., Solaro, R. J., and Sykes, B. D. (2001) Structure of the C-domain of human cardiac troponin C in complex with the Ca2+ sensitizing drug EMD 57033, *J. Biol. Chem. 276*, 25456-25466.

22. Solaro, R. J., Gambassi, G., Warshaw, D. M., Keller, M. R., Spurgeon, H. A., Beier, N., and Lakatta, E. G. (1993) Stereoselective Actions of Thiadiazinones on Canine Cardiac Myocytes and Myofilaments, *Circ. Res. 73*, 981-990.

23. Li, M. X., Spyracopoulos, L., Beier, N., Putkey, J. A., and Sykes, B. D. (2000) Interaction of cardiac troponin C with Ca2+ sensitizer EMD 57033 and cardiac troponin I inhibitory peptide, *Biochemistry 39*, 8782-8790.

24. Dweck, D., Hus, N., and Potter, J. D. (2008) Challenging Current Paradigms Related to Cardiomyopathies: ARE CHANGES IN THE Ca2+ SENSITIVITY OF MYOFILAMENTS CONTAINING CARDIAC TROPONIN C MUTATIONS (G159D AND L29Q) GOOD

PREDICTORS OF THE PHENOTYPIC OUTCOMES?, *J. Biol. Chem. 283*, 33119-33128.

25. Baryshnikova, O. K., Robertson, I. M., Mercier, P., and Sykes, B. D. (2008) Dilated cardiomyopathy G159D mutation in cardiac troponin C weakens the anchoring interaction with troponin I, *Biochemistry 47*, 10950-10960.

26. Hertog, M. G., Feskens, E. J., Hollman, P. C., Katan, M. B., and Kromhout, D. (1993) Dietary antioxidant flavonoids and risk of coronary heart disease: the Zutphen Elderly Study, *Lancet 342*, 1007-1011.

27. Keli, S. O., Hertog, M. G., Feskens, E. J., and Kromhout, D. (1996) Dietary flavonoids, antioxidant vitamins, and incidence of stroke: the Zutphen study, *Arch. Intern. Med. 156*, 637-642.

28. Liou, Y. M., Kuo, S. C., and Hsieh, S. R. (2008) Differential effects of a green tea-derived polyphenol (-)-epigallocatechin-3-gallate on the acidosis-induced decrease in the Ca(2+) sensitivity of cardiac and skeletal muscle, *Pflugers Arch. 456*, 787-800.

29. Hotta, Y., Huang, L., Muto, T., Yajima, M., Miyazeki, K., Ishikawa, N., Fukuzawa, Y., Wakida, Y., Tushima, H., Ando, H., and Nonogaki, T. (2006) Positive inotropic effect of purified green tea catechin derivative in guinea pig hearts: The measurements of cellular Ca2+ and nitric oxide release, *Eur. J. Pharmacol. 552*, 123-130.

30. Tadano, N., Yumoto, F., Tanokura, M., Ohtsuki, I., and Morimoto, S. (2005) EGCg, a major polyphenol in green tea, binds to the C-lobe of cardiac troponin and desensitizes cardiac muscle contraction to Ca2+, *Biophys. J. 88*, 314a-314a.

31. Chandra, M., Dong, W. J., Pan, B. S., Cheung, H. C., and Solaro, R. J. (1997) Effects of protein kinase A phosphorylation on signaling between cardiac troponin I and the N-terminal domain of cardiac troponin C, *Biochemistry 36*, 13305-13311.

32. Li, M. X., Gagne, S. M., Tsuda, S., Kay, C. M., Smillie, L. B., and Sykes, B. D. (1995) Calcium-Binding to the Regulatory N-Domain of Skeletal-Muscle Troponin-C Occurs in a Stepwise Manner, *Biochemistry 34*, 8330-8340.

33. Lykkesfeldt, J. (2000) Determination of ascorbic acid and dehydroascorbic acid in biological samples by high-performance liquid chromatography using subtraction methods: Reliable reduction with tris[2-carboxyethyl] phosphine hydrochloride, *Anal. Biochem. 282*, 89-93.

34. Delaglio, F., Grzesiek, S., Vuister, G. W., Zhu, G., Pfeifer, J., and Bax, A. (1995) Nmrpipe - a Multidimensional Spectral Processing System Based on Unix Pipes, *J. Biomol. NMR 6*, 277-293.

35. Johnson, B. A., and Blevins, R. A. (1994) Nmr View - a Computer-Program for the Visualization and Analysis of Nmr Data, *J. Biomol. NMR 4*, 603-614.

36.   Slupsky, C. M., Boyko, R. F., Booth, V. K., and Sykes, B. D. (2003) Smartnotebook: A semi-automated approach to protein sequential NMR resonance assignments, *J. Biomol. NMR 27*, 313-321.

37.   Schuttelkopf, A. W., and van Aalten, D. M. F. (2004) PRODRG: a tool for high-throughput crystallography of protein-ligand complexes, *Acta Crystallogr. Sect. D Biol. Crystallogr. 60*, 1355-1363.

38.   Guntert, P., Mumenthaler, C., and Wuthrich, K. (1997) Torsion angle dynamics for NMR structure calculation with the new program DYANA, *J. Mol. Biol. 273*, 283-298.

39.   Herrmann, T., Guntert, P., and Wuthrich, K. (2002) Protein NMR structure determination with automated NOE assignment using the new software CANDID and the torsion angle dynamics algorithm DYANA, *J. Mol. Biol. 319*, 209-227.

40.   Guntert, P. (2004) Automated NMR structure calculation with CYANA, *Methods Mol. Biol. 278*, 353-378.

41.   Jee, J., and Guntert, P. (2003) Influence of the completeness of chemical shift assignments on NMR structures obtained with automated NOE assignment, *J. Struct. Funct. Genomics 4*, 179-189.

42.   Cornilescu, G., Delaglio, F., and Bax, A. (1999) Protein backbone angle restraints from searching a database for chemical shift and sequence homology, *J. Biomol. NMR 13*, 289-302.

43.   Hoffman, R. M. B., Li, M. X., and Sykes, B. D. (2005) The bindin of W7, an inhibitor of striated muscle contraction, to cardiac troponin C, *Biochemistry 44*, 15750-15759.

44.   Lindhout, D. A., and Sykes, B. D. (2003) Structure and dynamics of the C-domain of human cardiac troponin C in complex with the inhibitory region of human cardiac troponin I, *J. Biol. Chem. 278*, 27024-27034.

45.   Ishizu, T., Hirata, C., Yamamoto, H., and Harano, K. (2006) Structure and intramolecular flexibility of beta-cyclodextrin complex with (-)-epigallocatechin gallate in aqueous solvent, *Magn. Reson. Chem. 44*, 776-783.

46.   Seidman, J. G., and Seidman, C. (2001) The genetic basis for cardiomyopathy: from mutation identification to mechanistic paradigms, *Cell 104*, 557-567.

47.   Maron, B. J. (2002) Hypertrophic cardiomyopathy - A systematic review, *JAMA 287*, 1308-1320.

48.   Sherrid, M. V. (2006) Pathophysiology and treatment of hypertrophic cardiomyopathy, *Prog. Cardiovasc. Dis. 49*, 123-151.

49.   McKinsey, T. A., and Kass, D. A. (2007) Small-molecule therapies for cardiac hypertrophy: moving beneath the cell surface, *Nat. Rev. Drug Discovery 6*, 617-635.

50.   Adhikari, B. B., and Wang, K. (2004) Interplay of troponin- and myosin-based pathways of calcium activation in skeletal and

cardiac muscle: The use of W7 as an inhibitor of thin filament activation, *Biophys. J. 86*, 359-370.

51. Silver, P. J., Pinto, P. B., and Dachiw, J. (1986) Modulation of Vascular and Cardiac Contractile Protein Regulatory Mechanisms by Calmodulin Inhibitors and Related-Compounds, *Biochem. Pharmacol. 35*, 2545-2551.

52. Li, M. X., Hoffman, R. M. B., and Sykes, B. D. (2006) Interaction of cardiac troponin C and troponin I with W7 in the presence of three functional regions of cardiac troponin I, *Biochemistry 45*, 9833-9840.

53. Kitano, K., Nam, K. Y., Kimura, S., Fujiki, H., and Imanishi, Y. (1997) Sealing effects of (-)-epigallocatechin gallate on protein kinase C and protein phosphatase 2A, *Biophys. Chem. 65*, 157-164.

54. Wroblewski, K., Muhandiram, R., Chakrabartty, A., and Bennick, A. (2001) The molecular interaction of human salivary histatins with polyphenolic compounds, *Eur. J. Biochem. 268*, 4384-4397.

55. Sorsa, T., Pollesello, P., Permi, P., Drakenberg, T., and Kilpelainen, I. (2003) Interaction of levosimendan with cardiac troponin C in the presence of cardiac troponin I peptides, *J. Mol. Cell. Cardiol. 35*, 1055-1061.

56. Kuhnle, G., Spencer, J. P. E., Schroeter, H., Shenoy, B., Debnam, E. S., Srai, S. K. S., Rice-Evans, C., and Hahn, U. (2000) Epicatechin and catechin are O-methylated and glucuronidated in the small intestine, *Biochem. Biophys. Res. Commun. 277*, 507-512.

57. Koehn, F. E., and Carter, G. T. (2005) The evolving role of natural products in drug discovery, *Nat. Rev. Drug Discov. 4*, 206-220.

58. Laskowski, R. A., Macarthur, M. W., Moss, D. S., and Thornton, J. M. (1993) Procheck - a Program to Check the Stereochemical Quality of Protein Structures, *J. Appl. Crystallogr. 26*, 283-291.

59. Laskowski, R. A., Rullmann, J. A. C., MacArthur, M. W., Kaptein, R., and Thornton, J. M. (1996) AQUA and PROCHECK-NMR: Programs for checking the quality of protein structures solved by NMR, *J. Biomol. NMR 8*, 477-486.

60. Archer, S. J., Ikura, M., Torchia, D. A., and Bax, A. (1991) An Alternative 3d-Nmr Technique for Correlating Backbone N-15 with Side-Chain H-Beta-Resonances in Larger Proteins, *J. Magn. Reson. B 95*, 636-641.

61. Kuboniwa, H., Grzesiek, S., Delaglio, F., and Bax, A. (1994) Measurement of HN-H alpha J couplings in calcium-free calmodulin using new 2D and 3D water-flip-back methods, *J. Biomol. NMR 4*, 871-878.

62. Muhandiram, D. R., and Kay, L. E. (1994) Gradient-Enhanced Triple-Resonance 3-Dimensional Nmr Experiments with Improved Sensitivity, *Journal of Magnetic Resonance Series B 103*, 203-216.

63. Kay, L. E., Xu, G. Y., Singer, A. U., Muhandiram, D. R., and Formankay, J. D. (1993) A Gradient-Enhanced Hcch Tocsy Experiment for Recording Side-Chain H-1 and C-13 Correlations in H2o Samples of Proteins, *J. Magn. Reson. B 101*, 333-337.

64. Grzesiek, S., Anglister, J., and Bax, A. (1993) Correlation of Backbone Amide and Aliphatic Side-Chain Resonances in C-13/N-15-Enriched Proteins by Isotropic Mixing of C-13 Magnetization, *J. Magn. Reson. B 101*, 114-119.

65. Zhang, O., Kay, L. E., Olivier, J. P., and Forman-Kay, J. D. (1994) Backbone 1H and 15N resonance assignments of the N-terminal SH3 domain of drk in folded and unfolded states using enhanced-sensitivity pulsed field gradient NMR techniques, *J. Biomol. NMR 4*, 845-858.

66. Stuart, A. C., Borzilleri, K. A., Withka, J. M., and Palmer, A. G. (1999) Compensating for variations in H-1-C-13 scalar coupling constants in isotope-filtered NMR experiments, *J. Am. Chem. Soc. 121*, 5346-5347.

67. Jeener, J., Meier, B. H., Bachmann, P., and Ernst, R. R. (1979) Investigation of Exchange Processes by 2-Dimensional Nmr-Spectroscopy, *J. Chem. Phys. 71*, 4546-4553.

68. Piantini, U., Sorensen, O. W., and Ernst, R. R. (1982) Multiple Quantum Filters for Elucidating Nmr Coupling Networks, *J. Am. Chem. Soc. 104*, 6800-6801.

Chapter 3

Structure of *trans*-resveratrol in complex with the cardiac regulatory protein troponin C*

Summary

Cardiac troponin – a heterotrimeric protein complex that regulates heart contraction – represents an attractive target for the development of drugs to treat heart disease. Cardiovascular diseases are one of the chief causes of morbidity and mortality worldwide. In France, however, the death rate from heart disease is remarkably low relative to fat consumption. This so-called "French paradox" has been attributed to the high consumption of wine in France; and the antioxidant *trans*-resveratrol is thought to be the primary basis for wine's cardioprotective nature. It has been demonstrated that *trans*-resveratrol increases the myofilament Ca^{2+}-sensitivity of guinea-pig myocytes (Liew, R., Stagg, M.A., MacLeod, K.T., and Collins, P., (2005) *Eur. J. Pharmacol.* 519, 1-8.), however, the specific mode of its action is unknown. In this study, the structure of *trans*-resveratrol free and bound to the calcium-binding protein, troponin C, was determined by NMR spectroscopy. The results indicate that *trans*-resveratrol undergoes a minor conformational change upon binding to the hydrophobic pocket of the C-domain of troponin C. The location occupied by *trans*-resveratrol coincides with the binding site of troponin I – troponin C's natural binding partner. This has been seen for other troponin C-targeting inotropes and implicates the modulation of the troponin C-troponin I interaction as a possible mechanism of action for *trans*-resveratrol.

Contribution: IMR and SEPS are coauthors. Experiments were planned by IMR, SEPS, and BDS. IMR and SEPS performed and analyzed the titrations. IMR and SEPS acquired the data for the structure refinement, and IMR did the structural calculations of free and bound resveratrol. Figures were made by IMR and SEPS. The manuscript was originally written by IMR and SEPS with BDS editing.

Introduction

The physiological function of the heart is to pump blood throughout the body in order to fulfill the oxygen and nutrient demands of the organism. The thin filament in heart muscle is made up of actin, tropomyosin, and troponin. Troponin is a heterotrimeric protein complex formed by the Ca^{2+}-binding subunit, troponin C (TnC); the inhibitory subunit, troponin I (TnI); and the tropomyosin-binding subunit, troponin T (TnT). Cardiac TnC (cTnC) has four EF-hand metal binding sites (I-IV) – two in each of its terminal domains. The C-terminal (cCTnC) and N-terminal (cNTnC) domains are connected by a flexible linker, as shown by the NMR (*1*) and X-ray structures (*2*). In cNTnC, site I is defunct and site II is a low-affinity Ca^{2+}-binding site; on the other hand, both site III and site IV in cCTnC are functional and can bind either Mg^{2+} or Ca^{2+}. During the contraction-relaxation cycle, cytosolic Ca^{2+} concentration dramatically oscillates: at high Ca^{2+} levels, cNTnC becomes Ca^{2+}-saturated, which primes cNTnC for binding with the "switch" region of cTnI ($cTnI_{147-163}$) (*3, 4*); at low Ca^{2+} concentration, Ca^{2+} dissociates from cNTnC leading to the release of $cTnI_{147-163}$. Alternatively, cCTnC remains saturated with either Mg^{2+} or Ca^{2+} throughout the contraction cycle and is associated with the "anchoring" region of cTnI ($cTnI_{34-71}$); an interaction which may play both a structural and regulatory role (*5*). Association of $cTnI_{147-163}$ with cNTnC drags the "inhibitory" region of cTnI ($cTnI_{128-147}$) off of actin, tropomyosin changes its orientation on the thin-filament, the myosin binding site is exposed on actin, and myosin binding to actin leads to contraction (for reviews see (*6, 7*)).

The strength of heart muscle contraction is regulated by the amount of Ca^{2+} released from the sarcoplasmic reticulum into the cytosol and by the response of the myofilaments to Ca^{2+}. Many popular cardiotonic agents (such as digitalis or dobutamine) improve contraction in the failing

heart by elevating intracellular Ca^{2+} concentration; however, intracellular Ca^{2+} modulation carries risks associated with Ca^{2+} overload such as cardiac arrhythmias, cell injury, or cell death. These limitations have shifted interest to a novel class of cardiotonic drugs: Ca^{2+}-sensitizers. Ca^{2+}-sensitizers induce a positive inotropic effect by modulating the myofilament's response to cytosolic Ca^{2+}, and consequently may circumvent the risks associated with altering Ca^{2+} homeostasis (*8*). The essential role cTnC plays in regulation of contraction makes it a logical target for the development of Ca^{2+}-sensitizers. Several ligands that have been found to have a Ca^{2+}-sensitizing ability through direct interaction with cTnC include trifluoperazine (TFP) (*9*), bepridil (*9, 10*), levosimendan (*11-13*), and EMD 57033 (*14-16*). While the majority of these compounds target cNTnC to elicit their Ca^{2+}-sensitizing effects, EMD 57033 functions by targeting cCTnC (*15*). In addition, the natural tea polyphenol, epigallocatechin gallate (EGCg), modulates heart muscle contractility through an interaction with cCTnC (*17-19*). These results suggest that both domains of cTnC represent targets for the development of Ca^{2+}-sensitizers to treat heart failure.

Cardiovascular diseases are the main cause of death worldwide. Interestingly, the mortality rate from heart disease is significantly lower in France than in other countries with comparable diets rich in fat and other risk factors. It has been suggested that this so called "French paradox" may be attributable to high wine consumption in France (*20*). *Trans*-resveratrol (3,4',5-trihydroxystilbene) is produced in grapevines after fungal infection and exposure to ultraviolet light (*21*), and Siemann and Creasy proposed that it might be the biologically active ingredient of red wine (*22*). *Trans*-resveratrol (resveratrol) has a variety of reported physiological effects including: antiplatelet aggregation, anti-inflammatory, and antioxidant activity linked to longevity (*23, 24*); protective effects in skin photosensitivity (*25*); neurodegenerative diseases (*26*); cancer chemoprevention (*27, 28*); and cardioprotection (*29*). Amongst its

cardioprotective effects, it has been shown that resveratrol improves recovery of ventricular function including developed pressure in the face of ischemia reperfusion injury (*30*). It was demonstrated that resveratrol directly affects the contractile function of guinea-pig myocytes, and it increased cell shortening in half the cells tested and decreased shortening in the other half. In the cells where it induced contraction, its relation with the Ca^{2+} transients was quantitatively determined indicating an increase in myofilament Ca^{2+}-sensitivity (*31*). These findings indicate a direct relation between resveratrol and the Ca^{2+} regulated elements in myocytes; however, structural details of this interaction remain unclear.

The present study investigates the interaction between cTnC and resveratrol using the structural technique, NMR spectroscopy. There have been a number of research groups that describe the applications of relatively sparse NMR data for the determination of protein-ligand complexes (*32-35*). Recently, Hoffman and Sykes described a procedure to determine the structure of W7 bound with cNTnC using a previously determined structure of cNTnC as a template (*36*). A similar protocol was followed here, and it was discovered that resveratrol binds to cCTnC in a similar manner as EGCg (*19*) and EMD 57033 (*14*). Several key hydrophobic interactions between cCTnC and resveratrol stabilize the binary structure. It also appears that resveratrol undergoes only a slight conformational change upon binding cCTnC. The solution structure provides clues into the cardioprotective mechanism of resveratrol, and molecular details of the interface between resveratrol and cCTnC may aid in the design of novel cCTnC-targeting drugs.

Experimental Procedures

Sample preparation – Labeled ^{15}N- and ^{15}N,^{13}C-cCTnC and ^{15}N-cTnC were obtained from *E. coli* strains containing the expression vector as previously described (*37, 38*). *Trans*-resveratrol was purchased from

Sigma-Aldrich Inc (99% purity as determined by gas chromatography). All NMR samples were 500 µL in volume and consisted of 100 mM KCl; 10 mM imidazole, or 8 mM imidazole-d_4 and 2 mM imidazole; and 0.5 mM DSS-d_6 as an NMR reference standard. Protein concentrations were ~0.2 mM for full length cTnC and ~0.5 mM for cCTnC with 20 mM or 10 mM CaCl$_2$ respectively. Sample pH was maintained at ~6.9 for all NMR experiments. Although resveratrol naturally exists in *cis* and *trans* isomeric forms, *trans*-resveratrol was used in this study due to its higher concentrations in red wine (0–15 µg/ml) in contrast with *cis*-resveratrol (0–5 µg/ml) (*24*). Stock solutions of 20 mM *trans*-resveratrol (resveratrol) in a 100 mM tris(2-carboxyethyl)phosphine (TCEP) - DMSO-d_6 solution were prepared. TCEP was used to allay oxidation of resveratrol as done for EGCg and Ascorbic Acid (*19, 39*). The concentration ratio of resveratrol:cCTnC was ~4:1 for NMR experiments of the complex. All the stock solutions were prepared fresh prior to each experiment and were wrapped with aluminum foil to prevent photo-degradation.

NMR spectroscopy and data processing – The NMR data used for this study was collected on Varian Inova 500-MHz and Unity 600-MHz spectrometers at 30 °C, or a Varian Inova 800-MHz spectrometer at 25 °C. All spectrometers have triple resonance probes with Z-pulsed field gradients. One-dimensional ^{1}H; and two-dimensional ^{1}H,^{1}H-NOESY and ^{1}H,^{1}H-ROESY experiments were acquired of resveratrol in D$_2$O with mixing times of 100 ms for the NOESY and 50, , 150, 200, and 300 ms mixing times for the ROESY experiments. Two-dimensional ^{1}H,^{13}C-HSQC and ^{1}H,^{15}N-HSQC experiments were acquired to monitor the titration of resveratrol into ^{13}C,^{15}N- or ^{15}N-labeled cCTnC. Intramolecular NOEs of resveratrol when in complex with cCTnC were measured with the two-dimensional ^{13}C,^{15}N-filtered NOESY experiment with a mixing time of 100 ms (*40, 41*); intermolecular distance restraints between resveratrol and cCTnC were derived from two-dimensional ^{13}C-edited/filtered NOESY-

HSQC (mixing times: 150, 200, 250 ms) (*42*) and three-dimensional ^{13}C-edited/filtered HMQC-NOESY (mixing times: 200, 250 ms) (*43, 44*) experiments. In order to check whether the conformation of cCTnC was perturbed by the presence of resveratrol, a two-dimensional ^{1}H,^{1}H-NOESY was acquired of cCTnC•resveratrol in D_2O with a mixing time of 150 ms. VNMRJ (Varian Inc.) was used for the analysis of one-dimensional NMR spectra, all two-dimensional and three-dimensional NMR data were processed with NMRPipe (*45*) and analyzed with NMRView (*46*). Chemical shifts of cCTnC were assigned using those deposited for cTnC (*1*) and the methionine methyls were assigned from assignments previously determined by mutagenesis (*47*). The interaction between resveratrol and cCTnC is in fast exchange, so the resonances from cCTnC could be followed throughout the titration of resveratrol and the assignments translated to the chemical shifts of the cCTnC•resveratrol complex.

Resveratrol assignment and assessment of stability –The proton chemical shifts of resveratrol were assigned in D_2O by the use of one-dimensional ^{1}H, two-dimensional ^{1}H,^{1}H-NOESY, and two-dimensional ^{1}H,^{1}H-ROESY NMR experiments. In order to test the stability of resveratrol in aqueous solution, 500 µL samples of ~0.3 mM resveratrol were prepared in D_2O. ^{1}H NMR spectra were acquired at one-hour increments to test for oxidative degradation. Another sample of resveratrol was prepared with 10 mM TCEP and reassessed the sample stability. In both samples, the pD was ~7.0.

NMR structure and ab initio calculations of resveratrol free in solution – The PRODRG web server (*48*) was used to create initial coordinates of resveratrol and XPLO-2D (*49*) was used to generate topology and parameter files for resveratrol. The structure of resveratrol was determined by ROE intensities of resveratrol at mixing time of 200 ms. XPLOR-NIH

(*50*) was used to calculate the solution structure of resveratrol. Four NOEs contributed to the structure calculation, which were binned from strong (2.00-1.80 Å), medium (2.80-1.80 Å), and weak (3.60-1.80 Å). The simulated annealing comprised square-well potentials for interproton distances and a patch to keep the aromatic rings and olefin bond planar; the aromatic rings of resveratrol were allowed to freely rotate around the C1'-Cα' and C1-Cα bonds. 100 structures were calculated, and the lowest 10 in energy were kept. The lowest energy solution structure of free resveratrol was used as an input structure in Gaussian03 (*51*) to calculate the total density and electrostatic potential (ESP). The energy calculation was performed in aqueous solvent with Becke's three-parameter Lee, Yang, Parr (B3LYP) hybrid functional with a split-valence basis set and polarization d- and p-orbitals added (B3LYP/6-311++G(d, p)). Final contour surfaces were represented using GaussView 3.0.

Resveratrol titrations into cTnC and cCTnC – The 20 mM resveratrol stock solution was titrated into an NMR tube containing full length ^{15}N-labeled cTnC, ^{15}N-, and ^{15}N,^{13}C-labeled cCTnC. Resveratrol additions were made to final concentrations of 60, 190, 370, 670, 960, 1520 and 2050 µM for the titration with cTnC and to final concentrations of 40, 170, 380, 580, 980, 1350 and 1700 µM for the titration with cCTnC. One-dimensional ^{1}H and two-dimensional ^{1}H,^{15}N-HSQC spectra were acquired at each titration point. Additionally, ^{1}H,^{13}C-HSQC spectra were acquired throughout the titration of resveratrol into ^{13}C,^{15}N-labeled cCTnC. At each titration point, the HSQC spectra were assigned, and residue specific chemical shift perturbations (CSPs) that were well resolved and underwent a large change were kept for the dissociation constant calculation. Chemical shift changes (Δδ) were calculated using the following equation:

$$\Delta \delta = \sqrt{(\Delta \delta_H)^2 + \frac{1}{25}(\Delta \delta_N)^2}$$

The dissociation constants (K_D) for resveratrol were calculated by using a global fitting approach with the program xcrvfit (www.bionmr.ualberta.ca/bds/software/xcrvfit), as described previously (*52*). Briefly, the set of kept titration curves were fit using a fixed K_D range and a floating final shift value (since residues were perturbed to a varying extent). The sum of squared error (SSE) was minimized by optimizing the K_D, and thus a global K_D was calculated that best fit all the CSPs. The binding of resveratrol to cTnC and cCTnC was fit with a 1:1 stoichiometry:

$$troponin + resveratrol \leftrightarrow troponin \bullet resveratrol$$
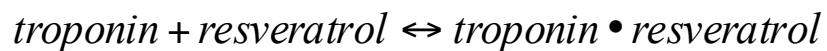
Concentrations of cTnC and cCTnC were calculated by integrating the one-dimensional-slice of the $^1H,^{15}N$-HSQC spectrum, and comparing the spectral intensity with that of a sample with a protein concentration determined by amino acid analysis. The concentrations of the resveratrol stock solutions were determined by comparing the proton spectral intensity of resveratrol peaks with the DSS proton intensity. Concentrations of cTnC, cCTnC, and resveratrol were then corrected for dilution that occurred during the titrations. Since the addition of resveratrol slowly decreased the pH of the sample, the pH was adjusted to ~6.9 with 1M NaOH when necessary.

J-surface mapping – The program Jsurf was used to localize the binding site of resveratrol on cCTnC. Jsurf approximates the origin of the CSP as a single point-dipole in the center of an aromatic ring from a ligand (*53*). With the coordinates of cTnC as input, Jsurf depicts the coordinates of a ligand ring as a dot based on the magnitude and sign of the CSPs. The region that shows the highest dot density is referred to as the j-surface, and is where the aromatic constituents of a ligand are most likely to reside. The chemical shifts in the $^1H,^{13}C$-HSQC spectrum of the final point in the

titration of cCTnC (CS_{PL}) with resveratrol were subtracted from the initial chemical shifts of cCTnC (CS_P).

$$CSP = CS_{PL} - CS_P$$

Only peaks that were well resolved and underwent a concentration-dependant CSP of ≥ 0.012 ppm in the proton dimension were used in the analysis; results were displayed in PyMOL.

Structure calculation of cCTnC•resveratrol – The structure of cCTnC•resveratrol was calculated using restraints for cCTnC from the complex of cCTnC•EGCg because the CSPs induced by both ligands are quite similar. A similar data-driven protocol has been used for the cNTnC•W7 complex (*36*). Distance restraints for cCTnC were calibrated with CYANA (*54*) using an upper limit of 6 Å. Dihedral angle restraints from TALOS (*55*) were used as well as 12 distance restraints from X-ray crystallographic data of chelating oxygen atoms to the two Ca^{2+} ions. CYANA was used to calculate 100 structures of cCTnC, of which the 30 conformers with the lowest target function were used to further refine the structure with XPLOR-NIH. The restraints were converted from CYANA format into XPLOR-NIH format. The simulated annealing protocol of XPLOR-NIH, with 10 000 high temperature steps and 6000 cooling steps, was used in the structure calculation. The NOEs were averaged using the R-6 with a soft well potential. Spin-diffusion was a concern because the mixing times of 200 ms and 250 ms for the measurement of intermolecular NOEs were high. Therefore, only NOEs that had an NOE intensity≥μ-1/2σ were kept for the structure calculation, and all were calibrated with the same distance. A total of 23 intermolecular NOEs (6.0-1.8 Å) and four intramolecular NOEs (2.6-1.8 Å) were used in the structure calculation. 100 structures were calculated, from which the lowest 50 in energy were kept for refinement in explicit solvent with a water box edge length of 18.8

Å. It has been shown that refinement in explicit solvent including electrostatic potentials can improve the quality of structures (*56*). Atomic charges calculated by Gaussian03 for resveratrol (see above) were included at this point in the structure calculation. The final ensemble is represented by the 20 lowest energy structures after water refinement and was validated by Procheck (*57*) available with the online Protein Structure Validation Software (PSVS) suite (http://psvs-1_4-dev.nesg.org/); and the structural statistics are available in Table 3-1.

Results

Stability of Resveratrol

NMR chemical shift assignments of *trans*-resveratrol (resveratrol), or *trans*-resveratrol derivatives have been previously reported in acetone (*58*), chloroform (*59*), DMSO-d_6 (*60*), and in a DMSO-d_6/D_2O mixture (*61*). Resveratrol (Figure 3-1) in D_2O was assigned by one-dimensional ^1H, two-dimensional $^1H,^1H$-NOESY, and two-dimensional $^1H,^1H$-ROESY NMR experiments. The aromatic protons were assigned using three and four bond couplings. H2'/H6' were distinguished from H3'/H5' by the acquisition of a two-dimensional NOESY and ROESY experiments; only the H2'/H6' made ROE contacts with the ethylene protons (Hα and Hα'). The unambiguous assignments of Hα and Hα' were facilitated with previously published assignments for resveratrol (*58-61*). The ethylene protons had a vicinal coupling constant of 16.4 Hz; consistent with a *trans*-ethylene bond (*62*).

The stability of resveratrol has been addressed previously (*63*). The authors found that under acidic conditions, resveratrol was stable for at least 42 hours; while at pH 10, resveratrol had a half-life of 1.6 Hrs. Since three-dimensional NMR experiments require a stable sample for 2-3 days, and the samples are at neutral pH; the necessity of a reducing agent was investigated. The degradation of resveratrol was measured by acquiring

Table 3-1. Structural statistics for 20 NMR structures of cCTnC•resveratrol.

	Backbone	Heavy Atoms
R.m.s.d. from the average structure		
All residues (Å)	0.93 ± 0.14	1.42 ± 0.13
Ordered residues [a] (Å)	0.72 ± 0.11	1.21 ± 0.13
Total Distance Restraints	925	
Short range (|*i-j*|=1) NOEs	519	
Medium range (1<|*i-j*|<5) NOEs	201	
Long range (|*i-j*|≥5) NOEs	179	
Intermolecular NOEs	23	
Intramolecular NOEs	4	
Ca^{2+} distance restraints	12	
Dihedral restraints (ϕ/ψ)	106	
NOE violations per structure		
> 0.5 Å	0	
> 0.3 Å	0	
> 0.1 Å	2.15	
Dihedral Violations > 5º	0	
Ramachadran plot statistics [b]		
ϕ/ψ in most favored regions (%)	83.2 %	
ϕ/ψ in additionally allowed regions (%)	15.3 %	
ϕ/ψ generously allowed regions (%)	1.4 %	
ϕ/ψ in disallowed regions (%)	0.1 %	

[a] Residues 92-105,111-124,and 131-158

[b] For all residues as determined by PROCHECK

Figure 3-1. Stability of resveratrol. **a.** Chemical structure of resveratrol. Torsion angles that were allowed to rotate during structure calculations are indicated. **b.** Degradation of resveratrol as a function of time. One-dimensional ^{1}H-NMR spectra acquired every 1 hour (bottom, first spectrum; top, last spectrum). **c.** The spectrum of resveratrol in the presence of 10 mM TCEP. Bottom spectrum is at time=0 and the top spectrum is of resveratrol after 24 hours. The unlabeled peak downfield from Hα' is from [1]H-imidazole which exchanged with D_2O over time.

one-dimensional ^{1}H-NMR spectra at one hour time points. Significant degradation of resveratrol was observed, primarily in the di-*meta*-hydroxyl (di-*m*-OH) ring (Figure 3-1b), and a half-life of 5-6 hours was estimated by monitoring the chemical shift change of the H2/H6 proton pair (Figure 3-2). The sample also changed color from clear to brown over the course of the 24 hours. Next, 10 mM of TCEP was added to a sample of resveratrol and no significant degradation occurred after one day (Figure 3-1c). There was some decrease in peak intensities; however, there was no change in chemical shift or sample color; even after 72 hours.

Structure of Resveratrol in D_2O

In order to determine the structure of resveratrol in solution, two-dimensional ROESY spectra were acquired with different mixing times (50, 150, 200, and 300 ms); the ROE build-up curve is shown in Figure 3-3. Two slices from the ROESY spectrum (mixing time = 200 ms) are shown in Figure 3-4a. The H2'/H6' protons make much stronger ROEs with the ethylene protons than the H2/H6 protons do (Table 3-2). The strong ROE between H2'/H6' and Hα is only consistent with a coplanar orientation of the *para*-hydroxyl (*p*-OH) ring and olefin. On the other hand, weak, approximately uniform ROEs between the ethylene protons and H2/H6 is indicative of roughly equal distance between H2/H6 and Hα and Hα'; consistent with a tilted and/or flexible di-*m*-OH ring. The ensemble of the 10 lowest energy structures is shown in Figure 3-4b. The torsion angles formed by Cα'-Cα-C1-C6 and Cα-Cα'-C1'-C6' can be used to describe the orientations of the two phenolic rings with respect to the olefin. In Table 3-3 the torsion angles for a number of structures of resveratrol are indicated. The *p*-OH ring is coplanar (0.5 ± 0.3°) with the olefin, whereas the di-*m*-OH ring is tilted by 43.9 ± 0.4°. The structure of free resveratrol has also been solved by NMR spectroscopy in DMSO (*60*) and by X-ray crystallography (*64*); both structures revealed an overall planar structure. The X-ray structure of a trimethoxy-derivative of resveratrol was less
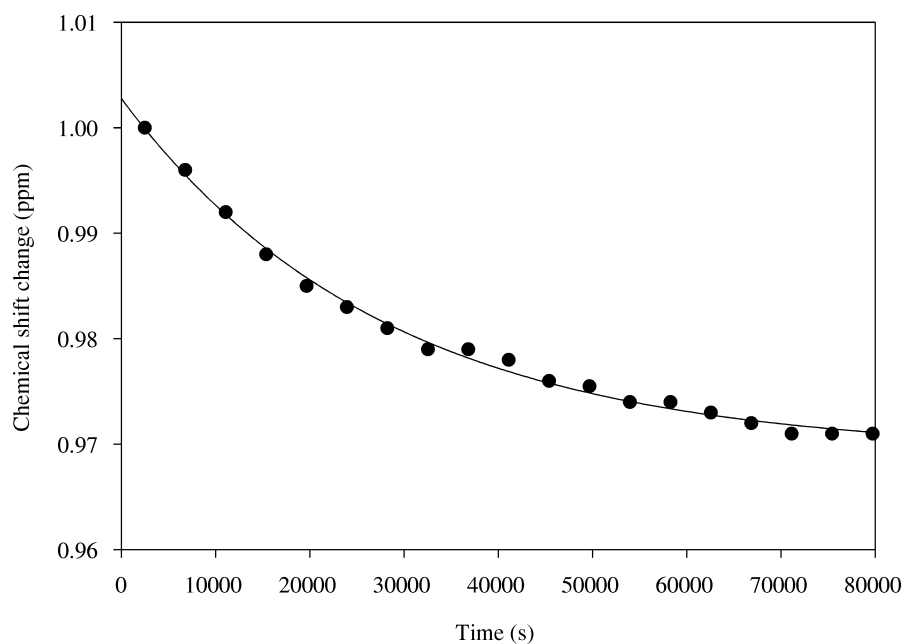
Figure 3-2. Oxidation rate of resveratrol determined by following the chemical shift change of H2/H6 over time. The initial starting chemical shift was normalized to one, and the chemical shift was measured at each time point. Since the H2/H6 is a doublet, the chemical shift from the further downfield peak of the doublet was measured.
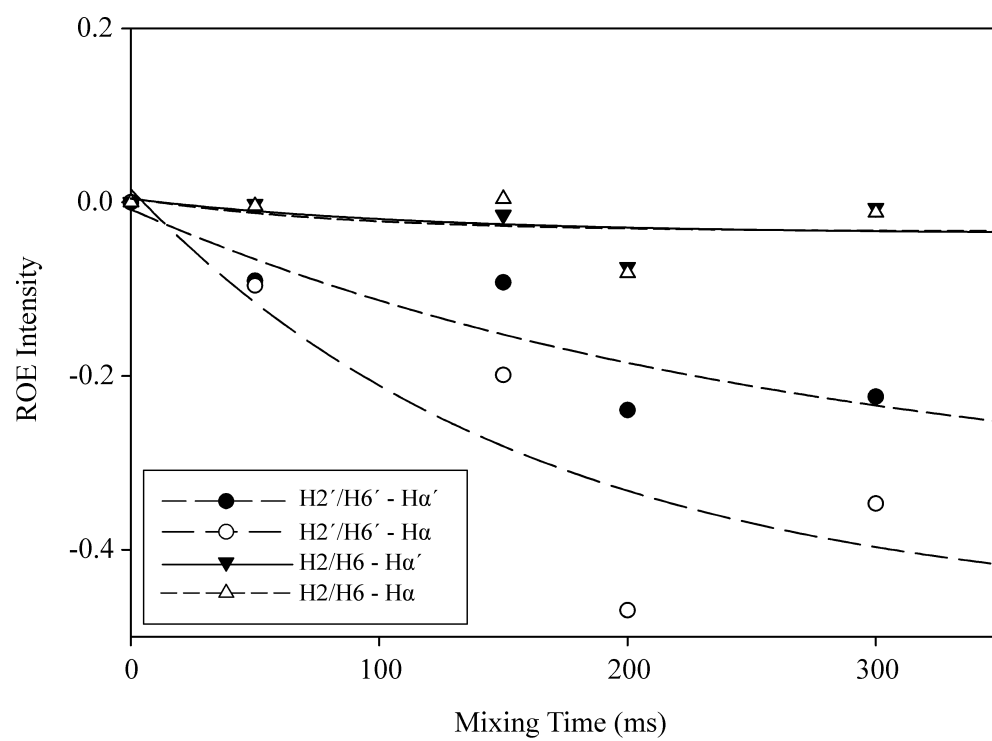
Figure 3-3. ROEs *versus* mixing time.

Table 3-2. Comparison of Relative ROE or NOE intensities.

Contact	Free resveratrol[a]	Bound Resveratrol
H2'/H6' - Hα'	0.51	0.67
H2'/H6' - Hα	1.00	0.84
H2/H6 – Hα	0.17	0.71
H2/H6 – Hα'	0.16	1.00

[a]At mixing time of 200 ms.

planar; particularly in respect to the orientation of the di-*m*-O-CH$_3$ ring (*65*). In the crystal structure of resveratrol, extensive hydrogen bonds contribute to the planarity of resveratrol, while the inability of 3,4',5-trimethoxystilbene to form intermolecular hydrogen bonds, resulted in a slight twist of the rings. It is possible that the presence of TCEP in the sample decreased the amount of intermolecular hydrogen bonding of resveratrol by perturbing stacking interactions, and may explain the somewhat tilted conformation of the di-*m*-OH ring. The lowest energy structure in the ensemble of resveratrol was used to calculate its electronic properties with the quantum chemistry program Gaussian03 (*51*) (Figure 3-4c).

Resveratrol binding to cTnC

To characterize resveratrol's interaction with troponin it was titrated into a sample containing ^{15}N-labeled cTnC. ^{1}H,^{15}N-HSQC NMR spectra were acquired throughout the titration and most of the large chemical shift perturbations (CSPs) were of backbone amides in the C-domain of cTnC (Figure 3-5). In addition, the residues that typically experience large perturbations upon cTnI or ligand binding to the N-domain (*4, 52*) such as Gly34, Gly42, Glu66, and Asp73 remained relatively unperturbed. The linear nature of the CSPs is indicative of a 1:1 stoichiometry for resveratrol binding to cTnC. Multiple binding would lead to non-linear CSPs, as was observed for TFP and bepridil binding to cTnC (*9*). Using the program xcrvfit, the CSPs of the backbone amides of Thr124, Gly125, Ile128, Thr129, Gly140, Gly159, and Glu161 were plotted as a function of resveratrol-to-cTnC concentration; a global dissociation constant (K_D) of 243 μM (SSE = 0.02) was determined (Figure 3-5b).

Resveratrol binding to cCTnC

To test whether the interaction between resveratrol and cTnC was the same as in the isolated C-domain, resveratrol was titrated into cCTnC.
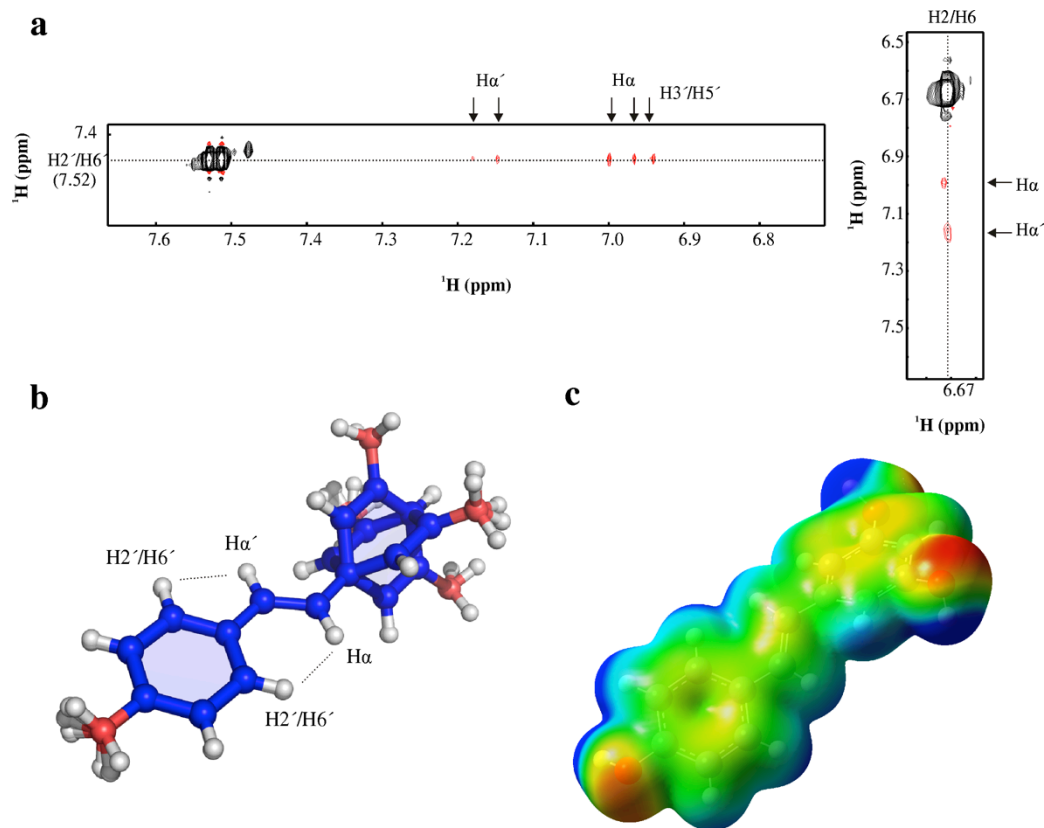
Figure 3-4. Structure of resveratrol. **a.** Two-dimensional-ROESY spectrum of resveratrol in D_2O. **b.** Ensemble of resveratrol aligned to the olefin atoms: Hα', Cα', Hα, and Cα. ROEs measured between H2'/H6' and Hα and Hα' are drawn on the structure to illustrate that the intensity of the ROE between H2'/H6' and Hα requires a planar orientation of phenol ring. **c.** Gaussian calculation from lowest energy structure of resveratrol. The electrostatic potential of resveratrol was mapped with an isovalue of 0.004 e/Å^3 (-7e^{-2} eV, red; 7e^{2+} eV, blue).
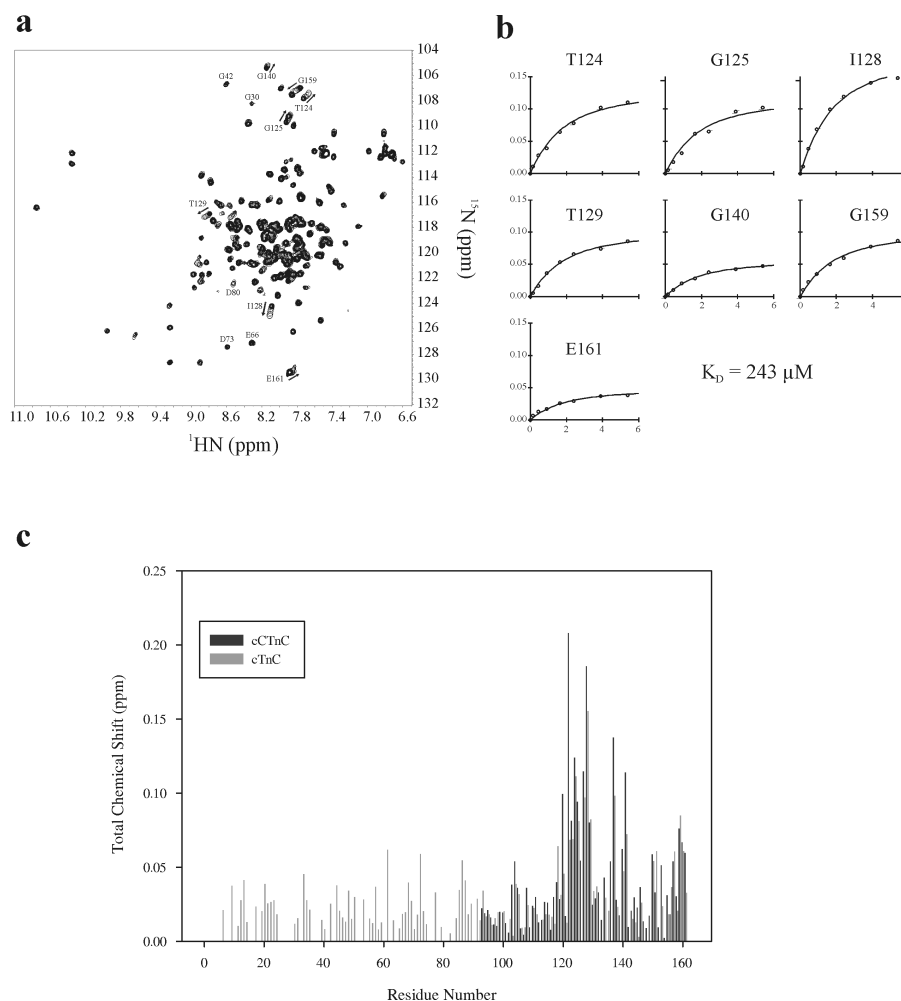
Figure 3-5. Binding of resveratrol to cTnC. **a.** ^{1}H,^{15}N-HSQC spectra of cCTnC acquired throughout the titration with resveratrol. The first point in the titration is represented with 20 contours; whereas, each titration point with resveratrol is represented by a single contour (O). Direction of CSPs are indicated by arrows for several peaks. **b.** fitting of ^{1}H,^{15}N-HSQC with xcrvfit to determine the dissociation constant. **c.** Bar graph of the total chemical shift change ($\Delta\delta = \sqrt{(\Delta\delta_H)^2 + \frac{1}{25}(\Delta\delta_N)^2}$) versus residue number for the titration of resveratrol into cTnC (light grey) and cCTnC (dark grey).

Two-dimensional ^{1}H,^{13}C and ^{1}H,^{15}N HSQC experiments were used to monitor the titration of resveratrol into a sample containing cCTnC (Figure 3-6a and 3-6b). The ^{1}H,^{13}C-HSQC (without resveratrol) was assigned using chemical shift assignments deposited for cTnC (1). Since resveratrol interacts with cCTnC in fast exchange, most assigned resonances could be easily followed throughout the titration. Global dissociation constants of 240 µM (SSE = 0.08); from the backbone amides, and 301 µM (SSE = 0.02); from the methyl groups of cCTnC were calculated (Figure 3-6). The residue specific CSPs are almost identical in both pattern and amplitude between the titrations of resveratrol to cCTnC and cTnC (Figure 3-5c). The comparable dissociation constants and CSP patterns suggest that resveratrol interacts with cCTnC the same as it does with full-length cTnC.

Following determination of the affinity and stoichiometry of resveratrol binding to cCTnC, a j-surface mapping was executed to predict resveratrol's binding location on cCTnC. J-surface mapping works to predict a binding site by assuming that the ring current from an aromatic constituent of a ligand is the primary source of ligand-induced CSPs (53). Typically, amide protons are used in the calculation; however, it is well established that cTnC undergoes a large conformational change upon ligand binding. Thus, most of the backbone CSPs are indicative of a global change in its structure rather than direct contact with a given ligand (66). In order to circumvent this difficulty, the CSPs of methyl protons were used in the j-surface calculation – as changes in these chemical shifts are more likely indicative of direct interactions with resveratrol. Methyl resonances used in the calculation were those that underwent ≥ |0.012| ppm in the proton dimension. These included: Ile112, Met120, Leu121, Ala123, Ile128, Ile148, Met157, and Val160. The structure of cTnC (pdb: 1aj4) (1) was used in the j-surface calculation, and the results localize the binding of resveratrol to the cleft formed by the four helices of cCTnC (Figure 3-7). There appears to be two j-surfaces: one near the surface of cCTnC and the other deeper in the core. Because the j-surface calculation is unable to
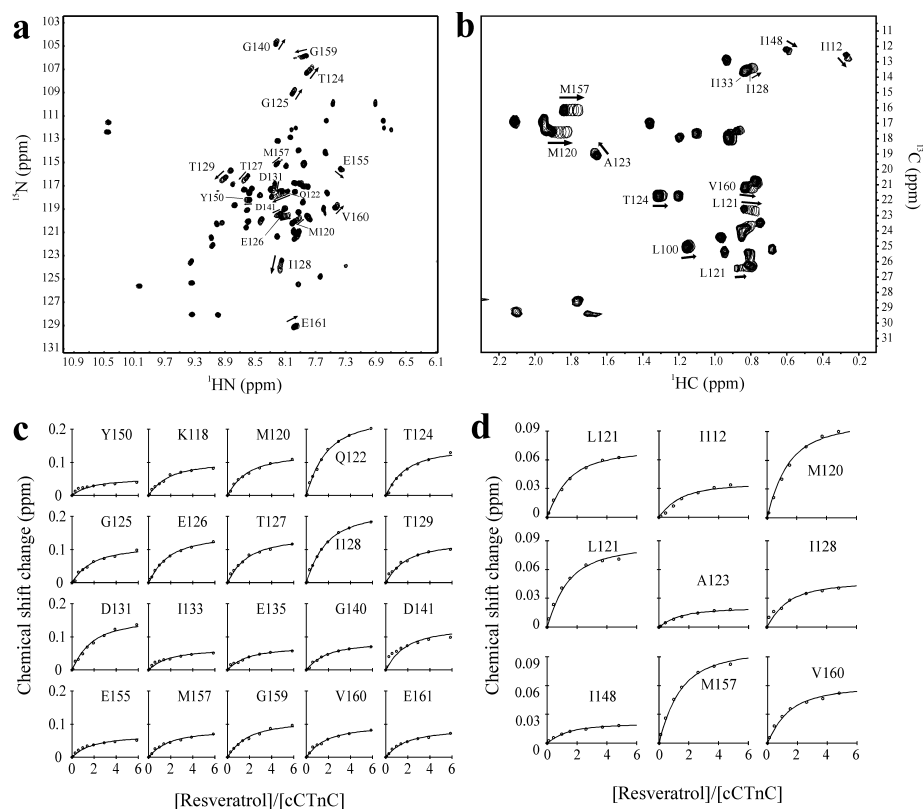
Figure 3-6. Binding of resveratrol to cCTnC. **a.** ^{1}H,^{15}N-HSQC and **b.** ^{1}H,^{13}C-HSQC (methyl-region) spectra of cCTnC acquired throughout the titration with resveratrol. The first point in the titration is represented with all 20 contours, whereas each titration point with resveratrol is represented by a single contour. Direction of CSPs are indicated by arrows for several peaks. **c.** fitting of ^{1}H,^{15}N-HSQC and **d.** ^{1}H,^{13}C-HSQC NMR data with xcrvfit to determine the dissociation constant.

120
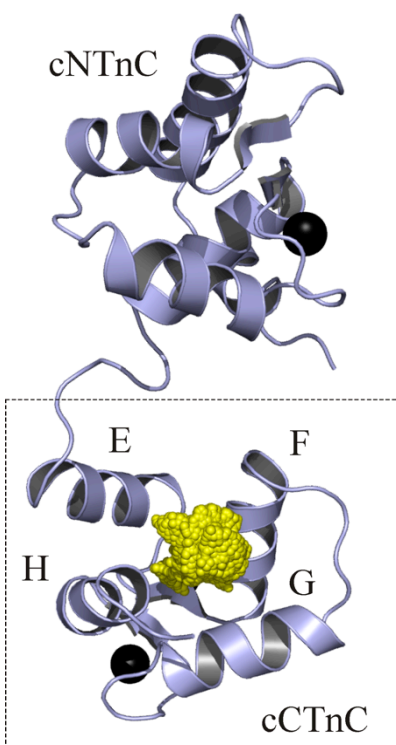
Figure 3-7. J-surface representation of resveratrol bound to cTnC. Results are mapped on the structure of cTnC (pdb: 1aj4). The backbone atoms are depicted in cartoon representation (light blue), Ca^{2+} ions are represented by black spheres, and the j-surface dot density is depicted using yellow spheres. Residues used in the j-surface calculation were: Leu121, Val160, Ala123, Ile148, Ile128, Met157, Met120, and Ile112.

identify the specific pose resveratrol adopts when bound to cCTnC, NMR spectroscopy was used to identify intermolecular contacts between resveratrol and cCTnC.

Structure of cCTnC•resveratrol complex

The structure of cCTnC free or in complex with a number of binding partners has been solved by both X-ray crystallography and NMR spectroscopy (*1, 2, 14, 19, 67-69*). Instead of determining the structure of cCTnC again, a data-driven docking approach was pursued. The ^{1}H,^{15}N-HSQC CSPs induced by resveratrol were compared with those induced by ligands that interact with cCTnC: cTnI$_{34-71}$, EMD 57033, and EGCg (Figure 3-8). The CSPs are most similar between resveratrol and EGCg (in both magnitude and pattern); hence the intramolecular NOEs and dihedrals restraints of cCTnC used in the structure calculation were taken from the cCTnC•EGCg complex (*19*). The only new restraints used in the structure calculation were those that defined the structure and pose of resveratrol in complex with cCTnC.

Intermolecular NOEs were measured between cCTnC and resveratrol with ^{13}C,^{15}N-edited/filtered NOESY experiments. These experiments measure solely NOEs between a ^{13}C/^{15}N-labeled molecule and an unlabeled molecule. Two-dimensional ^{13}C,^{15}N- filtered/edited NOESYHSQC (*42*) experiments were acquired with 150, 200, and 250 ms mixing times to establish the optimal mixing times to acquire the three-dimensional experiments. Since most of the intermolecular contacts observed were between methyl groups from cCTnC and the aromatic ring protons of resveratrol, the three-dimensional ^{13}C-edited/filtered HMQCNOESY experiment (*43, 44*) was acquired. This NMR experiment is optimized for the identification of intermolecular NOEs involving ^{13}C-methyls (*44*). Two three-dimensional ^{13}C-edited/filtered HMQCNOESY experiments were acquired: one with a mixing time of 250 ms and one with a mixing time of 200 ms. Intermolecular NOEs that had intensities ≥
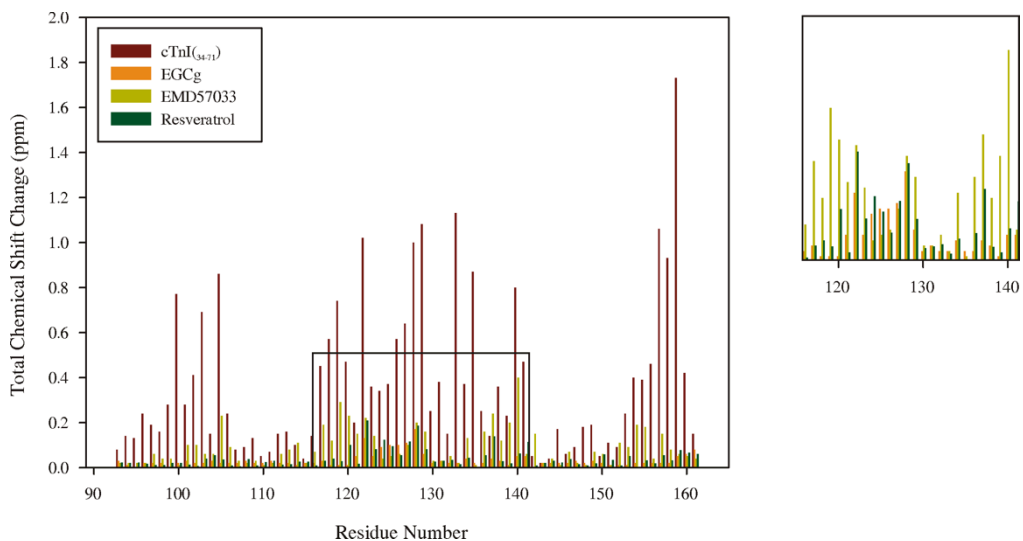
Figure 3-8. Ligand dependant chemical shift perturbations of cCTnC. Bar graph of the total chemical shift change ($\Delta\delta = \sqrt{(\Delta\delta_H)^2 + \frac{1}{25}(\Delta\delta_N)^2}$) *versus* residue number for the titration of cTnI$_{34\text{-}71}$ (red), EGCg (orange), EMD 57033 (yellow), and resveratrol (green) into cCTnC. Chart on the right is an expansion of the bar chart; cTnI$_{34\text{-}71}$ CSPs have been removed for clarity.

0.04 were included in the structure calculation. This is because of the long experimental mixing times of the intermolecular NOESY experiments and the tightly coupled nature of resveratrol increased the possibility of spin diffusion. When all NOEs were included in the structure run, many violations occurred, presumably because of spin diffusion. The intermolecular NOEs from a mixing time of 200 ms, used in the structure calculation are shown in Figure 3-9a. Initially, a structure calculation followed as was done for the EGCg calculation. The quality of the structure was subsequently improved by running a structure refinement in water; at this stage electrostatic potentials and atomic charges were included (*56*). The 20 lowest energy structures of the complex are shown in Figure 3-9b and c. The structure indicates that, congruent with the prediction by j-surface mapping, resveratrol is localized to the hydrophobic pocket of cCTnC. The resveratrol-cCTnC interaction site is populated primarily by non-polar contacts. Resveratrol contacts the side chains of Leu100, Leu117, Leu121, Thr124, Leu136, Met157, and Val160 (figure 5d). Weak NOEs between resveratrol and Ile148 and Ile112 (both β-sheet residues) – not used in the structure run because they did not meet the intensity cut-off criteria – were also consistent with the final structure. In addition to the methyl-resveratrol contacts, the structure indicates that arene-arene contacts made between resveratrol and Phe104, Phe153, and Phe156 contribute to the binding energy of resveratrol.

In addition to measuring intermolecular NOEs between resveratrol and cCTnC to determine their relative positions, the conformation of bound resveratrol was also determined. The intramolecular NOEs of resveratrol were measured with the ^{13}C,^{15}N-filtered NOESY experiment (*40, 41*), which works by removing signals from a ^{13}C,^{15}N-labeled molecule, keeping only signals from an unlabeled molecule. All structure-defining intramolecular NOEs were close to the same intensity, with the strongest being the H2/H6-Hα' contact (see Table 3-2 and Figure 3-10). This is in contrast with free resveratrol, where the strongest ROE was between
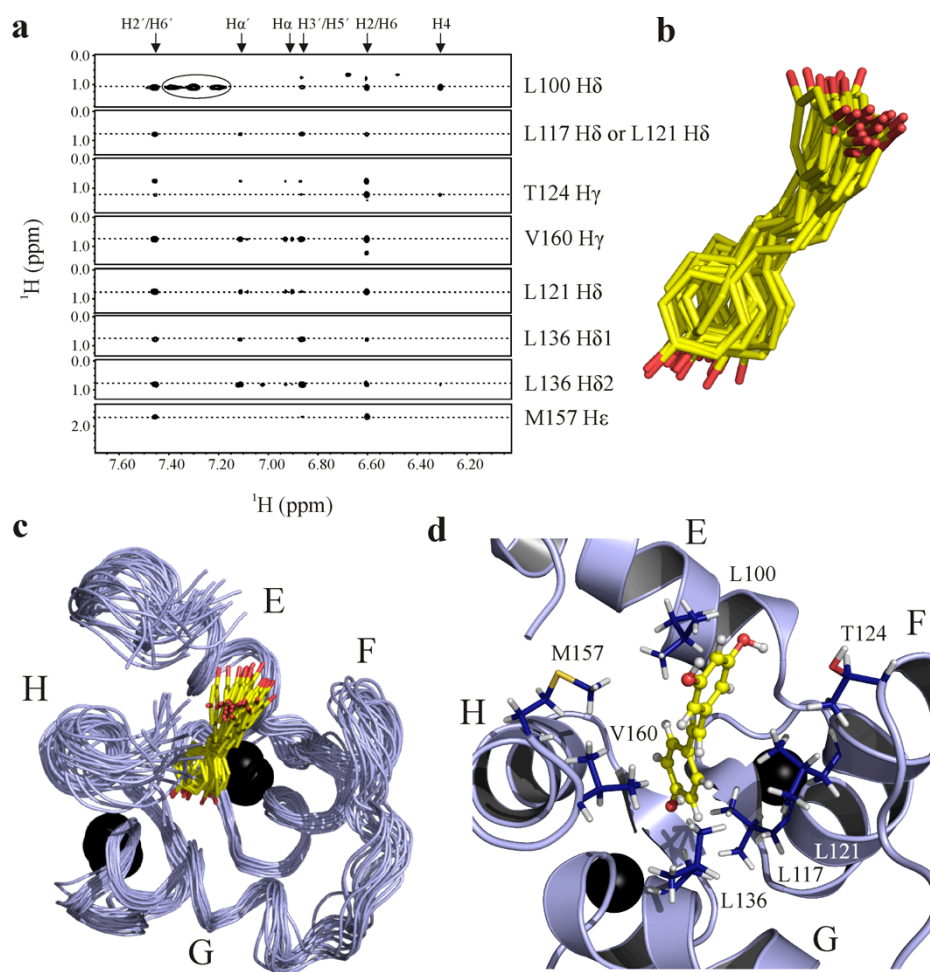
Figure 3-9. Structure of the binary complex of cCTnC•resveratrol. **a.** Strip plots showing the NOEs between resveratrol and cCTnC. The resveratrol assignments are at the top of the spectrum; cCTnC assignments are indicated on the right. Peaks that are circled represent intramolecular cCTnC NOEs that were not adequately filtered. **b.** Ensemble of resveratrol from the binary complex. The carbon atoms are shown in yellow and the oxygen atoms in red. **c.** 20 lowest energy structures of the cCTnC•resveratrol complex with the backbone trace of cCTnC in light blue; helices E to H are labeled. **d.** Resveratrol's binding pocket on the lowest energy structure of cCTnC. Residues for which NOEs were measured are labeled and depicted in stick representation with carbon atoms colored in dark blue; resveratrol is shown in ball-and-stick representation (hydrogen atoms in white). Calcium ions are shown as black spheres.
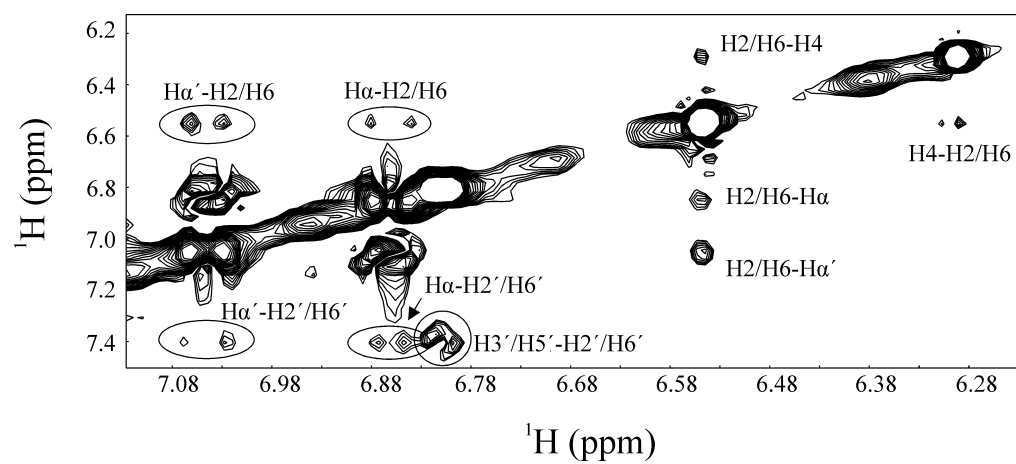
Figure 3-10. Intramolecular NOEs of resveratrol in complex with cCTnC.

H2'/H6' and Hα; and suggests that resveratrol undergoes a slight conformational change upon binding cCTnC. In order to limit biasing the structure of resveratrol during the calculation, one distance (2.6-1.8 Å) for the four intramolecular contacts was used; and the final structure was checked against the raw NOE data. Indeed, the results are consistent with the relative NOE intensities: the closest proton pair was the H2/H6-Hα' proton pair (2.24 ± 0.14 Å). The other distances are: H2/H6-Hα; 2.57 ± 0.05 Å, H2'/H6'-Hα'; 2.28 ± 0.06 Å, and H2'/H6'-Hα; 2.32 ± 0.07 Å. The torsion angles were measured for resveratrol when in complex with cCTnC and were compared to those determined for free resveratrol. The *p*-OH ring is more twisted than what was observed for free resveratrol (from 0.5 ± 0.3° to 18.6 ± 10.6°), whereas the torsion angle of the di-*m*-OH ring is not significantly different (from 43.9 ± 0.4° to 35.2 ± 8.7°).

There have been a number of crystal structures of resveratrol in complex with proteins solved, including: alfalfa chalcone synthase (CHS) (*70*), the fibril-forming transthyretin (TTR) (*71*), a variant of alfalfa CHS (*72*), quinone reductase 2 (QR2) (*73*), peanut stilbene synthase (STS) (*74*), bovine F1-ATPase (*75*), Leukotriene A4 hydrolase (*76*), and human cytosolic sulfotransferase (not published; but deposited in the PDB with the ID: 3ckl). In most of these structures resveratrol is planar or slightly distorted from a planar conformation with torsion angles no greater than 45°; the only exception is in the peanut STS-resveratrol complex, where both rings of resveratrol are twisted > 60° (*74*) (see Table 3-3). These results, in conjunction with the structures free resveratrol and resveratrol derivatives, point to a relatively rigid resveratrol framework. In accordance with the X-ray and NMR structures, Caruso *et al.* calculated single-point energy versus the torsion angle of the *p*-OH ring, and found the lowest energy structure is a planar conformation (*64*).

The structure of cCTnC in the cCTnC•resveratrol complex is not much different than that of cCTnC in other complexes. The Cα from residues in secondary structure elements of cCTnC•resveratrol were

Table 3-3. Comparison of resveratrol ring orientation with other structures. Ring twist illustrates the orientation of the ring with comparison to the central olefin of resveratrol. The p-OH ring twist is the Cα-Cα'-C1'-C6' torsion angle; the di-m-OH ring twist is the Cα'-Cα-C1-C6 torsion angle. For the NMR structures, both positive and negative torsions were measured so they are reported in absolute degrees. Multiple values are given when more than one resveratrol is present in the X-ray structures.

Structure	p-OH ring twist (°)	di-m-OH ring twist (°)
X-ray structure of resveratrol (64)	8.02	-2.98
X-ray structure of 3,5,4'-Trimethoxystilbene (65)	3.53/-9.16	21.13/-16.32
NMR structure of resveratrol (D$_2$O) [a]	0.5 ± 0.3	43.9 ± 0.4
NMR structure of cCTnC [a]	18.6 ± 10.6	35.2 ± 8.7
X-ray structure of Chalcone Synthase (pdb: 1CGZ)(70)	-9.21	-32.00
X-ray structure of Transthyretin (pdb: 1DVS)(71)	0.7/1.06	0.55/1.13
X-ray structure of Quinone Reductase 2 (pdb: 1SG0)(73)	0.23/0.23	3.11/2.15
X-ray structure of mutant Chalcone Synthase (pdb: 1U0W)(72)	-0.16/-2.98	0.18/-1.49
X-ray structure of Stilbene Synthase (pdb: 1Z1F)(74)	62.92	-66.97
X-ray structure of Cytosolic Sulfotransferase (pdb: 3CKL)	19.84/20.51	5.80/19.16
X-ray structure of Leukotriene A4 Hydrolase (pdb: 3FTS)(76)	-27.28	-17.65
X-ray structure of F$_1$-ATPase (pdb: 1JIZ)(75)[b]	27.68/19.90/-35.06/42.25	-9.25/7.60/45.69/-21.39

[a] This study.

[b] The authors could not distinguish between two binding modes, and therefore concluded that resveratrol may bind to F$_1$-ATPase in multiple poses.

128

superimposed with cCTnC (pdb: 3ctn), cCTnC•EMD57033 (pdb: 1ih0), cCTnC•EGCg (pdb: 2kdh), and cCTnC•cTnI$_{34-71}$ (pdb: 1j2d) and rmsds of: 1.17 Å, 1.50 Å, 1.02 Å, and 1.26 Å were determined, respectively. These values indicate that resveratrol does not significantly perturb the structure of cCTnC. The E-helix of cCTnC•resveratrol is shifted away from the hydrophobic cleft, similar to the cCTnC•EMD5033 complex. The position of the F-helix of cCTnC•resveratrol is in almost an identical position as in the cCTnC•EGCg and cCTnC•cTnI$_{34-71}$ complexes; however, is shifted further away from the E-helix of cCTnC and not as far away as in the cCTnC•EMD57033 structure.

Discussion

The regulatory role of the Ca^{2+}-dependant interaction between cTnI$_{147-163}$ and cNTnC is well established, and has been the interaction site primarily concentrated on for the development of Ca^{2+}-sensitizers (*77, 78*). However, the exclusive development of drugs that target cNTnC has been scrutinized as growing evidence indicates that cCTnC is also involved in contraction regulation. The dilated cardiomyopathy mutation of cCTnC, Gly159Asp, decreases myofilament Ca^{2+}-sensitivity (*79*) *via* its modulation of the cTnI$_{34-71}$-cCTnC interaction (*67*). The hypertrophic cardiomyopathy mutation, Asp145Glu, increases Ca^{2+}-sensitivity (*80*), presumably by decreasing Ca^{2+} and cTnI binding to cCTnC (*81*). The ablation of the Ca^{2+}-binding ability of the C-domain of cTnC increases the Ca^{2+}-sensitivity of muscle contraction (*82*). There are two isoforms of TnC in insect flight muscle: the F1 isoform, which regulates stretch-activated force, and the F2 isoform which is responsible for Ca^{2+}-activated contraction. Although it is not clear how F1 regulates stretch-activation, the interaction between the C-domain of F1 and TnH (an ortholog of cTnI) may play a role in regulation of stretch-activation (*83*). Finally, as previously mentioned, the

cardiotonic agents EMD 57033 (*15, 84*) and EGCg (*17, 18*) target cCTnC to modulate heart muscle contractility.

In this study, resveratrol was found to interact with the C-domain of cTnC, and the structure was determined by NMR spectroscopy. The *p*-OH group of resveratrol lies in the hydrophobic core of cCTnC, whereas the di-*m*-OH ring points towards the exterior of the protein. The stabilizing contacts between resveratrol and cCTnC are predominantly hydrophobic. In the other resveratrol-protein complexes, the binding site of resveratrol is also dominated by hydrophobic interactions; however, unlike the cCTnC•resveratrol structure, hydrogen bonds between the hydroxyls of resveratrol and the amino acids that line the binding pockets also contribute to the binding energy (*70-76*). The design of resveratrol with the *p*-OH converted to a hydrophobic constituent may therefore increase its affinity for cCTnC; for example, converting the hydroxyl to a fluorine atom would increase the lipophilicity of resveratrol without dramatically decreasing its size (*85, 86*). On the other hand, removing the *p*-OH would undoubtedly reduce the antioxidant ability of resveratrol, especially given that the *p*-OH has been implicated as being the principal hydroxyl responsible for resveratrol's antioxidant nature (*64, 87-89*).

The comparison of the cCTnC•resveratrol structure with the structures of cCTnC•EMD57033 and cCTnC•EGCg yields insights into several key functional groups. In the structure, the *p*-OH aromatic ring of resveratrol is positioned in a similar manner as the thiadiazinone ring of EMD 57033 – with the *para* hydroxyl pointed towards the cleft formed by helices G and H. The di-*m*-OH ring of resveratrol faces away from the hydrophobic cavity of cCTnC – much like the benzendiol of EGCg – which leaves its hydroxyl moieties free to hydrogen bond with the surrounding aqueous milieu. Therefore, the binding pose of resveratrol has features that uniquely resemble the structures of EGCg and EMD 57033 when bound to cCTnC. Resveratrol, EMD 57033, and EGCg all share their binding sites with the natural binding partner of cCTnC, $cTnI_{34-71}$ (Figure 3-
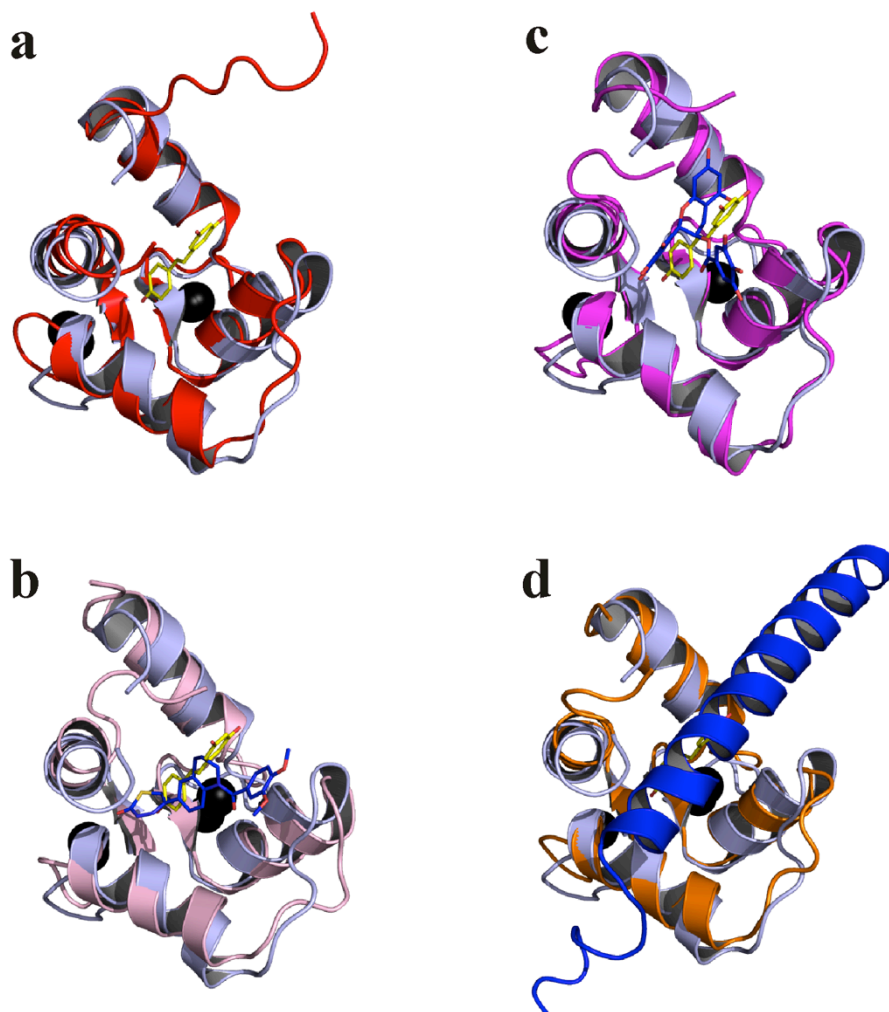
Figure 3-11. Structure comparisons. Superimposition between cCTnC•resveratrol (light blue) and **a.** cCTnC (red; pdb: 3ctn), **b.** cCTnC•EMD 57033 (pink; pdb: 1ih0), **c.** cCTnC•EGCg (magenta; pdb: 2kdh), and **d.** cCTnC•cTnI$_{34-71}$ (orange; pdb: 1j1d). The carbon atoms for resveratrol are colored in yellow, and the oxygen atoms are colored in red. For the other structures, ligand carbon atoms are colored in blue, oxygen atoms in red, nitrogen atoms in dark blue, and sulfur atoms in yellow. Ca^{2+} ions are shown as black spheres.

11), and as a result, may have a common mode of action. The troponin-dependant Ca^{2+}-sensitizing ability of EMD 57033 has been suggested to involve a competition between EMD 57033 and $cTnI_{34-71}$ for cCTnC (*90*). The perturbation of the $cTnI_{34-71}$-cCTnC interaction may lead to an increase in the affinity of $cTnI_{128-147}$ for cTnC and thus a decrease in contraction inhibition.

It was determined that resveratrol bound to cTnC and cCTnC with micromolar affinity. This relatively low affinity of resveratrol for cTnC was anticipated, since too high an affinity would lead to a marked increase in Ca^{2+}-sensitivity. This dramatic increase in Ca^{2+}-sensitivity over the long-term could lead to negative effects, such as hypertrophic cardiomyopathy. On the other hand, it may be useful to optimize the resveratrol-cCTnC interaction for the development of drugs to treat acute heart failure. One method for the analysis of whether a small molecule represents a good lead molecule is to determine its ligand efficiency (LE) (*91-93*). LE is described by the ratio of free energy of binding over the number of heavy atoms in a compound, and is based on the premise that as a drug is optimized, it often increases in molecular weight; a trend fraught with problems including a decrease in bioavailability through insolubility and membrane permeability (*94*).

The free energy (ΔG) of binding is:

$$\Delta G = -RT \ln K_D$$

and the ligand efficiency (binding energy per non-hydrogen atom) (LE) is:

$$LE = \Delta G / N$$

For resveratrol binding to cCTnC, a K_D of 240 µM has a binding energy of 4.97 kcal/mol. Resveratrol has 17 non-hydrogen atoms (14 carbon atoms and 3 oxygen atoms), so its ligand efficiency is 0.29 kcal/mol. This ligand

efficiency corresponds to a compound with 33 non-hydrogen atoms (approximately 2x the size of resveratrol: 450 MW) with a binding constant of 0.1 μM. The reasonably good ligand efficiency of resveratrol, suggests that the substitution or addition of a few atoms that enhance its affinity for cCTnC may lead toward novel therapies for the treatment of heart failure.

Conclusion

Resveratrol is a natural product found in wine that modulates the Ca^{2+}-sensitivity of myofilaments (*31*). In this study, the structure of resveratrol in complex with the cardiac regulatory protein troponin C was determined by NMR spectroscopy. Consistent with the small molecules EGCg and EMD 57033, resveratrol targeted the C-domain of troponin C. The binding of resveratrol is primarily stabilized by hydrophobic contacts such as methyl-arene and arene-arene interactions. In addition to providing clues into the cardioprotective nature of resveratrol, the structure highlights several functional groups that could be modified to optimize the binding efficacy of resveratrol. Recently, the polyphenol, propyl gallate, has also been identified to act as a Ca^{2+}-sensitizer as well (*95*); which alongside the functional and structural data for EGCg and resveratrol, points towards a common mechanism by which these natural compounds target the thin filament to protect against heart failure.

References

1. Sia, S. K., Li, M. X., Spyracopoulos, L., Gagne, S. M., Liu, W., Putkey, J. A., and Sykes, B. D. (1997) Structure of cardiac muscle troponin C unexpectedly reveals a closed regulatory domain, *J. Biol. Chem. 272*, 18216-18221.
2. Takeda, S., Yamashita, A., Maeda, K., and Maeda, Y. (2003) Structure of the core domain of human cardiac troponin in the Ca(2+)-saturated form, *Nature 424*, 35-41.
3. Spyracopoulos, L., Li, M. X., Sia, S. K., Gagne, S. M., Chandra, M., Solaro, R. J., and Sykes, B. D. (1997) Calcium-induced structural transition in the regulatory domain of human cardiac troponin C, *Biochemistry 36*, 12138-12146.
4. Li, M. X., Spyracopoulos, L., and Sykes, B. D. (1999) Binding of cardiac troponin-I147-163 induces a structural opening in human cardiac troponin-C, *Biochemistry 38*, 8289-8298.
5. Tripet, B., Van Eyk, J. E., and Hodges, R. S. (1997) Mapping of a second actin-tropomyosin and a second troponin C binding site within the C terminus of troponin I, and their importance in the Ca2+-dependent regulation of muscle contraction, *J. Mol. Biol. 271*, 728-750.
6. Li, M. X., Wang, X., and Sykes, B. D. (2004) Structural based insights into the role of troponin in cardiac muscle pathophysiology, *J. Muscle Res. Cell Motil. 25*, 559-579.
7. Kobayashi, T., Jin, L., and de Tombe, P. P. (2008) Cardiac thin filament regulation, *Pflugers Archiv-European Journal of Physiology 457*, 37-46.
8. Endoh, M. (2001) Mechanism of action of Ca2+ sensitizers--update 2001, *Cardiovasc. Drugs Ther. 15*, 397-403.
9. Kleerekoper, Q., Liu, W., Choi, D., and Putkey, J. A. (1998) Identification of binding sites for bepridil and trifluoperazine on cardiac troponin C, *J. Biol. Chem. 273*, 8153-8160.
10. Li, Y., Love, M. L., Putkey, J. A., and Cohen, C. (2000) Bepridil opens the regulatory N-terminal lobe of cardiac troponin C, *Proc. Natl. Acad. Sci. U. S. A. 97*, 5140-5145.
11. Haikala, H., Kaivola, J., Nissinen, E., Wall, P., Levijoki, J., and Linden, I. B. (1995) Cardiac Troponin-C as a Target Protein for a Novel Calcium Sensitizing Drug, Levosimendan, *J. Mol. Cell. Cardiol. 27*, 1859-1866.
12. Haikala, H., Nissinen, E., Etemadzadeh, E., Levijoki, J., and Linden, I. B. (1995) Troponin C-Mediated Calcium Sensitization Induced by Levosimendan Does Not Impair Relaxation, *J. Cardiovasc. Pharmacol. 25*, 794-801.
13. Haikala, H., Nissinen, E., Etemadzadeh, E., Linden, I. B., and Pohto, P. (1992) Levosimendan Increases Calcium Sensitivity

without Enhancing Myosin Atpase Activity and Impairing Relaxation, *J. Mol. Cell. Cardiol. 24*, S97-S97.

14.   Wang, X., Li, M. X., Spyracopoulos, L., Beier, N., Chandra, M., Solaro, R. J., and Sykes, B. D. (2001) Structure of the C-domain of human cardiac troponin C in complex with the Ca2+ sensitizing drug EMD 57033, *J. Biol. Chem. 276*, 25456-25466.

15.   Pan, B. S., and Johnson, R. G. (1996) Interaction of cardiotonic thiadiazinone derivatives with cardiac troponin C, *J. Biol. Chem. 271*, 817-823.

16.   Kleerekoper, Q., and Putkey, J. A. (1999) Drug binding to cardiac troponin C, *J. Biol. Chem. 274*, 23932-23939.

17.   Liou, Y. M., Kuo, S. C., and Hsieh, S. R. (2008) Differential effects of a green tea-derived polyphenol (-)-epigallocatechin-3-gallate on the acidosis-induced decrease in the Ca(2+) sensitivity of cardiac and skeletal muscle, *Pflugers Arch. 456*, 787-800.

18.   Tadano, N., Du, C. K., Yumoto, F., Morimoto, S., Ohta, M., Xie, M. F., Nagata, K., Zhan, D. Y., Lu, Q. W., Miwa, Y., Takahashi-Yanaga, F., Tanokura, M., Ohtsuki, I., and Sasaguri, T. (2010) Biological actions of green tea catechins on cardiac troponin C, *Br. J. Pharmacol. 161*, 1034-1043.

19.   Robertson, I. M., Li, M. X., and Sykes, B. D. (2009) Solution Structure of Human Cardiac Troponin C in Complex with the Green Tea Polyphenol, (-)-Epigallocatechin 3-Gallate, *J. Biol. Chem. 284*, 23012-23023.

20.   Renaud, S., and Delorgeril, M. (1992) Wine, Alcohol, Platelets, and the French Paradox for Coronary Heart-Disease, *Lancet 339*, 1523-1526.

21.   Langcake, P., and Pryce, R. J. (1976) Production of Resveratrol by Vitis-Vinifera and Other Members of Vitaceae as a Response to Infection or Injury, *Physiol. Plant Pathol. 9*, 77-86.

22.   Siemann, E. H., and Creasy, L. L. (1992) Concentration of the Phytoalexin Resveratrol in Wine, *Am. J. Enol. Vitic. 43*, 49-52.

23.   Das, D. K., Mukherjee, S., and Ray, D. (2010) Resveratrol and red wine, healthy heart and longevity, *Heart Failure Reviews 15*, 467-477.

24.   Lekli, I., Ray, D., and Das, D. K. (2010) Longevity nutrients resveratrol, wines and grapes, *Genes and Nutrition 5*, 55-60.

25.   Nichols, J. A., and Katiyar, S. K. (2010) Skin photoprotection by natural polyphenols: anti-inflammatory, antioxidant and DNA repair mechanisms, *Archives of Dermatological Research 302*, 71-83.

26.   Sun, A. Y., Wang, Q., Simonyi, A., and Sun, G. Y. (2010) Resveratrol as a Therapeutic Agent for Neurodegenerative Diseases, *Molecular Neurobiology 41*, 375-383.

27.   Jang, M. S., Cai, E. N., Udeani, G. O., Slowing, K. V., Thomas, C. F., Beecher, C. W. W., Fong, H. H. S., Farnsworth, N. R., Kinghorn, A. D., Mehta, R. G., Moon, R. C., and Pezzuto, J. M. (1997) Cancer

chemopreventive activity of resveratrol, a natural product derived from grapes, *Science 275*, 218-220.

28. Holme, A. L., and Pervaiz, S. (2007) Resveratrol in cell fate decisions, *J. Bioenerg. Biomembr. 39*, 59-63.

29. Das, D. K., and Maulik, N. (2006) Red wine and heart: A cardioprotective journey from grape to resveratrol, *Alcoholism-Clinical and Experimental Research 30*, 84a-84a.

30. Ray, P. S., Maulik, G., Cordis, G. A., Bertelli, A. A. E., Bertelli, A., and Das, D. K. (1999) The red wine antioxidant resveratrol protects isolated rat hearts from ischemia reperfusion injury, *Free Radical Biology and Medicine 27*, 160-169.

31. Liew, R., Stagg, M. A., MacLeod, K. T., and Collins, P. (2005) The red wine polyphenol, resveratrol, exerts acute direct actions on guinea-pig ventricular myocytes, *Eur. J. Pharmacol. 519*, 1-8.

32. Bertini, I., Fragai, M., Giachetti, A., Luchinat, C., Maletta, M., Parigi, G., and Yeo, K. J. (2005) Combining in silico tools and NMR data to validate protein-ligand structural models: Application to matrix metalloproteinases, *J. Med. Chem. 48*, 7544-7559.

33. Cioffi, M., Hunter, C. A., Packer, M. J., and Spitaleri, A. (2008) Determination of protein-ligand binding modes using complexation-induced changes in H-1 NMR chemical shift, *J. Med. Chem. 51*, 2512-2517.

34. Krishnamoorthy, J., Yu, V. C. K., and Mok, Y. K. (2010) Auto-FACE: An NMR Based Binding Site Mapping Program for Fast Chemical Exchange Protein-Ligand Systems, *PLoS ONE 5*, -.

35. Pintacuda, G., John, M., Su, X. C., and Otting, G. (2007) NMR structure determination of protein-ligand complexes by lanthanide labeling, *Acc. Chem. Res. 40*, 206-212.

36. Hoffman, R. M. B., and Sykes, B. D. (2009) Structure of the Inhibitor W7 Bound to the Regulatory Domain of Cardiac Troponin C, *Biochemistry 48*, 5541-5552.

37. Chandra, M., Dong, W. J., Pan, B. S., Cheung, H. C., and Solaro, R. J. (1997) Effects of protein kinase A phosphorylation on signaling between cardiac troponin I and the N-terminal domain of cardiac troponin C, *Biochemistry 36*, 13305-13311.

38. Li, M. X., Gagne, S. M., Tsuda, S., Kay, C. M., Smillie, L. B., and Sykes, B. D. (1995) Calcium-Binding to the Regulatory N-Domain of Skeletal-Muscle Troponin-C Occurs in a Stepwise Manner, *Biochemistry 34*, 8330-8340.

39. Lykkesfeldt, J. (2000) Determination of ascorbic acid and dehydroascorbic acid in biological samples by high-performance liquid chromatography using subtraction methods: Reliable reduction with tris[2-carboxyethyl] phosphine hydrochloride, *Anal. Biochem. 282*, 89-93.

40. Gemmecker, G., Olejniczak, E. T., and Fesik, S. W. (1992) An Improved Method for Selectively Observing Protons Attached to C-

12 in the Presence of H-1-C-13 Spin Pairs, *J. Magn. Reson. 96*, 199-204.

41. Ikura, M., and Bax, A. (1992) Isotope-Filtered 2d Nmr of a Protein Peptide Complex - Study of a Skeletal-Muscle Myosin Light Chain Kinase Fragment Bound to Calmodulin, *J. Am. Chem. Soc. 114*, 2433-2440.

42. Stuart, A. C., Borzilleri, K. A., Withka, J. M., and Palmer, A. G. (1999) Compensating for variations in H-1-C-13 scalar coupling constants in isotope-filtered NMR experiments, *J. Am. Chem. Soc. 121*, 5346-5347.

43. Lee, W., Revington, M. J., Arrowsmith, C., and Kay, L. E. (1994) A Pulsed-Field Gradient Isotope-Filtered 3d C-13 Hmqc-Noesy Experiment for Extracting Intermolecular Noe Contacts in Molecular-Complexes, *FEBS Lett. 350*, 87-90.

44. Robertson, I. M., Spyracopoulos, L., and Sykes, B. D. (2009) The Evaluation of Isotope Editing and Filtering for Protein-Ligand Interaction Elucidation by Nmr, *Biophysics and the Challenges of Emerging Threats*, 101-119.

45. Delaglio, F., Grzesiek, S., Vuister, G. W., Zhu, G., Pfeifer, J., and Bax, A. (1995) Nmrpipe - a Multidimensional Spectral Processing System Based on Unix Pipes, *J. Biomol. NMR 6*, 277-293.

46. Johnson, B. A., and Blevins, R. A. (1994) Nmr View - a Computer-Program for the Visualization and Analysis of Nmr Data, *J. Biomol. NMR 4*, 603-614.

47. Lin, X., Krudy, G. A., Howarth, J., Brito, R. M. M., Rosevear, P. R., and Putkey, J. A. (1994) Assignment and Calcium-Dependence of Methionyl Epsilon-C and Epsilon-H Resonances in Cardiac Troponin-C, *Biochemistry 33*, 14434-14442.

48. Schuttelkopf, A. W., and van Aalten, D. M. F. (2004) PRODRG: a tool for high-throughput crystallography of protein-ligand complexes, *Acta Crystallogr. Sect. D Biol. Crystallogr. 60*, 1355-1363.

49. Kleywegt, G. J., Zou, J.Y., Kjeldgaard, M., Jones, T.A., Around O. (2001   ) International Tables for Crystallography, Vol. F. Crystallography of Biological Macromolecules, (Rossmann, M. G., Arnold, E., Ed.), pp 353-356, 366-367, Dordrecht: Kluwer Academic Publishers, The Netherlands. .

50. Schwieters, C. D., Kuszewski, J. J., Tjandra, N., and Clore, G. M. (2003) The Xplor-NIH NMR molecular structure determination package, *J. Magn. Reson. 160*, 65-73.

51. M. J. Frisch, G. W. T., H. B. Schlegel, G. E. Scuseria, M. A. Robb, J. R. Cheeseman, J. A. Montgomery, Jr., T. Vreven, K. N. Kudin, J. C. Burant, J. M. Millam, S. S. Iyengar, J. Tomasi, V. Barone, B. Mennucci, M. Cossi, G. Scalmani, N. Rega, G. A. Petersson, H. Nakatsuji, M. Hada, M. Ehara, K. Toyota, R. Fukuda, J. Hasegawa, M. Ishida, T. Nakajima, Y. Honda, O. Kitao, H. Nakai, M. Klene, X.

Li, J. E. Knox, H. P. Hratchian, J. B. Cross, V. Bakken, C. Adamo, J. Jaramillo, R. Gomperts, R. E. Stratmann, O. Yazyev, A. J. Austin, R. Cammi, C. Pomelli, J. W. Ochterski, P. Y. Ayala, K. Morokuma, G. A. Voth, P. Salvador, J. J. Dannenberg, V. G. Zakrzewski, S. Dapprich, A. D. Daniels, M. C. Strain, O. Farkas, D. K. Malick, A. D. Rabuck, K. Raghavachari, J. B. Foresman, J. V. Ortiz, Q. Cui, A. G. Baboul, S. Clifford, J. Cioslowski, B. B. Stefanov, G. Liu, A. Liashenko, P. Piskorz, I. Komaromi, R. L. Martin, D. J. Fox, T. Keith, M. A. Al-Laham, C. Y. Peng, A. Nanayakkara, M. Challacombe, P. M. W. Gill, B. Johnson, W. Chen, M. W. Wong, C. Gonzalez, and J. A. Pople. (2004) Gaussian 03, Gaussian 03 ed., Gaussian, Inc., Wallingford CT.

52. Hoffman, R. M. B., Li, M. X., and Sykes, B. D. (2005) The bindin of W7, an inhibitor of striated muscle contraction, to cardiac troponin C, *Biochemistry 44*, 15750-15759.

53. McCoy, M. A., and Wyss, D. F. (2002) Spatial localization of ligand binding sites from electron current density surfaces calculated from NMR chemical shift perturbations, *J. Am. Chem. Soc. 124*, 11758-11763.

54. Guntert, P. (2004) Automated NMR structure calculation with CYANA, *Methods Mol. Biol. 278*, 353-378.

55. Cornilescu, G., Delaglio, F., and Bax, A. (1999) Protein backbone angle restraints from searching a database for chemical shift and sequence homology, *J. Biomol. NMR 13*, 289-302.

56. Linge, J. P., Williams, M. A., Spronk, C. A. E. M., Bonvin, A. M. J. J., and Nilges, M. (2003) Refinement of protein structures in explicit solvent, *Proteins-Structure Function and Bioinformatics 50*, 496-506.

57. Laskowski, R. A., Rullmann, J. A. C., MacArthur, M. W., Kaptein, R., and Thornton, J. M. (1996) AQUA and PROCHECK-NMR: Programs for checking the quality of protein structures solved by NMR, *J. Biomol. NMR 8*, 477-486.

58. Jayatilake, G. S., Jayasuriya, H., Lee, E. S., Koonchanok, N. M., Geahlen, R. L., Ashendel, C. L., Mclaughlin, J. L., and Chang, C. J. (1993) Kinase Inhibitors from Polygonum-Cuspidatum, *J. Nat. Prod. 56*, 1805-1810.

59. Koh, D., Park, K. H., Jung, J., Yang, H., Mok, K. H., and Lim, Y. (2001) Complete assignment of the H-1 and C-13 NMR spectra of resveratrol derivatives, *Magn. Reson. Chem. 39*, 768-770.

60. Commodari, F., Khiat, A., Ibrahimi, S., Brizius, A. R., and Kalkstein, N. (2005) Comparison of the phytoestrogen trans-resveratrol (3,4',5-trihydroxystilbene) structures from x-ray diffraction and solution NMR, *Magn. Reson. Chem. 43*, 567-572.

61. Bonechi, C., Martini, S., Magnani, A., and Rossi, C. (2008) Stacking interaction study of trans-resveratrol (trans-3,5,4'-trihydroxystilbene) in solution by nuclear magnetic resonance and

Fourier transform infrared spectroscopy, *Magn. Reson. Chem. 46*, 625-629.

62. Karplus, M. (1959) Contact Electron-Spin Coupling of Nuclear Magnetic Moments, *J. Chem. Phys. 30*, 11-15.

63. Trela, B. C., and Waterhouse, A. L. (1996) Resveratrol: Isomeric molar absorptivities and stability, *J. Agric. Food Chem. 44*, 1253-1257.

64. Caruso, F., Tanski, J., Villegas-Estrada, A., and Rossi, M. (2004) Structural basis for antioxidant activity of trans-resveratrol: Ab initio calculations and crystal and molecular structure, *J. Agric. Food Chem. 52*, 7279-7285.

65. Yin, Q., Shi, Y. M., Liu, H. M., Li, C. B., and Zhang, W. Q. (2002) (E)-3,5,4 '-Trimethoxystilbene, *Acta Crystallographica Section E-Structure Reports Online 58*, O1180-O1181.

66. Robertson, I. M., Pineda-Sanabria, S., and Sykes, B. D. (In Press) Approaches to protein-ligand structure determination by NMR spectroscopy: applications in drug binding to the cardiac regulatory protein troponin C, *Biophysics and Structure to Counter Threats and Challenges*.

67. Baryshnikova, O. K., Robertson, I. M., Mercier, P., and Sykes, B. D. (2008) Dilated cardiomyopathy G159D mutation in cardiac troponin C weakens the anchoring interaction with troponin I, *Biochemistry 47*, 10950-10960.

68. Gasmi-Seabrook, G. M., Howarth, J. W., Finley, N., Abusamhadneh, E., Gaponenko, V., Brito, R. M., Solaro, R. J., and Rosevear, P. R. (1999) Solution structures of the C-terminal domain of cardiac troponin C free and bound to the N-terminal domain of cardiac troponin I, *Biochemistry 38*, 8313-8322.

69. Lindhout, D. A., and Sykes, B. D. (2003) Structure and dynamics of the C-domain of human cardiac troponin C in complex with the inhibitory region of human cardiac troponin I, *J. Biol. Chem. 278*, 27024-27034.

70. Ferrer, J. L., Jez, J. M., Bowman, M. E., Dixon, R. A., and Noel, J. P. (1999) Structure of chalcone synthase and the molecular basis of plant polyketide biosynthesis, *Nat. Struct. Biol. 6*, 775-784.

71. Klabunde, T., Petrassi, H. M., Oza, V. B., Raman, P., Kelly, J. W., and Sacchettini, J. C. (2000) Rational design of potent human transthyretin amyloid disease inhibitors, *Nat. Struct. Biol. 7*, 312-321.

72. Austin, M. B., Bowman, M. E., Ferrer, J. L., Schroder, J., and Noel, J. P. (2004) An aldol switch discovered in stilbene synthases mediates cyclization specificity of type III polyketide synthases, *Chem. Biol. 11*, 1179-1194.

73. Buryanovskyy, L., Fu, Y., Boyd, M., Ma, Y. L., Hsieh, T. C., Wu, J. M., and Zhang, Z. T. (2004) Crystal structure of quinone reductase 2 in complex with resveratrol, *Biochemistry 43*, 11417-11426.

74.   Shomura, Y., Torayama, I., Suh, D. Y., Xiang, T., Kita, A., Sankawa, U., and Miki, K. (2005) Crystal structure of stilbene synthase from Arachis hypogaea, *Proteins-Structure Function and Bioinformatics 60*, 803-806.

75.   Gledhill, J. R., Montgomery, M. G., Leslie, A. G. W., and Walker, J. E. (2007) Mechanism of inhibition of bovine F-1-ATPase by resveratrol and related polyphenols, *Proc. Natl. Acad. Sci. U. S. A. 104*, 13632-13637.

76.   Davies, D. R., Mamat, B., Magnusson, O. T., Christensen, J., Haraldsson, M. H., Mishra, R., Pease, B., Hansen, E., Singh, J., Zembower, D., Kim, H., Kiselyov, A. S., Burgin, A. B., Gurney, M. E., and Stewart, L. J. (2010) Discovery of Leukotriene A4 Hydrolase Inhibitors Using Metabolomics Biased Fragment Crystallography (vol 52, pg 4694, 2009), *J. Med. Chem. 53*, 2330-2331.

77.   Li, M. X., Robertson, I. M., and Sykes, B. D. (2008) Interaction of cardiac troponin with cardiotonic drugs: a structural perspective, *Biochem. Biophys. Res. Commun. 369*, 88-99.

78.   Sorsa, T., Pollesello, P., and Solaro, R. J. (2004) The contractile apparatus as a target for drugs against heart failure: Interaction of levosimendan, a calcium sensitiser, with cardiac troponin c, *Mol. Cell. Biochem. 266*, 87-107.

79.   Mirza, M., Marston, S., Willott, R., Ashley, C., Mogensen, J., McKenna, W., Robinson, P., Redwood, C., and Watkins, H. (2005) Dilated cardiomyopathy mutations in three thin filament regulatory proteins result in a common functional phenotype, *J. Biol. Chem. 280*, 28498-28506.

80.   Landstrom, A. P., Parvatiyar, M. S., Pinto, J. R., Marquardt, M. L., Bos, J. M., Tester, D. J., Ornmen, S. R., Potter, J. D., and Ackerman, M. J. (2008) Molecular and functional characterization of novel hypertrophic cardiomyopathy susceptibility mutations in TNNC1-encoded troponin C, *J. Mol. Cell. Cardiol. 45*, 281-288.

81.   Swindle, N., and Tikunova, S. B. (2010) Hypertrophic Cardiomyopathy-Linked Mutation D145E Drastically Alters Calcium Binding by the C-Domain of Cardiac Troponin C, *Biochemistry 49*, 4813-4820.

82.   Szczesna, D., Guzman, G., Miller, T., Zhao, J. J., Farokhi, K., Ellemberger, H., and Potter, J. D. (1996) The role of the four Ca2+ binding sites of troponin C in the regulation of skeletal muscle contraction, *J. Biol. Chem. 271*, 8381-8386.

83.   Agianian, B., Krzic, U., Qiu, F., Linke, W. A., Leonard, K., and Bullard, B. (2004) A troponin switch that regulates muscle contraction by stretch instead of calcium, *EMBO J. 23*, 772-779.

84.   Solaro, R. J., Gambassi, G., Warshaw, D. M., Keller, M. R., Spurgeon, H. A., Beier, N., and Lakatta, E. G. (1993) Stereoselective Actions of Thiadiazinones on Canine Cardiac Myocytes and Myofilaments, *Circ. Res. 73*, 981-990.

85. Biffinger, J. C., Kim, H. W., and DiMagno, S. G. (2004) The polar hydrophobicity of fluorinated compounds, *Chembiochem 5*, 622-627.

86. Smart, B. E. (2001) Fluorine substituent effects (on bioactivity), *J. Fluorine Chem. 109*, 3-11.

87. Cao, H., Pan, X. L., Li, C., Zhou, C., Deng, F. Y., and Li, T. H. (2003) Density functional theory calculations for resveratrol, *Bioorg. Med. Chem. Lett. 13*, 1869-1871.

88. Del Nero, J., and De Melo, C. P. (2003) Investigation of the excited states of resveratrol and related molecules, *Int. J. Quantum Chem. 95*, 213-218.

89. Leopoldini, M., Marino, T., Russo, N., and Toscano, M. (2004) Antioxidant properties of phenolic compounds: H-atom versus electron transfer mechanism, *J. Phys. Chem. A 108*, 4916-4922.

90. Li, M. X., Spyracopoulos, L., Beier, N., Putkey, J. A., and Sykes, B. D. (2000) Interaction of cardiac troponin C with Ca2+ sensitizer EMD 57033 and cardiac troponin I inhibitory peptide, *Biochemistry 39*, 8782-8790.

91. Andrews, P. R., Craik, D. J., and Martin, J. L. (1984) Functional-Group Contributions to Drug Receptor Interactions, *J. Med. Chem. 27*, 1648-1657.

92. Hopkins, A. L., Groom, C. R., and Alex, A. (2004) Ligand efficiency: a useful metric for lead selection, *Drug Discov. Today 9*, 430-431.

93. Kuntz, I. D., Chen, K., Sharp, K. A., and Kollman, P. A. (1999) The maximal affinity of ligands, *Proc. Natl. Acad. Sci. U. S. A. 96*, 9997-10002.

94. Lipinski, C. A., Lombardo, F., Dominy, B. W., and Feeney, P. J. (1997) Experimental and computational approaches to estimate solubility and permeability in drug discovery and development settings, *Adv. Drug Delivery Rev. 23*, 3-25.

95. Tadano, N., Morimoto, S., Takahashi-Yanaga, F., Miwa, Y., Ohtsuki, I., and Sasaguri, T. (2009) Propyl Gallate, a Strong Antioxidant, Increases the Ca2+ Sensitivity of Cardiac Myofilament, *J. Pharmacol. Sci. 109*, 456-458.

Chapter 4

Defining the binding site of levosimendan and its analogs in a regulatory cardiac troponin C-I complex*

Summary

The interaction of cTnC and cTnI plays a critical role in transmitting the Ca^{2+}-signal to the other myofilament proteins in the activation of cardiac muscle contraction. As such, the cTnC-cTnI interface constitutes a logical target for cardiotonic agents such as levosimendan that can modulate the Ca^{2+}-sensitivity of the myofilaments. Evidence indicates that drug candidates may exert their effects by targeting a site formed by binding of the switch region of cTnI to the regulatory N-domain of cTnC (cNTnC). In this study, we utilized 2D $^{1}H,^{15}N$-HSQC NMR spectroscopy to monitor the binding of levosimendan and its analogs, CMDP, AMDP, CI-930, imazodan, and MPDP, to cNTnC•Ca^{2+} in complex with two versions of the switch region of cTnI ($cTnI_{147-163}$ and $cTnI_{144-163}$). Levosimendan, CMDP, AMDP, and CI-930 were found to bind to both cNTnC•Ca^{2+}•$cTnI_{147-163}$ and cNTnC•Ca^{2+}•$cTnI_{144-163}$. These compounds contain a methyl group that is absent in MPDP or imazodan. Thus, the methyl group constitutes one of the pharmacophores responsible for the action of these pyridazinone drugs on cTnC. Furthermore, the results showed that cNTnC•Ca^{2+}•$cTnI_{144-163}$ presents a higher affinity binding site for these compounds than cNTnC•Ca^{2+}•$cTnI_{147-163}$. This is consistent with our observation that the affinity of $cTnI_{144-163}$ for cNTnC•Ca^{2+} is ~10 fold stronger than that of $cTnI_{147-163}$, likely a result of electrostatic forces between the N-terminal RRV extension in $cTnI_{144-163}$ with the acidic residues in the C and D helices of cNTnC. These results will help in the delineation of the mode of action of levosimendan on the important functional unit of cardiac troponin that constitutes the regulatory domain of cTnC and the switch region of cTnI.

Introduction

Regulation of cardiac muscle contraction by intracellular Ca^{2+} is critical for normal heart function. This important task is accomplished by the heterotrimeric troponin complex anchored on the thin filament by its tropomyosin-binding subunit cTnT. The inhibitory subunit cTnI acts as a molecular switch moving from actin to the Ca^{2+}-binding subunit cTnC as intracellular Ca^{2+} concentration increases. This switch is essential for transmitting the Ca^{2+} signal to the other myofilament proteins, leading to tension producing cross bridges between actin and myosin, and ultimately activating cardiac muscle contraction (for recent reviews, see (*1, 2*)).

Structural studies of troponin have helped elucidate the molecular mechanism that governs the switching of cTnI to cTnC. cTnC is an 'elongated' molecule with two globular N- and C-domains connected by a flexible linker in solution (*3*). The apo cNTnC was shown to adopt a 'closed' conformation with most of its hydrophobic residues buried (*4*). The energy barrier for 'opening' is overcome by the binding of Ca^{2+} and the switch region of cTnI (residues ~147-163) (*5, 6*). In the NMR structure of the cNTnC•Ca^{2+}•$cTnI_{147-163}$ complex (*6*) and the X-ray structure of the cTnC•$3Ca^{2+}$•$cTnI_{31-210}$•$cTnT_{183-288}$ complex (*7*), $cTnI_{147-163}$ adopts an a-helical conformation and lies across the hydrophobic groove with contacts to key hydrophobic residues in cNTnC. This interaction initiates the movement of the adjoining inhibitory ($cTnI_{128-147}$) and the C-terminal ($cTnI_{163-210}$) regions of cTnI away from actin and releases the inhibition of the actomyosin ATPase, leading to muscle contraction (*1*). The $cTnI_{34-71}$ region binds tightly to cCTnC in the absence or presence of cytosolic Ca^{2+}. In the structure of cTnC•$3Ca^{2+}$•$cTnI_{31-210}$•$cTnT_{183-288}$, the 34-71 region of cTnI forms a long a-helix and makes extensive contacts with the hydrophobic surface of cCTnC. Most of the inhibitory region of cTnI is unobserved in cTnC•$3Ca^{2+}$•$cTnI_{31-210}$•$cTnT_{183-288}$, but the similar region of sTnI is shown to have an extended conformation and interact with the

central helix area of sTnC in the X-ray structure of the sTnC•$4Ca^{2+}$•$sTnI_{1-182}$•$sTnT_{156-262}$ complex (*8*). Specifically, the inhibitory region of sTnI was found to make electrostatic contacts with the acidic residues on the central DE-helix of sTnC, similar to those observed in the NMR solution structure of cCTnC•$2Ca^{2+}$•$cTnI_{128-147}$ (*9, 10*).

The Ca^{2+}-sensitive interaction between cNTnC and the switch region of cTnI has been proposed to be an important target for cardiotonic drugs (for reviews, see (*1, 11-15*)). These drugs are useful in the treatment of heart disease associated with depressed cardiac contractility. They act *via* a mechanism that modulates the Ca^{2+}-sensitivity of troponin without an overload of Ca^{2+} that would perturb the regulation of other Ca^{2+}-based signaling pathways in cardiomyocytes, leading to a series of undesirable side effects such as arrhythmia and death. A good example is levosimendan, which has proved to be a well-tolerated and effective treatment for patients with severe decompensated heart failure (for reviews, see (*13, 14*)). Several cardiotonic agents have been shown to target the binding site formed by cNTnC and the switch region of cTnI. In the NMR structure of the cNTnC•Ca^{2+}•$cTnI_{147-163}$•bepridil complex, bepridil and $cTnI_{147-163}$ bind concurrently to the hydrophobic pocket of the protein (*16*). In the structure of the sTnC•$4Ca^{2+}$•$sTnI_{1-182}$•$sTnT_{156-262}$ complex, a polyoxyethylene detergent molecule, anapoe, binds to sNTnC together with the switch region of sTnI ($sTnI_{115-131}$). This binding mode is likely responsible for the increase of the contractile force of muscle fibers in the presence of anapoe (*8*). Further, we have shown recently that a calmodulin antagonist, W7, binds to cNTnC and the binding can occur in the presence of the switch region of cTnI (*17*). Thus, these compounds, together with $cTnI_{147-163}$, may exert their effects by altering the dynamic equilibrium between 'closed' and 'open' cNTnC conformations, enhancing the affinity for cTnI and thereby modulating the calcium sensitivity of troponin. Structures of cNTnC•Ca^{2+}•levosimendan or cNTnC•Ca^{2+}•$cTnI_{147-163}$•levosimendan are not yet available. NMR chemical shift mapping has

shown that levosimendan's primary binding site is also located in the N-domain of cTnC in the presence of cTnI (*13, 18*), however, the exact binding geometry has not been established. In order to better delineate the binding site of levosimendan in cNTnC, we investigated the binding of levosimendan and its analogs (AMDP, CMDP, CI-930, MPDP, and imazodan) (Figure 4-1) to cNTnC•Ca^{2+}•cTnI$_{147\text{-}163}$ and cNTnC•Ca^{2+}•cTnI$_{144\text{-}163}$. The reason for using cTnI$_{144\text{-}163}$ is that the N-terminal RRV extension relative to cTnI$_{147\text{-}163}$ is expected to be important for a network of interactions responsible for the binding of drug molecules, on the basis of structural analysis of the cNTnC•Ca^{2+}•cTnI$_{147\text{-}163}$•bepridil and sTnC•4Ca^{2+}•sTnI$_{1\text{-}182}$•sTnT$_{156\text{-}262}$ complexes. We used 2D ^{1}H,^{15}N-HSQC NMR spectral changes to monitor the formation of the cNTnC•Ca^{2+}•cTnI$_{147\text{-}163}$ or cNTnC•Ca^{2+}•cTnI$_{144\text{-}163}$ complexes and the titration of these complexes with drug molecules. Our results revealed that only those compounds containing the methyl group induced chemical shift changes, suggesting that this group constitutes a key pharmacophore responsible for the binding of pyridazinone derivatives to cNTnC. The findings also showed that the pyridazinone compounds bound to cNTnC•Ca^{2+}•cTnI$_{144\text{-}163}$ with a higher affinity than to cNTnC•Ca^{2+}•cTnI$_{147\text{-}163}$. This correlates with our observation that the affinity of cTnI$_{144\text{-}163}$ for cNTnC•Ca^{2+} is ~10 fold stronger than that of cTnI$_{147\text{-}163}$, likely a result of electrostatic forces between the N-terminal RRV extension in cTnI$_{144\text{-}163}$ with the acidic residues in the C and D helices of cNTnC.

Experimental Procedures

Sample preparation:

Recombinant human cNTnC (residues 1-89) with the mutations C35S and C84S was used in this study. The engineering of the expression vector and the expression of ^{15}N-labeled proteins in *E. coli* were as described previously (*19*). Two synthetic cTnI peptides, cTnI$_{147\text{-}163}$, acetyl-
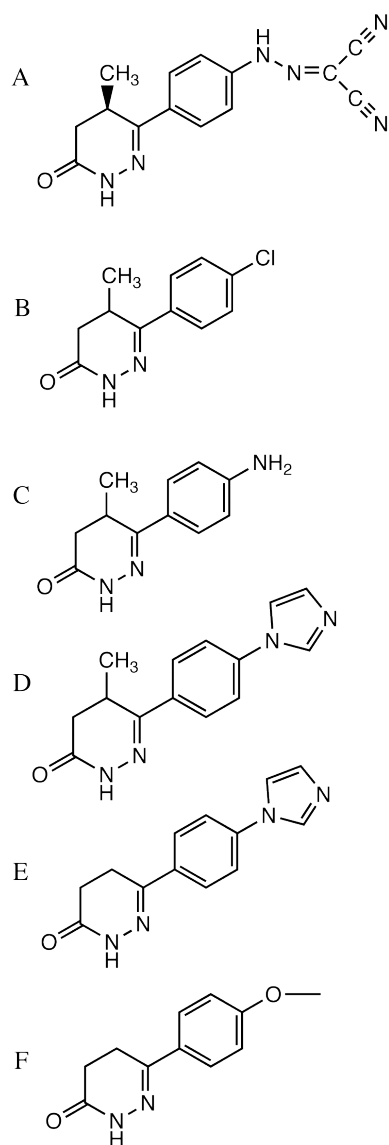
Figure 4-1. The chemical structures of (A) levosimendan, (B) CMDP, (C) AMDP, (D) CI-930, (E) imazodan, and (F) MPDP.

RISADAMMQALLGARAK-amide, and cTnI$_{144-163}$, acetyl-RRVRISADAMMQALLGARAK-amide, were obtained from GL Biochem Ltd. (Shanghai). The purity was verified by HPLC and the mass verified by electrospray mass spectrometry. CMDP (6-(4-chlorophenyl)-5-methyl-4,5-dihydro-3(2H)-pyridazinone), MPDP (6-(4-methoxyphenyl)-4,5-dihydro-3(2H)-pyridazinone), and imazodan (4,5-dihydro-6-[4-(1-imidazol-1-ly)phenyl]-3(2H)-pyridazinone) were purchased from Sigma-Aldrich. AMDP (6-(4–aminophenyl)-5-methyl-4,5-dihydro-3(2H)-pyridazinone) and levosimendan ((-)-[4-(1,4,5,6-tetrahydro-4-methyl-6-oxo-3-pyridazinyl)-phenyl] hydrazone propanedinitrile) were purchased from Kinbester Co. Ltd. (Hong Kong). CI-930 (4,5-dihydro-6-[4-(1-imidazol-1-ly)phenyl]-5-methyl-4,5-dihydro-3(2H)-pyridazinone) was obtained from Pfizer. Stock solutions of the compounds in DMSO-d$_6$ (Cambridge Isotopes Inc.) were prepared and the vials containing the solutions were wrapped in aluminum foil due to sensitivity to light. All drug stock solutions were made fresh for every titration to minimize possible time-induced degradation. The concentrations were determined gravimetrically. All NMR samples were ~500 µL in volume. The buffer conditions were 100 mM KCl, 10 mM imidazole, 5-10 mM Ca^{2+}, and 0.17 mM DSS in 90% H$_2$O/10% D$_2$O, and the pH was 6.7. DTT, NaN$_3$, and protease inhibitor cocktail were not used to avoid possible interactions with the drug compounds. Hamilton syringes and Gilson Pipetman P2 and P10 were used to deliver the drug solutions for all titrations.

Compound stereospecificity:

The chiral lanthanide shift reagent Eu-(hfc)$_3$ (Sigma-Aldrich) was titrated into NMR samples (all in CDCl$_3$, Cambridge Isotopes Inc.) of levosimendan, CMDP, AMDP, and CI-930 to determine whether the methyl on the pyridazinone ring was stereospecific, or if the compounds were enantiomer mixtures (for a review, see (*20*)). All of the NMR spectra were obtained using a Varian INOVA 500 MHz spectrometer at 30˚C. A

500 µL sample volume was used for each compound and TMS was used to reference the spectra at 0 ppm. For each titration, 16 transients were acquired at each point. A 16.5 mM sample of CI-930 was prepared and a 0.27 M stock solution of Eu-(hfc)$_3$ was titrated into the solution at the concentrations, 0.43, 0.86, 1.4, 1.94, 3.02, 4.1, 5.18, 6.26, 7.34, 8.42, 9.23, 12.47, and 15.17 mM. A 17 mM CMDP sample was prepared and titrated with a 0.322 M stock solution of Eu-(hfc)$_3$ to yield the Eu-(hfc)$_3$ concentrations of 1.28, 1.93, 2.6, 3.22, 4.5, 5.8, 11.6 and 17.6 mM. A 13.6 mM AMDP sample was prepared and titrated with a 0.4 M stock solution of Eu-(hfc)$_3$ to yield final concentrations of 1.73, 3.44, 5.14, 6.82, 8.5, and 10.2 mM. A 10 mM levosimendan sample was prepared and aliquots of Eu-(hfc)$_3$ were added to the sample to yield 1.82, 3.6, 5.4, 7.18, and 8.65 mM of Eu-(hfc)$_3$. The 1D ^{1}H NMR spectrum of each compound was assigned and the methyl was monitored throughout the titration with the chiral shift reagent, Eu-(hfc)$_3$ (Figure 4-2). The NMR signal from the methyl of levosimendan did not undergo splitting during the titration with Eu-(hfc)$_3$, indicating that the drug was of pure (R)- stereospecificity (Figure 4-2A). Meanwhile, the titration of Eu-(hfc)$_3$ into the NMR samples of CMDP, AMDP, and CI-930 revealed a splitting of the methyl resonance, indicating that these compounds are racemic mixtures of roughly equal (R)- and (S)- components (Figure 4-2B).

Titration of cNTnC•Ca^{2+} with cTnI$_{147-163}$ and cNTnC•Ca^{2+} with cTnI$_{144-163}$:

The titration of ^{15}N-cNTnC(WT)•Ca^{2+} with cTnI$_{147-163}$ was done previously (*6*) and the titration of ^{15}N-cNTnC•Ca^{2+} (0.6 mM and 0.7 mM, respectively) with cTnI$_{147-163}$ and cTnI$_{144-163}$ was done in this work. Both cTnI$_{147-163}$ and cTnI$_{144-163}$ are highly soluble in aqueous solution but tend to form gels at high concentrations, likely due to aggregation. Thus no stock solution was prepared; instead, solid peptide was added at every titration point. The concentrations of ^{15}N-cNTnC•Ca^{2+} and the peptides were determined by amino acid analysis at every titration point, giving the
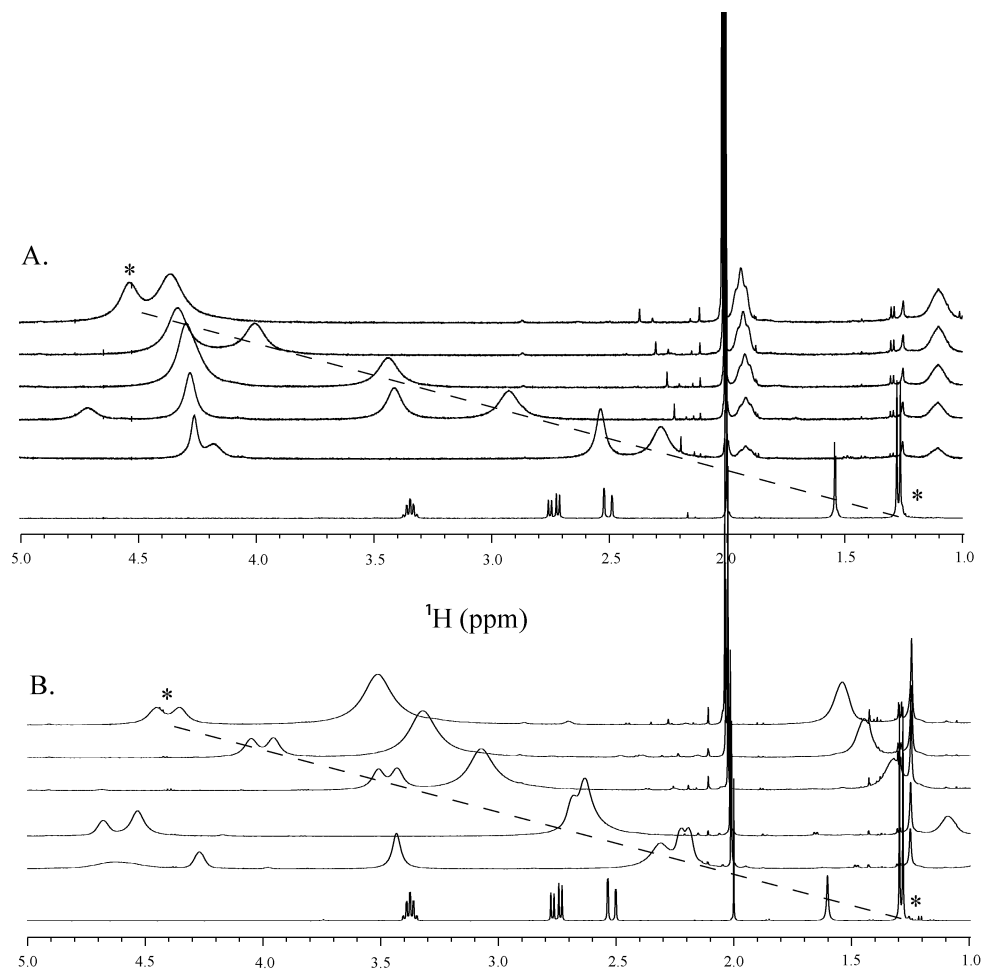
Figure 4-2. Stacked spectra of the titration of levosimendan (A) and CI-930 (B) with the shift reagent Eu-(hfc)$_3$ as monitored by 1D ^{1}H NMR spectroscopy. Starting from the lowest spectrum, the [Eu-(hfc)$_3$]/[CI-930] ratios for each titration point are 0, 0.25, 0.34, 0.54, 0.72, and 0.84. In the levosimendan titration series (A), no splitting of the methyl resonance (*) is observed, while in the case of CI-930 (B), splitting of the methyl resonance (*) is noticed, indicating an R/S mixture of enantiomers with roughly equal concentrations.

peptide/protein ratios. The decrease in pH associated with peptide additions was compensated by adjusting pH to 6.7 at every titration point. Both, 1D ^{1}H and 2D ^{1}H,^{15}N-HSQC NMR spectra were acquired and analyzed at every titration point. Like in the titration of ^{15}N-cNTnC(WT)•Ca^{2+} with cTnI$_{147-163}$ (6), 3 - 3.5 equivalents of cTnI$_{147-163}$ is required to saturate ^{15}N-cNTnC•Ca^{2+}, whereas 1 - 1.1 equivalents of cTnI$_{144-163}$ is required to saturate ^{15}N-cNTnC•Ca^{2+}.

Titration of cNTnC•Ca^{2+}•cTnI$_{147-163}$ and cNTnC•Ca^{2+}•cTnI$_{144-163}$ with levosimendan, CMDP, AMDP, CI-930, imazodan and MPDP:

The ^{15}N-cNTnC•Ca^{2+}•cTnI$_{147-163}$ complex was formed by dissolving 1 equivalent of solid protein (0.8 mM) and ~ 3.5 equivalents of solid peptide (2.8 mM) in NMR buffer and the ^{15}N-cNTnC•Ca^{2+}•cTnI$_{144-163}$ complex was formed by dissolving 1 equivalent of solid protein (1.0 mM) and ~ 1.1 equivalents of solid peptide (1.1 mM) in NMR buffer. For both complexes, 4 equivalents of CaCl$_2$ were added to saturate cNTnC, pH was adjusted to 6.7, and a slight amount of precipitate was eliminated by filtration. The final NMR sample volume was 500 mL. The protein and peptides concentrations were determined gravimetrically and calibrated based on amino acid analysis of each individual component. Both 1D ^{1}H and 2D ^{1}H, ^{15}N-HSQC NMR spectra were acquired and analyzed at every titration point.

A stock solution of 97 mM levosimendan was used for the titration of ^{15}N-cNTnC•Ca^{2+}•cTnI$_{147-163}$ in aliquots of 1.0, 1.0, 1.0, 1.0, 2.0, 4.0, 4.0, and 4.0 µL. A stock solution of 95 mM levosimendan was used for the titration of ^{15}N-cNTnC•Ca^{2+}•cTnI$_{144-163}$ in volumes of 1.0, 2.0, 5.0, 5.0, 10.0, and 10.0 µL. The sample was mixed thoroughly with each addition. In both cases, levosimendan started to precipitate when the drug to protein ratio reaches ~ 4:1. This precipitate is likely unbound levosimendan, which is insoluble in aqueous solution. The titrations were stopped shortly after the appearance of precipitation. Levosimendan

addition slightly decreased the pH, which was adjusted by adding 1 M NaOH to NMR samples.

Aliquots of 1 μL of 100 mM CMDP stock solution was added to ^{15}N-cNTnC•Ca^{2+}•cTnI$_{147-163}$ and ^{15}N-cNTnC•Ca^{2+}•cTnI$_{144-163}$. The titration was stopped when white precipitate started to appear (after the 8 μL addition). The change in pH from CMDP addition was negligible.

A stock of 100 mM AMDP was added in aliquots of 0.5, 1.5, 5.0, 5.0, 8.0, and 8.0 μL ^{15}N-cNTnC•Ca^{2+}•cTnI$_{147-163}$. AMDP is highly soluble in aqueous solution, and no precipitate was observed even after the final aliquot. A stock of 100 mM AMDP was added in aliquots of 0.5, 1.5, 5.0, 5.0, 8.0, and 10.0 μL to ^{15}N-cNTnC•Ca^{2+}•cTnI$_{144-163}$. Again, no precipitate was observed during or after the titration. The change in pH from AMDP addition was negligible.

To an NMR tube containing ^{15}N-cNTnC•Ca^{2+}•cTnI$_{147-163}$, aliquots of 1.0, 5.0, 5.0, 5.0, 5.0, and 5.0 μL of a 100 mM CI-930 stock solution were titrated into the sample. To the complex ^{15}N-cNTnC•Ca^{2+}•cTnI$_{144-163}$, aliquots of 0.25, 0.5, 2.5, 5.0, 5.0, 5.0, 5.0, and 5.0 μL of a 97 mM CI-930 stock solution were added. The change in pH from CI-930 addition was negligible.

Imazodan precipitated after an addition of 1 μL of 100 mM stock solution to the NMR sample of either ^{15}N-cNTnC•Ca^{2+}•cTnI$_{147-163}$ or ^{15}N-cNTnC•Ca^{2+}•cTnI$_{144-163}$. This was also the case with MPDP. Further additions resulted in more precipitation. No chemical shift changes were observed for the imazodan and MPDP titrations.

Pure DMSO-d$_6$ was added to an NMR sample containing ^{15}N-cNTnC to test if it would induce chemical shift changes of ^{15}N-cNTnC. No chemical shift perturbations were observed in the 2D ^{1}H, ^{15}N-HSQC spectrum upon addition of DMSO-d$_6$ (data not shown). To confirm that levosimendan was not interacting with free cTnI$_{147-163}$ or cTnI$_{144-163}$, levosimendan was titrated into solutions containing either peptide. 1D ^{1}H-NMR revealed no chemical shift change for cTnI$_{147-163}$ or cTnI$_{144-163}$ in the

presence of levosimendan, when compared to the spectra acquired in the absence of the drug (data not shown).

NMR spectroscopy:

All of the NMR spectra were obtained using a Varian INOVA 500 MHz spectrometer at 30°C. All 1D ^{1}H and 2D ^{1}H,^{15}N-HSQC spectra were acquired using the water and gNhsqc.c pulse sequences, respectively, (BioPack, Varian Inc.). The CBCA(CO)NNH and HNCACB NMR triple resonance experiments ([21]) were acquired for backbone assignment of the ^{13}C,^{15}N-cNTnC•Ca^{2+}•cTnI$_{144-163}$ complex. Spectral processing was accomplished with the program VNMRJ (Version 2.1B, Varian Inc.) and NMRPipe ([22]) and referenced according to the IUPAC conventions. Processed NMR spectra were analyzed using NMRView ([23]), and the backbone assignment of ^{13}C,^{15}N-cNTnC•Ca^{2+}•cTnI$_{144-163}$ complex was accomplished with the aid of the program Smartnotebook ([24]).

Results

Throughout this study, 2D ^{1}H,^{15}N-HSQC NMR spectra were used to monitor the binding of unlabeled ligands (such as the cTnI peptides, levosimendan, or its analogs) to ^{15}N-labeled cNTnC•Ca^{2+}. In these titrations, the chemical shifts of several assigned amide NH cross-peaks in the 2D ^{1}H,^{15}N-HSQC NMR spectrum of ^{15}N-cNTnC•Ca^{2+} were perturbed as a function of added ligand. In addition to the identification of ligands that associate with the ^{15}N-labeled protein, the changes in residue specific backbone shifts, which can be quantified to derive ligand stoichiometry and affinity, can be also used to locate the ligand-binding site on the protein. This procedure is commonly known as chemical shift mapping.

Interaction of cNTnC•Ca^{2+} with cTnI$_{147-163}$ and cTnI$_{144-163}$:

Previously, we titrated cTnI$_{147-163}$ into ^{15}N-cNTnC(WT)•Ca^{2+} and demonstrated that the binding of cTnI$_{147-163}$ to cNTnC(WT)•Ca^{2+} caused large chemical shift changes in the 2D ^{1}H,^{15}N-HSQC NMR spectrum of the protein, consistent with the structural transition in cNTnC from a 'closed' to an 'open' state (*6*). The dissociation constant (K_D) of cTnI$_{147-163}$ for cNTnC(WT)•Ca^{2+} was determined to be 154 ± 10 mM. In this study, we found that the binding of cTnI$_{147-163}$ to cNTnC•Ca^{2+} induced similar backbone amide ^{1}H or ^{15}N chemical shift changes, indicating a similar 'closed' to 'open' transition. The binding stoichiometry of cTnI$_{147-163}$ to cNTnC•Ca^{2+} was 1:1 in both the WT as well as the isoforms. An expanded region of the 2D ^{1}H,^{15}N-HSQC NMR spectra of cNTnC free and in the cNTnC•Ca^{2+}•cTnI$_{147-163}$ complex is depicted in Figure 4-3A, and peaks are labeled with residue assignments. Many peaks within this region of the spectrum including V28, G34, V64, G68, and T71 moved in the cTnI$_{147-163}$ complex to characteristic chemical shifts corresponding to an 'open' conformation of cNTnC (shown by arrows connecting multiple and first single contours). When the longer peptide cTnI$_{144-163}$ was titrated into cNTnC•Ca^{2+}, the majority of the cross peaks in the 2D ^{1}H,^{15}N-HSQC NMR spectrum of cNTnC shifted along nearly identical pathways as in the titration of cTnI$_{147-163}$ into cNTnC•Ca^{2+} but farther (shown by arrows connecting multiple and second single contours). The 2D ^{1}H,^{15}N-HSQC NMR spectrum of cNTnC in the cNTnC•Ca^{2+}•cTnI$_{144-163}$ complex has been assigned and the cross peaks are labeled with residue assignments (Figure 4-3A). The pattern of spectral changes is very similar for the two complexes (Figure 4-3B) except for larger backbone amide ^{1}H or ^{15}N chemical shift perturbations of cNTnC induced by cTnI$_{144-163}$ in comparison with cTnI$_{147-163}$. The additional movements of the residues indicate that the binding of cTnI$_{144-163}$ generates a more stable 'open' conformation for cNTnC•Ca^{2+} than cTnI$_{147-163}$. The average chemical shift changes of several residues that were perturbed the most during titration are plotted
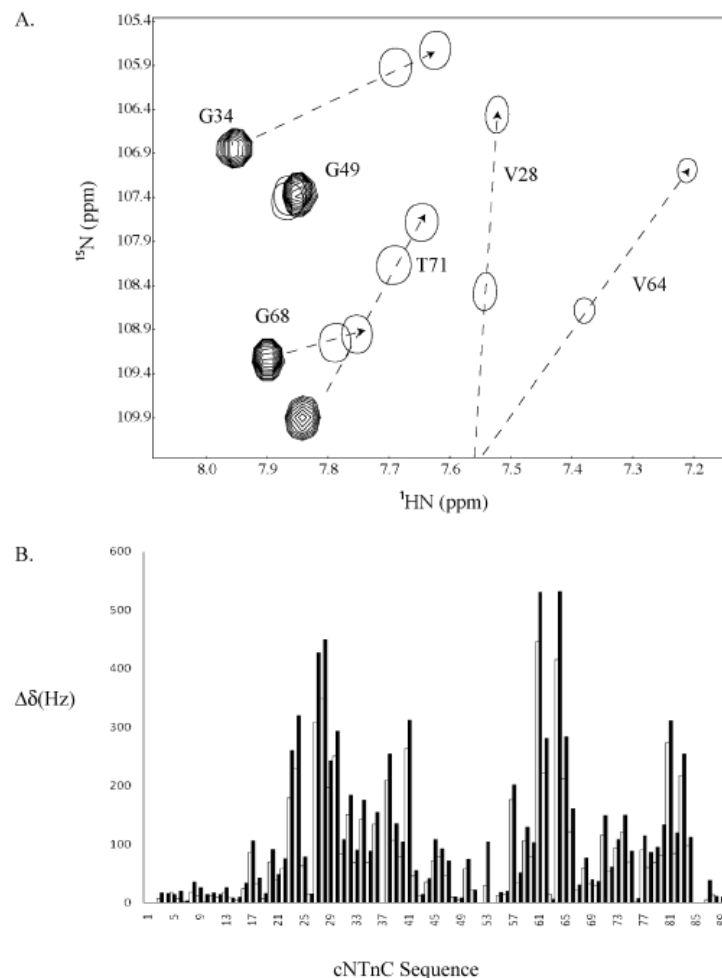
Figure 4-3. (A) An overlay of a well dispersed region of the 2D ^{1}H, ^{15}N-HSQC NMR spectra of cNTnC•Ca^{2+} (multiple contours), cNTnC•Ca^{2+}•cTnI$_{147\text{-}163}$ (first single contour), and cNTnC•Ca^{2+}•cTnI$_{144\text{-}163}$ (second single contour) complexes. The arrows indicate the direction of chemical shift change during cTnI titration into cNTnC•Ca^{2+}. Single contours represent the two cNTnC-cTnI complexes at the end points of titrations. The end points were determined by the cessation of chemical shift changes, which indicated a saturated complex. (B) The cTnI$_{147\text{-}163}$ (hollow bars) and cTnI$_{144\text{-}163}$ (solid bars) induced chemical shift changes of the backbone amides of cNTnC. Chemical shifts are presented in Hz and calculated as follows: $\Delta\delta = [(\Delta\delta_{\,1H})^2 + (\Delta\delta_{\,15N})^2]^{1/2}$. Since Hz is used instead of ppm to calculate the total chemical shift changes ($\Delta\delta$), a correction factor of 1/5 in the ^{15}N dimension is not needed.

as a function of $[cTnI_{144-163}]_{total}/[cNTnC \cdot Ca^{2+}]_{total}$ ratio (Figure 4-4) and the data were fit to the following equation:

$$cNTnC \cdot Ca^{2+} + cTnI_{144-163} \ D \ cNTnC \cdot Ca^{2+} \cdot cTnI_{144-163}$$

This yielded a macroscopic dissociation constant of 15 ± 5 mM, which is 10 times smaller than the dissociation constant of $cTnI_{147-163}$ binding to $cNTnC(WT) \cdot Ca^{2+}$ (*6*).

Interaction of $cNTnC \cdot Ca^{2+} \cdot cTnI_{147-163}$ and $cNTnC \cdot Ca^{2+} \cdot cTnI_{144-163}$ with levosimendan, CMDP, AMDP, and CI-930:

The formation of the $cNTnC \cdot Ca^{2+} \cdot cTnI_{147-163}$ and $cNTnC \cdot Ca^{2+} \cdot cTnI_{144-163}$ complexes were monitored by 2D ^1H, ^{15}N-HSQC NMR spectroscopy (Figure 4-3A). The assigned backbone amides of cNTnC in the $cNTnC \cdot Ca^{2+} \cdot cTnI_{147-163}$ and $cNTnC \cdot Ca^{2+} \cdot cTnI_{144-163}$ complexes were then used to follow the titration of levosimendan, CMDP, AMDP, and CI-930 (Figure 4-1). The initial (solid circles) and end points (open circles) from the titrations of $cNTnC \cdot Ca^{2+} \cdot cTnI_{144-163}$ with (A) levosimendan, (B) CMDP, (C) AMDP, and (D) CI-930 are shown in Figure 4-5. In contrast to the dramatic chemical shift changes induced by $cTnI_{147-163}$ or $cTnI_{144-163}$, those associated with drug binding are much smaller. This suggests that unlike the cTnI switch peptides, the drug compounds do not induce a large structural opening of cNTnC but rather cause subtle perturbations on the interface between cNTnC and the cTnI peptides. All four compounds induced backbone amide chemical shift changes in a common set of residues of both the $cNTnC \cdot Ca^{2+} \cdot cTnI_{147-163}$ and $cNTnC \cdot Ca^{2+} \cdot cTnI_{144-163}$ complexes. This suggests that the general location of binding is similar for these pyridazinone derivatives. It is interesting that although usually the same residues underwent perturbations throughout the different classes of ligands, the chemical shift changes were not always in the same direction. This may be due to the different moieties
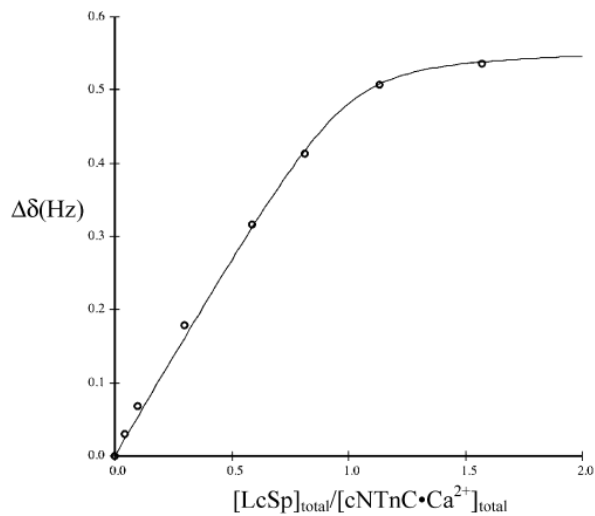
Figure 4-4. Titration of cNTnC•Ca^{2+} with cTnI$_{144-163}$. The data is averaged over several residues with significant chemical shift changes observed during titration. The best-fit curve to the data is shown by a solid line. Conditions are described under Experimental Procedures.
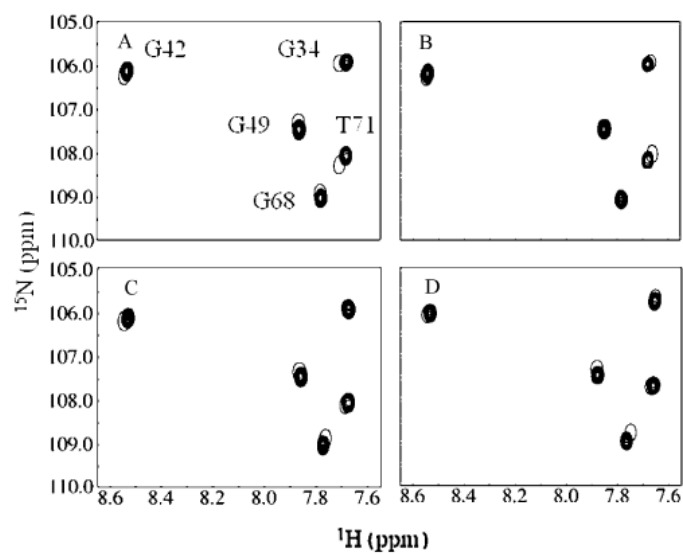
Figure 4-5. Titration of cNTnC•Ca^{2+}•cTnI$_{144-163}$ (1.0 mM cNTnC, 1.1 mM cTnI$_{144-163}$) with (A) levosimendan, (B) CMDP, (C) AMDP, (D) CI-930 as monitored by 2D ^{1}H, ^{15}N-HSQC NMR spectroscopy. The region of the 2D ^{1}H, ^{15}N-HSQC spectrum with well-dispersed resonances is shown. Conditions are described under Experimental Procedures.

present on the various pyridazinone derivatives. In order to correlate the drug induced chemical shift changes of cNTnC to conformational changes in the protein, we plotted the changes for backbone atoms against the protein sequence (Figure 4-6). The magnitude of the changes was generally small but similar to those reported in levosimendan binding to $cTnC \cdot 3Ca^{2+}$ (*25*) and to $cTnC \cdot 3Ca^{2+} \cdot cTnI_{32-79} \cdot cTnI_{128-180}$ (*18*). The changes induced by levosimendan (Figure 4-6A) or CMDP (Figure 4-6B) were relatively larger (≤ 60 Hz) than those (≤ 20 Hz) induced by AMDP (Figure 4-6C) and CI-930 (Figure 4-6D). This indicates that the group attached to the aromatic ring (mesoxalonitrile hydrazone in levosimendan, chloro in CMDP, amino in AMDP, and imidazole in CI-930, see Figure 4-1) influences the drug-protein-peptide interaction. These four molecules contain a chiral methyl group on the pyridazinone ring which may be in direct contact with the protein and involved in anchoring the drug molecules to $cNTnC \cdot Ca^{2+} \cdot cTnI_{144-163}$. This is supported by the observation that $cNTnC \cdot Ca^{2+} \cdot cTnI_{147-163}$ and $cNTnC \cdot Ca^{2+} \cdot cTnI_{144-163}$ do not interact with imazodan or MPDP, as represented by the lack of chemical shift perturbations.

In order to elucidate the binding site of levosimendan on $cNTnC \cdot Ca^{2+} \cdot cTnI_{144-163}$, chemical shift mapping is shown in Figure 4-7. The solution structure of $cNTnC \cdot Ca^{2+} \cdot cTnI_{147-163}$ (PDB:1MXL) was used to map the final chemical shift changes induced by the titration of levosimendan into $cNTnC \cdot Ca^{2+} \cdot cTnI_{144-163}$. The chemical shift perturbations are mapped on the structure by magnitude, such that the chemical shift changes for residues shown in pink were greater than the mean (μ), the chemical shift changes for residues shown in dark salmon were one standard deviation above the mean chemical shift change ($\mu + \sigma$), and the chemical shifts for residues shown in red were two standard deviations above the mean ($\mu + 2\sigma$) (see Figure 4-6A). Chemical shift mapping of CMDP on the structure of $cNTnC \cdot Ca^{2+} \cdot cTnI_{147-163}$ (PDB:1MXL) resulted in a nearly identical surface to that of levosimendan.
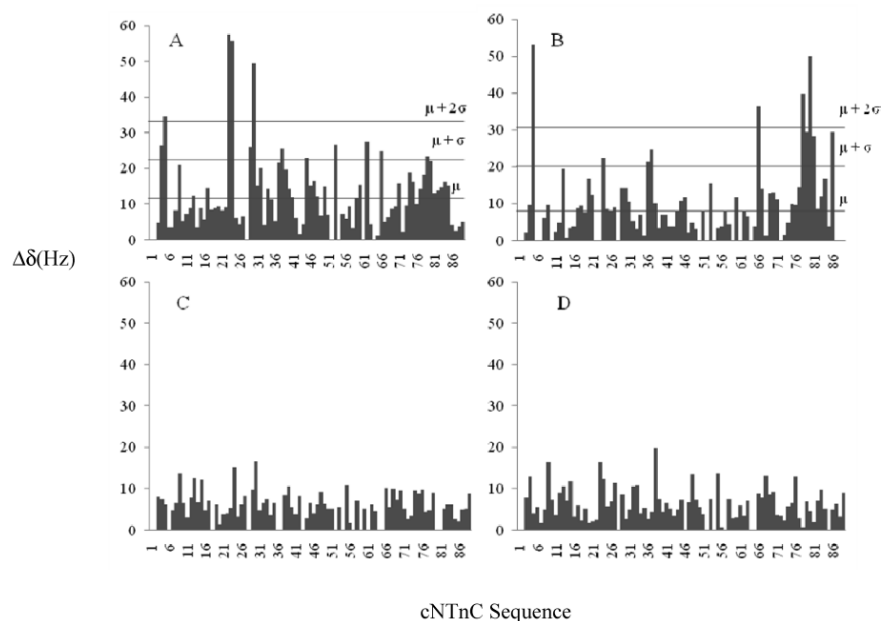
Figure 4-6. (A) Levosimendan, (B) CMDP, (C) AMDP, and (D) CI-930-induced chemical shift changes of the backbone amides of cNTnC in the cNTnC•Ca^{2+}•cTnI$_{144-163}$ complex (1.0 mM cNTnC, 1.1 mM cTnI$_{144-163}$). Chemical shift changes are presented in Hz and calculated as following: $\Delta\delta = [(\Delta\delta_{1H})^2 + (\Delta\delta_{15N})^2]^{1/2}$. Since Hz is used instead of ppm to calculate the total chemical shift changes ($\Delta\delta$), a correction factor of 1/5 in the ^{15}N dimension is not needed. Horizontal lines in the levosimendan and the CMDP bar diagrams (A,B) show total chemical shift perturbations larger than the mean (μ), the mean plus one standard deviation ($\mu + \sigma$), and the mean plus two standard deviations ($\mu + 2\sigma$). These values were used for chemical shift mapping.
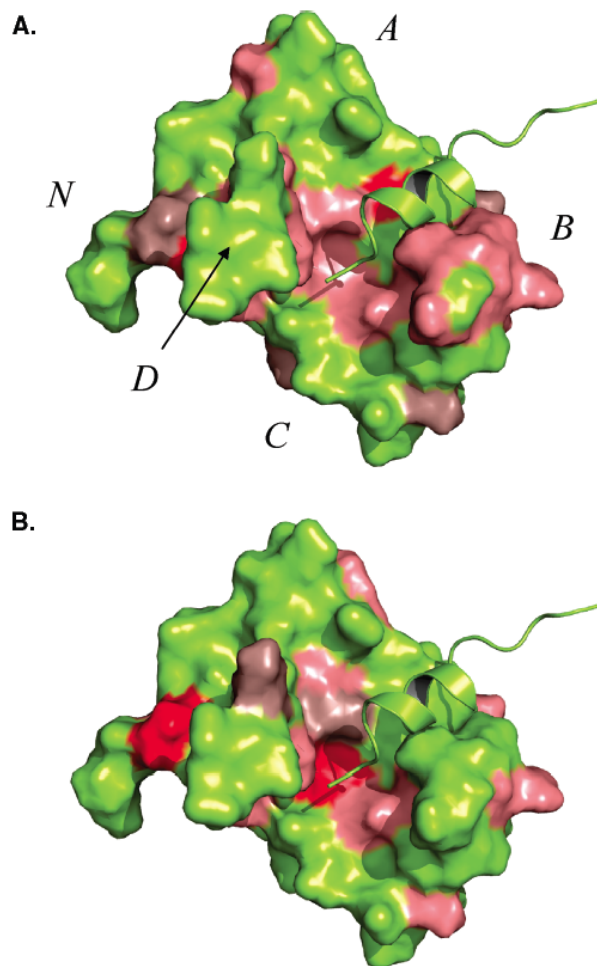
Figure 4-7. Chemical shift mapping on cNTnC•Ca^{2+}•cTnI$_{147\text{-}163}$ (PDB: 1MXL). The cNTnC•Ca^{2+}•cTnI$_{147\text{-}163}$ complex is shown in yellow with the helices of troponin C labeled. cNTnC•Ca^{2+} is depicted as a surface representation, whereas cTnI$_{147\text{-}163}$ is shown in ribbon format. Chemical shift perturbations induced by levosimendan (A) and CMDP (B) binding to cNTnC•Ca^{2+}•cTnI$_{144\text{-}163}$ are colored based on the magnitude of chemical shift. Chemical shifts greater than the mean plus two standard deviations ($\mu + 2\sigma$) are colored in red; greater than the mean plus one standard deviation ($\mu + \sigma$) are in dark salmon; and greater than the mean (μ) are in salmon.

Binding Affinity Determination:

The calculation of the affinities of the different drugs is illustrated in Figure 4-8. Data analysis of the titration of CI-930 into $cNTnC•Ca^{2+}•cTnI_{147-163}$ and $cNTnC•Ca^{2+}•cTnI_{144-163}$ are shown as an example. An expanded region of 2D $^1H,^{15}N$-HSQC NMR spectral changes induced by CI-930 is shown in Figure 4-8A and 8C, respectively. Plots of chemical shift changes of L48 as a function of [CI-930]$_{total}$/[$cNTnC•Ca^{2+}•cTnI_{147-163}$]$_{total}$ and [CI-930]$_{total}$/[$cNTnC•Ca^{2+}•cTnI_{144-163}$]$_{total}$ are shown in Figure 4-8B and 8D, respectively. In both cases, no plateau could be reached in the titration even at high protein-drug ratios, indicating weak binding. A global fitting approach (www.bionmr.ualberta.ca/bds/software/xcrvfit) was used, in which the data for residues perturbed during titration were fit to the following scheme:

$$Protein + ligand \leftrightarrow Protein•ligand$$
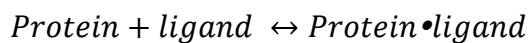
yielded a K_D of 11 mM for CI-930 binding to $cNTnC•Ca^{2+}•cTnI_{147-163}$ and 2.65 mM for CI-930 binding $cNTnC•Ca^{2+}•cTnI_{144-163}$. For levosimendan, the K_D's are 8 mM and 0.7 mM, respectively; and for AMDP, those are 6.5 mM and 1.5 mM, respectively. We were not able to obtain the dissociation constants for CMDP due to the precipitation of the ligand prior to reaching 1:1 stoichiometry. The results of levosimendan, AMDP, and CI-930 demonstrate that $cNTnC•Ca^{2+}•cTnI_{144-163}$ presents a more complete binding site for the drug molecules than $cNTnC•Ca^{2+}•cTnI_{147-163}$.

Discussion

The goal of this study was to define the binding site of levosimendan and several structural analogs (Figure 4-1) in the regulatory
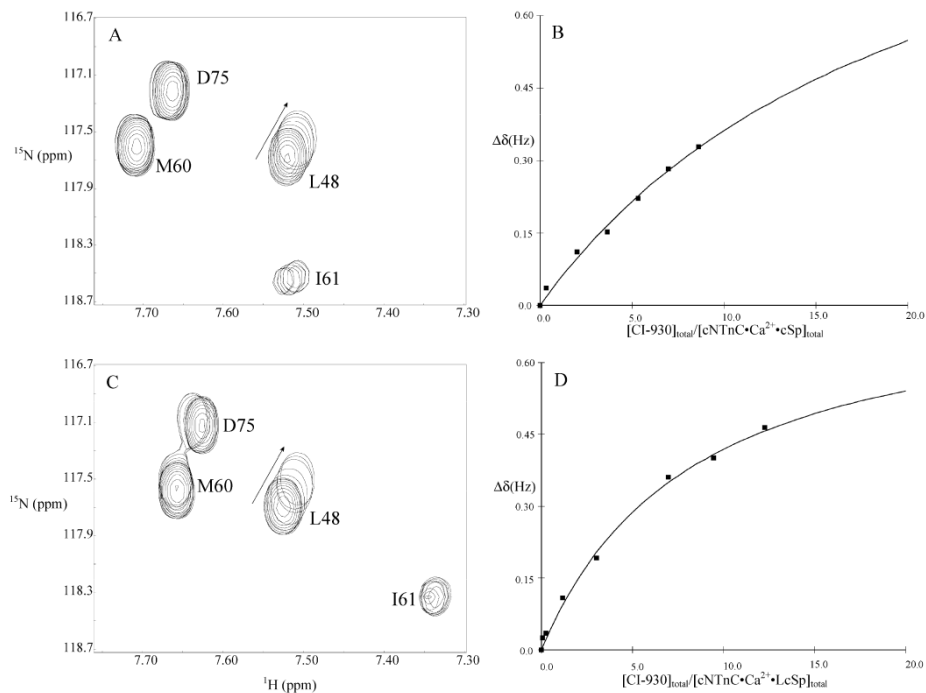
Figure 4-8. Selected region of 2D ^{1}H,^{15}N-HSQC NMR spectra demonstrating the progressive shifts of L48 during the CI-930 titration to cNTnC•Ca^{2+}•cTnI$_{147-163}$ (A) and to cNTnC•Ca^{2+}•cTnI$_{144-163}$ (C). Chemical shift changes of L48 were plotted as a function of [CI-930]$_{total}$/[cNTnC•Ca^{2+}•cTnI$_{147-163}$]$_{total}$ (B), and [CI-930]$_{total}$/[cNTnC•Ca^{2+}•cTnI$_{144-163}$]$_{total}$ (D), respectively. The best-fit curves to the data are shown as solid lines.

domain of cTnC in complex with the switch region of cTnI, as well as to gain insight into the particular pharmacophores responsible for the binding of the ligands to cNTnC-cTnI. An attractive aspect of this complex is that the interaction between cNTnC and the switch region of cTnI is Ca^{2+}-sensitive and the binding of Ca^{2+} and the cTnI switch are coupled to the 'opening' of the cNTnC hydrophobic pocket, revealing an important target for cardiotonic drugs. We utilized 2D $^1H,^{15}N$-HSQC NMR spectroscopy to monitor the formation of two cTnC-cTnI complexes, cNTnC•Ca^{2+}•$cTnI_{147-163}$ and cNTnC•Ca^{2+}•$cTnI_{144-163}$, and the titration of six drug compounds to those complexes. Since 2D $^1H,^{15}N$-HSQC NMR spectroscopy can report information pertaining to individual atoms throughout the protein sequence, we were able to detect the subtle chemical shift changes of drug binding on the backbone amides of cNTnC in the presence of $cTnI_{147-163}$ or $cTnI_{144-163}$ peptides. These measurements allowed the identification of a combination of specific amino acids in cNTnC and cTnI that form a binding pocket to accommodate the chiral methyl group on the pyridazinone ring of levosimendan and its analogs.

The structure of the cNTnC-cTnI has been characterized in several studies. We have shown that the binding of $cTnI_{147-163}$ induces a structural opening in cNTnC•Ca^{2+} (6). In the structure of cNTnC•Ca^{2+}•$cTnI_{147-163}$, the bound $cTnI_{147-163}$ peptide adopts an a-helical conformation spanning residues 4-12 in the 17-residue peptide. With the N-terminus of the peptide interacting with the center of the hydrophobic pocket, the a-helical region interacts with the AB helical interface and stabilizes the opening conformation of cNTnC•Ca^{2+}. The corresponding $sTnI_{115-131}$ peptide adopts a similar structure and a similar mode of interaction with sNTnC as observed in the structure of sNTnC(rhodamine)•$2Ca^{2+}$•$sTnI_{115-131}$ (26). The backbone atoms of the cNTnC•Ca^{2+}•$cTnI_{147-163}$ structure superimpose to 1.5 Å with the corresponding regions in the X-ray structure of cardiac troponin complex, cTnC•$3Ca^{2+}$•$cTnI_{31-210}$•$cTnT_{183-288}$. Addition of bepridil to cNTnC•Ca^{2+}•$cTnI_{147-163}$ resulted in the cNTnC•Ca^{2+}•$cTnI_{147-163}$•bepridil

ternary complex, with the binding site for $cTnI_{147-163}$ primarily located on the AB inter-helical interface and the binding site for bepridil in the center of the hydrophobic pocket (16). A similar binding scenario was observed in the X-ray structure of $sTnC \cdot 4Ca^{2+} \cdot sTnI_{1-182} \cdot sTnT_{156-262}$ complex (8); where a detergent molecule, anapoe, was found to bind together with the switch region of sTnI to $sNTnC \cdot 2Ca^{2+}$ (8). In the structure of $sTnC \cdot 4Ca^{2+} \cdot sTnI_{1-182} \cdot sTnT_{156-262}$, the three residue extension (R112, R113, and V114) in the N-terminus of $sTnI_{115-131}$ are involved in electrostatic contacts with a number of acidic residues in both the C and D helices of sNTnC (Figure 4-9), which may enhance the stability of the open conformation of $sNTnC \cdot 2Ca^{2+}$. Although R144, R145, and V146 are not visualized in both the $cNTnC \cdot Ca^{2+} \cdot cTnI_{147-163}$ and the $cTnC \cdot 3Ca^{2+} \cdot cTnI_{31-210} \cdot cTnT_{183-288}$ structures, these residues were expected to be located in close proximity to the corresponding acidic residues, D87 and D88, in the D-helix of cNTnC. This is based on the observation that the binding of the switch region of TnI to the N-domain of TnC is the same in all the structures mentioned above. Thus, it is reasonable to suggest that $cNTnC \cdot Ca^{2+} \cdot cTnI_{144-163}$ would present a more stable complex with a higher affinity binding site for drug compounds than $cNTnC \cdot Ca^{2+} \cdot cTnI_{147-163}$. This is in line with the observation in the current work.

An earlier study has shown that the binding site of levosimendan is in the N-domain of Ca^{2+}-saturated cTnC (27), although this was challenged by a different analysis showing that levosimendan did not bind to cTnC or a cTnC/cTnI complex (28). The later report showed that the inability to observe the levosimendan binding to cTnC was in part due to sample degradation and the use of a recombinant cTnC with C35 and C84 mutated to serines (25). It suggested that C84 is necessary for the interaction of levosimendan and cTnC. Furthermore, this report showed that levosimendan is capable of binding to both domains of cTnC. A recent investigation by Sorsa *et al.* (18) used NMR to demonstrate that levosimendan only bound to the N-domain of cTnC in the presence of
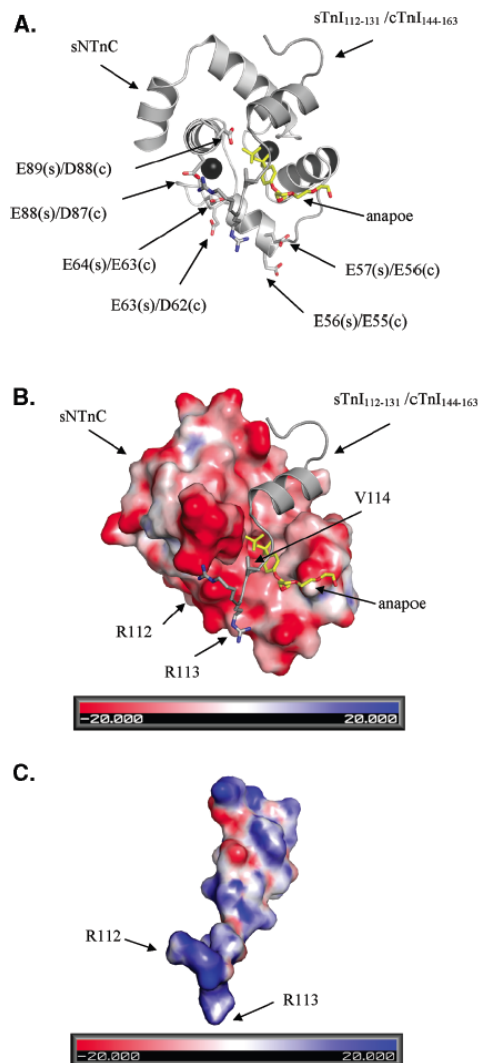
Figure 4-9. (A) Ribbon diagram of sNTnC•2Ca^{2+}•sTnI$_{112\text{-}131}$•anapoe (PDB entry 1YTZ). sNTnC is colored in light grey, and sTnI$_{112\text{-}132}$ is colored in dark grey, anapoe is in yellow, and calcium is in black. Six negatively charged residues of sNTnC (s) and cNTnC (c) are labeled. (B) Electrostatic surface map of sNTnC, with the potential contours shown at +20 k$_B$T/e (blue) and -20 k$_B$T/e (red). sTnI$_{112\text{-}131}$ is colored in dark grey and shown as a ribbon diagram, with the extra three residues from the inhibitory region of sTnI, R112, R113, and V114 depicted as sticks. (C) Electrostatic surface map of sTnI$_{112\text{-}131}$, with the potential contours shown at +20 k$_B$T/e (blue) and -20 k$_B$T/e (red). Positively charged R112 and R113 are labeled on the electrostatic surface map. Surface maps were generated with ABPS (*41*).

cTnI$_{32-79}$ and cTnI$_{128-180}$. Levosimendan induced amide chemical shift changes were detected throughout the N-domain of cTnC in the presence of the cTnI peptides. A number of the N-domain resonances were either broadened beyond detection or exhibited multiple chemical shifts. A large number of both polar and non-polar residues that exhibited chemical shift changes upon levosimendan binding precluded identification of the levosimendan-binding site on cNTnC. Sorsa *et al.* (*18*) attributed the numerous N-domain chemical shift changes to levosimendan altering either the dynamic equilibrium or the rate of exchange between 'open' and 'closed' N-domain conformations by partially stabilizing defunct Ca^{2+}-site I in cNTnC•Ca^{2+}. The exact binding location of levosimendan on cTnC remained unclear, although all the above studies suggested that its binding site is in the proximity of M81, M85, and F77 (residues on the D-helix) within the hydrophobic pocket of cNTnC. Our data is in agreement with these studies, and shows that levosimendan targets the hydrophobic pocket of cNTnC. The chemical shift mapping depicted in Figure 4-7 indicates that all backbone amide resonances perturbed modestly (in salmon) belong to the residues in the hydrophobic pocket, whereas the residues that are more significantly perturbed (dark salmon and red) belong to the N and A helices, away from the proposed binding surface. We suggest that the larger chemical shift perturbations of residues, such as Y5 and I4 on the N-helix and A23 and F24 on the A-helix, may be due to a slight conformational change of cNTnC•Ca^{2+}•cTnI$_{144-163}$ upon binding levosimendan, whereas the residues with smaller chemical shift changes identify the binding site of levosimendan in cNTnC•Ca^{2+}•cTnI$_{144-163}$ more accurately. The conformational change may be similar to that observed in the binding of bepridil to cNTnC•Ca^{2+}•cTnI$_{147-163}$, where in addition to the opening of cNTnC, there is a slight shift in the position of cTnI$_{147-163}$ (*15*). Our results demonstrated that the conserved positively charged N-terminal extension (RRV) in cTnI$_{144-163}$ is important for enhancing the affinity of levosimendan for cNTnC•Ca^{2+}. Thus, the network of electrostatic

interactions between R144/R145 of cTnI and D87/D88 of cNTnC, and the hydrophobic interactions between the helical region of $cTnI_{147-163}$ and the hydrophobic surface of $cNTnC \cdot Ca^{2+}$ creates the levosimendan binding site with enhanced affinity, with a net result of the stabilization of the hydrophobic pocket and the open conformation of $cNTnC \cdot Ca^{2+}$. We propose that the position of levosimendan in the cardiac troponin complex is analogous to that of anapoe in the skeletal troponin complex (Figure 4-9) based on the results of chemical shift mapping (Figure 4-7). The A-Cys version of cNTnC was used in this study and our results show that a cTnC-cTnI complex provides a favorable binding site for levosimendan in the absence of C84. The study (*25*) reporting that C84 is critical for the interaction of levosimendan and cNTnC suggested that the C84S mutation may slightly alter the conformation of the D-helix of cNTnC to render the levosimendan binding site unavailable. Our results show that electrostatic interactions between R144/R145 of cTnI and D87/D88 of cNTnC help to stabilize the D-helix and thereby the binding site for levosimendan. Covalent modification of C84 by levosimendan provides a plausible mechanism to account for the levosimendan-dependent effects (*e.g.* splitting of NMR peaks) observed by Sorsa et al. (*25*). This potential covalent interaction between C84 and levosimendan may not be required for its binding to the troponin complex, but may subsequently occur *in vivo* (*29*).

In order to understand the effect of the pharmacophores of levosimendan on binding to cNTnC, we investigated the binding of several levosimendan analogs to $cNTnC \cdot Ca^{2+} \cdot cTnI_{147-163}$ and $cNTnC \cdot Ca^{2+} \cdot cTnI_{144-163}$. Among the derivatives, only those containing the methyl group induced chemical shift changes, suggesting that this group constitutes a key pharmacophore responsible for the binding of pyridazinone derivatives to $cNTnC \cdot Ca^{2+}$. This is probably because this methyl group contributes to the hydrophobic packing in a stereo specific manner. This type of interaction is demonstrated in the binding of EMD 57033 to the C-domain of cTnC (*30,*

31). In the structure of cCTnC•2Ca^{2+}•EMD 57033, the drug molecule is oriented such that the chiral methyl group of EMD 57033 fits deep in the hydrophobic pocket and makes several key contacts with the protein. This stereospecifc interaction explains why the (-)-enantiomer of EMD 57033 (EMD 57439) is inactive. Studies on the action of stereoisomers of simendan (levosimendan and its (+) enantiomer, dextrosimendan) on cTnC have presented evidence that the Ca^{2+}-sensitizing effect of levosimendan is in part due to a stereoselective binding to the N-domain of cTnC (*32*). Another cardiotonic drug with structural characteristics similar to levosimendan, pimobendan, binds troponin and increases calcium sensitivity in a stereospecific manner as well (*33, 34*). The three levosimendan analogs that associated with cNTnC•Ca^{2+}•cTnI$_{147-163}$ and cNTnC•Ca^{2+}•cTnI$_{144-163}$, CMDP, AMDP, and CI-930 were shown in this work to be R/S mixtures (Figure 4-2); therefore it cannot be unambiguously concluded that binding to the complex is selective for one enantiomer over the other. However, it is possible that the affinity of one of the enantiomers of the pyridazinone compounds with cNTnC•Ca^{2+}•cTnI$_{144-163}$ is higher than the other.

In addition to the chiral methyl group on the pyridazinone ring, a group attached to the benzene ring may also be important in the binding. In levosimendan, this is a bulky group comprised of the mesoxalonitrile hydrazone moiety. Structure-to-activity analysis of levosimendan analogs has shown that this group is involved in hydrogen bonding with cTnC, indicating that both hydrogen bonds and van der Waals contacts are formed upon the binding of active levosimendan analogs to cTnC (*35*). Our data showed that levosimendan and CMDP induced larger chemical shift changes than AMDP and CI-930 (Figure 4-6). This demonstrates that the mesoxalonitrile hydrozone group in levosimendan and the chloro group in CMDP help to form stronger interaction with the binding site as compared to the amino group in AMDP or the imidazole group in CI-930. Chemical shift mapping (Figure 4-7) identifies a similar binding site

between levosimendan and CMDP located in the hydrophobic pocket of cNTnC• Ca^{2+}•$cTnI_{144-163}$. The large chemical shift perturbations of residues residing on the N-helix of cNTnC induced by CMDP suggests a structural opening of cNTnC•$cTnI_{144-163}$. The larger chemical shift changes of residues along the D-helix of cNTnC from CMDP binding when compared with levosimendan may be due to the proximity of these residues to the electronegative chloro group of CMDP, or a slightly different binding mode between the ligands. The perturbed chemical shifts along the B-helix induced by levosimendan may result from a larger displacement of $cTnI_{144-163}$ by the voluminous mesoxalonitrile hydrazone moiety when compared with CMDP. Assuming the binding mode of levosimendan and its analogs is similar to that of anapoe (Figure 4-9), the orientation of the pyridazinone molecules would be orthogonal to $cTnI_{144-163}$, *i.e.*, the chiral methyl group on the pyridazinone ring fits deep in the hydrophobic cavity whereas the group attached to the aromatic ring makes contacts with the residues in the N-terminus of $cTnI_{144-163}$ and the D-helix of cNTnC. Interestingly, EMD 57033 also binds into the hydrophobic pocket of cCTnC in a similar manner, with the chiral methyl group deep inside the protein core.

The affinities determined for the binding of levosimendan (K_D ~ 0.7 mM), AMDP (K_D ~ 1.5 mM), and CI-930 (K_D ~ 2.6 mM) to cNTnC•Ca^{2+}•$cTnI_{144-163}$ are comparable to the previous studies on levosimendan binding to cTnC•$3Ca^{2+}$•$cTnI_{32-79}$•$cTnI_{128-180}$ (K_D ≥ 0.2 mM) (*18*), W7 binding to cTnC•$3Ca^{2+}$•$cTnI_{34-71}$•$cTnI_{128-163}$ (K_D ~ 0.5 mM) (*17*), and anapoe binding to sTnC•$4Ca^{2+}$•$sTnI_{1-182}$•$sTnT_{156-262}$ (K_D ~ 0.64 mM) (*8*). This might support the notion that the binding of cardiotonic drugs to the regulatory unit of cardiac troponin occurs in a similar mode. These K_D values are in the high micromolar range, which is generally considered weak for protein-drug interactions. Levosimendan is known to exert multiple effects on perfused hearts at concentrations as low as 0.3 μM, the effect of levosimendan on skinned muscle fibers was half maximal by 0.3 μM, and maximal by 10 μM (*36*), and similar levels of levosimendan

modulated contractility in cardiomyocytes (*37*). Several factors could contribute to this phenomenon. Aggregation of drug molecules in aqueous solutions has been shown to cause low apparent affinities (*38, 39*). It is possible that cTnC in the highly organized and cooperative myofilaments may have a higher affinity for levosimendan than it does when cTnC is isolated in solution. On the other hand, the weak levosimendan-cTnC interaction may allow the drug to gently modulate cardiac contractility in a rhythmical fashion so that cardiac relaxation is not compromised. This is in accordance with a study reporting a K_D of > 2 mM for the interaction of pineal hormone melatonin and calmodulin. The low affinity has been used to explain many *in vitro* effects and pharmacological dosages of melatonin (*40*). The small chemical shift changes observed in this study suggest that these drug molecules do not induce large conformational changes in cNTnC•Ca^{2+}•$cTnI_{144-163}$. This feature is potentially useful for the rapid mapping of the drug molecules to the already determined structure of cNTnC•Ca^{2+}•$cTnI_{147-163}$ by measuring the intermolecular NOE restraints between cNTnC•Ca^{2+}•$cTnI_{147-163}$ and the drug molecules, a project currently in progress in our laboratory.

References

(1) Li, M. X., Wang, X., and Sykes, B. D. (2004) Structural based insights into the role of troponin in cardiac muscle pathophysiology. *J. Muscle Res. Cell Motil. 25*, 559-579.

(2) Kobayashi, T., and Solaro, R. J. (2005) Calcium, thin filaments, and the integrative biology of cardiac contractility. *Annu. Rev. Physiol. 67*, 39-67.

(3) Sia, S. K., Li, M. X., Spyracopoulos, L., Gagné, S. M., Liu, W., Putkey, J. A., and Sykes, B. D. (1997) NMR structure of cardiac troponin C reveals an unexpected closed regulatory domain. *J. Biol. Chem. 272*, 18216-18221.

(4) Spyracopoulos, L., Li, M. X., Sia, S. K., Gagné, S. M., Chandra, M., Solaro, R. J., and Sykes, B. D. (1997) Calcium-induced structural transition in the regulatory domain of human cardiac troponin C. *Biochemistry 36*, 12138-12146.

(5) McKay, R. T., Saltibus, L. F., Li, M. X., and Sykes, B. D. (2000) Energetics of the induced structural change in a Ca^{2+} regulatory protein: Ca^{2+} and troponin I peptide binding to the E41A mutant of the N-domain of skeletal troponin C. *Biochemistry 39*, 12731-12738.

(6) Li, M. X., Spyracopoulos, L., and Sykes, B. D. (1999) Binding of cardiac troponin-I 147-163 induces a structural opening in human cardiac troponin-C. *Biochemistry 38*, 8289-8298.

(7) Takeda, S., Yamashida, A., Maeda, K., and Maeda, Y. (2003) Structure of the core domain of human cardiac troponin in the Ca^{2+}-saturated form. *Nature 424*, 35-41.

(8) Vinogradova, M. V., Stone, D. B., Malanina, G. G., Karatzaferi, C., Cooke, R., Mendelson, R. A., and Fletterick, R. J. (2005) Ca^{2+}-regulated structural changes in troponin. *Proc Natl Acad Sci U S A. 102*, 5038-5043.

(9) Lindhout, D. A., and Sykes, B. D. (2003) Structure and dynamics of the C-domain of human cardiac troponin C in complex with the inhibitory region of human cardiac troponin I. *J. Biol. Chem. 278*, 27024-27034.

(10) Lindhout, D. A., Boyko, R. F., Corson, D. C., Li, M. X., and Sykes, B. D. (2005) The role of electrostatics in the interaction of the inhibitory region of troponin I with troponin C. *Biochemistry 44*, 14750-14759.

(11) Arteaga, G. M., Kobayashi, T., and Solaro, R. J. (2002) Molecular actions of drugs that sensitize cardiac myofilaments to Ca^{2+}. *Ann. Med. 34*, 248-258.

(12) Rosevear, P. R., and Finley, N. (2003) Molecular mechanism of levosimendan action: an update. *J. Mol. Cell. Cardiol. 35*, 1011-1015.

(13)   Sorsa, T., Pollesello, P., and Solaro, R. J. (2004) The contractile apparatus as a target for drugs against heart failure: interaction of levosimendan, a calcium sensitizer, with cardiac troponin C. *Mol. Cell Biochem. 266*, 87-107.

(14)   Kass, D. A., and Solaro, R. J. (2006) Mechanisms and use of calcium-sensitizing agents in the failing heart. *Circulation 113*, 305-315.

(15)   Li, M. X., Robertson, I. M., and Sykes, B. D. (2008) Interaction of cardiac troponin with cardiotonic drugs: A structural perspective. *Biochem. Biophys. Res. Commun. 369*, 88-99.

(16)   Wang, X., Li, M. X., and Sykes, B. D. (2002) Structure of the regulatory N-domain of human cardiac troponin C in complex with human cardiac troponin $I_{147-163}$ and bepridil. *J. Biol. Chem. 277*, 31124-31133.

(17)   Li, M. X., Hoffman, R. M. B., and Sykes, B. D. (2006) Interaction of cardiac troponin C with calmodulin antagonist W7 in the presence of three functional regions of cardiac troponin I. *Biochemistry 45*, 9833-9840.

(18)   Sorsa, T., Pollesello, P., Permi, P., Drakenberg, T., and Kilpelainen, I. (2003) Interaction of levosimendan with cardiac troponin C in the presence of cardiac troponin I peptides. *J. Mol. Cell Cardiol. 35*, 1055-1061.

(19)   Li, M. X., Saude, E. J., Wang, X., Pearlstone, J. R., Smillie, L. B., and Sykes, B. D. (2002) Kinetic studies of calcium and cardiac troponin I peptide binding to human cardiac troponin C using NMR spectroscopy. *Eur. Biophys. J. 31*, 245-256.

(20)   Parker, D. (1991) NMR determination of enantiomeric purity. *Chem. Rev. 91*, 1441-1457.

(21)   Muhandiram, D. R., and Kay, L. E. (1994) Gradient-enhanced triple-resonance three-dimensional NMR experiments with improved sensitivity. *J. Magn. Reson. B103*, 203-216.

(22)   Delaglio, F., Grzesiek, S., Vuister, G. W., Zhu, G., Pfeifer, J., and Bax, A. (1995) NMRPipe: A multidimensional spectral processing system based on UNIX pipes. *J. Biomol. NMR 6*, 277-293.

(23)   Johnson, B. A., and Blevins, R. A. (1994) NMRView: A computer program for teh visualization and analysis of NMR data. *J. Biomol. NMR 4*, 603-614.

(24)   Slupsky, C. M., Boyko, R. F., Booth, V. K., and Sykes, B. D. (2003) Smartnotebook: A semi-automated approach to protein sequential NMR
            resonance assignments. *J. Biomol. NMR 27*, 313-321.

(25)   Sorsa, T., Heikkinen, S., Abbott, M. B., Abusamhadneh, E., Laakso, T., Tilgmann, C., Serimaa, R., Annila, A., Rosevear, P. R., Drakenberg, T., Pollesello, P., and Kilpelainen, I. (2001) Binding of levosimendan, a calcium sensitizer, to cardiac troponin C. *J. Biol. Chem. 276*, 9337-9343.

(26)   Mercier, P., Ferguson, R. E., Corrie, J. E., Trenthem, D. R., and Sykes, B. D. (2003) Structure and dynamics of rhodamine labeled N-domain of skeletal troponin C in complex with with skeletal troponin I 115-131. *Biochemistry 42*, 4333-4348.

(27)   Pollesello, P., Ovaska, M., Kaivola, J., Tilgmann, C., Lundstrom, K., Kalkkinen, N., Ulmanen, I., Nissinen, E., and Taskinen, J. (1994) Binding of a new Ca^{2+} sensitizer, levosimendan, to recombinant human cardiac troponin C. A molecular modelling, fluorescence probe, and proton nuclear magnetic resonance study. *J. Biol. Chem. 269*, 28584-28590.

(28)   Kleerekoper, Q., and Putkey, J. A. (1999) Drug binding to cardiac troponin C. *J. Biol. Chem. 274*, 23932-23939.

(29)   Lehtonen, L., and Põder, P. (2007) The utility of levosimendan in the treatment of heart failure. *Ann. Med. 39*, 2-17.

(30)   Li, M. X., Spyracopoulos, L., Beier, N., Putkey, J. A., and Sykes, B. D. (2000) Interaction of cardiac troponin C with Ca^{2+} sensitizer EMD 57033 and cardiac troponin I inhibitory peptide. *Biochemistry 39*, 8782-8790.

(31)   Wang, X., Li, M. X., Spyracopoulos, L., Beier, N., Chandra, M., Solaro, R. J., and Sykes, B. D. (2001) Structure of the C-domain of human cardiac troponin C in complex with the Ca^{2+} sensitizing drug EMD 57033. *J. Biol. Chem. 276*, 25456-25466.

(32)   Sorsa, T., Pollesello, P., Rosevear, P. R., Drakenberg, T., and Kilpeläinen, I. (2003) Stereoselective binding of levosimendan to cardiac troponin C causes Ca^{2+}-sensitization. *Eur. J. Pharmacol. 486*, 1-8.

(33)   Solaro, R. J., Fujino, K., and Sperelakis, N. (1989) The positive inotropic effect of pimobendan involves stereospecific increases in the calcium sensitivity of cardiac myofilaments. *J. Cardiovasc. Pharmacol. 14*, S7-12.

(34)   Fujino, K., Sperelakis, N., and Solaro, R. J. (1988) Differential effects of d- and l-pimobendan on cardiac myofilament calcium sensitivity. *J. Pharmacol. Exp. Ther. 247*, 519-523.

(35)   Levijoki, J., Pollesello, P., Kaivola, J., Tilgmann, C., Sorsa, T., Annila, A., Kilpelainen, I., and Haikala, H. (2000) Further evidence for the cardiac troponin C mediated calcium sensitization by levosimendan: structure-response and binding analysis with analogs of levosimnedan. *J. Mol. Cell Cardiol. 32*, 479-491.

(36)   Edes, I., Kiss, E., Kitada, Y., Powers, F. M., Papp, J. G., Kranias, E. G., and Solaro, R. J. (1995) Effects of levosimendan, a cardiotonic agent targeted to troponin C, on cardiac function and on phosphorylation and Ca^{2+} sensitivity of cardiac myofibrils and sarcoplasmic reticulum in guinea pig heart. *Circ. Res. 77*, 107-113.

(37)   Sato, S., Talukder, M. A., Sugawara, H., Sawada, H., and Endoh, M. (1998) Effects of levosimendan on myocardial contractility and Ca^{2+} transients in aequorin-loaded right-ventricular papillary

muscles and indo-1-loaded single ventricular cardiomyocytes of the rabbit. *J. Mol. Cell. Cardiol. 30*, 1115-1128.

(38) Attwood, D., and Natarajan, R. (1981) Effect of pH on the micellar properties of amphiphilic drugs in aqueous solution. *J. Pharm. Pharmacol. 33*, 136-140.

(39) Ravin, L. J., and Warren, R. J. (1971) Micelle Formation and its significance in interpretation of NMR spectra of phenothiazine. *J. Pharm. Sci. 60*, 329.

(40) Turjanski, A. G., Estrin, D. A., Rosenstein, R. E., McCormick, J. E., Martin, S. R., Pastore, A., Biekofsky, R. R., and Martorana, V. (2004) NMR and molecular dynamics studies of the interaction of melatonin with calmodulin. *Prot. Sci. 13*, 2925-2938.

(41) Baker, N. A., Sept, D., Joseph, S., Holst, M. J., and McCammon, J. A. (2001) Electrostatics of nanosystems: application to microtubules and the ribosome. *Proc. Natl. Acad. Sci. U. S. A. 98*, 10037-10041.

Chapter 5

A structural and functional perspective into the mechanism of Ca^{2+}-sensitizers that target the cardiac troponin complex*

Summary

The Ca^{2+} dependent interaction between troponin I (cTnI) and troponin C (cTnC) triggers contraction in heart muscle. Heart failure is characterized by a decrease in cardiac output, and compounds that increase the sensitivity of cardiac muscle to Ca^{2+} have therapeutic potential. The Ca^{2+}-sensitizer, levosimendan, targets cTnC; however, detailed understanding of its mechanism has been obscured by its instability. In order to understand how this class of positive inotropes function, we investigated the mode of action of two fluorine containing novel analogs of levosimendan; 2′,4′-difluoro(1,1′-biphenyl)-4-yloxy acetic acid (dfbp-o) and 2′,4′-difluoro(1,1′-biphenyl)-4-yl acetic acid (dfbp). The affinities of dfbp and dfbp-o for the regulatory domain of cTnC were measured in the absence and presence of cTnI by NMR spectroscopy, and dfbp-o was found to bind more strongly than dfbp. Dfbp-o also increased the affinity of cTnI for cTnC. Dfbp-o increased the Ca^{2+}-sensitivity of demembranated cardiac trabeculae in a manner similar to levosimendan. The high resolution NMR solution structure of the cTnC–cTnI–dfbp-o ternary complex showed that dfbp-o bound at the hydrophobic interface formed by cTnC and cTnI making critical interactions with residues such as Arg147 of cTnI. In the absence of cTnI, docking localized dfbp-o to the same position in the hydrophobic groove of cTnC. The structural and functional data reveal that the levosimendan class of Ca^{2+}-sensitizers work by binding to the regulatory domain of cTnC and stabilizing the pivotal cTnC–cTnI regulatory unit via a network of hydrophobic and electrostatic interactions, in contrast to the destabilizing effects of antagonists such as W7 at the same interface.

Contribution: NMR experiments were planned by IMR and BDS. IMR and MXL did the titrations. IMR acquired the 3D experiments for the structure calculation and solved the structure and YBS performed the physiology experiments. IMR and BDS wrote the bulk of the manuscript, with YBS adding experimental details and conclusions from the fiber experiments.

Introduction

Cardiac muscle contraction is regulated by a Ca^{2+}-triggered cascade of thin and thick filament protein-protein interactions. The thin filament is comprised of three molecular units: troponin, tropomyosin, and f-actin. Troponin is a heterotrimeric protein complex consisting of troponin C (cTnC), a Ca^{2+}-binding protein with two EF-hand motifs in each terminal domain, troponin I (cTnI), the subunit which inhibits contraction via its interaction with f-actin, and troponin T (cTnT), a scaffolding protein that tethers troponin to the thin filament through association with cTnI and tropomyosin. The C-terminal, or "structural", domain of cTnC (cCTnC) is bound to two divalent cations (Mg^{2+} or Ca^{2+}) throughout the contraction-relaxation cycle of muscle contraction. Its primary function is to keep cTnC mounted on the thin filament via its tight association with the "anchoring" region of cTnI ($cTnI_{34-71}$). Like cCTnC, the regulatory domain of cTnC (cNTnC) contains two EF-hand motifs; however, Ca^{2+}-binding site I is defunct, leaving only site II available for Ca^{2+} association. During systole, Ca^{2+} enters the cytosol and binds to the N-domain of cTnC ($cNTnC \cdot Ca^{2+}$), which prompts a slight opening of cNTnC and the resultant interaction with the "switch" region of cTnI ($cTnI_{147-163}$). The association of $cTnI_{147-163}$ with $cNTnC \cdot Ca^{2+}$ is coupled with the separation of the inhibitory ($cTnI_{128-147}$) and C-terminal ($cTnI_{163-181}$) regions of cTnI from f-actin. Once cTnI dissociates from f-actin, tropomyosin changes its orientation to reveal the myosin binding surface on f-actin, the actin-myosin cross-bridge can subsequently form, and the ATPase dependant contraction occurs (for reviews on the regulation of contraction by troponin see (*1-3*)).

Heart failure is a condition that is characterized by compromised blood supply through the body. There are numerous drug therapies; however, many tend to have undesirable side effects. For example, therapeutic strategies which involve the increase of Ca^{2+} levels within the cardiomyocyte may result in arrhythmia, tachycardia, and mortality. In

response to the negative long-term performance of these drugs, another treatment scheme being explored is to increase the Ca^{2+}-sensitivity of the thin filament, and thus improve contractility without modulating Ca^{2+} concentration. This class of pharmaceuticals is referred to as Ca^{2+}-sensitizers (*4-6*). Levosimendan is a positive inotrope that binds cTnC to elicit its Ca^{2+}-sensitizing function (*7-9*). One current theory is that levosimendan functions by stabilizing the open conformation of cNTnC•Ca^{2+}, so that it is in a favorable conformation to bind cTnI$_{147-163}$ (*10*). Thus, levosimendan would increase the affinity of cTnI$_{147-163}$ for cNTnC•Ca^{2+} and as a result, the Ca^{2+}-sensitivity of the thin filament. Although the structure of levosimendan bound to cTnC has been modeled (*11*), there have not been any high resolution structures of levosimendan bound to cTnC or cTnC-cTnI solved. The unstable nature of levosimendan (*12*) is the major barrier preventing the determination of these structures and consequently is thwarting a complete understanding of its molecular mechanism.

In order to investigate the Ca^{2+}-sensitizing mechanism of levosimendan, we have elected to study the fluorine containing analogues, 2',4'-difluoro(1,1'-biphenyl)-4-yl acetic acid (dfbp) and 2',4'-difluorobiphenyl-4-yloxy acetic acid (dfbp-o). We conducted contractility measurements with demembranated trabeculae from rat ventricles and saw an increase in the Ca^{2+}-sensitivity of the cardiac muscle in the presence of dfbp-o. Thus, the chemical structure of dfbp-o constitutes a potential scaffold for the development of novel Ca^{2+}-sensitizers. Titration experiments done *in vitro* suggest that this enhanced contractility is caused by an increase in the affinity of cTnI$_{147-163}$ for cNTnC•Ca^{2+} by dfbp-o. In addition to determining the functional effects of dfbp-o, we investigated the structure of dfbp-o bound to cNTnC•Ca^{2+} and cNTnC•Ca^{2+}•cTnI$_{144-163}$. The structures highlight important pharmacophores of Ca^{2+}-sensitizing molecules and provide insight into the molecular mechanism of Ca^{2+}-sensitizers that target troponin.

Experimental Procedures

Sample preparation.

Recombinant human cNTnC (residues 1-89) was used in this study. The engineering of the expression vector and the expression of ^{15}N- and ^{13}C,^{15}N-labeled proteins in *E. coli* were as described previously (*13*). The two cTnI peptides, cTnI$_{147-163}$, acetyl-RISADAMMQALLGARAK-amide, and cTnI$_{144-163}$, acetyl-RRVRISADAMMQALLGARAK-amide, were synthesized by GL Biochem Ltd. (Shanghai, China). Peptide quality was verified by HPLC and ESI-Mass Spectrometry. Dfbp-o was purchased from Sigma-Aldrich and dfbp was purchased from Amatek Co. and purities and chemical structures were verified by NMR spectroscopy, ESI-Mass Spectrometry, MS/MS, and Infrared Spectroscopy. Stock solutions of the compounds in DMSO-d_6 (Cambridge Isotopes Inc.) were prepared and the vials containing the solutions were wrapped in aluminum foil to protect the molecules from light catalyzed degradation. All NMR samples prepared in 5 mm NMR tubes had a volume of 500 µL. The protein samples were solubilized in 100 mM KCl, 10 mM imidazole, and 0.2-0.25 mM 2,2-dimethyl-2-silapentane-5-sulfonate sodium salt (DSS) (Chenomix) in 95% H$_2$O/5% D$_2$O, 5-10 mM CaCl$_2$ (Fluka) and the pH was maintained at ~7.0. For the paramagnetic studies, 3 mm NMR tubes were used with a final volume of 200 µL, and the NMR buffer conditions were 100 mM KCl, 10 mM imidazole, and 0.2-0.25 mM DSS, 5-10 mM CaCl$_2$, 0.5 mM trifluoroacetic acid (TFA) in 99.9% D$_2$O and the pD was maintained at ~7.3.

Ab initio calculation details.

The minimum energy conformations and electronic properties were calculated with Gaussian03(*14*). The parameters implemented for the

calculations on dfbp, dfbp-o, and levosimendan were identical. Geometry optimization was performed using Becke's three-parameter Lee, Yang, Parr (B3LYP) hybrid functional with a split-valence basis set and polarization d-orbitals added (B3LYP/6-31G(d). The optimized geometries were subsequently used to calculate the total density and electrostatic potential (ESP), using the B3LYP/6-311+G(d, p) basis set in aqueous solvent. Final contour surfaces were represented using GaussView 3.0.

Computational Docking.

Autodock 4.0(*15*) was used to localize the binding site of dfbp-o on cNTnC. Autodock uses a genetic search algorithm as a global optimizer and energy minimization as a local search method. The target protein was kept rigid, and dfbp-o was given torsional flexibility around the ether bond. The spacing of 0.375 Å was used to generate the affinity grid maps. The Lamarckian genetic algorithm (LGA) and pseudo-Solis and Wets method were used for minimization. Default parameters were used for docking, unless otherwise specified. For the binding-site-centered docking, a grid map of 78 x 66 x 54 centered at 57.192, 2.138, and 0.939 was generated with each LGA job that consisted of 200 runs with 270000 generations in each run and maximum number of energy evaluations of 5.0×10^6. The resulting docked orientations with an rmsd of 2.0 Å were clustered together. AutoDockTools (http://www.scripps.edu/~sanner) was used to generate all of the necessary files and to analyze the results. The structure of dfbp-o used for the docking was generated by Gaussian03. Partial atomic charges were assigned automatically in AutoDockTools using the Gasteiger-Marsili method(*16*). The protein coordinates used in the calculation were taken from the X-ray structure of cTnC•3bepridil (PDB 1DTL)(*17*). The coordinates for the three bepridil molecules, the C-domain of cTnC (92-160), and the two Ca^{2+} bound to the C-domain were removed

prior to docking. Kollman united-atom partial charges and solvation parameters were added to the protein file using AutoDockTools.

NMR spectroscopy.

Titration Analysis.

All NMR experiments were run on either a Varian Inova 500 MHz spectrometer or a Unity 600 MHz spectrometer. All data were collected at 30 °C. Both spectrometers are equipped with a triple resonance $^{1}H^{13}C^{15}N$ probe and z-pulsed field gradients. Protein concentration was determined by amino acid analysis and by 1D $^{1}H,^{15}N$-HSQC NMR spectroscopy. Stock solutions of dfbp, dfbp-o, cTnI$_{147-163}$, and cTnI$_{144-163}$ were prepared in DMSO-d_6 and concentrations were calibrated by comparing their 1D ^{1}H NMR spectra with that of a DSS standard. In contrast to levosimendan(*12*), there was no noticeable degradation of dfbp-o and dfbp in the presence of DTT. The binding of the various ligands to cNTnC and to cNTnC in complex with a ligand was monitored by 2D-$^{1}H,^{15}N$-HSQC NMR spectroscopy. At each point in a titration, a 2D-$^{1}H, ^{15}N$-HSQC spectrum was acquired, and chemical shift changes were used to calculate the dissociation constant.

We titrated 0.17 mM ^{15}N-cNTnC with 0.11, 0.23, 0.45, 0.67, 1.22, 1.75, 2.28, 2.79, and 3.30 mM of dfbp. We titrated 0.08 mM ^{15}N-cNTnC in ~2x excess cTnI$_{144-163}$ with 0.23, 0.45, 0.67, 0.89, 1.43, 1.96, 2.49, 3.00, and 3.50 mM of dfbp. We titrated 0.24 mM ^{15}N-cNTnC with 0.10, 0.30, 0.69, 1.27, and 1.56 mM of dfbp-o. We titrated 0.34 mM ^{15}N-cNTnC in ~2x excess cTnI$_{144-163}$ with 0.05, 0.14, 0.28, 0.46, 0.64, 1.01, and 1.55 mM of dfbp-o. We titrated 0.61 mM ^{15}N-cNTnC in ~4x excess cTnI$_{147-163}$ with 0.09, 0.19, 0.28, 0.37, 0.46, 0.55, 0.64, and 1.09 mM of dfbp-o. We used a larger excess of cTnI$_{147-163}$ than cTnI$_{144-163}$ because cTnI$_{147-163}$ has a lower affinity for cNTnC, and we wanted to obtain saturation of cNTnC. We titrated 0.29 mM ^{15}N-cNTnC with 0.02, 0.03, 0.06, 0.12, 0.27, 0.44, 0.63,

and 0.74 mM of cTnI$_{144-163}$. We titrated 0.3 mM ^{15}N-cNTnC in ~4x excess dfbp-o with 0.03, 0.06, 0.18, 0.28, 0.37, 0.53, and 0.60 mM of cTnI$_{144-163}$. We titrated 0.11 mM ^{15}N-cNTnC in ~4x excess dfbp-o with 0.01, 0.02, 0.03, 0.05, 0.07, 0.09, 0.11, 0.14, 0.17, and 0.23 mM of cTnI$_{147-163}$. We titrated 0.10 mM ^{15}N-cNTnC with 0.01, 0.03, 0.05, 0.08, 0.11, 0.14, 0.17, 0.20, and 0.25 mM of cTnI$_{147-163}$. The titrations involving cTnI$_{147-163}$ were done at lower concentrations because it is difficult to get a concentrated stock solution of cTnI$_{147-163}$. During the titrations with the ligands the pH was maintained by adding small aliquots of NaOH to the samples.

The binding of the dfbp, dfbp-o, cTnI$_{147-163}$, and cTnI$_{144-163}$ to the target molecules or complexes were fit with a 1:1 stoichiometry. We corrected the concentrations of ^{15}N-cNTnC, cTnI$_{147-163}$, cTnI$_{144-163}$, dfbp, and dfbp-o for sample dilution that occurred during the various titrations. The dissociation constants were calculated by averaging the normalized individual chemical shifts as a function of the ligand to protein ratios and fitting was done using xcrvfit (www.bionmr.ualberta.ca/bds/software/xcrvfit). The amide resonances that were perturbed larger than the mean plus one standard deviation were chosen for the K_D calculation. The K_D was determined by fitting the data to the equation:

$$target + ligand \leftrightarrow target \cdot ligand$$
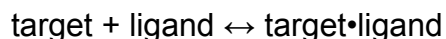
NMR experiments for Assignment and Structure Calculation.

The backbone atoms were assigned by the 2D-^{1}H,^{15}N-HSQC, 3D-CBCACONNH and 3D-HNCACB experiments and the side chain resonances were assigned by making use of the 2D-^{1}H,^{13}C-HSQC and 3D-CCONH and 3D-HCCONH experiments. Aromatic resonances were assigned by running a 2D-NOESY of the complex in D$_2$O. The HNHA experiment was run to unambiguously assign the α-protons of most residues. Intramolecular distance restraints for cNTnC were obtained by

the 3D-NOESYCHSQC and 3D-NOESYNHSQC experiments. We chose a mixing time of 100 ms for the 3D-NOESYCHSQC experiment and 150 ms for the 3D-NOESYNHSQC experiment. Structural distance restraints for cTnI$_{144-163}$ and dfbp-o were obtained with the 2D-^{13}C, ^{15}N filtered NOESY (mix = 200 ms) and the 2D-^{13}C,^{15}N filtered TOCSY (mix = 60 ms) experiments (18-20). Assignments of cTnI$_{144-163}$ were guided by the previously made assignments for cTnI$_{147-163}$ in the cNTnC•Ca^{2+}•cTnI$_{147-163}$•bepridil complex (21). The two fluorine nuclei of dfbp-o were assigned by running 1D ^{19}F and 2D ^{1}H,^{19}F – HOESY NMR spectroscopy (22, 23). In order to obtain distance restraints between the unlabeled ligands and labeled protein we employed the ^{13}C-edited, filtered HMQCNOESY experiment (24, 25) with a mixing time of 250 ms. Contacts between methionine methyls were crucial for the structure determination of this complex. They were assigned by the ^{13}C-edited NOESYHSQC and by comparing these assignments with those determined by Krudy *et al.* for the cTnC-cTnI complex(26) by the employment of site-specific mutagenesis of Met to Leu (27).

We used paramagnetic relaxation enhancement (PRE) to provide restraints between the metal ion bound to cNTnC and dfbp-o. The basic principle behind PRE is that the relaxation rates of nuclei surrounding the paramagnetic metal, such as gadolinium (Gd^{3+}), will be enhanced by the large contribution from the unpaired 4f electrons of the metal. The difference in relaxation rates between the diamagnetic and paramagnetic bound complexes can provide us with distance restraints to dfbp-o. In order to extract distances from the relaxation enhancement by Gd^{3+} we followed the procedures outlined by Gariépy *et al.* (28). Since Gd^{3+} has seven unpaired 4f electrons, the metal is a very efficient broadening agent and we did not need very much to elicit a strong response to dfbp-o. We prepared a stock solution of 0.3 mM cNTnC•Gd^{3+}•cTnI$_{144-163}$ and titrated it into an NMR tube containing 0.8 mM dfbp-o acquiring 1D ^{19}F or 1D ^{1}H spectra at each titration point. We repeated the titration with the

diamagnetic lanthanide (Ln^{3+}), lanthanum (La^{3+}), in complex with cNTnC and cTnI$_{144-163}$ to test for any diamagnetic contribution to the relaxation enhancement of dfbp-o. We found that diamagnetic relaxation enhancement was negligible at the low cNTnC•La^{3+}•cTnI$_{144-163}$ concentrations we were working with. We also added free Gd^{3+} into dfbp-o to see if excess Gd^{3+} (unbound to cNTnC•cTnI$_{144-163}$) would contribute to broadening via specific coordination with the carboxylate moiety of dfbp-o. Dfbp-o signals were broadened in the presence Gd^{3+}; however, only at concentrations greatly exceeding the cNTnC•Ln^{3+}•cTnI$_{144-163}$ concentration range we were working in. Since free Gd^{3+} only enhanced relaxation of dfbp-o nuclei at high concentrations and that ~1:1 cNTnC:Gd^{3+} complexes were prepared in order to limit the amount of free Gd^{3+}, we assumed that all paramagnetic effects were from bound dfbp-o. In order to determine the amount of dfbp-o bound, we took advantage of the situation where the total concentration of dfbp-o ($[L]_T$) greatly exceeds the concentration of the paramagnetic protein ($[P]_T$). The fraction of dfbp-o bound is then determined by the simple equation:

$$f_L^{bound} = \frac{[P]_T}{K_D + [L]_T}$$

This relationship requires that the total ligand concentration is approximately equal to free ligand. We determined the K_D of dfbp-o for cNTnC•Ca^{2+}•cTnI$_{144-163}$, and assumed that the affinity of dfbp-o for cNTnC•Gd^{3+}•cTnI$_{144-163}$ was unchanged.

Structure determination by NMR spectroscopy.

Generation of the structure file of dfbp-o.
The PRODRG web server(*29*) was used to create a PDB file for dfbp-o and XPLO-2D was used to create a topology file, a parameter file, and an XPLOR-NIH script which was used to generate a structure file. The

structure file of dfbp-o was manually altered to include the atomic charges predicted by Gaussian3.0 for water refinement.

Data processing and structure calculation.

VNMRJ (Varian Inc.) was used for the analysis of 1D NMR spectra, necessary for the assignment of dfbp-o and for the PRE measurements. All 2D and 3D NMR data were processed with NMRPipe(*30*). The assignment of chemical shifts was done with NMRView (*31*), and sequential assignment was done with the program SmartNoteBook (*32*). The ψ and φ dihedral angle restraints predicted by TALOS (*33*) were used for both cNTnC and cTnI$_{144-163}$. Six distance restrains derived from x-ray crystallographic data of Ca^{2+}-chelating oxygen atoms to Ca^{2+} were included, as well as, two distance restraints between Asp65 and Gly70 included to hold the Ca^{2+}-binding loop together. In order to help assign the 3D-NOESYCHSQC and 3D-NOESYNHSQC experiments, structures of cNTnC•Ca^{2+} were generated using the program CYANA(*34*). Distance restraints were calibrated in CYANA with an upper limit of 6 Å. Assignments were made manually and kept during the first four CYANA calculation cycles, after which they were open for automatic assignment with the "noeassign" command of CYANA. CYANA was used to calculate 100 structures, of which the 20 conformers with the lowest target function were used to further refine the structure. Following the CYANA refinement, peaklists were read back into NMRView, reviewed manually, and converted into XPLOR-NIH (*35*) format. The median method was used to calibrate interproton distances in the 3D-NOESYCHSQC and 3D-NOESYNHSQC experiments. The simulated annealing protocol of XPLOR-NIH was used, with 10,000 high temperature steps and 6000 cooling steps. The structure of cNTnC•Ca^{2+} was initially optimized, followed by the cNTnC•Ca^{2+}•cTnI$_{144-163}$ structure, and finally the cNTnC•Ca^{2+}•cTnI$_{144-163}$•dfbp-o complex. Intermolecular proton-proton distance restraints were calculated using loose restraints (1.8-6.0 Å).

There were 8 intermolecular NOE restraints between dfbp-o and cNTnC, 3 intramolecular NOEs of dfbp-o, 6 PRE distance restraints between dfbp-o and Gd^{3+}, and 4 intermolecular NOEs between dfbp-o and $cTnI_{144-163}$. We measured 30 intermolecular NOEs between $cTnI_{144-163}$ and cNTnC as well as 24 intramolecular NOEs. 200 structures were calculated and the 50 lowest energy structures were refined in water with a water box edge length of 18.8 Å(*36*). The final ensemble is represented by the 20 structures after the water refinement with the fewest dihedral violations, ordered by lowest energy prior to water refinement (see Supplementary Table II for statistics).The ensemble was validated by Procheck (*37*) available with the online Protein Structure Validation Software (PSVS) suite (http://psvs-1_4-dev.nesg.org/). The ensemble has been deposited in the protein data bank (www.rcsb.org) with the accession code of 2L1R.pdb.

Force measurement in ventricular trabeculae.

The methods for working with the ventricular trabeculae are the same as in Sun *et al.* (*38*). Wistar rats (200–250 g) were stunned and killed by cervical dislocation (Schedule 1 procedure in accordance with UK Animal (Scientific Procedures) Act 1986). The hearts were removed and rinsed free of blood in Krebs solution containing (mM): NaCl, 118; $NaHCO_3$, 24.8; Na_2HPO_4, 1.18; $MgSO_4$, 1.18; KCl, 4.75; $CaCl_2$, 2.54; glucose, 10; bubbled with 95% O_2–5% CO_2; pH 7.4 at 20 °C. Suitable trabeculae (free running, unbranched, diameter < 250 µm) were dissected from the right ventricle in Krebs solution containing 25 mM 2,3-butanedione-monoxime, permeabilised in relaxing solution (see below) containing 1% Triton X-100 for 30 min, and stored in relaxing solution containing 50% (vol/vol) glycerol at -20 °C for experiments, normally within 2 days of dissection. Demembranated trabeculae were mounted, via aluminium T-clips between a force transducer (AE 801) and a fixed hook

in a 60 µl glass trough containing relaxing solution. The sarcomere length of the relaxing muscle was set to 2.1–2.2 µm by laser diffraction. The experimental temperature was 20–22 °C.   Experimental   solutions contained 25 mM imidazole, 5 mM MgATP, 1 mM free Mg^{2+}, 10 mM EGTA (except pre-activating solution), 0 – 10 mM total calcium, 1 mM dithiothreitol and 0.1% (vol/vol) protease inhibitor cocktail (P8340, Sigma). All solutions also included an ATP backup system consisting of 15 mM phosphocreatine (P7936, Sigma) and 1 mg/ml creatine phosphokinase (C3755, Sigma). Ionic strength was adjusted to 200 mM with potassium propionate; pH was 7.1 at 20 °C. The concentration of free Ca^{2+} was calculated   using   the   program   WinMAXC   V2.5 (http://www.stanford.edu/~cpatton/maxc.html). When required, 0.5 mM dfbp-o was added from a 500 mM stock solution in DMSO and the pH was re-adjusted.

Each trabecular activation was preceded by a 1-min incubation in pre-activating solution. Isometric force and fluorescence intensities were measured after steady-state force had been established in each activation. The dependence of force on $[Ca^{2+}]$ was fit to data from individual trabeculae using nonlinear least-squares regression to the Hill equation:

$$Y = [Ca^{2+}]^{n_H} / (EC_{50}{}^{n_H} + [Ca^{2+}]^{n_H})$$

where EC_{50} is the $[Ca^{2+}]$ corresponding to half-maximal change in Y, and n_H is the Hill coefficient. All values are shown in Supplementary table I and given as mean ± standard error except where noted, with n representing the number of trabeculae.

Results

Structural Description of the Levosimendan Analogues

The short lifespan of levosimendan in aqueous solution has made it difficult to gain a thorough understanding of its mode of action. We chose to study two compounds (dfbp and dfbp-o) that were originally developed as analogues of the anti-inflammatory drug, flobufen (*39*). Although dfbp and dfbp-o are ostensibly structurally unique from levosimendan, we propose that these differences are mostly superficial, and the features that are exclusive to dfbp and dfbp-o may in fact contribute to their attractiveness as new lead compounds. Levosimendan, dfbp, and dfbp-o all contain a central phenyl constituent attached to a substituted ring structure and an electronegative moiety (Figure 5-1). We propose that the difluorophenyl group of dfbp and dfbp-o replaces of the pyridazinone ring of levosimendan and the carboxyl moiety, the malonodinitrile hydrazone group. Since fluorine has a van der Waals radius of 1.44 Å (*40*) it is isosteric with oxygen (*41*). Aromatic fluorine has a large dipole moment, similar to the carbonyl of levosimendan; however, unlike the carbonyl, it is not significantly polarizable. Therefore, although aromatic fluorine can take part in electrostatic interactions it does not take part in hydrogen bonding and consequently increases the overall lipophilicity of a molecule (*41, 42*). We propose that the second fluorine at the 2' position replaces the methyl on the pyridazinone ring of levosimendan. Given that levosimendan is predicted to bind to the hydrophobic pocket of cNTnC (*11, 43*) and that the substitution of a methyl with a fluorine can increase the metabolic stability of a compound (*44*), the replacement of the carbonyl and methyl groups with fluorines suggests these compounds may represent a novel chemical platform for the development of more suitable troponin targeting Ca^{2+}-sensitizers. The malonodinitrile group of levosimendan may be replaced by the carboxylate of dfbp and dfbp-o, and the aromatic ether of dfbp-o
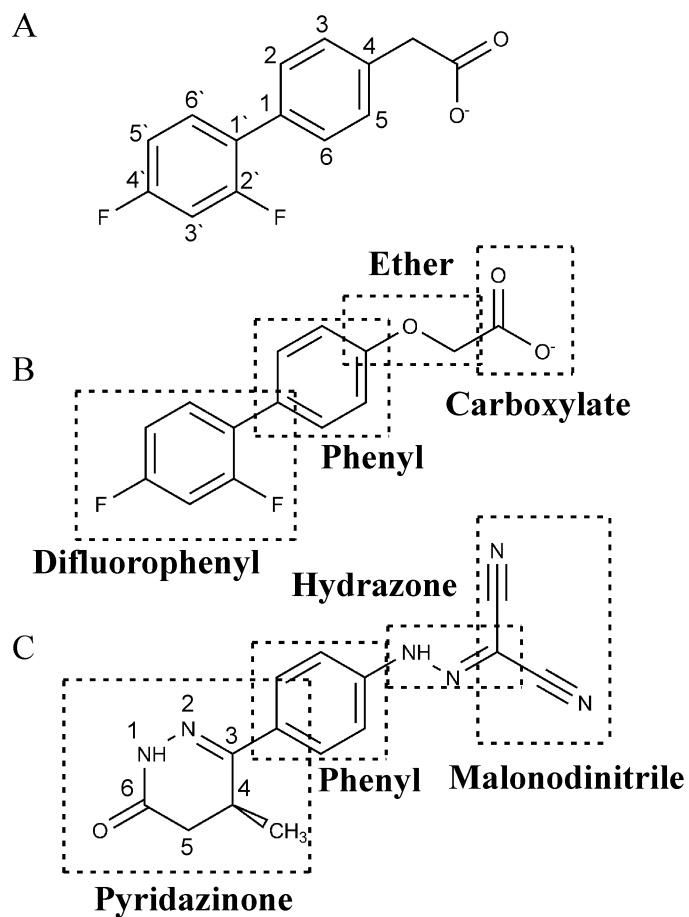
Figure 5-1. The chemical structures of (A) dfbp (B) dfbp-o and (C) levosimendan. Distinct chemical units of dfbp-o and levosimendan are labeled.

may serve as a hydrogen bond acceptor in a similar manner as the hydrazone group of levosimendan. In order to investigate the therapeutic prospect of these compounds, we monitored their interaction with the regulatory domain of cTnC in both the absence and presence of cTnI. Following these titrations, we chose the most potent of the ligands to pursue with a structural and functional analysis.

The Comparison of Dfbp and Dfbp-o

We monitored the binding of dfbp and dfbp-o to ^{15}N-labeled cNTnC ± cTnI$_{144-163}$ by acquiring ^{1}H,^{15}N-heteronuclear single quantum coherence (HSQC) NMR spectra at each point in the titrations. These data were used to determine the dissociation constants and stoichiometry of the ligands for the cNTnC•Ca^{2+} and the cNTnC•Ca^{2+}•cTnI$_{144-163}$ complexes (unless otherwise stated, all cTnC states are Ca^{2+}-saturated and thus the Ca^{2+} will be omitted). The ^{1}H,^{15}N-HSQC spectra also contribute information about changes in the chemical environment at each ^{15}N-labeled amide nucleus. When a ligand binds to a protein, the amide resonances of residues near the bound ligand will experience a change in chemical shift. A chemical shift change may also be induced by a conformational change in the protein rather than by direct contact with the ligand. In either scenario, the change in chemical shift may be used to characterize protein-ligand interactions. In this study, we calculated dissociation constants using all amide chemical shifts that were perturbed greater than the mean shift change plus one standard deviation. The data from these shifts were than normalized and averaged to calculate a final dissociation constant. We found that dfbp bound to cNTnC with a dissociation constant of 7150 ± 1160 µM, whereas dfbp-o bound to cNTnC with a K$_D$ of 820 ± 190 µM. Dfbp bound to the cNTnC•cTnI$_{144-163}$ complex with a K$_D$ = 2820 ± 480 µM, and dfbp-o bound to the same complex with a K$_D$ = 270 ± 30µM (Figure 5-

2). Since dfbp-o binds to cNTnC and cTnC•cTnI$_{144-163}$ ~10-fold tighter than dfbp we focused the rest of the study on characterizing its function.

The Inotropic Mechanism of Dfbp-o

In vitro analysis by NMR spectroscopy

The regulation of muscle contraction is linked to the opening and closing of cNTnC. The Ca^{2+}-triggered opening of cNTnC leads to a slight increase in the solvent exposure of a core hydrophobic patch. In the Ca^{2+}-saturated state, cNTnC does not fully open as is the case with sTnC (*45*), but rather its conformational equilibrium is shifted from the closed state towards the open state in the presence of Ca^{2+} (*46, 47*). Following Ca^{2+}-binding, the switch region of cTnI binds to cNTnC and stabilizes the open form of cNTnC (*48*). The development of ligands that likewise stabilize the open conformation of cNTnC might strengthen the interaction of cTnI with cNTnC, and thus augment contractility (*10*).   In order to test whether dfbp-o increased the affinity of cTnI$_{144-163}$ for cNTnC, we titrated cTnI$_{144-163}$ into cNTnC in the absence and presence of dfbp-o. The affinity of cTnI$_{144-163}$ for cNTnC was measured to be 26 ± 4 µM and in the presence of dfbp-o was measured to be 19 ± 10 µM. Since it is difficult to measure dissociation constants of low micromolar ranges by NMR spectroscopy, we chose to investigate an alternative cTnI segment with a lower affinity for cNTnC. The affinity of cTnI$_{147-163}$ for cNTnC was calculated to be 130 ± 10 µM and 60 ± 10 µM for cNTnC•dfbp-o (Figure 5-3A, B). The dissociation constant of dfbp-o was also enhanced by the presence of cTnI$_{147-163}$ from 820 ± 190 µM to 380 ± 80 µM (Figure 5-3C, D). The results indicate that dfbp-o and cTnI$_{147-163}$ bind reciprocally to cNTnC. We fit the data to a ternary complex model (Figure 5-3E), which is defined by a contribution of four equilibrium constants, two for dfbp-o (reactions C and D) and two for cTnI$_{147-163}$ (reactions A and B). The data meet the
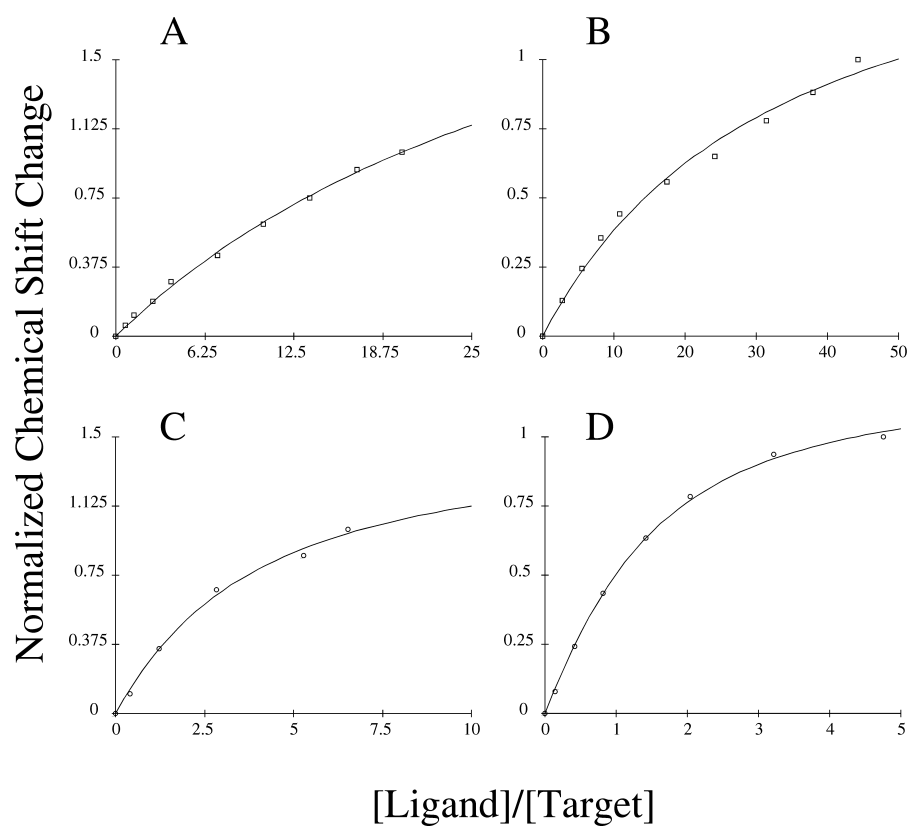
Figure 5-2. Comparison of the affinities of dfbp and dfbp-o. (A) Titration of dfbp into cNTnC. (B) Titration of dfbp into cNTnC•cTnI$_{144-163}$. (C) Titration of dfbp-o into cNTnC. (D) Titration of dfbp-o into cNTnC•cTnI$_{144-163}$.
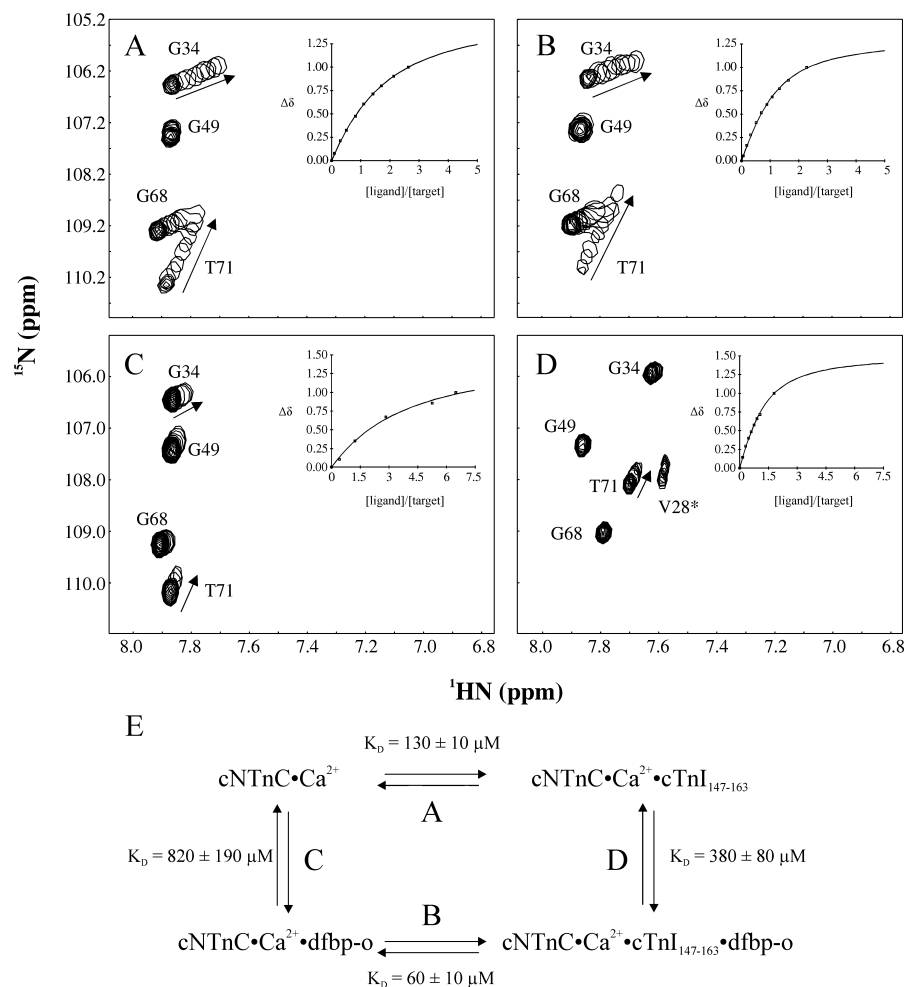
Figure 5-3. Titration series with dfbp-o. (A) Titration of cTnI$_{147-163}$ into cNTnC. (B) Titration of cTnI$_{147-163}$ into cNTnC•dfbp-o (4 fold excess of dfbp-o). (C) Titration of dfbp-o into cNTnC. (D) Titration of dfbp-o into cNTnC•cTnI$_{147-163}$ (2-3 fold excess of cTnI$_{147-163}$). The same expanded region of the two dimensional ^{1}H,^{15}N- HSQC NMR spectra of cNTnC for each ligand is shown. Spectra taken at the various titration points are superimposed. Arrows indicate the direction of chemical shift perturbation induced by the ligand. V28 is present in the spectrum (D) but not narrow enough to be seen in the other spectra. (E) The thermodynamic cycle of dfbp-o and cTnI$_{147-163}$ binding to cNTnC.

thermodynamic constraints of this model (C/D = 2.16 ± 0.95; A/B = 2.17 ± 0.53) and the cNTnC-cTnI interaction appears to be stabilized by dfbp-o.

In situ analysis by cardiac trabeculae contractility

The Ca^{2+}-sensitizing properties of dfbp-o were monitored using demembranated cardiac trabeculae from rat ventricles. Similar to previous results found for levosimendan (*9, 49, 50*), dfbp-o did not increase the maximal force of the trabeculae; however, at sub-maximal Ca^{2+} concentrations (1.0 – 1.5 µM) the force of contraction was significantly increased (Figure 5-4). The dependence of force on free $[Ca^{2+}]$ was fitted by the Hill equation. The $[Ca^{2+}]$ giving half-maximum force (EC_{50}) was decreased from 1.42 ± 0.03 µM to 1.23 ± 0.06 µM (SEM, n=4, *P* < 0.05, paired *t*-test) from the control to in the presence of 500 µM dfbp-o. The corresponding pCa (pCa_{50}; pCa=-$\log_{10}[Ca^{2+}]$) was 5.85 ± 0.01 and 5.91± 0.02 in the absence and presence of dfbp-o (Table 5-1), this change is similar to that induced by 10 µM levosimendan, where the pCa increased from 5.88 to 5.98(*49*). As the relationship between force and $[Ca^{2+}]$ is steep in the cardiac trabeculae, with Hill coefficients (n_H) of 5.7 and 4.6 in the absence and presence of dfbp-o, a decrease of 0.06 pCa units for pCa_{50} would result in an increase of force up to 20% of the maximum value during sub-maximal activation (dashed line in Figure 5-4). Similar results were also found with levosimendan [50].

The observation that dfbp-o has no influence on the force during relaxation and maximal Ca^{2+} activation suggests that dfbp-o is not altering the myosin-actin cross-bridge formation, and that dfbp-o would not impair relaxation. We chose to study trabeculae contraction in the presence of 500 µM dfbp-o, which is higher than the 10 µM of levosimendan used in previous studies (*9, 49*). This was done because the affinity of dfbp-o (820 ± 190 µM) for cNTnC is lower than what has been estimated for levosimendan (~ 10 µM (*10, 51*)).
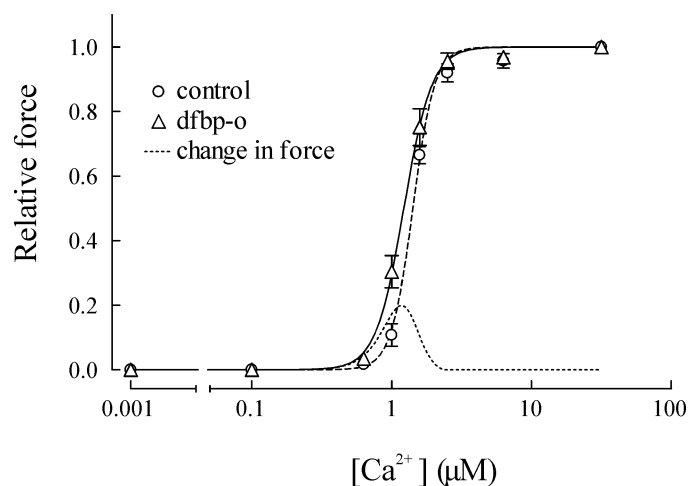
Figure 5-4. Effect on Ca^{2+}-sensitivity of skinned cardiac trabeculae by dfbp-o. The relationship between $[Ca^{2+}]$ and relative force at various $[Ca^{2+}]$ was determined in the absence (O) and presence of 500 µM dfbp-o (Δ). In the presence of dfbp-o, the relative force at Ca^{2+} concentrations of 1.0 µM and 1.5 µM were significantly higher than the control. Mean results were fit to the Hill equation and shown as dashed (control) or solid (dfbp-o) lines. The fine dashed line represents the change in force in the presence of dfbp-o.

Table 5-1. Effect on calcium sensitivity of skinned cardiac trabeculae by dfbp-o.

	Control	0.5 mM DFBP-O	p (one-tailed, paired t-test)
pCa_{50} (pCa corresponding to half maximum force)	5.85 ± 0.01	5.91 ± 0.02	0.012
EC_{50} (μM, Ca^{2+} concentration corresponding to pCa_{50})	1.42 ± 0.03	1.23 ± 0.06	0.008
n_H (Hill coefficient)	5.76 ± 0.72	4.60 ± 0.54	0.020

Structural Details of the Dfbp-o - Troponin Interaction

Dfbp-o binds to the hydrophobic surface of cNTnC

There are a number of structures of small molecules bound to cNTnC that have been solved by NMR spectroscopy and X-ray crystallography. Despite the markedly different chemical structures of the ligands, they all bind to the hydrophobic core of cNTnC and stabilize the open form of cNTnC. In this study, we titrated dfbp-o into cNTnC and followed the chemical shifts (^{1}H, ^{15}N) of each backbone amide resonance. The chemical shifts of all residues were averaged, and any resonance that moved greater than the mean change was mapped on the surface of cNTnC (Figure 5-5A). The results imply that dfbp-o binds in the hydrophobic groove of cNTnC, as does bepridil (1dtl.pdb) (*17, 52*), trifluoperazine (1wrk.pdb and 1wr1.pdb) (*52, 53*), and W7 (2kfx.pdb) (*54*).

In conjunction with the chemical shift mapping, we used AutoDock 4.0 (*15*) to predict the binding site and pose of dfbp-o on cNTnC. We docked dfbp-o onto the structure of the N-domain of the bepridil bound form of cTnC. We used a binding-site-centered docking approach for dfbp-o on the hydrophobic patch of cNTnC since the results from the chemical shift mapping identified this location as the binding site. To predict the binding mode of dfbp-o, the docking calculations generated clusters of binding modes and subsequently ranked them based on a lowest energy solution determined by the minimum docking energy. The lowest energy cluster predicted that the difluorophenyl ring binds in the hydrophobic core of cNTnC with the carboxyl moiety projecting towards the C-terminus of the D-helix (Figure 5-5B). AutoDock calculates the binding energy of each docked structure, and this energy can be converted to a binding constant. For the lowest energy cluster, the program predicted a K_D of 604 ± 145 μM, which is close to the experimentally determined K_D of 820 ± 190 μM, and thus gives additional credence to predicted binging mode.
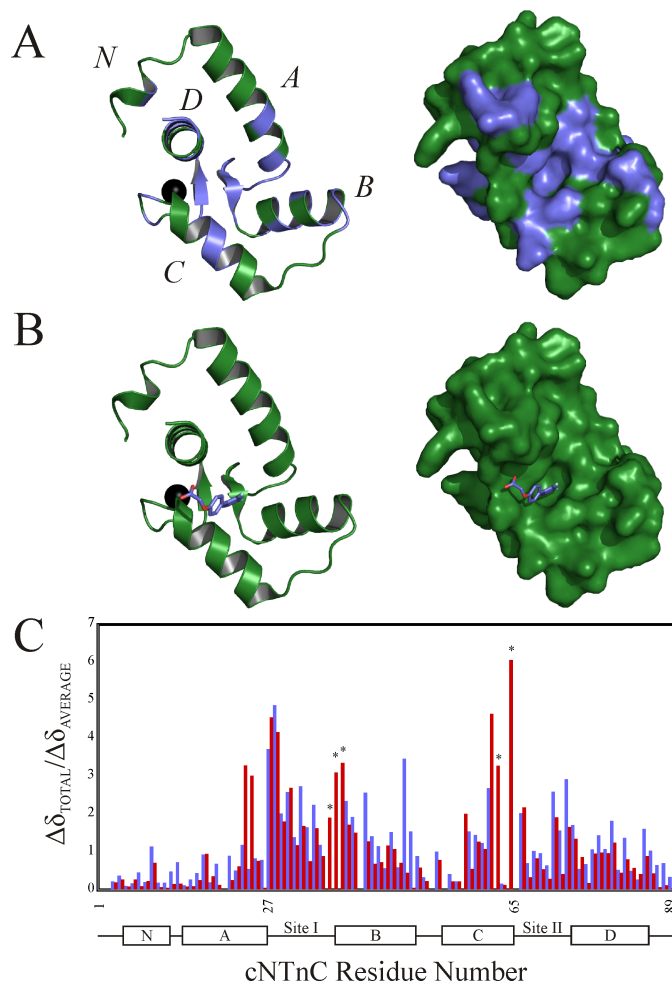
Figure 5-5. Binding of dfbp-o to cNTnC. (A) Mapping of the chemical shifts induced by the binding of dfbp-o to cNTnC onto the cartoon (left) and surface (right) representations of cNTnC taken from the cTnC•3Bep structure (1dtl.pdb). All residues perturbed more than the average chemical shift change are colored in slate, with the unperturbed residues colored in green; the Ca^{2+} is shown as a black sphere. (B) Localization of the binding site of dfbp-o on cNTnC by AutoDock 4.0. The lowest energy binding mode of dfbp-o (stick representation) is shown docked onto the cartoon (left) and surface (right) representations of cNTnC. (C) Bar diagram plotting the relative chemical shift perturbations of cNTnC induced by $cTnI_{147-163}$ (red bars) or dfbp-o (slate bars). Residues marked with a star were exchange broadened during the dfbp-o titration, and therefore final perturbed distances were not measured.

To investigate if dfbp-o induced an opening of cNTnC as do other ligands, we compared the relative chemical shift changes of dfbp-o with the relative chemical shift changes induced by cTnI$_{147-163}$ (Figure 5-5C). Although the total chemical shift changes induced by dfbp-o are smaller than what is caused by cTnI$_{147-163}$ (Figure 5-3), the patterns are quite similar. We propose that dfbp-o stabilizes the open state of cNTnC in a similar manner as cTnI$_{147-163}$. Therefore, the increase in the affinity of cNTnC•dfbp-o for cTnI$_{147-163}$ may be explained, in part, by the increase solvent exposure of the hydrophobic residues in the core of cNTnC. One goal of the design of Ca^{2+}-sensitizers is to select for ligands that increase the affinity of cTnI$_{147-163}$ for cNTnC, it has been proposed that the target molecule should be the cNTnC-cTnI complex (*55*). Accordingly, we have determined the structure of the cNTnC•cTnI$_{144-163}$•dfbp-o complex by NMR spectroscopy.

Solution Structure of cNTnC•cTnI$_{144-163}$•dfbp-o

The structure of cNTnC•cTnI$_{144-163}$•dfbp-o was determined by solution state NMR spectroscopy. See the online Methods for details on the NMR experiments we ran and references therein. For some of the less standard NMR experiments a brief discussion of the theory and expected results is included. Our discussion of the structure will start by considering each unit of the complex individually and then we will summarize the overall implications of the structure. The cNTnC•cTnI$_{144-163}$•dfbp-o structure discussed in the text is the lowest energy structure from the deposited ensemble of 20 structures (see Figure 5-6 and Table 5-2 for statistics).

Structural features of cNTnC.

The structure of cNTnC in the cNTnC•cTnI$_{144-163}$•dfbp-o complex is made up of five helical elements (N, A, B, C, D) and a short anti-parallel β-sheet (Figure 5-7A,B). This overall fold is conserved throughout all known
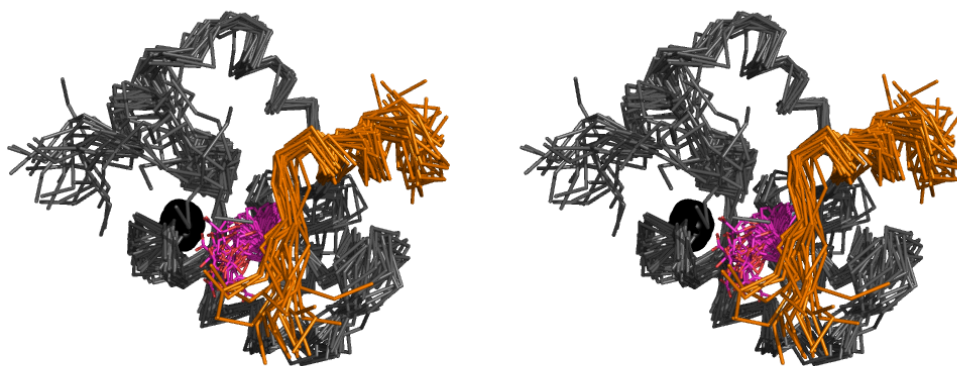
Figure 5-6. Cross-eye stereo view of the ensemble of 20 structures of cNTnC•cTnI$_{144-163}$•dfbp-o. cNTnC (grey) and cTnI$_{144-163}$ (orange) are shown in ribbon representation, dfbp-o (magenta) shown in stick representation, and Ca^{2+} is represented as a black sphere.

Table 5-2. Structural statistics for 20 NMR structures of cNTnC•cTnI$_{144-163}$•dfbp-o.

	Backbone atoms	Heavy Atoms
R.m.s.d. from the average structure		
All residues (Å)	1.7	2.3
Ordered residues [a] (Å)	0.9	1.4
Total Distance Restraints	1747	
Intra Residual NOEs	1030	
Short range (|*i-j*|=1) NOEs	309	
Medium range (1<|*i-j*|<5) NOEs	180	
Long range (|*i-j*|≥5) NOEs	147	
Intramolecular cTnI$_{144-163}$ NOEs	24	
NOEs between cTnI$_{144-163}$ and cNTnC	30	
NOEs between cTnI$_{144-163}$ and dfbp-o	4	
Intramolecular dfbp-o NOEs	3	
NOEs between dfbp-o and cNTnC	8	
PRE distance restraints to dfbp-o	6	
Ca^{2+} distance restraints	6	
Dihedral restraints (ϕ/ψ)	125	
NOE violations [b]		
> 0.5 Å	0	
> 0.3 Å	7	
> 0.1 Å	133	
Dihedral Violations > 5º	9	
Ramachadran plot statistics [c]		
ϕ/ψ in most favored regions (%)	94.8 %	
ϕ/ψ in additionally allowed regions	5.1 %	
ϕ/ψ generously allowed regions (%)	0.0 %	
ϕ/ψ in disallowed regions (%)	0.1 %	

[a] Residues 4-11, 14-29, 38-49,54-64,74-85, and 151-157

[b] Violations are for the 20 NMR lowest energy structures

[c] As determined by PROCHECK
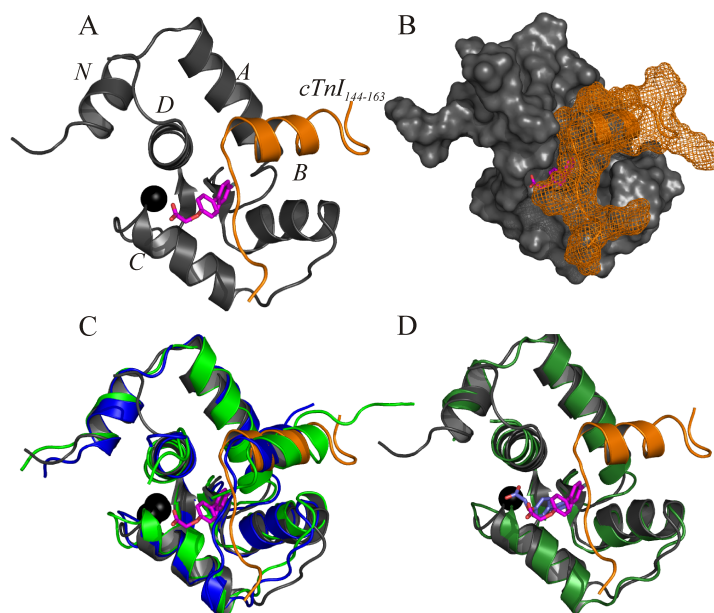
Figure 5-7. Structure of dfbp-o bound to cNTnC•cTnI$_{144-163}$. For all representations of cNTnC•cTnI$_{144-163}$•dfbp-o the backbone atoms for cNTnC are colored in grey and in orange for cTnI$_{144-163}$; dfbp-o is shown in stick representation with its carbon atoms colored in magenta, oxygen in red, and fluorine in aqua; and Ca^{2+} is shown as a black sphere. (A) Cartoon representation of the lowest energy structure of cNTnC•cTnI$_{144-163}$•dfbp-o. (B) The structure of cNTnC•cTnI$_{144-163}$•dfbp-o with cNTnC shown as a surface and cTnI$_{144-163}$ shown as a mesh. (C) Overlay of cNTnC•cTnI$_{144-163}$•dfbp-o with the X-ray crystal structure cNTnC•cTnI$_{144-163}$ (blue; 1j1d.pdb) and the NMR structure cNTnC•cTnI$_{147-163}$ (green; 1mxl.pdb). (D) Overlay of cNTnC•cTnI$_{144-163}$•dfbp-o with cNTnC•dfbp-o (forest green; predicted by AutoDock). The docked version of dfbp-o is colored in slate, and the dfbp-o from the NMR structure is shown in magenta.

structures of cNTnC and indicates that dfbp-o is not inducing any large structural perturbation of cNTnC. The backbone rmsd for cNTnC (residues 5-85) in this complex with the X-ray structure cNTnC•cTnI$_{144-163}$ (1j1d.pdb) (*56*) is 1.154 Å and with the NMR structure cNTnC•cTnI$_{147-163}$ (1mxl.pdb) (*48*) is 1.556 Å (Figure 5-7C). The only difference between cNTnC•cTnI$_{144-163}$•dfbp-o and the other structures is in the orientation of the C-helix, which has shifted slightly away from the D-helix to accommodate dfbp-o.

Structural features of cTnI$_{144-163}$.

The structure of cTnI$_{144-163}$ is bound in a similar conformation as in the crystal structure of cNTnC•cTnI$_{144-163}$ (1j1d.pdb) and the NMR structure of cNTnC•cTnI$_{147-163}$ (1mxl.pdb) with backbone rmsds for residues 150-157 of 0.504 Å and 1.278 Å, respectively. The assignment of the ^{1}H resonances of cTnI$_{144-163}$ when bound to cNTnC were obtained by the ^{13}C, ^{15}N-filtered nuclear overhauser effect spectroscopy (NOESY) and the ^{13}C, ^{15}N-filtered total correlation spectroscopy (TOCSY) (*18-20*). These experiments filter signals from the labeled-protein, while keeping signals from unlabeled ligands. We assigned 24 intramolecular NOEs belonging to cTnI$_{144-163}$ in the ^{13}C, ^{15}N-filtered NOESY. We determined the location of cTnI relative to cNTnC via the ^{13}C-edited, filtered HQMCNOESY NMR experiment (*24, 25*). This NMR experiment measures NOEs between a ^{13}C-labeled protein and an unlabeled ligand. We measured 30 intermolecular NOEs between cTnI$_{144-163}$ and ^{13}C, ^{15}N-labeled cNTnC (for examples see Figure 5-8), and the position of cTnI$_{144-163}$ relative to cNTnC is similar to that of cNTnC•cTnI$_{144-163}$. Since neither the structure of cTnI$_{144-163}$, nor the position of cTnI$_{144-163}$ is significantly perturbed by the presence of dfbp-o, it appears that dfbp-o is not competing for the same binding site on cNTnC. This is in contrast to W7 (*57*) and bepridil (*21*), which sterically clash with cTnI and subsequently perturb the position of cTnI on cNTnC.
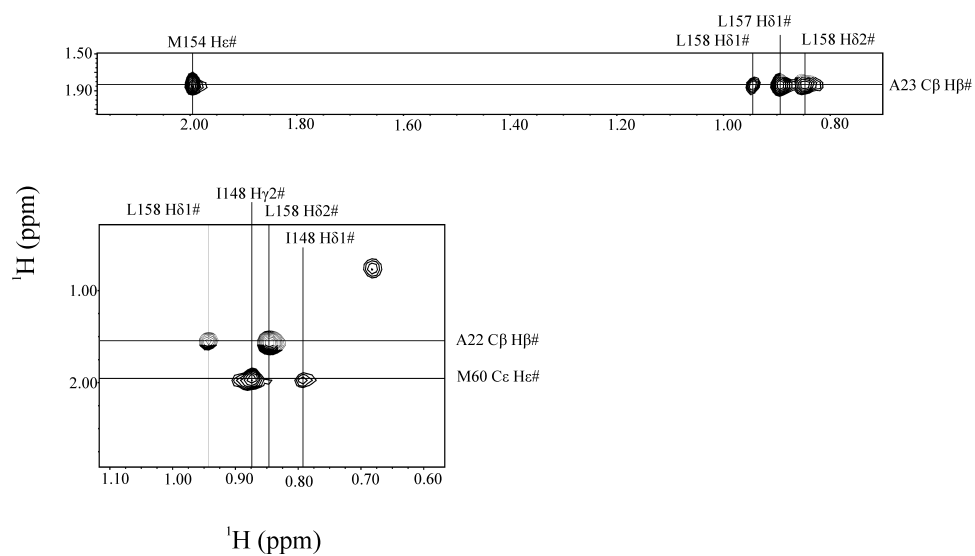
Figure 5-8. Intermolecular NOEs between cTnI$_{144\text{-}163}$ and ^{13}C, ^{15}N-labeled cNTnC. The right side of the spectra correspond to proton resonances from ^{13}C, ^{15}N-labeled cNTnC, and the vertical axis corresponds to proton resonances from cTnI$_{144\text{-}163}$.

Structural features of dfbp-o.

The binding site of dfbp-o is located in a well defined pocket formed by hydrophobic residues from cNTnC and cTnI$_{144-163}$. We used the filtered NOESY and TOCSY experiments to assign the ^{1}H chemical shifts of dfbp-o and we assigned the ^{19}F chemical shifts by one-dimensional ^{19}F and two-dimensional ^{1}H-^{19}F heteronuclear overhauser spectroscopy (HOESY) experiments (*23*). In addition to assigning the ^{1}H and ^{19}F chemical shifts of dfbp-o, the NOESY and HOESY experiments provided structural restraints for dfbp-o. In total we used three intramolecular distance restraints in the structure calculation, including one between F2' and H6/H2 and two between the phenyl protons (H2/H6 and H3/H5) and the CH$_2$ group. An important characteristic of dfbp-o is that its phenyl ring is symmetric, and so NOEs to H2 and H6 or H3 and H5 are indistinguishable and therefore were ambiguously assigned. The filtered NOESY also revealed NOEs between dfbp-o and cTnI$_{144-163}$. The terminal methyls of Met153 and Ile148 make NOE contacts with the aromatic H2/H6 and H3/H5 of dfbp-o (Figure 5-9). These NOEs added structural restraints between dfbp-o and cTnI$_{144-163}$, and gave us information into the relative orientations of the two molecules. Intermolecular NOEs between residues from cNTnC and dfbp-o helped position dfbp-o. We used the ^{13}C-edited, filtered HMQCNOESY NMR experiment to observe contacts between the dfbp-o H2/H6 and H3/H5 and the terminal methyls of Met60 and Met45 of ^{13}C,^{15}N-cNTnC. We also measured intermolecular contacts between Met80 and H6' and H3' as well as between Leu41 or Val72 and H3' and H5' (Figure 5-10).

The ambiguity of the NOE restraints and the lack of distance restraints between the fluorine atoms of dfbp-o and cNTnC left the orientation of dfbp-o poorly resolved. In an effort to improve the resolution of dfbp-o, we used paramagnetic relaxation enhancement (PRE). Lanthanide paramagnetism has recently been employed by the Otting group to determine the structure of thymidine bound to the ε exonuclease subunit of DNA polymerase III (*58*). Briefly, we used the principle that
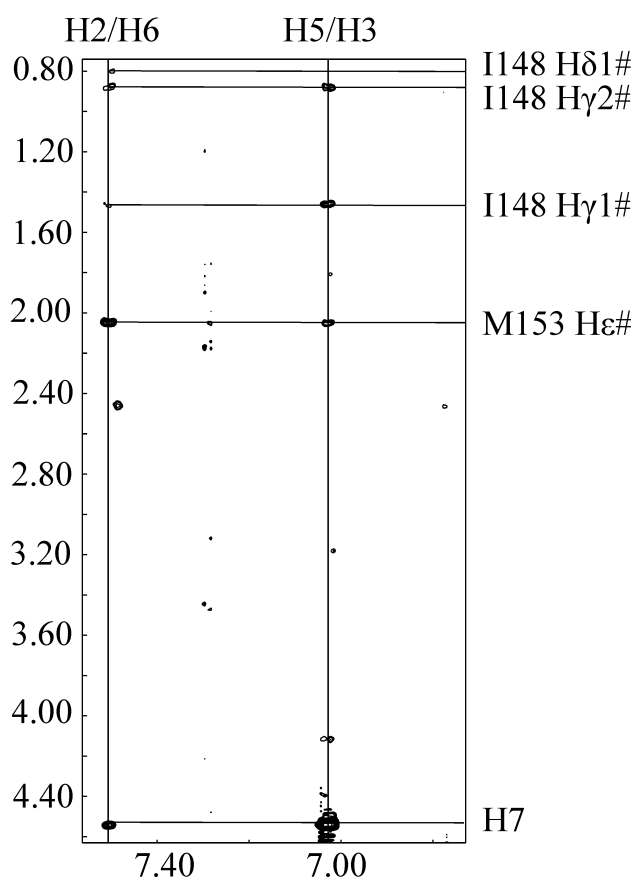
Figure 5-9. Intermolecular NOEs between cTnI$_{144-163}$ and dfbp-o. The right side of the spectra correspond to proton resonances from cTnI$_{144-163}$, and the vertical axis corresponds to proton resonances from dfbp-o.
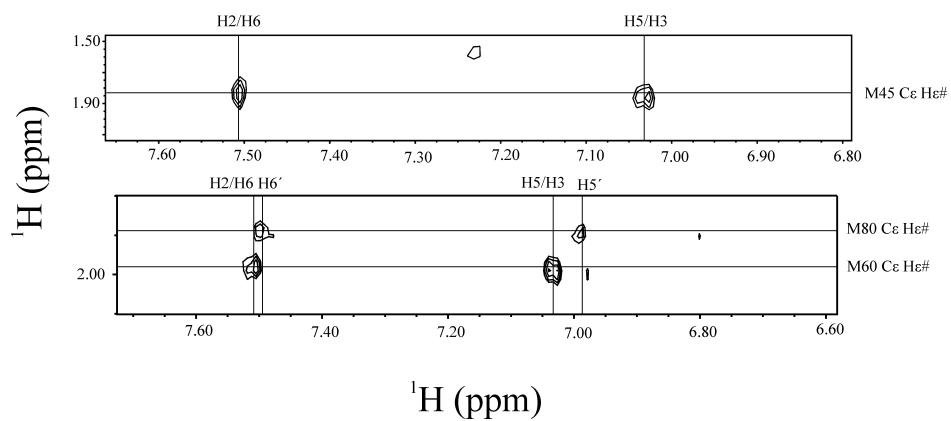
Figure 5-10. Intermolecular NOEs between dfbp-o and ^{13}C, ^{15}N-labeled cNTnC. The right side of the spectra correspond to proton resonances from ^{13}C, ^{15}N-labeled cNTnC, and the vertical axis corresponds to proton resonances from dfbp-o.

unpaired electrons from paramagnetic molecules will increase the relaxation rate of nuclei in a distance dependant manner. We titrated free dfbp-o with cNTnC•Gd^{3+}•cTnI$_{144\text{-}163}$ and cNTnC•La^{3+}•cTnI$_{144\text{-}163}$ and compared the relaxation rates of the two ^{19}F signals as well as the ^{1}H signals from H2/H6, H6', and CH$_2$ in the paramagnetic (Gd^{3+}) and diamagnetic (La^{3+}) systems. The broadening of the 1D ^{19}F and ^{1}H spectra of dfbp-o are shown in Figure 5-11. The differences in the relaxation rates were then used to calculate distances between the protons and the fluorines of dfbp-o and the Gd^{3+}.

The structure indicates that dfbp-o is bound in the hydrophobic pocket formed between cTnI$_{144\text{-}163}$ and cNTnC. The F4'of dfbp-o points towards the anti-parallel β-sheet of cNTnC and F2' points away from cTnI$_{144\text{-}163}$. The central phenyl ring of dfbp-o is near the N-terminus of cTnI$_{144\text{-}163}$ with the negatively charged carboxylate of dfbp-o positioned near the positively charged side-chains of Arg147 and Arg83. The overall orientation of dfbp-o is similar to the binding mode of dfbp-o in complex with cNTnC as predicted by AutoDock (Figure 5-7D). In summation, the structure reveals that dfbp-o binds deep enough within the hydrophobic pocket as to avoid sterically clashing with cTnI$_{144\text{-}163}$ and the negatively charged moiety of dfbp-o is in the vicinity of the positively charged N-terminus of cTnI$_{144\text{-}163}$.

Comparison of dfbp-o binding and other NTnC ligands.

There have been several structures determined of small molecules bound to the cTnC-cTnI complex. We have overlaid the secondary structures of these complexes with cNTnC•Ca^{2+}•cTnI$_{144\text{-}163}$•dfbp-o (Figure 5-12) and found that the most similar was the sNTnC•sTnI$_{112\text{-}131}$•anapoe (1ytz.pdb) X-ray crystal structure (*59*), with a backbone rmsd of 1.253 Å. The overlay of cNTnC•cTnI$_{144\text{-}163}$•dfbp-o with cNTnC•cTnI$_{147\text{-}163}$•bepridil (1lxf.pdb) (*21*) and cNTnC•cTnI$_{147\text{-}163}$•W7 (2krd.pdb) (*57*) yielded much larger rmsds (2.459 Å and 3.061 Å, respectively). These ligands all bind at
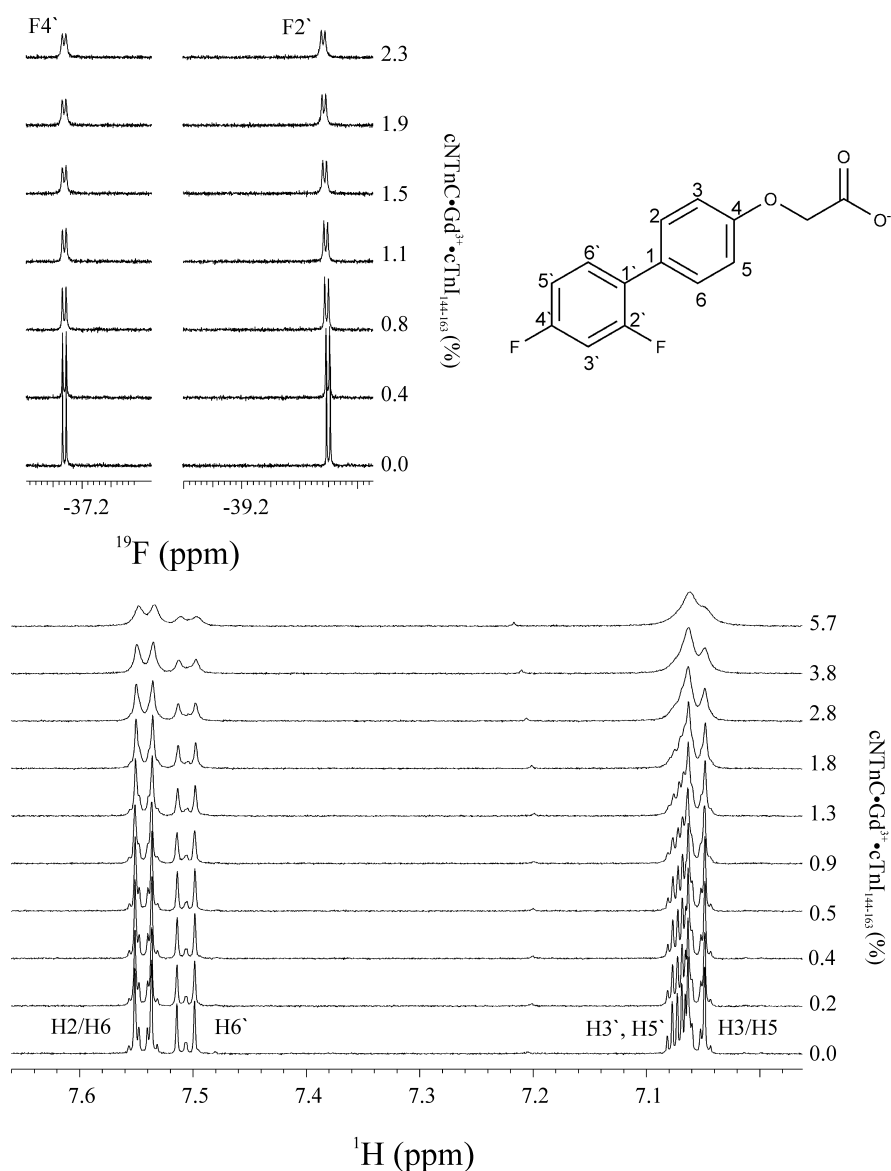
Figure 5-11. Paramagnetic relaxation enhancement of signals of dfbp-o by Gd^{3+} bound to cNTnC-cTnI$_{144-163}$. The stacked 1D ^{19}F spectrum of dfbp-o is shown in the upper left, and the stacked 1D ^{1}H spectrum of dfbp-o is shown at the bottom. Both stacked spectra are shown as a function of percentage dfbp-o bound to cNTnC•Gd^{3+}•cTnI$_{144-163}$. The numbering of dfbp-o is shown on its chemical structure as a reference.
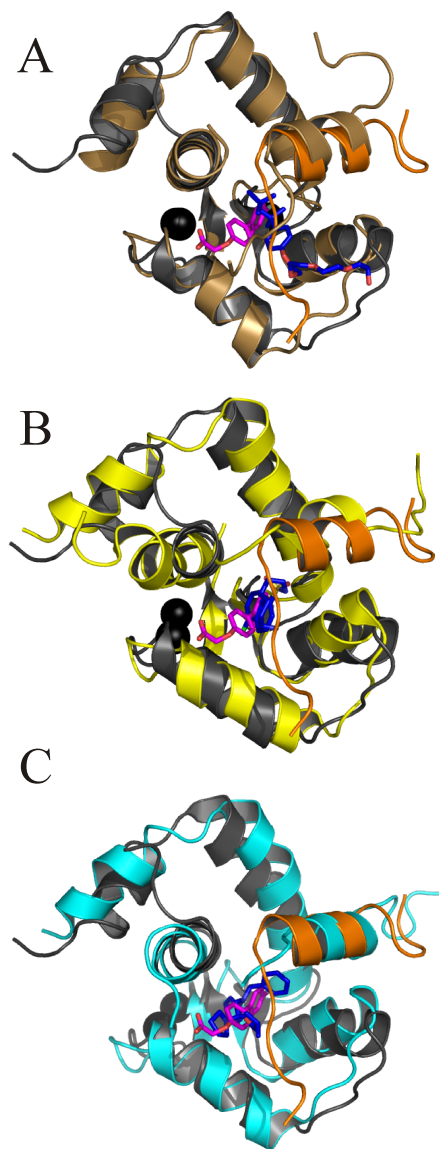
Figure 5-12. Overlay of the secondary structure backbone nuclei of cNTnC•cTnI$_{144-163}$•dfbp-o with (A) sNTn•sTnI$_{112-131}$•anapoe (1ytz.pdb), (B) cNTnC•cTnI$_{147-163}$•W7 (2krd.pdb), and (C) cNTnC•cTnI$_{147-163}$•bepridil (1lxf.pdb). Backbone atoms for cNTnC are colored in grey (cNTnC•cTnI$_{144-163}$•dfbp-o), brown (sNTnC•sTnI$_{112-131}$•anapoe), yellow (cNTnC•cTnI$_{147-163}$•W7), cyan (cNTnC•cTnI$_{147-163}$•bepridil). Only in cNTnC• cTnI$_{144-163}$•dfbp-o was cTnI colored differently than cNTnC (orange). Dfbp-o is shown in stick representation, with carbon atoms in magenta, oxygen in red, and fluorine in aqua. All other ligands are also shown in stick representation with carbon atoms colored in blue, oxygen in red, and nitrogen atoms in dark blue. Ca^{2+} ions are shown as black spheres.

the interface formed between cNTnC and cTnI, but only the Ca^{2+}-sensitizing agents, dfbp-o and anapoe do not perturb the quaternary structure of the troponin complex.

Discussion

The effectiveness of levosimendan in the treatment of heart failure has garnered much attention over the past few decades. Despite intense efforts to understand the molecular mechanism of levosimendan, its instability has circumvented knowledge of its precise mode of action *in vivo*. In this report, we described the molecular mechanism of the Ca^{2+}-sensitizing agent, dfbp-o, a stable analogue of levosimendan. The chemical structures of dfbp-o and levosimendan highlight several pharmacophores required for targeting the cTnC-cTnI complex. Firstly, a substituted ring system; in levosimendan it is a pyridazinone ring which contains a methyl and carbonyl oxygen, and in dfbp-o it is a phenyl ring with two fluorine atoms. The second functional moiety is a phenyl ring that serves as a hydrophobic scaffold to connect the substituted ring to a hydrophilic extension. The hydrophilic group contains a central H-bond acceptor (the ether oxygen in dfbp-o and the hydrazone nitrogen in levosimendan) and an electronegative moiety (the carboxylate in dfbp-o and malonodinitrile in levosimendan) coplanar with the central ring (Figure 5-13A-C). It was reported by Levijoki and coworkers that the hydrazone constituent of levosimendan is crucial for its full cardiotonic function (*43*). The authors removed the hydrogen accepting nitrogen from the hydrazone so that instead of NH-N it was NH-C and saw a drastic decrease in the Ca^{2+}-sensitizing and cTnC binding functionalities. Consistent with these findings, dfbp, which lacks the H-bond acceptor at this location has a ten-fold lower affinity for cTnC and the cTnC-cTnI complex than dfbp-o. In a recent study, Amin *et al*. identified a few more pharmacophores necessary to elicit cardiotonic activity (*60*). They found that carbonyl groups attached
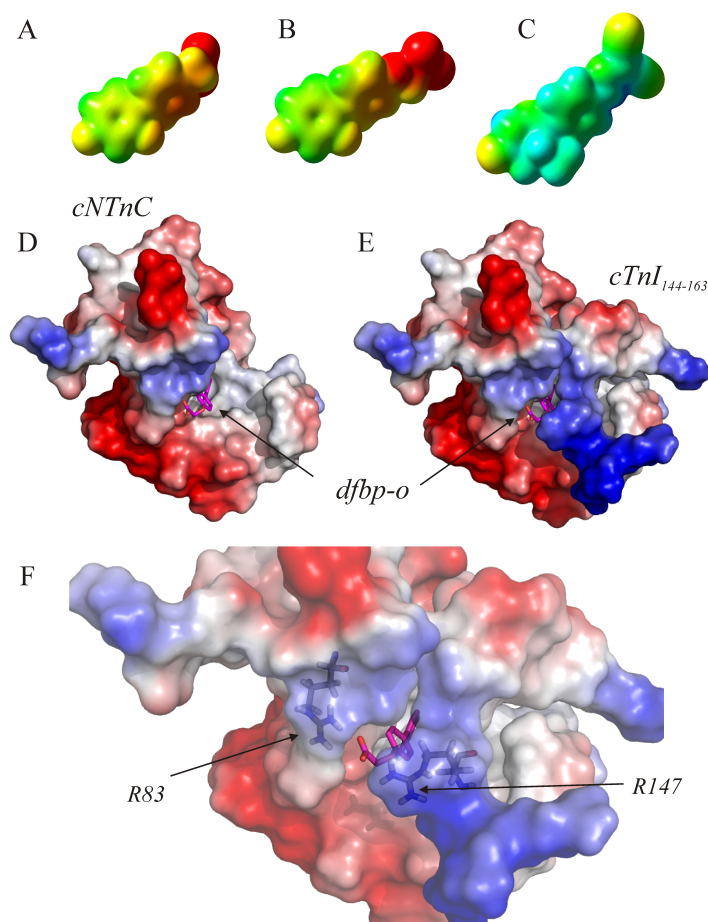
Figure 5-13. The role of electrostatics in dfbp-o Ca^{2+}-sensitization. The electron density isosurfaces of (A) dfbp, (B) dfbp-o, and (C) levosimendan calculated using the quantum chemistry program Gaussian03. The compounds are positioned so that the fluorine atoms of dfbp and dfbp-o are in a similar orientation as the methyl and carbonyl oxygen groups of levosimendan as in Figure 5-1. The mapped electrostatic potential is colored on the isosurfaces (negative – red, positive – blue, neutral – green). Electrostatic surface representation of the structure of cNTnC•cTnI$_{144-163}$•dfbp-o. (D) cTnI$_{144-163}$ has been omitted from the structure to indicate the location of dfbp-o. (E) Full ternary complex. (F) Close-up view of the electrostatic environment surrounding the carboxyl group of dfbp-o with Arg83 and Arg147 labeled. The electrostatic potential is shown on the surface of cNTnC and cTnI$_{144-163}$ as a color gradient from negatively charged (red) to positively charged (blue). Dfbp-o is shown in stick representation, with carbon atoms in magenta, oxygen in red, and fluorine in aqua.

to the hydrazone greatly improved the cardiotonic activity of the compounds. The location of the carbonyl groups is approximately in the same position as the carboxyl oxygen atoms of dfbp-o. All these data suggest that dfbp-o has a molecular framework similar to other well studied Ca^{2+}-sensitizers and presents a novel scaffold for the design of new Ca^{2+}-sensitizing agents.

Heart muscle experiments showed that dfbp-o has a Ca^{2+}-sensitizing function and NMR spectroscopy was employed to uncover the mechanism by which dfbp-o acts to enhance contractility. The muscle studies indicated that dfbp-o increased the Ca^{2+}-sensitivity of the muscle fiber without increasing the maximum force of contraction. These results are consistent with previous findings for levosimendan (*9, 49, 50*), and the lack of an increase in the maximal force suggests that dfbp-o targets troponin instead of the myosin-actin system. NMR spectroscopy showed that the affinity of $cTnI_{147-163}$ for cNTnC was enhanced by the presence of dfbp-o, and $cTnI_{147-163}$ bound to cNTnC also improved the binding of dfbp-o. These data indicate that dfbp-o may increase contractility by strengthening the cNTnC-cTnI interaction.

The docked structure of cNTnC•dfbp-o and the NMR structure of cNTnC•$cTnI_{144-163}$•dfbp-o have identified several of the important features of a Ca^{2+}-sensitizing agent that targets cNTnC. In the docked structure, dfbp-o is bound with its difluorophenyl ring in the hydrophobic core of cNTnC. The difluorophenyl ring comes in close contact with Leu41, Phe27, Phe77, Ile36, Val72, Met60 and Met80. The central phenyl component of dfbp-o is near Met60 and Met80, while the carboxylate forms an electrostatic interaction with Arg83 of cNTnC. The structure of levosimendan bound to cNTnC, has not been solved; however, there has been a data-driven model of levosimendan in complex with cNTnC (*11*). Although both levosimendan and dfbp-o models indicate the importance of the D-helix in forming the binding cleft, the binding site of dfbp-o is predicted to be located between helices B, C, and D; whereas, the binding

location of levosimendan was predicted to be nearer to the NAD helix bundle. The primary binding sites of W7 (*54*), bepridil (*17*), and trifluoperazine (*53*) are consistent to that predicted for dfbp-o, and it seems likely that the binding site of levosimendan is also in a similar location.

In the NMR ensemble of cNTnC•cTnI$_{144\text{-}163}$•dfbp-o, the fluorine-substituted phenyl ring of dfbp-o is buried deep in the hydrophobic pocket of cNTnC. The orientations of dfbp-o in the docked and the NMR structures are consistent, which emboldens the AutoDock model of cNTnC•dfbp-o. The biphenyl component of dfbp-o makes hydrophobic contacts to the same residues of cNTnC as in the docked model as well as the side chains of Met153 and Ile148 from cTnI$_{144\text{-}163}$. The carboxylate moiety is directed outward, away from the hydrophobic pocket towards the N-terminus of cTnI$_{144\text{-}163}$. The carboxylate is encapsulated by the positively charged side-chains of Arg83 from cNTnC and Arg147 from cTnI$_{144\text{-}163}$ (Figure 5-7). The distances between the carboxylate carbon of dfbp-o and the gaunidinyl group for Arg83 and Arg147 (CZ) over the ensemble are 8.3 ± 2.8 Å and 8.3 ± 2.5 Å, respectively. Given electrostatic potential can be exerted by a charged particle over a long range (≥ 20 Å) these electrostatic interactions may be critical for the Ca^{2+}-sensitizing mechanism of dfbp-o. In addition to the importance of Arg83 and Arg147, Arg145 and Arg144 are also near dfbp-o: 8.0 ± 4.1 Å and 11.6 ± 3.9 Å away from its carboxylate carbon. The malonodinitrile of levosimendan is also slightly electronegative (Figure 5-13C) and therefore the network of charge-charge interactions we observed between dfbp-o and cTnI might be the pervasive mode of action of all cNTnC-targeting Ca^{2+}-sensitizers.

The structural data we have presented here point towards a two-pronged mechanism of dfbp-o. Firstly, dfbp-o stabilizes a more open state of cNTnC and thus cNTnC is primed to bind cTnI$_{147\text{-}163}$. However, several structural studies have indicated that simply opening cNTnC does not necessarily promote binding of cTnI$_{147\text{-}163}$. W7 and bepridil were found to

bind to the hydrophobic surface of cNTnC and promote an opening similar to that induced by cTnI$_{147-163}$ (*17, 54*), yet they decreased the affinity of cTnI$_{147-163}$ (*21, 57*). Both W7 and bepridil have positively charged moieties that repel the positively charged N-terminal Arg147 of cTnI$_{147-163}$. In the same theme, the negatively charged carboxylate of dfbp-o may attract Arg147, therefore explaining how dfbp-o increases the affinity of cTnI$_{147-163}$ for cNTnC and enhances cardiac trabeculae Ca^{2+}-sensitivity.

The conclusion that levosimendan functions as a Ca^{2+}-sensitizer by the same mechanism as dfbp-o hinges on our assumption that dfbp-o is a good analogue of levosimendan; however, the affinity of dfbp-o for cNTnC was weaker than previously measured for levosimendan. The differences in affinities between dfbp-o and levosimendan may have several explanations. We initially proposed that the fluorine at the F2' position of dfbp-o may substitute for the stereospecific methyl group of levosimendan; however, the van der Waals radius of fluorine is significantly smaller than a methyl group and therefore may not be an optimal substitution. The second noteworthy and perhaps more critical difference between the two molecules is the hydrophilic region. The carboxyl group of dfbp-o is much more electronegative than the malonodinitrile moiety of levosimendan. While the negatively charged carboxyl moiety of dfbp-o may contribute to the increase in cTnI$_{147-163}$ affinity, it most likely decreases the affinity of dfbp-o for cNTnC, since cNTnC has a predominantly negative electrostatic surface (Figure 5-13A). Levosimendan is slightly longer than dfbp-o, and this may also contribute to its increase in affinity for cNTnC by promoting a stronger interaction with cTnI, or along the D-helix of cNTnC. For example, the side-chain of Cys84 has been implicated in being essential for levosimendan binding to cNTnC (*12*).

Conclusion

We have described the molecular mechanism of a novel Ca^{2+}-sensitizer, dfbp-o. We used *in silico* methods to compare aspects of dfbp-o with the well-known Ca^{2+}-sensitizing agent, levosimendan. Functional studies with cardiac trabeculae indicated that dfbp-o increased the Ca^{2+}-sensitivity in a similar manner as levosimendan. We also used NMR spectroscopy to show that dfbp-o enhanced the affinity of the switch region of cTnI for the Ca^{2+}-saturated N domain of cTnC. Chemical shift mapping and automated docking identified the hydrophobic core of cNTnC as the likely binding site of dfbp-o. The solution structure of cNTnC•cTnI$_{144-163}$•dfbp-o implicates an electrostatic attraction between dfbp-o and cTnI as a possible explanation for the Ca^{2+}-sensitizing effect of dfbp-o. The structure also gives insight into the possible orientation levosimendan might adopt when bound to troponin. Overall, these results indicate that Ca^{2+}-sensitizing agents may function by binding the hydrophobic surface of cNTnC, stabilizing its open conformation, and promoting the cTnI-cNTnC interaction. The data presented here contribute knowledge into the molecular mechanism of cTnC targeting inotropes, such as levosimendan, and highlight several of the key pharmacophores that direct their function.

References

1. Li, M. X., Wang, X., and Sykes, B. D. (2004) Structural based insights into the role of troponin in cardiac muscle pathophysiology, *J. Muscle Res. Cell Motil. 25*, 559-579.
2. Parmacek, M. S., and Solaro, R. J. (2004) Biology of the troponin complex in cardiac myocytes, *Prog. Cardiovasc. Dis. 47*, 159-176.
3. Gomes, A. V., Potter, J. D., and Szczesna-Cordary, D. (2002) The role of troponins in muscle contraction, *IUBMB Life 54*, 323-333.
4. Endoh, M. (2007) Could Ca2+ sensitizers rescue patients from chronic congestive heart failure?, *Br. J. Pharmacol. 150*, 826-828.
5. Kass, D. A., and Solaro, R. J. (2006) Mechanisms and use of calcium-sensitizing agents in the failing heart, *Circulation 113*, 305-315.
6. Li, M. X., Robertson, I. M., and Sykes, B. D. (2008) Interaction of cardiac troponin with cardiotonic drugs: a structural perspective, *Biochem. Biophys. Res. Commun. 369*, 88-99.
7. Haikala, H., Nissinen, E., Etemadzadeh, E., Linden, I. B., and Pohto, P. (1992) Levosimendan Increases Calcium Sensitivity without Enhancing Myosin Atpase Activity and Impairing Relaxation, *J. Mol. Cell. Cardiol. 24*, S97-S97.
8. Haikala, H., Kaivola, J., Nissinen, E., Wall, P., Levijoki, J., and Linden, I. B. (1995) Cardiac Troponin-C as a Target Protein for a Novel Calcium Sensitizing Drug, Levosimendan, *J. Mol. Cell. Cardiol. 27*, 1859-1866.
9. Haikala, H., Nissinen, E., Etemadzadeh, E., Levijoki, J., and Linden, I. B. (1995) Troponin C-Mediated Calcium Sensitization Induced by Levosimendan Does Not Impair Relaxation, *J. Cardiovasc. Pharmacol. 25*, 794-801.
10. Sorsa, T., Pollesello, P., and Solaro, R. J. (2004) The contractile apparatus as a target for drugs against heart failure: Interaction of levosimendan, a calcium sensitiser, with cardiac troponin c, *Mol. Cell. Biochem. 266*, 87-107.
11. Pollesello, P., Ovaska, M., Kaivola, J., Tilgmann, C., Lundstrom, K., Kalkkinen, N., Ulmanen, I., Nissinen, E., and Taskinen, J. (1994) Binding of a New Ca2+ Sensitizer, Levosimendan, to Recombinant Human Cardiac Troponin-C - a Molecular Modeling, Fluorescence Probe, and Proton Nuclear-Magnetic-Resonance Study, *J. Biol. Chem. 269*, 28584-28590.
12. Sorsa, T., Heikkinen, S., Abbott, M. B., Abusamhadneh, E., Laakso, T., Tilgmann, C., Serimaa, R., Annila, A., Rosevear, P. R., Drakenberg, T., Pollesello, P., and Kilpelainen, I. (2001) Binding of levosimendan, a calcium sensitizer, to cardiac troponin C, *J. Biol. Chem. 276*, 9337-9343.
13. Li, M. X., Saude, E. J., Wang, X., Pearlstone, J. R., Smillie, L. B., and Sykes, B. D. (2002) Kinetic studies of calcium and cardiac

troponin I peptide binding to human cardiac troponin C using NMR spectroscopy, *European Biophysics Journal with Biophysics Letters 31*, 245-256.

14. M. J. Frisch, G. W. T., H. B. Schlegel, G. E. Scuseria, M. A. Robb, J. R. Cheeseman, J. A. Montgomery, Jr., T. Vreven, K. N. Kudin, J. C. Burant, J. M. Millam, S. S. Iyengar, J. Tomasi, V. Barone, B. Mennucci, M. Cossi, G. Scalmani, N. Rega, G. A. Petersson, H. Nakatsuji, M. Hada, M. Ehara, K. Toyota, R. Fukuda, J. Hasegawa, M. Ishida, T. Nakajima, Y. Honda, O. Kitao, H. Nakai, M. Klene, X. Li, J. E. Knox, H. P. Hratchian, J. B. Cross, V. Bakken, C. Adamo, J. Jaramillo, R. Gomperts, R. E. Stratmann, O. Yazyev, A. J. Austin, R. Cammi, C. Pomelli, J. W. Ochterski, P. Y. Ayala, K. Morokuma, G. A. Voth, P. Salvador, J. J. Dannenberg, V. G. Zakrzewski, S. Dapprich, A. D. Daniels, M. C. Strain, O. Farkas, D. K. Malick, A. D. Rabuck, K. Raghavachari, J. B. Foresman, J. V. Ortiz, Q. Cui, A. G. Baboul, S. Clifford, J. Cioslowski, B. B. Stefanov, G. Liu, A. Liashenko, P. Piskorz, I. Komaromi, R. L. Martin, D. J. Fox, T. Keith, M. A. Al-Laham, C. Y. Peng, A. Nanayakkara, M. Challacombe, P. M. W. Gill, B. Johnson, W. Chen, M. W. Wong, C. Gonzalez, and J. A. Pople. (2004) Gaussian 03, Gaussian 03 ed., Gaussian, Inc., Wallingford CT.

15. Morris, G. M., Huey, R., Lindstrom, W., Sanner, M. F., Belew, R. K., Goodsell, D. S., and Olson, A. J. (2009) AutoDock4 and AutoDockTools4: Automated Docking with Selective Receptor Flexibility, *J. Comput. Chem. 30*, 2785-2791.

16. Gasteiger, J., and Marsili, M. (1980) Iterative Partial Equalization of Orbital Electronegativity - a Rapid Access to Atomic Charges, *Tetrahedron 36*, 3219-3228.

17. Li, Y., Love, M. L., Putkey, J. A., and Cohen, C. (2000) Bepridil opens the regulatory N-terminal lobe of cardiac troponin C, *Proc. Natl. Acad. Sci. U. S. A. 97*, 5140-5145.

18. Gemmecker, G., Olejniczak, E. T., and Fesik, S. W. (1992) An Improved Method for Selectively Observing Protons Attached to C-12 in the Presence of H-1-C-13 Spin Pairs, *J. Magn. Reson. 96*, 199-204.

19. Ikura, M., and Bax, A. (1992) Isotope-Filtered 2d Nmr of a Protein Peptide Complex - Study of a Skeletal-Muscle Myosin Light Chain Kinase Fragment Bound to Calmodulin, *J. Am. Chem. Soc. 114*, 2433-2440.

20. Ogura, K., Terasawa, H., and Inagaki, F. (1996) An improved double-tuned and isotope-filtered pulse scheme based on a pulsed field gradient and a wide-band inversion shaped pulse, *J. Biomol. NMR 8*, 492-498.

21. Wang, X., Li, M. X., and Sykes, B. D. (2002) Structure of the regulatory N-domain of human cardiac troponin C in complex with

human cardiac troponin I147-163 and bepridil, *J. Biol. Chem. 277*, 31124-31133.

22.	Yu, C., and Levy, G. C. (1983) Solvent and Intramolecular Proton Dipolar Relaxation of the 3 Phosphates of Atp - a Heteronuclear 2d Noe Study, *J. Am. Chem. Soc. 105*, 6994-6996.

23.	Rinaldi, P. L. (1983) Heteronuclear 2d-Noe Spectroscopy, *J. Am. Chem. Soc. 105*, 5167-5168.

24.	Lee, W., Revington, M. J., Arrowsmith, C., and Kay, L. E. (1994) A Pulsed-Field Gradient Isotope-Filtered 3d C-13 Hmqc-Noesy Experiment for Extracting Intermolecular Noe Contacts in Molecular-Complexes, *FEBS Lett. 350*, 87-90.

25.	Robertson, I. M., Spyracopoulos, L., and Sykes, B. D. (2009) The Evaluation of Isotope Editing and Filtering for Protein-Ligand Interaction Elucidation by Nmr, *Biophysics and the Challenges of Emerging Threats*, 101-119.

26.	Krudy, G. A., Kleerekoper, Q., Guo, X. D., Howarth, J. W., Solaro, R. J., and Rosevear, P. R. (1994) Nmr-Studies Delineating Spatial Relationships within the Cardiac Troponin-I Troponin-C Complex, *J. Biol. Chem. 269*, 23731-23735.

27.	Lin, X., Krudy, G. A., Howarth, J., Brito, R. M. M., Rosevear, P. R., and Putkey, J. A. (1994) Assignment and Calcium-Dependence of Methionyl Epsilon-C and Epsilon-H Resonances in Cardiac Troponin-C, *Biochemistry 33*, 14434-14442.

28.	Gariepy, J., Kay, L. E., Kuntz, I. D., Sykes, B. D., and Hodges, R. S. (1985) Nuclear Magnetic-Resonance Determination of Metal Proton Distances in a Synthetic Calcium-Binding Site of Rabbit Skeletal Troponin-C, *Biochemistry 24*, 544-550.

29.	Schuttelkopf, A. W., and van Aalten, D. M. F. (2004) PRODRG: a tool for high-throughput crystallography of protein-ligand complexes, *Acta Crystallogr. Sect. D Biol. Crystallogr. 60*, 1355-1363.

30.	Delaglio, F., Grzesiek, S., Vuister, G. W., Zhu, G., Pfeifer, J., and Bax, A. (1995) Nmrpipe - a Multidimensional Spectral Processing System Based on Unix Pipes, *J. Biomol. NMR 6*, 277-293.

31.	Johnson, B. A., and Blevins, R. A. (1994) Nmr View - a Computer-Program for the Visualization and Analysis of Nmr Data, *J. Biomol. NMR 4*, 603-614.

32.	Slupsky, C. M., Boyko, R. F., Booth, V. K., and Sykes, B. D. (2003) Smartnotebook: A semi-automated approach to protein sequential NMR resonance assignments, *J. Biomol. NMR 27*, 313-321.

33.	Cornilescu, G., Delaglio, F., and Bax, A. (1999) Protein backbone angle restraints from searching a database for chemical shift and sequence homology, *J. Biomol. NMR 13*, 289-302.

34.	Guntert, P. (2004) Automated NMR structure calculation with CYANA, *Methods Mol. Biol. 278*, 353-378.

35. Schwieters, C. D., Kuszewski, J. J., and Clore, G. M. (2006) Using Xplor-NIH for NMR molecular structure determination, *Prog. Nucl. Magn. Reson. Spectrosc. 48*, 47-62.

36. Linge, J. P., Williams, M. A., Spronk, C. A. E. M., Bonvin, A. M. J. J., and Nilges, M. (2003) Refinement of protein structures in explicit solvent, *Proteins-Structure Function and Bioinformatics 50*, 496-506.

37. Laskowski, R. A., Rullmann, J. A. C., MacArthur, M. W., Kaptein, R., and Thornton, J. M. (1996) AQUA and PROCHECK-NMR: Programs for checking the quality of protein structures solved by NMR, *J. Biomol. NMR 8*, 477-486.

38. Sun, Y. B., Lou, F., and Irving, M. (2009) Calcium- and myosin-dependent changes in troponin structure during activation of heart muscle, *Journal of Physiology-London 587*, 155-163.

39. Lapka, R., Smolik, S., and Rejholec, V. (1990) Pharmacokinetics of Flobufen and Its Main Active Metabolite in the Rat, *Drug Metab. Dispos. 18*, 1060-1064.

40. Williams, D. E., and Houpt, D. J. (1986) Fluorine Nonbonded Potential Parameters Derived from Crystalline Perfluorocarbons, *Acta Crystallographica Section B-Structural Science 42*, 286-295.

41. Smart, B. E. (2001) Fluorine substituent effects (on bioactivity), *J. Fluorine Chem. 109*, 3-11.

42. DiMagno, S. G., and Sun, H. R. (2006) The strength of weak interactions: Aromatic fluorine in drug design, *Curr. Top. Med. Chem. 6*, 1473-1482.

43. Levijoki, J., Pollesello, P., Kaivola, J., Tilgmann, C., Sorsa, T., Annila, A., Kilpelainen, I., and Haikala, H. (2000) Further evidence for the cardiac troponin C mediated calcium sensitization by levosimendan: Structure-response and binding analysis with analogs of levosimendan, *J. Mol. Cell. Cardiol. 32*, 479-491.

44. Bohm, H. J., Banner, D., Bendels, S., Kansy, M., Kuhn, B., Muller, K., Obst-Sander, U., and Stahl, M. (2004) Fluorine in medicinal chemistry, *Chembiochem 5*, 637-643.

45. Spyracopoulos, L., Li, M. X., Sia, S. K., Gagne, S. M., Chandra, M., Solaro, R. J., and Sykes, B. D. (1997) Calcium-induced structural transition in the regulatory domain of human cardiac troponin C, *Biochemistry 36*, 12138-12146.

46. McKay, R. T., Saltibus, L. F., Li, M. X., and Sykes, B. D. (2000) Energetics of the induced structural change in a Ca2+ regulatory protein: Ca2+ and troponin I peptide binding to the E41A mutant of the N-domain of skeletal troponin C, *Biochemistry 39*, 12731-12738.

47. Paakkonen, K., Sorsa, T., Drakenberg, T., Pollesello, P., Tilgmann, C., Permi, P., Heikkinen, S., Kilpelainen, I., and Annila, A. (2000) Conformations of the regulatory domain of cardiac troponin C

examined by residual dipolar couplings, *Eur. J. Biochem. 267*, 6665-6672.

48. Li, M. X., Spyracopoulos, L., and Sykes, B. D. (1999) Binding of cardiac troponin-I147-163 induces a structural opening in human cardiac troponin-C, *Biochemistry 38*, 8289-8298.

49. Szilagyi, S., Pollesello, P., Levijoki, J., Kaheinen, P., Haikala, H., Edes, I., and Papp, Z. (2004) The effects of levosimendan and OR-1896 on isolated hearts, myocyte-sized preparations and phosphodiesterase enzymes of the guinea pig, *Eur. J. Pharmacol. 486*, 67-74.

50. Edes, I., Kiss, E., Kitada, Y., Powers, F. M., Papp, J. G., Kranias, E. G., and Solaro, R. J. (1995) Effects of Levosimendan, a Cardiotonic Agent Targeted to Troponin-C, on Cardiac-Function and on Phosphorylation and Ca2+ Sensitivity of Cardiac Myofibrils and Sarcoplasmic-Reticulum in Guinea-Pig Heart, *Circ. Res. 77*, 107-113.

51. Sorsa, T., Pollesello, P., Rosevear, P. R., Drakenberg, T., and Kilpelainen, L. (2004) Stereoselective binding of levosimendan to cardiac troponin C causes Ca2+-sensitization, *Eur. J. Pharmacol. 486*, 1-8.

52. Kleerekoper, Q., Liu, W., Choi, D., and Putkey, J. A. (1998) Identification of binding sites for bepridil and trifluoperazine on cardiac troponin C, *J. Biol. Chem. 273*, 8153-8160.

53. Igarashi, T., Takeda, S., and Mori, H. (2005) Crystal structure of the N-terminal domain of human cardiac troponin C in complex with a calcium-sensitizer; trifluoperazine, *J. Mol. Cell. Cardiol. 39*, 1016-1016.

54. Hoffman, R. M. B., and Sykes, B. D. (2009) Structure of the Inhibitor W7 Bound to the Regulatory Domain of Cardiac Troponin C, *Biochemistry 48*, 5541-5552.

55. Robertson, I. M., Baryshnikova, O. K., Li, M. X., and Sykes, B. D. (2008) Defining the binding site of levosimendan and its analogues in a regulatory cardiac troponin C-troponin I complex, *Biochemistry 47*, 7485-7495.

56. Takeda, S., Yamashita, A., Maeda, K., and Maeda, Y. (2003) Structure of the core domain of human cardiac troponin in the Ca(2+)-saturated form, *Nature 424*, 35-41.

57. Oleszczuk, M., Robertson, I. M., Li, M. X., and Sykes, B. D. (2010) Solution structure of the regulatory domain of human cardiac troponin C in complex with the switch region of cardiac troponin I and W7: The basis of W7 as an inhibitor of cardiac muscle contraction, *J. Mol. Cell. Cardiol. 48*, 925-933.

58. John, M., Pintacuda, G., Park, A. Y., Dixon, N. E., and Otting, G. (2006) Structure determination of protein-ligand complexes by transferred paramagnetic shifts, *J. Am. Chem. Soc. 128*, 12910-12916.

59. Vinogradova, M. V., Stone, D. B., Malanina, G. G., Karatzaferi, C., Cooke, R., Mendelson, R. A., and Fletterick, R. J. (2005) Ca(2+)-regulated structural changes in troponin, *Proc. Natl. Acad. Sci. U. S. A. 102*, 5038-5043.

60. Amin, E. N., Abdel-Alim, A. A. M., Abdel-Moty, S. G., El-Shorbagi, A. N. A., and Abdel-Rahman, M. S. (2010) Synthesis of New 4,5-3(2H)pyridazinone Derivatives and Their Cardiotonic, Hypotensive, and Platelet Aggregation Inhibition Activities, *Arch. Pharmacal Res. 33*, 25-46.

Chapter 6

The structure-activity relationship of a new set of inotropes that target troponin

Summary

A series of naphthalenesulfonamides were prepared and their modulation of cardiac troponin I (cTnI) binding to cardiac troponin C (cTnC) was evaluated. The cTnC-cTnI interaction is responsible for stimulation of contraction in heart muscle and the design of molecules that target this interaction hold potential as treatments for heart failure. The naphthalenesulfonamide, W7, is a calmodulin antagonist that also inhibits muscle contractility. Recent NMR studies suggest that W7 may decrease contractility by binding to the regulatory domain of cTnC (cNTnC) and inhibiting its interaction with cTnI. The structure of cNTnC•Ca^{2+}•cTnI$_{147-163}$•W7 revealed that the competition between W7 and cTnI$_{147-163}$ stems, at least in part, from an electrostatic repulsion between the positively charged terminal amino of W7 and the positively charged side-chain of R147 from cTnI$_{147-163}$. We prepared three molecules to test the role of electrostatics on the function of W7: A6, A7, and A8. These compounds contained a carboxyl group (in place of the amino group of W7) connected to the naphthalene moiety by varying lengths of a hydrocarbon chain (5, 6, or 7 methylene groups). We measured the affinities of these compounds for cNTnC•Ca^{2+} and cNTnC•Ca^{2+} in complex cTnI$_{147-163}$, as well as the affinity of cTnI$_{147-163}$ for the respective cNTnC•Ca^{2+}•A-compound complex. A7 was found to slightly decrease the binding of cTnI$_{147-163}$, but much less than that observed for W7, whereas A6 did not affect binding of cTnI$_{147-163}$. These results suggest that the negative inotropic effect of W7 may result from a combination of electrostatic repulsion and steric hindrance with cTnI.

Introduction

Heart muscle contraction is regulated by Ca^{2+} binding to the heterotrimeric thin filament protein complex, troponin. The thin filament is made up of primarily two proteins, the double helical F-actin filament and tropomyosin. Troponin is tethered to the thin filament every seventh actin monomer and is composed of three components. Troponin T (cTnT) anchors the complex to the thin filament by interactions with tropomyosin and troponin I. Troponin I (cTnI) is the inhibitory subunit of troponin, and toggles between the actin and troponin C (cTnC), depending on the Ca^{2+} concentration. At low Ca^{2+} levels, cTnI is bound to actin and contraction is inhibited because tropomyosin is oriented such that the myosin binding sites on actin are blocked. When Ca^{2+} concentration increases during systole, Ca^{2+} binds to the regulatory domain of cTnC (cNTnC) to promote association with the switch region of cTnI ($cTnI_{147-163}$). The binding of $cTnI_{147-163}$ drags cTnI off of actin and inhibition is released, resulting in actin-myosin cross-bridge formation and muscle contraction (for reviews see (1-4)). The Ca^{2+}-sensitive $cNTnC$-$cTnI_{147-163}$ interaction therefore triggers contraction, and fine-tuning either Ca^{2+}-binding to cNTnC or the $cNTnC$-$cTnI_{147-163}$ complex formation by drugs represents plausible treatments of heart failure (5, 6). Molecules that enhance these interactions are called Ca^{2+}-sensitizers and they stimulate an increase in contractility. On the other hand, molecules that impede these interactions decrease contractility by Ca^{2+}-desensitization.

In the last few years the solution structures of cNTnC-cTnI bound to the negative inotrope (decreases contractility), W7 (N-(6-aminohexyl)-5-chloro-1-naphthalenesulfonamide), or the positive inotrope (increases contractility), dfbp-o (2′,4′-difluoro(1,1′-biphenyl)-4-yloxy acetic acid), have been solved (7, 8). Although both molecules bound to the hydrophobic pocket formed by cNTnC-cTnI, the structures of cNTnC and cTnI were markedly different in the two ternary complexes when compared to the

solution structure of cNTnC•Ca^{2+}•cTnI$_{147-163}$ (*9*) or X-ray structure of the core troponin complex (*10*). W7 significantly perturbed the structure of cNTnC and pushed cTnI$_{147-163}$ away from the binding pocket. On the other hand, dfbp-o caused little perturbation in the structure of cNTnC or in the structure and position of cTnI$_{144-163}$. These structural variances were paralleled by changes in the affinity of cTnI$_{147-163}$ for the cNTnC-drug complexes. The affinity of cTnI$_{147-163}$ was markedly reduced in the presence of W7, but enhanced in the presence of dfbp-o. These differences were discussed in terms of the charge alteration between dfbp-o and W7 (see Figure 6-1). The positively charged terminal amino group of W7 appeared to repel the guanidinium group of R147 of cTnI$_{147-163}$. Conversely, the negatively charged carboxyl group of dfbp-o attracted R147's side chain. Therefore, the functional distinctions between these two compounds were rationalized to be primarily the result of differences in the charge of the two molecules (*7, 8*). Although, the chemical structures of dfbp-o and W7 have differences other than the charge (Figure 6-1).

In order to test our postulate that electrostatics are important in tuning the contraction dependent cNTnC-cTnI association, we have synthesized a new set of compounds. The molecules prepared have a carboxyl group in place of the amino of W7. Additionally we varied the hydrocarbon linker lengths, since several structure-activity relationship (SAR) studies on W7 indicated that the longer the methylene moiety, the larger the inhibitory action of the molecules (*11, 12*). We synthesized three molecules: N-(5-carboxylhexyl)-5-chloro-1-naphthalenesulfonamide (A6), N-(6-carboxylhexyl)-5-chloro-1-naphthalenesulfonamide (A7), and N-(7-carboxylhexyl)-5-chloro-1-naphthalenesulfonamide (A8) and examined their affinity for cNTnC•Ca^{2+} and cNTnC•Ca^{2+} in complex cTnI$_{147-163}$, as well as their effect on the strength of cTnI$_{147-163}$ binding to Ca^{2+}-saturated cNTnC (cNTnC•Ca^{2+}) by NMR spectroscopy. A8 turned out to be too hydrophobic to be soluble under the conditions used. We found A7 slightly
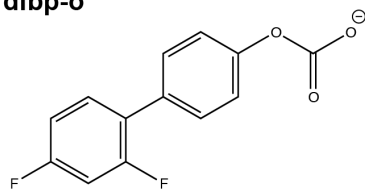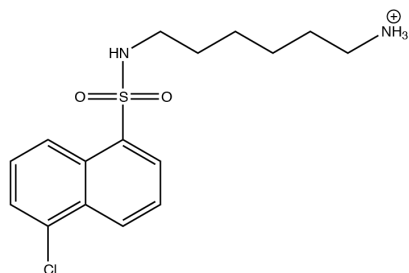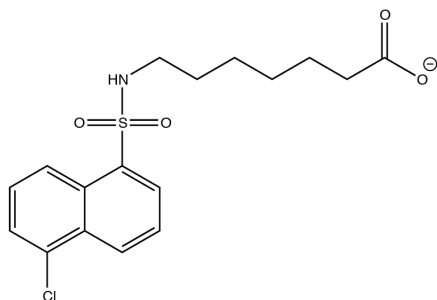
Figure 6-1. Chemical structures of dfbp-o, W7, and A7.

competed with $cTnI_{147-163}$, but very much less than W7, whereas A6 did not. Thus, in addition to charge, the length of the methylene tail is important in determining the affinity of $cTnI_{147-163}$. We used ^{13}C-NMR chemical shift mapping to predict the binding site of A6 in a cNTnC-cTnI complex. The results suggest that A6 binds to the hydrophobic pocket made by cNTnC and cTnI in a similar site as W7.

Experimental procedures

Sample preparation: Recombinant human cNTnC (residues 1-89) was used in this study. The engineering of the expression vector and the expression of ^{15}N- and ^{13}C,^{15}N-labeled proteins in *E. coli* was described previously (*13*). $cTnI_{147-163}$ (acetyl-RISADAMMQALLGARAK-amide) and $cTnI_{144-163}$ (acetyl-RRVRISADAMMQALLGARAK-amide) were synthesized by GL Biochem Ltd. (Shanghai, China) and their quality was assessed by HPLC, NMR spectroscopy, and ESI-Mass Spectrometry. All NMR samples for the titrations were prepared in 5 mm NMR tubes to a final volume of ~500 µL. The protein samples were solubilized in 100 mM KCl, 10 mM imidazole, and 0.2-0.25 mM 2,2-dimethyl-2-silapentane-5-sulfonate sodium salt (DSS) (Chenomx) in 95% H_2O/5% D_2O, 5-10 mM $CaCl_2$ (Fluka) and the pH was maintained at 6.7-6.9.

Synthesis of A7: The reaction scheme for the synthesis of A7 is shown in figure 1A. The reaction procedure is similar to that outlined previously (*14*). 68.3 mg (470.4 µmol) of 7-aminoheptanoic acid (AHA) (Sigma-Aldrich) was dissolved in 2 mL of 0.5 M Na_2CO_3/$NaHCO_3$ buffer, pH 9.4 and was heated to 60°C. 9.57 mg (36.7 µmol) of 5-chloro-napthalene-1-sulfonyl chloride (CNSC) (Toronto Research Chemicals) was dissolved in 1 mL of acetonitrile and added to the 60°C AHA mixture and reacted for 1 hour with vigorous mixing every 15 minutes. ^{1}H NMR spectroscopy was used to confirm the reaction was complete (i.e. all of CNSC was reacted). A7 was

purified by two ethyl acetate extractions done at low pH. The organic solution was dried, and A7 crystals were stored at 4°C. The product verified by Liquid Chromatography-Mass Spectrometry (LC-MS). Signals were observed at 370.09 (M+H) and 352.07 (M-H_2O+H) m/z (Theoretical molecular weight = 369.08 g/mol). The ^{1}H NMR spectrum of purified A7 is shown in figure 6-2B.

Synthesis of A6: 68 mg (518.4 µmol) of ε-aminocaproic acid (ACA) (Sigma-Aldrich) was reacted with 9.78 mg (37.5 µmol) of CNSC in acetonitrile as described above. LC-MS indicated peaks at 356.07 (M+H) and 338.06 (M-H_2O+H) m/z (exact mass = 355.06 g/mol).

Synthesis of A8: 68.9 mg (432.7 µmol) of 8-aminooctanoic acid (AOA) (Sigma-Aldrich) was reacted with 9.68 mg (37.1 µmol) of CNSC as above. LC-MS indicated peaks at 384.10 (M+H) and 366.09 (M-H_2O+H) m/z (exact mass = 383.10 g/mol).

Titrations: All NMR data were collected at 30°C on either a Varian Inova 500 MHz spectrometer or a Unity 600 MHz spectrometer (Both spectrometers are equipped with a triple resonance ^{1}H^{13}C^{15}N probe and z-pulsed field gradients). Peptide and drug stocks were prepared in DMSO-d_6 (Cambridge Isotopes) and concentrations were determined by 1D ^{1}H NMR spectroscopy, using DSS as an internal standard. cNTnC concentration was determined by NMR as outlined before by Robertson *et al.* (*8*). Titrations of A6, A7, and A8 into cNTnC•Ca^{2+} and cNTnC•Ca^{2+}•cTnI$_{147-163}$ complex were monitored by NMR spectroscopy; at each aliquot, a ^{1}H,^{15}N-HSQC spectrum was acquired. A7 was titrated into 0.14 mM of cNTnC•Ca^{2+} to final concentrations of 0.07, 0.14, 0.21, 0.28, 0.37, 0.56, and 0.84 mM. A7 was titrated into 0.3 mM of cNTnC•Ca^{2+}•cTnI$_{147-163}$ to final concentrations of 0.08, 0.15, 0.23, 0.30, 0.38, 0.45, and 0.60 mM. cTnI$_{147-163}$ was titrated into a sample containing

0.13 mM of cNTnC•Ca^{2+}•A7 to final concentrations of 0.03, 0.06, 0.09, 0.13, 0.17, 0.23, 0.28, 0.35, 0.48 mM. A6 was titrated into 0.2 mM of cNTnC•Ca^{2+} to final concentrations of 0.05, 0.10, 0.20, 0.30, 0.35, 0.40, and 0.50 mM. A6 was titrated into 0.2 mM of cNTnC•Ca^{2+}•cTnI$_{147-163}$ to final concentrations of 0.10, 0.20, 0.30, 0.40, 0.6, 0.70, 0.90 1.1 and 1.3 mM. cTnI$_{147-163}$ was titrated into 0.15 mM of cNTnC•Ca^{2+}•A6 to final concentrations of 0.03, 0.06, 0.09, 0.11, 0.15, 0.19, 0.23, 0.28, 0.35 mM. The titrations were analyzed using the data fitting program, xcrvfit (www.bionmr.ualberta.ca/bds/software/xcrvfit). Binding was fit as described previously (*9*). Five residues that were well resolved throughout each titration were monitored, and their dissociation constants were calculated (Tables 6-1 and 6-2).

Results and discussion

Synthesis:

The preparation of the A-series compounds was accomplished by a modified protocol described by Guo and Li (*14*). 5-chloro-napthalene-1-sulfonyl chloride (CNSC) was mixed with ~10x excess 7-Aminoheptanoic Acid (AHA). It is believed that the formation of the S-N bond occurs *via* an S$_N$2 mechanism (*18*). A solution of AHA in Na$_2$CO$_3$/NaHCO$_3$ buffer at pH 9.4 was heated to 60°C. Once the temperature had equilibrated, CNSC dissolved in acetonitrile was rapidly mixed with the AHA solution. The two-step procedure was followed because aromatic sulfonyl chlorides are prone to hydrolysis at alkaline pH (*15*). Excess AHA was added to simplify purification of the product. The CNSC peaks were monitored throughout the titration until all resonances had disappeared. After 1 hour at 60°C, the sample was cooled and the pH lowered until the product precipitated (concomitant with protonation of the terminal carboxyl). The product was purified by an organic extraction with ethyl acetate. The organic solution
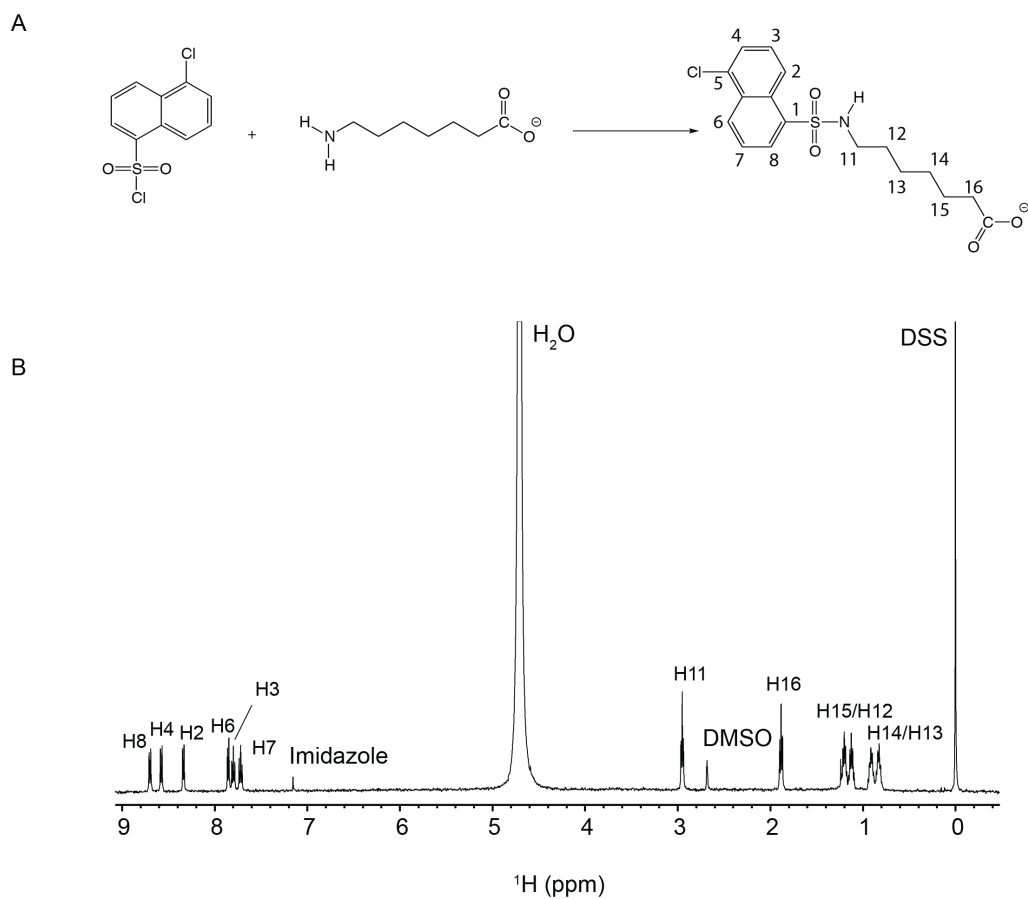
Figure 6-2. Synthesis and NMR spectrum of A7. **A**. The reaction scheme used in the synthesis of A7. 5-chloro-napthalene-1-sulfonyl chloride (CNSC) was reacted with 7-aminoheptanoic acid (AHA). **B**. ^{1}H NMR spectrum of A7 with assignments taken from W7 (*19*).

was dried, and the product was identified by mass spectrometry and its purity was verified by NMR spectroscopy (Figure 6-2).

Titrations with A7:

It was postulated by Oleszczuk *et al.* that the terminal amino group of W7 was chiefly responsible for its competition with $cTnI_{147-163}$ for $cNTnC\cdot Ca^{2+}$ (7). To address this possibility, A7 was titrated into $cNTnC\cdot Ca^{2+}$ in the absence (Figure 6-3a,di) and presence of $cTnI_{147-163}$ (Figure 6-3b,dii). The presence of $cTnI_{147-163}$ had a slight negative effect on the affinity of A7, K_D^{cNTnC} = 260 ± 140 µM and $K_D^{cNTnC-cTnI(147-163)}$ = 320 ± 140 µM (Table 6-1). The same competitive interaction was seen when $cTnI_{147-163}$ was titrated into $cNTnC\cdot Ca^{2+}\cdot A7$ (Figure 6-3c, diii), $K_D^{cNTnC-A7}$ = 230 ± 50 µM compared to K_D^{cNTnC} = 150 ± 30 µM (data not shown; in agreement with previously reported values (*8, 9*)). The dissociation constants were estimated by averaging the K_DS for the five residues shown in Figure 6-3d(i,ii,iii). Although the affinities of A7 for the $cNTnC\cdot Ca^{2+}$ and $cNTnC\cdot Ca^{2+}\cdot cTnI_{147-163}$ are within experimental error, the decreased affinity (320 ± 140 µM/260 ± 140 µM = 1.2 ± 1.0 fold) is consistent with decreased affinity of $cTnI_{147-163}$ (230 ± 50 µM /150 ± 30 µM = 1.5 ± 0.4 fold). These data are indicative of a moderate competition between A7 and $cTnI_{147-163}$; however, the affinity of $cTnI_{147-163}$ is still approximately 9 fold tighter than the affinity of $cTnI_{147-163}$ in the presence of W7 (W7 increased the dissociation constant from 150 ± 30 µM to 2000 ± 50 µM (7)). Therefore, the charge of ligands that target the cNTnC-cTnI complex seems to be a central feature of their function.

Titrations with A8 and A6:

The competition between A7 and $cTnI_{147-163}$ led us to consider whether the hydrocarbon tail competed with $cTnI_{147-163}$ by a steric hindrance. We synthesized ligands with +1 and -1 methylenes (A8 and A6, respectively). We titrated A8 into cNTnC; however it was very hydrophobic
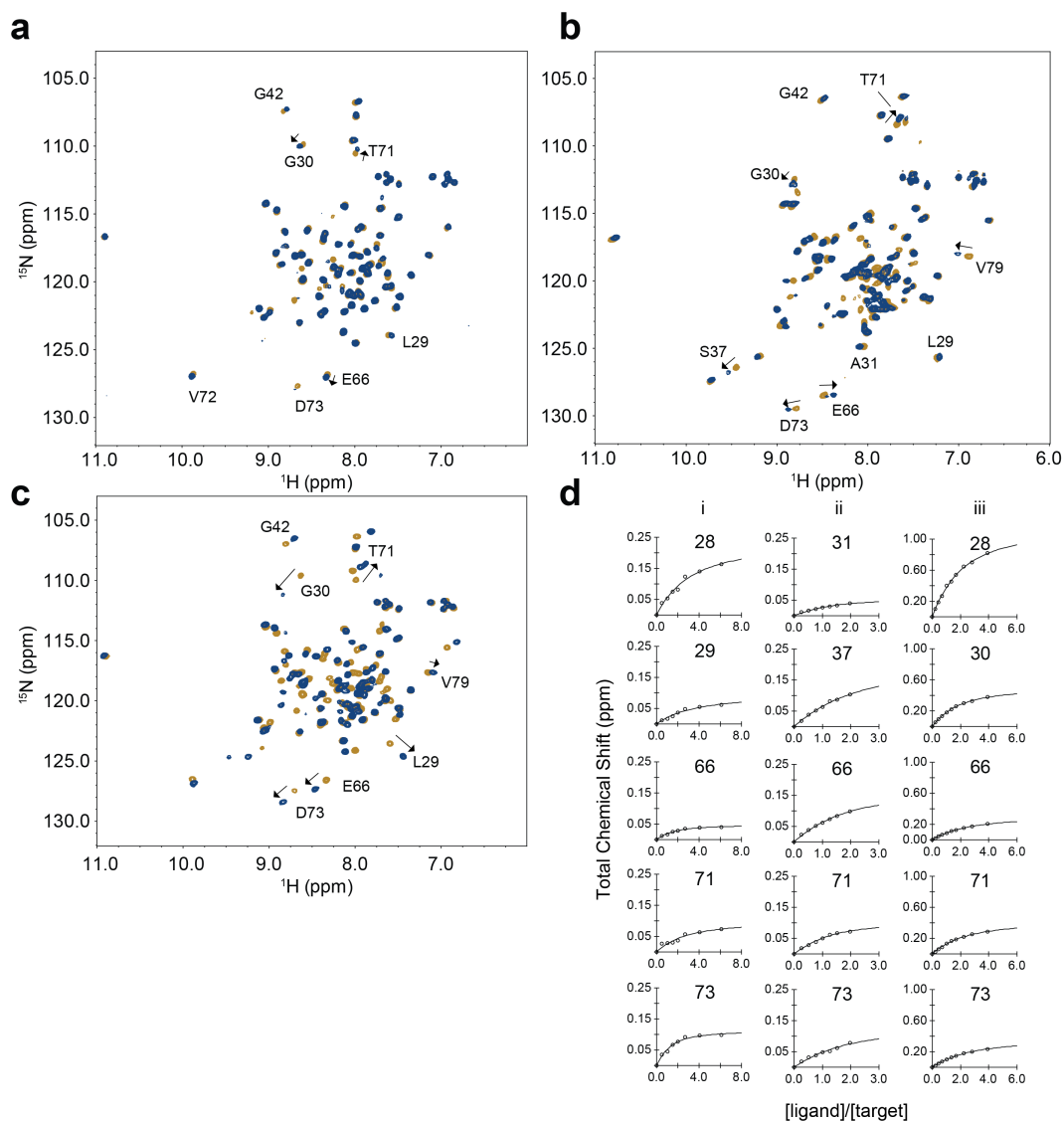
Figure 6-3. Titration with A7. $^1H,^{15}N$-HSQC NMR spectra of **a.** the titration of A7 into cNTnC•Ca^{2+}; **b.** the titration of A7 into cNTnC•Ca^{2+}•cTnI$_{147-163}$ and **c.** the titration of cTnI$_{147-163}$ into cNTnC•Ca^{2+}•A7. **d.** Analysis of the titration data of i. A7 into cNTnC•Ca^{2+} (a.); ii. A7 into cNTnC•Ca^{2+}•cTnI$_{147-163}$ (b.); and iii. cTnI$_{147-163}$ into cNTnC•Ca^{2+}•A7 (c.). Dissociation constants are reported in Table 6-1.

and precipitated at < 0.1 mM making it difficult to measure a reliable dissociation constant by NMR spectroscopy. A6 is less hydrophobic than A7 and accordingly was easily monitored by NMR. The titration of A6 into cNTnC•Ca^{2+} and cNTnC•Ca^{2+}•cTnI$_{147-163}$ (Figure 6-4a, di; and 6-4b,dii, respectively), as well as the titration of cTnI$_{147-163}$ into cNTnC•Ca^{2+}•A6 (Figure 6-4c, diii) were done as for A7. The affinity of cTnI$_{147-163}$ was less significantly perturbed by A6 than it was by A7, K$_D$$^{cNTnC-A6}$ = 180 ± 30 µM, which is not significantly different than to free cNTnC•Ca^{2+}, 150 ± 30 µM. In addition, the binding of A6 to cNTnC•Ca^{2+} or cNTnC•Ca^{2+}•cTnI$_{147-163}$ did not seem perturbed: K$_D$^{cNTnC} = 420 ± 350 µM *versus* K$_D$$^{cNTnC-cTnI}$ = 390 ± 50 µM. The lack of competition between A6 and cTnI$_{147-163}$ implies the longer the chain the more it clashes with cTnI$_{147-163}$. A7 bound with a higher affinity than A6 to cNTnC•Ca^{2+}, which could be the result of a corresponding increase in hydrophobicity. A similar observation was made of W7 analogues binding to calmodulin (*11, 12*).

Structural insights:

To predict the binding site of A6 to the ternary complex, ^{1}H,^{13}C-HSQC spectra were acquired for cNTnC•Ca^{2+}•cTnI$_{144-163}$ with and without A6. The methyl region of the ^{1}H,^{13}C-HSQC spectrum is shown in Figure 6-5a. The chemical shifts were assigned based on previously published assignments for cTnC-cTnI and cNTnC-cTnI (*9, 16*). The residues that experienced large chemical shift perturbations in their methyl resonances are shown in stick representation on the structure of cNTnC•Ca^{2+}•cTnI$_{147-163}$•W7. These residues are: M60, M45, M80, V64, I36 and I61 (several resonances in the more dense regions also shifted, however, were left unassigned because we were not certain of their assignment). The methyls that were perturbed upon A6 binding are from residues that encapsulate the W7 molecule in cNTnC•Ca^{2+}•cTnI$_{147-163}$•W7 (Figure 6-5b,c). This trend may indicate that the naphthalene moiety establishes the
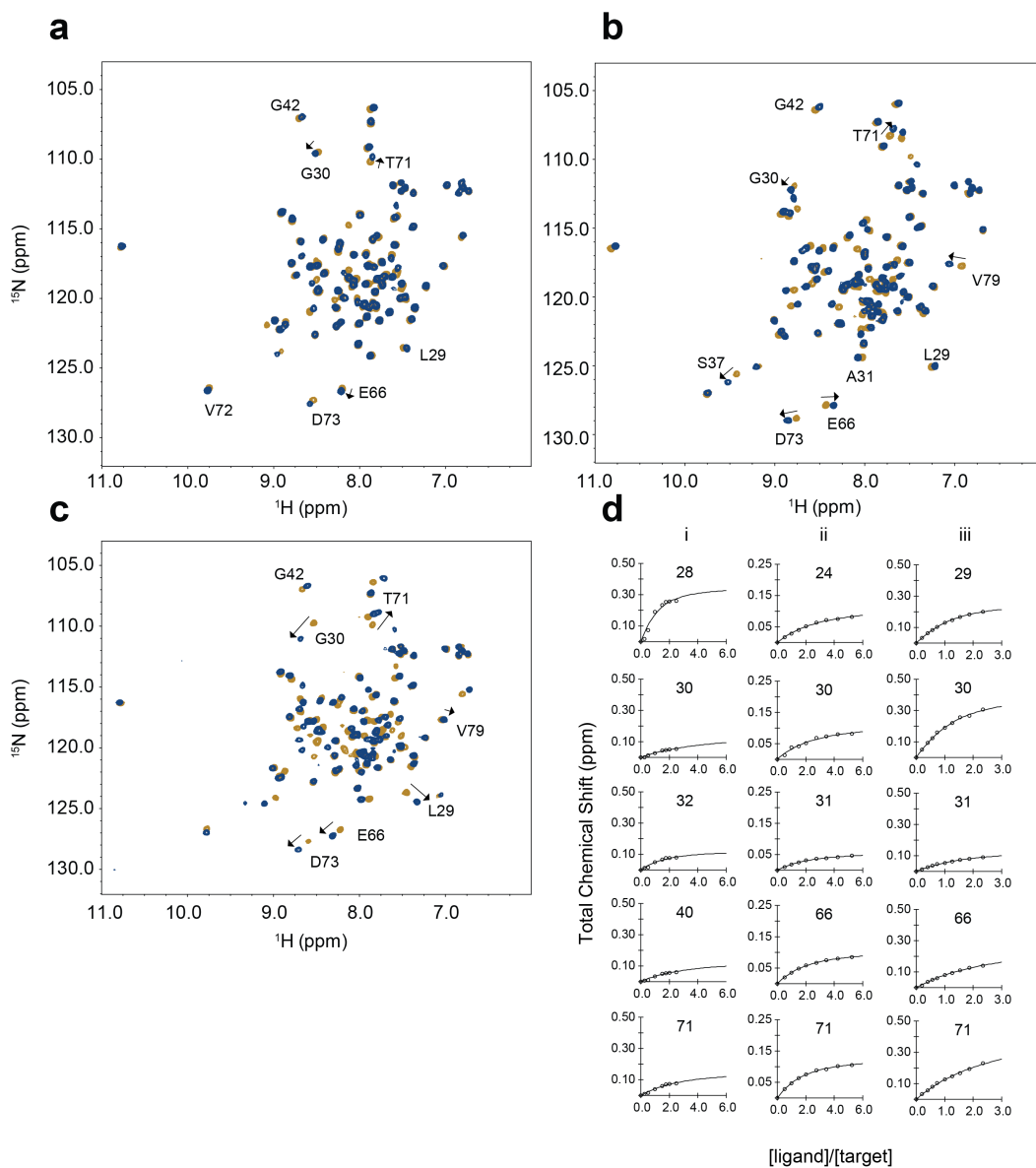
Figure 6-4. Titration with A6. ^{1}H,^{15}N-HSQC NMR spectra of **a.** the titration of A6 into cNTnC•Ca^{2+}; **b.** the titration of A6 into cNTnC•Ca^{2+}•cTnI$_{147-163}$ and **c.** the titration of cTnI$_{147-163}$ into cNTnC•Ca^{2+}•A6. **d.** Analysis of the titration data of i. A6 into cNTnC•Ca^{2+} (a); ii. A6 into cNTnC•Ca^{2+}•cTnI$_{147-163}$ (b); and iii. cTnI$_{147-163}$ into cNTnC•Ca^{2+}•A6 (c). Dissociation constants are reported in Table 6-2.

Table 6-1. Dissociation constants for A7 and cTnI$_{147-163}$ binding.

Ligand/Target	Dissociation Constant
A7/cNTnC•Ca^{2+}	260 ± 140 µM
A7/cNTnC•Ca^{2+}•cTnI$_{147-163}$	320 ± 140 µM
cTnI$_{147-163}$/cNTnC•Ca^{2+}	150 ± 30 µM
cTnI$_{147-163}$/cNTnC•Ca^{2+}•A7	230 ± 50 µM

Table 6-2. Dissociation constants for A6 and cTnI$_{147-163}$ binding.

Ligand/Target	Dissociation Constant
A6/cNTnC•Ca^{2+}	420 ± 350 µM
A6/cNTnC•Ca^{2+}•cTnI$_{147-163}$	390 ± 50 µM
cTnI$_{147-163}$/cNTnC•Ca^{2+}	150 ± 30 µM
cTnI$_{147-163}$/cNTnC•Ca^{2+}•A6	180 ± 30 µM

binding pose of these compounds whereas the length and charge of the hydrocarbon chain controls the function of these compounds.

Conclusion

The results presented here increase our understanding of the pharmacophores responsible for the function of ligands that target troponin to modulate contractility. The charge of the molecule clearly seems important; however, charge alone is not enough to enhance cTnI$_{147\text{-}163}$ binding to cNTnC. Decreasing the length of the hydrophobic tail of A7 by one methylene decreased the impairment of cTnI$_{147\text{-}163}$ binding, and thus it is likely that W7 may both sterically hinder cTnI binding as well as electrostatically repel R147. Importantly, as we decreased the length of A7 the affinity of A6 for cNTnC•Ca^{2+} was also decreased. This observation suggests that drug binding to cNTnC in the absence of cTnI is driven by hydrophobic interactions. This is not surprising given cNTnC is lined by hydrophobic residues. Therefore, when designing Ca^{2+}-sensitizing molecules that target cNTnC, a drug should have as large a hydrophobic surface as possible to enhance its binding to cNTnC without compromising the binding of cTnI. Given the rigid nature of the naphthalene group, it may be not be the best scaffold to build off of. The biphenyl structure of dfbp-o or the pyridazinone-phenyl structure of levosimendan may represent better pharmacophores because they can twist to accommodate the shape of the binding pocket and avoid clashing with cTnI$_{147\text{-}163}$. Finally, the negatively charged group of the A compounds or dfbp-o is not ideal in designing molecules that bind cNTnC, which is negatively charged (pI ~4.1). A better template may be a molecule with an electron dense region that may still attract R147 (or at least not repel it) without dramatically reducing the drug's interaction with cNTnC•Ca^{2+}. Levosimendan (*17*) may function by this means since it is uncharged but has a slightly negative electrostatic potential surrounding the nitrile groups (*8*). Finally, to verify our
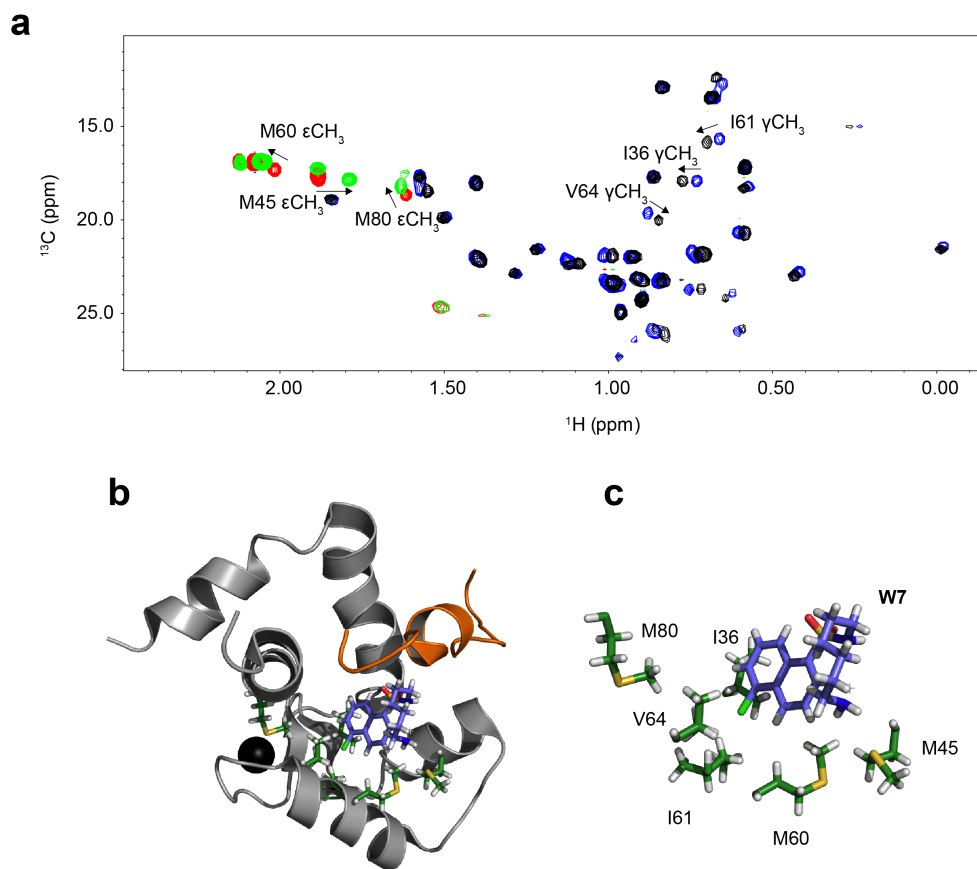
Figure 6-5. Prediction of the binding site of A6. **a.** The ^{1}H,^{13}C-HSQC NMR spectrum of 0.2 mM sample of cNTnC•Ca^{2+}•cTnI$_{144\text{-}163}$ in the absence (blue – positive peaks; red – negative peaks) and presence of 0.6 mM A6 (black – positive peaks; green – negative peaks). **b.** The structure of W7 bound to cNTnC•Ca^{2+}•cTnI$_{147\text{-}163}$ (cNTnC in grey, Ca^{2+} ion in sphere representation, cTnI in orange, and W7 in stick representation colored slate) with the labeled residues from **a.** shown in stick representation (green). **c**. Close-up of the residues perturbed upon A6 binding in relation to the location of W7 in the cNTnC•Ca^{2+}•W7•cTnI$_{147\text{-}163}$ complex.

electrostatic model, we plan to test this series of compounds on demembranated myofilaments as what was done for dfbp-o (*8*).

References

1. Gordon, A. M., Homsher, E., and Regnier, M. (2000) Regulation of contraction in striated muscle, *Physiol. Rev. 80*, 853-924.

2. Parmacek, M. S., and Solaro, R. J. (2004) Biology of the troponin complex in cardiac myocytes, *Prog. Cardiovasc. Dis. 47*, 159-176.

3. Tobacman, L. S. (1996) Thin filament-mediated regulation of cardiac contraction, *Annu. Rev. Physiol. 58*, 447-481.

4. Kobayashi, T., Jin, L., and de Tombe, P. P. (2008) Cardiac thin filament regulation, *Pflugers Archiv-European Journal of Physiology 457*, 37-46.

5. Endoh, M. (2002) Mechanisms of action of novel cardiotonic agents, *J. Cardiovasc. Pharmacol. 40*, 323-338.

6. Kass, D. A., and Solaro, R. J. (2006) Mechanisms and use of calcium-sensitizing agents in the failing heart, *Circulation 113*, 305-315.

7. Oleszczuk, M., Robertson, I. M., Li, M. X., and Sykes, B. D. (2010) Solution structure of the regulatory domain of human cardiac troponin C in complex with the switch region of cardiac troponin I and W7: The basis of W7 as an inhibitor of cardiac muscle contraction, *J. Mol. Cell. Cardiol. 48*, 925-933.

8. Robertson, I. M., Sun, Y. B., Li, M. X., and Sykes, B. D. (2010) A structural and functional perspective into the mechanism of Ca2+-sensitizers that target the cardiac troponin complex, *J. Mol. Cell. Cardiol. 49*, 1031-1041.

9. Li, M. X., Spyracopoulos, L., and Sykes, B. D. (1999) Binding of cardiac troponin-I147-163 induces a structural opening in human cardiac troponin-C, *Biochemistry 38*, 8289-8298.

10. Takeda, S., Yamashita, A., Maeda, K., and Maeda, Y. (2003) Structure of the core domain of human cardiac troponin in the Ca(2+)-saturated form, *Nature 424*, 35-41.

11. Hidaka, H., Asano, M., and Tanaka, T. (1981) Activity-structure relationship of calmodulin antagonists, Naphthalenesulfonamide derivatives, *Mol. Pharmacol. 20*, 571-578.

12. MacNeil, S., Griffin, M., Cooke, A. M., Pettett, N. J., Dawson, R. A., Owen, R., and Blackburn, G. M. (1988) Calmodulin antagonists of improved potency and specificity for use in the study of calmodulin biochemistry, *Biochem. Pharmacol. 37*, 1717-1723.

13. Li, M. X., Saude, E. J., Wang, X., Pearlstone, J. R., Smillie, L. B., and Sykes, B. D. (2002) Kinetic studies of calcium and cardiac troponin I peptide binding to human cardiac troponin C using NMR spectroscopy, *European Biophysics Journal with Biophysics Letters 31*, 245-256.

14. Guo, K., and Li, L. (2009) Differential C-12/C-13-Isotope Dansylation Labeling and Fast Liquid Chromatography/Mass

Spectrometry for Absolute and Relative Quantification of the Metabolome, *Anal. Chem. 81*, 3919-3932.

15. Rogne, O. (1968) Kinetics of Neutral and Alkaline Hydrolysis of Aromatic Sulphonyl Chlorides in Water, *Journal of the Chemical Society B-Physical Organic*, 1294-&.

16. Krudy, G. A., Kleerekoper, Q., Guo, X. D., Howarth, J. W., Solaro, R. J., and Rosevear, P. R. (1994) Nmr-Studies Delineating Spatial Relationships within the Cardiac Troponin-I Troponin-C Complex, *J. Biol. Chem. 269*, 23731-23735.

17. Pollesello, P., Ovaska, M., Kaivola, J., Tilgmann, C., Lundstrom, K., Kalkkinen, N., Ulmanen, I., Nissinen, E., and Taskinen, J. (1994) Binding of a New Ca2+ Sensitizer, Levosimendan, to Recombinant Human Cardiac Troponin-C - a Molecular Modeling, Fluorescence Probe, and Proton Nuclear-Magnetic-Resonance Study, *J. Biol. Chem. 269*, 28584-28590.

18. Kustova, T. P., Sterlikova, I. O., and Klyuev, M. V. (2002) Arylsulfonylation of N-isobutylaniline and its derivatives: experimental study and quantum-chemical calculations, *Russian Chemical Bulletin 51*, 2157-2160.

19. Hoffman, R. M. B., and Sykes, B. D. (2009) Structure of the Inhibitor W7 Bound to the Regulatory Domain of Cardiac Troponin C, *Biochemistry 48*, 5541-5552.

Chapter 7

The structural and functional consequences of the Ca^{2+}-sensitizing mutation, L48Q, on cardiac troponin C*

Summary

Ca^{2+} binding to the regulatory domain of cardiac troponin C (cNTnC) prompts a series of protein-protein interactions that culminate in muscle contraction. Following Ca^{2+} association with cNTnC, there is a subtle conformational change that partially exposes a hydrophobic surface to which troponin I (cTnI) binds. At low Ca^{2+} levels, apo cNTnC is closed and cTnI binds to actin, inhibiting contraction. Hence, cNTnC is involved in two crucial regulatory steps, Ca^{2+} and cTnI binding. In recent years, there have been a number of mutations found in the troponin complex linked to disease. These include several in cNTnC, such as A8V, L29Q, E59D/D75Y, and C84Y. These mutations have been shown to alter the Ca^{2+}-sensitivity of the thin filament. Recently, Tikunova and Davis engineered a series of cNTnC mutations with the aim of modulating the Ca^{2+} sensitivity of the thin filament (Tikunova, S. B., and Davis, J. P. (2004) Designing calcium-sensitizing mutations in the regulatory domain of cardiac troponin C, *J Biol Chem 279*, 35341-35352). The mutation L48Q showed a pronounced increase in Ca^{2+} sensitivity. While the authors speculate this is through a stabilization of the open state of cNTnC, there has not been any structural study investigating this possibility. In this work, we sought structural and mechanistic explanations for the increased Ca^{2+} sensitivity of L48Q. We used an array of biophysical techniques to characterize its interaction with Ca^{2+} and cTnI. We found that the L48Q mutation enhanced binding of both Ca^{2+} and cTnI to troponin C. NMR chemical shift and relaxation data provided evidence that the L48Q variant of cNTnC is more open than the wild-type cNTnC. Finally, molecular dynamics simulations suggest that the mutation of Leu48 to a glutamine disrupts a network of crucial hydrophobic interactions that stabilize the closed form of cNTnC. The findings presented herein emphasize the importance of cNTnC's conformation in the regulation of contraction, and suggests that mutations in cNTnC that alter myofilament Ca^{2+} sensitivity can do so by either modulating Ca^{2+} affinity, cTnI affinity, or as is the case for L48Q, both.

Introduction

Striated muscle contraction is triggered by a transient increase in intracellular Ca^{2+} that binds to troponin C (TnC) – the Ca^{2+}-binding subunit of the cardiac troponin (cTn) complex on thin filaments. TnC is a dumbbell shaped protein that consists of N-terminal and C-terminal EF-hand motifs connected by a long flexible linker (*1*). There are two isoforms of troponin C in striated muscle: skeletal (sTnC) and cardiac (cTnC). The regulatory lobe of sTnC (sNTnC) undergoes a large structural "opening" when it binds two Ca^{2+} (*2*). The structural change is much smaller in cNTnC upon binding Ca^{2+} and it remains essentially "closed" (*3*). This difference is the result of cNTnC having only one functional Ca^{2+} binding site (site II) (*4*). The C-terminus of cTnC (cCTnC) contains high affinity Ca^{2+} binding sites, III and IV. Although these sites are thought to play primarily a structural role by anchoring the Tn complex to the thin filament, they may also be involved in the Ca^{2+} signaling pathway, since disease related mutations in this region of cTnC affect cardiac muscle function (*5-7*). cTnC interacts with the other two components of cTn: cardiac troponin I (cTnI) and troponin T (cTnT). Following Ca^{2+} binding to site II of cNTnC, the "switch" region of cTnI (residues 147-163, $cTnI_{147-163}$) binds to cNTnC and consequently the "inhibitory" region of cTnI (residues 112-146) dissociates from actin. The detachment of $cTnI_{112-146}$ from actin permits increased mobility of tropomyosin over the surface of the thin filament. The repositioning of tropomyosin leads to the exposure of the myosin head binding sites on actin and the actomyosin cross-bridges form generating contractile force and cell shortening (*8, 9*).

A growing number of genetically identified variants (mutations) in cTn subunits associated with cardiomyopathies have been shown to the alter protein-protein interactions involved in thin filament activation (*10*). Thus far, at least 84 mutations in cTn proteins have been identified in patients with hypertrophic, restrictive, and dilated cardiomyopathy (HCM,

RCM, and DCM, respectively) (*11, 12*). Functional studies of HCM associated mutations have, in most cases, been found to result in increased Ca^{2+} sensitivity of contraction of skinned myocardium, and at least three variants are located in cTnC (A8V, C84Y and D145E). While the increase in the Ca^{2+}-sensitivity may not cause HCM, it is possible that the augmented contractility is associated with the progression and severity of HCM over time (*13*). Thus, understanding how altered Ca^{2+} binding influences cTn subunit interactions and signaling of thin filament activation has considerable medical relevance.

In this study we have focused on a cTnC variant, cTnC(L48Q), which was engineered to enhance the Ca^{2+}-sensitivity of cTnC (it has not been identified in HCM patients to date). Previously, Davis and Tikunova showed that human cTnC(L48Q) increased the Ca^{2+} affinity of the Tn complex and thin filament (*14, 15*). Parvatiyar *et al.* (*16*) showed it increased in both Ca^{2+} sensitivity of skinned porcine trabeculae contraction and ATPase sensitivity. Recently, Kreutziger *et al.* (*17*) reported that the rat L48Q variant of cTnC had similar effects in solution and increased Ca^{2+} sensitivity of contraction in rat trabeculae and myofibrils. Korte *et al.* demonstrated that cTnC(L48Q) increased intact myocyte contractility without affecting relaxation or intracellular Ca^{2+} transients (paper in review). Despite this wealth of functional data, the precise molecular mechanism of this single residue mutation has yet to be elucidated.

Leu48 makes a number of crucial hydrophobic contacts that contribute to stabilizing a closed form of cNTnC (*1*) – in both the apo and Ca^{2+}-saturated states (*3*). The mutation of this leucine to a glutamine is therefore expected have a significant destabilizing effect on the structure. We have employed an integrative approach to understand how the L48Q mutation of cTnC results in an increased myofilament Ca^{2+} sensitivity. Fluorescence spectroscopy, isothermal titration calorimetry (ITC), and nuclear magnetic resonance (NMR) spectroscopy experiments confirm

that an increase in both Ca^{2+} and cTnI affinity was observed by mutating L48 to glutamine. The isolated cNTnC L48Q variant, cNTnC(L48Q), dimerized in a concentration dependent manner consistent with a more open conformation of the domain and this was quantitated using chemical shift changes. Molecular dynamics (MD) simulations and NMR relaxation experiments were used to probe the relationship between structure and function. The MD simulations suggested that L48Q increases the binding affinity of the switch region of cTnI ($cTnI_{147-163}$) to cNTnC by stabilizing its open conformation. Furthermore, the L48Q mutation significantly perturbed the relaxation of site I residues (which are far from the mutation site) and supported the conclusion that cNTnC(L48Q) undergoes a conformational perturbation. Overall, our results are consistent with L48Q stabilizing a more open conformation of cNTnC, which has the multifarious consequences of enhancing the Ca^{2+} and cTnI binding to cNTnC.

Experimental Procedures

Protein preparation and labeling

Protein Mutagenesis and Purification

Construction and expression of wild-type rat cTnC, cTnI and cTnT in PET 24A vector has been described in a previous publication(*18*). $cTnC^{C35S}$ and $cTnC(L48Q)^{C35S}$ were constructed from the rat wild-type cTnC plasmid by a primer based site-directed mutagenesis kit and confirmed by DNA sequence analysis. The plasmids for cTnC mutants were then transformed into *Escherichia Coli* BL21 cells and expressed and purified. The DNA encoding cNTnC (residues 1-89) was into the pET-3a expression vector as previously described (*19*). The L48Q mutation was engineered using a site-directed mutagenesis kit. The expression vectors were transformed into *Escherichia Coli* BL21 cells, expressed, and

purified. ^{15}N-labeled cNTnC and cNTnC(L48Q) were expressed in minimal media enriched with (^{15}NH$_4$)$_2$SO$_4$ (20).

Fluorescent Labeling of Protein

The labeling procedure used here is similar as previous described [15]. Briefly, cTnC^{C35S} and cTnC(L48Q)^{C35S},respectively, were first dialyzed against 1mM DTT in a buffer containing 6M urea, 25mM TRIS, 1mM ethylenediamine-N,N,N9,N9-tetraacetic acid (EDTA) at pH8.0. 5mM DTT was added and the proteins were then dialyzed against the same buffer but without DTT for at least 12h with 3 times buffer changes.100mM IANBD (N-(2-(iodoacetoxy)ethyl)-N-methyl)amino-7-nitrobenz-2-oxa-1,3-diozole Mw=406.14) (in dimethylformamide) was added in 3 fold molar excess over TnC^{C35S} or cTnC(L48Q)^{C35S} and the protein solutions were gently shaken in the dark for >4h at 4°C.The labeling reaction was terminated by addition of 10mM DTT and the labeled protein solution was dialyzed against buffer containing 20mM MOPS,150mM KCl,3mM MgCl$_2$,2mM EGTA,1mM DTT, pH7.0 to remove unreacted IANBD (3 times for at least 12h). Finally, cTnC^{C35S} and cTnC(L48Q)^{C35S} were labeled at C84 of cTnC with IANBD and we have demonstrated that the fluorescence probe at this position monitors cTnC N-terminal Ca^{2+} binding (21). The labeling efficiency was 90% determined by comparison of the concentration of the protein before and after labeling.

Reconstitution of Tn Complexes.

The Tn subunits (TnI, and TnT) were first dialyzed separately against 6M urea, 25mM TRIS, 1mM EDTA at pH8. After dialysis, IANBD-cTnC^{C35S}/cTnI/cTnT were then mixed at the molar ratio of 1:1:1. After incubating at room temperature for 30 min, the protein solution were dialyzed through a series of steps against (1)2M urea, 0.75M KCl, 20mM MOPS, 3mM MgCl$_2$, 1mM CaCl$_2$,pH 7.0 (2) 1M urea, 0.75M KCl, 20mM MOPS, 3mM MgCl$_2$, 2mM EGTA, pH 7.0 (3) 0.75M KCl, 20mM MOPS,

3mM MgCl$_2$, 2mM EGTA, pH 7.0 (4) 0.5M KCl, 20mM MOPS, 3mM MgCl$_2$, 2mM EGTA, pH 7.0 (5) 0.25M KCl, 20mM MOPS, 3mM MgCl$_2$, 2mM EGTA, pH 7.0 (6) Finally, 150mM KCl, 20mM MOPS, 3mM MgCl$_2$, 2mM EGTA, ,1mM DTT, pH 7.0. All dialysis were done in dark without stirring at 4°C. Proteins that precipitated during the dialysis with decreasing KCl concentration were removed by centrifugation (22).

Steady-state Fluorescence Measurements

All steady-state fluorescence measurements were performed using Perkin Elmer Luminescence Spectrometer LS50B at 15°C. IANBD fluorescence was excited at 490nm and monitored at ~530 nm (Both bandwidths set at ~8nm). Protein buffer solutions contained 20mM MOPS, 150mM KCl, 3mM MgCl$_2$, 2mM EGTA, 1mM DTT (pH 7.0). Fluorescence signal of 2 ml IANBD-cTnC^{C35S} or IANBD-cTn^{C35S} (0.6 µM) was monitored with titration of microliter amounts of Ca^{2+} or cTnI in the presence (100 µM) or absence of Ca^{2+}. The free Ca^{2+} concentration was calculated using Maxchelator program (http://maxchelator.stanford.edu) (23). Ca^{2+} sensitivities of conformational changes (pCa value at half maximal fluorescence signal change) and dissociation constant K$_D$ of cTnI for cTnC were obtained by fitting the binding curve with sigmoid Hill equation as previously described (24). The value reported here were the mean of three to five successive titrations.

Isothermal Titration Microcalorimetry

All experiments were performed using a Microcal Inc isothermal titration microcalorimeter (ITC-200). Experimental conditions were 30 °C, 20 mM MOPS, pH 7.0, 150 mM KCl, 3 mM MgCl$_2$, 2 mM EGTA, 1 mM CaCl$_2$. The sample cell was filled with 200 µL of 3 µM cTnI (with 1 mM Ca^{2+}) and titrated with 2 µl per injection of 50-70 µM cTnC (WT or L48Q,

Ca^{2+} saturated). Control titration of cTnC (WT or L48Q) to buffer was performed for each independent experiment. Binding parameters were calculated by the Origin-ITC data analysis software package using single set of sites mode.

NMR Spectroscopy

Sample Preparation and data analysis

All NMR samples had starting volumes of 500 µL. The protein samples were dissolved in 100 mM KCl, 10 mM Imidazole, and 0.2-0.25 mM 2,2-dimethyl-2-silapentane-5-sulfonate sodium salt (DSS) (Chenomx) with 0.01 % NaN_3 in 95% H_2O/5% D_2O with 2-8 mM $CaCl_2$ (Fluka). Concentrations of cNTnC(L48Q) varied from 0.5 mM for assignment experiments to 0.1 mM for $cTnI_{147-163}$ titrations. The pH was kept constant between 6.7-7.0. All experiments were run on either a Varian Inova 500 MHz spectrometer of a Unity 600 MHz spectrometer. All data were collected at 30°C. All NMR data were processed with NMRPipe (*25*) and visualized with NMRViewJ (*26*). ^{15}N-T_1, ^{15}N-T_2, and NOE experiments were analyzed with the Rate Analysis and HetNOE modules in NMRViewJ. The analysis of titration data and dimerization data was done with xcrvfit (www.bionmr.ualberta.ca/bds/software/xcrvfit). Model-free analysis of the data was done using Mathematica notebooks prepared by Leo Spyracopoulos (*27*). Models were chosen using Akaike's Information Criteria (AIC) (*28*), and Monte Carlo analysis was done on the chosen model to get errors (*29*).

Titrations

The titration of Ca^{2+} and $cTnI_{147-163}$ into cNTnC(L48Q) was monitored by the ^1H,^{15}N-HSQC NMR experiment. At each titration point spectra were recorded, and the concentration dependent chemical shift perturbations were used to determine dissociation constants. For the Ca^{2+}

titration, initially Ca^{2+}-free buffer was prepared with Chelex 100 (Bio-Rad), which was used to chelate any free metal ions. The protein was run down a desalting column in the presence of EGTA. We prepared a 50 mM $CaCl_2$ stock solution and titrated the solution into the apo-cNTnC(L48Q) NMR sample to final concentrations of: 0.10, 0.15, 0.20, 0.25, 0.30, 0.35, 0.40, 0.45, 0.50, 0.60, 0.80, 1.41, 2.63 mM. We prepared a 3.8 mM stock of $cTnI_{147-163}$ in DMSO-d6 (Cambridge Isotopes Inc.) and the concentration of cNTnC(L48Q) was determined to be 84 µM. We titrated $cTnI_{147-163}$ into cNTnC(L48Q) to final concentrations of: 7, 14, 22, 29, 36, 43, 57, 71, 85, 99, 120, 140, 173, 205, and 269 µM. The pH was kept between 6.9 and 7.0 throughout the titration by adding 1M HCl or 1M NaOH.

NMR experiments for assignment

The $^1H,^{15}N$-HSQC NMR spectra of ^{15}N-labeled cNTnC(L48Q) were assigned for all three states of L48Q: Apo, Ca^{2+}-bound, and $cTnI_{147-163}$-bound. The $^1H,^{15}N$-HSQC spectra for the different states of L48Q were assigned with the aid of the three-dimensional ^{15}N-NOESYHSQC and ^{15}N-TOCSYHSQC NMR experiments. The TOCSYHSQC experiment correlates intraresidue backbone amides with side-chain protons; and the NOESYHSQC experiment correlates backbone amide nuclei with nearby nuclei – either intraresidue or interresidue. Through the combination of these two NMR experiments, and previously published assignments for cNTnC (*3, 30*), we were able to completely assign the backbone amides of cNTnC(L48Q) (Figure 7-4).

^{15}N Backbone Relaxation experiments

To assess the concentration-dependent aggregation of cNTnC(L48Q)•Ca^{2+}, T_2 experiments were acquired at four protein concentrations: 0.15, 0.33, 0.7, and 1.2 mM. The T_1 and NOE values were recorded with a cNTnC(L48Q)•Ca^{2+} concentration of 0.33 mM on the 500 and 600 MHz spectrometers; and with a concentration of 0.15 mM on the

500 MHz spectrometer. All experiments were recorded with the same experimental parameters: T_1 values were determined using relaxation delays of 10, 50, 100, 200, 300, and 400 ms; T_2 values were acquired using relaxation delays of 10, 30, 50, 70, 90, and 110 ms. Delays between transients for T_1 and T_2 experiments was set to 3 s. The ^{1}H-^{15}N NOE experiments had a delay of 3s without the proton saturation and when proton saturation was on, it was set to 3s.

Molecular Dynamics Simulations and Analysis

The starting structure of the N-terminus of cTnC (cNTnC, from residue 1 to 89) in the Ca^{2+} saturated was from model 14 of NMR structure (PDB entry 1ap4) (*3*), and the model 13 of the NMR structure (PDB entry 1spy) (*3*) was used for apo state cNTnC starting structure. The L48Q mutation was created *in silico* by UCSF Chimera (*31*) in all three structures. All-atom, explicit solvent molecular dynamics (MD) simulations were performed at 288 K in the microcanonical (NVE, constant number of particles, volume, and energy) ensemble using the *in lucem* molecular mechanics (*il*mm) program (*32*) with the Levitt *et al.* force field(*33*). The starting structures, minimized for 1000 steps with the steepest descent minimization, were solvated in a rectangular box of flexible three-center (F3C) waters (*34*) with walls located at least 10 Å from any protein atom. The solvent density of the box was adjusted to 0.999129 g/mL according to the simulation temperature (*35*). A 2 fs time step was used and structures were saved every 1ps. Multiple (n≥3) simulations for the WT and L48Q of complexes, apo cNTnC and Ca^{2+} saturated cNTnC, respectively, were performed to write out independent trajectories, up to 70ns each. Analysis of MD trajectories was performed with *il*mm(*32*). Contacts between residues were identified where the distance between two carbon atoms was ≤ 5.4 Å or any other non-carbon atoms were ≤4.6 Å. Distances were measured between specific atom pairs or between the

centers of mass of groups of atoms (e.g. two helices). Root-mean-square deviation (RMSD) of the Cα atoms of helices A (residues 14-28) and B (residues 41-48) to the starting structure were calculated. Protein images were generated using UCSF Chimera (*31*). Interhelical angles were calculated using the program interhlx (K. Yap, University of Toronto).

Results

Ca^{2+} and cTnI titrations into cTnC(L48Q) and cTnC monitored by fluorescence spectroscopy.

To assess the Ca^{2+} binding affinity of the L48Q variant, a C35S mutation was used to allow for site-specific labeling at C84 of cTnC with the fluorescence probe IANBD (IANBD-cTnC^{C35S}). C84 is located at the end of helix D, whereas C35 is exposed to the solvent and is near the nonfunctional Ca^{2+} binding loop I. Mechanical and fluorescence studies have demonstrated that both Ca^{2+} and cross-bridge cycling influence the structure of the N-terminal domain of cTnC at C84 and that the probe at this position monitors Ca^{2+} binding to cNTnC (*21*). Thus, fluorescence labeling at C84 reports on conformational changes in cNTnC (*36*). Ca^{2+}-binding to cNTnC causes the B and C helices to move away from the N, A, and D helix bundle resulting in the exposure of a hydrophobic surface. The fluorescence of IANBD increases as this conformational change occurs, presumably because it binds to the exposed hydrophobic patch of cNTnC•Ca^{2+}.

We compared the Ca^{2+}-dependent conformational changes of IANBD-cTnC(L48Q)^{C35S} and IANBD-cTnC^{C35S}. As shown in the inset graph of Figure 7-1, IANBD-cTnC(L48Q)^{C35S} underwent ~1.33 fold maximal increase in IANBD fluorescence when saturated with Ca^{2+} and IANBD-cTnC^{C35S} experienced a ~1.25 fold increase in fluorescence. The enhanced magnitude of total fluorescence change for IANBD-
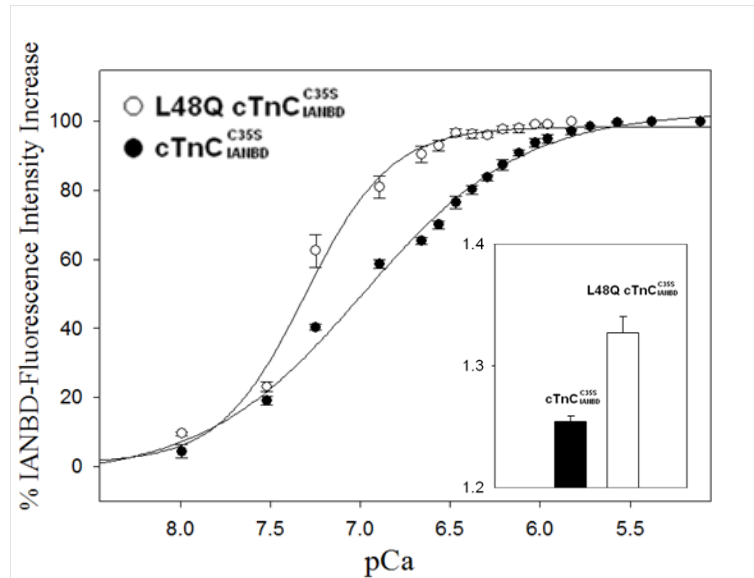
Figure 7-1. Effects of L48Q on the Ca^{2+} dependent changes in the fluorescence of IANBD-cTn^{C35S} complexes. (○) Ca^{2+} binding to IANBD-cTn(L48Q)^{C35S}; (●) Ca^{2+} binding to IANBD-cTn^{C35S}. Inset graph, effects of L48Q on the magnitude IANBD fluorescence increase of IANBD-cTnC(L48Q)^{C35S}. Excitation was at 490 nm and the emission was monitored at 530 nm. The error bars represent the standard error of 3-5 experiments.

cTnC(L48Q)^{C35S} implies the structural change of the regulatory domain of cTnC upon Ca^{2+} binding is slightly larger in the mutant. We next added IANBD-cTnC(L48Q)^{C35S} or IANBD-cTnC^{C35S} to cTnI and cTnT to form whole cTn complexes to determine if the L48Q variant influenced Ca^{2+} binding to the complex. The Ca^{2+} affinities for cTn(L48Q) and cTn were determined by measuring Ca^{2+} induced increases in IANBD fluorescence associated with the conformational changes within the cTn complexes. Consistent with a previous report using recombinant human cTnC variants, the L48Q variant enhanced Ca^{2+} binding affinity (*15*). Ca^{2+} sensitivity of the fluorescence signal (reported as pCa at half-fluorescence increase) was shifted +0.32 pCa unit, from 6.99±0.03 (IANBD-cTn^{C35S}) to 7.31±0.03 (IANBD-cTn(L48Q)^{C35S}) (curves in Figure 7-1). This matches well the 0.38 pCa unit increase in Ca^{2+} sensitivity of contraction recently reported upon exchanging cTn(L48Q)^{C35S} into skinned rat trabeculae (*17*).

Increased interaction between cTnC and cTnI plays a critical role in transferring the Ca^{2+}-signal to other myofilament proteins to initiate cardiac muscle contraction. Thus, in addition to examining Ca^{2+} affinity, we tested whether the L48Q variant also altered cTnI affinity. Binding of cTnI to cTnC was measured by titrating labeled IANBD-cTnC^{C35S} with cTnI in the presence or absence of Ca^{2+}. cTnI binding to IANBD-cTnC^{C35S} and IANBD-cTnC(L48Q)^{C35S}, in the apo (panel A) and Ca^{2+} saturated (panel B) states increased IANBD fluorescence (Figure 7-2). For both control and IANBD-cTnC(L48Q)^{C35S}, the magnitude of maximal IANBD fluorescence change was greater for the Ca^{2+} saturated states than the apo state, indicating a larger conformational change. The magnitude of fluorescence increase for IANBD-cTnC(L48Q)^{C35S} in the apo and Ca^{2+} saturated states was 2.27±0.07 and 3.73 ± 0.18 fold, respectively, which were greater than IANBD-cTnC^{C35S} for both conditions (2.14 ± 0.06 fold without Ca^{2+} and 3.29 ± 0.11 fold with Ca^{2+}), suggesting that the regulatory domain of cTnC(L48Q) is more open when bound to cTnI. cTnI bound to IANBD-
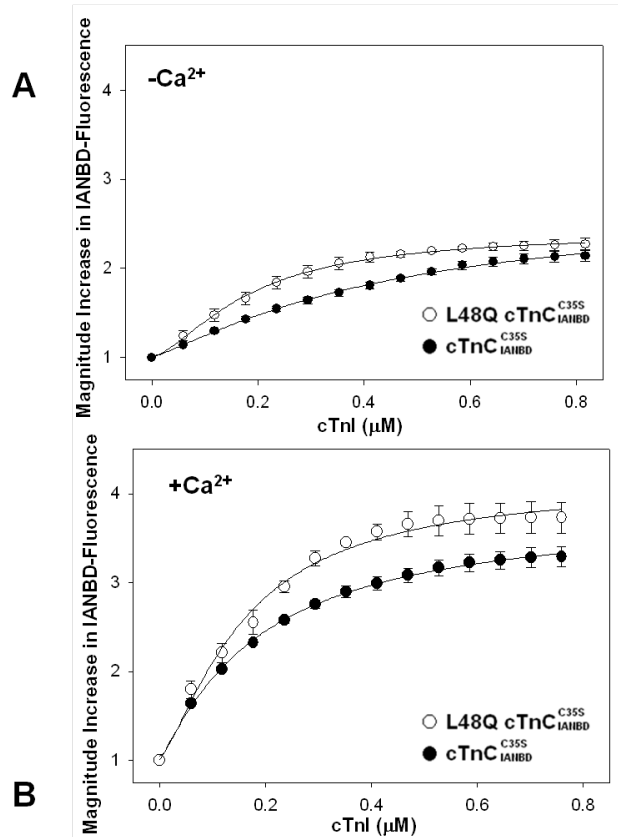
Figure 7-2. Effects of L48Q on the binding of cTnI to IANBD-cTnC^{C35S}. The binding was determined by measuring the changes in IANBD fluorescence emission intensity of IANBD-cTnC^{C35S} titrating with cTnI in A. the absence of Ca^{2+} and B. the presence of Ca^{2+}: ($\circ$) IANBD-cTnC^{C35S} ($\bullet$) IANBD-cTnC(L48Q)^{C35S}. Excitation was at 490nm and the emission was monitored at 530nm. The error bars represent the standard error of 3-5 experiments.

cTnC(L48Q)^{C35S}•3Ca^{2+} more tightly than to IANBD-cTnC^{C35S}•3Ca^{2+}, with dissociations constants of 174 ± 8 nM and 198 ± 5 nM, respectively.

Binding of cTnI to cTnC bound to calcium by ITC.

We used isothermal titration calorimetry (ITC) to get a more comprehensive picture of cTnI binding to cTnC. ITC permits the monitoring of protein-protein interactions without the need for chemical modifications which may detrimentally modify the interaction surface. The titration of cTnI with Ca^{2+} saturated cTnC(L48Q) as monitored by ITC is shown in Figure 7-3. For each titration point, the quantity of heat released (as indicated by the negative deflection) is directly proportional to the amount of binding between the two proteins. The complete binding isotherm was obtained by plotting the integrated heat against the molar ratio of cTnC added to cTnI in the reaction cell. The stoichiometry (*n*), binding dissociation constant (*K$_D$*) and enthalpy (*ΔH*) of the binding were directly obtained by fitting these data using the Origin-ITC package. The results from a minimum of three independent ITC binding experiments for cTnC or cTnC(L48Q) binding to cTnI, in the presence of Ca^{2+}, suggested that the binding stoichiometry was approximately 1:1 for both WT and cTnC(L48Q). Consistent with the fluorescence data, the affinity of cTnC(L48Q) for cTnI was higher than cTnC, K$_D$ ~131 nM for cTnC(L48Q) and K$_D$ ~159 nM for cTnC. Furthermore, the total heat released upon binding to cTnI (ΔH) for cTnC(L48Q) was -22.1 ± 1.47 kJ·mol^{-1}, and -16.1 ± 3.9 kJ·mol^{-1} for cTnC.

Ca^{2+} and cTnI$_{147-163}$ titrations into cNTnC(L48Q) by NMR spectroscopy.

To understand the structural significance of L48Q on the N-lobe regulatory domain of cTnC, we expressed ^{15}N-labeled cNTnC(L48Q) for NMR experiments. The ^{1}H,^{15}N-HSQC NMR spectrum of ^{15}N-labeled
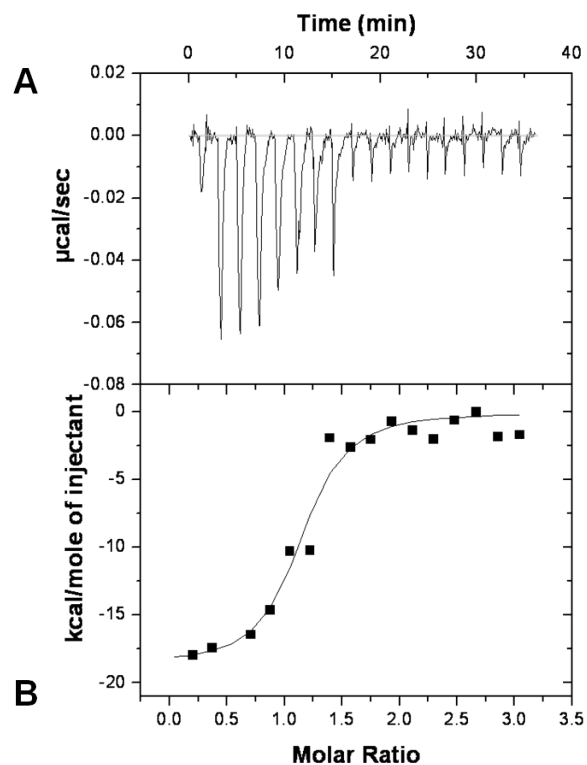
Figure 7-3. Microcalorimetric titration of cTnI with cTnC(L48Q) in the presence of Ca^{2+}. A, an example trace of the titration of 3 μM cTnI with 50 μM - 70 μM cTnC(L48Q) at 30 °C. B, Integrated heats for each injection obtained from the raw data in panel A *versus* the molar ratio of cTnC(L48Q) to cTnI. The data were fit to the data using a 1:1 binding model, the fit is shown by the solid line.

cNTnC(L48Q)[1] was assigned in its apo; Ca^{2+} saturated; and Ca^{2+} and cTnI$_{147-163}$ bound states using the three-dimensional ^{15}N-NOESYHSQC and ^{15}N-TOCSYHSQC NMR experiments (Figure 7-4). NMR spectroscopy was used to measure the affinity of cNTnC(L48Q) for Ca^{2+} and the affinity of Ca^{2+} saturated cNTnC(L48Q) for cTnI$_{147-163}$ (Figure 7-5A, 5B). Ca^{2+} was titrated into an NMR sample containing apo cNTnC(L48Q) and ^{1}H,^{15}N-HSQC spectra were acquired at each point. The concentration-dependent chemical shift perturbations of five well-resolved resonances were used to determine the dissociation constant of Ca^{2+} based on the global fitting method developed by Hoffman and Sykes (*37*). The protocol involves determining a global dissociation constant that fits all the data with a minimum sum of squared error (SSE). Ca^{2+} bound to cNTnC(L48Q) with a dissociation constant of 0.6 µM (SSE=0.055) (Figure 7-5C and 5D), which is lower than the dissociation constant for cNTnC(wt), 2.6 ± 1 µM (*38*). This result is consistent with our findings in intact troponin and with Tikunova and Davis for cTnC(L48Q) (*39*), and supports the use of the isolated domain to ascertain the effects of the L48Q mutation.

We next measured the affinity of the cTnI$_{147-163}$ peptide for cNTnC(L48Q)•Ca^{2+}. This fragment of cTnI is also called the switch region, i.e. the sequence of cTnI responsible for triggering contraction through specific binding to cNTnC•Ca^{2+} (*40*). The dissociation constant of cTnI$_{147-163}$ was determined in a similar manner as described for the Ca^{2+} titration. The global fit yielded a cTnI$_{147-163}$ dissociation constant of 61 µM (SSE=0.2) (Figure 7-5E and 5F), which is approximately 2x tighter than the dissociation constant of 150 ± 10 µM measured for cNTnC by NMR (*41*). The significantly weaker interaction between the fragment of cTnI (cTnI$_{147-163}$) and the isolated domain of cTnC (cNTnC) than what was measured by ITC and fluorescence for the full-length constructs is

---

[1] All protein analyzed by NMR was ^{15}N-labeled, so further mention of it will be excluded for brevity.
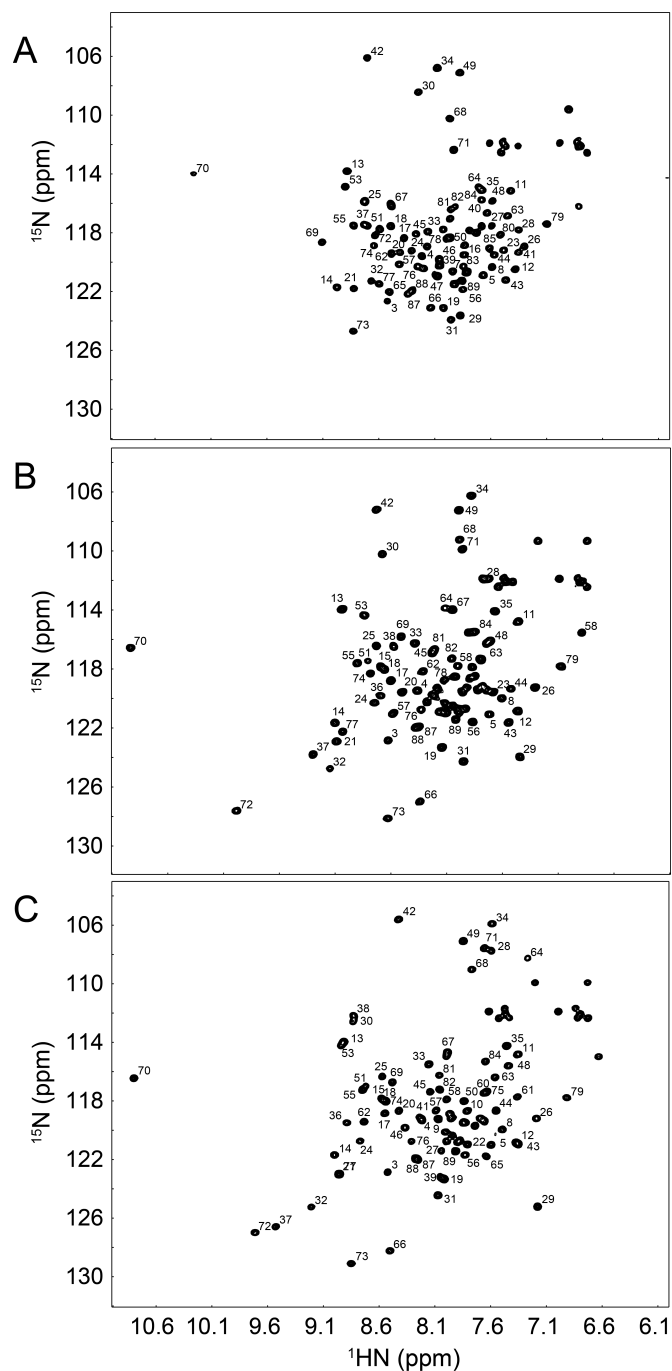
Figure 7-4. Assigned ^{1}H,^{15}N-HSQC spectra of A. Apo cNTnC(L48Q), B. cNTnC(L48Q)•Ca^{2+}, and cNTnC (L48Q)•Ca^{2+}•cTnI$_{147\text{-}163}$. All well resolved backbone amide peaks are labeled (side chain NH$_2$ were not assigned).
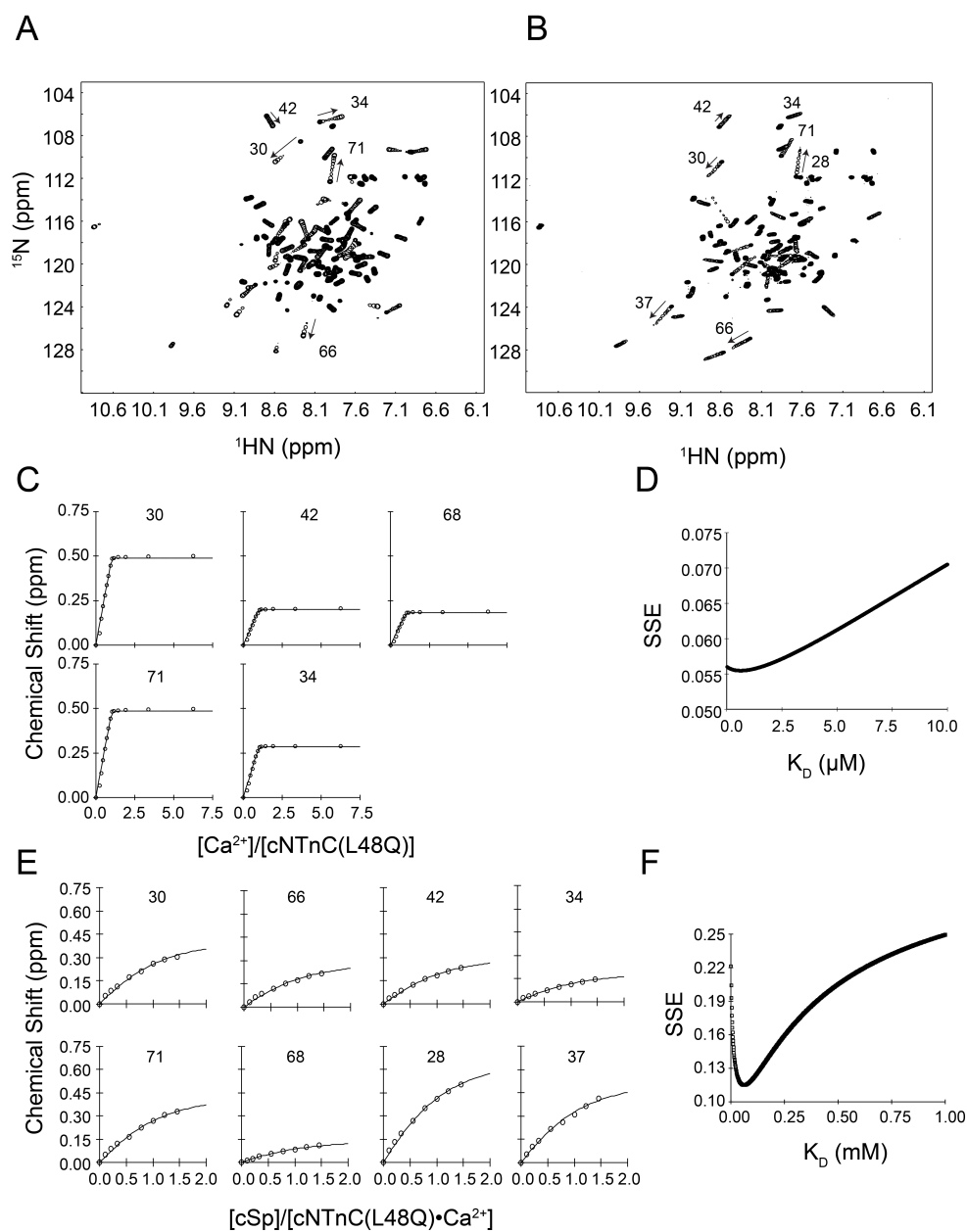
Figure 7-5. ^{1}H,^{15}N-HSQC spectra of A. the Ca^{2+} titration into Apo-cNTnC(L48Q) and B. the cTnI$_{147-163}$ titration into cNTnC(L48Q)•Ca^{2+}. C. Binding curves of the Ca^{2+} titration into cNTnC(L48Q) that were used in the global fit to determine the dissociation constant and D. the corresponding sum of squared error (SSE) for the global fit. E. Representative binding curves of the cTnI$_{147-163}$ titration into cNTnC(L48Q)•Ca^{2+} that were used in the global fit to determine the dissociation constant and F. the corresponding SSE for the global fit.

expected since full-length cTnI binds to both domains of cTnC; the interaction of cTnI$_{34-71}$ with cCTnC is in the nanomolar range (*42*).

Amide chemical shift comparison of cNTnC(L48Q)•Ca^{2+} with other troponin states.

In the apo state of cNTnC is in a closed conformation, with its hydrophobic residues buried in the core of the protein. The NMR structure of cNTnC•Ca^{2+} indicates that when Ca^{2+}-binds, a minor opening occurs (*3*). However, it is not until cTnI$_{147-163}$ binds that the fully open state of cNTnC is stabilized (Figure 7-6). The conformation of cNTnC is described by the A/B and C/D interhelical angles (90° means the helices are orthogonal and thus the protein is open; and an angle nearer to 180° indicates a more closed conformation – see Table 7-1). Therefore, the protein is fully open when both the A/B and C/D interhelical angles are ~90°. Although it is convenient to discuss the conformation of cNTnC in terms of angles, it must be stressed that a structure is a static representation of cNTnC. For example, the conformation of cNTnC•Ca^{2+} is thought to be in a dynamic equilibrium, fluxing between closed and open states (*43-45*).

Chemical shift differences between nuclei are caused by a change in the local magnetic environment such as by local structure or solvent exposure. So, in addition to their applicability in discerning the affinity and stoichiometry of Ca^{2+} or cTnI binding, chemical shifts may be able to provide insight into the conformation of cNTnC. The Ca^{2+}-sensitizing agent, bepridil, has been shown to stabilize the open form of cNTnC in a similar manner as cTnI$_{147-163}$ (*46*) (Table 7-1). Although they are structurally distinct molecules (bepridil is a small hydrophobic molecule and cTnI$_{147-163}$ is an amphipathic peptide), they induce similar amide chemical shift perturbations in the ^{1}H,^{15}N-HSQC spectrum of cNTnC, most likely because they both the stabilize the open state of cNTnC•Ca^{2+}. We
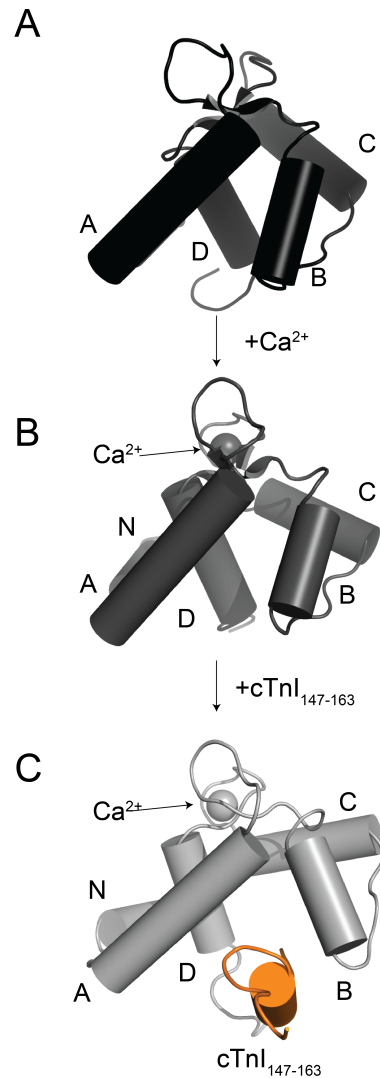
Figure 7-6. Conformational change of cNTnC from A. closed in the apo state (pdb: 1spy) through B. slightly open in the Ca^{2+}-bound state (pdb: 1ap4) to C. fully open when $cTnI_{147-163}$ is bound (pdb: 1mxl). cNTnC is depicted in cartoon mode with the helices shown in cylinder representation and are labeled (the N helix is pointing directly into the page in panel A. and is therefore not visible).

Table 7-1. Interhelical Angles.

		cNTnC apo	cNTnC+Ca2+	Bepridil
	Original NMR Structure Accession code(PDB)	1SPY	1AP4	1DTL
	Interhelical angles(°)	A/B	A/B	A/B
Exp.		140±3	132±3	92
WT		103±7	98±8	-
L48Q		97±8	89±7	-

overlaid the ^{1}H,^{15}N-HSQC spectra of cNTnC•Ca^{2+}, cNTnC•Ca^{2+}•cTnI$_{147-163}$, cNTnC•Ca^{2+}•bepridil, and cNTnC(L48Q)•Ca^{2+} to estimate the conformation of the L48Q variant (Figure 7-7). The chemical shifts of cNTnC(L48Q)•Ca^{2+} were intermediate between those for cNTnC•Ca^{2+} and the bepridil or cTnI$_{147-163}$ cNTnC•Ca^{2+} complexes. This suggests the L48Q mutation moves the conformational equilibrium of cNTnC•Ca^{2+} towards the open state; however, not as much as bepridil or cTnI$_{147-163}$. We recently developed a program, ORBplus, to analyze the relationship between the interhelical angles of cNTnC and amide chemical shifts. ORBplus predicted that the A/B interhelical angle of cNTnC(L48Q)•Ca^{2+} is more open than cNTnC•Ca^{2+} by approximately 10° from ~130° to ~120° (Robertson *et al.*, J. Bio. NMR, *in press* – See Appendix C).

^{15}N-T$_2$ and amide chemical shift as a function of concentration.

The Ca^{2+}-triggered conformational change of cNTnC is less than sNTnC because only one Ca^{2+} ion binds to cNTnC whereas two Ca^{2+} ions bind to the skeletal isoform. The biological role of the exposed hydrophobic surface is to promote binding of TnI$_{147-163}$ to cNTnC. The exposed hydrophobic surface also serves as an interface for *in vitro* dimerization (in the absence of troponin I). The NMR relaxation rate R$_2$ (=T$_2$) is proportional to the rotational correlation time of a protein and, hence, to its size. It has been shown that as the apparent sizes of cNTnC•Ca^{2+} or sNTnC•2Ca^{2+} increase as a function of concentration (*47*). The dissociation constant for dimer formation (K$_{dimer}$=[monomer]^2/[dimer]) was previously determined to be 7.3 mM for cNTnC(wt)•Ca^{2+} and 1.3 mM for sNTnC•2Ca^{2+} (*47*). To determine the dimerization constant of cNTnC(L48Q)•Ca^{2+} we measured the T$_2$ relaxation time of L48Q at four different concentrations (1.2, 0.72, 0.33, and 0.14 mM) and plotted R$_2$ (1/T$_2$) as a function of protein concentration (*48*) (Figure 7-8A). The
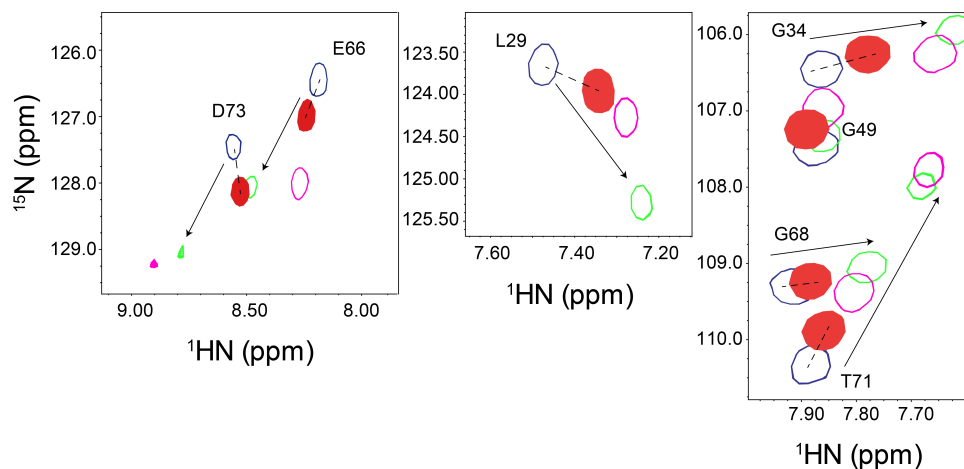
Figure 7-7. Comparison of ^{1}H,^{15}N-HSQC spectra from cNTnC(L48Q)•Ca^{2+} (filled red) with cNTnC•Ca^{2+} (blue), cNTnC•Ca^{2+}•cTnI$_{147-163}$ (green) and cNTnC•Ca^{2+}•bepridil (magenta). The resonances of cNTnC(L48Q)•Ca^{2+} are shifted intermediately between cNTnC(wt)•Ca^{2+} and the cTnI$_{147-163}$ or bepridil bound forms of cNTnC.

dimerization constant of cNTnC(L48Q)•Ca^{2+} was determined to be ~2 mM with an R$_2$ (monomer) of 6.2 s^{-1} and a R$_2$ (dimer) of 8.4 s^{-1}. We also compared amide chemical shifts as a function of concentration (Figure 7-8B). By comparing chemical shift as a function of protein concentration for a number of residues we obtained a range of dimerization constants (1.2-12 mM). The increased in dimerization efficacy of cNTnC(L48Q)•Ca^{2+} when compared to cNTnC•Ca^{2+} is most likely due to an increase in exposed hydrophobic surface. However, the data also indicate that cNTnC(L48Q)•Ca^{2+} is still not as open as sNTnC•2Ca^{2+} (K$_{dimer}$ = 1.3 mM).

Backbone ^{15}N relaxation data.

NMR relaxation data is a valuable source of experimental evidence for protein dynamics. The ^{15}N backbone NMR relaxation parameters T$_1$, T$_2$, and nuclear Overhauser effect (NOE) depend on the tumbling of the protein as a whole as well as on internal motions within the protein. The measured relaxation data for cNTnC(L48Q)•Ca^{2+} at 0.33 mM are shown on a per residue basis in Figure 7-9. The results indicate that cNTnC(L48Q) is a highly structured and rigid protein. The dramatic increase in T$_1$ and T$_2$ as well as a drop in NOE at the C-terminus of cNTnC(L48Q), is consistent with disorder. The average T$_1$^{500} (superscript indicates the magnetic field the relaxation data were acquired at, expressed as the frequency of ^{1}H in MHz) for all residues was 408 ± 87 ms with an average error of 15 ms, and the average T$_1$^{600} was 466 ± 62 ms with an average error of 27 ms. The average T$_2$^{500} for all residues was 151 ± 102 ms with an average error of 8 ms, and the average T$_2$^{600} was 142 ± 69 ms with an average error of 7 ms. The average NOE^{500} was 0.60 ± 0.52 (average error of 0.023) and the average NOE^{600} was 0.70 ± 0.31 (average error of 0.011).

The relaxation parameters for 0.15 mM cNTnC•Ca^{2+} have been previously published by Spyracopoulos *et al.* (*49*). They found the average
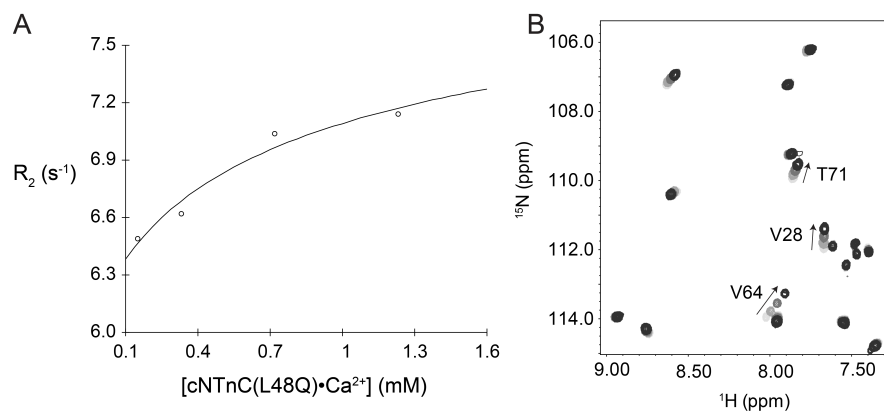
Figure 7-8. Dependence of the A. average ^{15}N-T_2 and B. ^{1}H,^{15}N-HSQC as a function of cNTnC(L48Q)•Ca^{2+} concentration. In the ^{1}H,^{15}N-HSQC spectrum, contours are colored from light grey to black as cNTnC(L48Q)•Ca^{2+} concentration increases.
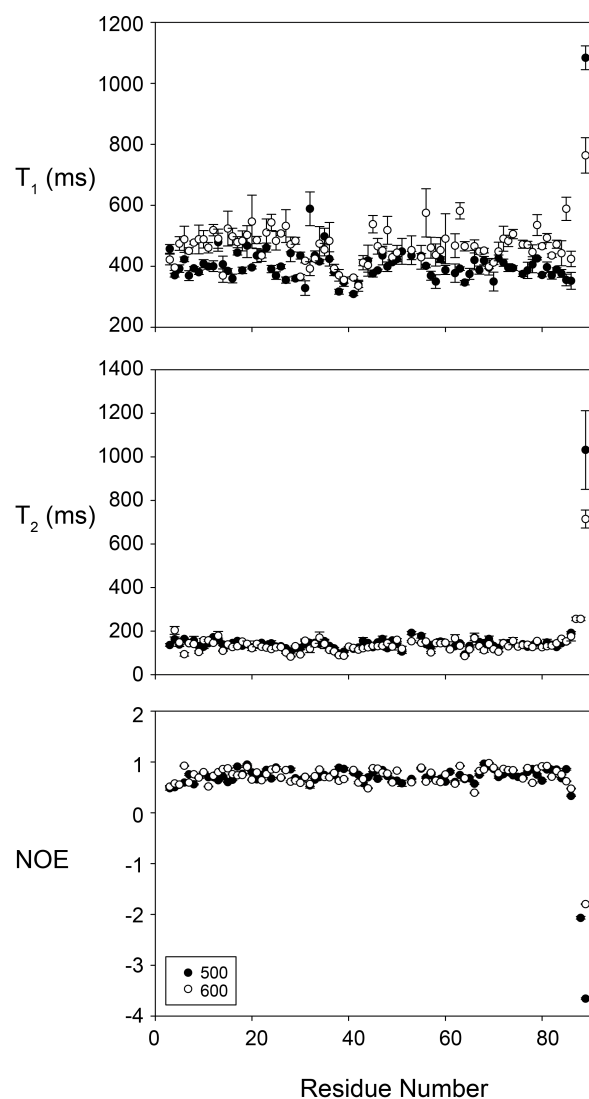
Figure 7-9. Plots of ^{15}N-T$_2$, ^{15}N-T$_1$, and {^{1}H}^{15}N NOE (500 MHz and 600 MHz relaxation data are superimposed) for 0.33 mM cNTnC(L48Q)•Ca^{2+}. T$_1$ and T$_2$ increase with an increase internal motion, and NOE decreases with an increase in internal motion. Residues 87-89, at the C-terminus of cNTnC(L48Q) have high T$_1$ and T$_2$ and low NOE, which indicate that the C-terminus of cNTnC(L48Q) is disordered.

T_1^{500} was 440 ± 106 ms with an average error of 12 ms, the average T_2^{500} was 166 ± 82 ms with an average error of 5 ms, and the average NOE^{500} was 0.57 ± 0.27 with an average error of 0.04. In order to directly compare cNTnC(L48Q)•Ca^{2+} with cNTnC•Ca^{2+} we prepared a 0.15 mM sample and recorded the relaxation data at 500 MHz. The average T_1^{500} was 408 ± 97 ms with an average error of 20 ms, the average T_2^{500} was 154 ± 80 ms with an average error of 9 ms, and the average NOE was 0.70 ± 0.44 ms with an average error of 0.11 ms. We have superimposed the data from cNTnC•Ca^{2+} with the L48Q mutant in Figure 7-10A.

While most of the relaxation data between cNTnC•Ca^{2+} and cNTnC(L48Q)•Ca^{2+} are not different, inspection of residues in site I suggests that the L48Q mutation specifically modulates the dynamics of this loop (residues 29-40). We used a suite of *Mathematica* notebooks to perform model-free analysis of the ^{15}N relaxation data to determine the order parameters for residues in site I (*27*). Models for each residue were chosen according to Akaike's information criteria (AIC) (*28*). The average S^2 for loop 1 is 0.85 ± 0.11 for cNTnC(L48Q)Ca^{2+}, whereas the S^2 for the loop is 0.77 ± 0.08 for cNTnC•Ca^{2+}. Therefore, an explanation of the differences in relaxation parameters is that the conformation of cNTnC(L48Q) is slightly different than the wild-type domain, making the residues in loop 1 more rigid.

MD simulations of cNTnC(L48Q) and cNTnC.

To further validate the conformational change in cNTnC by the L48Q mutation, we performed MD simulations on apo and Ca^{2+}-saturated cNTnC structures (PDB entries: 1SPY and 1AP4, respectively) for both wild-type and L48Q. In Figure 7-11, the starting structures are compared with the structures at 60 ns for cNTnC(L48Q) and cNTnC. For both the apo and Ca^{2+}-saturated simulations, the B-helix of cNTnC(L48Q) underwent a large movement away from the core of the domain. In cNTnC, no
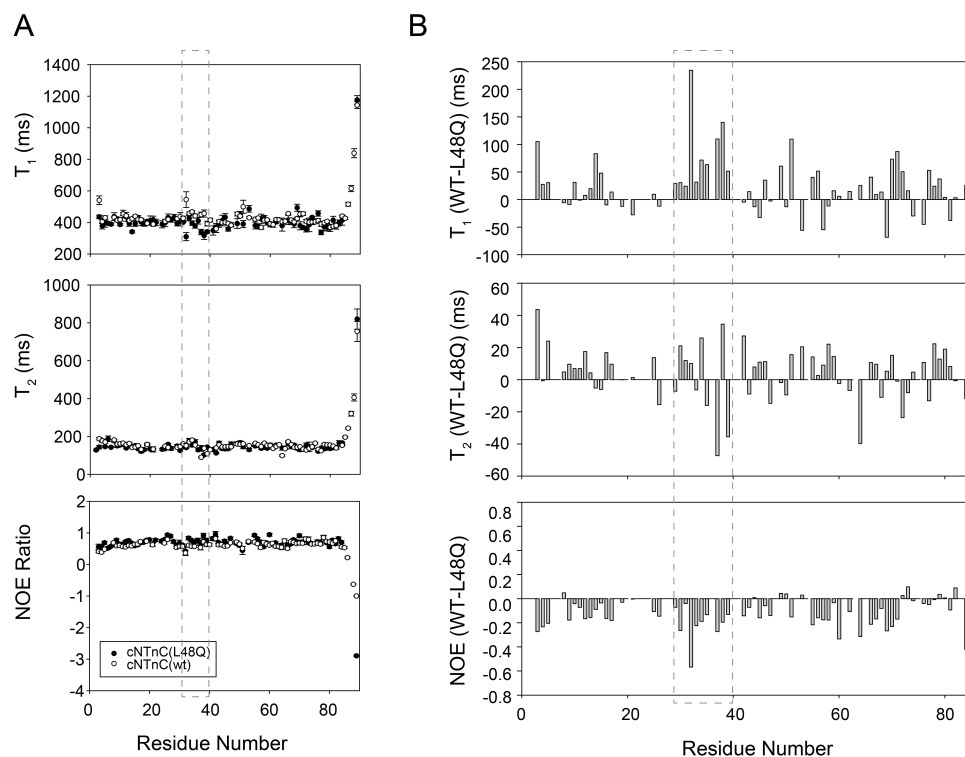
Figure 7-10. A. Plots of $^{15}N\text{-}T_2$, $^{15}N\text{-}T_1$, and $\{^1H\}^{15}N$ NOE of cNTnC•Ca^{2+} superimposed with cNTnC(L48Q)•Ca^{2+}. The concentrations of cNTnC•Ca^{2+} and cNTnC(L48Q)•Ca^{2+} were both 0.15 mM in order to limit the influence any aggregation may have on the relaxation data. B. Differences in T_1, T_2, and NOE data between cNTnC(L48Q)•Ca^{2+} and cNTnC•Ca^{2+} are plotted. Overall, the data are consistent; however, there is a significant deviation between the two proteins in residues of site I (residues 29-40; highlighted in dashed box), which may represent a change in conformation and/or dynamics of this site.
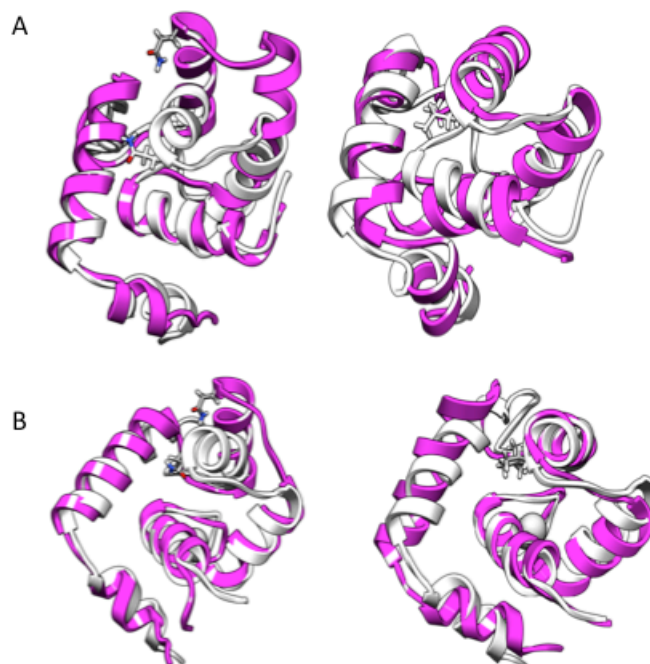
Figure 7-11. L48Q induced movement of the B helix in both apo and Ca^{2+} saturated states of cNTnC. A. Apo State: cNTnC(L48Q) (left) *versus* cNTnC (0 ns shown in white and 60 ns shown in purple). B.Ca^{2+} Saturated State: cNTnC(L48Q)•Ca^{2+} (left) *versus* cNTnC•Ca^{2+} (0 ns shown in white and 60 ns shown in purple). L48 and Q48 are shown in stick representation.

movement of the helix was observed. The differences in the motion of the B-helix between cNTnC(L48Q) and cNTnC is presumably due to the L48Q mutation at the end of the B-helix disrupts key hydrophobic contacts L48 makes with residues on the A-helix, such as F20, A23, and F27 (Figure 7-12). The interhelical angle between A and B helices was used to quantify the conformation of cNTnC and is summarized in Table 7-1. The hydrophobic patch was more exposed for L48Q than wild-type in apo and Ca^{2+}-saturated states. In the apo and Ca^{2+} saturated simulations, A/B interhelical angle in both wild-type and L48Q decreased, indicating an opening of both structures; however, the A/B helices in L48Q generally were more open than wild-type for both apo and Ca^{2+} saturated states.

The distance between the backbone α-carbons of Met 81 (on the helix D) and Asn 50 (on the loop that connects the B and C helices) was used to quantify the opening of cNTnC, as was previously done to monitor the opening of cNTnC when $cTnI_{147-163}$ bound or when or Ca^{2+} bound to sNTnC (*30*). Table 7-2 lists the averaged distances between M81 and N50 for 70 ns multiple simulations. M81-D50 distances were generally larger in the cNTnC(L48Q) compared to cNTnC, as calculated from the MD simulations of the apo and Ca^{2+}-saturated states. The increase in the distance between M81-D50 of cNTnC(L48Q) is consistent with the results from the interhelical angle and the distances between helices A/B, which suggest that the L48Q variant induced a more open conformation of cNTnC.

Discussion

The results presented in this manuscript give structural rationale for the Ca^{2+}-sensitizing effect of the mutation L48Q of cTnC. We first measured the effect of the mutation had on the Ca^{2+}-sensitivity of the troponin complex by fluorescence. The pCa of the troponin complex was leftward shifted from 6.99 to 7.31 indicating an increase in Ca^{2+}-sensitivity.
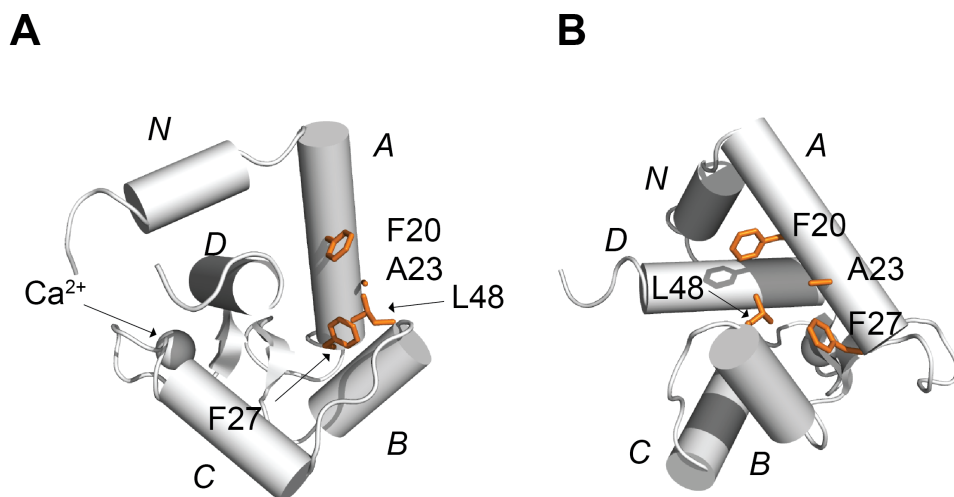
Figure 7-12. The stabilizing role of L48. A. Cartoon representation of cNTnC•Ca^{2+} (PDB: 1AP4) is shown with helices labeled and the side chains of L48, F20, A23, and F27 are colored in orange. B. -90° rotation about the y-axis of A.

Table 7-2. Distances between M81 and A50.

Protein	Original NMR PDB code	Original NMR (Å)	WT	L48Q
			70ns MD Simulations (n=3) (Å)	70ns MD Simulations (n=3) (Å)
cNTnC apo	1SPY	8	9.8 ± 1.3	11.7 ± 1.9
cNTnC+Ca^{2+}	1AP4	10	10.7 ± 1.3	13.5 ± 1.9

Fluorescence spectroscopy and ITC also indicated that cTnC(L48Q) had an increased affinity for cTnI, a change in affinity that was localized by NMR spectroscopy to the interaction between cNTnC and cTnI$_{147-163}$.

To explain the enhanced affinity of cTnI$_{147-163}$ for cNTnC(L48Q) we turned to NMR spectroscopy and MD. We compared the amide chemical shifts of D73, E66, L29, G34, G68, and T71 from cNTnC(L48Q)•Ca^{2+} with the shifts of the closed state, cNTnC•Ca^{2+} and two open states, cNTnC•Ca^{2+}•cTnI$_{147-163}$ and cNTnC•Ca^{2+}•bepridil. The chemical shifts suggest that cNTnC(L48Q)•Ca^{2+} is in a conformational somewhere between the closed and open states, closer to the closed state. Furthermore, cNTnC(L48Q) was found to dimerize more than cNTnC•Ca^{2+}, but less than sNTnC•2Ca^{2+}, which also supports the notion that L48Q stabilizes a slightly more open state of cNTnC.

The dynamics and MD data also suggest that a conformational change is induced by L48Q. The relaxation data, particularly the NOE and T$_1$ data were quite different than the data for cNTnC•Ca^{2+}. This may be the result of slightly different dynamics and/or orientation of the loop residues. The MD simulations strongly support the opening of cNTnC by the L48Q mutation. The B-helix swings away from the hydrophobic core of cNTnC after 60 ns of simulation. Interestingly, L48Q has been correlated to suppressed relaxation and activity at even low Ca^{2+}. The MD simulations suggest that even in the apo state of cNTnC, L48Q disrupts the packing of cNTnC and therefore may explain the observed binding of cTnI to cTnC(L48Q) in the apo state. Overall, the results presented herein suggest that the mechanism by which the L48Q mutation modulates the Ca^{2+} sensitivity is by disrupting the structure of cNTnC. By destabilizing the closed conformation of cNTnC, L48Q decreases the energetic barrier of opening, enhancing both Ca^{2+} and cTnI binding, culminating in an increase in muscle fiber contractility (Figure 7-13).
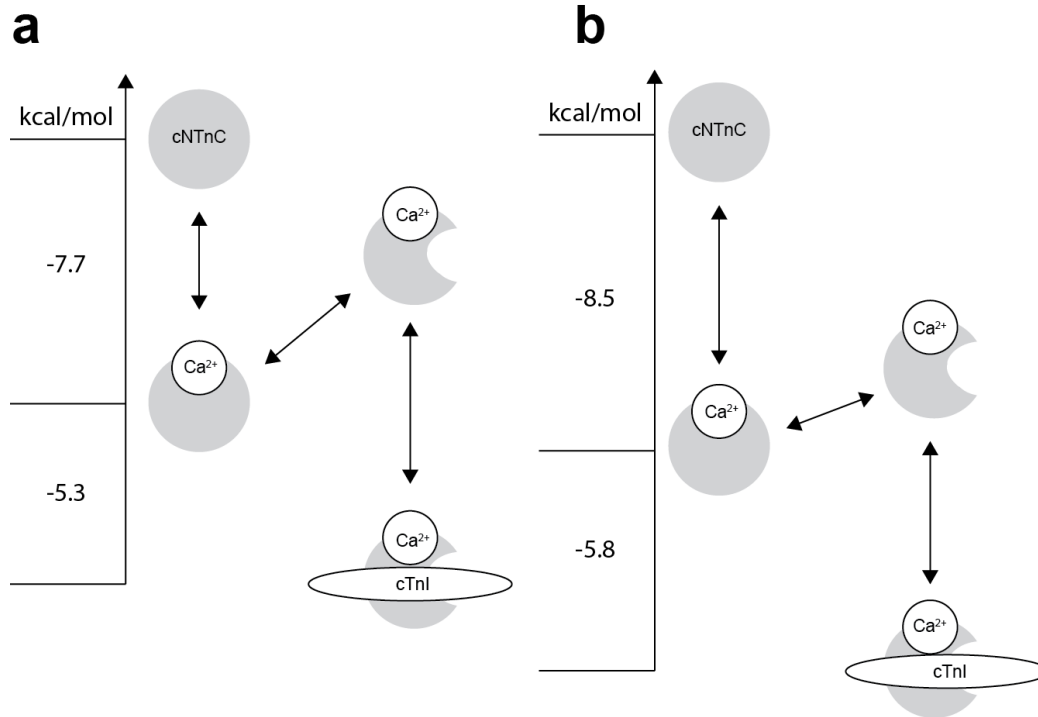
Figure 7-13. Energy level diagram highlighting the Ca^{2+}-sensitizing mechanism of the L48Q mutation of cTnC. **a.** In apo cNTnC, cNTnC is closed, once Ca^{2+}-binds to cNTnC, cNTnC oscillates between open and closed states, but the domain remains in predominantly the closed state. $cTnI_{147-163}$ binds to the open state of cNTnC to stabilize its open conformation (*45, 50, 51*). **b.** The L48Q mutation shifts the closed-to-open equilibrium towards the open state enhancing both the Ca^{2+} and $cTnI_{147-163}$ affinities. The free energy for **a.** is from McKay et al. (*45*), and for **b.** the NMR data in this work are used to calculate the free energy of binding. The relationship: $\Delta G°=-RTlnK_D$ was used to calculate the binding energies.

References

1. Sia, S. K., Li, M. X., Spyracopoulos, L., Gagne, S. M., Liu, W., Putkey, J. A., and Sykes, B. D. (1997) Structure of cardiac muscle troponin C unexpectedly reveals a closed regulatory domain, *J. Biol. Chem. 272*, 18216-18221.
2. Gagne, S. M., Tsuda, S., Li, M. X., Smillie, L. B., and Sykes, B. D. (1995) Structures of the Troponin-C Regulatory Domains in the Apo and Calcium-Saturated States, *Nat. Struct. Biol. 2*, 784-789.
3. Spyracopoulos, L., Li, M. X., Sia, S. K., Gagne, S. M., Chandra, M., Solaro, R. J., and Sykes, B. D. (1997) Calcium-induced structural transition in the regulatory domain of human cardiac troponin C, *Biochemistry 36*, 12138-12146.
4. Putkey, J. A., Sweeney, H. L., and Campbell, S. T. (1989) Site-Directed Mutation of the Trigger Calcium-Binding Sites in Cardiac Troponin-C, *J. Biol. Chem. 264*, 12370-12378.
5. Baryshnikova, O. K., Robertson, I. M., Mercier, P., and Sykes, B. D. (2008) The dilated cardiomyopathy G159D mutation in cardiac troponin C weakens the anchoring interaction with troponin I, *Biochemistry 47*, 10950-10960.
6. Ramakrishnan, S., and Hitchcock-DeGregori, S. E. (1996) Structural and functional significance of aspartic acid 89 of the troponin C central helix in Ca2+ signaling, *Biochemistry 35*, 15515-15521.
7. Biesiadecki, B. J., Kobayashi, T., Walker, J. S., John Solaro, R., and de Tombe, P. P. (2007) The troponin C G159D mutation blunts myofilament desensitization induced by troponin I Ser23/24 phosphorylation, *Circ Res 100*, 1486-1493.
8. Gordon, A. M., Homsher, E., and Regnier, M. (2000) Regulation of contraction in striated muscle, *Physiol. Rev. 80*, 853-924.
9. Rarick, H. M., Tu, X. H., Solaro, R. J., and Martin, A. F. (1997) The C terminus of cardiac troponin I is essential for full inhibitory activity and Ca2+ sensitivity of rat myofibrils, *J. Biol. Chem. 272*, 26887-26892.
10. Willott, R. H., Gomes, A. V., Chang, A. N., Parvatiyar, M. S., Pinto, J. R., and Potter, J. D. (2010) Mutations in Troponin that cause HCM, DCM AND RCM: what can we learn about thin filament function?, *J. Mol. Cell. Cardiol. 48*, 882-892.
11. Hoffmann, B., Schmidt-Traub, H., Perrot, A., Osterziel, K. J., and Gessner, R. (2001) First mutation in cardiac troponin C, L29Q, in a patient with hypertrophic cardiomyopathy, *Hum. Mutat. 17*, 524.
12. Tardiff, J. C. (2011) Thin filament mutations: developing an integrative approach to a complex disorder, *Circ Res 108*, 765-782.

13. Gomes, A. V., and Potter, J. D. (2004) Molecular and cellular aspects of troponin cardiomyopathies, *Ann. N. Y. Acad. Sci. 1015*, 214-224.

14. Tikunova, S. B., Liu, B., Swindle, N., Little, S. C., Gomes, A. V., Swartz, D. R., and Davis, J. P. (2010) Effect of calcium-sensitizing mutations on calcium binding and exchange with troponin C in increasingly complex biochemical systems, *Biochemistry 49*, 1975-1984.

15. Tikunova, S. B., and Davis, J. P. (2004) Designing calcium-sensitizing mutations in the regulatory domain of cardiac troponin C, *J Biol Chem 279*, 35341-35352.

16. Parvatiyar, M. S., Pinto, J. R., Liang, J., and Potter, J. D. (2010) Predicting cardiomyopathic phenotypes by altering Ca2+ affinity of cardiac troponin C, *J. Biol. Chem. 285*, 27785-27797.

17. Kreutziger, K. L., Piroddi, N., McMichael, J. T., Tesi, C., Poggesi, C., and Regnier, M. (2011) Calcium binding kinetics of troponin C strongly modulate cooperative activation and tension kinetics in cardiac muscle, *J. Mol. Cell. Cardiol. 50*, 165-174.

18. Dong, W. J., Rosenfeld, S. S., Wang, C. K., Gordon, A. M., and Cheung, H. C. (1996) Kinetic studies of calcium binding to the regulatory site of troponin C from cardiac muscle, *J. Biol. Chem. 271*, 688-694.

19. Pearlstone, J. R., Chandra, M., Sorenson, M. M., and Smillie, L. B. (2000) Biological function and site IICa2+-induced opening of the regulatory domain of skeletal troponin C are impaired by invariant site I or II Glu mutations, *J. Biol. Chem. 275*, 35106-35115.

20. Li, M. X., Corson, D. C., and Sykes, B. D. (2002) Structure determination by NMR. Isotope labeling, *Methods Mol. Biol. 173*, 255-265.

21. Martyn, D. A., Regnier, M., Xu, D., and Gordon, A. M. (2001) Ca2+- and cross-bridge-dependent changes in N- and C-terminal structure of troponin C in rat cardiac muscle, *Biophys. J. 80*, 360-370.

22. Dong, W. J., Robinson, J. M., Stagg, S., Xing, J., and Cheung, H. C. (2003) Ca2+-induced conformational transition in the inhibitory and regulatory regions of cardiac troponin I, *J. Biol. Chem. 278*, 8686-8692.

23. Patton, C., Thompson, S., and Epel, D. (2004) Some precautions in using chelators to buffer metals in biological solutions, *Cell Calcium 35*, 427-431.

24. George, S. E., Su, Z., Fan, D., Wang, S., and Johnson, J. D. (1996) The Fourth EF-Hand of Calmodulin and Its Helix−Loop−Helix Components: Impact on Calcium Binding and Enzyme Activation†, *Biochemistry 35*, 8307-8313.

25. Delaglio, F., Grzesiek, S., Vuister, G. W., Zhu, G., Pfeifer, J., and Bax, A. (1995) Nmrpipe - a Multidimensional Spectral Processing System Based on Unix Pipes, *J. Biomol. NMR 6*, 277-293.

26. Johnson, B. A., and Blevins, R. A. (1994) Nmr View - a Computer-Program for the Visualization and Analysis of Nmr Data, *J. Biomol. NMR 4*, 603-614.

27. Spyracopoulos, L. (2006) A suite of Mathematica notebooks for the analysis of protein main chain N-15 NMR relaxation data, *J. Biomol. NMR 36*, 215-224.

28. d'Auvergne, E. J., and Gooley, P. R. (2003) The use of model selection in the model-free analysis of protein dynamics, *J. Biomol. NMR 25*, 25-39.

29. Palmer, A. G., Rance, M., and Wright, P. E. (1991) Intramolecular Motions of a Zinc Finger DNA-Binding Domain from Xfin Characterized by Proton-Detected Natural Abundance C-12 Heteronuclear Nmr-Spectroscopy, *J. Am. Chem. Soc. 113*, 4371-4380.

30. Li, M. X., Spyracopoulos, L., and Sykes, B. D. (1999) Binding of cardiac troponin-I147-163 induces a structural opening in human cardiac tropoin-C, *Biochemistry 38*, 8289-8298.

31. Pettersen, E. F., Goddard, T. D., Huang, C. C., Couch, G. S., Greenblatt, D. M., Meng, E. C., and Ferrin, T. E. (2004) UCSF chimera - A visualization system for exploratory research and analysis, *J. Comput. Chem. 25*, 1605-1612.

32. Beck, D. A. C., Alonso, D. O. V., and Daggett, V. (2000-2010) in lucem molecular mechanics (ilmm).

33. Levitt, M., Hirshberg, M., Sharon, R. & Daggett, V. (1995) Potential-energy function and parameters for simulations of the molecular-dynamics of proteins and nucleic-acids in solution, *Comput. Phys. Commun. 91*, 215-231.

34. Levitt, M., Hirshberg, M., Sharon, R., Laidig, K. E., and Daggett, V. (1997) Calibration and testing of a water model for simulation of the molecular dynamics of proteins and nucleic acids in solution, *J. Phys. Chem. B 101*, 5051-5061.

35. Kell, G. S. (1967) Precise Representation of Volume Properties of Water at 1 Atmosphere, *J. Chem. Eng. Data 12*, 66-&.

36. Dong, W. J., and Cheung, H. C. (1996) Calcium-induced conformational change in cardiac troponin C studied by fluorescence probes attached to Cys-84, *Biochim Biophys Acta 1295*, 139-146.

37. Hoffman, R. M. B., Li, M. X., and Sykes, B. D. (2005) The bindin of W7, an inhibitor of striated muscle contraction, to cardiac troponin C, *Biochemistry 44*, 15750-15759.

38. Li, M. X., Gagne, S. M., Spyracopoulos, L., Kloks, C. P., Audette, G., Chandra, M., Solaro, R. J., Smillie, L. B., and Sykes, B. D. (1997) NMR studies of Ca2+ binding to the regulatory domains of

cardiac and E41A skeletal muscle troponin C reveal the importance of site I to energetics of the induced structural changes, *Biochemistry 36*, 12519-12525.

39. Tikunova, S. B., and Davis, J. P. (2004) Designing calcium-sensitizing mutations in the regulatory domain of cardiac troponin C, *J. Biol. Chem. 279*, 35341-35352.

40. Tripet, B., Van Eyk, J. E., and Hodges, R. S. (1997) Mapping of a second actin-tropomyosin and a second troponin C binding site within the C terminus of troponin I, and their importance in the Ca2+-dependent regulation of muscle contraction, *J. Mol. Biol. 271*, 728-750.

41. Li, M. X., Spyracopoulos, L., and Sykes, B. D. (1999) Binding of cardiac troponin-I147-163 induces a structural opening in human cardiac troponin-C, *Biochemistry 38*, 8289-8298.

42. Li, M. X., Saude, E. J., Wang, X., Pearlstone, J. R., Smillie, L. B., and Sykes, B. D. (2002) Kinetic studies of calcium and cardiac troponin I peptide binding to human cardiac troponin C using NMR spectroscopy, *Eur. Biophys. J. Biophy. 31*, 245-256.

43. Paakkonen, K., Sorsa, T., Drakenberg, T., Pollesello, P., Tilgmann, C., Permi, P., Heikkinen, S., Kilpelainen, I., and Annila, A. (2000) Conformations of the regulatory domain of cardiac troponin C examined by residual dipolar couplings, *Eur. J. Biochem. 267*, 6665-6672.

44. Eichmueller, C., and Skrynnikov, N. R. (2007) Observation of mu s time-scale protein dynamics in the presence of Ln(3+)stop ions: application to the N-terminal domain of cardiac troponin C, *J. Biomol. NMR 37*, 79-95.

45. McKay, R. T., Saltibus, L. F., Li, M. X., and Sykes, B. D. (2000) Energetics of the induced structural change in a Ca2+ regulatory protein: Ca2+ and troponin I peptide binding to the E41A mutant of the N-domain of skeletal troponin C, *Biochemistry 39*, 12731-12738.

46. Li, Y., Love, M. L., Putkey, J. A., and Cohen, C. (2000) Bepridil opens the regulatory N-terminal lobe of cardiac troponin C, *Proc. Natl. Acad. Sci. U. S. A. 97*, 5140-5145.

47. Spyracopoulos, L., S.M. Gagne, and B.D. Sykes. (2001) in Proceedings of the International School of Structural Biology and Magnetic Resonance, pp 37-44 (Jardetzky, O., and Lefevre, J. F., Eds.) Plenum Press, New York. 37-44.

48. Baryshnikova, O. K., and Sykes, B. D. (2006) Backbone dynamics of SDF-1 alpha determined by NMR: Interpretation in the presence of monomer-dimer equilibrium, *Protein Sci. 15*, 2568-2578.

49. Spyracopoulos, L., Gagne, S. M., Li, M. X., and Sykes, B. D. (1998) Dynamics and thermodynamics of the regulatory domain of human cardiac troponin C in the apo- and calcium-saturated states, *Biochemistry 37*, 18032-18044.

50. Paakkonen, K., Sorsa, T., Drakenberg, T., Pollesello, P., Tilgmann, C., Permi, P., Heikkinen, S., Kilpelainen, I., and Annila, A. (2000) Conformations of the regulatory domain of cardiac troponin C examined by residual dipolar couplings, *Eur. J. Biochem. 267*, 6665-6672.

51. Sorsa, T., Pollesello, P., and Solaro, R. J. (2004) The contractile apparatus as a target for drugs against heart failure: Interaction of levosimendan, a calcium sensitiser, with cardiac troponin c, *Mol. Cell. Biochem. 266*, 87-107.

Chapter 8

Understanding the histidine button: structural evidence for the isoform-dependent pH sensitivity of troponin I

Summary

Myocardial ischemia is characterized by reduced blood flow to cardiac muscle cells. This can lead to acidosis, a condition where intracellular pH is decreased. Acidosis compromises the cardiac muscle by decreasing its calcium sensitivity and contractile efficiency. By contrast, skeletal and neonatal muscles are much less sensitive to changes in pH. The pH sensitivity of cardiac muscle can be reduced by replacing cardiac troponin I with its skeletal or neonatal counterparts. The isoform specific response of troponin I is dictated by a single histidine in both neonatal and skeletal isoforms of troponin I – dubbed the histidine button – which is replaced by an alanine in cardiac troponin I. In this study we probed the role of this histidine (H130) in the skeletal isoform of troponin I by measuring its acid dissociation constant in the absence and presence of troponin C by NMR spectroscopy. We also determined acid dissociation constants of glutamate residues of troponin C lining the troponin I binding interface under a variety of conditions, including the skeletal troponin I bound form. The results indicate H130 makes an electrostatic interaction with E19 of troponin C. Furthermore, we show that the skeletal troponin I switch peptide (sTnI$_{115-131}$) binds to troponin C in a pH-dependent manner: at pH 7.5 its dissociation constant is 360 µM and at pH 6.1 its affinity is dramatically increased, with a dissociation constant of 100 µM. The pH-dependent change in affinity of troponin I is directly correlated to the protonation state of H130. Our data provide insight into the molecular mechanisms of pH sensitivity for different troponin I isoforms.

Introduction

Heart failure is characterized by a decline in cardiac contractile force. In myocardial ischemia, cardiomyocytes do not receive adequate oxygen supply, which culminates in acidosis, a significant drop in intracellular pH. Acidosis incurs a dramatic reduction in the Ca^{2+}-sensitivity of muscle contraction (*1, 2*). Cardiomyocyte contraction is regulated through Ca^{2+} entering the cytosol following muscle cell excitation. Ca^{2+} influx triggers a series of thin and thick filament protein-protein interactions that leads to muscle contraction. The thin filament is composed of three proteins – actin, tropomyosin, and the Ca^{2+}-binding molecule, troponin. Troponin is a heterotrimeric molecule, its three subunits are: cardiac troponin C (cTnC), responsible for binding Ca^{2+}; cardiac troponin I (cTnI), the inhibitory subunit; and cardiac troponin T (cTnT), the subunit that attaches troponin to the thin filament *via* interactions with troponin I and tropomyosin. During muscle relaxation (diastole), the 'inhibitory' and C-terminal regions of cTnI interact with actin preventing contraction. The binding of Ca^{2+} to N-terminal domain of cTnC (cNTnC) leads to the binding of the 'switch' region of cTnI ($cTnI_{147-163}$) to cNTnC. This binding prompts the dissociation of the inhibitory and C-terminal regions of cTnI from actin, resulting in contraction (for reviews see (*3, 4*)).

The negative inotropic effect (decrease in contractility) of acidosis (pH ≤ 6.5) is due, in part, to a decrease in the Ca^{2+}(*5-7*) and cTnI (*8*) affinity for cTnC. Cardiomyocytes of neonatal rats are less sensitive to low pH than adult heart cells (*9*). Westfall *et al*. have noticed that the pH sensitivity of cardiac muscle cells is dramatically reduced by the substitution of cTnI with the neonatal myofilament troponin I, slow skeletal TnI (ssTnI) (*10*). Furthermore, the fast skeletal isoform of TnI (sTnI) has been shown to make the myofilament less sensitive to acidic conditions (low pH) (*7, 11, 12*). The regions of ssTnI and sTnI that are responsible for the isoform specific response to pH were initially localized to the C-

terminal region (which includes the switch region of TnI) (*11, 13*). It was later determined that the difference in pH sensitivity between TnI isoforms largely arises from a single histidine in sTnI and ssTnI, which is replaced by an alanine in cTnI (*12, 14*) (see scheme 1). Smillie and coworkers found that when this alanine of cTnI (A162) was replaced by a histidine, a dramatic reduction in pH sensitivity was observed(*12*). Furthermore, when H130 of sTnI was replaced with the parallel alanine (the numbering is different between the isoforms, because cTnI has an extra 32 residues at its N-terminus not present in sTnI and ssTnI), the pH sensitivity of muscle containing sTnI was similar to cTnI. Recently, this alanine to histidine substitution (termed the histidine button) has been shown to partially blunt the negative effects of acidosis in intact myocytes, isolated hearts, and whole mice (*14*).

The conveyed pH resistance of sTnI has been suggested to stem from the buffering capacity of histidine over a pH range that is near to acidosis pH. When histidine is protonated (at low pH) its positive charge will interact with negatively charged side chains of cNTnC, and thus increases its affinity for cNTnC. The ability of this histidine to buffer the cardiomyocyte's function over a range of pH values has led it to be referred to as a "molecular pH rheostat" (*15*). In the skeletal X-ray crystal structure, H130 of sTnI forms a salt bridge with E20 of sNTnC (numbering is taken from the deposited X-ray crystal structure)(*16*). Solution NMR relaxation (*17*) and chemical shift (*18*) data of sTnI in complex with sTnC confirm that this region of sTnI is rigid, consistent with the formation of this salt bridge in solution. The X-ray and NMR structures of cardiac troponin indicate that the corresponding glutamate in cTnC, E19, does not make a homologous interaction with cTnI (*19, 20*).

The focus of the present study was to define the molecular basis for the increase in pH sensitivity caused by this single histidine residue of sTnI. We use NMR spectroscopy to investigate the role of electrostatic interactions between sTnI and cNTnC. The pK_a of glutamates were

determined for four different states of cNTnC: Ca^{2+}-free (apo), Ca^{2+}-bound, Ca^{2+} and cTnI$_{147-163}$-bound, and the complex of cNTnC bound to Ca^{2+} and the switch region of sTnI (sTnI$_{115-131}$). The pK$_a$ of H130 of sTnI$_{115-131}$was also monitored in both free and bound states. The pK$_a$ of E19 was constant for apo, Ca^{2+}-bound, cTnI$_{147-163}$-bound states; however, when in complex with sTnI$_{115-131}$, two ionization events were observed (one being the protonation of the carboxylate of E19 and the other being the ionization of the imidazole of H130). The pK$_a$ of H130 increased when sTnI$_{115-131}$ was bound to cNTnC, which indicates that it is involved in making an electrostatic interaction with cNTnC. Moreover, the pH dependent differences in the affinity of sTnI$_{115-131}$ for cNTnC reveals that the ionization state of H130 fine tunes the affinity of sTnI$_{115-131}$ for cNTnC. These results provide evidence for the mechanism by which a single histidine in sTnI can protect the heart during acidosis.

Experimental Procedures

Sample Preparation: Recombinant human cNTnC (residues 1-89, C84S, C35S, a-cys form). The engineering of the expression vector and the expression of ^{15}N- and ^{13}C, ^{15}N-labeled proteins in *E. coli* were as described previously (*21*). GL Biochem Ltd. (Shanghai, China) synthesized cTnI$_{147-163}$(acetyl-RISADAMMQALLGARAK-amide) and Alberta Peptide Institute (API) synthesized sTnI$_{115-131}$ (acetyl-RMSADAMLKALLGSKHK-amide). HPLC and ESI-Mass Spectrometry were employed to verify peptide quality.

cTnI$_{147-163}$ 147- R I S A D A M M Q A L L G A R A K -163
　　　　　　　 | * | | | | | | * * | | | |　* | |
sTnI$_{115-131}$ 115- R M S A D A M L K A L L G S K H K -131
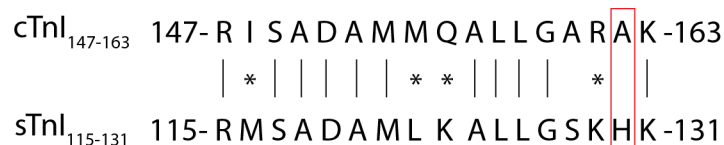
All NMR samples were prepared in 5 mm NMR tubes and had a volume of ~500 µL. Protein samples were solubilized in an NMR buffer containing 90% H_2O/10% D_2O, 100 mM KCl, 10 mM imidazole, 5-10 mM $CaCl_2$ (Fluka), and 0.5 mM 2,2-dimethyl-2-silapentane-5-sulfonate-d_6 sodium salt (DSS) (Chenomx).

NMR spectroscopy: All NMR experiments were run on either a Varian Inova 500 MHz or Unity 600 MHz NMR spectrometers at 30 °C. Prior to each multidimensional experiment, 1D ^1H and 2D ^1H,^{15}N-HSQC NMR spectra were acquired. The 3D CBCA(CO)NNH, 3D HNCACB, and 3D HCCONH NMR experiments were acquired for backbone and side chain proton assignment (Figure 8-1) of ^{13}C,^{15}N-cNTnC (apo) and ^{13}C,^{15}N-cNTnC-sTnI$_{115-131}$. The 2D ^1H, ^{13}C-HCBCGCO NMR experiment (*22*) was acquired to follow side chain carboxylate carbon signals of ^{13}C,^{15}N-cNTnC(apo), ^{13}C,^{15}N-cNTnC-Ca^{2+}, ^{13}C,^{15}N-cNTnC-Ca^{2+}-cTnI$_{147-163}$, and ^{13}C,^{15}N-cNTnC-Ca^{2+}-sTnI$_{115-131}$ during the pH titrations. Spectral processing was accomplished with the programs VNMRJ (Version 2.21B, Varian Inc.) and NMRPipe (*23*) and referenced according to the IUPAC conventions. Processed NMR spectra were analyzed using NMRView (*24*). The backbone resonances of ^{13}C,^{15}N-cNTnC(apo) and ^{13}C,^{15}N-cNTnC-sTnI$_{115-131}$ were assigned with the program Smartnotebook(*25*).

pH titrations: The pH was gradually adjusted by adding aliquots of 1M NaOH or 1M HCl covering a range from 3.5 to 7.5. The pH at each titration point was verified by the chemical shift of tris, imidazole, piperazine, or formate in the NMR buffer (*26*). At each titration point, 1D ^1H, 2D ^{15}N-HSQC and 2D ^1H, ^{13}C-HCBCGCO NMR spectra were acquired. The pH titration data were analyzed using xcrvfit (www.bionmr.ualberta.ca/bds/software/xcrvfit). Datasets showing a single pK$_a$ were fit to the following equation:

$$\delta_{obs} = \delta_{HA} + \frac{\Delta\delta_1}{1 + 10^{(pKa1-pH)}}$$

Where δ_{obs} is the observed chemical shift at a given pH, δ_{HA} is the chemical shift for the protonated form, and $\Delta\delta_1$ is the total shift from unprotonated to protonated forms. For two pK_a datasets the equation used was (27):

$$\delta_{obs} = \delta_{HA} + \frac{\Delta\delta_1}{1 + 10^{(pKa1-pH)}} + \frac{\Delta\delta_2}{1 + 10^{(pKa2-pH)}}$$

sTnI$_{115-131}$ titrations at pH 6.1 and pH 7.5: The titration with sTnI$_{115-131}$ was performed at two different pH values. For both titrations, fresh stocks of sTnI$_{115-131}$ were prepared in NMR buffer. The sTnI$_{115-131}$ stock solution concentrations were determined by preparing an NMR sample containing 5 µL of sTnI$_{115-131}$ stock in 500 µL of NMR buffer in 99.9% D$_2$O and 25 µL of 4.963 mM DSS in 98% D$_2$O. 1D ^{1}H NMR spectra were acquired with an acquisition time of 8 seconds, and a relaxation delay of 4 seconds; thus providing enough time for DSS and sTnI$_{115-131}$ to return to equilibrium in between transients. In order to determine the concentration of cNTnC, the intensity of the ^{1}H,^{15}N-HSQC spectrum was compared to that of another sample of cNTnC for which amino acid analysis was used to determine concentration (data from previously published(28)). Any subtle variations in pH during the titrations were corrected for by adding aliquots of 1M HCl or 1M NaOH. At each aliquot, ^{1}H,^{15}N-HSQC spectra were acquired and the amide chemical shift changes ($\Delta\delta$) were calculated by the following equation:

$$\Delta\delta = \sqrt{(\Delta\delta_H)^2 + \frac{1}{25}(\Delta\delta_N)^2}$$

$\Delta\delta_H$ and $\Delta\delta_N$ are the change in proton and nitrogen chemical shifts, respectively, for each titration point. The dissociation constants of sTnI$_{115-131}$ binding to cNTnC were fit to a 1:1 stoichiometry to the following scheme:

$$P + L \longleftrightarrow PL$$
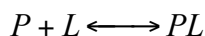
P is free protein and L is free ligand, and PL is the protein-ligand complex. Concentrations of sTnI$_{115-131}$ and cNTnC were corrected for dilution during the titration. The dissociation constant for sTnI$_{115-131}$ binding to cNTnC was determined by fitting all amide chemical shift perturbations for all non-overlapping residues. The dissociation constants were determined by using the global fitting protocol in xcrvfit, which has been described elsewhere(28). Instead of fitting NMR chemical shift data to each individual residue and then averaging the individual dissociation constants as is typically done, the shift data were fit to obtain a global dissociation constant that best fitted the ensemble of titration curves (i.e. had the lowest sum of squared error (SSE)).

Results

cNTnC glutamate pK$_a$ values as a function of structure

The dissociation constants for ionizable residues can provide insight into the molecular interactions within the protein complex. The shift in pK$_a$ can indicate an electrostatic interaction or hydrogen bonds (29). To investigate the electrostatic forces between cNTnC and cTnI or sTnI; we measured the pK$_a$ values of the glutamates of cNTnC for a variety of troponin complexes. 2D ^{1}H,^{15}N-HSQC and 2D ^{1}H,^{13}C-HCBCGCONMR spectra were acquired over a range of pH values for four different

complexes of cNTnC: cNTnC(apo), cNTnC-Ca^{2+} [1], cNTnC-cTnI$_{147-163}$, cNTnC-sTnI$_{115-131}$. The ^{1}H,^{15}N-HSQC NMR experiment correlates backbone amide ^{1}H with ^{15}N nuclei so that each signal in the ^{1}H,^{15}N-HSQC spectrum belongs to a single residue in the ^{15}N-labeled protein. The 2D ^{1}H,^{13}C-HCBCGCO NMR experiment (22), correlates the aliphatic protons of a residue with its terminal ^{13}C-carboxyl nucleus (or carbonyl). The glutamates of cNTnC(apo) and cNTnC-sTnI$_{115-131}$were assigned in this work (the assignments of cNTnC and cNTnC-cTnI$_{147-163}$ have been done previously) (20, 30, 31). The assignments of cNTnC(apo) and cNTnC-sTnI$_{115-131}$ are shown in Figure 8-1; some glutamates could not be assigned due to signal overlap. Surprisingly, the pattern of chemical shifts for all complexes of cNTnC were relatively constant (Figures 8-1 and 8-2), with the only exception of the E76 ^{13}C-carboxyl, which was shifted from 182.7 ppm in cNTnC(apo) to 188.8 ppm in the other states of cNTnC (Figure 8-1). This large downfield shift would be expected for a bidentate ligand, such as E76, complexed to Ca^{2+} (32, 33).

At low pH, the cNTnC solutions were not stable. In the case of the Ca^{2+}-bound complexes, precipitation was observed below pH 4.25 and the ^{1}H,^{15}N-HSQC spectra resembled the apo form. Since it was not possible to measure the glutamate chemical shifts at pH values below 4.25, in most instances the pK$_a$ values reported probably represent an upper limit. Many of the pK$_a$ values obtained from the ^{1}H,^{15}N-HSQC spectra were difficult to interpret since the change in amide chemical shifts can stem from several phenomena, such as intraresidue ionization, pH-dependent conformational changes, or the ionization of nearby residues (27). For this reason, we also used the 2D ^{1}H,^{13}C-HCBCGCO NMR experiment to track the pH-dependent chemical shift perturbations of the carboxyl carbons and the aliphatic γ protons of the glutamate residues of cNTnC (Figure 8-2). Since

---

[1] Unless otherwise stated, cNTnC will be assumed to be Ca^{2+}-saturated, and therefore, the Ca^{2+} will be omitted when discussing the different states of cNTnC.
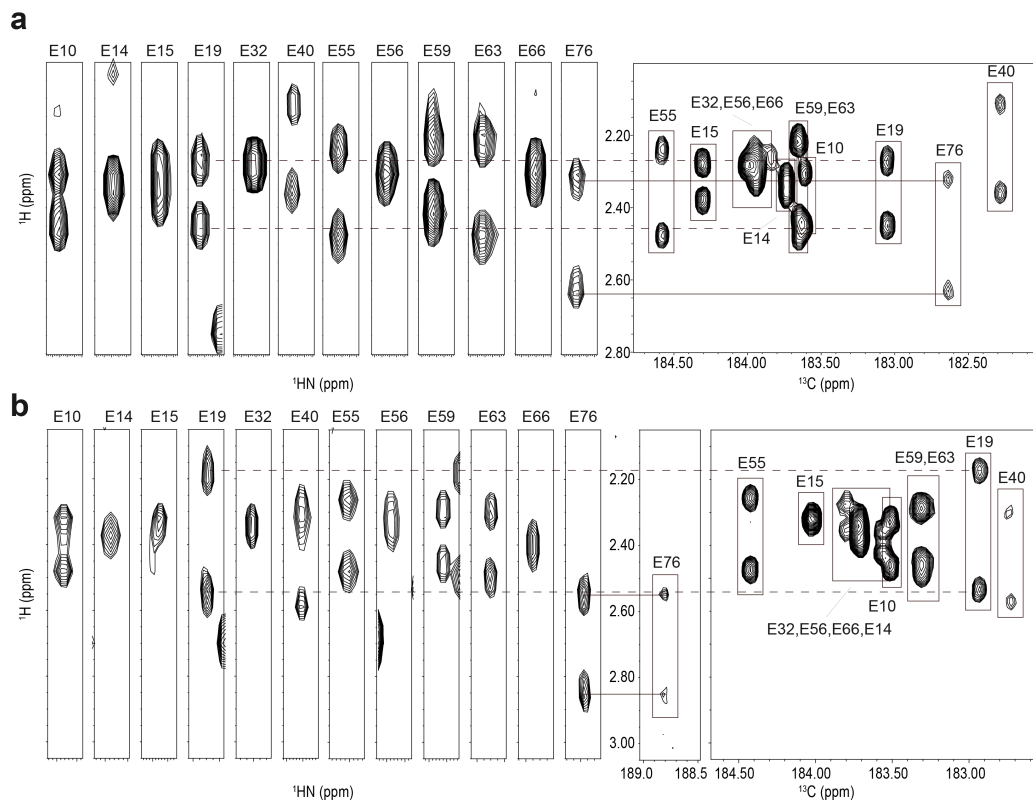
Figure 8-1. The assignment of glutamate carboxyl carbons of **a.** cNTnC(apo) and **b.** cNTnC-sTnI$_{115-131}$. The glutamate region of the 2D ^{1}H,^{13}C-HCBCGCO spectrum of cNTnCis shown on the right.Slices from the 3D ^{1}H,^{13}C, ^{1}HN-HCCONH NMR experiment are shown on the left. The carboxyl carbon chemical shifts were assigned by matching the γ proton chemical shifts.
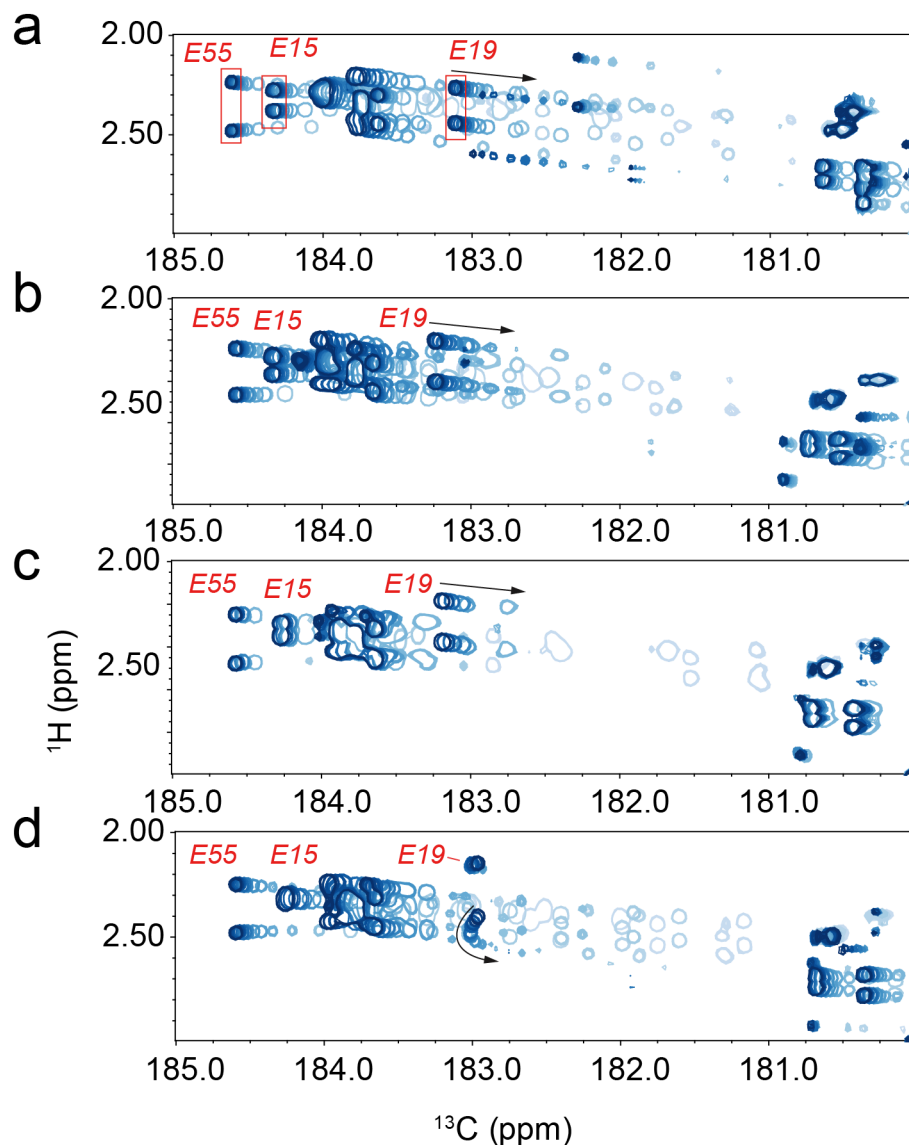
Figure 8-2. Superimposed 2D ^{1}H,^{13}C-HCBCGCO NMR spectra acquired throughout the pH titrations of **a.** cNTnC(apo), **b.** cNTnC, **c.** cNTnC-cTnI$_{147-163}$, and **d.** cNTnC-sTnI$_{115-131}$. As the pH decreases the spectra color changes from dark blue to light blue contours. See Figure 8-3 for pK$_a$ values. The resonances of three glutamates are labeled in red.

the 2D ^{1}H,^{13}C-HCBCGCO NMR experiment directly monitors the chemical shift of each carboxyl group, the pK_a values obtained from this experiment will likely arise from intraresidue ionization.

The results for the pK_a values calculated using the ^{1}H,^{15}N-HSQC and ^{1}H,^{13}C-HCBCGCO NMR data for all cNTnC glutamates are listed in Table 8-1 and Table 8-2, respectively. Residues with missing pK_as had overlapping signals or did not titrate over the pH range tested. Titration data for E55 (a residue far from the binding site of TnI), E19 (a residue possibly interacting with H130 based on the crystal structure of the skeletal complex), and E15 (a residue in close proximity to H130 in the skeletal crystal structure, and may interact with H130) are shown in Figure 8-3 for the cTnI$_{147-163}$ and sTnI$_{115-131}$ bound complexes. The pK_a values of E55 and E15 are not significantly perturbed across the four different states of cNTnC (Tables 8-1 and 8-2). The titration curves of E19 are monophasic in the apo, Ca^{2+}-bound, and cTnI$_{147-163}$-bound complexes; however, it is clearly biphasic when sTnI$_{115-131}$ is bound. The pK_a of E19 is 5.09 ± 0.04 in the apo state, 5.07 ± 0.03 in the Ca^{2+} bound state, and 5.10 ± 0.03 when cTnI$_{147-163}$ is bound. The two pK_a values measured for E19 when sTnI$_{115-131}$ is bound are 4.84 ± 0.05 and 6.73 ± 0.11. Since the lower pK_a was fitted to the large ^{13}C perturbation we assumed it represented the pK_a of the intraresidue carboxyl group. The second higher pK_a was determined by fitting a much smaller chemical shift perturbation, and probably represents the titration of a nearby ionizable group. Since the major difference between the different complexes is the presence of a histidine in sTnI$_{115-131}$, it is possible that the pK_a of 6.73 ± 0.11 is from H130 of sTnI$_{115-131}$. The pK_a of E19 decreases from 5.10 ± 0.03 when cTnI$_{147-163}$ is bound to 4.84 ± 0.05 when sTnI$_{115-131}$ is bound (a difference of 0.26 ± 0.08). The reduction in the pK_a of E19 suggests that it is involved in the formation of an electrostatic interaction, and that the residue it forms an interaction with has a pK_a of 6.73 ± 0.11. In order to investigate if the

Table 8-1. Three-parameter or four-parameter fits of titration data for glutamate residues using 2D ^{1}H,^{15}N-HSQC NMR spectra[a].

Residue	Apo		Ca^{2+}		cTnI$_{147\text{-}163}$		sTnI$_{115\text{-}131}$	
	HN	N	HN	N	HN	N	HN	N
E10	4.57 (0.18)	4.93 (0.09)	-	4.89 (0.09)	-	4.92 (0.1)	4.15 (0.09) 8.65(6.14)	3.92 (0.17)
E14	-	4.67 (0.32)	-	-	-	-	-	-
E15	5.09 (0.04)	5.22 (0.03)	5.03 (0.03)	-	5.00 (0.05)	-	-	-
E19	5.08 (0.05)	5.14 (0.06)	4.82 (0.03)	5.22 (0.02)	5.00 (0.04)	5.00 (0.03)	5.03 (0.02) 6.77 (0.04)	4.72 (0.05) 6.87 (0.11)
E32	4.28 (0.11)	4.68 (0.08) 6.29 (0.11)	4.32 (0.06)	4.22 (0.04)	3.64 (0.56)	3.16 (1.16)	3.69 (0.19)	-
E40	4.13 (0.18)	-	-	3.29 (0.45) 5.10 (0.06)	-	-	5.74 (0.1)	4.65 (0.11)
E55	4.67 (0.06)	4.13 (0.19)	4.64 (0.04)	4.64 (0.02)	4.73 (0.06)	4.43 (0.12)	4.86 (0.036)	4.28 (0.06)
E56	4.85 (0.08)	-	-	4.51 (0.02)	-	4.3 (0.03)	4.77 (0.06)	4.25 (0.07)
E59	4.89 (0.03)	5.63 (0.11)	4.63 (0.05)	-	-	-	-	-
E63	5.31 (0.06)	4.06 (0.156) 6.53 (0.08)	4.05 (0.19) 8.04 (0.25)	2.98 (1.0) 5.29 (0.08)	-	-	4.85 (0.07) 6.49 (0.09)	-
E66	4.49 (0.33)	4.86 (0.06)	-	-	-	-	5.93 (0.08)	4.37 (0.045)
E76	4.57 (0.08)	4.98 (0.09) 6.77 (0.11)	4.38 (0.03)	4.57 (0.06)	4.92 (0.07)	4.63 (0.09)	4.97 (0.05)	4.93 (0.03) 7.13(0.18)

[a]Data were fit to equation 1 or 2, setting hill coefficient to 1.

Table 8-2. Three-parameter or four-parameter fits of titration data for glutamate residues using 2D ^{1}H,^{13}C-HCBCGCO spectra[a].

Residue	Apo			Ca^{2+}			cTnI$_{147-163}$			sTnI$_{115-131}$		
	Hγ1	Hγ2	Cδ	Hγ1	Hγ2	Cδ	Hγ1	Hγ2	Cδ	Hγ1	Hγ2	Cδ
E10	-	4.58 (0.18)	4.66 (0.03)	4.73 (0.06)	4.88 (0.09)	4.62 (0.02)	4.74 (0.03)	4.83 (0.16)	4.67 (0.03)	-	-	-
E14	-	-	-	-	-	-	-	-	-	-	-	-
E15	4.49 (0.09)	-	4.88 (0.03)	4.37 (0.05)	-	4.84 (0.03)	4.36 (0.10)	4.43 (0.22)	4.83 (0.06)	-	4.83 (0.09)	4.87 (0.03)
E19	5.06 (0.04)	5.09 (0.03)	5.06 (0.03)	-	5.17 (0.03)	5.06 (0.02)	-	5.15 (0.05)	5.23 (0.01)	4.60 (0.11) 6.44 (0.32)	5.15 (0.05) 6.8 (0.05)	4.70 (0.01) 6.78 (0.05)
E32	-	-	-	-	-	-	-	-	-	-	-	-
E40	4.85 (0.06)	-	4.57 (0.03)	-	-	-	-	-	-	-	-	4.07 (0.22)
E55	4.58 (0.07)	-	4.75 (0.04)	4.60 (0.05)	-	4.63 (0.04)	4.58 (0.06)	-	4.66 (0.06)	4.62 (0.05)	-	4.68 (0.03)
E56	-	-	-	-	-	-	-	-	-	-	-	-
E59	5.44 (0.05)	5.15 (0.08)	5.43 (0.05)	5.38 (0.03)	4.97 (0.05)	5.31 (0.03)	5.40 (0.02)	5.02 (0.09)	5.38 (0.04)	5.43 (0.03)	5.21 (0.06)	5.37 (0.022)
E63	5.40 (0.06)	5.64 (0.06)	5.26 (0.05)	5.42 (0.05)	5.71 (0.08)	5.34 (0.03)	5.29 (0.13)	5.71 (0.09)	5.19 (0.04)	5.22 (0.05)	5.55 (0.04)	5.05 (0.03)
E66	-	-	-	-	-	-	4.96 (0.03)	5.40 (0.06)	4.97 (0.02)	-	-	-
E76	-	6.35 (0.06)	6.06 (0.07)	-	-	-	-	-	-	-	-	-

[a]Data were fit to equation 1 or 2, setting hill coefficient to 1.
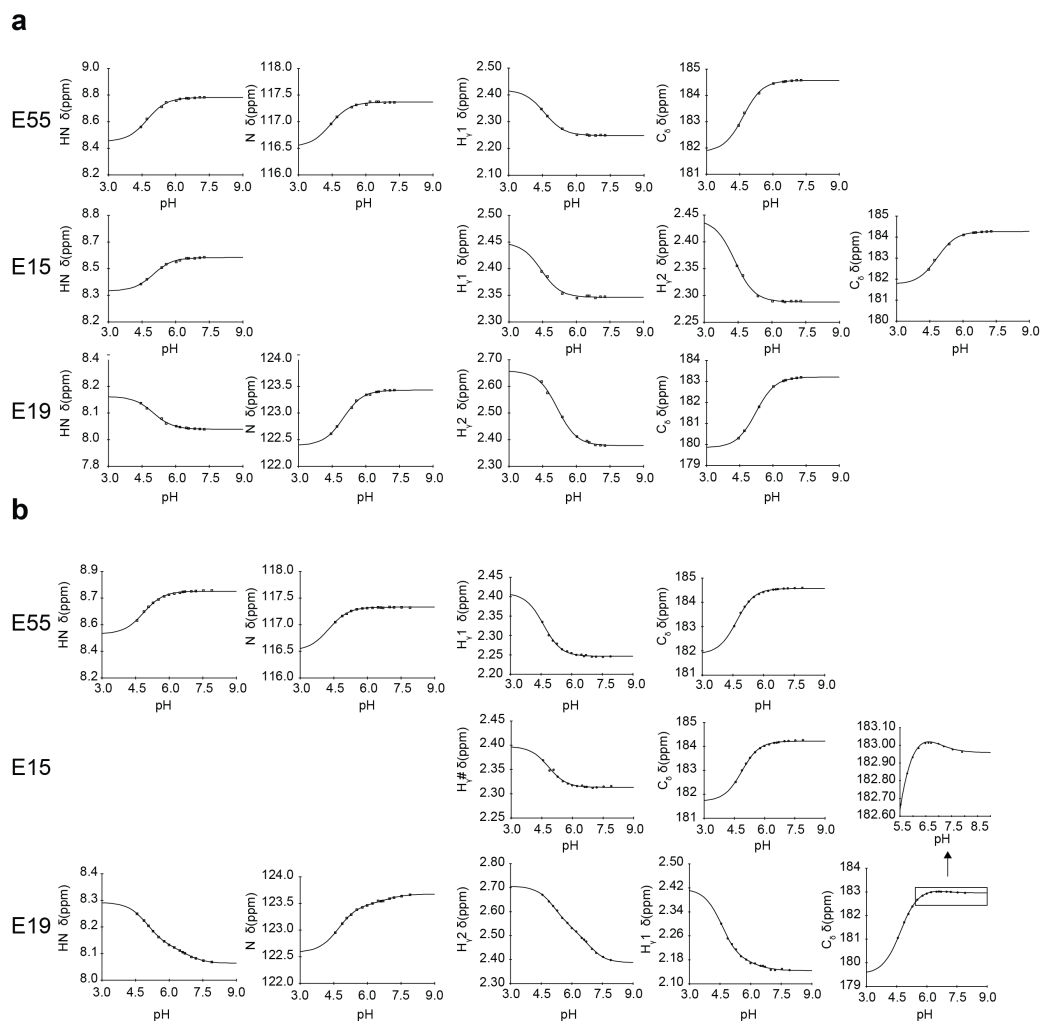
Figure 8-3. The pH dependence of the HN, N, C_δ, and H_γ resonances of E55, E15, and E19 of cNTnC when bound to **a.** cTnI$_{147-163}$ and **b.** sTnI$_{115-131}$. The pK$_a$ curves of the amide resonances are shown in the left two columns and the aliphatic proton and carboxylate carbon resonances in the right three columns. Peaks that were overlapped with other signals, or that did not titrate were omitted. The HN, N, C_δ, $H_\gamma 1$, and $H_\gamma 2$ resonances of E19 are fitted to two pK$_a$ values in the sTnI$_{115-131}$ bound state. The second inflection of the C_δ chemical shift of E19 is expanded. For the pK$_a$ values measured refer to Tables 1 and 2.

second ionization event monitored by E19 corresponds to the histidine on sTnI$_{115-131}$, we measured the pK$_a$ of histidine in its free and bound states.

sTnI$_{115-131}$ histidine pK$_a$ values as a function of structure

The results above suggest that E19 interacts with H130 on sTnI$_{115-131}$; to further investigate this possibility, the pK$_a$ of H130 was measured for sTnI$_{115-131}$ in the absence and presence of cNTnC. The stacked 1D ^{1}H-NMR spectra for the pH titration are shown in Figure 8-4a. The pK$_a$ of H130, using the histidine aromatic protons H2 and H5, was determined to be 6.12 ± 0.01 and 6.13 ± 0.03, respectively. The pK$_a$ of H130 was measured again, in the presence of cNTnC. The relative concentrations of sTnI$_{115-131}$ to cNTnC were ~4:1. Excess sTnI$_{115-131}$ made it easier to follow the chemical shift perturbations of H2 and H5 as a function of pH. Spectra and curves are shown in Figure 8-4b. H2 underwent a large pK$_a$ shift of 0.15 units from 6.12 ± 0.01 to 6.27 ± 0.01, whereas the pK$_a$ shift of H5 diminished 0.17 units to 5.96 ± 0.02. The pK$_a$ values were determined using the modified Hill equation (also fitting the Hill coefficient (*n*)). This was because the pK$_a$ curves did not fit the simple pK$_a$ model. Low Hill coefficients fit for H2 (n=0.8) and H5 (n=0.66) indicated that H130 is most likely interacts with other ionizable group(s). For example, as a nearby residue (such as E19 or E15) is deprotonated the protonated form of H130 is stabilized – this will result in a flattened pK$_a$ curve (n < 1). The different pK$_a$ values for H2 and H5 is abnormal; the low pK$_a$ observed for H5 may be the result of two ionization events nearby: one from H130 and one from E19. Fitting the curve of H5 to two pK$_a$'s yields pK$_a^1$ = 5.16 ± 0.07 and pK$_a^2$ = 6.46 ± 0.03. There was a minor peak present in the 1D ^{1}H spectrum from pH 7.31 to pH 5.06. The pK$_a$ of this secondary peak was 6.07 ± 0.07 (n=1), and is probably from a secondary bound conformation of H130 in slow exchange (*34*). Similar observations have been made for histidine residues in neurophysin II (*35*) and Staphylococcal Nuclease (*36*). In line
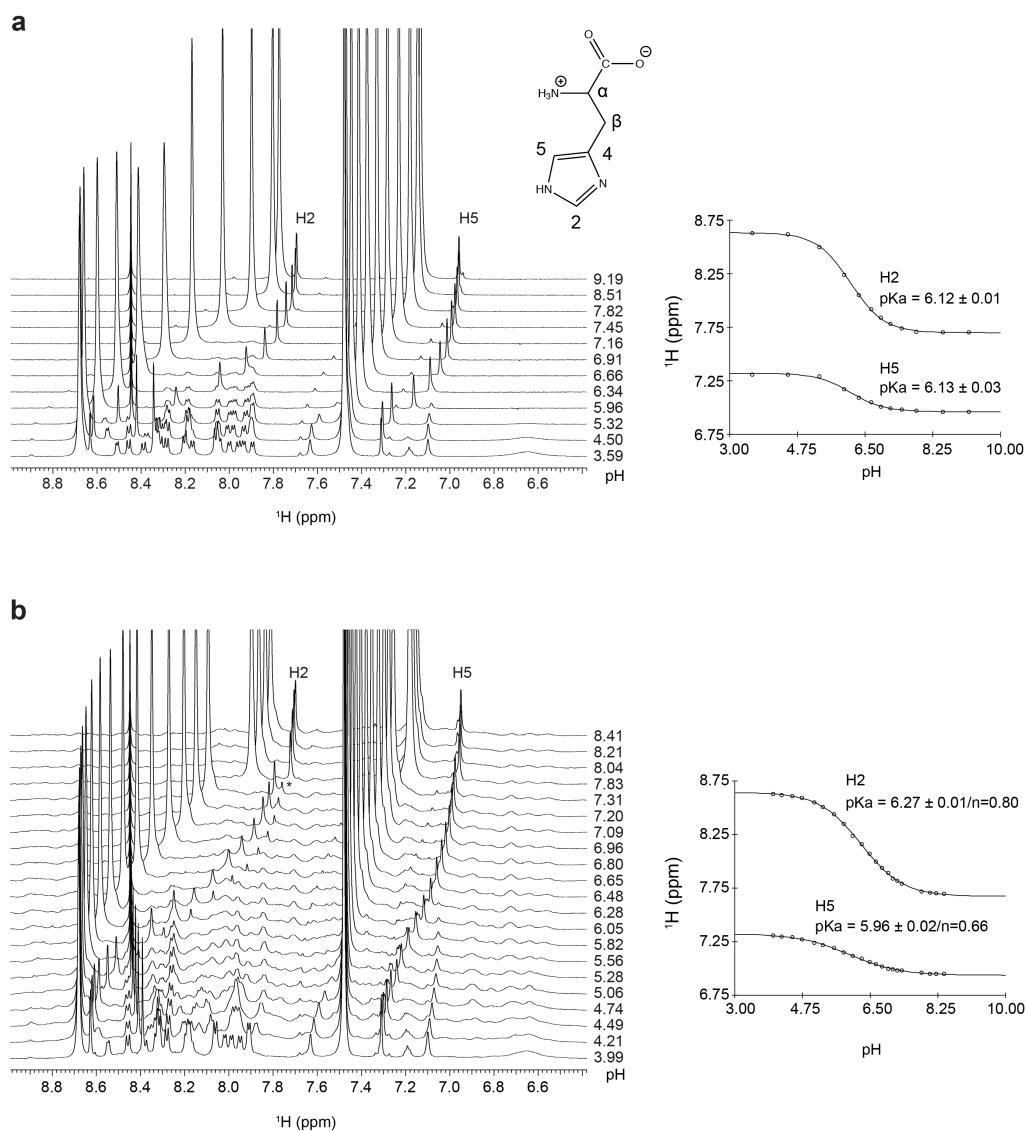
Figure 8-4. pH titrations of His_{130} of $sTnI_{115-131}$ when **a.** free and **b.** bound to cNTnC. ^{1}H NMR spectra are shown on the left with histidine aromatic protons assigned. The pK_a curves for H2 and H5 in the free and bound states are shown on the right. The pH sensitive peak near H2 in **b.** designated with an asterisk has a pKa of 6.08 +/- 0.01 and a Hill coefficient of 0.92. This is very close to H2 in free $sTnI_{115-131}$ (pKa = 6.12; n=1) and most likely represents a second conformation of H130 not making an electrostatic interaction with cNTnC.

with this conclusion, sTnI has been shown by NMR experiments to be in two conformations when bound to sNTnC (*18*). For H130 the pK_a values of H2 is upwards shifted, but not all the way to the values measured from cNTnC glutamates pK_a curves. This is explained by the fact that the sTnI$_{115-131}$ is in excess of cNTnC, and therefore the chemical shifts being monitored represent a combination of free and bound pK_a values. Whereas, the second pK_a measured by monitoring the chemical shift of E19 represents the pK_a of bound H130.

The pH-dependent dissociation constants of sTnI$_{115-131}$

Since the pK_a H130 is perturbed when bound to cNTnC, it follows that the protonation state of H130 should influence the binding equilibrium. sTnI$_{115-131}$ was titrated into cNTnC at two pH values (6.1 and 7.5). At each aliquot of sTnI$_{115-131}$, 2D ^{1}H,^{15}N-HSQC spectra were acquired. The global dissociation constant (K_D) was determined to be 100 µM (SSE^2 = 0.066) at pH=6.1 and K_D=360 µM (SSE=0.076) at pH=7.5. For an overlay of fits at the two pH values for residue T71 see Figure 8-5. For the global fits see Figures 8-6 and 8-7. We fitted the dissociation data to the simple model to investigate whether the pK_a shifts of H130 are directly correlated to the modulation of the K_D of sTnI$_{115-131}$.

$$
\begin{array}{ccc}
& K_a & \\
\text{Peptide} & \rightleftharpoons & \text{Peptide-H} \\
K_D \updownarrow & & \updownarrow K_{D-H} \\
& K_a^* & \\
\text{cNTnC-Peptide} & \rightleftharpoons & \text{cNTnC-Peptide-H}
\end{array}
$$
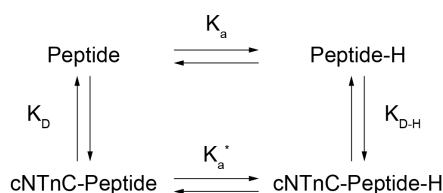
Protonation constants are represented by K_a (free) and K_a^* (bound) and the peptide dissociation constants are indicated by K_D (unprotonated peptide) and K_{D-H} (protonated peptide). The same model has been fitted to analyze the pH dependence of a peptide binding to calmodulin (*37*). For

---

^{2} Sum of squared error (see materials and methods).
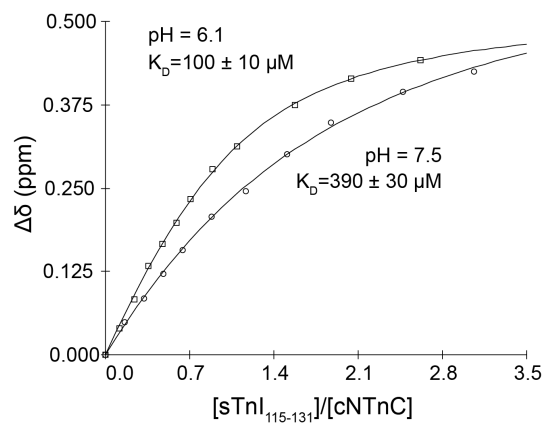
Figure 8-5. Titration of sTnI[115-131] into cNTnC at two different pH values. The dissociation curves fit to the amide ^{1}H NMR chemical shift data of T71. sTnI[115-131] binds to cNTnC with a significantly higher affinity at the lower pH.
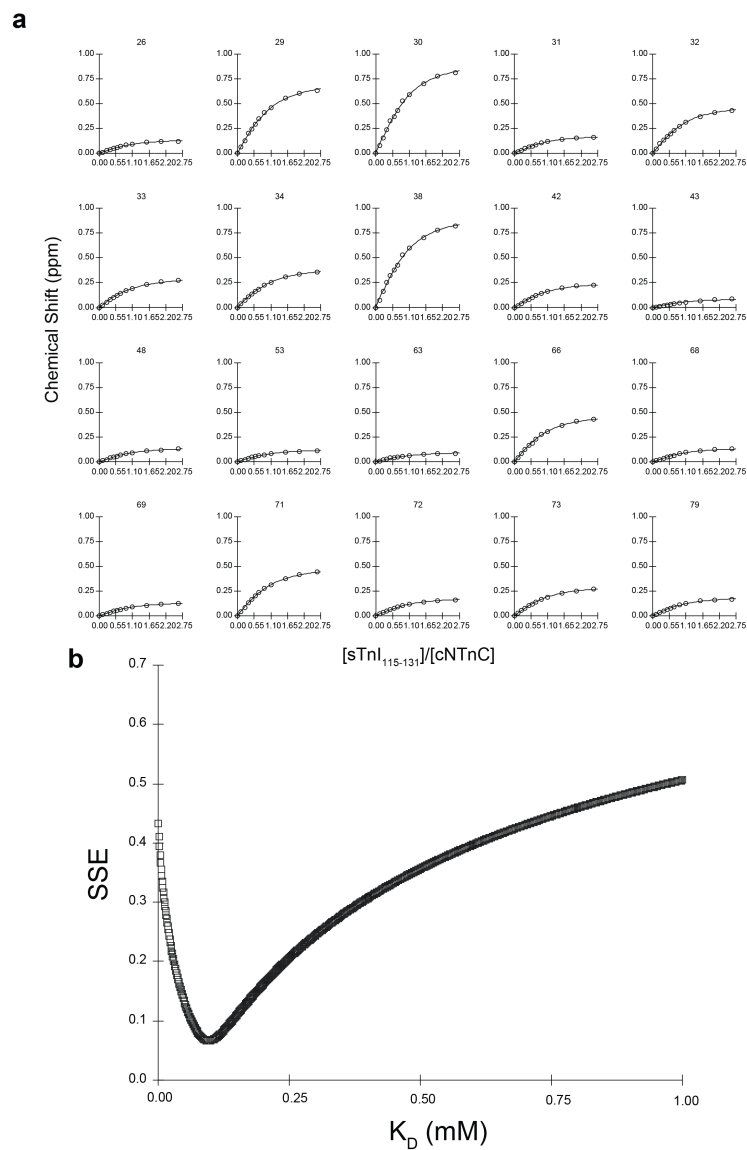
Figure 8-6. **a.** Global fit of the amide chemical shift changes of cNTnC when sTnI$_{115-131}$ is titrated to cNTnC at pH 6.1. **b.** The minimum SSE for the global fit in a is at K$_D$= 100µM (SSE = 0.066).
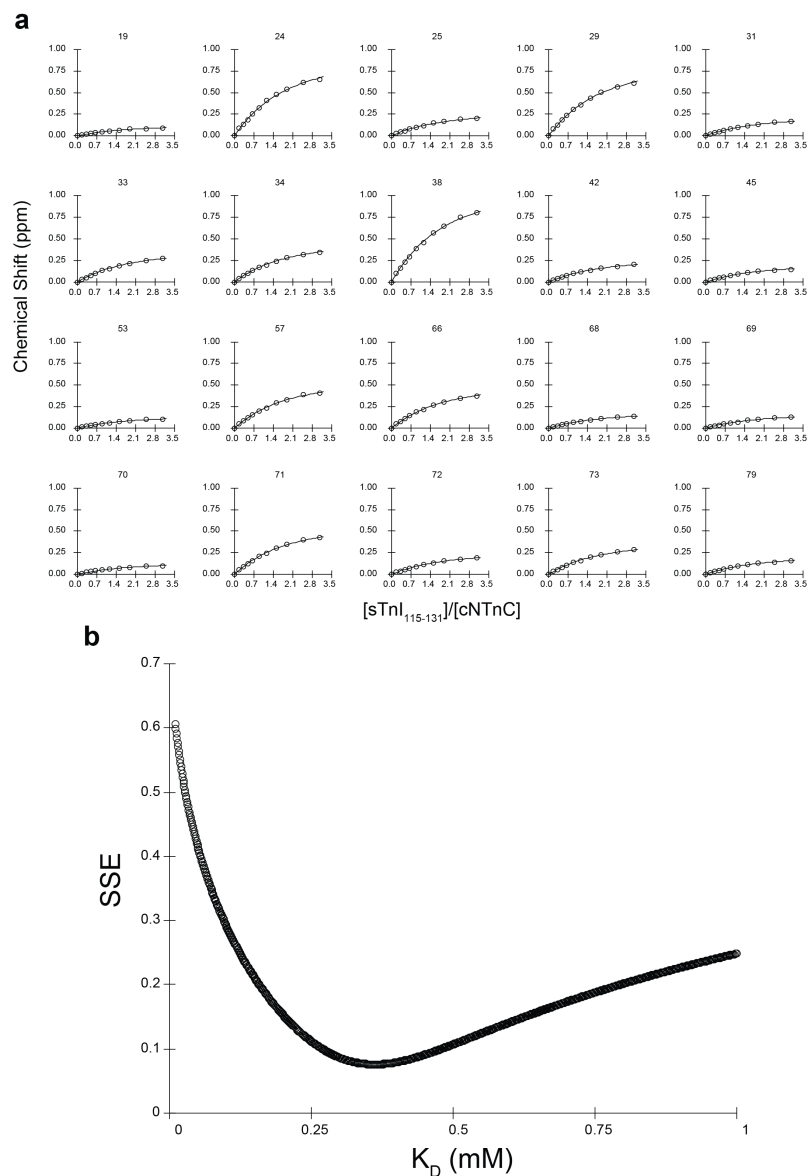
Figure 8-7. **a.** Global fit of the amide chemical shift changes of cNTnC when sTnI$_{115-131}$ is titrated to cNTnC at pH 7.5. **b.** The minimum SSE for the global fit in a is at K$_D$= 360µM (SSE = 0.076).

H130, K_a = 7.59 x 10^{-7} M (pKa = 6.12) and K_a^*= 1.86 x 10^{-7} M (pKa = 6.73). K_D = 3.90 x 10^{-4} M and K_D = 1.00 x 10^{-4} M. Indeed, K_a/K_a^* (4.1) is approximately equal to K_D/K_{D-H} (3.9), which is consistent with scheme 1.This result implies that the protonation state of H130 directly tunes the pH dependent affinity of sTnI$_{115-131}$.

Discussion

The data presented herein illustrates how a single hisitidine on sTnI can protect against acidosis. The affinity of sTnI$_{115-131}$ is directly related to the ionization state of H130, which can be explained in part by an interaction made between E19 of cNTnC and H130 of sTnI$_{115-131}$.We postulate that the electrostatic interaction between E19 and H130 is analogous to the interaction between E20 of sTnC and H130 of sTnI observed in the crystal structure of the skeletal complex (*16*). This interaction is probably not an artifact of crystal packing, since NMR relaxation data indicate that residues 124-130 of sTnI are rigid in solution (*17*). In the crystal structure, the imidazole N3 of H130 is only 4.1 Å from the carboxylate carbon of E20. The pK$_a$ shift of H130 presented in this work (ΔpK$_a$ = 0.605 ± 0.13) is significantly larger than that of E19 (ΔpK$_a$ = 0.26 ± 0.08); H130 is likely interacting with other negatively charged residues. The carboxylate of D119 of sTnI in the X-ray structure is only 3.7 Å from N4 of H130. If this interaction occurs when sTnI$_{115-131}$ is bound to cNTnC, then it will also contribute to the increase in the pK$_a$ of H130. E16 is also in close proximity to H130 (10.1 Å); and may also be involved in driving sTnI binding to sTnC, since electrostatic forces can span distances > 10 Å(*38-42*). Conversely, in the NMR and X-ray structures of cardiac troponin, this interaction does not occur, presumably because the histidine is replaced by an alanine (*19, 20*). Comparison of the crystal structures of the cardiac and skeletal troponin complexes in Figure 8-8 illustrates that in the cardiac system A162 is much further from E15 and E19 (11.8 and 16.4
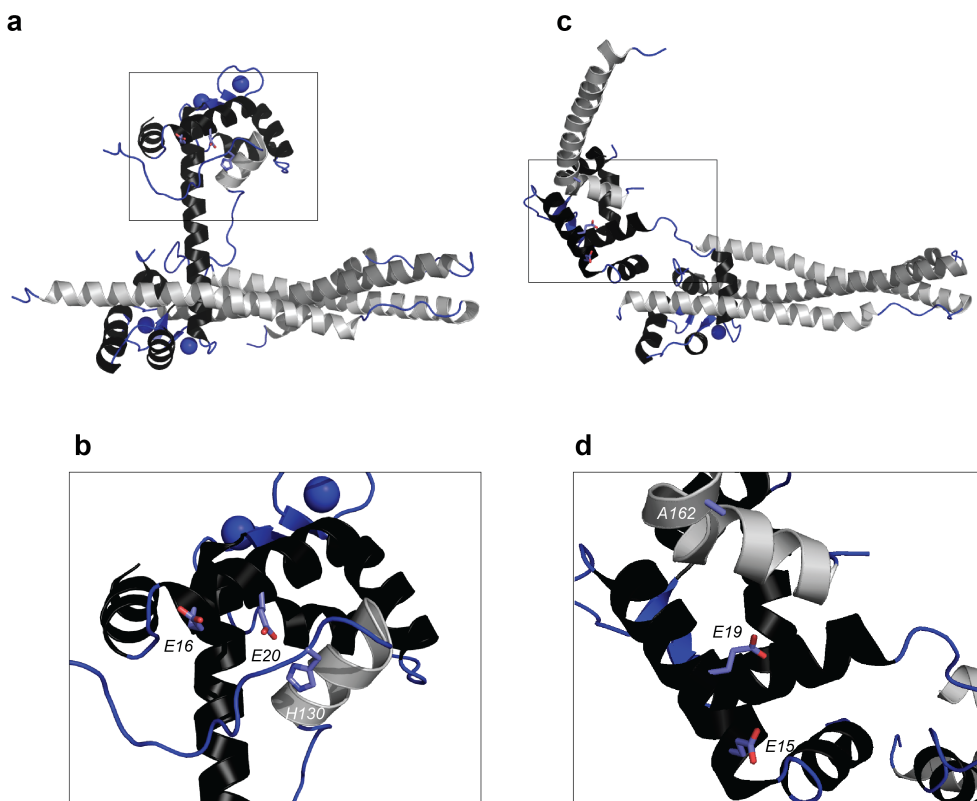
Figure 8-8. Cartoon representations of the **a, b** core skeletal complex (pdb: 1YTZ) and the **c, d** core cardiac complex (pdb: 1J1E) from the X-ray structures. In both structures, TnC is shown in black, TnI in dark grey, and TnT in light grey. The loops and unstructured regions are colored in blue, and Ca^{2+} ions are depicted as blue spheres. E16, E20, and H130 (E15, E19, and A162 in the cardiac system) are shown in stick representation. Expanded regions of **a.** and **c.** are shown in **b.** and **d.**, respectively.

Å, respectively). Thus, it is likely that when sTnI or cTnI(A162H) binds to cTnC, it adopts a conformation similar to that in the skeletal complex.

The simple interpretation of the data presented herein would suggest that at acidic pH, muscle fibers bearing the skeletal isoform of TnI should have enhanced contractility, when compared with an equivalent muscle at physiological pH. Functional studies of cardiac myofilaments replaced by sTnI clearly demonstrate quite the reverse; while sTnI partially depresses the negative inotropic effects of acidosis, it does not enhance the Ca^{2+} sensitivity when compared at neutral pH (*11, 12*). This discrepancy can be explained if low pH values encountered during acidosis dramatically reduce the affinity of Ca^{2+} affinity of cTnC (*5-7*). Reduction in Ca^{2+}-affinity would be partially compensated for by the concomitant enhancement in the affinity of sTnI for cTnC at low pH. Our results are consistent with findings that sTnI enhances the Ca^{2+} affinity of cTnC at low pH values by its enhanced affinity for cTnC(*7*). The improved affinity of sTnI for cTnC at low pH would stabilize the open state of cTnC more than when cTnI is bound, which would therefore increase the affinity of cTnC at low pH, when compared to the cTnI bound state. It is important to stress that while the protonation state of H130 modifies the affinity of sTnI$_{115-131}$ for cNTnC, it is also possible that its charge state may have other functional effects in an intact muscle fiber. For example, the protonation may both enhance the interaction between sTnI and cTnC and diminish sTnI binding to actin.

References

1. Donaldson, S. K., Hermansen, L., and Bolles, L. (1978) Differential, direct effects of H+ on Ca2+ -activated force of skinned fibers from the soleus, cardiac and adductor magnus muscles of rabbits, *Pflugers Arch. 376*, 55-65.

2. Fabiato, A., and Fabiato, F. (1978) Effects of pH on the myofilaments and the sarcoplasmic reticulum of skinned cells from cardiace and skeletal muscles, *The Journal of physiology 276*, 233-255.

3. Gordon, A. M., Homsher, E., and Regnier, M. (2000) Regulation of contraction in striated muscle, *Physiol. Rev. 80*, 853-924.

4. Kobayashi, T., Jin, L., and de Tombe, P. P. (2008) Cardiac thin filament regulation, *Pflugers Archiv-European Journal of Physiology 457*, 37-46.

5. Blanchard, E. M., and Solaro, R. J. (1984) Inhibition of the activation and troponin calcium binding of dog cardiac myofibrils by acidic pH, *Circ. Res. 55*, 382-391.

6. Parsons, B., Szczesna, D., Zhao, J. J., VanSlooten, G., Kerrick, W. G. L., Putkey, J. A., and Potter, J. D. (1997) The effect of pH on the Ca2+ affinity of the Ca2+ regulatory sites of skeletal and cardiac troponin C in skinned muscle fibres, *J. Muscle Res. Cell Motil. 18*, 599-609.

7. Liou, Y. M., and Chang, J. C. (2004) Differential pH effect on calcium-induced conformational changes of cardiac troponin C complexed with cardiac and fast skeletal isoforms of troponin I and troponin T, *J Biochem 136*, 683-692.

8. el-Saleh, S. C., and Solaro, R. J. (1988) Troponin I enhances acidic pH-induced depression of Ca2+ binding to the regulatory sites in skeletal troponin C, *J. Biol. Chem. 263*, 3274-3278.

9. Solaro, R. J., Lee, J. A., Kentish, J. C., and Allen, D. G. (1988) Effects of acidosis on ventricular muscle from adult and neonatal rats, *Circ. Res. 63*, 779-787.

10. Westfall, M. V., Rust, E. M., and Metzger, J. M. (1997) Slow skeletal troponin I gene transfer, expression, and myofilament incorporation enhances adult cardiac myocyte contractile function, *Proc. Natl. Acad. Sci. U. S. A. 94*, 5444-5449.

11. Li, G., Martin, A. F., and Solaro, J. R. (2001) Localization of regions of troponin I important in deactivation of cardiac myofilaments by acidic pH, *J. Mol. Cell. Cardiol. 33*, 1309-1320.

12. Dargis, R., Pearlstone, J. R., Barrette-Ng, I., Edwards, H., and Smillie, L. B. (2002) Single mutation (A162H) in human cardiac troponin I corrects acid pH sensitivity of Ca2+-regulated actomyosin S1 ATPase, *J. Biol. Chem. 277*, 34662-34665.

13.   Westfall, M. V., Albayya, F. P., Turner, II, and Metzger, J. M. (2000) Chimera analysis of troponin I domains that influence Ca(2+)-activated myofilament tension in adult cardiac myocytes, *Circ. Res. 86*, 470-477.

14.   Day, S. M., Westfall, M. V., Fomicheva, E. V., Hoyer, K., Yasuda, S., La Cross, N. C., D'Alecy, L. G., Ingwall, J. S., and Metzger, J. M. (2006) Histidine button engineered into cardiac troponin I protects the ischemic and failing heart, *Nat. Med. 12*, 181-189.

15.   Palpant, N. J., D'Alecy, L. G., and Metzger, J. M. (2009) Single histidine button in cardiac troponin I sustains heart performance in response to severe hypercapnic respiratory acidosis in vivo, *FASEB J. 23*, 1529-1540.

16.   Vinogradova, M. V., Stone, D. B., Malanina, G. G., Karatzaferi, C., Cooke, R., Mendelson, R. A., and Fletterick, R. J. (2005) Ca(2+)-regulated structural changes in troponin, *Proc. Natl. Acad. Sci. U. S. A. 102*, 5038-5043.

17.   Julien, O., Mercier, P., Allen, C. N., Fisette, O., Ramos, C. H. I., Lague, P., Blumenschein, T. M. A., and Sykes, B. D. (2011) Is there nascent structure in the intrinsically disordered region of troponin I?, *Proteins-Structure Function and Bioinformatics 79*, 1240-1250.

18.   McKay, R. T., Tripet, B. P., Pearlstone, J. R., Smillie, L. B., and Sykes, B. D. (1999) Defining the region of troponin-I that binds to troponin-C, *Biochemistry 38*, 5478-5489.

19.   Takeda, S., Yamashita, A., Maeda, K., and Maeda, Y. (2003) Structure of the core domain of human cardiac troponin in the Ca(2+)-saturated form, *Nature 424*, 35-41.

20.   Li, M. X., Spyracopoulos, L., and Sykes, B. D. (1999) Binding of cardiac troponin-I147-163 induces a structural opening in human cardiac troponin-C, *Biochemistry 38*, 8289-8298.

21.   Li, M. X., Saude, E. J., Wang, X., Pearlstone, J. R., Smillie, L. B., and Sykes, B. D. (2002) Kinetic studies of calcium and cardiac troponin I peptide binding to human cardiac troponin C using NMR spectroscopy, *European Biophysics Journal with Biophysics Letters 31*, 245-256.

22.   Yamazaki, T., Yoshida, M., and Nagayama, K. (1993) Complete Assignments of Magnetic Resonances of Ribonuclease-H from Escherichia-Coli by Double-Resonance and Triple-Resonance 2d and 3d Nmr Spectroscopies, *Biochemistry 32*, 5656-5669.

23.   Delaglio, F., Grzesiek, S., Vuister, G. W., Zhu, G., Pfeifer, J., and Bax, A. (1995) Nmrpipe - a Multidimensional Spectral Processing System Based on Unix Pipes, *J. Biomol. NMR 6*, 277-293.

24.   Johnson, B. A., and Blevins, R. A. (1994) Nmr View - a Computer-Program for the Visualization and Analysis of Nmr Data, *J. Biomol. NMR 4*, 603-614.

25. Slupsky, C. M., Boyko, R. F., Booth, V. K., and Sykes, B. D. (2003) Smartnotebook: A semi-automated approach to protein sequential NMR resonance assignments, *J. Biomol. NMR 27*, 313-321.

26. Baryshnikova, O. K., Williams, T. C., and Sykes, B. D. (2008) Internal pH indicators for biomolecular NMR, *J. Biomol. NMR 41*, 5-7.

27. Farrell, D., Miranda, E. S., Webb, H., Georgi, N., Crowley, P. B., McIntosh, L. P., and Nielsen, J. E. Titration_DB: storage and analysis of NMR-monitored protein pH titration curves, *Proteins 78*, 843-857.

28. Hoffman, R. M. B., Li, M. X., and Sykes, B. D. (2005) The bindin of W7, an inhibitor of striated muscle contraction, to cardiac troponin C, *Biochemistry 44*, 15750-15759.

29. Russell, S. T., and Warshel, A. (1985) Calculations of Electrostatic Energies in Proteins - the Energetics of Ionized Groups in Bovine Pancreatic Trypsin-Inhibitor, *J. Mol. Biol. 185*, 389-404.

30. Sia, S. K., Li, M. X., Spyracopoulos, L., Gagne, S. M., Liu, W., Putkey, J. A., and Sykes, B. D. (1997) Structure of cardiac muscle troponin C unexpectedly reveals a closed regulatory domain, *J. Biol. Chem. 272*, 18216-18221.

31. Spyracopoulos, L., Li, M. X., Sia, S. K., Gagne, S. M., Chandra, M., Solaro, R. J., and Sykes, B. D. (1997) Calcium-induced structural transition in the regulatory domain of human cardiac troponin C, *Biochemistry 36*, 12138-12146.

32. Bjornson, M. E., Corson, D. C., and Sykes, B. D. (1985) C-13 and Cd-113 Nmr-Studies of the Chelation of Metal-Ions by the Calcium-Binding Protein Parvalbumin, *J. Inorg. Biochem. 25*, 141-149.

33. Nelson, D. J., Theoharides, A. D., Nieburgs, A. C., Murray, R. K., Gonzalezfernandez, F., and Brenner, D. S. (1979) C-13 Magnetic-Resonance Study of Lanthanide-Substituted Muscle Calcium-Binding Parvalbumins, *Int. J. Quantum Chem. 16*, 159-174.

34. Markley, J. L. (1975) Observation of Histidine Residues in Proteins by Means of Nuclear Magnetic-Resonance Spectroscopy, *Acc. Chem. Res. 8*, 70-80.

35. Cohen, P., Griffin, J. H., Camier, M., Caizergues, M., Fromageot, P., and Cohen, J. S. (1972) Hormonal interactions at the molecular level: A high resolution proton magnetic resonance study of bovine neurophysins and their interactions with oxytocin, *FEBS Lett. 25*, 282-286.

36. Markley, J. L., Williams, M. N., and Jardetzk.O. (1970) Nuclear Magnetic Resonance Studies of Structure and Binding Sites of Enzymes .12. A Conformational Equilibrium in Staphylococcal Nuclease Involving a Histidine Residue, *Proc. Natl. Acad. Sci. U. S. A. 65*, 645-&.

37. Martin, S. R., Biekofsky, R. R., Skinner, M. A., Guerrini, R., Salvadori, S., Feeney, J., and Bayley, P. M. (2004) Interaction of

calmodulin with the phosphofructokinase target sequence, *FEBS Lett. 577*, 284-288.

38. Rees, D. C. (1980) Experimental Evaluation of the Effective Dielectric-Constant of Proteins, *J. Mol. Biol. 141*, 323-326.

39. Russell, A. J., Thomas, P. G., and Fersht, A. R. (1987) Electrostatic Effects on Modification of Charged Groups in the Active-Site Cleft of Subtilisin by Protein Engineering, *J. Mol. Biol. 193*, 803-813.

40. Sternberg, M. J. E., Hayes, F. R. F., Russell, A. J., Thomas, P. G., and Fersht, A. R. (1987) Prediction of Electrostatic Effects of Engineering of Protein Charges, *Nature 330*, 86-88.

41. Jackson, S. E., and Fersht, A. R. (1993) Contribution of Long-Range Electrostatic Interactions to the Stabilization of the Catalytic Transition-State of the Serine-Protease Subtilisin Bpn', *Biochemistry 32*, 13909-13916.

42. Cederholm, M. T., Stuckey, J. A., Doscher, M. S., and Lee, L. (1991) Histidine Pka Shifts Accompanying the Inactivating Asp121-] Asn Substitution in a Semisynthetic Bovine Pancreatic Ribonuclease, *Proc. Natl. Acad. Sci. U. S. A. 88*, 8116-8120.

Chapter 9

"My Brain is open"
- Paul Erdős

Conclusions

Summary

In this thesis I focused in large part on expanding our knowledge of how modulating the critical troponin C-troponin I interaction leads to a change in the apparent Ca^{2+}-sensitivity of cardiac muscle. In the first chapter, the role of heart in maintaining human health was reviewed. The integral regulatory role of troponin during contraction and its potential as a drug target were also discussed. In Chapters 2 and 3 the natural compounds, resveratrol and EGCg, were shown to bind to the C-domain of troponin C (cCTnC). These structures, as well as the EMD 57033-cCTnC structure, point to a mechanism by which drugs bind to cCTnC and modulate its interaction with the anchoring and/or inhibitory region of troponin I (cTnI). The next section of the thesis (Chapters 4-6) looked at the N-domain of troponin C (cNTnC) as a drug target. Several critical chemical elements of drugs that dictate their function were highlighted. We show that Ca^{2+}-sensitizers work, in part, by enhancing binding of the switch region of cTnI to cNTnC. In the final two chapters, the influence a single residue (either in cNTnC or in cTnI) had on the modulation of Ca^{2+}-sensitivity was investigated. The mutation of a leucine to a glutamine in cNTnC has been found to increase Ca^{2+}-sensitivity. Our results support the idea that this substitution stabilizes a more open conformation of cNTnC to enhance both Ca^{2+} and cTnI binding. The final chapter looked at the modulation of Ca^{2+}-sensitivity during acidosis. The decreased Ca^{2+}-sensitivity in the cardiac myofilament at low pH can be almost completely reversed when the cardiac TnI isoform is replaced by the skeletal or neonatal isoforms of TnI (sTnI or ssTnI, respectively). This phenomenon has been unambiguously linked to a single histidine (which is an alanine in the cardiac system). We show that the ionized state of this histidine directly determines the affinity of sTnI for cNTnC, which we attribute to an electrostatic interaction it makes with E19 of cNTnC. Since each chapter contained a detailed discussion, I will only briefly review the results and present a final mechanism in this final chapter. I will finish by discussing some future experiments that may help unravel the *in vivo* mode of action of inotropic compounds that target troponin.

The mechanism of drugs that target the C-domain of troponin C

The NMR studies investigating the interactions of EGCg and resveratrol with cCTnC have expanded our understanding of the pharmacophores responsible for small molecules binding to cCTnC. For a long time cCTnC has been thought to serve a structural purpose. However, recent hypertrophic and dilated cardiomyopathies (HCM and DCM, respectively) identified in cCTnC have questioned this dogma (see Chapter 3 for a detailed discussion). EGCg, resveratrol, and EMD 57033 were all shown to explicitly target the C-domain of cTnC, even in full-length cTnC (*1-3*). While all three compounds bind to the hydrophobic surface of cCTnC, they have different *in vivo* functions. EMD 57033 and resveratrol increase the Ca^{2+}-sensitivity (*4, 5*), whereas EGCg has been shown to decrease Ca^{2+}-sensitivity (*6*). A proposed mechanism for the troponin-dependent Ca^{2+}-sensitization of EMD 57033 is that it competes with the anchoring region of cTnI ($cTnI_{34-71}$) and thereby enhances binding of the inhibitory region of cTnI ($cTnI_{129-146}$) thus increasing contractility (*3*). EGCg did not bind as "deep" in the hydrophobic pocket as EMD 57033, and instead laid across the hydrophobic surface (Chapter 2, (*2*)). While EMD 57033 did not compete with $cTnI_{129-146}$ for cCTnC (*7*), based on the structure of cCTnC-EGCg, it is likely that EGCg would also compete with $cTnI_{129-146}$ for binding to cCTnC. Therefore, a plausible explanation for the differences in the function of EGCg and EMD 57033 (and resveratrol) is that all three compounds compete with $cTnI_{34-71}$ for cCTnC, however, EMD 57033 and resveratrol (which binds in a similar orientation as EMD 57033 (*1*)) would bind concurrently with $cTnI_{129-146}$ but EGCg would not. In order to test this theory, titrations with $cTnI_{129-146}$ to EGCg and resveratrol-bound forms of cCTnC need to be done.

The mechanism of drugs that target the N-domain of troponin C

A possible mechanism of Ca^{2+} inotropes that affect contractility through the cNTnC-mediated pathway has been previously outlined (*8*). The model proposes that drugs bind to Ca^{2+}-saturated cNTnC, stabilize its open conformation and enhance cTnI binding to cNTnC. Based on the results presented in this thesis, and those by Hoffman and Sykes (*9*) and Oleszczuk et al. (*10*), we have provided experimental evidence for the validity of this model. The novel levosimendan analog, dfbp-o, shifts the open-to-closed equilibrium towards the open state, enhanced the binding of the switch region of cTnI ($cTnI_{147-163}$), which resulted in an increase in contractility (Chapter 5, (*11*)). In the ternary structure, $cNTnC \cdot Ca^{2+} \cdot cTnI_{144-163}$, the negatively charged carboxyl group of dfbp-o is located near the positively charged guanidinium side chain of R147, implying an electrostatic attraction between these two groups may explain the activity of dfbp-o. The negative inotrope, W7, also stabilized the open conformation of cNTnC (*9*), but decreased the binding of $cTnI_{147-163}$ primarily *via* a charge repulsion between R147 and its terminal amino group (*10*). Therefore, the relationship between the inotrope and $cTnI_{147-163}$ binding to cNTnC seems to be the determining factor of their influence on muscle contraction. Furthermore, the change in the charge of W7 from positive to negative dramatically reduced the competition between the drug and $cTnI_{147-163}$ (Chapter 6). This supports the electrostatic model of competition, although steric interference also plays a role in the drug-cTnI relationship (Figure 9-1).

The results presented in Chapter 7 and 8 reinforce the significance of the cNTnC-cTnI interaction in governing contraction. The Ca^{2+}-sensitizing mutation, L48Q in cNTnC, disrupts hydrophobic interactions made between L48 and F20, A23, and F27 that are critical in keeping $cNTnC \cdot Ca^{2+}$ in a more closed conformation (*12*). Our work indicates that akin to Ca^{2+}-sensitizing drugs, L48Q stabilizes an open state of cNTnC
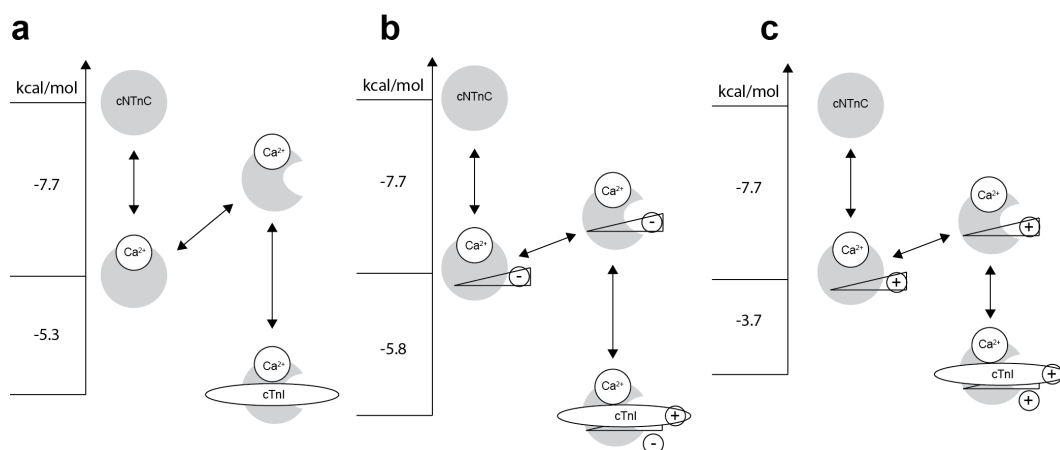
Figure 9-1. The energy level diagram illustrating the proposed mechanism of Ca^{2+} inotropes (modified from Sorsa *et al*. (*8*)). **a.** Normal energy levels in the cardiac troponin system (ΔG's for Ca^{2+} and cTnI binding are from (*37*)). **b.** The energy level diagram for a Ca^{2+}-sensitizer (i.e. dfbp-o) that stabilizes the open state of Ca^{2+}-saturated state of cNTnC and enhances cTnI binding by an electrostatic interaction (ΔG for cTnI binding is calculated from the K_D ~ 60 µM from Robertson *et al.* (11) using the equation ΔG = -RTlnK$_D$). **c.** The energy level diagram for a Ca^{2+}-desensitizer (i.e. W7) that stabilizes the open state of Ca^{2+}-saturated state of cNTnC but decreases the binding of cTnI by an electrostatic repulsion (ΔG for cTnI binding is calculated from the K_D ~ 2000 µM from Olesczcuk *et al.* (*10*) for W7). The presence of W7 or dfbp-o could alter the Ca^{2+} affinity of cNTnC as is the case for bepridil (*15*); however, since these values have not been measured, in this simple model they are assumed to be unchanged.

enhancing its affinity for Ca^{2+} and cTnI (Chapter 7). The replacement of cTnI with the skeletal isoform (sTnI) is known to reduce the Ca^{2+}-desensitizing effect of low pH (*13*). We have shown in Chapter 8 that the protonation of H130 on sTnI enhances the switch peptide's affinity for $cNTnC•Ca^{2+}$ through the formation of an electrostatic interaction with E19 of cNTnC. This result may explain the protective effects of sTnI against myocardial ischemia.

All these results bolster the importance of the cNTnC-cTnI interaction in dictating contraction and suggest it represents a genuine drug target worthy of a high-throughput screening program. Varughese and Li have used a computational screening approach to identify a novel group of compounds that may be interesting to investigate experimentally (*14*). However, before we scream *Geronimo!* and dive head first into a drug screening program, it would be nice to address several unanswered questions. Primarily, what is the troponin-mediated mode of action of levosimendan? Since levosimendan is the most successful Ca^{2+}-sensitizer to date, having a detailed understanding of its molecular mechanism will give credence to the development of molecules that target troponin. Another related, lingering question is: do these inotropes bind troponin in an intact muscle fiber? There have been some studies that addressed this question; for example, bepridil was shown to enhance contractility only in the presence of troponin and tropomyosin (*15*). Structural studies that could unequivocally identify the binding sites of inotropes on the thin filament would help to reconcile some of the uncertainty regarding the *in vivo* mode of action of these compounds.

Structure and function of levosimendan – a new hope?

The exact inotropic mode of action of levosimendan remains unknown despite considerable effort. Most likely, levosimendan has multifarious *in vivo* actions that contribute to its positive inotropic effect

(*16, 17*). Levosimendan's binding to cTnC has been identified as one of these inotropic activities (*18-21*). Based on sparse NOE data and using the X-ray structure of skeletal troponin C as a model (*22*), Pollesello *et al.* predicted that levosimendan bound to a pocket formed by F20, A22, A23, F24, V28, and F77 (*19*). However, later Kleerekoper and Putkey failed to witness any association between levosimendan and cTnC, which had both of its cysteines mutated to serines (*23*). In 2001, Sorsa *et al.* indicated that the source of this controversy stemmed from the fact that C84 is critical for levosimendan binding to cTnC (*24*). They also found that levosimendan reacts with DTT and NaN_3 (*24*). In Chapter 4 we show that levosimendan can bind to cNTnC(C35S,C84S) in the presence of the switch region of cTnI. The affinity we measured, however, was lower than that for binding to wild-type cTnC, suggesting that the presence of cTnI does not fully compensate for the absence of C84 (*25*). From these studies several questions emerge that would be interesting to investigate and which we have begun to answer: what is the structure of levosimendan bound to cTnC and why is C84 compulsory for levosimendan binding?

What is the structure of the complex of cNTnC with levosimendan?

Since levosimendan degrades in the presence of cTnC after several days (*24*) it has been difficult to solve the structure of the troponin-levosimendan complex. We have employed a technique that avoids the prerequisite of having a long lasting complex, discussed in Chapter 5 (*11*). Instead of relying on intermolecular NOEs between cNTnC and levosimendan, which can take days-weeks to acquire, we could use paramagnetic relaxation enhancement (PRE). In this experiment, 1D spectra of levosimendan are acquired at varying concentrations of cNTnC bound to the paramagnetic ion Gd^{3+} (instead of Ca^{2+}). The extent of relaxation enhancement a nucleus experiences is correlated to its distance from the paramagnetic ion. I have done preliminary PRE experiments for levosimendan and have manually docked levosimendan on $cNTnC \cdot Ca^{2+}$

(Figure 9-2). The isotropic electronic environment of Gd^{3+} means that it only perturbs the relaxation of protons, not their chemical shift and thus only provides distance restraints not orientation information. Hence, in the model in Figure 9-2, levosimendan is assumed to bind to the core of cNTnC and the PRE restraints were used to refine its position. If Gd^{3+} were replaced with a different lanthanide, such as Europium or Dysprosium, with nonisotropic distributions of their f electrons, orientation and distance information could be obtained using pseudocontact shifts (PCS) (26). Nevertheless, the model is probably reasonable since all other inotropes that bind cNTnC target this pocket (see Chapter 1). In the model, the pyridazinone and phenyl rings are in the hydrophobic pocket while the dinitrile moiety points towards the solvent. Future PCS experiments should improve this preliminary model, and may provide us with a high-resolution structure of levosimendan bound to cNTnC.

Why is C84 required for levosimendan binding to cTnC?

An attractive explanation for the importance of C84 is the formation of a covalent bond between the thiol group of C84 and one of the dinitrile moieties of levosimendan. In general, nitriles are known to react with thiols to form thioimidates (27, 28). Crystal structures of the cysteine protease, cathepsin K, bound to nitrile-containing inhibitors unambiguously reveals the formation of a thioimidate (29, 30) (see Figure 9-3 for an example). The general reaction scheme is as follows (31, 32):
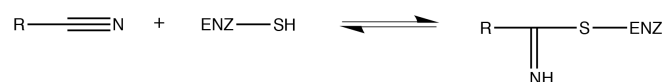
In addition to the established precedence for this type of reaction in cysteine proteases, there are a number of lines of indirect evidence that support this mechanism. Levosimendan has been shown to react vigorously with DTT, presumably *via* and interaction with its thiol groups (24). Furthermore, the major metabolic product of levosimendan is
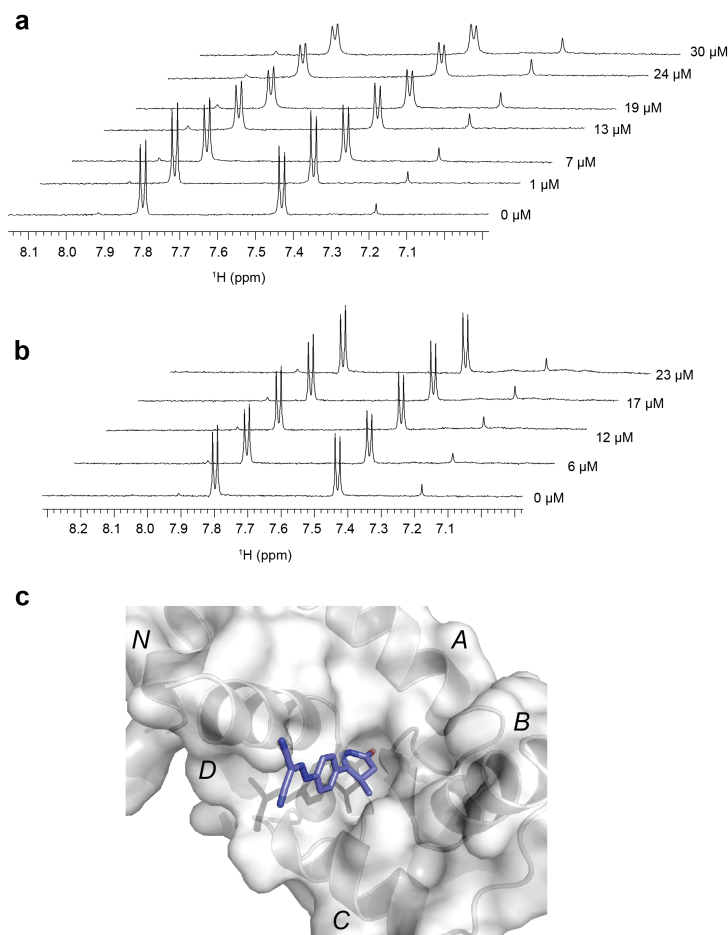
Figure 9-2. Levosimendan manually docked into cNTnC using PRE derived distances. **a.** Titration of 0.3 mM levosimendan with cNTnC•Gd³⁺. **b**. Titration of 0.3 mM levosimendan with cNTnC•La³⁺. Final concentrations of cNTnC are shown on the right. Note the significant broadening induced by Gd³⁺ but not by La³⁺. **c**. Manually docked levosimendan into cNTnC (pdb: 1dtl; bepridil bound X-ray structure) using PRE distances: Methyl – Gd³⁺ ~ 12-13 Å, the aromatic protons and the Gd³⁺ ~ 11-12 Å. We assume levosimendan binds to the hydrophobic pocket of cNTnC.

generated by the formation of a covalent adduct with glutathione, specifically at its cysteine residue (*17*). As noted by Sorsa *et al*., after several days at 40°C levosimendan dissociated from cTnC (*24*), this could be explained by the fact that thioimidate esters can undergo hydrolysis (*33*). Finally, the docked structure positions the nitrile moiety adjacent to the side chain of C84 (see Figure 9-3).

The fact that levosimendan activity can be reversed by washing it out (*21*), would seem to preclude the possibility of the thioimidate ester linkage; however, in the case of the cysteine protease inhibitors, it was shown by NMR that the formation of the thioimidate is reversible (*31, 32*). Mass spectrometry of levosimendan-cTnC solutions did not show the presence of a covalent adduct (*24*); however, since thioimidates are prone to acid hydrolysis (or base elimination) (*33*), it is possible that during the sample preparation the thioimidate was broken down. The formation of a thioimidate between a nitrile inhibitor (benzoylamidoacetonitrile) and papain has been monitored by ^{13}C-NMR (Figure 9-4) (*31, 32*). I have run some preliminary ^{13}C-NMR experiments using natural abundance ^{13}C-levosimendan; while a change in the ^{13}C-spectra was noticed upon addition of glutathione, it was not possible to unambiguously assign the ^{13}C-nitrile peaks in the reacted form of levosimendan. A possible solution to this problem would be to synthesize ^{13}C-labeled levosimendan solely at the nitriles. This would permit direct observation of solely the nitrile chemical shifts as a function of glutathione or troponin C as done for benzoylamidoacetonitrile binding to papain (*31, 32*).

In situ mode of action of Ca^{2+}-sensitizers.

Given the uncertainty surrounding levosimendan's *in vivo* mode of action, it would be valuable to have direct structural confirmation of its binding to troponin in an intact muscle fiber. We have used broad line 1D ^{19}F NMR methods examine if dfbp-o interactes with rabbit psoas muscle
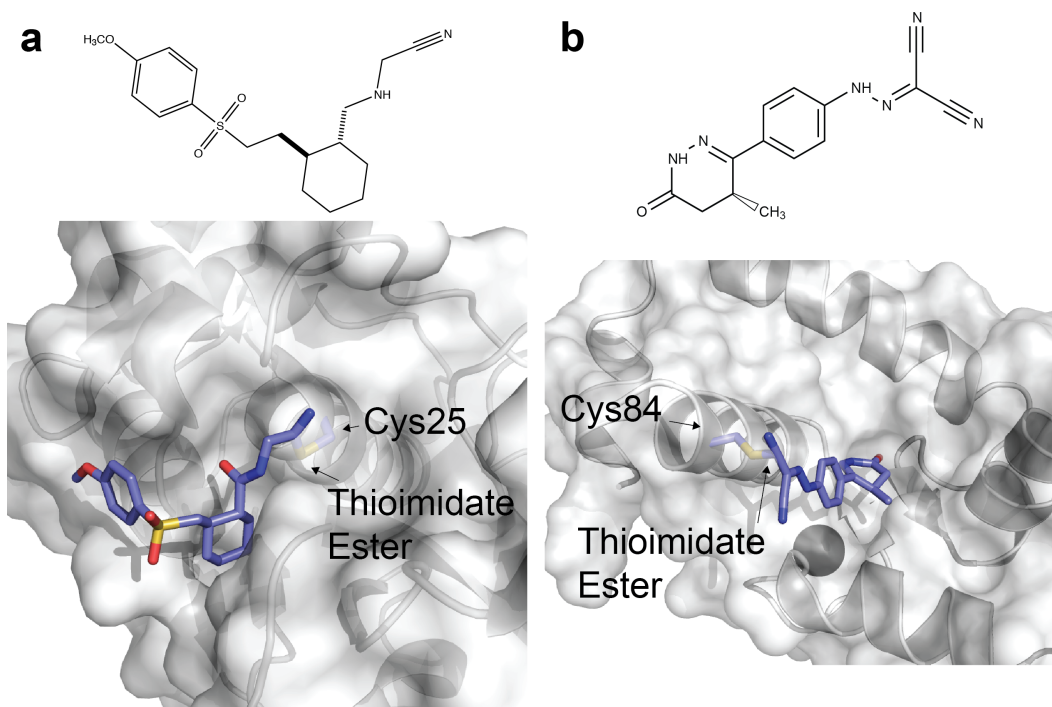
Figure 9-3. a. The X-ray structure of the cysteine protease, cathepsin K, bound to a nitrile inhibitor. The inhibitor forms a reversible thioimidate ester with C25 of cathepsin K (pdb: 2f7d). **b.** using the docked structure (Figure 9-2), the nitrile moiety of levosimendan is in close proximity of C84, and may form a similar thioimidate bond.
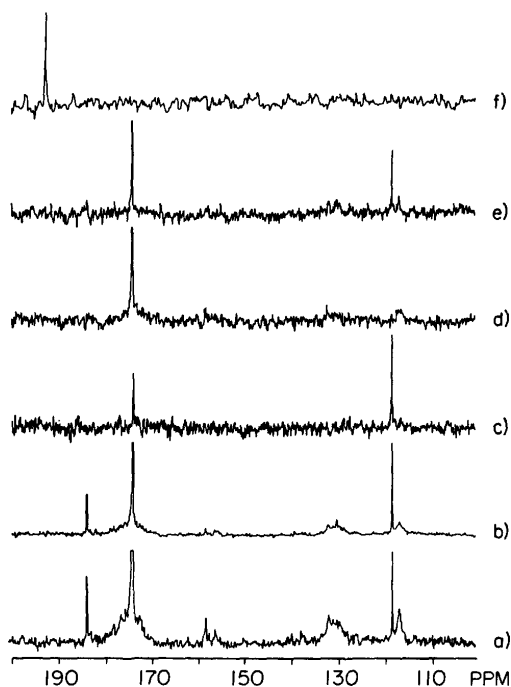
Figure 9-4. ^{13}C NMR spectrum of benzoylamidoacetonitrile, ^{13}C-labeled at its nitrile carbon. **a.** 0.3 mM papain and 0.5 mM benzoylamidoacetonitrile; **b.** 0.3 mM papain, 1 mM benzoylamidoacetonitrile; **c.** 1 mM benzoylamidoacetonitrile; **d.** 0.3 mM papain; **e.** repeat of **b**., 1 month after mixing; **f.** 5% ethyl acetothioimidate in DMSO-d$_6$. In spectra **a, b, c**, and **e,** the unbound benzoylamidoacetonitrile (^{13}CN)-labeled peak is observed at 117 ppm, and in spectra **a** and **b**, the labeled peak of the bound species appears at 183 ppm. In spectra **a, b, d,** and **e,** the broad features are due to enzyme, and in spectra **a-e**, the peak at ~173 ppm is due to EDTA. (Figure and legend adapted from (*31*)).

(Appendix E). The effectiveness of using ^{19}F NMR experiments lies in the utility of ^{19}F as a nucleus to study by NMR spectroscopy. Like ^{1}H, it is 100% abundant in nature and like ^{1}H it has a high gyromagnetic ratio. ^{19}F is a good alternative to ^{1}H as a nucleus to study in a muscle fiber, since there are ^{1}H nuclei from all the muscle proteins, which would overwhelm the drug's signal. The NMR spectra suggested that dfbp-o was immobilized in the fiber. If we perfused the fiber with TFP, the concentration of signal of dfbp-o diminished. Furthermore, parallel with an overnight incubation in dfbp-o, the fiber contracted from 3 cm to 1 cm. Although these observations are not unambiguous, they support our hypothesis that dfbp-o targets cTnC to elicit its Ca^{2+}-sensitization *in situ*. Since the chemical structure of dfbp-o is different than levosimendan, we have synthesized another ^{19}F-containing analog (OR1896-CF$_3$) that more closely resembles levosimendan (Appendix F). We could repeat the same set of experiments we developed with dfbp-o to investigate whether the pyridazinone-class of drugs also function in a similar manner.

There are several limitations with the above ^{19}F experiments. 1) we still cannot say with certainty that the molecules are binding to troponin and 2) we are not answering the question everyone wants to know: *where does levosimendan bind in a muscle fiber?*. An alternative method that may shed light on this question is the technique developed by Irving, Sun, and colleagues called fluorescence for in situ structure (FISS), which can determine the conformation of troponin in working trabeculae (*34-36*). In FISS, cTnC is expressed with pairs of residues changed to cysteines that are then cross-linked by a bifunctional rhodamine (BR). The native cTnC in trabeculae is replaced by BR-labeled cTnC (BR-cTnC) and fluorescence polarization is used to determine the orientation of the BR dipole, and thus of the part of cTnC where it is attached in the trabeculae (*36*). FISS could be used to monitor the changes in the relative orientation of the N- and C-terminal domains of cTnC in trabeculae in response to binding drugs shown to bind cTnC *in vitro*. The differential effects on the domains of

cTnC revealed by these studies could allow the site of action and mechanism of the drugs to be determined *in situ*. Not only could we identify the binding site of levosimendan and other proposed N-terminal domain targeting drugs, but we could also investigate the role of the C-terminal domain of troponin in the mode of action of EMD 57033, EGCg, and resveratrol. This type of study would bridge the gap between the structural and functional studies of Ca^{2+}-sensitizers and significantly extend our understanding of the mechanism of these agents *in vivo*.

References

1.   Pineda-Sanabria, S. E., Robertson, I. M., and Sykes, B. D. (2011) Structure of trans-Resveratrol in Complex with the Cardiac Regulatory Protein Troponin C, *Biochemistry 50*, 1309-1320.

2.   Robertson, I. M., Li, M. X., and Sykes, B. D. (2009) Solution Structure of Human Cardiac Troponin C in Complex with the Green Tea Polyphenol, (-)-Epigallocatechin 3-Gallate, *J. Biol. Chem. 284*, 23012-23023.

3.   Wang, X., Li, M. X., Spyracopoulos, L., Beier, N., Chandra, M., Solaro, R. J., and Sykes, B. D. (2001) Structure of the C-domain of human cardiac troponin C in complex with the Ca2+ sensitizing drug EMD 57033, *J. Biol. Chem. 276*, 25456-25466.

4.   Liew, R., Stagg, M. A., MacLeod, K. T., and Collins, P. (2005) The red wine polyphenol, resveratrol, exerts acute direct actions on guinea-pig ventricular myocytes, *Eur. J. Pharmacol. 519*, 1-8.

5.   Solaro, R. J., Gambassi, G., Warshaw, D. M., Keller, M. R., Spurgeon, H. A., Beier, N., and Lakatta, E. G. (1993) Stereoselective Actions of Thiadiazinones on Canine Cardiac Myocytes and Myofilaments, *Circ. Res. 73*, 981-990.

6.   Tadano, N., Du, C. K., Yumoto, F., Morimoto, S., Ohta, M., Xie, M. F., Nagata, K., Zhan, D. Y., Lu, Q. W., Miwa, Y., Takahashi-Yanaga, F., Tanokura, M., Ohtsuki, I., and Sasaguri, T. (2010) Biological actions of green tea catechins on cardiac troponin C, *Br. J. Pharmacol. 161*, 1034-1043.

7.   Li, M. X., Spyracopoulos, L., Beier, N., Putkey, J. A., and Sykes, B. D. (2000) Interaction of cardiac troponin C with Ca2+ sensitizer EMD 57033 and cardiac troponin I inhibitory peptide, *Biochemistry 39*, 8782-8790.

8.   Sorsa, T., Pollesello, P., and Solaro, R. J. (2004) The contractile apparatus as a target for drugs against heart failure: Interaction of levosimendan, a calcium sensitiser, with cardiac troponin c, *Mol. Cell. Biochem. 266*, 87-107.

9.   Hoffman, R. M. B., and Sykes, B. D. (2009) Structure of the Inhibitor W7 Bound to the Regulatory Domain of Cardiac Troponin C, *Biochemistry 48*, 5541-5552.

10.   Oleszczuk, M., Robertson, I. M., Li, M. X., and Sykes, B. D. (2010) Solution structure of the regulatory domain of human cardiac troponin C in complex with the switch region of cardiac troponin I and W7: The basis of W7 as an inhibitor of cardiac muscle contraction, *J. Mol. Cell. Cardiol. 48*, 925-933.

11.   Robertson, I. M., Sun, Y. B., Li, M. X., and Sykes, B. D. (2010) A structural and functional perspective into the mechanism of Ca2+-sensitizers that target the cardiac troponin complex, *J. Mol. Cell. Cardiol. 49*, 1031-1041.

12. Sia, S. K., Li, M. X., Spyracopoulos, L., Gagne, S. M., Liu, W., Putkey, J. A., and Sykes, B. D. (1997) Structure of cardiac muscle troponin C unexpectedly reveals a closed regulatory domain, *J. Biol. Chem. 272*, 18216-18221.

13. Li, G., Martin, A. F., and Solaro, J. R. (2001) Localization of regions of troponin I important in deactivation of cardiac myofilaments by acidic pH, *J. Mol. Cell. Cardiol. 33*, 1309-1320.

14. Varughese, J. F., Baxley, T., Chalovich, J. M., and Li, Y. (2011) A computational and experimental approach to investigate bepridil binding with cardiac troponin, *J. Phys. Chem. B 115*, 2392-2400.

15. Solaro, R. J., Bousquet, P., and Johnson, J. D. (1986) Stimulation of Cardiac Myofilament Force, Atpase Activity and Troponin-C Ca++ Binding by Bepridil, *J. Pharmacol. Exp. Ther. 238*, 502-507.

16. Endoh, M. (2002) Mechanisms of action of novel cardiotonic agents, *J. Cardiovasc. Pharmacol. 40*, 323-338.

17. Lehtonen, L., and Poder, P. (2007) The utility of levosimendan in the treatment of heart failure, *Ann. Med. 39*, 2-17.

18. Edes, I., Kiss, E., Kitada, Y., Powers, F. M., Papp, J. G., Kranias, E. G., and Solaro, R. J. (1995) Effects of Levosimendan, a Cardiotonic Agent Targeted to Troponin-C, on Cardiac-Function and on Phosphorylation and Ca2+ Sensitivity of Cardiac Myofibrils and Sarcoplasmic-Reticulum in Guinea-Pig Heart, *Circ. Res. 77*, 107-113.

19. Pollesello, P., Ovaska, M., Kaivola, J., Tilgmann, C., Lundstrom, K., Kalkkinen, N., Ulmanen, I., Nissinen, E., and Taskinen, J. (1994) Binding of a New Ca2+ Sensitizer, Levosimendan, to Recombinant Human Cardiac Troponin-C - a Molecular Modeling, Fluorescence Probe, and Proton Nuclear-Magnetic-Resonance Study, *J. Biol. Chem. 269*, 28584-28590.

20. Haikala, H., Kaivola, J., Nissinen, E., Wall, P., Levijoki, J., and Linden, I. B. (1995) Cardiac Troponin-C as a Target Protein for a Novel Calcium Sensitizing Drug, Levosimendan, *J. Mol. Cell. Cardiol. 27*, 1859-1866.

21. Haikala, H., Nissinen, E., Etemadzadeh, E., Levijoki, J., and Linden, I. B. (1995) Troponin C-Mediated Calcium Sensitization Induced by Levosimendan Does Not Impair Relaxation, *J. Cardiovasc. Pharmacol. 25*, 794-801.

22. Satyshur, K. A., Rao, S. T., Pyzalska, D., Drendel, W., Greaser, M., and Sundaralingam, M. (1988) Refined structure of chicken skeletal muscle troponin C in the two-calcium state at 2-A resolution, *J. Biol. Chem. 263*, 1628-1647.

23. Kleerekoper, Q., and Putkey, J. A. (1999) Drug binding to cardiac troponin C, *J. Biol. Chem. 274*, 23932-23939.

24. Sorsa, T., Heikkinen, S., Abbott, M. B., Abusamhadneh, E., Laakso, T., Tilgmann, C., Serimaa, R., Annila, A., Rosevear, P. R., Drakenberg, T., Pollesello, P., and Kilpelainen, I. (2001) Binding of

levosimendan, a calcium sensitizer, to cardiac troponin C, *J. Biol. Chem. 276*, 9337-9343.

25. Robertson, I. M., Baryshnikova, O. K., Li, M. X., and Sykes, B. D. (2008) Defining the binding site of levosimendan and its analogues in a regulatory cardiac troponin C-troponin I complex, *Biochemistry 47*, 7485-7495.

26. Pintacuda, G., John, M., Su, X. C., and Otting, G. (2007) NMR structure determination of protein-ligand complexes by lanthanide labeling, *Acc. Chem. Res. 40*, 206-212.

27. Peach, M. E. (1974) *The Chemistry of the Thiol Group, Part 2*, John Wright & Sons Ltd.

28. Schaefer, F. C. (1970) *The Chemistry of the Cyano Group*, John Wiley & Sons.

29. Crane, S. N., Black, W. C., Palmer, J. T., Davis, D. E., Setti, E., Robichaud, J., Paquet, J., Oballa, R. M., Bayly, C. I., McKay, D. J., Somoza, J. R., Chauret, N., Seto, C., Scheigetz, J., Wesolowski, G., Masse, F., Desmarais, S., and Ouellet, M. (2006) beta-substituted cyclohexanecarboxamide: A nonpeptidic framework for the design of potent inhibitors of cathepsin K, *J. Med. Chem. 49*, 1066-1079.

30. Altmann, E., Cowan-Jacob, S. W., and Missbach, M. (2004) Novel purine nitrile derived inhibitors of the cysteine protease cathepsin K, *J. Med. Chem. 47*, 5833-5836.

31. Brisson, J. R., Carey, P. R., and Storer, A. C. (1986) Benzoylamidoacetonitrile Is Bound as a Thioimidate in the Active-Site of Papain, *J. Biol. Chem. 261*, 9087-9089.

32. Moon, J. B., Coleman, R. S., and Hanzlik, R. P. (1986) Reversible Covalent Inhibition of Papain by a Peptide Nitrile - C-13 Nmr Evidence for a Thioimidate Ester Adduct, *J. Am. Chem. Soc. 108*, 1350-1351.

33. Chaturve.Rk, Macmahon, A. E., and Schmir, G. L. (1967) Hydrolysis of Thioimidate Esters . Tetrahedral Intermediates and General Acid Catalysis, *J. Am. Chem. Soc. 89*, 6984-&.

34. Ferguson, R. E., Sun, Y. B., Mercier, P., Brack, A. S., Sykes, B. D., Corrie, J. E. T., Trentham, D. R., and Irving, M. (2003) In situ orientations of protein domains: Troponin C in skeletal muscle fibers, *Mol. Cell 11*, 865-874.

35. Corrie, J. E. T., Brandmeier, B. D., Ferguson, R. E., Trentham, D. R., Kendrick-Jones, I., Hopkins, S. C., van der Heide, U. A., Goldman, Y. E., Sabido-David, C., Dale, R. E., Criddle, S., and Irving, M. (1999) Dynamic measurement of myosin light-chain-domain tilt and twist in muscle contraction, *Nature 400*, 425-430.

36. Sun, Y. B., Lou, F., and Irving, M. (2009) Calcium- and myosin-dependent changes in troponin structure during activation of heart muscle, *Journal of Physiology-London 587*, 155-163.

37.   McKay, R. T., Saltibus, L. F., Li, M. X., and Sykes, B. D. (2000) Energetics of the induced structural change in a Ca2+ regulatory protein: Ca2+ and troponin I peptide binding to the E41A mutant of the N-domain of skeletal troponin C, *Biochemistry 39*, 12731-12738.

Appendix A.

The evaluation of isotope editing and filtering for protein-ligand interaction elucidation by NMR*

Summary

A series of experiments that aid in the structural characterization of protein-ligand complexes by NMR have been assessed. Methods have been established to identify intermolecular NOEs between labeled proteins and unlabeled peptides and/or drug ligands, while omitting signal from intramolecular NOEs within both labeled and unlabeled constituents. The protein-peptide complex chosen to illustrate the value of such techniques is the C-terminal domain of the cardiac muscle regulatory protein Troponin C ($cCTnC_{91-161}$) bound to the N-terminal domain of the inhibitory protein Troponin I ($cTnI_{35-72}$). The measurement of intermolecular NOE contacts between cCTnC and $cTnI_{35-72}$ was accomplished by the ^{13}C-edited/filtered NOESY-HSQC (19) and ^{13}C-edited/filtered HMQC-NOESY (9) experiments. The assignment of the bound peptide was facilitated by the ^{13}C, ^{15}N-filtered TOCSY, and ^{13}C, ^{15}N-filtered NOESY experiments (4, 6, 15).

Introduction

The determination of structures of protein-ligand complexes is an important role of structural biology, but is also one of the most experimentally challenging aspects of solution NMR. Of particular interest is the structural assessment of unlabeled ligands such as peptides and/or drugs associated with uniformly labeled proteins by isotope filtering (16). Characterizing the binding interface can be difficult, especially when trying to elucidate intermolecular contacts between an unlabeled ligand and a labeled protein. Several methods have been designed in which the signals from the labeled protein are filtered, leaving only signals from the unlabeled ligand to be detected, or the reverse. The wide variation of ^{1}H-^{13}C scalar coupling constants (120-220 Hz) make isotope-based NMR spectral purging experiments difficult to design. In this review, isotope filtering strategies will be introduced, experimentally tested, and compared.

The ^{13}C-edited/filtered HMQC-NOESY (9) and ^{13}C-edited/filtered NOESY-HSQC (19) are variations of edited/filtered NOESY schemes that isolate NOEs between a labeled protein and an unlabeled ligand, while filtering out intramolecular NOE contacts either within the labeled protein or unlabeled ligand. The other series of experiments that will be described, the two-dimensional (2D) ^{13}C,^{15}N-filtered TOCSY and 2D ^{13}C,^{15}N-filtered NOESY (4, 6, 15) display spectra of the unlabeled ligand with no intramolecular or intermolecular NOEs from the labeled protein. The ^{13}C-edited/filtered HMQC-NOESY, and two 2D ^{13}C,^{15}N-filtered experiments use a similar approach to filter signals from the labeled protein. The experiments use nominal one-bond ^{1}J-couplings between a labeled isotope (^{13}C, or ^{15}N) and a ^{1}H to tune delay periods. The tuned delays generate multiple quantum coherences (MQCs) via the ^{1}J-coupling Hamiltonian ($\hat{H}$), which are unobservable and also purged using pulsed field gradients (PFGs). The ^{13}C-edited/filtered NOESY-HSQC uses an

elegant approach; delays are used that allow the one-bond ^{1}H-^{13}C coupling Ĥ to mimic the effect of a broad-band composite 90° pulse, such that a wide range of $^1J_{HC}$ values can be filtered.

The two edited/filtered experiments; the ^{13}C-edited/filtered HMQC-NOESY and ^{13}C-edited/filtered NOESY-HSQC are examples of experiments that should yield similar results, but attain them via different routes. The ^{13}C-edited/filtered HMQC-NOESY first selects for ^{1}H resonance signals coupled to ^{13}C (F_1-edited) and then after the mixing period filters out the same ^{1}H-^{13}C signals (F_3-filtered) detection of the unlabeled ligand ^{1}H signals occurs during t_3. In the ^{13}C-edited/filtered NOESY-HSQC the opposite path of magnetization transfer is followed; first the ^{1}H-^{12}C nuclei is selected for (F_1-filtered) and following the NOE transfer the ^{1}H-^{13}C is selected (F_3-edited). In the ^{13}C-edited/filtered NOESY-HSQC, the final signal detected during acquisition is the ^{1}H-^{13}C coupled nuclei. Figure A-1 presents a schematic explanation of the two different experiments described above.

Other methods have been developed to improve the efficiency of the edited/filtered experiments. Zwahlen *et al.* (22) and Kupče *et al.* (8) used the approximate correlation between $^1J_{HC}$ and ^{13}C chemical shift to design an isotope-filter. An adiabatic pulse is applied, such that the frequency is swept according to the ^{13}C chemical shift range, and the signal from the labeled protein is inverted according to $^1J_{HC}$. More recently, Valentine *et al*. (21) have developed a new procedure in which they have combined the composite-rotation and adiabatic-sweeping techniques to improve signal filtering and the removal of artifacts. In practice we have found that the simpler pulse sequences can be easily implemented on modern NMR spectrometers and can effectively filter protein signals.

The biological system chosen to examine the efficiency of the isotope edited/filtered experiments is the cardiac contractile network. The C-terminal domain of the contractile regulatory protein Troponin C (cCTnC) and the N-terminal region of the inhibitory protein Troponin I

Protein   Ligand

$^{13}C-^1H$ $^1H-^{12}C$ $^{13}C-^1H$ $^1H-^{12}C$

F_1-edited, F_3-filtered HMQC-NOESY   **F_1-filtered, F_3-edited NOESY-HMQC**
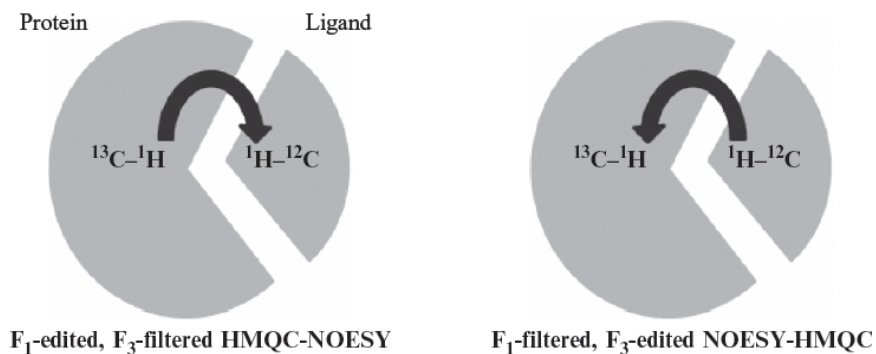
Figure A-1. An introduction into the edited/filtered experiment nomenclature. The *F_1-edited, F_3-filtered* HMQC-NOESY is an experiment that first detects the signals from a proton attached on the ^{13}C nuclei, and then after the NOE transfer, filters out the ^{13}C attached protons prior to detection. *F_1-filtered, F_3-edited* NOESY-HSQC initially suppresses the signal from an attached proton to the heteronuclei, and following the NOE mixing period detects the $^1H^{-13}C$ signal.

(cTnI$_{35-72}$) associate to form a tight complex (11). Contraction in cardiac muscle is stimulated by the binding of Ca^{2+} to the N-terminal domain of cTnC (cNTnC), subsequently cNTnC opens and binds the C-terminal region of cTnI (otherwise associated with actin) (12). The interaction between cCTnC and cTnI$_{35-72}$ is maintained during the contraction and relaxation cycle of muscle. The complex has a dissociation constant of 1 μM (11), making it ideal for studying efficacy of the edited/filtered experiments. The previously determined structure of cCTnC-cTnI$_{40-71}$ (20) will also help gauge the efficiency of the filter, and accuracy of the NOE assignments. Of course, the experiments described here may be successfully applied to observe contacts made between a labeled protein and other unlabeled ligands, such as a drug. The object of this report is to use the cCTnC-cTnI$_{35-72}$ system as a model to compare the advantages of the two edited/filtered experiments, as well as describe a technique for generating a structure of a protein associated with a ligand.

Experimental procedures

The expression vector for cardiac Troponin C$_{91-161}$ (cCTnC) was designed (2) and uniformly labeled ^{13}C, ^{15}N cCTnC was isolated from *E. coli* as previously described (10). The unlabeled peptide cTnI$_{35-72}$, Ac-AKKKSKISASRKLQLKT-LLLQIAKQELEREAEERRGEK-NH$_2$ was synthetically prepared by GL Biochem Ltd. All NMR experiments described in the article were run at 30ºC on Varian Inova 600 MHz and 800 MHz spectrometers. Details for the particular experiments are given in the corresponding figure legends. Figure A-2 shows the ^{13}C *F$_1$-edited, F$_3$-filtered* HMQC-NOESY, and the ^{13}C *F$_1$-filtered, F$_3$-edited* NOESY-HSQC as well as the ^{13}C,^{15}N-filtered NOESY. Detailed discussions of the pulse schemes may be found in references (4, 6, 9, 15, 19). All acquired spectra were processed with NMRPipe (3), and analyzed with NMRView (7). The previously determined structures used to illustrate the topics

presented in this paper are the Ca^{2+} saturated chicken cCTnC (18) (pdb: 3CTN) and the troponin complex core structure (20) (pdb:1J1E).

Theory

The two ^{13}C edited/filtered experiments, the ^{13}C-edited/filtered HMQC-NOESY and the ^{13}C-edited/filtered NOESY-HSQC as well as the ^{13}C,^{15}N-filtered NOESY are illustrated in Figure A-2. In the text below a brief description of each of the experiments is provided. A product operator analysis on the purging technique used in the ^{13}C-edited/filtered HMQC-NOESY is also provided at the end of the chapter.

^{13}C-edited/filtered NOESY-HSQC (F$_1$-filtered, F$_3$-edited)

In this experiment, the general pulse scheme (Figure A-2(A)) proceeds as follows. Initially a filter removes any signal originating from either ^{1}H-^{13}C or ^{1}H-^{15}N. The filter period uses a semi-constant time technique to frequency label a ^{1}H attached to ^{12}C. Following the initial filter and semi-CT time, a mixing period allows for the build-up of NOEs between unlabeled ligand and labeled protein.

After the NOE mixing period, ^{1}H magnetization is transferred to ^{13}C of the labeled protein by the standard INEPT (employing composite 180º ^{13}C pulses). The ^{13}C - spins are frequency labeled and the magnetization is transferred back to the protons via a reverse INEPT for detection during acquisition (t_3). Since detection occurs on the labeled protein, the ^{13}C must be decoupled, therefore the length of the acquisition time/resolution in t_3 is limited.

The main concept behind the filter applied in the ^{13}C-edited/filtered NOESY-HSQC is that the sequence uses composite rotations generated by the ^{1}H-^{13}C ^{1}J-coupling Ĥ to compensate for a range of ^{1}J$_{HC}$ instead of

Figure A-2. Examples of pulse sequences that filter out signals from isotropically labeled proteins. For all of the pulse sequences, the narrow rectangles represent 90º pulses, and the wide rectangles are indicative of 180º pulses. All the pulse phases are along x, unless otherwise indicated. For simplicity, the phase cycling from the pulse sequences has been omitted. The delay τ_m represents the NOE mixing time present in all three of the experiments. (A) The ^{13}C-edited/filtered NOESY-HSQC pulse scheme as presented by Stuart *et al.* (19). The unfilled pulses represent composite 180º pulses that function to invert over the wide range of ^{13}C resonances. The pulse sequence also purges ^{15}N coupled protons, and not show here is the [13]CO decoupling applied during t_2. The delays selected for the selection of the coupling constant J_{HC} = 140 Hz are τ = 3.57 ms, τ_a = 5.355 ms + $0.5\tau_{c0}$ – $n\Delta\tau$, τ_b = 0.5(3.57ms - τ_{c0}) + $n\Delta\tau$, τ_c = τ_{c0} + n(1/SW1 – $2\Delta\tau$), $\Delta\tau$ = (5.425 ms – τ_{a0})/(N-1), τ_{a0} = 0.9 ms, τ_{c0} = 0.65 ms, τ_d = 1.785 ms and τ_e = 1.785 ms. In order to optimize the filter efficiency for $^1J_{HN}$, the delays should be set to τ_a - τ_b + 2ζ = $1/(2J_{HN})$. For more detailed descriptions on the selection of the different delays refer to Stuart *et al.* (19). The decoupling of the ^{13}C nuclei during acquisition is accomplished by the GARP method (17). The gradients applied are g1 = (1.5 ms, 17 G/cm); g2 = (450 μs 10.4 G/cm); g3 = (450 μs 24 G/cm); g4 = (450 μs -13.8 G/cm); g5 = (450 μs 27.6 G/cm); g6 = (1 ms, 7 G/cm); g7 = (500 μs 7 G/cm); g8 = (500 μs 10.4 G/cm); g9 = (1.2 ms, -17.6 G/cm); g10 = (300 μs 20.7 G/cm). (B) The ^{13}C-edited/filtered HMQC-NOESY pulse scheme. This pulse scheme has been simplified from the original (9) including the removal of the ^{15}N purging and [13]CO decoupling. This simplified version is optimized for methyl-methyl NOEs, and is best run in D_2O. The delay τ_a = 3.57 ms during the HMQC transfer was chosen to select for aliphatic ^{13}C coupled protons (J_{HC} = 140 Hz). The delays in the filtering period after the NOE mixing time; τ_b = 4.17 ms, τ_c = 3.33 ms and τ_d = 0.84 ms were chosen to cover a range of aliphatic ^{13}C coupled ^1H signals (120-150 Hz). The gradient strengths and lengths are: g1 = (0.1 ms, 10 G/cm); g2 = (1 ms, 5 G/cm); g3 = (0.4 ms, 8 G/cm). (C) The pulse sequence applied for observing NOEs within the unlabeled ligand, the ^{13}C, ^{15}N filtered NOESY experiment (4, 5, 15). The pulse sequence was written by L.E. Kay 1996, and incorporated into the Varian BioPack pulse sequence suite. The delays chosen to filter the aliphatic and aromatic [13]C-^1H, as well as the ^1H scalar coupled to ^{15}N were; τ_a = 4.0 ms, τ_b = 0.43 ms, τ_c = 1.07 ms, τ_d = 3.125 ms, τ_e = 0.625 ms, τ_f = 1.75 ms. The gradients lengths and strengths are; g1 = (300 μs 20.420 G/cm); g2 = (1.0 ms, 30.630 G/cm); g3 = (500 μs 4.084 G/cm); g4 = (500 μs 51.050 G/cm).
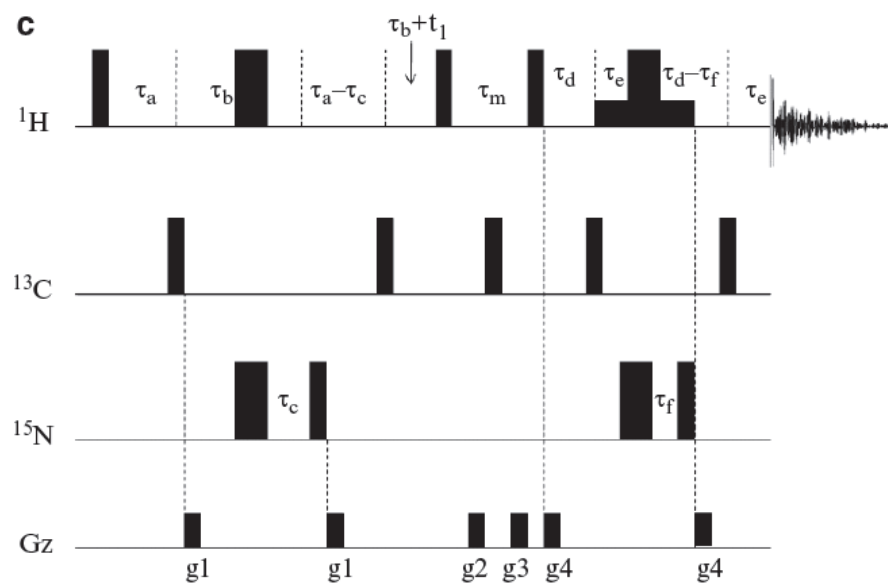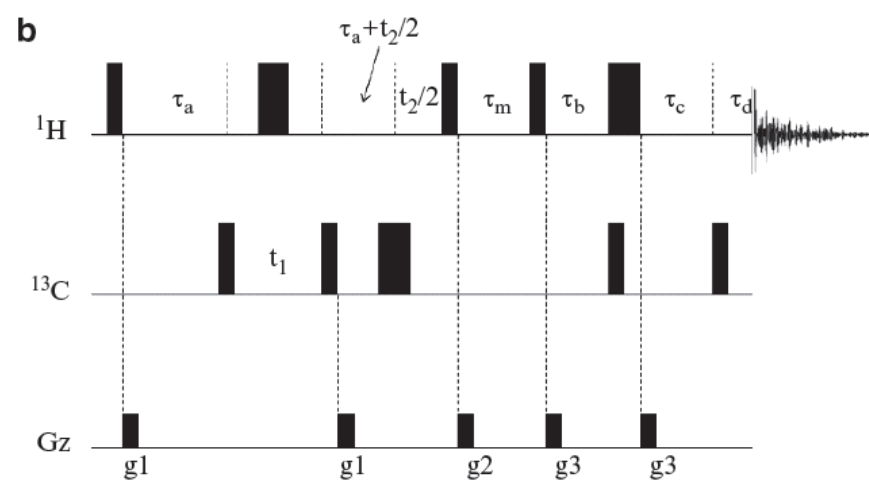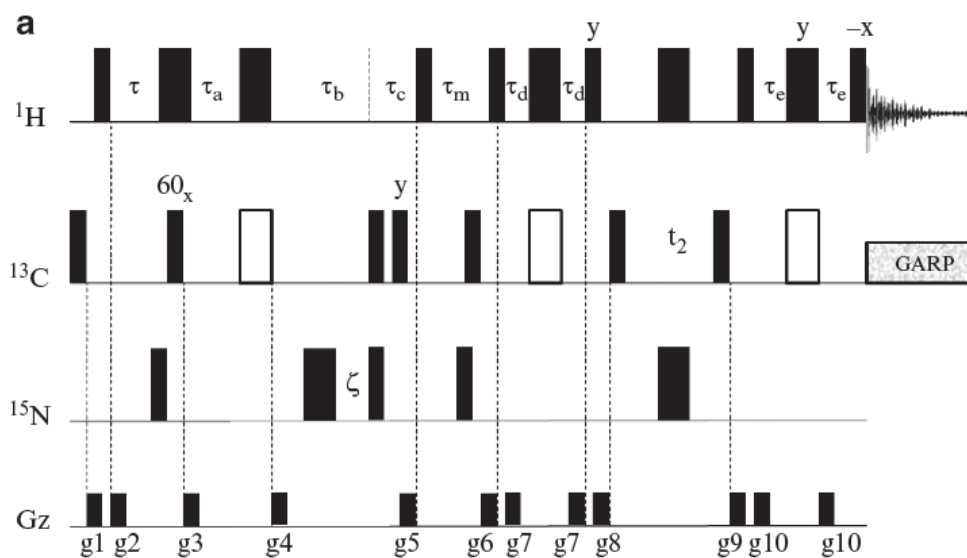
relying on the precise selection of delays to filter signals from the labeled protein (see below).

The efficiency (ε) of the filter is given by the following expression (1):

$$\varepsilon = \cos(\pi\,^1J_{HC}\tau)\cos(2\pi\,^1J_{HC}\tau) + 0.5\sin(\pi\,^1J_{HC}\tau)\sin(2\pi\,^1J_{HC}\tau) = \cos^3(\pi\,^1J_{HC}\tau)$$

where the filter is tuned to $^1J_0 = 1/(2\tau)$. The efficiency of the filter (ε) is equal to 1 when $^1J_{HC} = 0$ (uncoupled proton), and equal to 0 when $^1J_{HC} = {}^1J_0$. The filter has a high filtering efficiency for a range of 50 Hz; so that for the selection of $^1J_0 = 140$ Hz, the filter exhibits good signal suppression from 115 – 165 Hz. For more details regarding the efficiency of the isotope filter or other aspects of the pulse sequence see Stuart *et al.* (19).

^{13}C-edited/filtered HMQC-NOESY (F_1-edited, F_3-filtered)

The ^{13}C-edited/filtered HMQC-NOESY represents a different method to detect intermolecular NOE contacts between a labeled protein and unlabeled ligand (refer to Figure A-2(B) for the pulse scheme). The magnetization is first transferred from the ^{1}H to the attached ^{13}C *via* an HMQC transfer, and is subsequently labeled with the ^{13}C chemical shift during t_1. The delay τ_a is set to $1/(2\,^1J_{HC})$, where $^1J_{HC} = 140$ Hz for aliphatic ^{1}H-^{13}C. Following t_1, the magnetization is transferred back to ^{1}H and the chemical shifts are recorded during t_2.

Following ^{1}H chemical shift labeling, the magnetization is rotated along the z-axis for NOE transfer wherein the ^{1}H-^{13}C magnetization is transferred to the ^{1}H-^{12}C. After the mixing time the magnetization is returned to the transverse plane, now labeled with ^{13}C attached ^{1}H (t_2) and ^{13}C (t_1) chemical shifts, as well as the ^{1}H-^{13}C $\leftrightarrow$ ^{1}H-^{12}C NOE. The final stage prior to detection involved a purging period tuned to two different coupling constants (120 Hz, and 150 Hz). This double-tuned filter removes

isotope labeled signals leaving behind only the uncoupled protons for detection (t_3).

The disadvantage of the double-tuned filter is that the coupling constants do not cover the entire range of $^1J_{HC}$ possibly present in a protein. In the pulse sequence put forth by Palmer and colleagues (19) discussed earlier, the selection of a single coupling constant provides filtration for a range of $^1J_{HC}$ values. The advantage of the ^{13}C edited/filtered HMQC-NOESY is that since no ^{13}C decoupling is present during t_3, there is no limitation on the acquisition time (t_3) and therefore the resolution for the unlabeled ligand.

$^{13}C,^{15}N$ filtered NOESY and $^{13}C,^{15}N$ filtered TOCSY

The pulse sequence employed for the detection of intramolecular NOE contacts within the unlabeled peptide is displayed in Figure A-2(c). The magnetization transfer up until the mixing time is the exact same in the ^{13}C,^{15}N filtered TOCSY and therefore theoretical discussion will focus on the filtering in the ^{13}C,^{15}N filtered NOESY. The first ^{1}H 90_x pulse will flip I_z into the transverse plane. If the delay τ_a is tuned correctly, after the evolution period ($\tau_a = 1/2^1J_{HC}$) the magnetization is in complete anti-phase with respect to the ^{1}J-coupled ^{13}C. In the scenario where the delay is not tuned accurately, the magnetization will be a mixture of anti-phase and in-phase operators. The $^1J_{HN}$ coupling will also generate proton nitrogen anti-phase/in-phase mixture that has evolved under the ^{15}N-^{1}H scalar coupling for the duration τ_a.

The subsequent ^{13}C 90_x pulse produces the unobservable MQC for the properly tuned delay. The gradient will de-phase all transverse magnetization. The next delay, $\tau_b = \tau_a - 1/2^1J_{HC2}$ is tuned to a slightly different $^1J_{HC}$, so that if τ_a was inaccurately tuned, by the second ^{13}C 90_x pulse the in-phase magnetization not purged previously, will have evolved into anti-phase magnetization. Following the ^{13}C 90_x pulse, the

magnetization is converted into MQC; which is not detected during the acquisition (t_3). After the delay τ_c ($\tau_c = 1/2{}^1J_{HN} - \tau_a - \tau_b$), the ^{15}N one-bond coupled protons will have evolved into anti-phase magnetization. So the applied 90_x pulse on the ^{15}N will yield MQC, which is subsequently de-phased by a gradient.

In order to refocus the proton chemical shift, time periods $\tau_a - \tau_c$ and τ_b are followed. The delay $\tau_a - \tau_c$ is also necessary to convert the magnetization not completely removed in the first purging period (τ_a) to anti-phase prior to the second carbon 90_x pulse. Finally, just preceding the mixing period, ^{1}H (on ^{12}C nuclei) chemical shift is recorded during t_1. After the mixing time the signal is in the transverse plane, and there is another filtering period (in the ^{13}C,^{15}N filtered NOESY, but not in the ^{13}C,^{15}N filtered TOCSY). In this period, larger coupling constants are chosen for the delays in order to filter signals originating from aromatic couplings, $^1J_{HC1}$ and $^1J_{HC2} \sim 160$ and 200 Hz. In this fashion, one can obtain an artifact-free "finger-print" spectrum with purging of aliphatic signals in the F_1 dimension, and purging of amide and aromatic protein signals in the F_2 dimension. In the ^{13}C,^{15}N filtered TOCSY pulse sequence (pulse scheme not shown), the ^{1}H-^{13}C magnetization is initially filtered as in the ^{13}C,^{15}N filtered NOESY, and then the ^{1}H-^{12}C signal undergoes a DIPSI mixing (1) in order to observe ^{1}H-^{1}H correlations from intraresidue ^{1}H spin systems.

Results and discussion

The structure of the calcium saturated cCTnC bound with the N-terminal region of cTnI (cTnI$_{40-71}$) is displayed in Figure A-3(A) (20). The tight association and known structure of this complex makes this system a perfect model to study the efficacy of the various filtering techniques. An alignment of the X-ray crystal structure of cCTnC bound to cNTnI (cTnI$_{40-71}$) with the solution structure of the chicken cCTnC (18) (Figure A-3(B)) demonstrates the high degree of similarity between the two structures
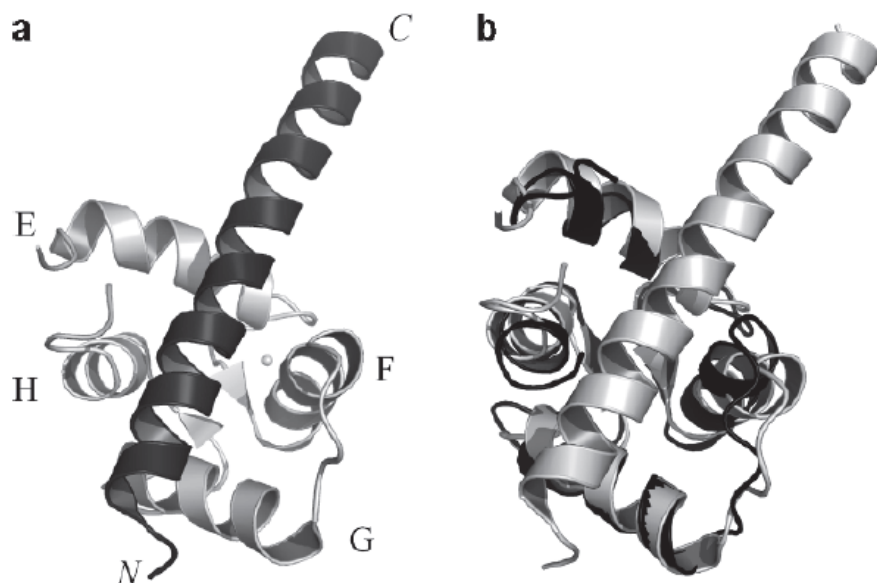
Figure A-3. A ribbon diagram of the C domain of the human cardiac Troponin C in complex with cardiac Troponin I (40-71) (pdb: 1J1E). (A) In light grey is the calcium saturated cCTnC, and in black is $cTnI_{40-71}$. The C domain diagram is taken from the X-ray crystal structure of the core domain of the troponin complex (cTnC-cTnI-cTnT) (20). The helices are labeled on the cCTnC, and the N and C termini are labeled on the $cTnI_{40-71}$. (B) The $cCTnC$-$cTnI_{40-71}$ complex from (A) is colored completely in light grey. The structure is aligned with the chicken C domain of cTnC (in black) described by Sia *et al.* (18) (pdb: 3CTN) in the absence of $cTnI_{40-71}$. The only sequence difference between the two domains is in amino acid 93 (near the N terminus of the C domain). In cCTnC (light grey) the amino acid is S93, while T93 (black). The RMSD for the backbone Cα was 1.5 Å and produced by PYMOL.

(RMSD = 1.5 Å for the backbone Cα). The minimal structural change between the two proteins highlights the significance of these different techniques in solving protein structure. If the structural change of a protein is small when binding a ligand, then the elucidation of the protein-ligand contacts in the binding interface represents a crucial aspect in determining an accurate complex structure. Another important principle in protein-ligand complexes is exemplified in Figure A-4. The interface between the cCTnC-cTnI$_{40-71}$ contains almost exclusively hydrophobic methyl-methyl interactions. The prevalence of aliphatic ^{1}H in the protein-peptide interface allows for the selection of small sweep widths, and the use of a double-tuned filter (as is in the ^{13}C-edited/filtered HMQC-NOESY) is sufficient to cover the expected range of aliphatic ^{1}J$_{HC}$-couplings (120-150 Hz).

Before discussing the edited/filtered experiments we will briefly review the ^{13}C, ^{15}N filtered experiments. Figure A-5 shows the filtered (A) and unfiltered NOESY (B) spectra. The signal removed by employing the simple approach described in the theory section is evident. The selection of four different delays for four different coupling constants (125 Hz, 140 Hz, 160 Hz, and 200 Hz), and pulsed field gradients allows for exquisite filtering in the 'finger print' region. In the ^{13}C,^{15}N filtered TOCSY the aromatic purging period was not included, but still displayed good filtering (data not shown). In Figure A-6 the H$_N$-H$_\alpha$ region of the ^{13}C,^{15}N filtered NOESY and ^{13}C,^{15}N filtered TOCSY are overlaid and the sequential assignment strategy for the bound unlabeled peptide is illustrated. For a smaller ligand like a drug the assignment of the resonances would be simpler and the use of these filtered experiments may not be required if a one-dimensional spectrum can be unambiguously assigned.

The two edited/filtered experiments chosen for comparison of NOE transfer between unlabeled ligands and labeled proteins are the classical approach (4, 6, 9, 15, 16), which utilizes the evolution of the heteronuclear scalar coupling Ĥ to filter out signals from the isotropically labeled proteins, and the more recent approach discussed in Stuart *et al.* (19),
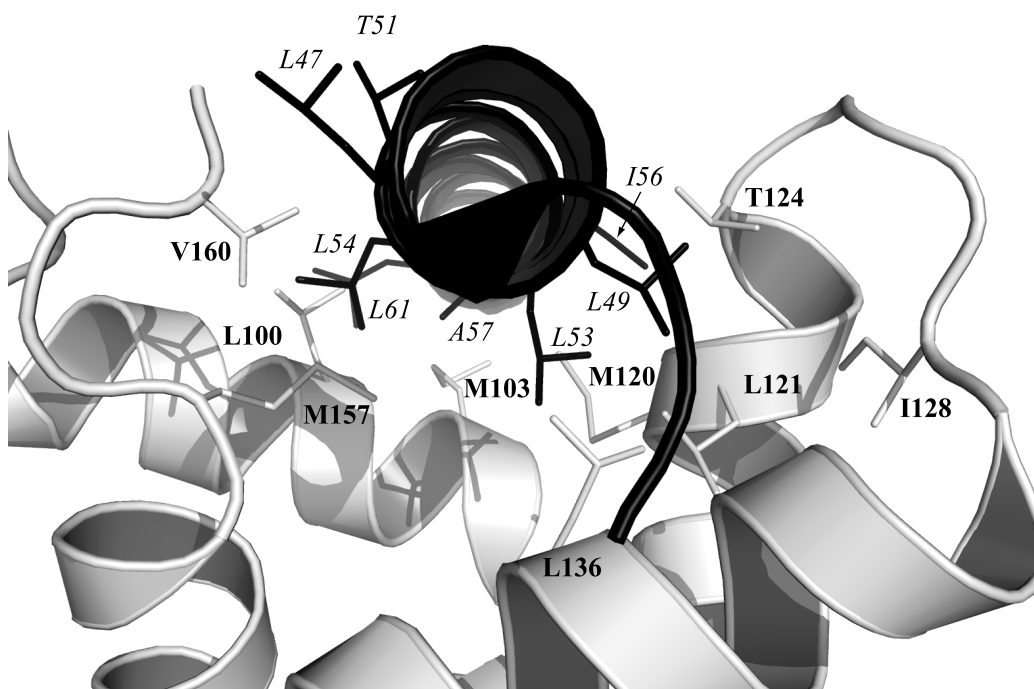
Figure A-4. A close up view of the ribbon diagram in Figure A-3 (A), rotated by 90º along the horizontal axis to emphasize the cCTnC-cTnI$_{35-72}$ interface. The color scheme employed in Figure A-3(A) is adopted here. An interesting aspect of the cCTnC-cTnI$_{40-71}$ interface is the predominance of methyl-methyl hydrophobic interactions. This feature of the protein-peptide interaction was considered when selecting the region to focus on for the ^{13}C-edited/filtered experiments (see text).
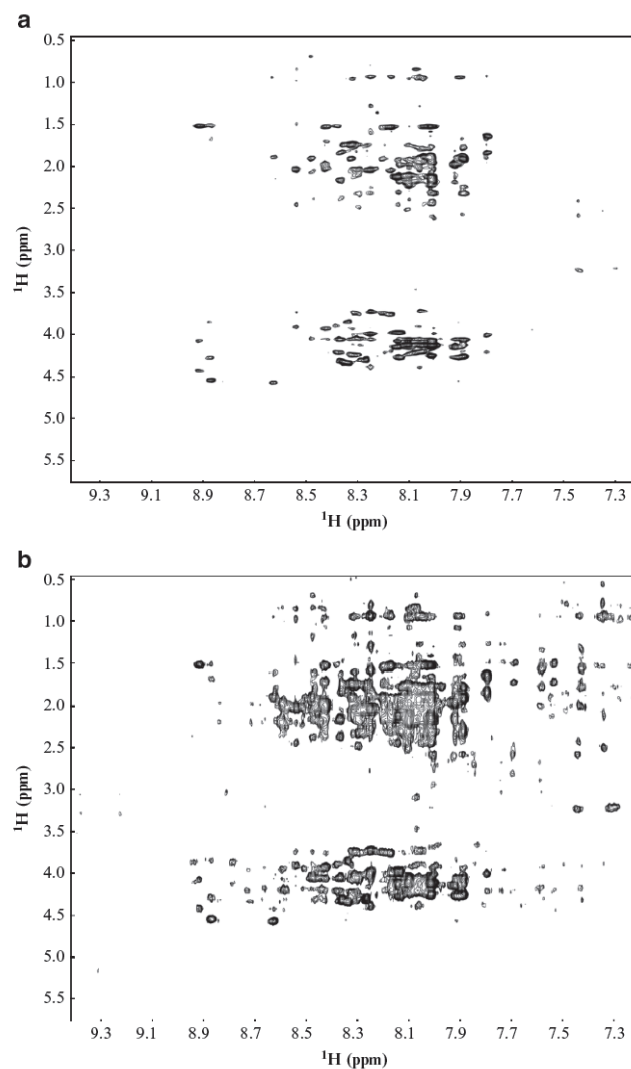
Figure A-5. The efficiency of the ^{13}C, ^{15}N filtered NOESY of the cCTnC•cTnI$_{35\text{-}72}$. The pulse scheme is presented in Figure A-2(C). The different $^1J_{HC}$ chosen for filtering out were 125 Hz, 140 Hz (both selected for filtering of aliphatic protons), 160 Hz and 200 Hz (for removal of ^{13}C aromatic protons). (A) A two-dimensional spectrum of the ^{13}C, ^{15}N filtered NOESY, with the filtering turned on, and in (B) the filtering was turned off. The number of points acquired in t_3 was 4096 and the number of increments was 256. The total number of transients was 64. (C) The filtering efficiency is visualized by the overlay of one-dimensional spectra acquired with 4096 points in detected dimension and 128 transients. In light grey is the unfiltered NOESY, ^{13}C and ^{15}N pulses have been turned to 0 dB, and in black is the ^{13}C, ^{15}N filtered NOESY. Notice the loss of signal within the amide region (inset in (C)), and the H$_N$-H$_{sidechain}$ region of the ^{13}C,^{15}N filtered NOESY spectrum (A).
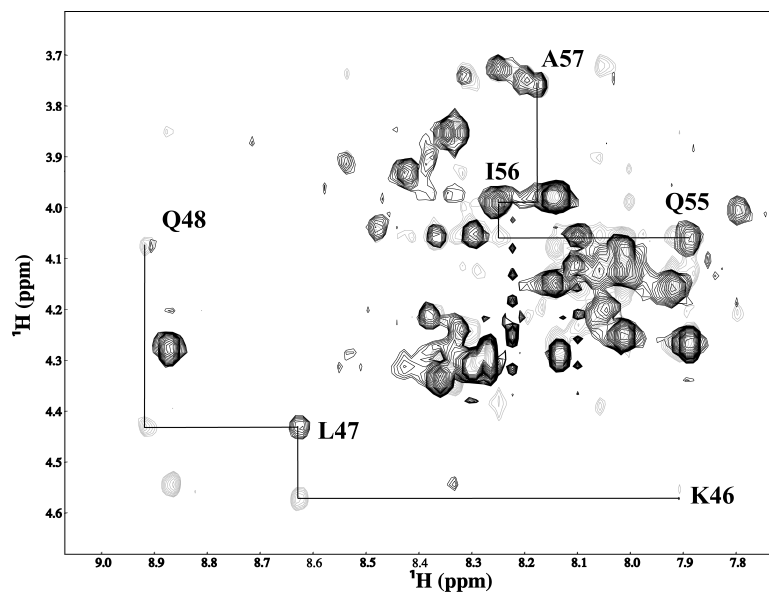
Figure A-6. The $^{13}C,^{15}N$ filtered NOESY (light grey) and $^{13}C,^{15}N$ filtered TOCSY (black) overlapped to illustrate the assignment of the unlabeled peptide when bound to the labeled protein. Both experiments had 32 transients, 512 increments and 4096 points acquired. The mixing times in the above spectra were, 80 ms for the $^{13}C,^{15}N$ filtered TOCSY, and 100 ms for the $^{13}C,^{15}N$ filtered NOESY. The region viewed here designates the amide protons coupled to the intraresidue Cα, and the interresidue Cα. Several small chains are labeled at the TOCSY peaks (intraresidue H_N - H_α).

which uses composite pulses to rotate the operators without relying on a specific ^{1}H-^{13}C coupling constant. See the theory section for a detailed description of the filtering strategies employed by the different methods. In Figure A-7, an expanded view of the two-dimensional spectrum from the ^{13}C-edited/filtered NOESY-HSQC is shown. The diagonal represents the signal that was not filtered during acquisition. Although not shown, the ^{13}C-edited/filtered HMQC-NOESY reveals an almost identical spectrum verifying the labeled peaks in Figure A-7 are NOEs. The labeled protein methyls were unambiguously assigned by the use of a 3D-^{13}C-edited/filtered HMQC-NOESY experiment and the conventional triple resonance experiments, such as the 3D-CBCACONNH (14), 3D-HNCACB (14), 3D-CCONH (5), and 3D-HCCONH (13). Care must be taken, however when attempting to assign peaks along the diagonal. In Figure A-7(B) the view from Figure A-4 is rotated by 180º about the vertical axis, so that now we are looking down the C terminus of the cTnI$_{40-71}$ peptide. The figure confirms the assigned contact in Figure A-7(A) between the L100 and M120 terminal methyls and the β-methyl of A57 of the peptide.

In order to address the potential advantages of the two filtering techniques, identical experiments were set up (see Figure A-8). The same number of increments and transients for each experiment were acquired. The only difference between the two experimental parameters lied within the number of points in the acquired dimension (t_3). This is due to the fact that in the ^{13}C-edited/filtered NOESY-HSQC experiment decoupling along the carbon channel is required during acquisition. In the ^{13}C-edited/filtered HMQC-NOESY no decoupling during detection permits the number of points acquired to depend solely on the resolution desired. The increase in resolution in the F_3 dimension (unlabeled ligand) is evident in the ^{13}C-edited/filtered HMQC-NOESY spectrum (Figure A-8(B)). There is an improvement on the labeled protein resolution of the ^{13}C-edited/filtered NOESY-HSQC when compared with the ^{13}C-edited/filtered HMQC-NOESY experiment. The improvement is because, even though there is
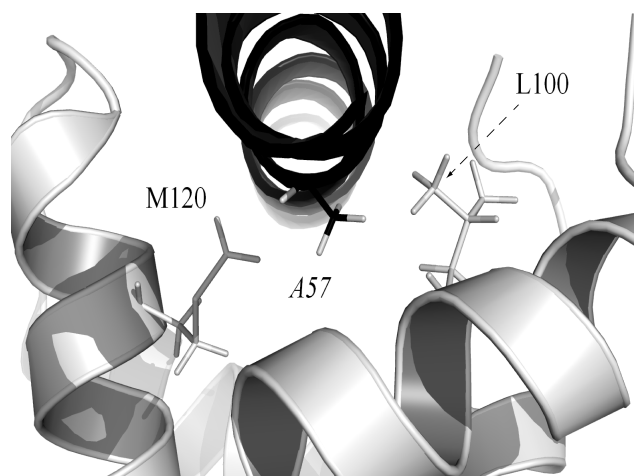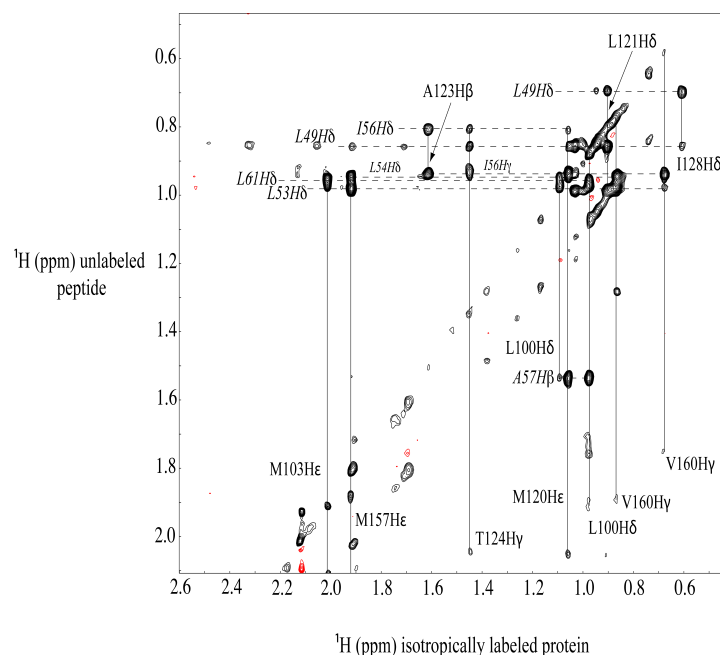
Figure A-7. (A) The assigned spectrum acquired from the ^{13}C-edited/filtered NOESY-HSQC experiment. The assigned peaks represent intermolecular NOEs between the labeled cCTnC and the unlabeled cTnI$_{35-72}$. Vertical lines represent peaks from the labeled protein, while the horizontal dotted lines are from the peptide. Peak labels shown in italics originate from the peptide. The number of transients taken was 64, 256 increments during F_1 and 392 points during the acquisition. The NOE mixing time was set to 150 ms. The sweep widths were 5.0 ppm in the F_1 and 5.0 ppm in F_3. (B) The coloring scheme is the same as in Figure A-3 (A). The peptide is in black, while the labeled protein is in grey. The NOE between A57 from the peptide and M120 and L100 from the peptide is assigned in (A) and then identified in (B) using the structure from Takeda *et al.* (pdb: 1J1E) (20).

decoupling during t_3 in the ^{13}C-edited/filtered NOESY-HSQC experiment, the time restriction prevents the experimentalist to acquire as many increments in the ^{13}C-edited/filtered HMQC-NOESY during F_1.

The filtering efficiency is not immediately clear when comparing the two spectra in Figure A-8. Since there is a high proportion of methyl-methyl contacts in the interface between the cCTnC and cTnI$_{35-72}$ (see Figure A-4), the sweep widths and carrier frequencies selected focus on the aliphatic region. Thus the increased efficiency of the filter as discussed in Stuart *et al.* (19), is of less value in the overall performance of the experiments. Instead, other considerations such as resolution and acquisition time become more relevant when selecting the appropriate pulse sequence.

Conclusion

In the present review, an overview of several of the different methods applied to filter signals from a uniformly labeled protein, while maintaining the signal from an unlabeled bound ligand is provided. The large range in the one-bond ^{1}J-couplings between ^{1}H and ^{13}C and ^{13}C chemical shift makes the efficient purging of ^{13}C,^{15}N isotropically labeled protein signals challenging. More recent approaches have been described (8, 21-22) which attempt to improve on the filtering efficiency of the approaches described here. In many situations involving protein-ligand interactions, however, the binding interface is predominated with methyl-methyl contacts. Given this aspect, often the selection of small sweep widths and specific coupling constants that focus on the relevant interactions render a wide filtering range less crucial. The system used as a model to describe the filtering techniques was the cCTnC-cTnI$_{35-72}$ complex; however, the utility of purging isotropically labeled protein signals can also provide rapid identification of the binding location of unlabeled drugs to their target proteins. The knowledge of the binding location
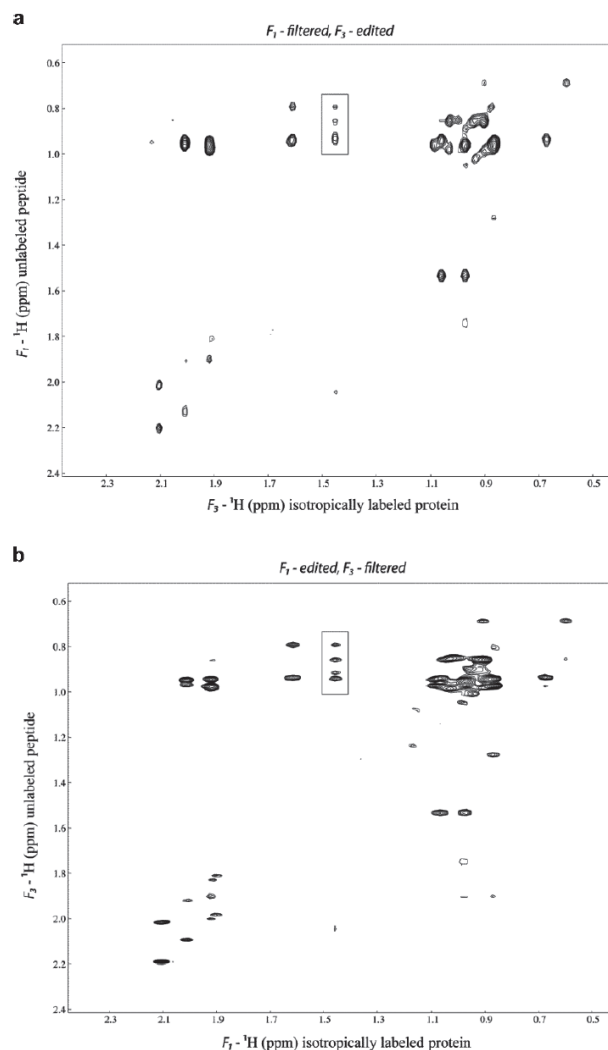
Figure A-8. A comparison of the two ^{13}C-edited/filtered experiments. Both experiments were acquired at 30ºC on a Varian Inova 800 MHz with identical sweep widths (5.0 ppm x 5.0 ppm). The carrier frequency was set to 2.42 ppm, and in the three-dimensional experiment (not shown) the carbon carrier was 20.0 ppm with a sweep width of 20 ppm. The mixing time for both experiments was set to 200 ms. (A) ^{13}C-edited/filtered NOSEY-HSQC experiment with 392 points in the F_3 dimension (labeled protein), 128 increments in the F_1 (unlabeled peptide) dimension, the 32 transients. (B) ^{13}C-edited/filtered HMQC-NOESY experiment also acquired 32 transients with 128 increments in the F_1 dimension. The large difference between the two experiments is 1024 points were acquired in the F_3 dimension, rather than the 392 points in the ^{13}C-edited/filtered NOESY-HSQC. The ^{13}C-edited/filtered NOESY-HSQC provides slightly higher resolution in the labeled protein dimension, but greatly diminished resolution in the unlabeled ligand dimension when compared to the ^{13}C-edited/filtered HMQC-NOESY (see the boxed in area in the above figure).

between a drug and its target protein may greatly enhance the design of new more potent drugs.

Product Operator Analysis

The purging period employed in the ^{13}C-edited/filtered HMQC-NOESY experiment (Figure A-2(B)) is a common filtering method and will be discussed in detail using the product operator formalism. The product operator representing the ^{1}H magnetization after the mixing period (τ_m) is I_z and following the 90_x ^{1}H pulse it becomes transverse magnetization (I_y). During this final filtering section of the pulse sequence any signal from ^{1}H one-bond ^{1}J-coupled to ^{13}C will be purged. In principle, ^{1}H ^{1}J-coupled to ^{15}N could also be removed by making minor revisions to the pulse sequence; however, for simplicity these will be omitted from detailed discussion.

The pulse sequence was designed so that the two delays, τ_b and τ_c are tuned to different ^{1}J$_{HC}$ couplings. The two values selected were 120 Hz and 150 Hz to cover the range of aliphatic ^{1}H-^{13}C ^{1}J-couplings. The assumption made was that most protein-protein interactions involve methyl-methyl contacts, thus we are not concerned with protons coupled to aromatic residues (see *results and discussion*).

We will examine three separate scenarios during the purging period. The situation for an incorrectly tuned delay is not discussed, but would result in incomplete signal suppression.

(a) The delay τ_b is tuned correctly for ^{1}J$_{HC}$

(b) The delay τ_b is incorrectly tuned for ^{1}J$_{HC}$, but τ_c is tuned correctly for ^{1}J$_{HC}$

(c) ^{1}H is not ^{1}J-coupled to any ^{13}C

Since the ^{1}H 180_x pulse is flanked by equal delays (τ_b, and $\tau_c + \tau_d$), where τ_d is a delay after the final ^{13}C 90_x pulse tuned to completely refocus the proton chemical shift ($\tau_d = \tau_b - \tau_c$). The gradients (g4) surrounding the ^{1}H 180_x pulse function to clean up artifacts, as well as dephase multiple quantum coherences.

(a) $\tau_b = 1/(2J_{HC})$: $-I_y \xrightarrow{\ 2\pi J_{HC}I_zS_z\tau_b\ } -[\cos(\pi J_{HC}\tau_b)I_y - \sin(\pi J_{HC}\tau_b)2I_xS_z]$

Given $\tau_b = 1/(2J_{HC})$ the operator prior to the ^{13}C 90_x pulse is the anti-phase term: $2I_xS_z$

Since the S_z commutes with the ^{13}C chemical shift Hamiltonian ($\hat{H}$), it is not considered. Given the ^{1}H 180_x pulse refocuses the ^{1}H chemical shift, it will also be neglected. After the ^{13}C 90_x pulse the term generated is the multiple quantum operator.

$$-2I_xS_z \longrightarrow 2I_xS_y$$

The MQC term is unobservable and also subsequently de-phased by the g4 pulse, and the following time period (τ_c) is of no significance, given all the signal has been eliminated.

(b) $\tau_b \neq 1/(2J_{HC})$; $\tau_c = 1/(2J_{HC})$:

$$-I_y \xrightarrow{\ 2\pi J_{HC}I_zS_z\tau_b\ } -[\cos(\pi J_{HC}\tau_b)I_y - \sin(\pi J_{HC}\tau_b)2I_xS_z]$$

The next ^{13}C 90_x and ^{1}H 180_x pulses will produce both in-phase ^{1}H magnetization and MQC.

$$-\cos(\pi J_{HC}\tau_b)I_y + \sin(\pi J_{HC}\tau_b)2I_xS_z \xrightarrow{\ 90_S^x,180_I^x\ } +\cos(\pi J_{HC}\tau_b)I_y - \sin(\pi J_{HC}\tau_b)2I_xS_y$$

The gradient pulse (g4) will de-phase the multiple quantum operators, but re-phase the in-phase ^{1}H operators. If we follow the in-phase term,

$$+\cos(\pi J_{HC}\tau_b)I_y \xrightarrow{\ 2\pi J_{HC}I_zS_z\tau_c\ } +\cos(\pi J_{HC}\tau_b)[\cos(\pi J_{HC}\tau_c)I_y - \sin(\pi J_{HC}\tau_c)2I_xS_z]$$

Given $\tau_c = 1/(2J_{HC})$ the signal just prior to the ^{13}C 90_x pulse is:

$$- \cos(\pi J_{HC}\tau_b)2I_x S_z$$

As in the previous example, the ^{13}C 90$_x$ pulse will generate MQC:

$$\cos(\pi J_{HC}\tau_b)2I_x S_y$$

During the remaining delay (τ_d = τ_b - τ_c) and the detection period the multiple quantum operators are not observable.

(c) The signal is not coupled to ^{13}C:

In the final example, where the signal did not originate from a proton on a ^{13}C the case is rather simple. The ^{1}H 180$_x$ pulse will refocus the chemical shift during the purging period, as well as invert the sign of the ^{1}H operator. The final in-phase ^{1}H magnetization is detected during acquisition (t_3).

$$- I_y \xrightarrow{\ 180_I^x\ } + I_y$$

References

1.   Cavanagh, J., and Rance, M. (1992) Suppression of Cross-Relaxation Effects in Tocsy Spectra Via a Modified Dipsi-2 Mixing Sequence, *Journal of Magnetic Resonance 96*, 670-678.

2.   Chandra, M., Dong, W. J., Pan, B. S., Cheung, H. C., and Solaro, R. J. (1997) Effects of protein kinase A phosphorylation on signaling between cardiac troponin I and the N-terminal domain of cardiac troponin C, *Biochemistry 36*, 13305-13311.

3.   Delaglio, F., Grzesiek, S., Vuister, G. W., Zhu, G., Pfeifer, J., and Bax, A. (1995) NMRpipe - a Multidimensional Spectral Processing System Based on Unix Pipes, *Journal of Biomolecular NMR 6*, 277-293.

4.   Gemmecker, G., Olejniczak, E. T., and Fesik, S. W. (1992) An Improved Method for Selectively Observing Protons Attached to C-12 in the Presence of H-1-C-13 Spin Pairs, *Journal of Magnetic Resonance 96*, 199-204.

5.   Grzesiek, S., Anglister, J., and Bax, A. (1993) Correlation of Backbone Amide and Aliphatic Side-Chain Resonances in $^{13}C/^{15}N$-Enriched Proteins by Isotropic Mixing of ^{13}C Magnetization, *Journal of Magnetic Resonance Series B 101*, 114-119.

6.   Ikura, M., and Bax, A. (1992) Isotope-Filtered 2d NMR of a Protein Peptide Complex - Study of a Skeletal-Muscle Myosin Light Chain Kinase Fragment Bound to Calmodulin, *Journal of the American Chemical Society 114*, 2433-2440.

7.   Johnson, B. A., and Blevins, R. A. (1994) NMR View - a Computer-Program for the Visualization and Analysis of NMR Data, *Journal of Biomolecular NMR 4*, 603-614.

8.   Kupče, E., and Freeman, R. (1997) Compensation for spin-spin coupling effects during adiabatic pulses, *Journal of Magnetic Resonance 127*, 36-48.

9.   Lee, W., Revington, M. J., Arrowsmith, C., and Kay, L. E. (1994) A pulsed field gradient isotope-filtered 3D ^{13}C HMQC-NOESY experiment for extracting intermolecular NOE contacts in molecular complexes, *FEBS letters 350*, 87-90.

10.   Li, M. X., Gagné, S. M., Tsuda, S., Kay, C. M., Smillie, L. B., and Sykes, B. D. (1995) Calcium-Binding to the Regulatory N-Domain of Skeletal-Muscle Troponin-C Occurs in a Stepwise Manner, *Biochemistry 34*, 8330-8340.

11.   Li, M. X., Wang, X., Lindhout, D. A., Buscemi, N., Van Eyk, J. E., and Sykes, B. D. (2003) Phosphorylation and mutation of human cardiac

troponin I deferentially destabilize the interaction of the functional regions of troponin I with troponin C, *Biochemistry 42*, 14460-14468.

12.   Li, M. X., Wang, X., and Sykes, B. D. (2004) Structural based insights into the role of troponin in cardiac muscle pathophysiology, *Journal of muscle research and cell motility 25*, 559-579.

13.   Lyons, B. A., and Montelione, G. T. (1993) An Hccnh Triple-Resonance Experiment Using [13]C Isotropic Mixing for Correlating Backbone Amide and Side-Chain Aliphatic Resonances in Isotopically Enriched Proteins, *Journal of Magnetic Resonance Series B 101*, 206-209.

14.   Muhandiram, D. R., and Kay, L. E. (1994) Gradient-Enhanced Triple-Resonance 3-Dimensional NMR Experiments with Improved Sensitivity, *Journal of Magnetic Resonance Series B 103*, 203-216.

15.   Ogura, K., Terasawa, H., and Inagaki, F. (1996) An improved double-tuned and isotope-filtered pulse scheme based on a pulsed field gradient and a wide-band inversion shaped pulse, *Journal of Biomolecular NMR 8*, 492-498.

16.   Otting, G., and Wüthrich, K. (1990) Heteronuclear filters in two-dimensional (1H,1H)-NMR spectroscopy: combined use with isotope labelling for studies of macromolecular conformation and intermolecular interactions, *Quarterly reviews of biophysics 23*, 39-96.

17.   Shaka, A. J., Barker, P. B., and Freeman, R. (1985) Computer-Optimized Decoupling Scheme for Wideband Applications and Low-Level Operation, *Journal of Magnetic Resonance 64*, 547-552.

18.   Sia, S. K., Li, M. X., Spyracopoulos, L., Gagné, S. M., Liu, W., Putkey, J. A., and Sykes, B. D. (1997) Structure of cardiac muscle troponin C unexpectedly reveals a closed regulatory domain, *The Journal of biological chemistry 272*, 18216-18221.

19.   Stuart, A. C., Borzilleri, K. A., Withka, J. M., and Palmer, A. G. (1999) Compensating for variations in H-1-C-13 scalar coupling constants in isotope-filtered NMR experiments, *Journal of the American Chemical Society 121*, 5346-5347.

20.   Takeda, S., Yamashita, A., Maeda, K., and Maeda, Y. (2003) Structure of the core domain of human cardiac troponin in the Ca(2+)-saturated form, *Nature 424*, 35-41.

21.   Valentine, E. R., Ferrage, F., Massi, F., Cowburn, D., and Palmer, A. G., 3rd. (2007) Joint composite-rotation adiabatic-sweep isotope filtration, *Journal of biomolecular NMR 38*, 11-22.

22.   Zwahlen, C., Legault, P., Vincent, S. J. F., Greenblatt, J., Konrat, R., and Kay, L. E. (1997) Methods for measurement of intermolecular NOEs by multinuclear NMR spectroscopy: Application to a bacteriophage

lambda N-peptide/boxB RNA complex, *Journal of the American Chemical Society 119*, 6711-6721.

Appendix B.

Approaches to protein-ligand structure determination by NMR spectroscopy: applications in drug binding to the cardiac regulatory protein troponin C*

Summary

NMR spectroscopy is an effective tool employed by medicinal chemists in the drug discovery pipeline. NMR spectroscopy is convenient because it can provide structural information relatively easily. For example, chemical shift mapping has been a tool employed for many years to identifying ligand-binding sites and to determine the stoichiometry and affinity of ligand binding. However, the determination of a high resolution solution structure of a target-drug complex can be much more laborious and time consuming. This is especially inconvenient in comparison with the crystal soak difference Fourier methods used for X-ray structures. Over the years, we have sought methods which are more rapid when the general overall structure of the target is known. We discuss the application of some of these methods herein; including a number of *in silico* methods developed to augment traditional NOE based NMR methods.

Contribution: IMR performed the majority of the NMR experiments. SEPS analyzed the titration data of resveratrol, IMR performed and analyzed the automated docking, JSURF calculations, and PRE experiments. IMR and SEPS wrote the manuscript with BDS.

Introduction

A key element in rational drug design is the rapid determination of protein-ligand structures. X-ray crystallography and NMR Spectroscopy are the most commonly used techniques to determine high-resolution structures of protein-ligand complexes. While NMR spectroscopy has the advantage that different drugs can easily be titrated into the protein in solution, the determination of the full high resolution solution structure involves the assignment of thousands of nuclear Overhauser effect contacts (NOEs) and other data, which tends to be a time-consuming task. If the structure of a target protein is known and the NMR spectra of the $^{13}C,^{15}N$-labeled protein are assigned, the measurement of intermolecular NOEs between the ligand and the protein may be enough to faithfully localize the orientation of the ligand in the complex. This procedure can drastically reduce the overall time for determining the orientation of the ligand on its target, while still providing invaluable structural details about the important pharmacophores of a molecule. There are situations; however, when this method is still too laborious (*e.g.* for high-throughput applications) or not possible (*e.g.* for a low affinity ligand, resulting in weak of NOEs).

NMR spectroscopy is unique from other screening and structural methods in that it can determine binding constants as well as identify the ligand binding site on a protein by monitoring residue specific changes in chemical shifts upon ligand binding. This approach is called chemical shift mapping and it is routinely used for rapidly identifying the binding site of a ligand on a protein and is a critical step in SAR-by-NMR (*1*). Chemical shift mapping is most typically done by following the amide nuclei of an ^{15}N-labeled target molecule, and then highlighting the residues that are significantly shifted on the van der Waals surface of the target protein. These results can also be used as ambiguous distance restraints by docking programs, such as HADDOCK (*2*) or the mapped surface can be

used for a binding-site centered docking with an automated docking program such as AutoDock (*3*). Since chemical shift perturbations are a response to a change in the local chemical environment induced by ligand binding, it is possible to predict the location of the ligand rings from the magnitude and sign of the chemical shift changes if we assume these changes are caused predominantly by proximity to aromatic groups of a ligand. Finally, the use of a protein with a paramagnetic center can provide distance restraints between the ligand and the protein. A number of groups have investigated the efficacy of combining a variety of these methods to accurately and rapidly resolve protein-ligand structures (*4-7*). In order to examine the usefulness of these techniques, we shall study their applications in regards to drug binding into the cardiac muscle contractile regulatory protein, troponin C (cTnC).

cTnC is a dumbbell shaped Ca^{2+}-binding protein that triggers contraction upon Ca^{2+}-binding its regulatory N-lobe (cNTnC). Ca^{2+} enters the cytosol of a muscle cell and binds to cNTnC, which induces a slight opening of cNTnC. Following Ca^{2+} association with cNTnC, the "switch region" of the protein troponin I (cTnI) binds to cNTnC, stabilizing the fully open conformation of cNTnC. The "inhibitory region" of cTnI is subsequently released from actin, which results in the contraction-dependent actin-myosin interaction. During relaxation, Ca^{2+} dissociates from cNTnC as it leaves the cytosol, cTnI translocates from cNTnC back to actin, which blocks the actin-myosin interface to inhibit contraction. The C-domain of cTnC (cCTnC) has two high-affinity metal binding sites that are occupied throughout the contraction-relaxation cycle. The binding partner of cCTnC is a different segment of cTnI, the "anchoring region". The primary role of the cCTnC-cTnI interaction is to tether cTnC to the thin filament, but recent insights into the structure and function of insect flight muscle troponin suggest this interaction may also play a role in regulation of contraction (*8, 9*). For recent reviews into the molecular mechanism of contraction, see (*10-12*). Given both the C- and N-lobes of cTnC interact

with cTnI to regulate contraction, the design of small molecules that bind cTnC and modulate its interaction with cTnI have therapeutic potential (*13-15*).

Intermolecular NOEs

The identification of NOEs between a protein and a ligand is a crucial step in solving the structure of the complex by NMR spectroscopy. Knowledge of the high-resolution structure of a protein-ligand complex can provide insights into the mechanism of a ligand as well as help in the design of new pharmaceuticals. The standard scheme of determining a protein-ligand structure by NMR spectroscopy begins by assigning the resonances of a $^{13}C,^{15}N$- or ^{15}N-labeled protein. Following the resonance assignment, the structure of the protein is solved by assigning intramolecular NOEs to obtain distance restraints. Once the tertiary structure of the target is known, the unlabeled ligand is assigned when in complex with the protein using a variety of isotope filtered experiments (*16-18*). Finally, NOE contacts between the unlabeled ligand and labeled target are measured to obtain distance restraints between the ligand and protein (*19-21*). Frequently, the protein structure is not significantly altered upon binding to the ligand making the re-determination of the protein structure superfluous. In these cases, it may be sufficient to use only intermolecular NOEs to provide distance restraints between the labeled protein and unlabeled ligand. Unfortunately, the target molecule does often undergo structural changes when binding a ligand. If there has been a structure of the target molecule in complex with a related ligand, it may be possible to use intermolecular NOEs to localize the ligand onto the complex structure, with the homologous ligand removed. We have recently employed this technique to a complex with cNTnC and the small molecule, W7 (*22*). The structure of cNTnC was obtained from the NMR solution structure of cNTnC-cTnI (*23*), with cTnI removed prior to the docking of

W7. The complex we will focus on in this report is cCTnC bound to the polyphenol, resveratrol (Figure B-1a).

Resveratrol is an antioxidant present at high concentrations in red wine and in the skins of grapes (*24*) and it has been studied intensely due to its benefits to cardiovascular health (*25*). The low incidence of cardiovascular disease among Mediterranean populations despite a diet rich in fat, has prompted some researchers to suggest that the high consumption of red wine offers protection against heart disease, and has been dubbed, the "French paradox" (*26, 27*). We have found that resveratrol targets cCTnC, and this interaction may impart some of its protective properties (*28*). The structure of cCTnC bound to the green tea polyphenol, epigallocatechin gallate (EGCg) (*29*), the anchoring region of cTnI (cTnI$_{34-71}$) (*30, 31*), and the cardiotonic drug EMD 57033 (*32*) have been solved by either NMR spectroscopy or X-ray crystallography. Even though the ligands of cCTnC are chemically dissimilar, they all induce an analogous conformational change of cCTnC (*29*). Instead of solving the structure of cCTnC again, we measured intermolecular NOEs between resveratrol and cCTnC and docked resveratrol onto the cCTnC-EGCg structure (Figure B-1b-d). In order to dock resveratrol, we repeated the simulated annealing procedure in Xplor-NIH (*33, 34*) using the intramolecular NOEs for cCTnC from the cCTnC-EGCg structure, and replaced the intermolecular NOEs from EGCg to cCTnC with restraints between resveratrol and cCTnC. We propose that this procedure is better than simply performing a rigid docking since it allows for some flexibility of cCTnC. We chose the cCTnC-EGCg structure because both EGCg and resveratrol are polyphenols and thus may induce similar structural perturbations of cCTnC.

Monitoring strong protein-ligand complexes can be a fruitful source of structural information. However, problems can arise when the unlabeled ligand is too large so that it contains an abundance of overlapping signals, or when the intermolecular NOEs are weak, making it difficult to
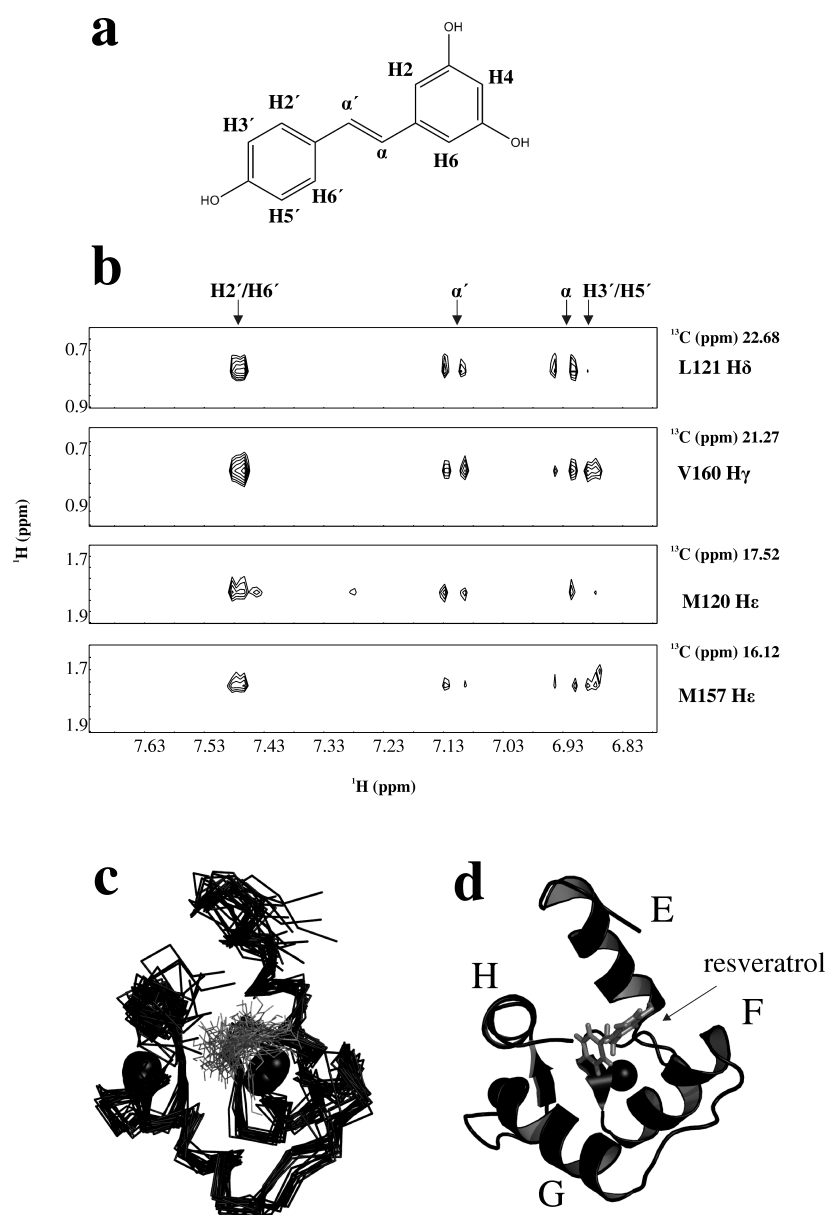
Figure B-1. Structure of cCTnC in complex with resveratrol as determined by intermolecular NOEs. (a) chemical structure of resveratrol. (b) several strips from the ^{13}C-edited-filtered NOESY NMR experiment that identifies NOEs between an unlabeled ligand and a ^{13}C-labeled protein. (c) Ensemble of the 20 lowest energy structures of cCTnC-resveratrol. (d) the lowest energy structure from the ensemble. cCTnC is shown in black with the helices labeled and resveratrol is colored in grey. Black spheres represent Ca^{2+}.

distinguish noise from NOEs. Therefore, it is often necessary to make use of other methods to assist in the determination of protein-ligand structures. We will assess some of these approaches, by comparing the predictions from these methods with the cCTnC-resveratrol structure as determined with the NOE data.

Chemical Shift Mapping

Chemical shift mapping is a frequently used application of NMR spectroscopy, which allows the estimation of a binding site of a ligand on a target molecule. Typically the perturbations of ^{15}N-amide chemical shifts are used, which can provide information on the binding location of the compound on the protein as well as its binding constant. While chemical shift mapping is a rapid method to estimate the binding surface on a protein, it has several pitfalls, including a lack of resolution, and is hampered by any allosteric effects induced by a ligand binding. This is because chemical shifts are perturbed in response to a change in local chemical environment, which may be due to proximity to a ligand or because of a conformational change induced by the ligand binding.

The use of amide chemical shift mapping with the interaction between cCTnC and resveratrol is shown in Figure B-2a. While, perturbations seem to point towards the central groove as the binding site of resveratrol, the largest shifts are from residues residing in the F-G linker are not near to resveratrol in the structure (Figure B-1c,d). Investigation of the chemical shifts perturbed by resveratrol, and compared to those induced by other ligands of cCTnC: EGCg, EMD 57033, and cTnI$_{34-71}$ we see that all these residues induce the same pattern of amide chemical shift change (Figure B-2c). These ligands have unique structural features, and while they all bind in the core of the protein the orientations they adopt are quite varied. Alternatively, the similar amide chemical shift perturbations are more likely from a similar conformational perturbation
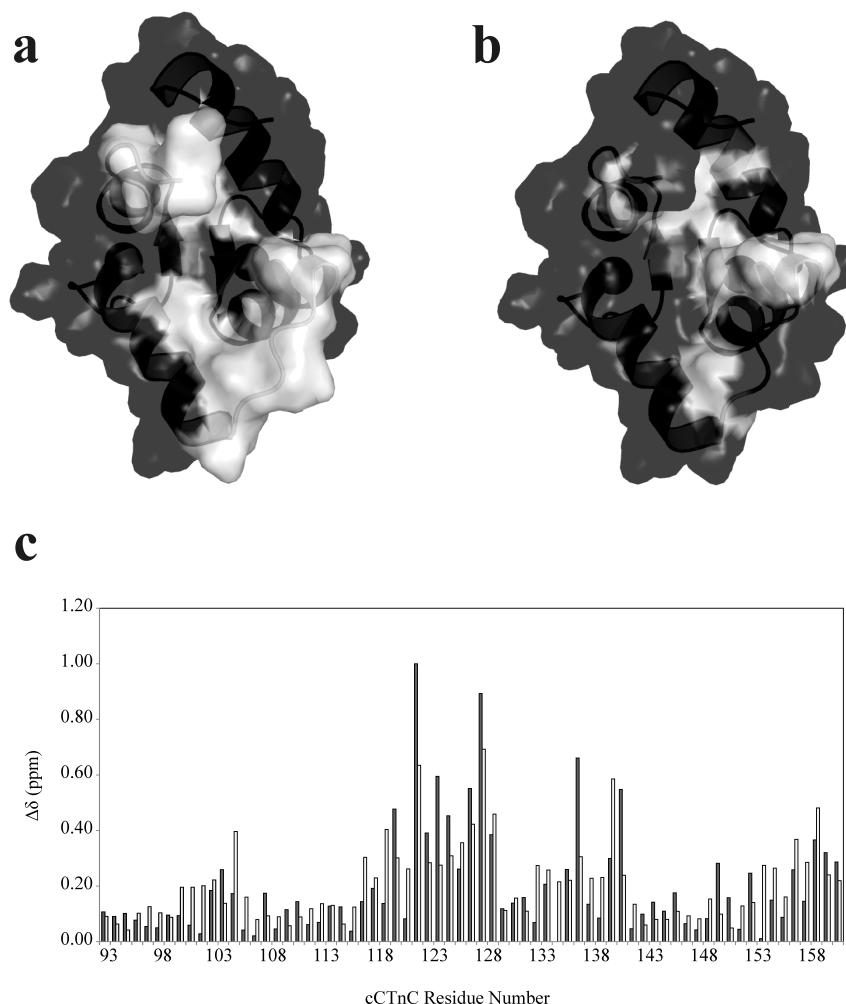
Figure B-2. Chemical shift mapping of resveratrol induced shifts on cCTnC from the cCTnC-EGCg structure (2kdh.pdb). (a) ^{15}N-amide chemical shifts that were perturbed larger than the mean chemical shift perturbation. (b) residues that were perturbed in the methyl region of the ^{1}H,^{13}C-HSQC spectrum. cCTnC is shown as a transparent surface (black), with the perturbed resonances highlighted in white. (c) bar diagram that compares the total amide chemical shift ($\Delta\delta$) pattern induced by resveratrol (black bars) and the average chemical shift perturbation induced by EMD 57033, cTnI$_{34\text{-}71}$, and EGCg (white bars). $\Delta\delta = ((\Delta\delta^{1}\text{H})^{2} + 1/25(\Delta\delta^{15}\text{N})^{2})^{1/2}$.

since all ligand bound forms of cCTnC in an open state (the F-G and E-H helix pairs are moved apart to accommodate the ligands). Although the amide shifts may they tell us very little about the specific binding site of resveratrol, they do give us some idea of the conformation of cCTnC.

Another way to map the binding surface of a ligand on a target molecule is to look at the ^{13}C-methyl chemical shift perturbations. Since most protein-ligand structures are stabilized via hydrophobic interactions, following methyl perturbations when a ligand binds to the protein may be more informative that using ^{15}N-amide chemical shifts. In Figure B-2b we show mapped residues that underwent perturbations in the terminal methyls. Most of the perturbed residues, are on the E-, F-, and H-helices, as well as on the β-sheet of cCTnC. These results are more consistent with the structure we determined with intermolecular NOEs. In fact, many of the methyls that were perturbed during the titration were also involved in making NOEs with resveratrol. Chemical shift mapping of the methyls clearly do a better job than amide nuclei of identifying the binding site of resveratrol, but the predictions are still qualitative.

J-surface mapping

To supplement the qualitative chemical shift mapping, we have mapped the J-surface of resveratrol on cCTnC. The ring current effect from aromatic ligands can induce chemical shift perturbations of nuclei proximal to the ligand. McCoy and Wyss described the application of this phenomenon to identify the binding surface of a ligand to the hepatitis C virus NS3 protease (*35*). Caveats of using this method to identify the ligand binding site are that the ligand must contain an aromatic group and that the ring current effect from the ligand is the primary source of chemical shift perturbation. In order to localize the binding site of resveratrol on cCTnC we performed J-surface mapping with the program Jsurf using the amide and methyl chemical shift perturbation data (Figure

B-3). Jsurf approximates the origin of chemical shift perturbations as a single point-dipole at the center of the aromatic ring of a ligand (*36*). The center of the aromatic ring is then predicted based on the magnitude and sign of the proton perturbation. For each perturbed residue, the aromatic ring inducing the chemical shift change can be at any number of places and for each additional residue considered this location is narrowed down until finally a surface is identified where the ligand rings is likely to reside.

We used the amide protons chemical shift perturbations to see if Jsurf could accurately predict the binding of resveratrol (Figure B-3a). The predicted J-surface runs through the F and G helices, which is not consistent with the NOEs and for resveratrol to lie here would violate many van der Waals forces. While it is likely that some of the amide resonances perturbed in the presence of resveratrol are due to ring current effects, evidently many are caused not by direct contact with the ring, but rather by an allosteric perturbation induced by resveratrol binding. We repeated the J-surface analysis using the methyl protons (Figure B-3b). The result of using the methyl protons was a binding site localized to the hydrophobic pocket in a very similar location as calculate by the intermolecular NOEs. As an aside, Jsurf requires an input file that has atom numbers from the protein structure file (i.e. PDB file format) with the corresponding shift for that atom. In contrast to amide protons, there are three protons associated with each methyl. So the input file we used for Jsurf had three protons for each methyl perturbation included in the calculation.

Automated Docking

While Jsurf does a reasonable job of predicting the binding site of resveratrol on cCTnC using the methyl proton perturbations, it does not predict the actual binding pose of resveratrol. In order to do this, we used AutoDock4.2 which predicts the conformations of a ligand bound to a macromolecular target of known structure as well as the free energy of
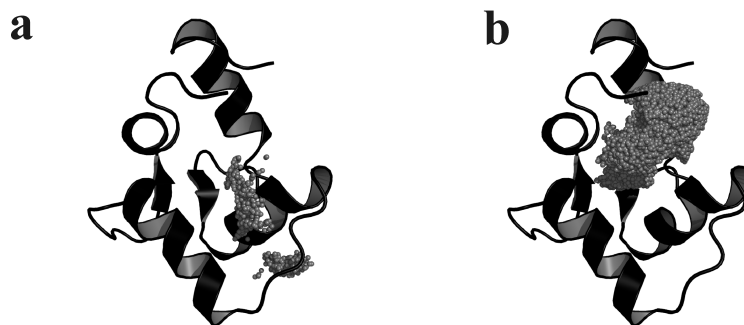
Figure B-3. The J-surface (grey spheres) from the amide (a) and methyl (b) chemical shift perturbations mapped on the structure of cCTnC (black cartoon) from the cCTnC-EGCg structure (2kdh.pdb).

binding. AutoDock4.2 allows flexibility for both the ligand and for a limited number of residues in the target protein indicated by the user, it also allows the user to select a region of the target molecule to perform the conformation searching (the grid volume) (*37, 38*). AutoDock 4.2 with the AutoDockTools graphical interface was used to predict 150 binding conformations using a population size of 500 and 5000000 energy evaluations. The docking was guided by limiting the grid volume to encompass residues of cCTnC that the chemical shift and J-surface mappings predicted to be involved in binding resveratrol. Residues which showed chemical shifts greater than one standard deviation from the mean in the ^{1}H,^{13}C HSQC NMR experiment were defined as flexible residues.

A total of 15 clusters were predicted for resveratrol using an r.m.s.d. tolerance of 2.0 Å for each cluster. All 150 structures predict that resveratrol binds in the hydrophobic groove of cCTnC (Figure B-4a). This is not surprising, considering the grid volume chosen from the experimental data encompassed primarily this region of cCTnC. In AutoDock identifying the lowest-energy cluster and the most populated cluster are two ways of choosing the best conformer (*39, 40*). The ten lowest energy structures are shown in Figure B-4b, and include two different conformations of resveratrol as having the lowest energy. The lowest energy conformer has resveratrol oriented parallel to the β-sheet of cCTnC, whereas the next lowest energy cluster predicts resveratrol binds in the hydrophobic pocket of cCTnC pointed towards the β-sheet. The buried structure of resveratrol more closely resembles the methyl-based Jsurf prediction and NOE data; however, the NOE data has the diphenol ring oriented away from the protein, not deep within the hydrophobic pocket calculated by AutoDock.
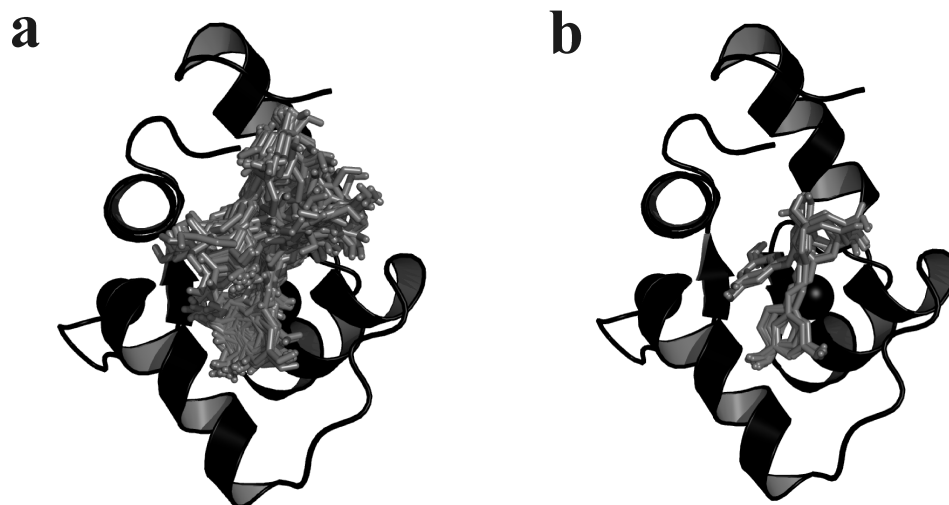
Figure B-4. Overlay of the poses of resveratrol (grey sticks) on cCTnC (black cartoon) from the cCTnC-EGCg structure (2kdh.pdb). (a) all 150 poses and (b) the ten lowest energy poses generated using AutoDock.

Restraints derived from paramagnetic restraints

The prediction of the binding site of resveratrol on cCTnC by chemical shift mapping, J-surface mapping, and docking had some success; but, in the end it would be difficult to validate the results without less ambiguous data, such as NOEs. The use of paramagnetic relaxation enhancement (PRE) has been used extensively to aide in protein structure determination (*41*), in protein-protein structure determination (*42*), and in protein-ligand structure determination (*43*). PRE is a phenomenon which arises when unpaired electrons from a paramagnetic center, such as a lanthanide ion, increase the relaxation of nuclei in a distance dependant manner. Pseudocontact shifts (PCS) induced by paramagnetic lanthanide ions with anisotropic magnetic susceptibility tensors can also tell the user information about the orientation of the ligand with respect to the metal. The Otting group has recently employed PCS to determine the structure of a protein-drug complex (*44*). On the other hand, the lanthanide gadolinium (Gd^{3+}) has an isotropic paramagnetic environment, so it does not yield information about the orientation between the nuclei and metal, but does provide distance information.

It has been shown that the trivalent lanthanides can substitute for calcium in troponin C (*45, 46*). The C-terminal domain of troponin C binds two metal ions, and therefore it would be difficult to obtain structural restraints between resveratrol and both of these ions. Fortuitously, the cNTnC contains only one Ca^{2+} binding site. In a recent publication (*47*), we have used PRE to obtain distance restraints between Gd^{3+} and the cardiotonic agent, 2',4'-difluoro(1,1'-biphenyl)-4-yloxy acetic acid (dfbp-o). In this type of experiment, free dfbp-o was titrated with Gd^{3+}-bound cNTnC-cTnI, and at each titration point we measured the transverse and longitudinal relaxation rates of ^{19}F and ^{1}H of dfbp-o. As the concentration of cNTnC-cTnI-Gd^{3+} increased, the relaxation rates of dfbp-o increased (see Figure B-5 for signal broadening), and this increase in relaxation
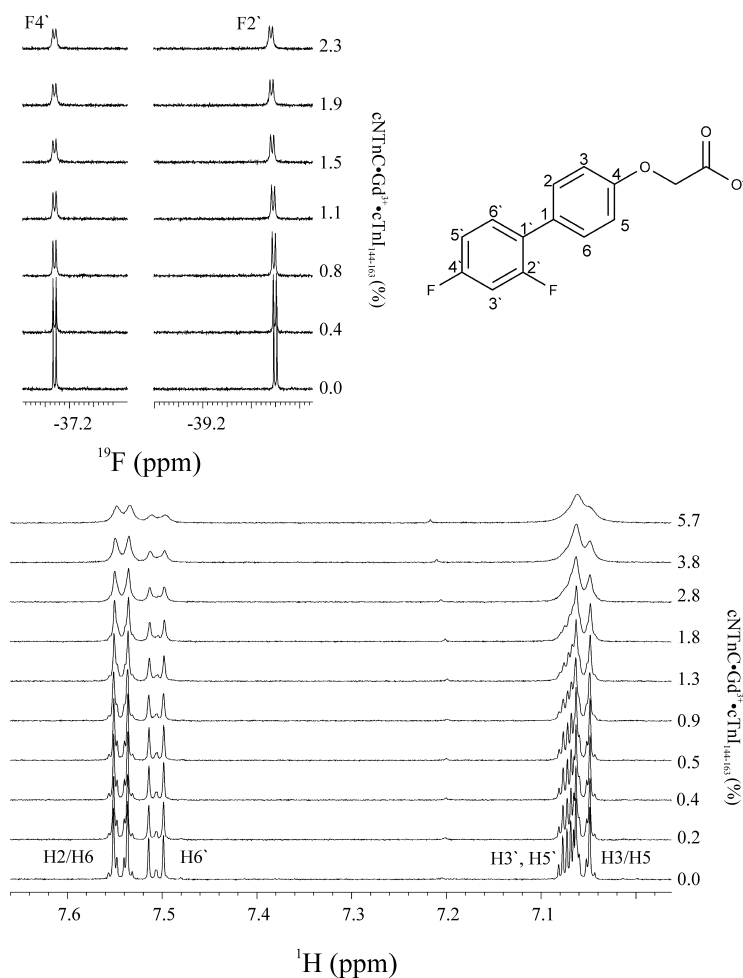
Figure B-5. Paramagnetic relaxation enhancement of signals of dfbp-o by Gd^{3+} bound to cNTnC-cTnI. The stacked 1D ^{19}F spectrum of dfbp-o is shown in the upper left, and the stacked 1D ^{1}H spectrum of dfbp-o is shown at the bottom. Both stacked spectra are shown as a function of percentage dfbp-o bound to cNTnC•Gd^{3+}•cTnI. The numbering of dfbp-o is shown on its chemical structure as a reference (Figure adapted from (*47*)).

rates were used to calculate this distance between dfbp-o and Gd^{3+} as previously described (*48*). We calculated the structure of the tertiary complex, cNTnC-cTnI-dfbp-o using only NOE restraints, and NOE and PRE restraints (Figure B-6). The addition of the PRE restraints radically improved the resolution of dfbp-o in the structure, and illustrates the usefulness of this technique to aid in protein-ligand structure refinement.

Conclusion

The calculation of protein-ligand structures is an important step in the development of novel pharmaceuticals. The high resolution description of the binding site and pose of a ligand is a crucial step in the rationale design of novel drugs. In this review we have surveyed a few approaches available to scientists to help in the resolving of protein-ligand structures. Intermolecular NOEs are a crucial step in solving protein-ligand structures; however, they are not always attainable. Reasons for this include but are not limited to: time-constraints, no ^{13}C-labeled protein available, or a weak binding constant. There are other techniques that can validate structures solved with few NOEs, or substitute for NOEs when none exist. While ^{15}N-amide nuclei are the most used nucleus for estimating the binding site of a ligand, conformational changes in the protein upon ligand binding can be misleading. We show that the use of ^{13}C-methyl chemical shift mapping and J-surface prediction using methyl perturbations more accurately identify the binding site of a ligand. Identification of the binding pose of the ligand in the absence of NOE data can be done with AutoDock; however, it is difficult to choose the cluster that most closely resembles the real structure. Other experimentally derived restraints, such as PREs can significantly improve protein-ligand structures when either NOEs are not sufficient to define the binding pose of the ligand or when NOEs are not available.

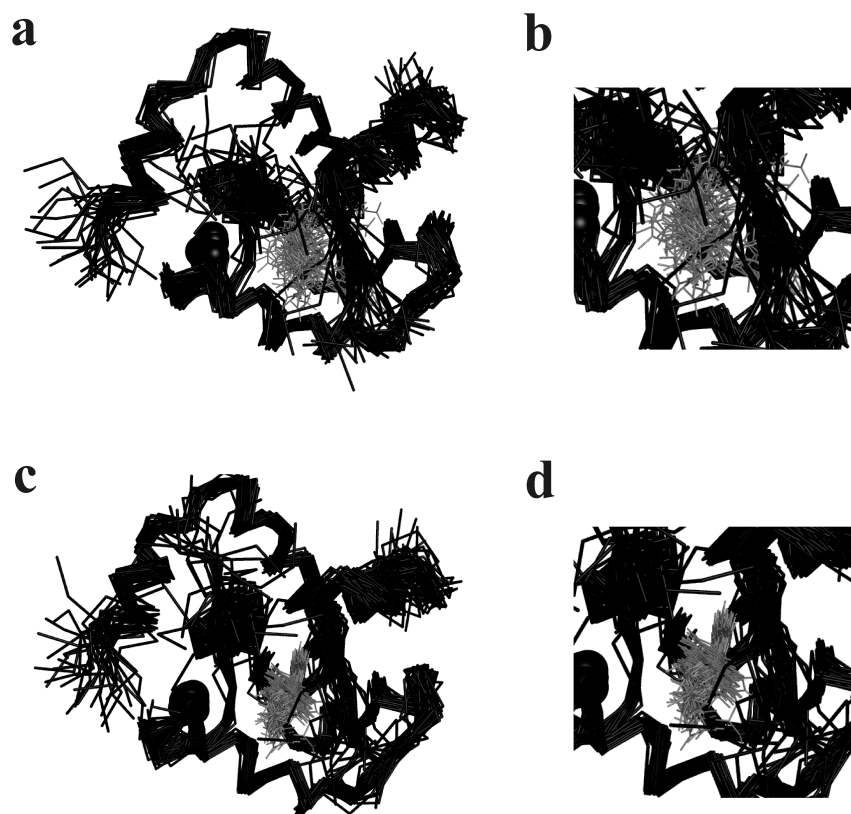**Figure B-6**. Ribbon diagram of cNTnC bound to cTnI (both in black) and dfbp-o (grey) in stick representation. (a) Refinement of the complex using only intermolecular NOEs. (b) close-up view of the binding site, highlighting the disorder of dfbp-o. (c) Refinement of the complex using intermolecular NOEs and PRE distance restraints. (d) close-up view of the binding site in (c).

References

1. Shuker, S. B., Hajduk, P. J., Meadows, R. P., and Fesik, S. W. (1996) Discovering high-affinity ligands for proteins: SAR by NMR, *Science 274*, 1531-1534.

2. Dominguez, C., Boelens, R., and Bonvin, A. M. J. J. (2003) HADDOCK: A protein-protein docking approach based on biochemical or biophysical information, *J. Am. Chem. Soc. 125*, 1731-1737.

3. Morris, G. M., Huey, R., Lindstrom, W., Sanner, M. F., Belew, R. K., Goodsell, D. S., and Olson, A. J. (2009) AutoDock4 and AutoDockTools4: Automated Docking with Selective Receptor Flexibility, *J. Comput. Chem. 30*, 2785-2791.

4. Bertini, I., Fragai, M., Giachetti, A., Luchinat, C., Maletta, M., Parigi, G., and Yeo, K. J. (2005) Combining in silico tools and NMR data to validate protein-ligand structural models: Application to matrix metalloproteinases, *J. Med. Chem. 48*, 7544-7559.

5. Cioffi, M., Hunter, C. A., Packer, M. J., Pandya, M. J., and Williamson, M. P. (2009) Use of quantitative H-1 NMR chemical shift changes for ligand docking into barnase, *J. Biomol. NMR 43*, 11-19.

6. Krishnamoorthy, J., Yu, V. C. K., and Mok, Y. K. (2010) Auto-FACE: An NMR Based Binding Site Mapping Program for Fast Chemical Exchange Protein-Ligand Systems, *PLoS ONE 5*, -.

7. Cioffi, M., Hunter, C. A., Packer, M. J., and Spitaleri, A. (2008) Determination of protein-ligand binding modes using complexation-induced changes in H-1 NMR chemical shift, *J. Med. Chem. 51*, 2512-2517.

8. Bullard, B., Agianian, B., Krzic, U., Linke, W. A., and Leonard, K. R. (2004) Independent regulation of insect flight muscle by two isoforms of troponin C, *Biophys. J. 86*, 215a-216a.

9. De Nicola, G., Burkart, C., Qiu, F., Agianian, B., Labeit, S., Martin, S., Bullard, B., and Pastore, A. (2007) The structure of Lethocerus troponin C: Insights into the mechanism of stretch activation in muscles, *Structure 15*, 813-824.

10. Gomes, A. V., Potter, J. D., and Szczesna-Cordary, D. (2002) The role of troponins in muscle contraction, *IUBMB Life 54*, 323-333.

11. Li, M. X., Wang, X., and Sykes, B. D. (2004) Structural based insights into the role of troponin in cardiac muscle pathophysiology, *J. Muscle Res. Cell Motil. 25*, 559-579.

12. Parmacek, M. S., and Solaro, R. J. (2004) Biology of the troponin complex in cardiac myocytes, *Prog. Cardiovasc. Dis. 47*, 159-176.

13. Kass, D. A., and Solaro, R. J. (2006) Mechanisms and use of calcium-sensitizing agents in the failing heart, *Circulation 113*, 305-315.

14. Li, M. X., Robertson, I. M., and Sykes, B. D. (2008) Interaction of cardiac troponin with cardiotonic drugs: a structural perspective, *Biochem. Biophys. Res. Commun. 369*, 88-99.

15. Sorsa, T., Pollesello, P., and Solaro, R. J. (2004) The contractile apparatus as a target for drugs against heart failure: Interaction of

levosimendan, a calcium sensitiser, with cardiac troponin c, *Mol. Cell. Biochem. 266*, 87-107.

16. Gemmecker, G., Olejniczak, E. T., and Fesik, S. W. (1992) An Improved Method for Selectively Observing Protons Attached to C-12 in the Presence of H-1-C-13 Spin Pairs, *J. Magn. Reson. 96*, 199-204.

17. Ikura, M., and Bax, A. (1992) Isotope-Filtered 2d Nmr of a Protein Peptide Complex - Study of a Skeletal-Muscle Myosin Light Chain Kinase Fragment Bound to Calmodulin, *J. Am. Chem. Soc. 114*, 2433-2440.

18. Ogura, K., Terasawa, H., and Inagaki, F. (1996) An improved double-tuned and isotope-filtered pulse scheme based on a pulsed field gradient and a wide-band inversion shaped pulse, *J. Biomol. NMR 8*, 492-498.

19. Lee, W., Revington, M. J., Arrowsmith, C., and Kay, L. E. (1994) A Pulsed-Field Gradient Isotope-Filtered 3d C-13 Hmqc-Noesy Experiment for Extracting Intermolecular Noe Contacts in Molecular-Complexes, *FEBS Lett. 350*, 87-90.

20. Robertson, I. M., Spyracopoulos, L., and Sykes, B. D. (2009) The Evaluation of Isotope Editing and Filtering for Protein-Ligand Interaction Elucidation by Nmr, *Biophysics and the Challenges of Emerging Threats*, 101-119.

21. Stuart, A. C., Borzilleri, K. A., Withka, J. M., and Palmer, A. G. (1999) Compensating for variations in H-1-C-13 scalar coupling constants in isotope-filtered NMR experiments, *J. Am. Chem. Soc. 121*, 5346-5347.

22. Hoffman, R. M. B., and Sykes, B. D. (2009) Structure of the Inhibitor W7 Bound to the Regulatory Domain of Cardiac Troponin C, *Biochemistry 48*, 5541-5552.

23. Li, M. X., Spyracopoulos, L., and Sykes, B. D. (1999) Binding of cardiac troponin-I147-163 induces a structural opening in human cardiac troponin-C, *Biochemistry 38*, 8289-8298.

24. Jang, M. S., Cai, E. N., Udeani, G. O., Slowing, K. V., Thomas, C. F., Beecher, C. W. W., Fong, H. H. S., Farnsworth, N. R., Kinghorn, A. D., Mehta, R. G., Moon, R. C., and Pezzuto, J. M. (1997) Cancer chemopreventive activity of resveratrol, a natural product derived from grapes, *Science 275*, 218-220.

25. Corder, R., Douthwaite, J. A., Lees, D. M., Khan, N. Q., dos Santos, A. C. V., Wood, E. G., and Carrier, M. J. (2001) Endothelin-1 synthesis reduced by red wine - Red wines confer extra benefit when it comes to preventing coronary heart disease., *Nature 414*, 863-864.

26. Kopp, P. (1998) Resveratrol, a phytoestrogen found in red wine. A possible explanation for the conundrum of the 'French paradox'?, *Eur. J. Endocrinol. 138*, 619-620.

27. Goldberg, D. M., Hahn, S. E., and Parkes, J. G. (1995) Beyond Alcohol - Beverage Consumption and Cardiovascular Mortality, *Clin. Chim. Acta 237*, 155-187.

28. Pineda-Sanabria, S. E., Robertson, I. M., and Sykes, B. D. (2011) Structure of trans-Resveratrol in Complex with the Cardiac Regulatory Protein Troponin C, *Biochemistry 50*, 1309-1320.

29. Robertson, I. M., Li, M. X., and Sykes, B. D. (2009) Solution Structure of Human Cardiac Troponin C in Complex with the Green Tea Polyphenol, (-)-Epigallocatechin 3-Gallate, *J. Biol. Chem. 284*, 23012-23023.

30. Takeda, S., Yamashita, A., Maeda, K., and Maeda, Y. (2003) Structure of the core domain of human cardiac troponin in the Ca(2+)-saturated form, *Nature 424*, 35-41.

31. Gasmi-Seabrook, G. M., Howarth, J. W., Finley, N., Abusamhadneh, E., Gaponenko, V., Brito, R. M., Solaro, R. J., and Rosevear, P. R. (1999) Solution structures of the C-terminal domain of cardiac troponin C free and bound to the N-terminal domain of cardiac troponin I, *Biochemistry 38*, 8313-8322.

32. Wang, X., Li, M. X., Spyracopoulos, L., Beier, N., Chandra, M., Solaro, R. J., and Sykes, B. D. (2001) Structure of the C-domain of human cardiac troponin C in complex with the Ca2+ sensitizing drug EMD 57033, *J. Biol. Chem. 276*, 25456-25466.

33. Schwieters, C. D., Kuszewski, J. J., and Clore, G. M. (2006) Using Xplor-NIH for NMR molecular structure determination, *Prog. Nucl. Magn. Reson. Spectrosc. 48*, 47-62.

34. Schwieters, C. D., Kuszewski, J. J., Tjandra, N., and Clore, G. M. (2003) The Xplor-NIH NMR molecular structure determination package, *J. Magn. Reson. 160*, 65-73.

35. McCoy, M. A., and Wyss, D. F. (2002) Spatial localization of ligand binding sites from electron current density surfaces calculated from NMR chemical shift perturbations, *J. Am. Chem. Soc. 124*, 11758-11763.

36. Moyna, G., Zauhar, R. J., Williams, H. J., Nachman, R. J., and Scott, A. I. (1998) Comparison of ring current methods for use in molecular modeling refinement of NMR derived three-dimensional structures, *J. Chem. Inf. Comput. Sci. 38*, 702-709.

37. Morris, G. M., Goodsell, D. S., Huey, R., and Olson, A. J. (1996) Distributed automated docking of flexible ligands to proteins: Parallel applications of AutoDock 2.4, *J. Comput. Aided Mol. Des. 10*, 293-304.

38. Huey, R., Morris, G. M., Olson, A. J., and Goodsell, D. S. (2007) A semiempirical free energy force field with charge-based desolvation, *Journal of Computational Chemistry 28*, 1145-1152.

39. Morris, G. M., Goodsell, D. S., Halliday, R. S., Huey, R., Hart, W. E., Belew, R. K., and Olson, A. J. (1998) Automated docking using a Lamarckian genetic algorithm and an empirical binding free energy function, *J. Comput. Chem. 19*, 1639-1662.

40. Rosenfeld, R. J., Goodsell, D. S., Musah, R. A., Morris, G. M., Goodin, D. B., and Olson, A. J. (2003) Automated docking of ligands to an artificial active site: augmenting crystallographic analysis with computer modeling, *J. Comput. Aided Mol. Des. 17*, 525-536.

41. Bertini, I., Donaire, A., Luchinat, C., and Rosato, A. (1997) Paramagnetic relaxation as a tool for solution structure determination: Clostridium pasteurianum ferredoxin as an example, *Proteins-Structure Function and Genetics 29*, 348-358.

42. Clore, G. M., and Iwahara, J. (2009) Theory, Practice, and Applications of Paramagnetic Relaxation Enhancement for the Characterization of Transient Low-Population States of Biological Macromolecules and Their Complexes, *Chem. Rev. 109*, 4108-4139.

43. Pintacuda, G., John, M., Su, X. C., and Otting, G. (2007) NMR structure determination of protein-ligand complexes by lanthanide labeling, *Acc. Chem. Res. 40*, 206-212.

44.   John, M., Pintacuda, G., Park, A. Y., Dixon, N. E., and Otting, G. (2006) Structure determination of protein-ligand complexes by transferred paramagnetic shifts, *J. Am. Chem. Soc. 128*, 12910-12916.
45.   Gay, G. L., Lindhout, D. A., and Sykes, B. D. (2004) Using lanthanide ions to align troponin complexes in solution: Order of lanthanide occupancy in cardiac troponin C, *Protein Sci. 13*, 640-651.
46.   Wang, C. L. A., Leavis, P. C., Dehorrocks, W., and Gergely, J. (1981) Binding of Lanthanide Ions to Troponin-C, *Biochemistry 20*, 2439-2444.
47.   Robertson, I. M., Sun, Y. B., Li, M. X., and Sykes, B. D. (2010) A structural and functional perspective into the mechanism of Ca2+-sensitizers that target the cardiac troponin complex, *J. Mol. Cell. Cardiol. 49*, 1031-1041.
48.   Marsden, B. J., Hodges, R. S., and Sykes, B. D. (1988) H-1-Nmr Studies of Synthetic Peptide Analogs of Calcium-Binding Site-Iii of Rabbit Skeletal Troponin-C - Effect on the Lanthanum Affinity of the Interchange of Aspartic-Acid and Asparagine Residues at the Metal-Ion Coordinating Positions, *Biochemistry 27*, 4198-4206.

Appendix C.

Visualizing the principal component of ^{1}H,^{15}N-HSQC NMR spectral changes that reflect protein structural or functional properties: Application to Troponin C*

Summary

Laboratories often repeatedly determine the structure of a given protein under a variety of conditions, mutations, modifications, or in a number of states. This approach can be cumbersome and tedious. Given then a database of structures, identifiers, and corresponding ^{1}H,^{15}N-HSQC NMR spectra for homologous proteins, we investigated whether structural information could be ascertained for a new homolog solely from its ^{1}H,^{15}N-HSQC NMR spectrum. We addressed this question with two different approaches. First, we used a semi-automated approach with the program, ORBplus. ORBplus looks for patterns in the chemical shifts and correlates these commonalities to the explicit property of interest. ORBplus ranks resonances based on consistency of the magnitude and direction of the chemical shifts within the database, and the chemical shift correlation of the unknown protein with the database. ORBplus visualizes the results by a histogram and a vector diagram, and provides residue specific predictions on structural similarities with the database. The second method we used was partial least squares (PLS), which is a multivariate statistical technique used to correlate response and predictor variables. We investigated the ability of these methods to predict the tertiary structure of the contractile regulatory protein troponin C. Troponin C undergoes a closed-to-open conformational change, which is coupled to its function in muscle. We found that both ORBplus and PLS were able to identify patterns in the ^{1}H,^{15}N-HSQC NMR data from different states of troponin C that correlated to its conformation.

Introduction

The determination of protein structures by NMR spectroscopy is a valuable tool used by scientists that span a wide array of disciplines. Laboratories often repeatedly determine the structure of a protein under a variety of conditions, mutations, modifications, or in a number of ligand-bound states; however, this can be tedious. For example, medicinal chemists are interested in protein-drug structures to aid in the design of novel drugs, but determination of many similar structures with different drugs can be too slow to be effective in the discovery pipeline. As a result, several other approaches have been adopted over the years to help rapidly characterize protein and protein-ligand structures. Chemical shift mapping utilizes the basic hypothesis that if a ligand binds a target the chemical environment surrounding residues lining the interaction surface will be changed as a consequence of binding (for reviews on this and other NMR screening methods see (*1, 2*)). Typically, researches use ^{15}N-labeled protein to rapidly scan these interactions in order to localize a binding site and quantitate ligand stoichiometry and affinity. The benefit of this approach is it can readily distinguish whether the target and ligand are interacting and may be able to predict a binding surface. The downside is that amide chemical shifts are sensitive to a variety of sources including structure, dynamics, hydrogen bonding, and solvent accessibility; therefore, chemical shift perturbations induced by ligand binding may be remote from its binding site. For example, chemical shift perturbations of amide resonances may stem from an overall conformational or stability change in the target upon binding a ligand. In this case, simply chemical shift mapping will not be effective at localizing the binding site of a ligand. On the other hand, if a series of compounds induce a similar conformational change in the target, then this perceived limitation of amide chemical shift mapping can be utilized to the user's advantage. Given then a database of structures, identifiers (i.e. target conformation), and

corresponding $^1H,^{15}N$-HSQC NMR spectra for set of homologous proteins, it is interesting to ask: can structural information be ascertained for a new homolog solely from its $^1H,^{15}N$-HSQC NMR spectrum?

We address this possibility in the context of the cardiac regulatory protein troponin C. Cardiac troponin C (cTnC) is the Ca^{2+}-binding subunit of the heterotrimeric troponin complex. The two other proteins in the complex are: troponin I (cTnI), the inhibitory subunit, and troponin T (cTnT), the subunit that tethers the complex to the muscle fiber. cTnC has two high-affinity metal binding sites in its C-terminal lobe (cCTnC) that remain bound to Ca^{2+} or Mg^{2+} during contraction and relaxation; and one lower affinity Ca^{2+} binding site in its N-terminal lobe (cNTnC). Muscle contraction is triggered when Ca^{2+} binds to cNTnC and induces a large conformational change from a 'closed' to a 'partially open' state so that cNTnC can bind cTnI. At low Ca^{2+} levels, cNTnC is in its apo state and cTnI is bound to actin, preventing contraction from occurring. When Ca^{2+} binds cNTnC the switch region of cTnI (cTnI$_{147-163}$) interacts with and stabilizes the 'fully open' state of cNTnC and its inhibition of contraction is abrogated. The structures of a number of these physiological states of cNTnC have been solved by NMR spectroscopy and X-ray crystallography. The apo and Ca^{2+} bound states of cNTnC and cTnC were solved by NMR spectroscopy (*3, 4*). The NMR structure of cNTnC-Ca^{2+} in complex with cTnI$_{147-163}$ was also solved by NMR (*5*). Later, the X-ray structure of the core troponin complex (cTnC-3Ca^{2+}-cTnI$_{31-210}$-cTnT$_{183-288}$) was solved (*6*). In addition to these natural states of cTnC, a number of structures have been solved for cNTnC-Ca^{2+}-drug (*7-9*) and cNTnC-Ca^{2+}-cTnI-drug (*10-12*) complexes.

The tertiary structure of troponin C can be defined by the AB and CD inter-helical angles. While it is convenient to discuss the structure of cNTnC in terms of a single static conformation, it is important to emphasize that the structures are dynamic and are more correctly viewed as an ensemble. For example, the Ca^{2+}-saturated state of cNTnC is not

actually 'partially open' but rather is in a dynamic equilibrium between open and closed states (*13-15*). When cTnI$_{147-163}$ binds cNTnC it stabilizes its open state (see Figure C-1a). The corresponding ^{1}H,^{15}N-HSQC is shown in Figure C-1b – which highlights the large chemical shift perturbations induced by the addition of cTnI$_{147-163}$. The side chain of residue Leu48 of cNTnC makes intramolecular hydrophobic contacts with A23, F20, and F27 which stabilizes the closed conformation of the AB inter-helical angle observed for cNTnC-Ca^{2+} (*3*). Tikunova and Davis postulated that the mutation of this residue to the hydrophilic residue, glutamine, should disrupt these hydrophobic interactions and thus stabilize a more open form of cNTnC (*16*). Their functional studies on this mutation indicated that cNTnC(L48Q) was more active than cNTnC, probably due to its more open conformation. In Figure C-1c we overlay the ^{1}H,^{15}N-HSQC spectra of cNTnC-Ca^{2+} with cNTnC(L48Q)-Ca^{2+}. Many of the same residues that are perturbed by cTnI$_{147-163}$ are also shifted by this leucine to glutamine mutation. This protein thus serves as a query protein for the data mining approaches we investigate herein to answer the straightforward but subtle question: *can we confidently define the inter-helical angles that define the troponin C's tertiary structure from chemical shift data in lieu of complete structure determination*?

We used two different approaches to look for patterns in ^{1}H,^{15}N HSQC spectra: a semi-automated program ORBplus and the multivariate statistical analysis - partial least squares (PLS). ORBplus looks for patterns in the chemical shifts and correlates these commonalities to the explicit property of interest. The program ranks resonances based on consistency of the magnitude and direction of the chemical shifts within the database, and the chemical shift correlation of the unknown protein with the database and visualizes the results by a histogram and a vector diagram, and provides residue specific predictions on structural similarities with the database. The PLS approach is a statistical technique that is used to maximize covariance between responses and predictors of
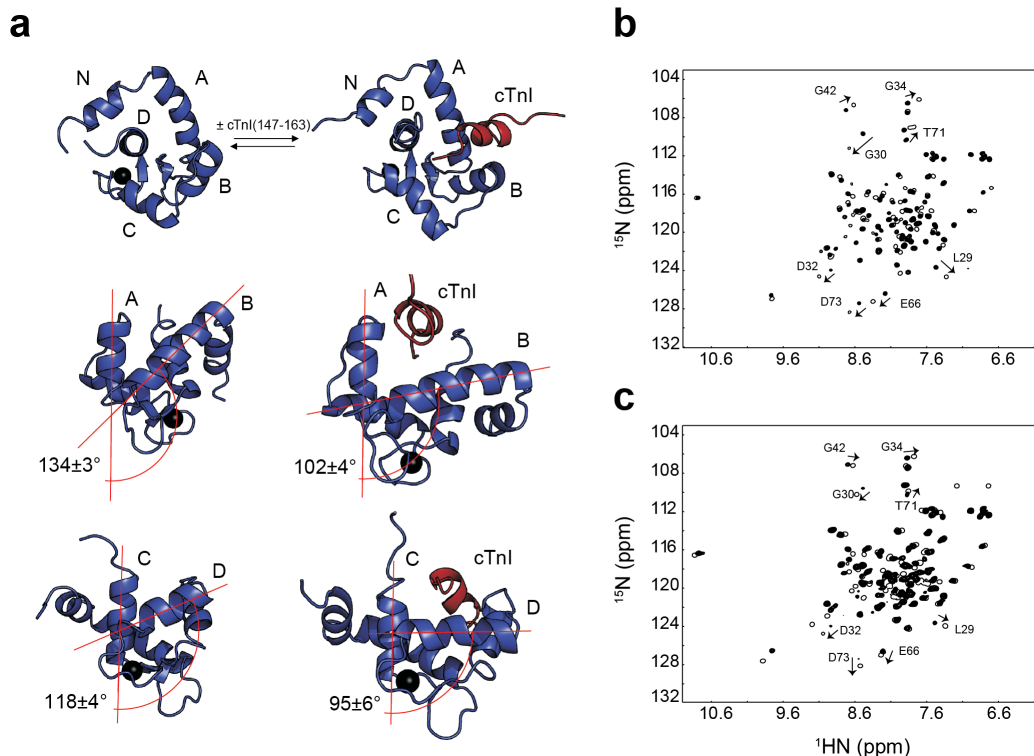
Figure C-1. The closed-to-open transition of cardiac troponin C upon binding troponin I. **a.** The structures of cNTnC and the cNTnC-cTnI$_{147\text{-}163}$ complex are shown. The five helices of cNTnC are labeled (N, A, B, C, D). The inter-helical angles, AB and CD, for the two states of cNTnC are shown below the corresponding structures. As the interhelical angles decrease towards 90°, cNTnC is more open. **b.** The overlay of ^{1}H,^{15}N-HSQC spectra from cNTnC (filled contours) and the cNTnC -cTnI$_{147\text{-}163}$ complex (open contours). **c.** The overlay of ^{1}H,^{15}N-HSQC spectra from cNTnC (filled contours) and cNTnC(L48Q) (open contours). Several of the residues that are significantly perturbed by cTnI$_{147\text{-}163}$ and the L48Q mutation are labeled.

corresponding observable variables. PLS and other multivariate analyses, such as principal component analysis, are popular in the analysis of large databases such as identifying interesting motions in a molecular dynamics trajectory (*17-20*) and metabolic foot-printing in metabolomics (*21, 22*).

Study Case Results

Semi-automated Analysis with ORBplus

ORBplus is a semi-automated tool for the identification of patterns within ^{1}H,^{15}N-HSQC spectra that correspond to structural or functional properties of a protein [1]. ORBplus follows a similar semi-automated approach and design utilized by the NMR assignment tool, Smartnotebook (*23*), and the NMR chemical shift predictor tool, ORB (*24*). ORBplus works by comparing the assigned ^{1}H,^{15}N-HSQC NMR spectrum of a query protein of unknown properties with a database of ^{1}H,^{15}N-HSQC NMR spectra from proteins with corresponding known properties. The feature in question can be, but is not limited to, a structural property. ORBplus takes NMRView (*25*) peaklist files or Biological Magnetic Resonance Bank (BMRB) formatted files as input for both the database ^{1}H,^{15}N-HSQC data and the query chemical shift data. It requires at least two datasets that represent two different states (i.e. open and closed or active and inactive). ORBplus treats each chemical shift in the ^{1}H,^{15}N-HSQCs as coordinates and connects them *via* a vector. In the case where many datasets exist for a given state, the ^{1}H,^{15}N-HSQC data are averaged and a vector is drawn to the averaged ^{1}H,^{15}N-HSQC data point by default; however, the user may decide to compare the query dataset to just one database dataset as well. ORBplus makes projections by automatically ranking residues as good predictors by four criteria: (1) the magnitude of chemical shift in the

---

[1] The ORBplus program and extensive documentation is freely available at
http://www.bionmr.ualberta.ca/bds/software/orbplus/

database files, (2) similarity of chemical shift within the database files, (3) magnitude of chemical shift for the query dataset, and (4) the direction of chemical shift for the query data in comparison with the database datasets. ORBplus also has the option for the user to manually select residues of interest that may not have been automatically selected by ORBplus. Once the predictor residues have been chosen, ORBplus predicts the query data's properties by projecting the query chemical shift onto the average database vector and comparing the fraction length of the query shift to the average. For example, in the case where we are considering inter-helical angles, if the projection of the query data is 75% the length of the average vector, then ORBplus predicts for that residue, the inter-helical angle of the query protein is 75% that of the average angle in the database.

We provided ORBplus with ^{1}H,^{15}N-HSQC data for corresponding cNTnC structures with known AB and CD interhelical angles (see Table C-1). First we looked to see how ORBplus would perform given ^{1}H,^{15}N-HSQC of the cNTnC-Ca^{2+}-cTnI$_{147\text{-}163}$ complex (unless otherwise stated all forms of cNTnC mentioned will assume Ca^{2+} is bound). Although ORBplus will automatically pick the top ten residues to predict the unknown query protein's properties, we wanted to probe for specific changes in the two inter-helical angles. To do this, we chose to separately follow residues from, or directly adjacent to, Ca^{2+}-binding site I (residues 27-40), and Ca^{2+}-binding site II (residues 64-74), because it has been shown that these regions experience large chemical shift perturbations when cNTnC's conformation changes (*5*). Using these residues, ORBplus predicted an AB inter-helical angle of 104° and a CD angle of 90°. These results are within the error of those determined experimentally: 102 ± 4° and 95 ± 6° (NMR) or 104° and 96° (X-ray)[2]. The vector diagrams for residues in site I and site II are shown in Figure C-2.

---

[2]Angles calculated with the program Interhlx (K. Yap, University of Toronto)

Table C-1. Inter-helical angles of cNTnC structures [a]. The smaller the interhelical angle, the more open the cNTnC structure is (see Figure C-1a). The reference closed state of cNTnC used by ORBplus (Figure C-2) is highlighted in grey.

| | | | | Interhelical Angles | |
cNTnC structures			PDB code	AB[b]	CD[c]
cNTnC(apo)		(NMR)	1SPY	140 ± 3°	127 ± 5°
cNTnC-Ca^{2+}		(NMR)	1AP4	134 ± 3°	118 ± 4°
cNTnC(acys)-Ca^{2+}		(NMR)	2CTN	142 ± 3°	109 ± 4°
cNTnC-Ca^{2+}-$cTnI_{147-163}$		(NMR)	1MXL	102 ± 4°	95 ± 6°
cTnC(acys)-$3Ca^{2+}$-$cTnI_{31-210}$-$cTnT_{183-288}$	(X-ray)		1J1D	104°	96°
cNTnC(F77W,V82A)-Ca^{2+}		(NMR)	2JXL	108 ± 5°	95 ± 4°
cTnC(acys)-$3Ca^{2+}$-3bepridil		(X-ray)	1DTL	93°	89°
cNTnC-Ca^{2+}-$cTnI_{147-163}$-bepridil		(NMR)	1LXF	121 ± 4°	85 ± 4°
cNTnC(acys)-Ca^{2+}-2TFP		(X-ray)	1WRK	107°	104°
cNTnC(acys)-Ca^{2+}-W7		(NMR)	2KFX	114 ± 3°	86 ± 2°
cNTnC(acys)-Ca^{2+}- $cTnI_{147-163}$-W7		(NMR)	2KRD	112 ± 5°	63 ± 6°
cNTnC(acys)-Ca^{2+}- $cTnI_{144-163}$-dfbp-o		(NMR)	2L1R	96 ± 6°	89 ± 6°

[a]Angles calculated with the program Interhlx (K. Yap, University of Toronto)
[b]AB interhelical angles were determined by defining the C helix as residues 17-26, and the D helix was defined as residues 40-46 for all structures.
[c]CD interhelical angles were determined by defining the C helix as residues 54-62, and the D helix was defined as residues 75-83 for all structures.
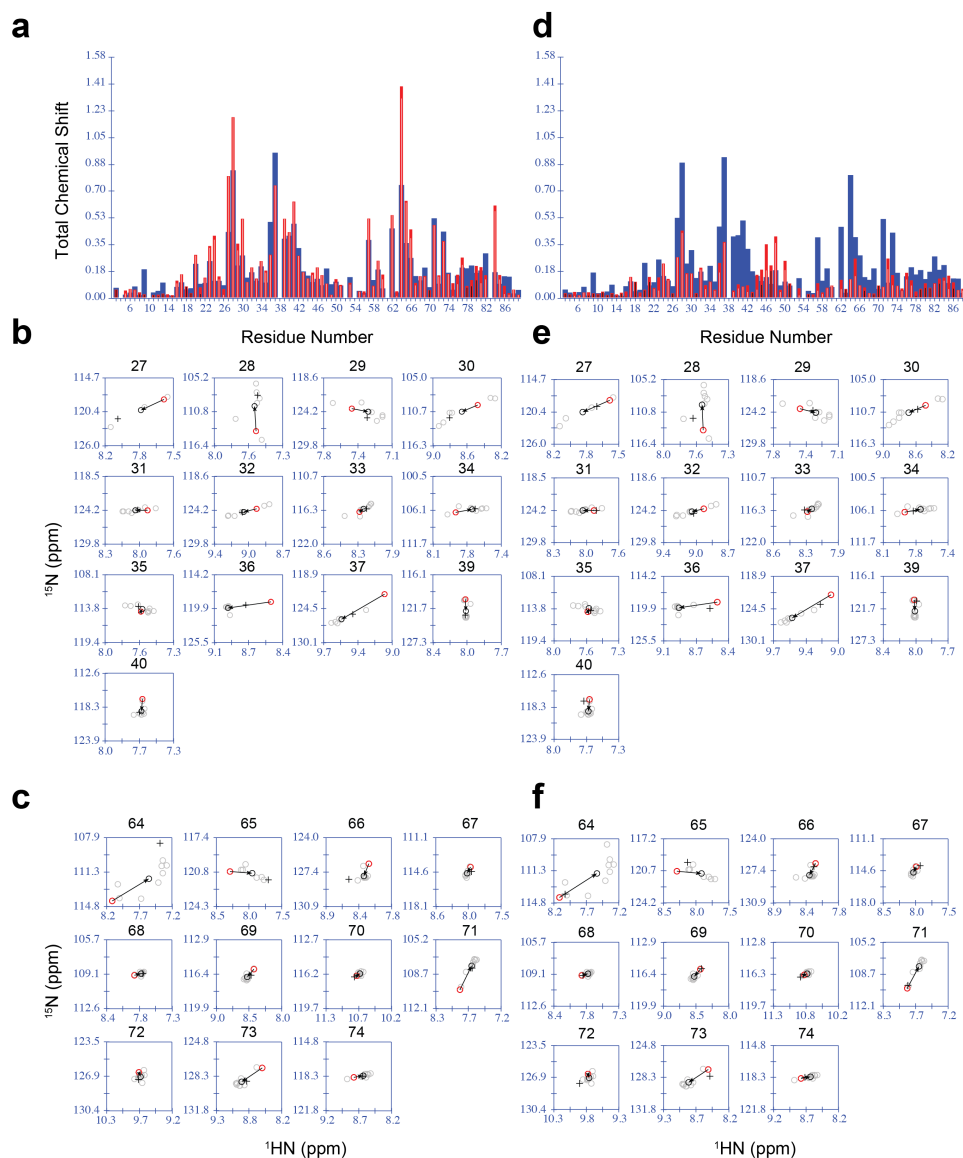
Figure C-2. ORBplus chemical shift histogram and spectral plots displaying the prediction of the conformation of (a-c) the cNTnC-cTnI$_{147-163}$ complex and (d-f) for cNTnC(L48Q). (**a,d**) Histograms compare the magnitude of chemical shift changes of the query protein (red) and the average chemical shift of the database proteins (blue) from the reference closed state (see Table C-1). The histograms also compare the direction of chemical shift change with the average chemical shift change (white inner bar indicates the same direction and blue inner bar indicates opposite direction – see ORBplus documentation for details). Spectral perturbations for residues (**b, e**) in site I and (**c, f**) site II are shown. The red circles represent the chemical shift of the reference closed state (see table I), the light grey circles represent the chemical shifts for the database proteins, and the black circles the average chemical shift of the database proteins. The cross is the chemical shift of the query protein.

Once we established that ORBplus could predict the inter-helical angles of cNTnC when in complex with cTnI$_{147-163}$ we tested it on cNTnC(L48Q). Leu48 lies at the end of the B helix of cNTnC and makes several hydrophobic interactions with residues along the A helix thereby stabilizing the closed conformation of cNTnC, even in the presence of Ca^{2+} (see Table C-1). The mutation of leu48 to a glutamine is thought to disrupt these crucial hydrophobic interactions: the strong NOEs that were observed by Sia *et al.* between the terminal methyls of Ala23 and Leu48 (*3*) are not observed between the terminal NH$_2$ of Gln48 and the β-methyl of Ala23 (Figure C-3). The top ten automatically chosen residues by ORBplus are displayed in Table C-2. For the same reasons described above, we manually selected residues in sites I and II for the calculation of the AB and CD interhelical angles. ORBplus predicted that the AB inter-helical angle of cNTnC(L48Q) is slightly more open than cNTnC(wt) (124° *versus* 134 ± 3°), whereas the CD interhelical angle is practically unchanged (113° *versus* 118 ± 4°). These results are as anticipated and illustrate the efficacy of ORBplus at predicting even subtle perturbations in the conformation of cNTnC.

Multivariate Analysis with partial least squares

Multivariate analysis is a useful method used to extract a fundamental property from a large amount of data, and recently it has been used to look at 2D-NMR data. Sakurai and Goto used principal component analysis (PCA) to correlate the pH-dependent conformation of β-lactoglobulin with ^{1}H,^{15}N-HSQC spectra (*26*). They were able to identify a key subset of residues that underwent chemical shift changes as a function of pH – an observation they were able to link to several structural transitions. Jaumot *et al.* utilized multivariate curve resolution alternating least squares analysis to understand the underlying mechanism of a chemical reaction monitored by ^{1}H,^{15}N-HSQC spectroscopy (*27*).
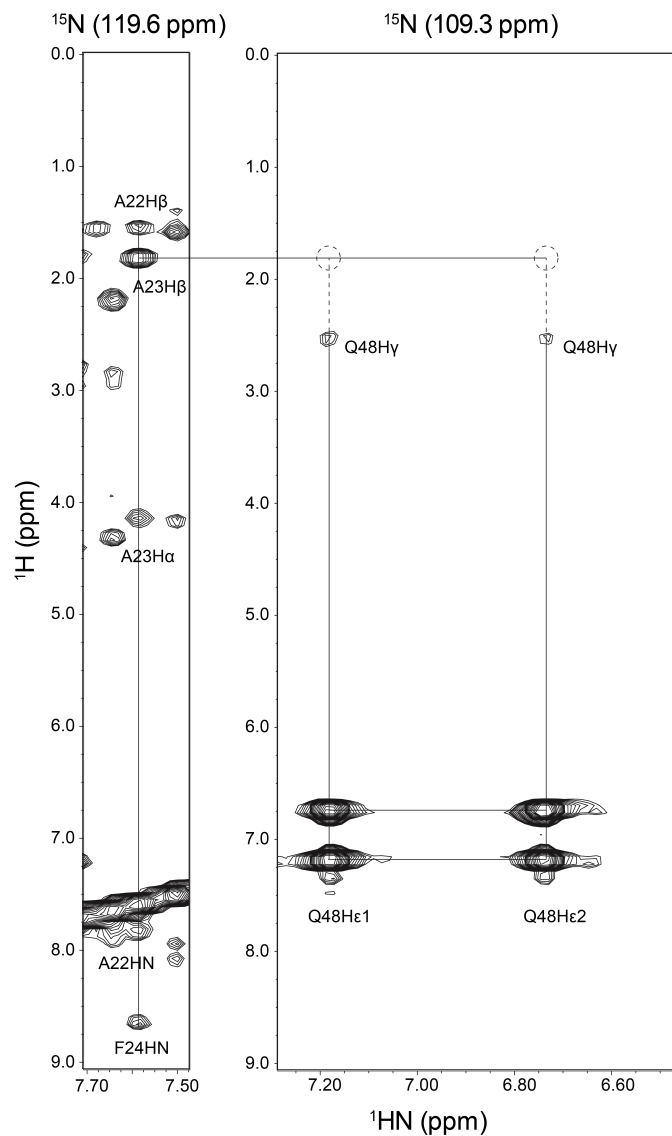
Figure C-3. Regions of ^{1}HN-^{1}H slices taken from 3D-^{15}N-NOESYHSQC spectrum of cNTnC(L48Q). The spectrum was recorded with 0.3-0.4 mM cNTnC(L48Q). The number of total points were 32 x 128 x 512 and the experiment took ~60 hours to acquire.

Table C-2. Top ten residues as indicators of the conformation of cNTnC. Residues in site I or site II are identified. The first column lists the ten most predictive residues of conformation of cNTnC(L48Q) as automatically chosen by ORBplus (using the default parameters) based on the correlation of the chemical shift magnitude and direction of cNTnC(L48Q) with the database chemical shifts. The second and third columns are the top ten residues from the VIP plot for the ^{1}HN (Figure C-4b) and ^{15}N (Figure C-4c) chemical shifts.

ORBplus	PLS (^{1}HN chemical shifts)	PLS (^{15}N chemical shifts)
S37 (site I)	F74 (site II)	A22
V28 (site I)	G34 (site I)	F77
I36 (site I)	G68 (site II)	E59
V64 (site II)	E32 (site I)	D73 (site II)
F27 (site I)	E59	S37 (site I)
E66 (site II)	L29 (site I)	T38 (site I)
L41	S37 (site I)	E40 (site I)
T71 (site II)	L41	V28 (site I)
D73 (site II)	D62	E66 (site II)
D65 (site II)	A31 (site I)	E32 (site I)

Multivariate analysis has also been used in other aspects of structural biology, for example it resolved the crucial intermolecular features of diubiquitin involved in stabilizing the different lysine-linked ubiquitin chains (*28*).

We subjected the same ^{1}H,^{15}N-HSQC NMR chemical shift data used in ORBplus to a PLS analysis using the statistical software Simca P+ v12.0.1 (Umetrics, Umeå, Sweden)(*29*). PLS was used to maximize the correlation between the NMR data and the conformation of cNTnC. We designated the chemical shift data as the X variables and the inter-helical angle data as the Y variables and allowed Simca to use the standard defaults for mean centering and scaling. All residues were given a corresponding angle: residues 3-52 were associated with the AB inter-helical angle and residues 53-89 were given CD inter-helical angles (cNTnC(L48Q) data only included chemical shifts since we do not have experimentally derived inter-helical angles). The scatter plot is shown in Figure C-4a. The plot indicates that there are two groupings: one including the closed states of cNTnC (2CTN, 1AP4) and the other more dispersed various open states of cNTnC (2JXL, 1WRK, 1MXL, 2KFX, 1DTL, 1LXF, 2KRD, and 2L1R).

The variable influence on projection (VIP) plots (Figure C-4b,c) can be used to highlight the most important residues for fitting the PLS model; the higher the VIP score the more the residue contributes to the model. The results from the ^{1}HN and ^{15}N nuclei clearly indicate that the most important chemical shifts reside in the two loops (sites I and II) of cNTnC (see Table C-2 for a list of the top 10 residues). To compare the predictions from PLS with those from ORBplus, we used the PLS model to predict the angles of cNTnC-cTnI$_{147-163}$ and cNTnC(L48Q). We only looked at predictions for residues in site I and site II, as was done in ORBplus. PLS predicted an AB inter-helical angle of 105 ± 1º and a CD inter-helical angle of 89 ± 0.1º. These results are similar to those determined by Interhlx (AB: 102 ± 4º and CD: 95 ± 6º (NMR); AB: 104º and CD: 96º (X-
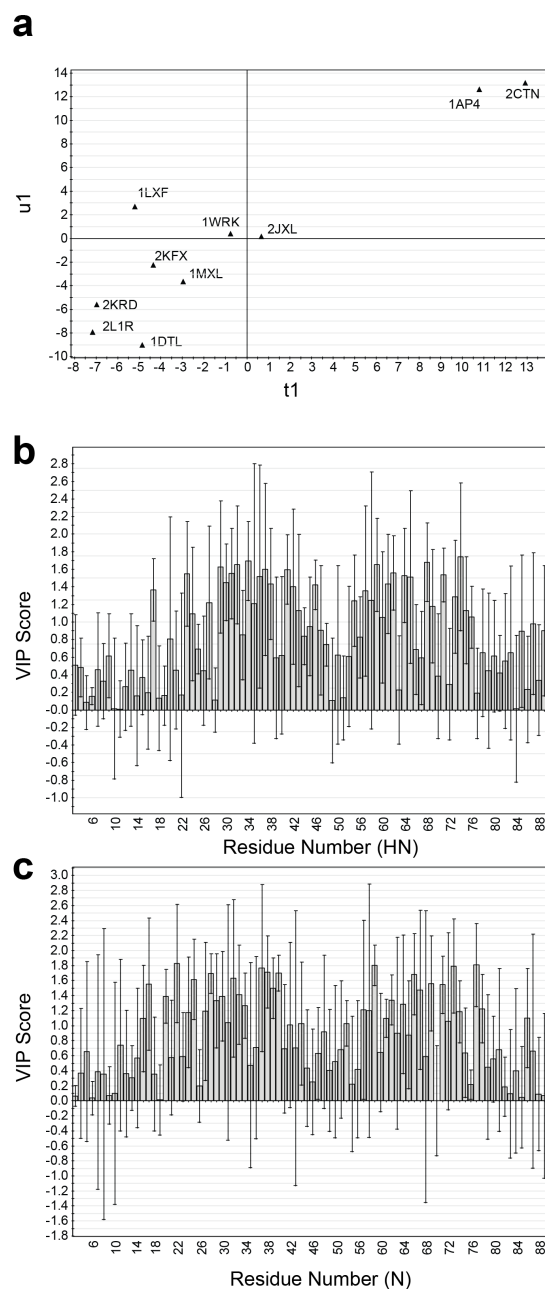
Figure C-4. PLS scatter and VIP plots of the ^{1}H,^{15}N-HSQC data for the cNTnC structures. **a**. u_1/t_1 scatter plot shows the correlation between inter-helical angles and chemical shifts. The cNTnC structures are labeled by their protein databank (PDB) codes (see Table C-1). The PLS analysis used a one component model with $R^2Y=0.509$ and $Q^2=0.303$. (**b, c**) Variable influence on projection (VIP) scores for ^{1}H,^{15}N-HSQC data versus the sequence of cNTnC.

ray)). The angles predicted by the model for cNTnC(L48Q) were 123 ± 2º for the AB inter-helical angle and 105 ± 0.4º for the CD inter-helical angle. The AB inter-helical angle is very close between the ORBplus and PLS predictions; however, the CD inter-helical angle prediction has a variance between the two methods of ~8º (ORBplus = 113º; PLS = 105 ± 0.4º).

Discussion

The use of chemical shifts to predict protein structure has been employed by others (30-32); however, these methods all require the assignment of ^{13}C-labeled protein to predict tertiary structure. In a previously published study, Biekofsky *et al.* used *ab initio* methods to correlate ^{15}N chemical shift differences to Ca^{2+}-coordination and protein conformation in troponin C and other EF-hand proteins (33). In this work, detailed analysis of solely ^{1}H,^{15}N-HSQC NMR spectra from a variety of conformational states of cNTnC was able to provide insight into the tertiary structure of cNTnC(L48Q). We used two methods to analyze the NMR data: a semi-automated program, ORBplus; and the multivariate statistical method, PLS. Both programs predicted that cNTnC(L48Q) was more open than cNTnC at the AB inter-helical interface, but differed in their prediction of the effect of the mutation on the CD inter-helical angle. ORBplus predicted only a minor perturbation, while the PLS model predicted a slightly more open angle.

The quality factors (R^{2}Y=0.509 and Q^2=0.303) for the PLS model were slightly less than that expected for a biological sample (R^{2}Y=0.5 and Q^2=0.4) (29), which illustrates the model's limitations in its fit and predictability. There are several explanations for PLS's mediocre predictability: slight variations in sample conditions (pH, protein concentration, protein-ligand ratios), lack of consistency between the conditions used in the structure determination and in the ^{1}H,^{15}N-HSQC experiments (X-ray structures vs. NMR data), ^{1}H,^{15}N-HSQC data were

acquired with just cNTnC whereas X-ray structures often included full length cTnC, missing data in the $^1H,^{15}N$-HSQC spectra (TFP binds to cNTnC in the intermediate exchange regime, and some peaks were not able to be followed throughout the titration), and perhaps most importantly, the conformational model is simplistic. Clearly some of the chemical shift changes could result from proximity to the different ligands/mutations and *not* solely from a conformational change, such as ring current effects induced by aromatic rings present on the ligands. In fact, this phenomenon has been exploited by McCoy and Wyss to predict the binding site of a ligand on a protein with the program Jsurf (*34*). However, in the case of troponin C, trying to predict a binding site by ring current effects using amide chemical shifts has led to erroneous binding site predictions, because the large chemical shifts induced by ligand binding are largely dominated by the opening and closing of troponin C (*35*). It may be that the more straightforward approach of ORBplus, augmented by the interactive GUI and human intuition, is a better method when dealing with noisy data. One may envision a two pronged approach: (1) use PLS to identify the residues that correlate to the predictor variable, and (2) switch to ORBplus to analyze the data in a semi-automated way – selecting the most important residues chosen by PLS – to predict structure or function. ORBplus is not meant to compete with other multivariate methods of analysis, but to provide the user with a detailed visualization of the spectral changes that most reflect a change in a given property (such as activity, stability, structure, etc.) for the protein in question. In our system, it led to the immediate demonstration that the closed-to-open transition could be different for the AB and CD hinges depending upon the mutation or ligand.

There are a number of obvious advantages to using these types of computational approaches in predicting protein structure. For example, understanding how a large number of mutations perturb protein structure without repeating the cumbersome task of structure determination.

Another application may be in pharmaceutical research; multivariate analysis is already being utilized by medicinal chemists for lead optimization (for a review see (*36*)). The ability of multivariate techniques to predict the conformational change induced when a protein binds a lead compound may be very useful, particularly if the compound of interest is designed to modulate the protein's tertiary structure in a specific manner. These models need not replace structure determination either: the conformational predictions could be used as restraints in a structure calculation to aid in refinement. It is important to note that although this work has emphasized the role ^{1}H,^{15}N-HSQC analysis can play on predicting protein structure it does not have to be limited to this; in any situation where NMR chemical shifts and an observable (i.e. enzyme kinetics, ligand binding) are correlated, this type of investigation could be applied.

References

1. Pellecchia, M., Sem, D. S., and Wuthrich, K. (2002) NMR in drug discovery, *Nat. Rev. Drug Discovery 1*, 211-219.
2. Stockman, B. J., and Dalvit, C. (2002) NMR screening techniques in drug discovery and drug design, *Prog. Nucl. Magn. Reson. Spectrosc. 41*, 187-231.
3. Sia, S. K., Li, M. X., Spyracopoulos, L., Gagne, S. M., Liu, W., Putkey, J. A., and Sykes, B. D. (1997) Structure of cardiac muscle troponin C unexpectedly reveals a closed regulatory domain, *J. Biol. Chem. 272*, 18216-18221.
4. Spyracopoulos, L., Li, M. X., Sia, S. K., Gagne, S. M., Chandra, M., Solaro, R. J., and Sykes, B. D. (1997) Calcium-induced structural transition in the regulatory domain of human cardiac troponin C, *Biochemistry 36*, 12138-12146.
5. Li, M. X., Spyracopoulos, L., and Sykes, B. D. (1999) Binding of cardiac troponin-I147-163 induces a structural opening in human cardiac troponin-C, *Biochemistry 38*, 8289-8298.
6. Takeda, S., Yamashita, A., Maeda, K., and Maeda, Y. (2003) Structure of the core domain of human cardiac troponin in the Ca(2+)-saturated form, *Nature 424*, 35-41.
7. Hoffman, R. M. B., and Sykes, B. D. (2009) Structure of the Inhibitor W7 Bound to the Regulatory Domain of Cardiac Troponin C, *Biochemistry 48*, 5541-5552.
8. Li, Y., Love, M. L., Putkey, J. A., and Cohen, C. (2000) Bepridil opens the regulatory N-terminal lobe of cardiac troponin C, *Proc. Natl. Acad. Sci. U. S. A. 97*, 5140-5145.
9. Igarashi, T., Takeda, S., and Mori, H. (2005) Crystal structure of the N-terminal domain of human cardiac troponin C in complex with a calcium-sensitizer; trifluoperazine, *J. Mol. Cell. Cardiol. 39*, 1016-1016.
10. Oleszczuk, M., Robertson, I. M., Li, M. X., and Sykes, B. D. (2010) Solution structure of the regulatory domain of human cardiac troponin C in complex with the switch region of cardiac troponin I and W7: The basis of W7 as an inhibitor of cardiac muscle contraction, *J. Mol. Cell. Cardiol. 48*, 925-933.
11. Robertson, I. M., Sun, Y. B., Li, M. X., and Sykes, B. D. (2010) A structural and functional perspective into the mechanism of Ca2+-sensitizers that target the cardiac troponin complex, *J. Mol. Cell. Cardiol. 49*, 1031-1041.
12. Wang, X., Li, M. X., and Sykes, B. D. (2002) Structure of the regulatory N-domain of human cardiac troponin C in complex with human cardiac troponin I147-163 and bepridil, *J. Biol. Chem. 277*, 31124-31133.
13. Paakkonen, K., Sorsa, T., Drakenberg, T., Pollesello, P., Tilgmann, C., Permi, P., Heikkinen, S., Kilpelainen, I., and Annila, A. (2000) Conformations of the regulatory domain of cardiac troponin C

examined by residual dipolar couplings, *Eur. J. Biochem. 267*, 6665-6672.

14. McKay, R. T., Saltibus, L. F., Li, M. X., and Sykes, B. D. (2000) Energetics of the induced structural change in a Ca2+ regulatory protein: Ca2+ and troponin I peptide binding to the E41A mutant of the N-domain of skeletal troponin C, *Biochemistry 39*, 12731-12738.

15. Eichmueller, C., and Skrynnikov, N. R. (2007) Observation of mu s time-scale protein dynamics in the presence of Ln(3+)stop ions: application to the N-terminal domain of cardiac troponin C, *J. Biomol. NMR 37*, 79-95.

16. Tikunova, S. B., and Davis, J. P. (2004) Designing calcium-sensitizing mutations in the regulatory domain of cardiac troponin C, *J. Biol. Chem. 279*, 35341-35352.

17. Caves, L. S. D., Evanseck, J. D., and Karplus, M. (1998) Locally accessible conformations of proteins: Multiple molecular dynamics simulations of crambin, *Protein Sci. 7*, 649-666.

18. Ichiye, T., and Karplus, M. (1991) Collective Motions in Proteins - a Covariance Analysis of Atomic Fluctuations in Molecular-Dynamics and Normal Mode Simulations, *Proteins-Structure Function and Genetics 11*, 205-217.

19. Mu, Y. G., Nguyen, P. H., and Stock, G. (2005) Energy landscape of a small peptide revealed by dihedral angle principal component analysis, *Proteins-Structure Function and Bioinformatics 58*, 45-52.

20. Kitao, A., Hayward, S., and Go, N. (1998) Energy landscape of a native protein: Jumping-among-minima model, *Proteins-Structure Function and Genetics 33*, 496-517.

21. Stoyanova, R., and Brown, T. R. (2001) NMR spectral quantitation by principal component analysis, *NMR Biomed. 14*, 271-277.

22. Lindon, J. C., Holmes, E., and Nicholson, J. K. (2001) Pattern recognition methods and applications in biomedical magnetic resonance, *Prog. Nucl. Magn. Reson. Spectrosc. 39*, 1-40.

23. Slupsky, C. M., Boyko, R. F., Booth, V. K., and Sykes, B. D. (2003) Smartnotebook: A semi-automated approach to protein sequential NMR resonance assignments, *J. Biomol. NMR 27*, 313-321.

24. Gronwald, W., Boyko, R. F., Sonnichsen, F. D., Wishart, D. S., and Sykes, B. D. (1997) ORB, a homology-based program for the prediction of protein NMR chemical shifts, *J. Biomol. NMR 10*, 165-179.

25. Johnson, B. A., and Blevins, R. A. (1994) Nmr View - a Computer-Program for the Visualization and Analysis of Nmr Data, *J. Biomol. NMR 4*, 603-614.

26. Sakurai, K., and Goto, Y. J. (2007) Principal component analysis of the pH-dependent conformational transitions of bovine beta-lactoglobulin monitored by heteronuclear NMR, *Proc. Natl. Acad. Sci. U. S. A. 104*, 15346-15351.

27. Jaumot, J., Marchan, V., Gargallo, R., Grandas, A., and Tauler, R. (2004) Multivariate curve resolution applied to the analysis and resolution of

two-dimensional [H-1,N-15] NMR reaction spectra, *Anal. Chem. 76*, 7094-7101.

28. Fushman, D., and Walker, O. (2010) Exploring the Linkage Dependence of Polyubiquitin Conformations Using Molecular Modeling, *J. Mol. Biol. 395*, 803-814.

29. Eriksson, L. J. E., Kettaneh-Wold, N., Trygg, J., Wikstrom, C., Wold, S. (2001) *Multi- and megavariate data analysis. Part 1: Principles and applications*, 2nd ed., Umetrics Academy: Umeå, Sweden.

30. Shen, Y., Vernon, R., Baker, D., and Bax, A. (2009) De novo protein structure generation from incomplete chemical shift assignments, *J. Biomol. NMR 43*, 63-78.

31. Shen, Y., Lange, O., Delaglio, F., Rossi, P., Aramini, J. M., Liu, G. H., Eletsky, A., Wu, Y. B., Singarapu, K. K., Lemak, A., Ignatchenko, A., Arrowsmith, C. H., Szyperski, T., Montelione, G. T., Baker, D., and Bax, A. (2008) Consistent blind protein structure generation from NMR chemical shift data, *Proc. Natl. Acad. Sci. U. S. A. 105*, 4685-4690.

32. Wishart, D. S., Arndt, D., Berjanskii, M., Tang, P., Zhou, J., and Lin, G. (2008) CS23D: a web server for rapid protein structure generation using NMR chemical shifts and sequence data, *Nucleic Acids Res. 36*, W496-W502.

33. Biekofsky, R. R., Turjanski, A. G., Estrin, D. A., Feeney, J., and Pastore, A. (2004) Ab initio study of NMR N-15 chemical shift differences induced by Ca2+ binding to EF-hand proteins, *Biochemistry 43*, 6554-6564.

34. McCoy, M. A., and Wyss, D. F. (2002) Spatial localization of ligand binding sites from electron current density surfaces calculated from NMR chemical shift perturbations, *J. Am. Chem. Soc. 124*, 11758-11763.

35. Robertson, I. M., Pineda-Sanabria, S., and Sykes, B. D. (In Press) Approaches to protein-ligand structure determination by NMR spectroscopy: applications in drug binding to the cardiac regulatory protein troponin C, *Biophysics and Structure to Counter Threats and Challenges*.

36. Gabrielsson, J., Lindberg, N. O., and Lundstedt, T. (2002) Multivariate methods in pharmaceutical applications, *J. Chemom. 16*, 141-160.

Appendix D.

The dilated cardiomyopathy mutation G159D in cardiac troponin C weakens the anchoring interaction with troponin I*

Summary

NMR spectroscopy has been employed to elucidate the molecular consequences of the DCM mutation G159D on the structure and dynamics of troponin C, and its interaction with troponin I. Since the molecular effects of human mutations are often subtle, all NMR experiments were run as direct side-by-side comparisons of the wild type C-domain of troponin C (cCTnC) and the mutant protein, G159D. In the presence of mutation, the affinity towards the anchoring region of cTnI ($cTnI_{34-71}$) was weakened ($K_D = 3.0 \pm 0.6$ µM) as compared to the wild type ($K_D < 1$ µM). Overall structure and dynamics of the $G159D \cdot cTnI_{34-71}$ complex were very similar to those of $cCTnC \cdot cTnI_{34-71}$. There were, however, significant changes in the ^1H, ^{13}C, and ^{15}N NMR chemical shifts, especially for the residues in direct contact with $cTnI_{34-71}$, and the changes in NOE connectivity patterns between $G159D \cdot cTnI_{34-71}$ and $cCTnC \cdot cTnI_{34-71}$. Thus, the most parsimonious hypothesis is that the development of disease results from the poor anchoring of cTnI to cCTnC, with the resulting increase in acto-myosin inhibition in agreement with physiological data. Another possibility is that long-range electrostatic interactions affect the binding of the inhibitory and switch regions of cTnI ($cTnI_{128-147}$ and $cTnI_{147-163}$) and/or the cardiac specific N-terminus of cTnI ($cTnI_{1-29}$) to the N-domain of cTnC. These important interactions are all spatially close in the X-ray structure of the cardiac TnC core.

*This work has been published elsewhere. Baryshnikova, OK, Robertson, IM, Mercier, P, Sykes, BD. (2008) The dilated cardiomyopathy mutation G159D in cardiac troponin C weakens the anchoring interaction with troponin I. *Biochemistry.* 47, 10950-10960.

Contributions: OKB and IMR are coauthors. OKB, IMR, and BDS designed the NMR experiments. IMR and OKB acquired the NMR data, assigned the chemical shifts, solved the structures of cCTnC and G159D, and wrote the manuscript with BDS. PM aided in the structure calculation. Dave Corson and OKB expressed and purified the protein.

Introduction

Calcium regulation of contraction in cardiac muscle is a fine tuned process that depends on the reliable function of its protein parts. The presence of mutations in contractile proteins can cause the development of cardiac disorders. Indeed, as revealed by genetic analysis, a large number of mutations in b-myosin, a-tropomyosin, troponin I (cTnI), and troponin T (cTnT) causes various forms of cardiomyopathy (*1, 2*). Troponin C (cTnC), the protein directly responsible for Ca^{2+} sensitivity of the thin filament, is highly conserved among mammals and was thought to have fewer mutations until recently (*3-5*).

Troponin C is a dumbbell shaped molecule with its structural domain, cCTnC, linked to its regulatory domain, cNTnC, through a stretch of 11 residues. During the contracting-relaxing cycle, cCTnC stays saturated with Ca^{2+} due to its high Ca^{2+} affinity. This domain is thought to be bound at all time to the anchoring region of cTnI (~ residues 34-71), which tethers cTnC to the thin filament. The Ca^{2+} binding site of cNTnC is occupied only when the concentration of Ca^{2+} is relatively high. This happens upon the release of Ca^{2+} from the sarcoplasmic reticulum resulting from muscle stimulation. Upon Ca^{2+} binding, cNTnC binds to the switch region of cTnI (~ residues 147-163), which pulls the inhibitory region of cTnI (~ residues 128-147) away from its binding site on actin, leading to the movement of tropomyosin and the exposure of myosin binding sites on actin, allowing the contraction (for reviews see (*6, 7*)).

Two mutations found in cNTnC, L29Q and E59D/D75Y, were linked to hypertrophic cardiomyopathy (FHC) and dilated cardiomyopathy (DCM), respectively (*3, 8*). As demonstrated in physiological experiments, L29Q resulted in a slight increase of Ca^{2+} sensitivity of the force development (*9*). L29Q also abolished the impact of phosphorylation on the activity of ATPase, the sliding velocity of the thin filament (*10*), and the kinetics of Ca^{2+} binding to the troponin complex (*11*). The presence of E59D/D75Y

resulted in a reduced ability to activate myosin ATPase (*12*) and a decreased Ca^{2+} sensitivity of force development (*8*). In structural studies (*13*), mutations L29Q and E59D/D75Y affected the interplay between the cardiac specific N-terminus of cTnI (~ residues 1-29) and the switch region of cTnI (~ residues 147-163), the binding of which is crucial for the transferring of Ca^{2+} signal through cTnC and further along the thin filament. In L29Q, the affinity towards $cTnI_{147\text{-}163}$ was not affected by the $cTnI_{1\text{-}29}$ phosphorylation and in the presence of $cTnI_{1\text{-}29}$ was stronger than the wild type value. In E59D/D75Y, the affinity towards $cTnI_{147\text{-}163}$ was weakened in the presence of $cTnI_{1\text{-}29}$. Thus, the physiological consequences of the L29Q and E59D/D75Y mutations and disease development can be related to the impaired thermodynamics of the cNTnC interactions with its binding partners, $cTnI_{1\text{-}29}$ and $cTnI_{147\text{-}163}$.

Another mutation, G159D, linked to DCM, was found in cCTnC (*4*). In reconstituted rat (*14*) and rabbit (*15*) cardiac trabeculae, the presence of G159D did not significantly alter myofilament Ca^{2+} sensitivity. However, the presence of G159D in guinea pig trabeculae resulted in the reduced Ca^{2+} sensitivity (*16*). Available physiological data on G159D reported the reduced activity of ATPase (*16*); however, the Ca^{2+} sensitivity of ATPase was not affected (*14*). It might be difficult to interpret physiological results on the molecular level, especially since Ca^{2+} sensitivity is a complex function of many consequential events, such as the binding of Ca^{2+}, binding of $cTnI_{147\text{-}163}$, and the attachment of cross-bridges, and since the reproducibility of results was mentioned to be dependent on the muscle fiber type (*15*). We have attempted to address this question using the G159D mutant of cCTnC and the cTnI peptide ($cTnI_{34\text{-}71}$), so that the interactions between troponin parts can be unambiguously traced. The knowledge of these interactions can be compiled afterwards into the overall picture assisting the interpretation of the physiological data.

There are several functions attributed to cCTnC, which could be affected by the presence of G159D: first, in its Ca^{2+} bound form, cCTnC

binds to the anchoring region of cTnI (~ residues 34-71) and tethers the entire troponin complex to the thin filament; second, cCTnC binds the inhibitory region of cTnI (~ residues 128-147), the location of which has not been visualized in available crystal structures (*17*) and is suspected to be driven by electrostatics (*18, 19*). The binding of cTnI$_{128-147}$ occurs without replacement of cTnI$_{34-71}$ and is hypothesized to be localized next to the highly charged E-D linker connecting two domains of cTnC. Third, cCTnC was also shown to interact with cTnT (*20*). Fourth, G159D might affect the interaction with the cardiac specific N-terminus of cTnI (~ residues 1-34), as was suspected in experiments with skinned rat trabeculae (*14*) and with reconstituted troponin complex (*11*). In the crystal structure, Gly^{159} is located at the very end of the H-helix, 5 Å away from Leu^{47} of the anchoring region of cTnI (~residues 34-71) (*17*). This suggests that the presence of mutation might first of all affect the interaction with cTnI$_{34-71}$, which has not been addressed previously. Using NMR spectroscopy we have determined the affinity of G159D towards cTnI$_{34-71}$ and examined the consequences of this mutation on the structure and dynamics of the G159D•cTnI$_{34-71}$ complex. Based on NOE connectivity patterns, NMR chemical shifts changes, dynamics, and 3D structures we conclude that compared to cCTnC, G159D binds to cTnI$_{34-71}$ in a similar fashion, albeit with a lower affinity. This interaction is a key function of cCTnC, and when impaired, can perturb the function of the entire Tn complex and lead to severe physiological consequences, such as the development of cardiomyopathy.

Experimental Procedures

*Protein Expression and Purification*

The DNA encoding cCTnC (91-161) was subcloned previously into pET-3a expression vector similarly to Pearlstone et al. (*21*). Using cCTnC as a template, the G159D mutation was engineered using a site-directed

mutagenesis kit (QuikChange purchased from Stratagene). E. coli strain BL21(DE3)pLysS was transformed with the expression vector and incubated at 37°C to the OD_{600} of 0.6-0.9. Cell cultures were induced with IPTG and harvested after incubation for 3 hours. Uniformly ^{15}N-labeled or ^{13}C,^{15}N-labeled cCTnC and G159D were expressed in a minimal media enriched with $(^{15}NH_4)_2SO_4$ or $(^{15}NH_4)_2SO_4$ and (^{13}C) glucose (22). Cell pellet was lysed using French press and applied to a DEAE column (50 mM Tris, 0.1 M NaCl, pH 8.0). Proteins were further purified using a Superdex-75 size exclusion column (50 mM Tris, 0.15 M NaCl, pH 8.0), desalted using Sephadex G25 column (10 mM NH_4HCO_3), and lyophilized. Molecular masses for unlabeled proteins, cCTnC and G159D, as determined by MALDI mass spectrometry were equal to the expected values. Amino acid composition was confirmed independently by amino acid analysis.

cTnI$_{34-71}$ titration of cCTnC and G159D monitored by 2D {^{1}H, ^{15}N}-HSQC NMR spectroscopy

The peptide, cTnI$_{34-71}$, (acetyl-AKKKSKISASRKLQLKTLLLQ IAKQELEREAEERRGEK-amide) was synthesized using standard methodology for a typical TnI peptide (23). The sequence was confirmed by amino acid analysis and the mass was verified by electrospray mass spectrometry. During titration, the peptide was added in the form of powder to the 500 mL solution of 0.57 mM cCTnC and 0.56 mM G159D. The buffer consisted of 100 mM KCl, 10 mM imidazole, 2 mM $CaCl_2$, 5 mM NaN_3, and 0.2 mM DSS in 90% H_2O/10% D_2O. The pH was adjusted to 6.7 ± 0.05 at every titration point. Concentrations of proteins and peptides were determined by weight and confirmed by amino-acid analysis. Since the reaction proceeds within the slow exchange limits for both cCTnC and G159D, the chemical shifts for two species (cCTnC or G159D alone and in complex with cTnI$_{34-71}$) were observed during titrations. The decreasing intensity of individual amide resonances of

uncomplexed cCTnC or G159D were used to calculate K_D. The cTnI$_{34-71}$ induced decrease in amide intensities was averaged for all monitored amides and plotted as a function of [cTnI$_{34-71}$]$_{total}$/[cCTnC]$_{total}$ or [cTnI$_{34-71}$]$_{total}$/[G159D]$_{total}$. The normalized curve for all monitored amides was fit for both titrations to the equation:

$$\text{Troponin C + Troponin I} \leftrightarrow \text{Troponin C-Troponin I}$$
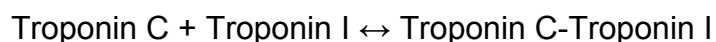
The dissociation constants measured were in the micromolar range, and since the concentrations of G159D and cCTnC were in the millimolar range, precise comparison of the data was difficult. Therefore, the titration of cTnI$_{34-71}$ was repeated at a much lower G159D concentration. Samples of 42 µM unlabeled G159D and 2 mM unlabeled cTnI$_{34-71}$ were prepared in the buffer conditions summarized above. The titration was performed until ~3:1 cTnI$_{34-71}$-G159D was reached. 1D ^{1}H NMR spectra of G159D were acquired at each titration point. Isolated peaks in the 1D ^{1}H spectrum were monitored throughout the titration, and changes in peak intensities as a function of cTnI$_{34-71}$ were used to calculate the K_D. The data were averaged and normalized and fit using the curve fitting program xcrvfit, v. 4.0.12 (http://www.bionmr.ualberta.ca/bds/software/xcrvfit).

^{15}N backbone amide NMR relaxation data

Relaxation data were acquired at 30 ^{o}C on a Varian Inova 500 MHz spectrometer from ^{15}N-T$_1$, ^{15}N-T$_2$, and {^{1}H-^{15}N}-NOE experiments (Biopack, Varian Associates) for 500 mL samples containing 0.57 mM of cCTnC or 0.56 mM G159D and 1.2 mM of cTnI$_{34-71}$. T$_1$ data were acquired using relaxation delays of 10, 50, 100, 200, 300, and 400 ms, and T$_2$ data were acquired using relaxation delays of 10, 30, 50, 70, 90, and 110 ms. Delays between transients in ^{15}N-T$_2$ and ^{15}N-T$_1$ experiments were set to 3 s. {^{1}H-^{15}N}-NOE experiments were performed using delays of 5 s for spectra recorded without proton saturation and delays of 2 s for

spectra recorded with proton saturation. Proton saturation was set to 3 s so that the total time between transients was equal to 5 s. Relaxation parameters, T_1, T_2, and NOE, were extracted using the rate analysis module built in NMRView (*24*) and analyzed using Mathematica scripts provided by Dr. Leo Spyracopuolos (www.bionmr.ualberta.ca/~lspy/) (*25*). Overall rotational tumbling time, τ_m, was averaged from the per residue fitting of relaxation data to the Lipari-Szabo S^2-τ_m-τ_f model (*26*). Relaxation data for residues with significant internal motions, as judged by NOE<0.65, and data for residues with possible slow motions, as judged by significantly decreased T_2, were excluded in this method of τ_m calculation.

Assignment and structure calculation for cCTnC•cTnI$_{34-71}$ and G159D•cTnI$_{34-71}$

Samples used for NMR data acquisition contained ~0.5 mM of G159D or cCTnC, ~1.2 mM of cTnI$_{34-71}$ in the buffer consisted of 100 mM KCl, 10 mM imidazole, 2 mM CaCl$_2$, 5 mM NaN$_3$, and 0.2 mM DSS in 90% H$_2$O/10% D$_2$O. Buffer used for data acquisition in D$_2$O contained 100 mM KCl, 0.5 mM imidazole, 9.5 mM deuterated imidazole, 2 mM CaCl$_2$, 5 mM NaN$_3$, and 0.2 mM DSS. NMR spectra were acquired at 30^0C on Varian INOVA 500, Unity 600, or INOVA 800 spectrometers equipped with 5 mm triple resonance probes and z axis pulsed field gradients (Table D-1). NMR data was processed using NMRPipe (*27*) and analyzed with NMRView (*24*). The backbone resonances for cCTnC and G159D in the [^{13}C,^{15}N] cCTnC•cTnI$_{34-71}$ and [^{13}C,^{15}N] G159D•cTnI$_{34-71}$ complexes were assigned using SmartNotebook v5.1.3 (*28*). Side chain assignment was carried out using HCCH-TOCSY, HCCONH, CCONH, HNHA, HNHB, and ^{15}N TOCSY HSQC. The majority of side chain resonances were unambiguously assigned. Resonances for aromatic residues were assigned using 2D homonuclear DQF-COSY and NOESY experiments in D$_2$O. Resonances for the cTnI$_{34-71}$ peptide were not dispersed well enough in 2D ^{13}C/^{15}N-filtered TOCSY and NOESY experiments to allow for the

Table D-1. NMR experiments acquired for structure calculations and chemical shift assignments.

Experiment	nuclei	^1H	x-pts	y-pts	z-pts	x-sw	y-sw	z-sw	Mix (ms)
^{15}N-HSQC	^1H, ^{15}N	500	1074	192		8384.9		2026.3	–
HCCH-TOCSY	^1H, ^{13}C, ^1H	500	1024	128	104	8384.9	5998.5	10057.8	–
CBCA(CO)NNH	^1H, ^{13}C, ^{15}N	500	1024	118	64	8384.9	10057.2	2026.3	–
HNCACB	^1H, ^{13}C, ^{15}N	500	1024	118	64	8384.9	10057.2	2026.3	–
HCCONH	^1H, ^{13}C, ^{15}N	600	1024	160	64	8398.1	5998.5	2431.6	–
CCONH	^1H, ^{13}C, ^{15}N	600	1024	184	64	8398.1	12067.2	2431.6	–
^{13}C NOESY HSQC	^1H, ^1H, ^{13}C	600	1024	160	80	8398.1	5998.7	6033.7	100
^{15}N NOESY HSQC	^1H, ^1H, ^{15}N	600	1024	160	80	8398.1	5998.7	2431.6	150
^{15}N TOCSY HSQC	^1H, ^1H, ^{15}N	600	1024	160	64	8398.1	5998.7	2431.6	50
HNHA	^1H, ^1H, ^{15}N	600	1024	160	64	8398.1	5998.7	2431.6	–
HNHB	^1H, ^1H, ^{15}N	500	1024	160	64	8384.9	4998.8	2026.3	–
DQF-COSY (D$_2$0)	^1H, ^1H	800							
NOESY (D$_2$0)	^1H, ^1H	800							
^{13}C/^{15}N-filt. TOCSY	^1H, ^1H	600	4096	512	–	8384.9	8385.7	–	60
^{13}C/^{15}N-filt. NOESY	^1H, ^1H	600	4096	512	–	8384.9	8385.7	–	250
^{13}C-filt., ed. NOESY	^1H, ^1H, ^{13}C	600	1024	240	64	3595.9	3595.9	3014.0	150

assignment of many residues except for amide protons, HN, for residues 41-64, Ha protons for residues 41-59, Hb protons for residues 41-43, 50, 53, 56, and Hd/g protons for residues 46-53, 55, and 58-60.

Structure calculations were performed with CYANA (*29*) using the 'noeassign' automatic assignment procedure (*30*) and distance restraints from ^{13}C NOESY HSQC and ^{15}N NOESY HSQC experiments. Unambiguous restraints were assigned manually and were forced to keep their assignments during the first four runs of CYANA calculations, after which they were open for automatic assignment by CYANA. Distance restraints were calibrated with CYANA standard procedure using upper limits of 6 Å. TALOS dihedral restraints for helical regions for G159D and cCTnC (*31*), and Ca^{2+} restraints for Ca^{2+} binding loops were obtained from X-ray crystallographic data and added into the calculation (Table D-3). TALOS restraints did not affect the overall fold of the structures (data not shown). In the final structure calculations of G159D, however, the TALOS restraints were truncated up to residue 151. This was done to avoid artifactual secondary structure fabrication from TALOS, since it only uses chemical shift homology from other proteins to predict backbone angles. CYANA was used to calculate 50 structures, of which the 20 conformers with the lowest target function were refined in explicit solvent by XPLOR-NIH (*32, 33*) with a water box edge length of 18.8 Å. The final ensembles were averaged and refined using the same water refinement protocol as done previously, and are the structures discussed herein and deposited (PDBs). Structures were validated using PROCHECK (*34*) and WHATCHECK (*35*).

Results

cTnI₃₄₋₇₁ titrations of cCTnC and G159D

In a 2D {^{1}H, ^{15}N}-HSQC NMR spectrum, cross peaks correlate the ^{15}N and ^{1}H chemical shifts of backbone amide NH. Chemical shifts are

exceptionally sensitive to changes in the structure and dynamics of a protein. 2D {^{1}H, ^{15}N}-HSQC spectra obtained for G159D (Figure D-1a) and cCTnC (Figure D-1b), with and without their binding partner, cTnI$_{34-71}$, demonstrate the difference in the positions of several {^{1}H, ^{15}N}-HSQC cross peaks, corresponding to the residues adjacent to the site of mutation. The rest of the amide chemical shifts, and the changes they undergo during the titration with cTnI$_{34-71}$, are similar, suggesting a resemblance in overall structural folds for G159D and cCTnC, in agreement with the structure determined herein (see below). The kinetics of the binding of cTnI$_{34-71}$ to G159D (Figure D-1a) and cCTnC (Figure D-1b) is on the NMR slow exchange time scale, in which the intensities of cross-peaks for complexed and uncomplexed species vary depending on the degree of binding. Binding curves were obtained by measuring the intensity decrease for several representative cross-peaks corresponding to the unliganded protein, which were averaged and fit to a single binding site model (Figure D-1d). K_D's were found to be 6 ± 3 µM in the case of G159D and < 1 µM in the case of cCTnC. The later is in agreement with literature data (*36*).

In order to more accurately determine the dissociation constant of cTnI$_{34-71}$ for G159D, the titration was repeated at the concentration of G159D equal to 42 µM, which was too low for an adequate acquisition of 2D {^{1}H, ^{15}N}-HSQC NMR spectra at each titration point (in a realistic time frame). However, there were several peaks isolated in the 1D ^{1}H NMR spectrum of G159D, which could be monitored throughout the titration (Figure D-1c). Intensities at each titration point were measured for the isolated peaks, averaged, normalized, and plotted against the ratio of total cTnI$_{34-71}$ to total G159D (Figure D-1d). The dissociation constant was determined to be 3.0 ± 0.6 µM, which is within experimental error to that determined at the higher concentration.
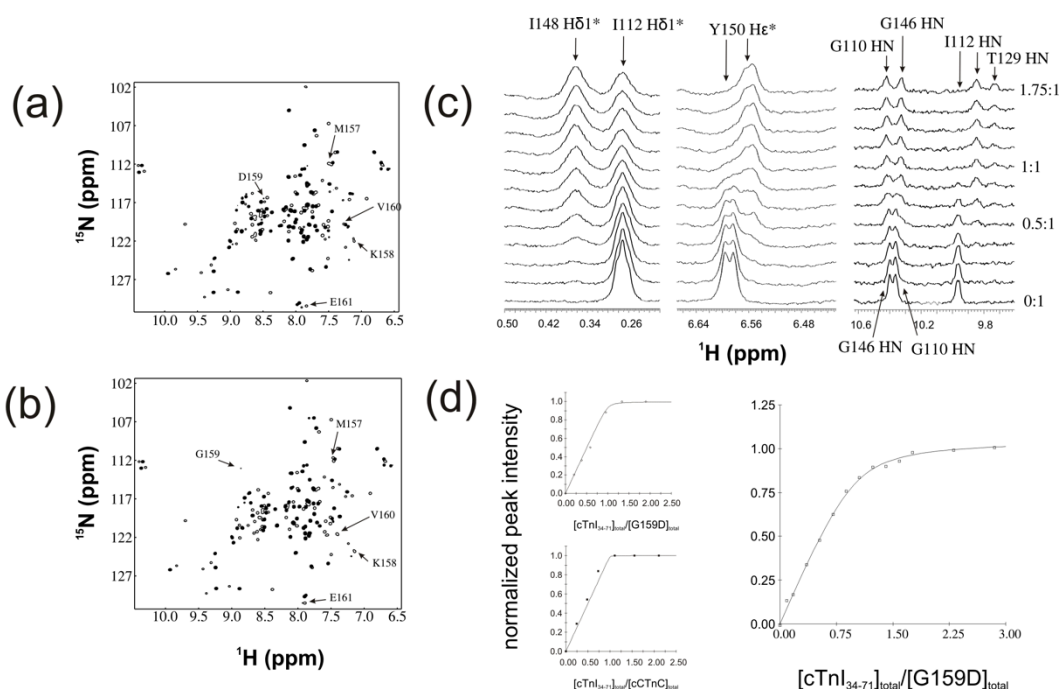
Figure D-1. Titration of (a) G159D and (b) cCTnC with cTnI$_{34-71}$ using 2D {^{1}H, ^{15}N}-HSQC NMR spectroscopy. The NMR samples contained 0.57 mM and 0.56 mM of cCTnC and G159D, respectively. Filled cross-peaks correspond to uncomplexed cCTnC or G159D and open cross-peaks correspond to the complex of cCTnC or G159D with cTnI$_{34-71}$. Annotated residues have the largest ^{15}N chemical shift differences and are adjacent to the mutation site. (c) 1D ^{1}H NMR stacked spectra acquired during the titration of G159D with cTnI$_{34-71}$. The concentration of G159D was reduced to 42 µM in order to more accurately determine the dissociation constant of cTnI$_{34-71}$ for G159D. ^{1}H resonances are labeled for residues that were isolated in the 1D spectra and used to determine the K$_D$. The ratios of G159D to cTnI$_{34-71}$ for a few key points in the titration are given on the right side of the spectra. The titration was continued until a cTnI$_{34-71}$-G159D ratio of ~3:1 was reached; however the stacked 1D plots are shown up to a ratio of 1.75:1 since the peak intensities remained mostly unchanged at higher ratios. Binding curves (d) corresponding to the titration of G159D (open circles) and cCTnC (closed squares) with cTnI$_{34-71}$ as monitored by 2D {^{1}H, ^{15}N}-HSQC NMR spectroscopy are provided in the smaller plots on the left. The large plot on the right (d) reflects the changes in signal intensity during the titration of 42 µM G159D with cTnI$_{34-71}$ (open squares). The binding data were averaged and normalized and then fit using the program xcrvfit (see *experimental procedures* for details).

^{15}N backbone relaxation data

^{15}N backbone NMR relaxation parameters, T_1, T_2, and NOE, are the complex functions of the protein motions, including the tumbling of a protein as a whole, the motions of its independent parts, and the chemical exchange processes. Per residue T_1, T_2, and NOE were determined for G159D and cCTnC alone, and in complex with cTnI$_{34-71}$ (Figure D-2). T_1, T_2, and NOE for cCTnC•cTnI$_{34-71}$ and G159D•cTnI$_{34-71}$ were virtually identical within the errors of the experiments (Figure D-2), implying that the presence of the mutation did not affect the dynamic properties, as well as the conformational flexibility, of the complex. Importantly, ^{15}N backbone T_1, T_2, and NOE for cCTnC•cTnI$_{34-71}$ and G159D•cTnI$_{34-71}$ were also similar in the area adjacent to the mutation site. Relaxation data for cCTnC was in agreement with qualitative data presented earlier (*37, 38*).

T_1, T_2, and NOE are per residue parameters, whereas the overall correlation time, t_m, calculated from T_1, T_2, and NOE (Table D-2), is the function of the hydrated radius of the entire protein, r_h, and consequently its molecular weight. According to the Stokes-Einstein-Debye theory (*39*),

$$\tau_m = \frac{4}{3}\pi\eta r_h^3 / k_B T,$$

where η is the solvent viscosity, k_B is the Boltzmann constant, and T is temperature. As a rule of thumb, t_m (ns) is approximated to the half of the molecular weight of a protein (kDa), provided that the protein tumbling is mostly isotropic. This can serve as a good estimate of the molecular weight of a protein or its complexes (*18*). An increase in t_m, as compared to the calculated molecular weight can result from issues such as dimerization (*40*), which is the case for skeletal protein, sCTnC (*41*). We have determined t_m's for G159D and cCTnC alone, and in complex with cTnI$_{34-71}$ (Table D-2). For cCTnC and G159D, t_m's are comparable to each
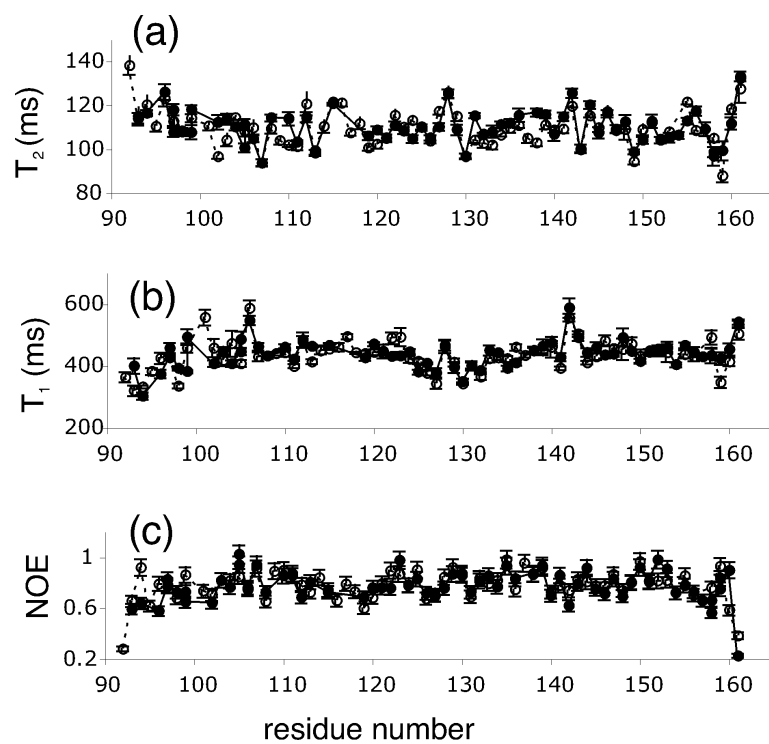
Figure D-2. Per residue NMR relaxation parameters T_2 (a), T_1 (b), NOE (c) for G159D (closed circles) and cCTnC (open circles) in complexes with $cTnI_{34-71}$.

Table D-2. NMR relaxation parameters T_1, T_2, and τ_m determined for G159D and cCTnC alone and in complexes with cTnI$_{34-71}$. Theoretical estimate for correlation time τ_m is equal to the half of the molecular weight in kDa.

	Average of per residue T_1 (ms)	Average of per residue T_2 (ms)	Overall correlation time, τ_m (ns)	Theoretical estimate for correlation time, τ_m (ns)
G159D	356 ± 47	193 ± 31	3.3	4.2
G159D•cTnI$_{34-71}$	436 ± 46	112 ± 9	6.6	6.4
cCTnC	348 ± 42	185 ± 25	3.4	4.2
cCTnC•cTnI$_{34-71}$	438 ± 53	109 ± 13	6.5	6.4

other and smaller than the rule of thumb estimate, which could be explained by a lesser degree of bound water, for example (*42, 43*). The values of t_m's determined for G159D•cTnI$_{34-71}$ and cCTnC•cTnI$_{34-71}$ were comparable to each other and to the theoretical estimate, which suggests the formation of 1:1 complexes in both cases, and the absence of dimerization and significant conformational exchange.

Differences in the chemical shifts of cCTnC and G159D in the complexes with cTnI$_{34-71}$

Chemical shifts changes are uniquely indicative of changes in chemical environment of nuclei and hence, in protein structure and dynamics. We have calculated the chemical shift changes of ^{15}N, ^{13}C, and ^{1}H for G159D and cCTnC in complexes with cTnI$_{34-71}$ (Figure D-3 and D-4). Backbone amide ^{15}N chemical shifts underwent the most significant perturbations at the end of the H-helix near to the mutation site (Figure D-3a and D-4a). ^{15}N chemical shifts in the region where the H-helix is contacting the E-helix (residues 93-97) are also affected by the presence of mutation but to a much lesser degree. As demonstrated by ^{15}N chemical shifts changes, the overall fold of G159D and cCTnC remains similar with the only significant perturbation being near to the mutation site. Changes in ^{1}H and ^{13}C chemical shifts, especially those for the side chains, are sensitive not only to the changes in overall fold but also to the changes in the configurational patterns, e.g. the number, energetics, and the geometry of connections that stabilize protein core or protein complex. As demonstrated by ^{13}C chemical shifts changes (Figure D-3b and D-4b), the major perturbations occurred at the several hydrophobic residues (for example Leu^{100}, Met^{120}, Leu^{121}, Ile^{128}) known to be responsible for the interaction with cTnI$_{34-71}$ (*17*). ^{1}H, atoms directly responsible for the majority of van der Waals and hydrophobic contacts in proteins, are the most sensitive indicators of changes in protein core and binding interfaces.
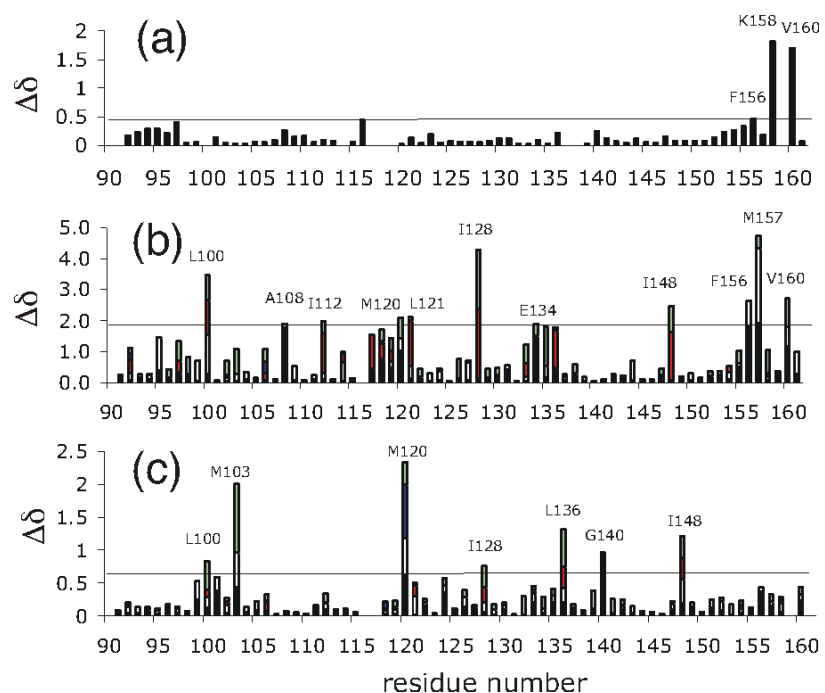
Figure D-3. Chemical shifts differences between G159D and cCTnC in complexes with cTnI$_{34-71}$ for backbone amide ^{15}N (a), side chain ^{13}C (b), and side chain ^{1}H (c). Side chain chemical shift changes for ^{13}C and ^{1}H are added together for every residue, with Ca and Ha in black, Cb and Hb in white, Cd and Hd in red, Ce and He in dark blue, and Cd and Hd in green. Horizontal lines correspond to the average value plus one standard deviation.
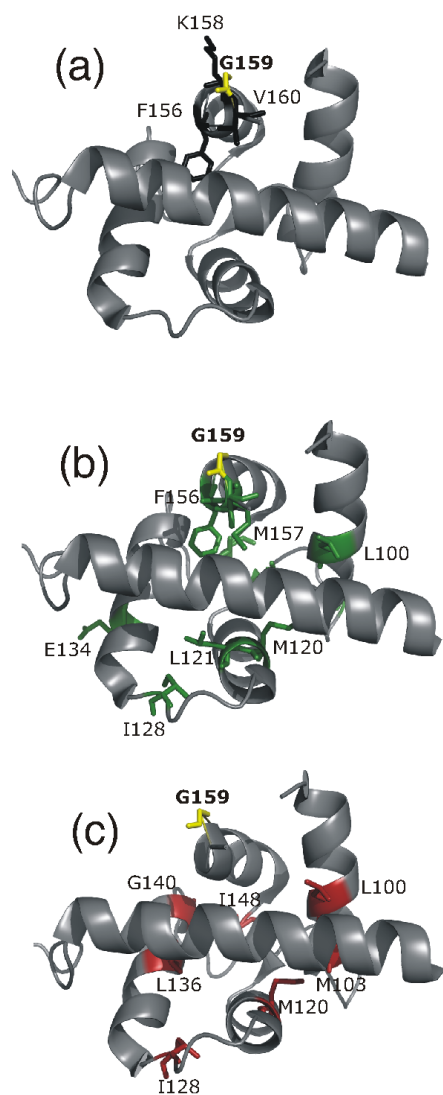
Figure D-4. Residues with chemical shift changes visualized on the structure of cCTnC determined by X-ray crystallography (1J1D). Residues with the significant ^{15}N chemical shift changes are shown in black (a). Residues with the significant side chain ^{13}C chemical shift changes are shown in green (b). Residues with the significant side chain ^1H chemical shift changes are shown in red (c). Gly^{159} is shown in yellow in all three panels.

As demonstrated by ^{1}H chemical shifts differences (Figure D-3c and D-4c), significant changes occurred with the residues forming the interface between cCTnC and cTnI$_{34-71}$ (for example Leu^{100}, Met^{103}, Met^{120}, Leu^{121}, Ile^{128}, Leu^{136}), implying that the binding of cTnI$_{34-71}$ to cCTnC is perturbed in the presence of the mutation (*17*). Interestingly, the chemical shifts of two interior residues, Ile^{148} and Ile^{112}, which form the hydrophobic core of cCTnC, have also undergone perturbations.

Differences in the NOE connectivities of cCTnC and G159D in the complexes with cTnI$_{34-71}$

NOE connectivites obtained from 3D ^{13}C NOESY HSQC and ^{15}N NOESYHSQC NMR spectra are typically used as distance restraints during structure calculations. It is often informative therefore to make pair-wise comparisons of NOE patterns. NOE, however, is a less sensitive parameter to long range perturbations as compared to a chemical shift since the intensity of NOE decreases rapidly with the distance between two nuclei:

$$NOE \propto \frac{1}{r^6} \text{ (44)}.$$

We have compared strips from 3D ^{13}C NOESY HSQC and ^{15}N NOESY HSQC NMR spectra for G159D and cCTnC for residues with the significant chemical shift changes. Spectra were acquired using identical parameters, such as mixing time, which is crucial for such a comparison. The vast majority of contacts in the cCTnC spectra were accurately reproduced in the G159D spectra; however, there were some differences (Figure D-5). For example, in the ^{13}C NOESY HSQC spectrum, the g-proton of Met^{103} has more contacts in cCTnC compared to G159D, with some of these contacts being tentatively assigned to the peptide resonances (Figure D-5a). The g-proton of Ile^{112} contacted the a-proton of Asp^{149} in G159D, and the a-proton of Asp^{105} and the d-proton of Tyr^{150} in
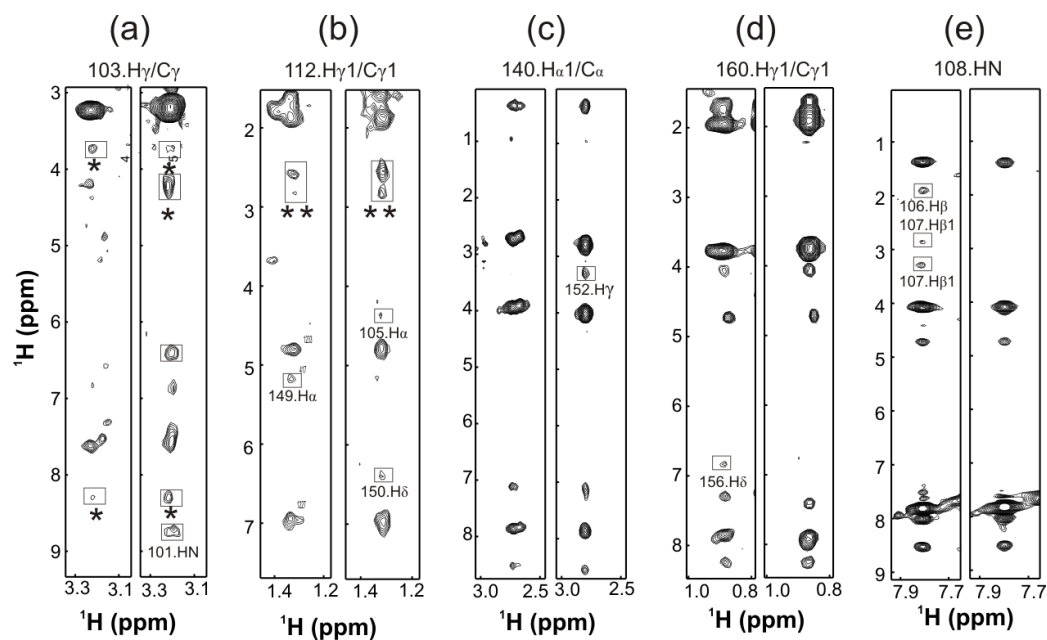
Figure D-5. NOE strips for G159D (left) and cCTnC (right) in complexes with cTnI$_{34-71}$ obtained in 3D ^{13}C NOESY HSQC NMR spectra (a-d) and ^{15}N NOESY HSQC NMR spectra (e), where stars represent the resonances tentatively assigned to the peptide, and double stars represent resonances tentatively assigned to the protein. Assignments are indicated below each pair of plots.

cCTnC (Figure D-5b). The a-proton of Gly[140] contacted the g-proton of Glu[152] in cCTnC but not in G159D (Figure D-5c). The g-proton of Val[160] contacted the e-proton of Phe[156] in G159D but not in cCTnC (Figure D-5d). In the ^{15}N NOESY HSQC NMR spectrum, the differences in NOE patterns were less significant, with the noticeable change observed in the amide proton of Ala[108], which had contacts with the b-protons of Lys[106] and Asn[107] in G159D but not in cCTnC. These results demonstrate that the residues with the large chemical shift differences (Figure D-5) had also distinct NOE connectivities in ^{13}C NOESY HSQC and ^{15}N NOESY HSQC spectra.

Structures of cCTnC and G159D in the complexes with cTnI$_{34-71}$

The ensemble containing 20 best NMR structures out of 50 calculated was analyzed for G159D and cCTnC. All structures had a good geometry after water refinement with > 92 % in most favorable and > 7 % in additionally allowed regions of the Ramachandran plot for G159D and cCTnC (Table D-3). Structures of both proteins converged with rmsd < 1.4 Å for all atoms for residues 95-155, including loops. The overall topology and the secondary structure for G159D and cCTnC were similar to the cCTnC structure obtained by X-ray crystallography, PDB code 1J1D (*17*) and previously by NMR, PDB code 1FI5 (*38*). Rmsd's for backbone atoms between cCTnC and 1J1D was 1.2 Å for all residues, and between cCTnC and 1FI5 1.4 Å (Figure D-6A). Similar rmsd of 1.7 Å was between reported 1FI5 and 1J1D. The G159D structure, although similar overall, overlapped with 1J1D with rmsd of 1.7 Å for backbone atoms for all residues (Figure D-6B). G159D overlapped with cCTnC with rmsd of 1.4 Å and with 1FI5 with 1.3 Å (Figure D-6B). The resolution of X-ray diffraction data for 1J1D was 2.6 Å (*17*), within which, structures determined in this work and reported previously have similar folds.

Table D-3. Statistics for 20 NMR structures of G159D and cCTnC in complex with cTnI$_{34-71}$. Structures were calculated using CYANA (*29*), refined using XPLOR-NIH (*32, 33*), and analyzed using PROCHECK (*34*) and WHATCHECK (*35*).

	G159D	cCTnC
NOE restraints	1075	957
Short range (|*i-j*|=1)	624	561
Medium range (1<|*i-j*|<5)	231	215
Long range (|*i-j*|≥5)	220	181
Ca^{2+} binding restraints	16	16
Dihedral restraints (φ/ψ)[a]	84	86
NOE violations		
> 0.5 Å	0.15 ± 0.37	0.0 ± 0.0
> 0.3 Å	0.25 ± 0.55	1.8 ± 1.20
> 0.1 Å	6.3 ± 1.95	10.45 ± 2.28
Dihedral Violations (º)	0.0 ± 0.0	0.0 ± 0.0
Ramachadran plot statistics[b]		
φ/ψ in most favorable regions (%)	93 ± 4	92 ± 4
φ/ψ in additionally allowed regions (%)	7 ± 3	7 ± 3
φ/ψ in generously allowed regions (%)	0 ± 1	1 ± 1
φ/ψ in disallowed regions (%)	0 ± 1	1 ± 1
Pairwise RMSD (Å)[c]		
Before water refinement	0.71 ± 0.13	0.59 ± 0.12
After water refinement	1.29 ± 0.28	1.31 ± 0.24
WHAT CHECK structure Z-scores after water refinement		
Second-generation packing quality	-0.9 ± 0.4	-0.9 ± 0.3
Ramachandran plot appearance	0.9 ± 0.7	1.8 ± 0.8

[a]Predicted from chemical shifts using TALOS
[b]PROCHECK was used over all the residues (90-161)
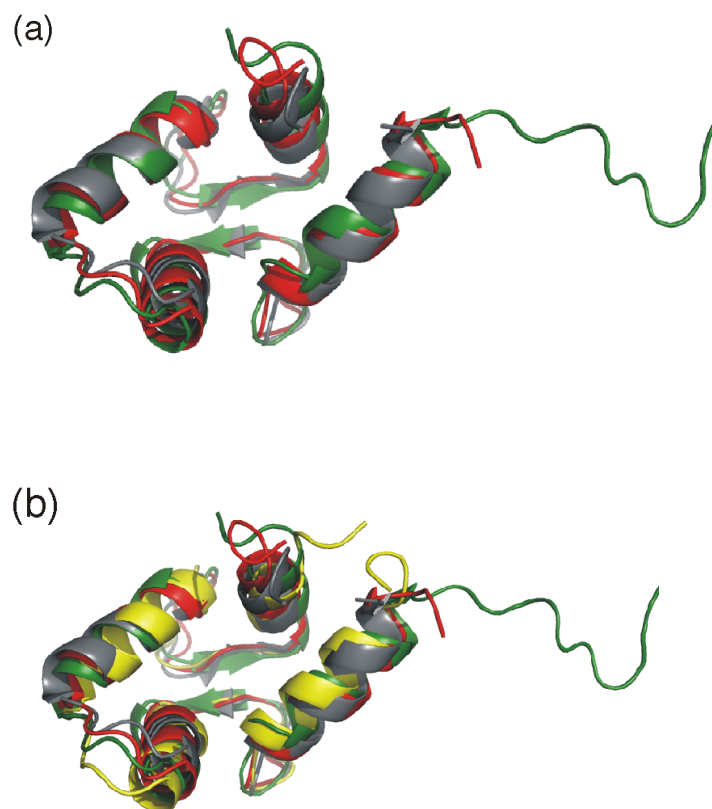[c]Main chain nuclei over the residues 95-155

(a)

(b)

Figure D-6. Secondary structures of cCTnC (a) and G159D (b) in complexes with the anchoring region of cTnI in comparison with previously determined structures 1J1D (grey) and 1FI5 (green). The structure of cCTnC determined in this work is shown on both panels in red and the structure of G159D is in yellow.

The packing of the cCTnC core occurs between the hydrophobic residues of a-helical regions (Leu[97], Phe[101], Leu[117], Met[120], Leu[121], Ile[133], Leu[136], Phe[153], and Met[157]) and the two residues of the b-sheet region (Ile[112] and Ile[148]). Orientation of these key residues did not change in the cCTnC and G159D structures calculated in this work as compared to 1J1D and 1FI5. Several residues such as Phe[104] and Phe[156] in cCTnC and G159D are lacking the restraints with the peptide and thus their positions are more flexible, but are in the good agreement with the NMR structure, 1FI5. The packing interactions between helices and the protein cores of cCTnC have not been affected by the presence of G159D as demonstrated by the resultant structures. In spite of some differences in NOE contacts for Ile[112] and Ile[148], the calculated structures were similar within the limits of the method. This demonstrates that among the restraints used (Table D-3), many were identical, which determined the similarity between the structures.

Differences in the NOE connectivities between cCTnC (and G159D) and cTnI$_{34-71}$ in ^{13}C-edited, filtered NOESY spectra

The NOE connectivities between ^{15}N, ^{13}C-labeled cCTnC and the unlabeled peptide cTnI$_{34-71}$ were obtained using the ^{13}C-edited, filtered NOESY pulse sequence (*45*) optimized in our laboratory for this particular complex (*46*). In this experiment, each cross peak corresponds to a ^{1}H protein resonance on the vertical axis and to a ^{1}H peptide resonance on the horizontal axis. ^{13}C resonance in the third dimension connects to the corresponding ^{1}H resonances on the protein, which allows for the assignment. Peptide ^{1}H assignments can be typically obtained with the 2D ^{15}N, ^{13}C-filtered TOCSY and 2D ^{15}N, ^{13}C-filtered NOESY (*47-49*); however, in our case, few resonances can be unambiguously assigned due to the poor dispersion of peptide chemical shifts, which precluded the structure calculation for the entire complex. Similarly to previous NMR

studies (*38, 41, 50*), structure determination of the entire complex was difficult to achieve without the additional restraints between a protein and a peptide, which might be found in crystal structures but are not always desirable to use due to the possibility of introducing artifacts. The peptide in complex is predominantly a-helical, which is supported by the values of peptide chemical shifts in 2D ^{15}N, ^{13}C-filtered TOCSY and 2D ^{15}N, ^{13}C-filtered NOESY and their poor dispersion. The superposition of ^{13}C-edited, filtered NOESY spectra for G159D and cCTnC in complexes with cTnI$_{34-71}$ shows a similarity between contacts formed (Figure D-7). Some contacts are virtually identical, for example, the contacts between Ala^{57} of cTnI$_{34-71}$ and Leu^{100} and Met^{120} of cCTnC and G159D (Figure D-7a) or the contact between Leu^{62} of cTnI$_{34-71}$ and Met^{103} of cCTnC and G159D (Figure D-7c). Some contacts were slightly changed, for example, the contacts between Ile^{56} of cTnI$_{34-71}$ and Thr^{124} of cCTnC and G159D (Figure D-7c). One contact, between Leu^{54} of cTnI$_{34-71}$ and Val^{160} of cCTnC, was clearly missing in G159D (Figure D-7b). No contacts were observed in the spectrum of G159D that were missing in case of cCTnC. Also, the intensities of existing connectivities were not stronger in the case of G159D. This demonstrates that G159D interacts with cTnI$_{34-71}$ similarly to cCTnC, without making new connections between the protein and the peptide and with the existing connections being qualitatively not stronger.

Discussion

The task of defining the impact of mutations on the structure and function of the sarcomeric proteins and the resultant physiological behavior of the sarcomere represents a substantial challenge, especially for non-lethal human mutations where the effect on the protein has to be mild to allow an individual to survive even in disease. Structural approaches, including the determination of structure using NMR or crystallography might not bring conclusive answers when the differences
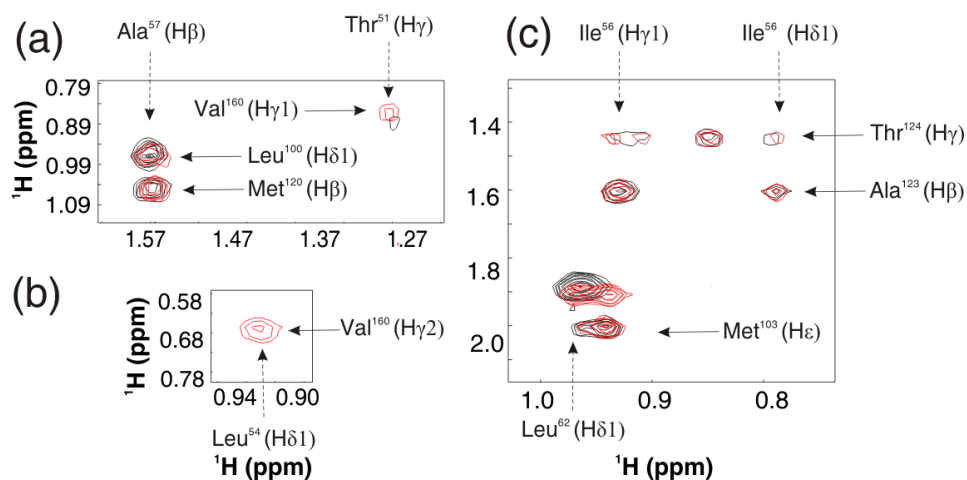
Figure D-7. Overlap of the regions of 2D projections of the 3D ^{13}C-filtered, edited NOESY spectra, showing direct contacts between G159D (black contours) and cCTnC (red contours) with cTnI$_{34\text{-}71}$. The resonances of proteins are shown with the horizontal solid arrows, the resonances for the peptide are shown with the vertical dashed arrows. The contact for G159D in the panel B is missing.

in structures of mutant and wild type proteins are not significant enough to be resolved within the resolution of the chosen technique. Often the affinities of mutated and wild type proteins for their targets and/or ligands are unchanged. It remains unknown, therefore, whether the mutant phenotype has been brought about by the changes undetectable within the limits of methods. However, the necessity to study individual human mutations is evident by the growing interest in genetically tailored nutrition and medicine, and in general, will be beneficial to our understanding of current biochemical models, in our example, cardiac muscle contraction.

We have attempted to dissect the effect of the G159D mutation on the structure, dynamics, and interactions of troponin C using solution state NMR. This technique allows not only for the structure determination but also provides a wealth of information pertaining to the chemical environment and dynamics of individual residues. Since the effects are expected to be subtle, all NMR experiments were run as direct side-by-side comparisons of the wild type and G159D mutant proteins. We have found that the secondary structure, tertiary structure, and the packing of the protein core have not changed for G159D in complex with $cTnI_{34-71}$ in comparison to the $cCTnC \cdot cTnI_{34-71}$ complex. Dynamic behavior for G159D is also unchanged, even in the vicinity of the mutation. However, the affinity of G159D towards $cTnI_{34-71}$ is reduced, and the NMR chemical shifts of protein residues in the complex are perturbed. The K_D of G159D towards $cTnI_{34-71}$ has been increased to 3 μM. The K_D of $cTnI_{34-71}$ for wild type cCTnC is < 1 μM (*36, 51*). Furthermore, the analogous region of skeletal TnI ($sTnI_{1-40}$) has been shown to bind the C-domain of skeletal TnC with a K_D of ~50 nm (*52*). Both results are significantly tighter than established here for G159D. The differences in NMR chemical shifts were well beyond the resolution in ^{1}H dimension (0.03 ppm), ^{13}C dimension (0.3 ppm), and ^{15}N dimension (0.2 ppm) in our experiments, with the most significant changes observed for residues directly involved in binding to $cTnI_{34-71}$. We have also observed the changes in NOE connectivities

between the protein and the peptide, with some connectivities changed or missing. All of the above evidence indicates the weakened binding and perturbed interaction between G159D and the anchoring region of cTnI (cTnI$_{34-71}$). The structure and dynamics of the protein core remain the same, however, in agreement with the G159D mutation locating at the very end of the H-helix, away from the protein core.

The binding of cCTnC to cTnI$_{34-71}$ is a key function of the C-domain. In skeletal TnC, the binding of the inhibitory region of sTnI is dependent upon the presence of the anchoring region of sTnI, with the anchoring region modulating the binding of the inhibitory region (*52-54*), which directly influences contractility. In insect flight muscle, the regulation of contraction is achieved entirely through the C-domain of TnC without the involvement of the N-domain and binding of the region analogous to the switch region of cTnI (*55*). The C-domain of cTnC has also been proposed to be the target of the regulatory molecule, EMD 57033, which binds exclusively to the C-domain of cTnC (*56-58*) and modulates the affinity cCTnC towards cTnI$_{34-71}$ (*59*). Thus our data supports the interpretation that the G159D mutation leads to impaired contractility and disease through an impaired anchoring of cTnC to the thin filament. The weaker binding to cTnI$_{34-71}$ might lead to a weaker anchoring of troponin C to the thin filament, lower k$_{on}$ for the switch region of cTnI (~residues 147-163) due to the decrease in proximity effect, and a more pronounced inhibition of the acto-myosin ATPase. This is in agreement with a slower activation kinetics in rabbit psoas fibers (*15*), which might be a more important parameter than the steady state force development (*60, 61*). Our conclusions are also in agreement with the decrease in actin-tropomyosin activated ATPase rate and the decrease in sliding velocity (*16*).

A second possibility is that impaired function is caused by perturbations of other important long-range electrostatic interactions within the troponin complex. Electrostatic potential drops off as a function of 1/r, where r is the distance from the charge, so that it can be active 10-20 Å
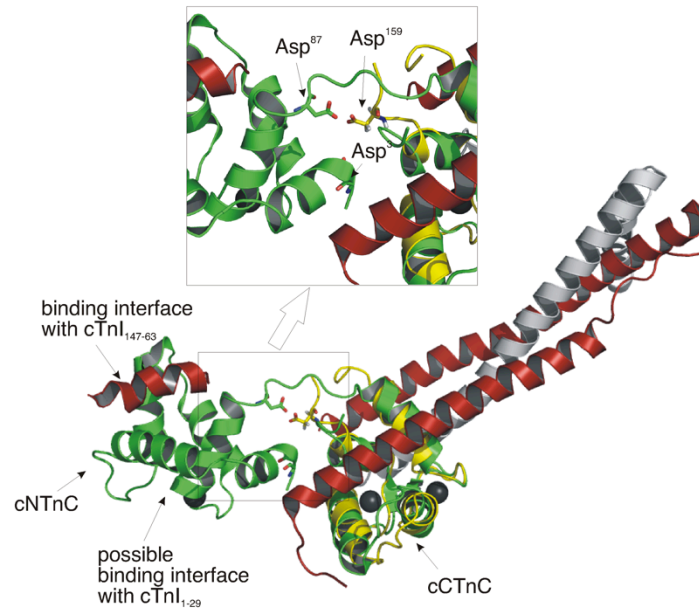
Figure D-8. X-ray structure of troponin complex (1JID) overlaid with G159D to demonstrate the proximity of Asp^{159} to cNTnC. Ribbon diagram in shown for cTnC (green), cTnI (red), cTnT (grey) and G159D (yellow). The cNTnC binding site for cTnI$_{147-163}$ and the possible cNTnC binding site for cTnI$_{1-29}$ are indicated. Electrostatic residues of cNTnC in close proximity to Asp^{159} are shown in sticks (Asp^{87} and Asp^{3}).

away from the site of mutation. In crystal structure (*17*), the N-domain of cTnC is folded over the C-domain of cTnC (Figure D-8), so that Gly159 is in reasonable proximity to the binding site for the switch region of cTnI (~residues 147-163) (*62*), to the binding site of the inhibitory region of cTnI (~residues 128-147), and to the possible binding site for the cardiac specific N-terminus of cTnI (~ residues 1-29) (*63, 64*). The binding of the N-terminus and the inhibitory region of cTnI are suspected to be electrostatically driven (*18, 19*), as well as influenced by phosphorylation (*65*), and the change in electrostatic potential of cCTnC might affect these interactions. A perturbed interaction of G159D with the N-terminus of cTnI has been reported (*11, 14*), which resulted in blunting the effect of PKA phosphorylation. Interestingly, the L29Q mutation has also blunted the effect of PKA phosphorylation (*10, 11, 13*) but lead to hypertrophy instead (*3*). The physical parameter crucial for the development of hyper- *versus* hypocontractility may be the resultant affinity towards the switch region of cTnI (~residues 147-163) (*13*) and the kinetics of this binding interaction (*11*). Another possibility to consider is that the clustering of the negatively charged residues Asp^3, Asp^{87}, and Asp^{159} might produce a cation binding site. The binding of a cation to this site could modify the interaction of troponin C with troponin I, or perhaps the flexibility of the D-E linker, either of which could impair contraction efficiency. In this work, we have determined that G159D binds to $cTnI_{34-71}$ with weaker affinity, supported by structural data, such as changes in chemical shifts and NOE connectivities. This weakened interaction is likely to modulate the anchoring of troponin C, with the resulting increase of acto-myosin inhibition. Other possibilities such as perturbed binding of the N-terminus of cTnI (~ residues 1-29) to cNTnC through the long-range electrostatic interactions or binding of the inhibitory region of cTnI cannot be excluded (~ residues 128-147).

References

1.	Redwood, C. S., Moolman-Smook, J. C., and Watkins, H. (1999) Properties of mutant contractile proteins that cause hypertrophic cardiomyopathy, *Cardiovasc Res 44*, 20-36.
2.	Seidman, J. G., and Seidman, C. (2001) The genetic basis for cardiomyopathy: from mutation identification to mechanistic paradigms, *Cell 104*, 557-567.
3.	Hoffmann, B., Schmidt-Traub, H., Perrot, A., Osterziel, K. J., and Gessner, R. (2001) First mutation in cardiac troponin C, L29Q, in a patient with hypertrophic cardiomyopathy, *Hum. Mutat. 17*, 524.
4.	Mogensen, J., Murphy, R. T., Shaw, T., Bahl, A., Redwood, C., Watkins, H., Burke, M., Elliott, P. M., and McKenna, W. J. (2004) Severe disease expression of cardiac troponin C and T mutations in patients with idiopathic dilated cardiomyopathy, *J Am Coll Cardiol 44*, 2033-2040.
5.	Lim, C. C., Yang, H., Yang, M., Wang, C. K., Shi, J., Berg, E. A., Pimentel, D. R., Gwathmey, J. K., Hajjar, R. J., Helmes, M., Costello, C. E., Huo, S., and Liao, R. (2008) A novel mutant cardiac troponin C disrupts molecular motions critical for calcium binding affinity and cardiomyocyte contractility, *Biophys J 94*, 3577-3589.
6.	Li, M. X., Wang, X., and Sykes, B. D. (2004) Structural based insights into the role of troponin in cardiac muscle pathophysiology, *J. Muscle Res. Cell Motil. 25*, 559-579.
7.	Sykes, B. D. (2003) Pulling the calcium trigger, *Nat Struct Biol 10*, 588-589.
8.	Lim, C. C., Yang, H., Yang, M., Wang, C. K., Shi, J., Berg, E. A., Pimentel, D. R., Gwathmey, J. K., Hajjar, R. J., Helmes, M., Costello, C. E., Huo, S., and Liao, R. (2008) A Novel Mutant Cardiac Troponin C Disrupts Molecular Motions Critical For Calcium Binding Affinity And Cardiomyocyte Contractility, *Biophys J*.
9.	Muir, L. A., Tschirgi, M. L., Rajapakse, I., and Chandra, M. (2006) Rat Cardiac Troponin C Mutations L29Q and G159D Decrease Myofilament Calcium Sensitivity Without Affecting Cooperativity, In *Biophysical Society, Annual Meeting*, p 529, Salt Lake City, Utah.
10.	Schmidtmann, A., Lindow, C., Villard, S., Heuser, A., Mugge, A., Gessner, R., Granier, C., and Jaquet, K. (2005) Cardiac troponin C-L29Q, related to hypertrophic cardiomyopathy, hinders the transduction of the protein kinase A dependent phosphorylation signal from cardiac troponin I to C, *Febs J 272*, 6087-6097.
11.	Dong, W. J., Xing, J., Ouyang, Y., An, J., and Cheung, H. C. (2008) Structural kinetics of cardiac troponin C mutants linked to familial hypertrophic and dilated cardiomyopathy in troponin complexes, *J Biol Chem 283*, 3424-3432.
12.	Dweck, D., Gomes, A. V., and Potter, J. D. (2005) Functional effects of human cardiac troponin C mutations linked to familial and

dilated cardiomyopathis, In *Biophysical Society, Annual Meeting*, p 317a, Long Beach, CA.

13. Baryshnikova, O. K., Li, M. X., and Sykes, B. D. (2008) Modulation of cardiac troponin C function by the cardiac-specific N-terminus of troponin I: influence of PKA phosphorylation and involvement in cardiomyopathies, *J Mol Biol 375*, 735-751.

14. Biesiadecki, B. J., Kobayashi, T., Walker, J. S., John Solaro, R., and de Tombe, P. P. (2007) The Troponin C G159D Mutation Blunts Myofilament Desensitization Induced by Troponin I Ser23/24 Phosphorylation, *Circ Res 100*, 1486-1493.

15. Preston, L. C., Ashley, C. C., and Redwood, C. S. L. (2007) DCM troponin C mutant Gly159Asp blunts the response to troponin phosphorylation, *Biochem Biophys Res Commun 360*, 27-32.

16. Mirza, M., Marston, S., Willott, R., Ashley, C., Mogensen, J., McKenna, W., Robinson, P., Redwood, C., and Watkins, H. (2005) Dilated cardiomyopathy mutations in three thin filament regulatory proteins result in a common functional phenotype, *J Biol Chem 280*, 28498-28506.

17. Takeda, S., Yamashita, A., Maeda, K., and Maeda, Y. (2003) Structure of the core domain of human cardiac troponin in the Ca(2+)-saturated form, *Nature 424*, 35-41.

18. Lindhout, D. A., Boyko, R. F., Corson, D. C., Li, M. X., and Sykes, B. D. (2005) The role of electrostatics in the interaction of the inhibitory region of troponin I with troponin C, *Biochemistry 44*, 14750-14759.

19. Vinogradova, M. V., Stone, D. B., Malanina, G. G., Karatzaferi, C., Cooke, R., Mendelson, R. A., and Fletterick, R. J. (2005) Ca(2+)-regulated structural changes in troponin, *Proc. Natl. Acad. Sci. U. S. A. 102*, 5038-5043.

20. Blumenschein, T. M., Tripet, B. P., Hodges, R. S., and Sykes, B. D. (2001) Mapping the interacting regions between troponins T and C. Binding of TnT and TnI peptides to TnC and NMR mapping of the TnT-binding site on TnC, *J Biol Chem 276*, 36606-36612.

21. Pearlstone, J. R., Chandra, M., Sorenson, M. M., and Smillie, L. B. (2000) Biological function and site II Ca2+-induced opening of the regulatory domain of skeletal troponin C are impaired by invariant site I or II Glu mutations, *J Biol Chem 275*, 35106-35115.

22. Li, M. X., Corson, D. C., and Sykes, B. D. (2002) Structure determination by NMR. Isotope labeling, *Methods Mol. Biol. 173*, 255-265.

23. Tripet, B., Van Eyk, J. E., and Hodges, R. S. (1997) Mapping of a second actin-tropomyosin and a second troponin C binding site within the C terminus of troponin I, and their importance in the Ca2+-dependent regulation of muscle contraction, *J. Mol. Biol. 271*, 728-750.

24.   Johnson, B. A., and Blevins, R. A. (1994) NMRView: A computer program for the visualization and analysis of NMR data, *J Biomol NMR 4*, 603-614.

25.   Spyracopoulos, L. (2006) A suite of Mathematica notebooks for the analysis of protein main chain 15N NMR relaxation data, *J Biomol NMR 36*, 215-224.

26.   Lipari, G., and Szabo, a. (1982) Model-Free Approach to the Interpretation of Nuclear Magnetic-Resonance Relaxation in Macromolecules .1. Theory and Range of Validity, *J Am Chem Soc 104*, 4546-4559.

27.   Delaglio, F., Grzesiek, S., Vuister, G. W., Zhu, G., Pfeifer, J., and Bax, A. (1995) NMRPipe: a multidimensional spectral processing system based on UNIX pipes, *J Biomol NMR 6*, 277-293.

28.   Slupsky, C. M., Boyko, R. F., Booth, V. K., and Sykes, B. D. (2003) Smartnotebook: a semi-automated approach to protein sequential NMR resonance assignments, *J Biomol NMR 27*, 313-321.

29.   Guntert, P. (2004) Automated NMR strucutre calculation with CYANA, *Methods Mol Biol 278*, 353-378.

30.   Jee, J., and Guntert, P. (2003) Influence of the completeness of chemical shift assignments on NMR structures obtained with automated NOE assignment, *J. Struct. Funct. Genomics 4*, 179-189.

31.   Cornilescu, G., Delaglio, F., and Bax, A. (1999) Protein backbone angle restraints from searching a database for chemical shift and sequence homology, *J Biomol NMR 13*, 289-302.

32.   Linge, J. P., Williams, M. A., Spronk, C. A., Bonvin, A. M., and Nilges, M. (2003) Refinement of protein structures in explicit solvent, *Proteins 50*, 496-506.

33.   Schwieters, C. D., Kuszewski, J. J., Tjandra, N., and Clore, G. M. (2003) The Xplor-NIH NMR molecular structure determination package, *J Magn Reson 160*, 65-73.

34.   Laskowski, R. A., MacArthur, M. W., Moss, D. S., and Thornton, J. M. (1993) PROCHECK: a program to check the stereochemical quality of protein structures., *J. Appl. Cryst. 26P*, 283-291.

35.   Hooft, R. W., Vriend, G., Sander, C., and Abola, E. E. (1996) Errors in protein structures, *Nature 381*, 272.

36.   Li, M. X., Wang, X., Lindhout, D. A., Buscemi, N., Van Eyk, J. E., and Sykes, B. D. (2003) Phosphorylation and mutation of human cardiac troponin I deferentially destabilize the interaction of the functional regions of troponin I with troponin C, *Biochemistry 42*, 14460-14468.

37.   Lindhout, D. A., and Sykes, B. D. (2003) Structure and dynamics of the C-domain of human cardiac troponin C in complex with the inhibitory region of human cardiac troponin I, *J Biol Chem 278*, 27024-27034.

38. Gasmi-Seabrook, G. M., Howarth, J. W., Finley, N., Abusamhadneh, E., Gaponenko, V., Brito, R. M., Solaro, R. J., and Rosevear, P. R. (1999) Solution structures of the C-terminal domain of cardiac troponin C free and bound to the N-terminal domain of cardiac troponin I, *Biochemistry 38*, 8313-8322.

39. Bloembergen, N., Purcell, E. M., and Pound, R. V. (1948) Relaxation Effects in Nuclear Magnetic Resonance Absorption, *Physical Review 73*, 679-712.

40. Baryshnikova, O. K., and Sykes, B. D. (2006) Backbone dynamics of SDF-1alpha determined by NMR: interpretation in the presence of monomer-dimer equilibrium, *Protein Sci 15*, 2568-2578.

41. Mercier, P., Spyracopoulos, L., and Sykes, B. D. (2001) Structure, dynamics, and thermodynamics of the structural domain of troponin C in complex with the regulatory peptide 1-40 of troponin I, *Biochemistry 40*, 10063-10077.

42. Cantor, C. R., and Schimmel, P. R. (1980) *Biophysical Chemistry, Part II, Techniques for the study of biological structure and function*, W.H. Freeman, New York.

43. Tanford, C. (1961) *Physical chemistry of macromolecules*, John Wiley & Sons, Inc., New York.

44. Wuthrich, K. (1986) *NMR of Proteins and Nucleic Acids*, John Wiley & Sons, New York.

45. Lee, W., Revington, M. J., Arrowsmith, C., and Kay, L. E. (1994) A pulsed field gradient isotope-filtered 3D 13C HMQC-NOESY experiment for extracting intermolecular NOE contacts in molecular complexes, *FEBS Lett 350*, 87-90.

46. Robertson, I. M., Spyracopoulos, L., and Sykes, B. D. (2007) The evaluation of isotope editing and filtering for protein-ligand interaction elucidation by NMR, In *Proceedings for the international School of Biological Magnetic Resonanse, 8th Course on Biophysics and the Challenges of Emerging Threats* (Puglisi, J. D., Ed.), NATO Science Series: Life and Behavioural Sciences, IOS press, The Nethrlands.

47. Gemmecker, G., Olejniczak, E. T., and Fesik, S. W. (1992) An Improved Method for Selectively Observing Protons Attached to C-12 in the Presence of H-1-C-13 spin Pairs, *Journal of Magnetic Resonance 96*, 199-204.

48. Ikura, M., and Bax, A. (1992) Isotope-Filtered 2d NMR of a Protein Peptide Complex - Study of a Skeletal-Muscle Myosin Light Chain Kinase Fragment Bound to Calmodulin, *J Am Chem Soc 114*, 2433-2440.

49. Ogura, K., Terasawa, H., and Inagaki, F. (1996) An improved double-tuned and isotope-filtered pulse scheme based on a pulsed field gradient and a wide-band inversion shaped pulse, *J Biomol NMR 8*, 492-498.

50. Finley, N. L., Howarth, J. W., and Rosevear, P. R. (2004) Structure of the Mg2+-loaded C-lobe of cardiac troponin C bound to the N-domain of cardiac troponin I: comparison with the Ca2+-loaded structure, *Biochemistry 43*, 11371-11379.

51. Li, M. X., Saude, E. J., Wang, X., Pearlstone, J. R., Smillie, L. B., and Sykes, B. D. (2002) Kinetic studies of calcium and cardiac troponin I peptide binding to human cardiac troponin C using NMR spectroscopy, *Eur Biophys J 31*, 245-256.

52. Tripet, B., De Crescenzo, G., Grothe, S., O'Connor-McCourt, M., and Hodges, R. S. (2003) Kinetic analysis of the interactions between troponin C (TnC) and troponin I (TnI) binding peptides: evidence for separate binding sites for the 'structural' N-terminus and the 'regulatory' C-terminus of TnI on TnC, *J Mol Recognit 16*, 37-53.

53. Sheng, Z., Pan, B. S., Miller, T. E., and Potter, J. D. (1992) Isolation, expression, and mutation of a rabbit skeletal muscle cDNA clone for troponin I. The role of the NH2 terminus of fast skeletal muscle troponin I in its biological activity, *J Biol Chem 267*, 25407-25413.

54. Potter, J. D., Sheng, Z., Pan, B. S., and Zhao, J. (1995) A direct regulatory role for troponin T and a dual role for troponin C in the Ca2+ regulation of muscle contraction, *J Biol Chem 270*, 2557-2562.

55. De Nicola, G., Burkart, C., Qiu, F., Agianian, B., Labeit, S., Martin, S., Bullard, B., and Pastore, A. (2007) The structure of Lethocerus troponin C: Insights into the mechanism of stretch activation in muscles, *Structure 15*, 813-824.

56. Pan, B. S., and Johnson, R. G., Jr. (1996) Interaction of cardiotonic thiadiazinone derivatives with cardiac troponin C, *J Biol Chem 271*, 817-823.

57. Kleerekoper, Q., and Putkey, J. A. (1999) Drug binding to cardiac troponin C, *J Biol Chem 274*, 23932-23939.

58. Lipinski, C. A. (2000) Drug-like properties and the causes of poor solubility and poor permeability, *J. Pharmacol. Toxicol. Methods 44*, 235-249.

59. Wang, X., Li, M. X., Spyracopoulos, L., Beier, N., Chandra, M., Solaro, R. J., and Sykes, B. D. (2001) Structure of the C-domain of human cardiac troponin C in complex with the Ca2+ sensitizing drug EMD 57033, *J. Biol. Chem. 276*, 25456-25466.

60. Cheng, H., Lederer, M. R., Lederer, W. J., and Cannell, M. B. (1996) Calcium sparks and [Ca2+]i waves in cardiac myocytes, *Am J Physiol 270*, C148-159.

61. Takamatsu, T., and Wier, W. G. (1990) Calcium waves in mammalian heart: quantification of origin, magnitude, waveform, and velocity, *Faseb J 4*, 1519-1525.

62. Li, M. X., Spyracopoulos, L., and Sykes, B. D. (1999) Binding of cardiac troponin-I147-163 induces a structural opening in human cardiac troponin-C, *Biochemistry 38*, 8289-8298.

63. Finley, N., Abbott, M. B., Abusamhadneh, E., Gaponenko, V., Dong, W., Gasmi-Seabrook, G., Howarth, J. W., Rance, M., Solaro, R. J., Cheung, H. C., and Rosevear, P. R. (1999) NMR analysis of cardiac troponin C-troponin I complexes: effects of phosphorylation, *FEBS Lett 453*, 107-112.

64. Gaponenko, V., Abusamhadneh, E., Abbott, M. B., Finley, N., Gasmi-Seabrook, G., Solaro, R. J., Rance, M., and Rosevear, P. R. (1999) Effects of troponin I phosphorylation on conformational exchange in the regulatory domain of cardiac troponin C, *J Biol Chem 274*, 16681-16684.

65. Keane, N. E., Quirk, P. G., Gao, Y., Patchell, V. B., Perry, S. V., and Levine, B. A. (1997) The ordered phosphorylation of cardiac troponin I by the cAMP-dependent protein kinase--structural consequences and functional implications, *Eur J Biochem 248*, 329-337.

Appendix E.

NMR characterization of the novel inotrope dfbp-o in solution, solid state, membrane bilayers, and muscle fibers

Summary

Levosimendan is the most widely used calcium sensitizers, but since it is unstable, its exact mode of action has yet to be identified. Recently, we compared the function of two stable analogs of levosimendan, dfbp and dfbp-o (Chapter 5). In this chapter, we characterize dfbp and dfbp-o by mass spectrometry, infrared spectroscopy, and NMR spectroscopy. Since dfbp-o has an enhanced affinity over dfbp for troponin and functions as a Ca^{2+}-sensitizer (Chapter 5), we decided to study it in more detail. We present the complete ^{1}H, ^{13}C, and ^{19}F NMR chemical shift assignments of dfbp-o in solution. The two fluorine atoms on dfbp-o can be used to obtain useful structural information *via* ^{19}F-NMR spectroscopy. [19]F is a particularly attractive nucleus for study by NMR spectroscopy because like [1]H: it is ~100% naturally abundant, has a spin of 1/2, and has a large gyromagnetic ratio. In addition, ^{19}F chemical shifts are normally characterized by large anisotropies. Following the assignment, we use solid-state NMR spectroscopy and theoretical techniques to identify the ^{19}F chemical shift tensors. Next, we illustrate the potential of how ^{19}F NMR can be used to calculate molecular orientation in oriented systems. Finally, we present the ^{19}F NMR spectrum of dfbp-o in demembranated psoas muscle fibers. Although we were not able to establish the orientation of dfbp-o in the muscle, we were able to make some interesting observations. 1) dfbp-o decreased the length of the muscle fiber from 3 cm to 1 cm; 2) the ^{19}F NMR spectrum had a broad and narrow resonances, possible from bound and free dfbp-o; and 3) perfusion of the fiber with TFP (which also binds cNTnC) washed out the dfbp-o signal. These results suggest dfbp-o binds to troponin in the intact muscle fiber.

Characterization of dfbp and dfbp-o by MS, and FT-IR

The electrospray ionization mass (ESI-MS), Fourier transform infrared (FT-IR), and NMR spectra of dfbp (Figure E-1) and dfbp-o (Figure E-2) were acquired to confirm the identification of the two molecules. Techniques other than NMR were needed because the compounds differed only by an ether oxygen and thus had the same number of ^{1}H, ^{19}F, and ^{13}C nuclei. We also used MS/MS with the help of Professor Liang Li (Department of Chemistry, University of Alberta, results not shown) to confirm the identity of the compounds. The assignment of the IR spectra was accomplished by side-by-side comparison with IR spectra for phenyloxyacetic acid and benzoic acid taken from the spectral database for organic compounds (SDBS) (http://riodb01.ibase.aist.go.jp/sdbs/ (National Institute of Advanced Industrial Science and Technology, July 12, 2011)) (Figure E-3).

Assignment of dfbp-o in DMSO-d$_6$ and D$_2$O by NMR

Dfbp-o was analyzed by NMR spectroscopy in DMSO-d_6. The relative intensities of ^{1}H peaks in the 1D spectrum and chemical shifts allowed partial assignment of dfbp-o (Figure E-4). Identification of the ^{1}H nuclei on the difluorophenyl ring was verified by the ^{19}F-decoupled ^{1}H 1D spectrum in Figure E-2. ^{1}H resonances for the difluorophenyl ring were assigned using a 2D DQF-COSY NMR spectrum (Figure E-5). However, there were some ambiguities (for example assignment of H2/H6 *versus* H3/H5) that required heteronuclear NMR experiments to assign. The solvent was changed from DMSO-d$_6$ to D$_2$O since the protein experiments in Chapter 5 and muscle fiber experiments were done in an aqueous environment.

The ^{19}F NMR spectra of dfbp-o in DMSO-d$_6$ and D$_2$O are shown in Figure E-6. The fluorine peaks dramatically changed positions from -34.4
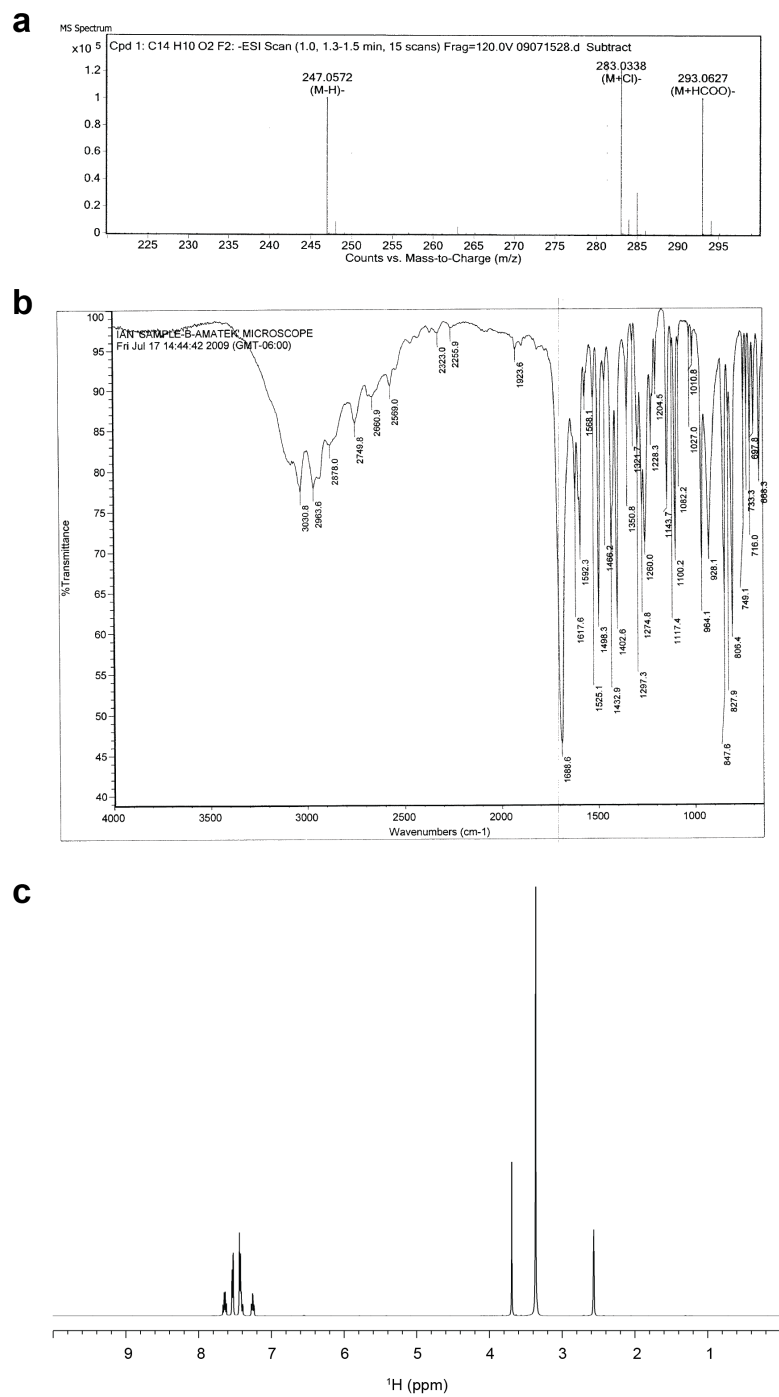
Figure E-1. a. ESI-MS, **b.** FT-IR, and **c.** 1D ^{1}H NMR spectra of dfbp.
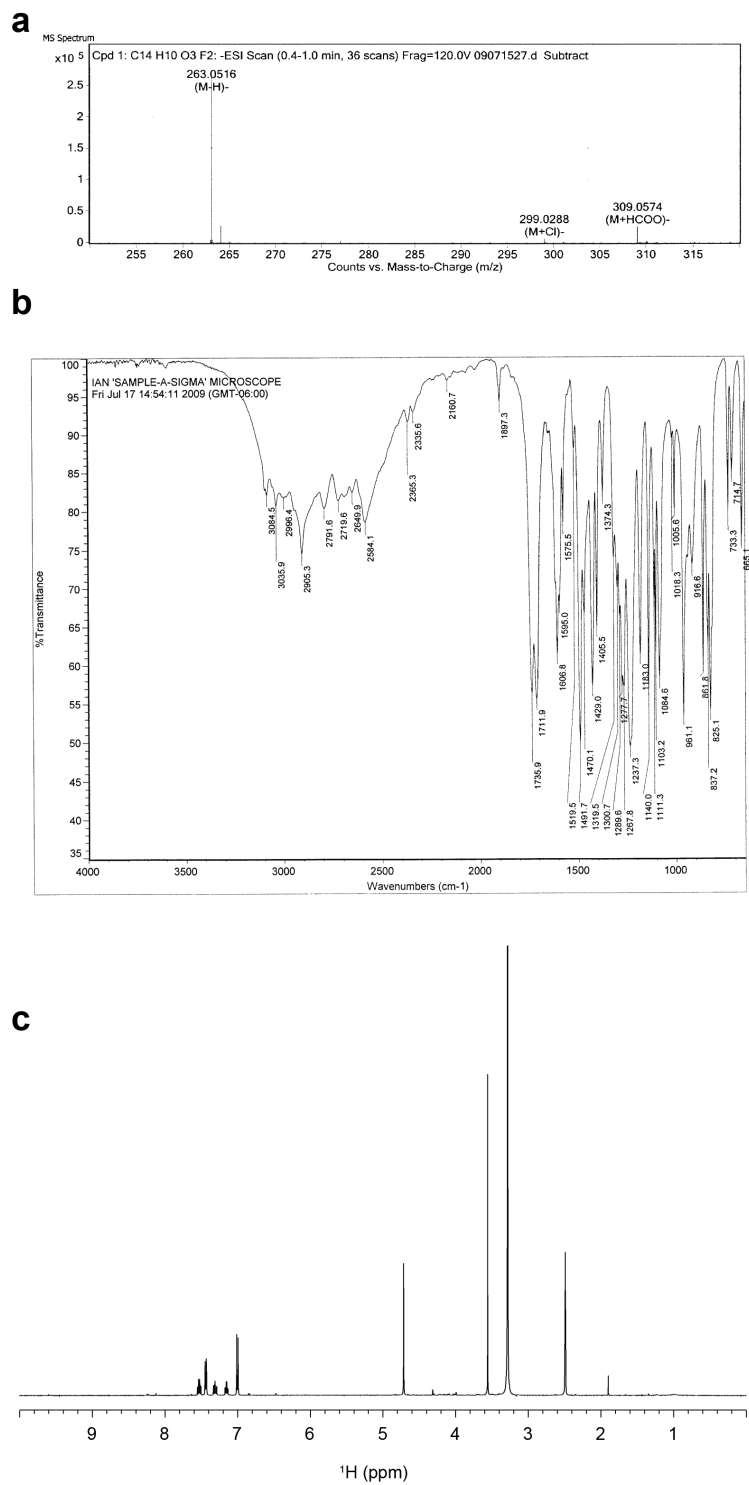
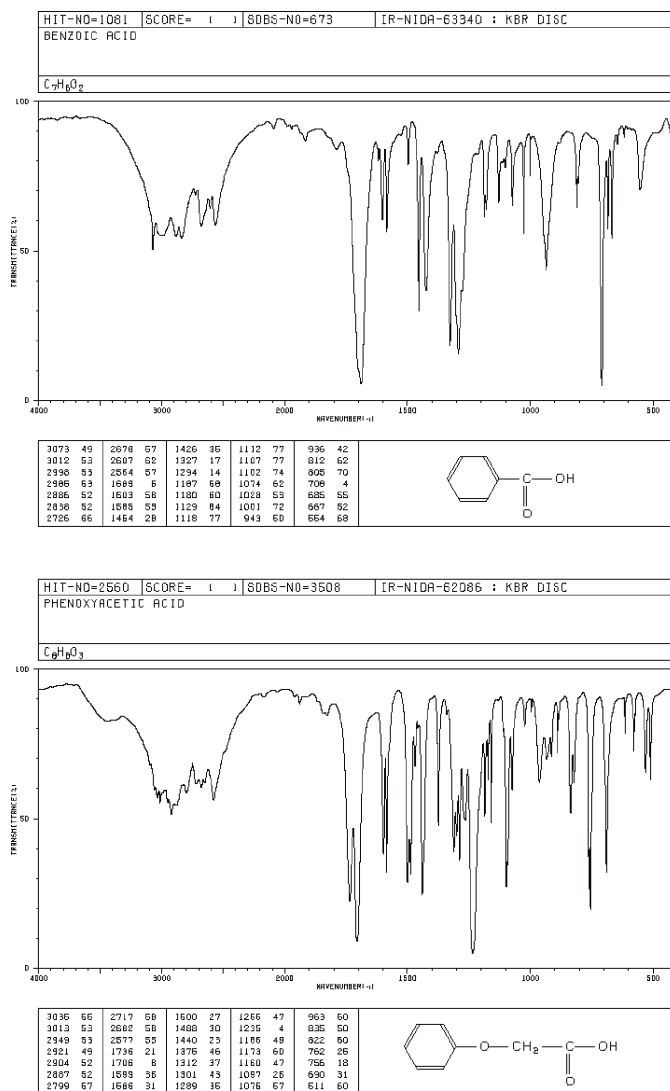**Figure E-2. a.** ESI-MS, **b.** FT-IR, and **c.** 1D ^{1}H NMR spectra of dfbp-o.

Figure E-3: IR spectra of benzoic acid and phenyloxyacetic acid (SDBS). Note the two bands around 1700 cm^{-1} for phenyloxyacetic acid (only one band for benzoic acid) is similar to what was observed for dfbp-o (Figure E-2).
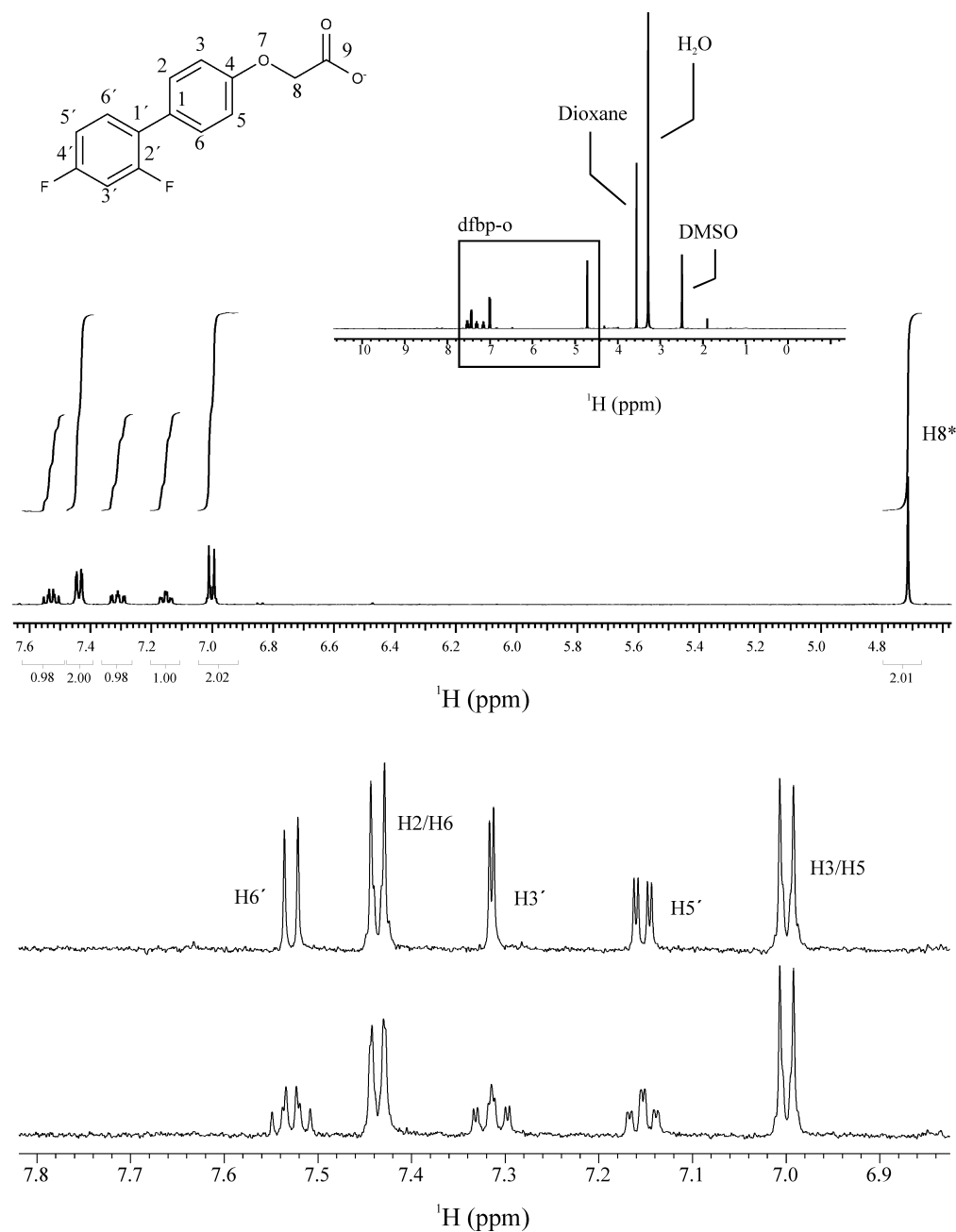
Figure E-4. ^{1}H NMR spectra of dfbp-o in DMSO-d_6. Bottom two spectra: the difference between the ^{1}H spectrum of dfbp-o with ^{19}F decoupling turned on (upper) or off (lower). The resonances that underwent significant simplification upon decoupling were identified as those on the difluorophenyl ring.

and -36.4 ppm in DMSO-d_6 to -37.2 and -39.5 ppm in D_2O (referenced to TFA). This is probably due to differences in van der Waals interactions, the solvent electric fields, and possibly hydrogen bonding to the fluorine nuclei (1). We also saw large differences in the ^{1}H chemical shifts corresponding to the solvent change (Figure E-7 *versus* E-4).

Since aromatic ligands (such as dfbp-o) can undergo stacking in solution (2), the ligand's dissociation constant for its target protein may be concealed its the self-association constant. In order to investigate if dfbp-o stacks in D_2O, a serial dilution of dfbp-o was performed; however, we saw no concentration dependent chemical shift change (not shown).

To confirm dfbp-o is negatively charged at neutral conditions, the pH was lowered. Around pH < 5 precipitate appeared, presumably because dfbp-o is less soluble when protonated. The doublet near 7.0 ppm underwent the largest chemical shift change upon protonation of dfbp-o (Figure E-7), and was therefore tentatively assigned to H3/H5. Assignment of the ^{19}F and ^{1}H resonances was confirmed with the ^{1}H, ^{19}F-HOESY (mixing time = 350 ms) (Figure E-8). F2' makes an HOE contact with H2/H6 of the benzene ring, which confirmed the assignment of H3/H5 by the pH experiment, and unambiguously separated the two phenyl proton assignments. Additionally, the lack of an HOE to H6' distinguished it as the one proton on the difluorophenyl ring not adjacent to a ^{19}F nucleus. The assignments were also verified by comparing with assignments for the analogous molecule, flobufen (3).

The ^{13}C resonances were assigned by the ^{1}H,^{13}C-HSQC (Figure E-9) and the [9]F,^{13}C-HMQC (Figure E-10) NMR experiments. Since the H3' and H5' were overlapped in the 1D ^{1}H spectrum, it was not possible to assign the corresponding C3' and C5' even though the two ^{13}C are well resolved in the ^{1}H,^{13}C-HSQC spectrum. In order to resolve these assignments, an HMBC type experiment may be useful.
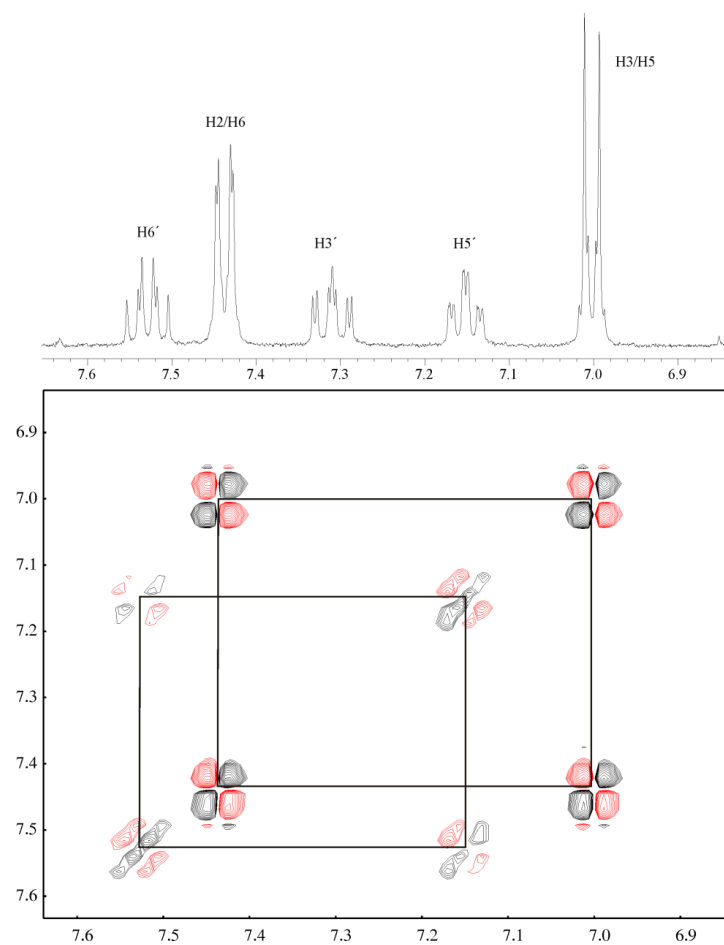
Figure E-5. The 2D ^{1}H-^{1}H DQF-COSY of dfbp-o DMSO-d$_6$. We could identify coupled protons, such as H2/H6-H3/H5 and H6'-H5'; however, it was not possible to assign the nuclei further.
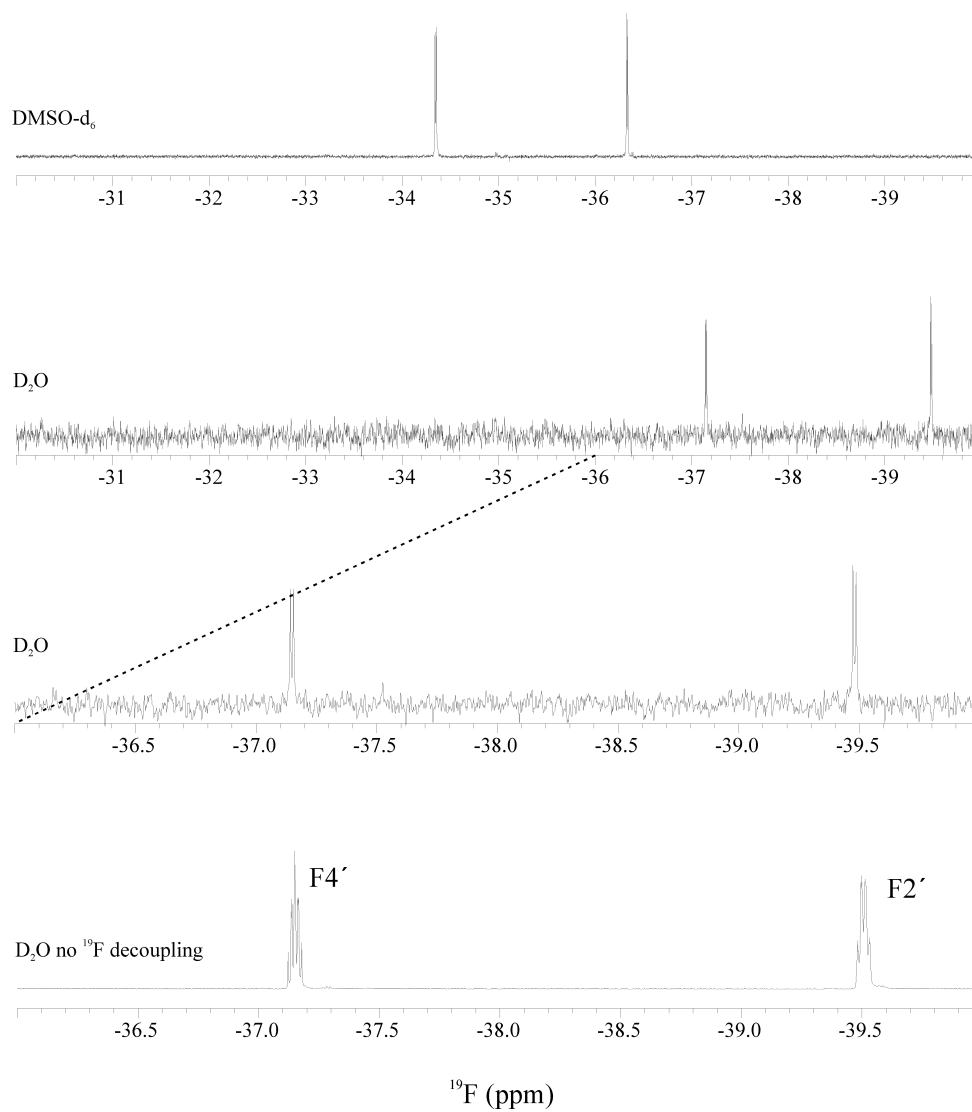
Figure E-6. ^{19}F NMR spectra of dfbp-o in DMOS-d$_6$ or D$_2$O. Again note the simplification of the fluorine spectra upon proton decoupling. After ^{1}H decoupling, the ^{19}F coupling could be resolved (^{4}J$_{FF}$ = 7.5 Hz).
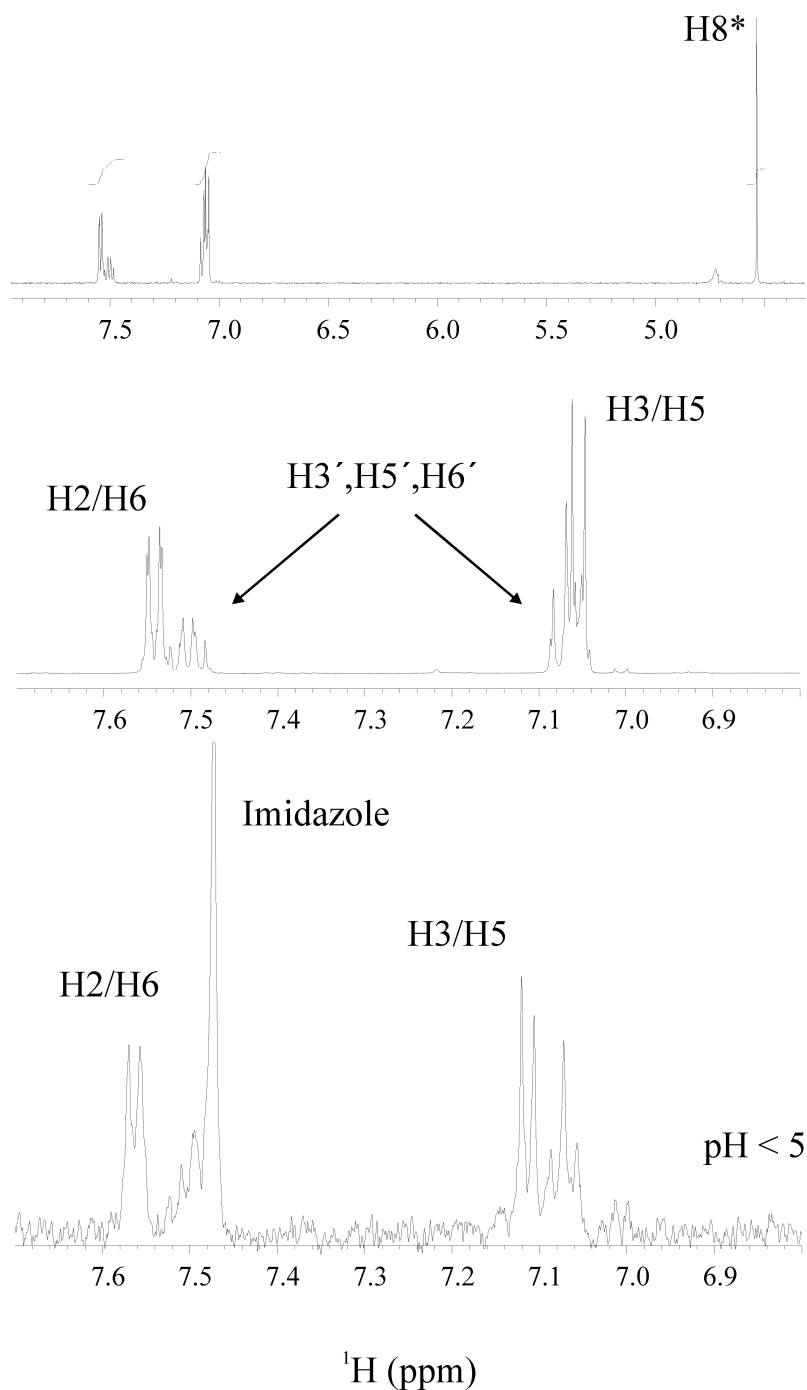
Figure E-7. ^{1}H NMR spectrum of dfbp-o in D_2O. The upper and middle spectra were acquired at neutral pH. In the bottom spectrum, in acidic conditions the carboxylate is protonated and the ^{1}H spetrum changed, primarily at the most upfield aromatic proton pair assigned to H3/H5.
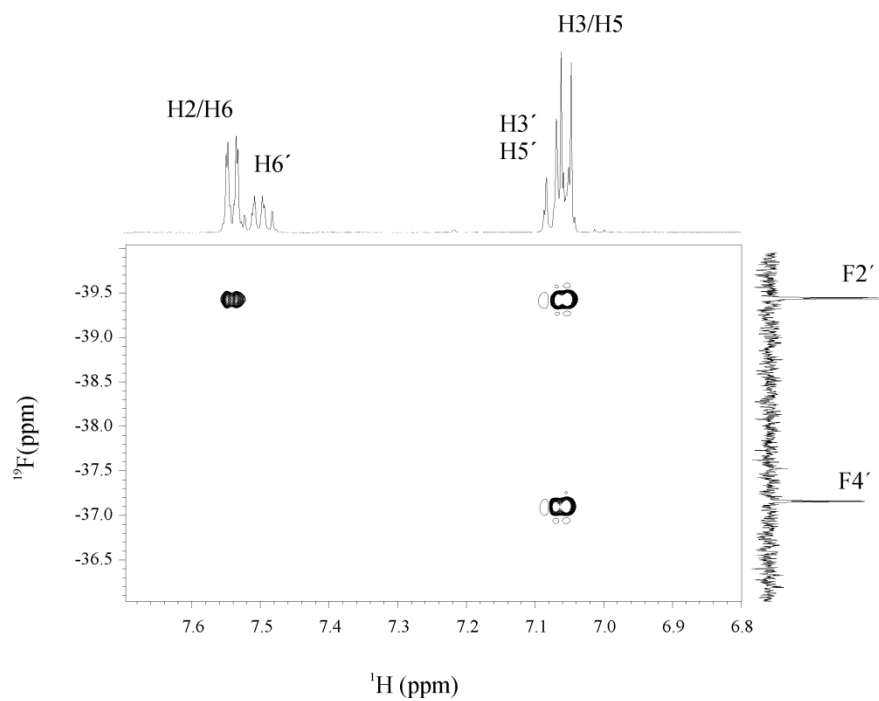
Figure E-8. 2D ^{1}H-^{19}F HOESY NMR spectrum of dfbp-o in D_2O.
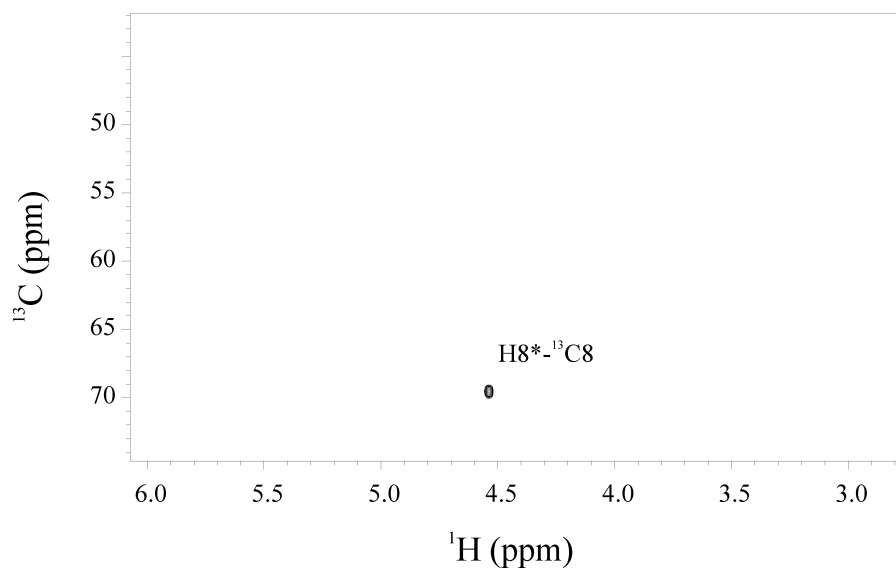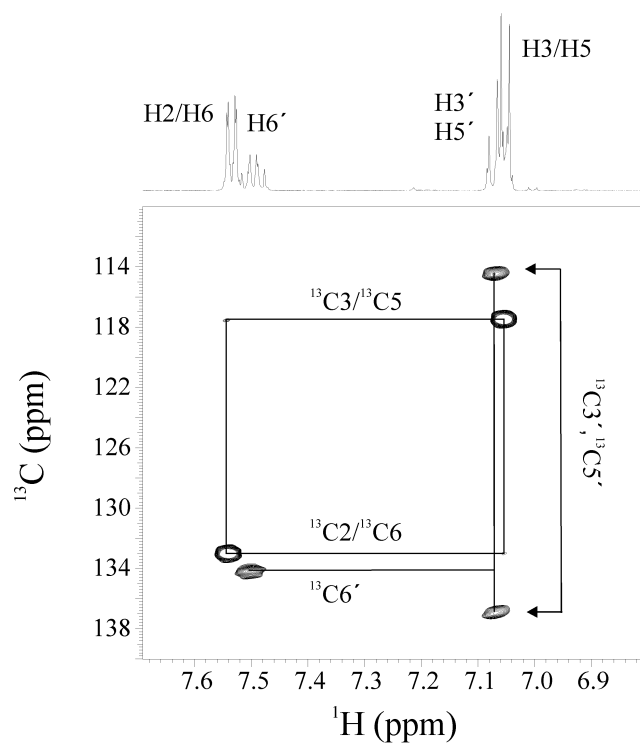
Figure E-9. ^{1}H,^{13}C-HSQC NMR spectra of dfbp-o in D$_2$O.
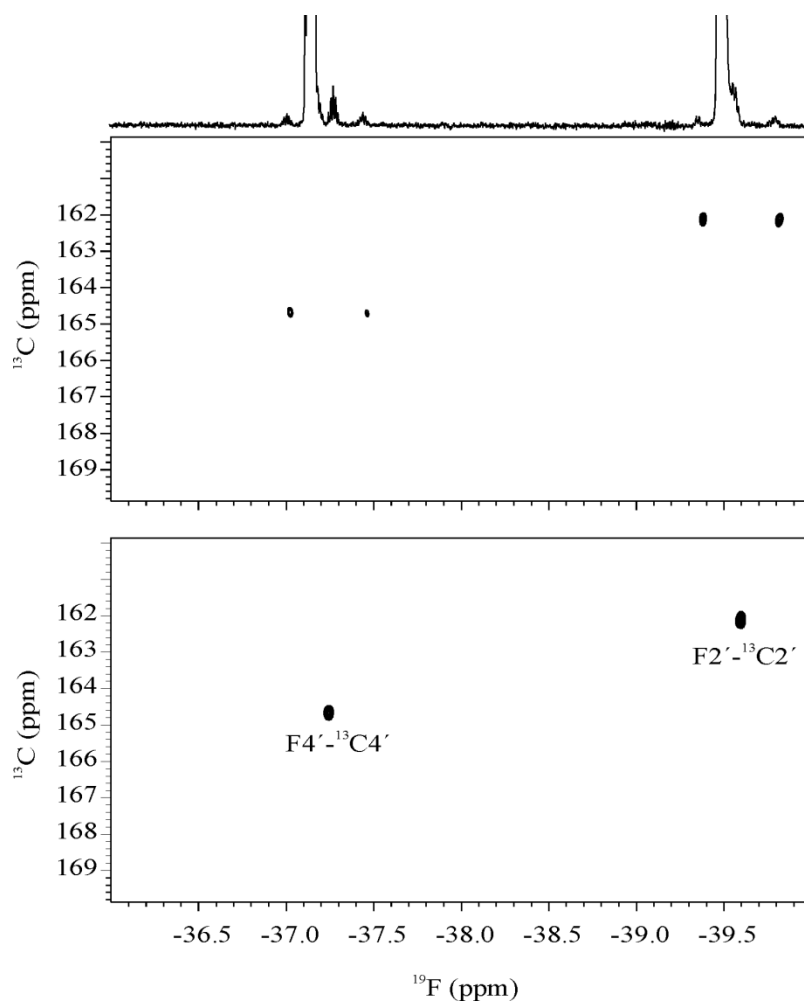
Figure E-10. ^{19}F,^{13}C-HMQC NMR spectra of dfbp-o in D$_2$O. (top) ^{19}F decoupling was turned off to measure the one-bond C-F coupling constant ($^1J_{CF}$ ~ 250 Hz).

Analysis of dfbp-o by solid-state NMR spectroscopy

The high power (100 KHz) [1]H-decoupled powder spectrum of dfbp-o is shown in Figure E-11. To obtain the ^{19}F chemical shift anisotropy (CSA) principal axis system with respect to the molecular frame of dfbp-o both Hartree-Fock gauge including atomic orbitals (HF-GIAO) and Density Functional Theory GIAO (DFT-GIAO) methods were used as previously described (4). The *ab initio* DFT optimized structure of dfbp-o (Chapter 5) was used to calculate the ^{19}F chemical shift tensors of F2' and F4' with Gaussian 03 (5). The HF-GIAO calculation best fit the experimental data and the ^{19}F CSA tensor values are plotted on the powder spectrum (Figure E-11). Neither of the DFT and HF calculations fit the experimental ^{19}F CSA tensor values, particularly in the calculation of δ_{22}. Therefore, the calculated ^{19}F principal axis directions with respect to the molecular frame may not be accurate. This failure may reflect that the best starting structure was not used for the calculations or a limitation of the theoretical methods in the more complicated fluorinated systems such as ours (as compared to the success of these calculations with other aromatic fluorines (4)). To address the issue of an inappropriate structure, we used X-ray coordinates of a related molecule (1-(2',4'-Difluorobiphenyl-4-yl)ethanone, (6)); however, the calculations did not improve (data not shown). The ^{19}F CSA directions from the HF-GIAO calculation for F4' deviate from the local molecular frame by: $\delta_{11} < 1°$ (perpendicular to the C-F bond), $\delta_{22} = 3°$ (parallel to the C-F bond) and $\delta_{33} < 3°$ (perpendicular to the plane of the aromatic ring) - see Figure E-12c for the orientation of the principal axes with respect to the molecular frame. The orientation of F2' [19]F CSA principal axes deviated significantly more than F4' (probably due to the adjacent phenyl ring): $\delta_{11} = 1°$, $\delta_{22} = 16°$, and $\delta_{33} = 16°$.

We next attempted to predict the orientation of dfbp-o in dimyristoylphosphatidylcholine (DMPC). The goal was to see if we could use just ^{19}F chemical shifts to predict orientation. We suspended dfbp-o in
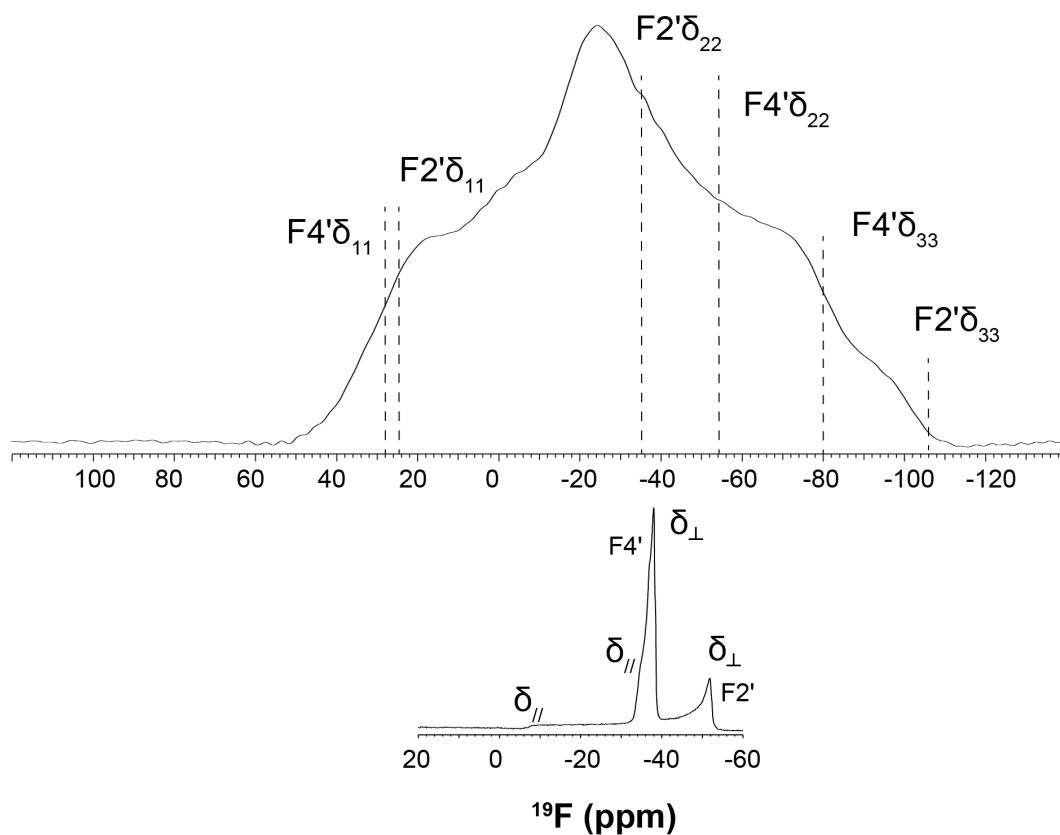
Figure E-11. Solid-state ^{19}F spectra of dfbp-o. (top) ^{19}F spectrum of dfbp-o powder; 1D ^{19}F DEPTH spectrum with high power ^{1}H decoupling (100 KHz). The spectrum is labeled with the HF-GIAO calculated ^{19}F CSA tensors. (bottom) ^{19}F spectrum of dfbp-o in DMPC bilayers. The axially symmetric spectrum indicates that dfbp-o undergoes axial rotation in the membrane.
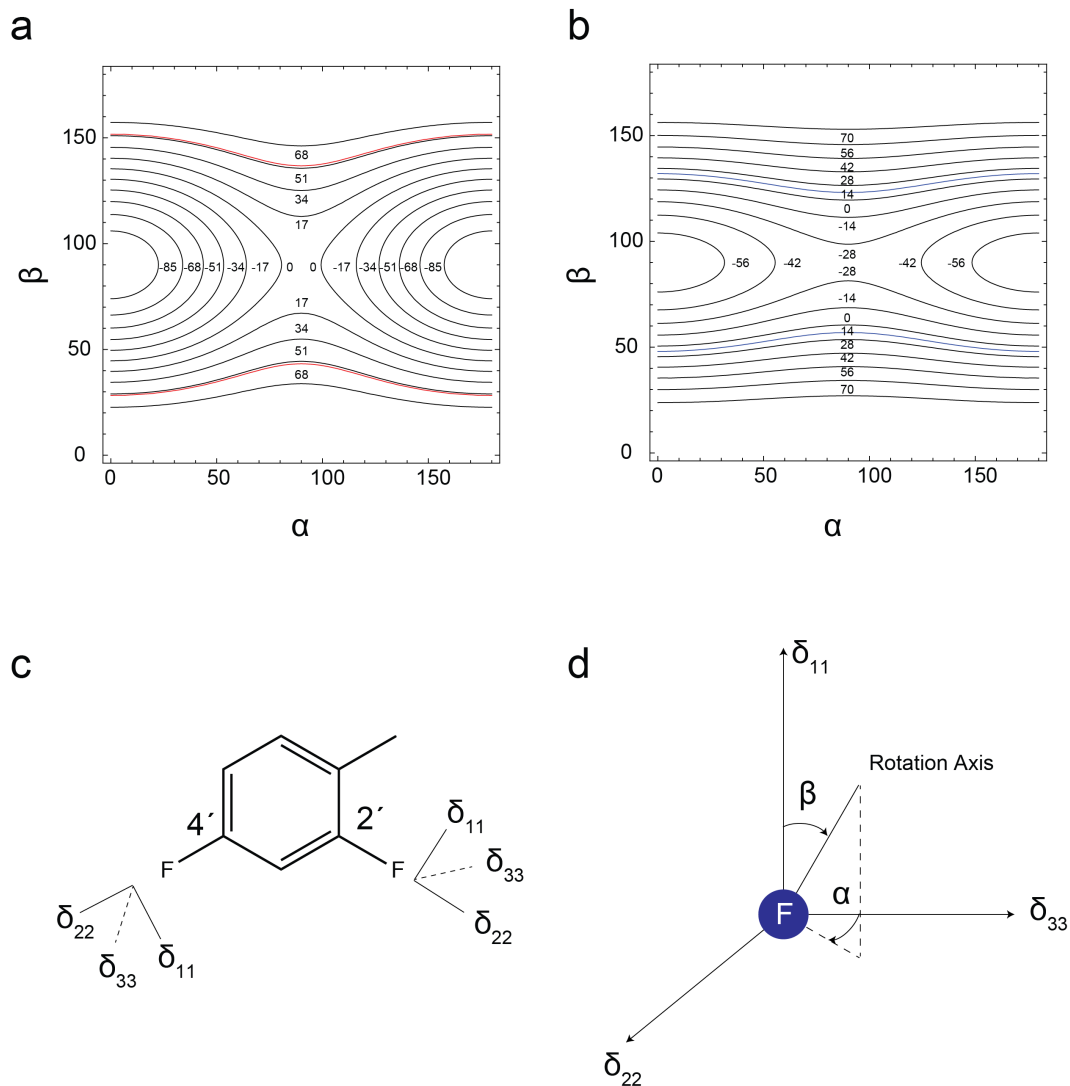
Figure E-12. Calculated Δδ values (ppm) of simulated axially symmetric spectra for the fluorine atoms of dfbp-o (a. F2' and b. F4') as a function of the azimuthal (α) and polar (β) angles that relate the rotation axis to ^{19}F CSA tensor (see c. and d.). Red and Blue lines correspond to the calculated ^{19}F tensors, labeled on the spectra in Figure E-12.

a hydrated DMPC sample (*7*). The ^{19}F spectrum of dfbp-o in the DMPC sample is in Figure E-11. The spectrum is much narrower than the powder spectrum, and shows two unique axially symmetric patterns, ostensibly from each ^{19}F nuclei. These axially symmetric patterns mean that dfbp-o is rapidly rotating about at least one axis in the membrane. In Figure E-12 we outline the way the axially symmetric chemical shifts can be used to calculate orientation of dfbp-o. For details on the calculations see Matsumori *et al*. (*8*). Although we have not completed a detailed analysis of the data, the rotation axis of dfbp-o in DMPC seems to lie near the C4'-F bond.

Muscle fiber studies of dfbp-o

Since we established that it is possible to determine the orientation of dfbp-o in an ideal system, we wanted to investigate whether dfbp-o aligned in muscle and if we could predict its orientation when bound. We soaked a psoas muscle fibre with 500 µM dfbp-o in relaxing buffer for ~12 hours (Figure E-13). The muscle fiber decreased in length from 3 cm to 1 cm following the soak. Following the soak the muscle fiber was carefully pulled through a capillary tube and then placed in a 3 mm NMR tube. The 1D ^{19}F NMR spectrum of dfbp-o free in D_2O and of dfbp-o bound to the muscle fibre are shown in Figure E-13b. Note the isotropic shifts are still observable in the muscle fibre spectrum suggesting a free and bound species. A competition assay between dfbp-o and TFP was also conducted. The muscle fibre from the dfbp-o soak was removed from the 3 mm NMR tube, but left in the capillary tube. The capillary tube was than perfused with relaxing buffer containing 150 µM TFP. Note that post TFP perfusion, dfbp-o peak intensity was greatly reduced (Figure E-13c).
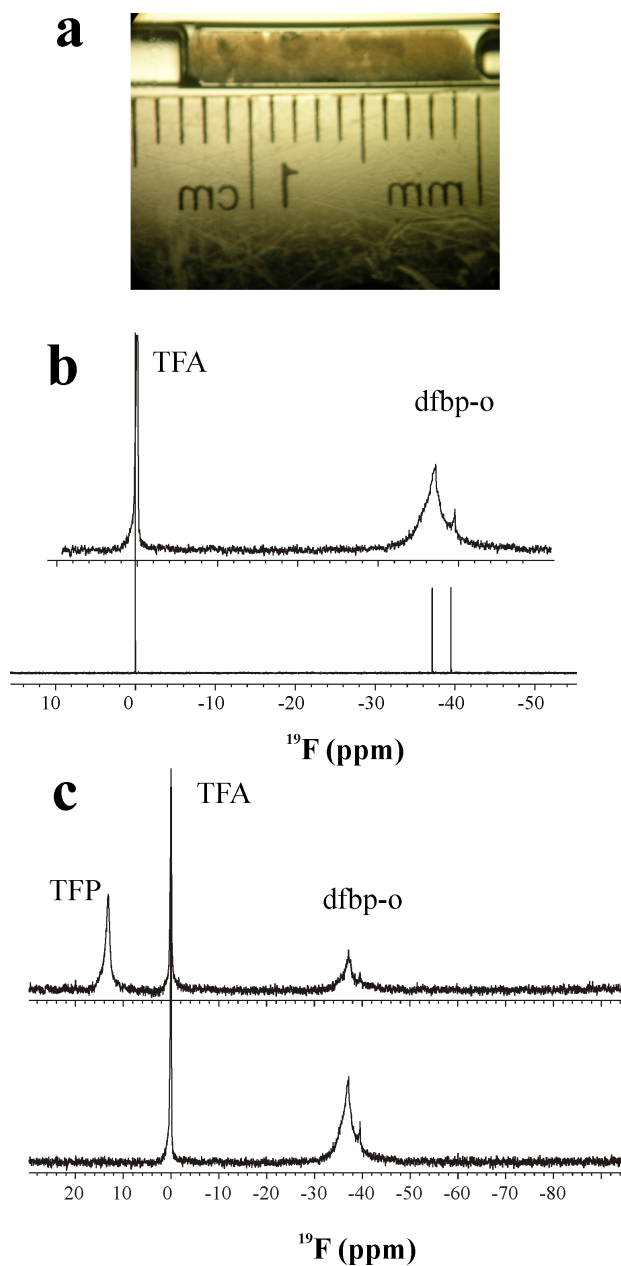
Figure E-13. [9]F NMR spectra of dfbp-o in a muscle fiber. a. psoas muscle fiber in a 3 mm NMR tube after soaking the fiber in 0.5 mM dfbp-o overnight. b. the ^{19}F NMR spectrum of dfbp-o in (top) a psoas muscle fibre and (bottom) the spectrum of dfbp-o free in solution. c. (bottom) same spectra as in b. and (top) following perfusion with 150 µM TFP.

Conclusions

In this chapter we assigned the ^{1}H,^{13}C, and ^{19}F NMR spectrum of dfbp-o, which was necessary for determining its structure bound to the troponin C-troponin I complex (Chapter 5). We used theoretical methods to calculate the ^{19}F CSA principal values and axes, and then acquired the axially symmetric ^{19}F spectra of dfbp-o to show that it's possible to predict its rotation axis in DMPC. Finally we soaked a psoas muscle fiber in 0.5 mM dfbp-o and acquired ^{19}F spectra of the contracted fiber. Several conclusions can be drawn from the ^{19}F spectra in Figure E-13.

The presence of narrow and broad peaks may represent free and bound species of dfbp-o. It is unlikely that this is not nonspecific binding for several reasons: the TFA peak is narrow compared to the dfbp-o signal, the spectra of dfbp-o is not as broad as the powder spectrum (Figure E-11), nor is it as broad as the membrane spectrum (Figure E-11). The ability of TFP to wash off dfbp-o suggested they competed for the same binding site (such as sNTnC). It is difficult to explain the contraction of the psoas muscle fibers in the absence of Ca^{2+}. Several possibilities may explain this result: dfbp-o bound to TnC and competed with TnI like TFP to wash off TnC over time, or dfbp-o actually induces contraction in the apo state of sTnC. Although more experiments are needed to verify if the broad ^{19}F signals in the spectrum are indeed from dfbp-o in complex with TnC, we have developed a technique of preparing muscle fibers for ^{19}F-NMR studies.

References

1. Lau, E. Y., and Gerig, J. T. (1996) Solvent effects on fluorine shielding in fluorobenzene, *J. Am. Chem. Soc. 118*, 1194-1200.
2. Martin, R. B. (1996) Comparisons of Indefinite Self-Association Models, *Chem. Rev. 96*, 3043-3064.
3. Jegorov, A., Sedmera, P., Havlicek, V., Husak, M., Pakhomova, S., Kratochvil, B., Kuchar, M., and Bulej, P. (1995) Spectroscopic and Structural Study of Flobufen, *J. Fluorine Chem. 73*, 213-219.
4. Sanders, L. K., and Oldfield, E. (2001) Theoretical investigation of F-19 NMR chemical shielding tensors in fluorobenzenes, *J. Phys. Chem. A 105*, 8098-8104.
5. Frisch, M. J., Trucks, G. W., Schlegel, H. B., G. E. Scuseria, M. A. Robb, J. R. Cheeseman, J. A. Montgomery, Jr., T. Vreven, K. N. Kudin, J. C. Burant, J. M. Millam, S. S. Iyengar, J. Tomasi, V. Barone, B. Mennucci, M. Cossi, G. Scalmani, N. Rega, G. A. Petersson, H. Nakatsuji, M. Hada, M. Ehara, K. Toyota, R. Fukuda, J. Hasegawa, M. Ishida, T. Nakajima, Y. Honda, O. Kitao, H. Nakai, M. Klene, X. Li, J. E. Knox, H. P. Hratchian, J. B. Cross, V. Bakken, C. Adamo, J. Jaramillo, R. Gomperts, R. E. Stratmann, O. Yazyev, A. J. Austin, R. Cammi, C. Pomelli, J. W. Ochterski, P. Y. Ayala, K. Morokuma, G. A. Voth, P. Salvador, J. J. Dannenberg, V. G. Zakrzewski, S. Dapprich, A. D. Daniels, M. C. Strain, O. Farkas, D. K. Malick, A. D. Rabuck, K. Raghavachari, J. B. Foresman, J. V. Ortiz, Q. Cui, A. G. Baboul, S. Clifford, J. Cioslowski, B. B. Stefanov, G. Liu, A. Liashenko, P. Piskorz, I. Komaromi, R. L. Martin, D. J. Fox, T. Keith, M. A. Al-Laham, C. Y. Peng, A. Nanayakkara, M. Challacombe, P. M. W. Gill, B. Johnson, W. Chen, M. W. Wong, C. Gonzalez, and J. A. Pople. (2004) Gaussian 03, Gaussian 03 ed., Gaussian, Inc., Wallingford CT.
6. Guo, M. P., Deng, J. H., Zhang, Q. C., Guo, H. R., and Yuan, L. (2008) 1-(2 ',4 '-difluorobiphenyl-4-yl)ethanone, *Acta Crystallographica Section E-Structure Reports Online 64*, O1923-U3759.
7. Grage, S. L., and Ulrich, A. S. (1999) Structural parameters from F-19 homonuclear dipolar couplings, obtained by multipulse solid-state NMR on static and oriented systems, *J. Magn. Reson. 138*, 98-106.
8. Matsumori, N., Kasai, Y., Oishi, T., Murata, M., and Nomura, K. (2008) Orientation of fluorinated cholesterol in lipid bilayers analyzed by 19F tensor calculation and solid-state NMR, *J. Am. Chem. Soc. 130*, 4757-4766.

Appendix F.

Synthesis of a fluorinated analog of the cardiotonic compound OR1896.

Summary

The preparation of a fluorinated analog of the Ca^{2+}-sensitizing agent OR1896 is described. OR1896 is the natural metabolite of levosimendan and has been shown to increase the Ca^{2+} sensitivity (*1*). It has been proposed to act by a combination of sensitizing cardiac troponin C (cTnC) and inhibiting phosphodiesterase (PDE) III (*2*). The purpose of this work was to build upon the approach discussed in Appendix E; that is, can we identify if the pyridazinone-class of ligands (that encompass levosimendan and pimobendan) bind to the thin filament in a muscle fiber by ^{19}F-NMR spectroscopy (described for dfbp-o in Appendix E). In the following chapter, we review the synthesis of OR1896-CF$_3$ and the assignment of its ^{1}H and ^{19}F NMR spectra. Finally, we study its interaction with cTnC, the regulatory domain of troponin C (cNTnC), and cNTnC in complex with the switch region of troponin I (cTnI$_{144-163}$).

Experimental Procedures

Sample Preparations.

Recombinant human cTnC (residues 1-161), cNTnC (residues 1-89) with the mutations C35S and C84S was used in this study. The engineering of the expression vector and the expression of ^{15}N-labeled proteins in *E. coli* were as described previously (*3, 4*). The synthetic peptide, cTnI$_{144-163}$ (acetyl-RRVRISADAMMQALLGARAK-amide), was prepared by GL Biochem Ltd. (Shanghai). The purity was verified by HPLC and the mass verified by electrospray mass spectrometry. AMDP (6-(4–aminophenyl)-5-methyl-4,5-dihydro-3(2H)-pyridazinone) was purchased from Kinbester Co. Ltd. (Hong Kong). Stock solutions of the compounds in DMSO-d$_6$ (Cambridge Isotopes Inc.) were prepared and the vials containing the solutions were wrapped in aluminum foil due to sensitivity to light. All NMR samples were 500 mL in volume. The buffer conditions were 100 mM KCl, 10 mM imidazole, and 0.2-0.25 mM DSS in 95% H$_2$O/5% D$_2$O, and the pH was 6.7-6.9. For the ^{19}F-NMR spectroscopy, a 3 mm NMR sample with a final volume of 200 μL was prepared, 0.5 mM trifluoroacetic acid (TFA) was used as the chemical shift reference.
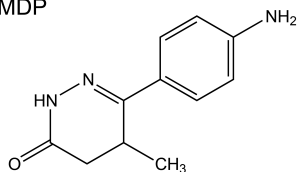
Synthesis of OR1896-CF$_3$.

The synthesis of OR1896-CF$_3$ (Figure F-1) was modified from the protocol described by Prashad *et al*. for the trifluoroacetylation of aniline (*5*). We dissolved 1.0 g of AMDP (MW = 142.08 g/mol) and 296 mg of 4-dimethylaminopyridine (DMAP) (MW=122.17 g/mol) in 80.0 mL of tetrahydrofuran (THF) and 4 mL of ethyl trifluoroacetate. The sample was kept at 70-80°C for 24 Hours. Thin layer chromatography was used to monitor the course of the reaction. OR1896-CF$_3$ was purified by mixing ethyl acetate with the reaction mixture and performing 7 separate acid washes. Subsequent drying of ethyl acetate yielded crystals of OR1896-CF$_3$, which was characterized by ESI-MS and NMR spectroscopy (Figure F-2).
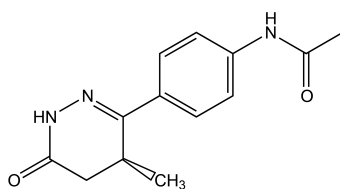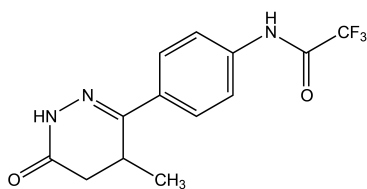
Figure F-1. Chemical structures of two metabolites of levosimendan, OR1896 and AMDP (the racemate of OR1855); and of the fluorinated analog of OR1896, OR1896-CF$_3$.
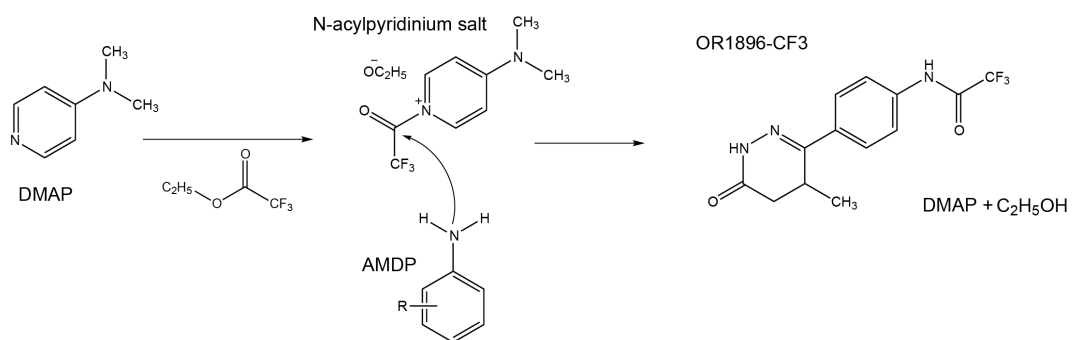
Figure F-2. Proposed reaction scheme for the synthesis of OR1896-CF$_3$ (*5*).

NMR spectroscopy.

All of the NMR spectra were obtained at 30°C. ^{1}H and ^{1}H,^{15}N spectra were acquired using a Varian INOVA 500 MHz spectrometer. The ^{19}F spectra were acquired on a Unity 600 MHz spectrometer. All 1D ^{1}H and 2D ^{1}H,^{15}N-HSQC spectra were acquired using the water and gNhsqc.c pulse sequences, respectively, (BioPack, Varian Inc.). Spectral processing was accomplished with the program VNMRJ (Version 2.1B, Varian Inc.) and NMRPipe (*6*) and referenced according to the IUPAC conventions. Processed NMR spectra were analyzed using NMRViewJ (*7*) and assignments for cTnC•3Ca^{2+}, cNTnC•Ca^{2+}, and cNTnC•Ca^{2+}•cTnI$_{144-163}$ were taken from that done previously (*8, 9*).

Results and Discussion

The chemical structures OR1896 (*N*-(4-(1,4,5,6-tetrahydro-4-methyl-6-oxo-3-pyridazinyl)phenyl) acetamide), AMDP (6-(4–aminophenyl)-5-methyl-4,5-dihydro-3(2H)-pyridazinone), and OR1896-CF$_3$ (*N*-(4-(1,4,5,6-tetrahydro-4-methyl-6-oxo-3-pyridazinyl)phenyl) trifluoroacetamide) are shown in Figure F-1. OR1896 is a metabolite and has been shown to function as a Ca^{2+}-sensitizer by much the same means as levosimendan (*1, 2*). OR1896-CF$_3$ was prepared using AMDP s starting material, following a procedure outlined for the selective trifluoroacetylation of aniline (*5*). AMDP was dissolved in 80 mL of THF. The proposed mechanism of OR1896-CF$_3$ synthesis adapted from (*5*) is shown in Figure F-2. Briefly, the aniline moiety of AMDP attacks the N-acylpyridinium salt to make a tetrahedral intermediate that results in the release of the fluorinated product, OR1896-CF$_3$ and ethanol. The assigned ^{1}H and ^{19}F NMR spectra of OR1896-CF$_3$ are shown in Figure F-3. The assignment of OR1896-CF$_3$ was done using 2D ^{1}H,^{1}H-NOESY and ^{1}H,^{19}F HOESY spectra. The assignment was also aided by comparison with the spectrum of levosimendan (*10*).

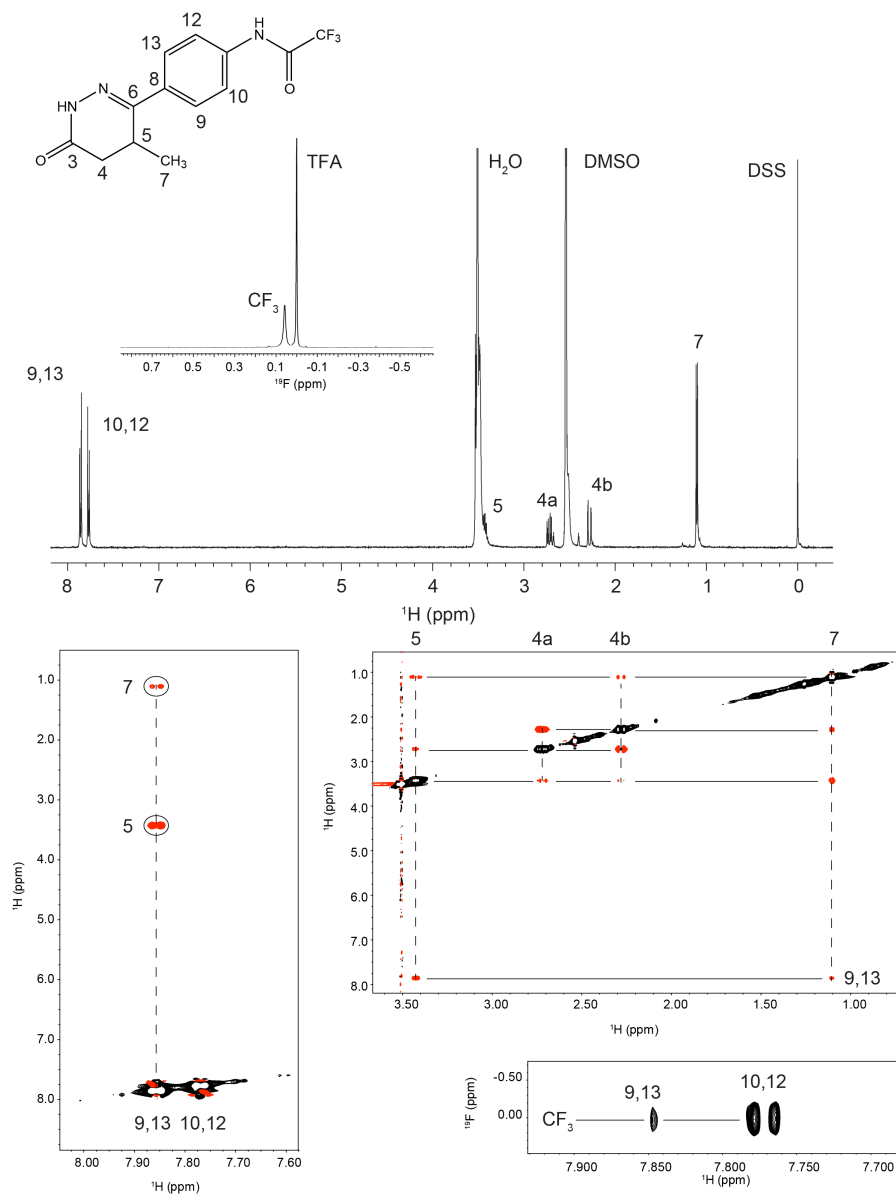**Figure F-3**. Assignment of the ^{1}H and ^{19}F NMR spectra of OR1896-CF$_3$. Top: 1D ^{19}F NMR and ^{1}H spectra of OR1896-CF$_3$ acquired at 564 and 600 MHz, respectively. Middle: two slices from the 2D ^{1}H-^{1}H NOESY spectrum (mixing time = 400 ms). Bottom right: 2D ^{1}H,^{19}F HOESY spectrum (mixing time = 400 ms).

OR1896-CF$_3$ was added to a sample containing cTnC•3Ca^{3+}. The superimposition of the ^{1}H,^{15}N HSQC spectra are shown in Figure F-4. OR1896-CF$_3$ perturbed residues in both domains (also noted for levosimendan (*11*) and W7 (*4*)). However, since cTnI precludes the C-domain binding site (*4, 12*), we investigated whether OR1896-CF$_3$ bound to the isolated regulatory domain of cTnC (cNTnC•Ca^{2+}) in the absence and presence of cTnI$_{144-163}$. Many of the same peaks in the N-domain that were perturbed when OR1896-CF$_3$ was added to cTnC were also shifted in cNTnC•Ca^{2+} (Figure F-5). When cTnI$_{144-163}$ was present, the perturbations caused by the addition of OR189-CF$_3$ were much smaller. There are two possible explanations for this observation. The first is that OR1896-CF$_3$ binding to the cNTnC-cTnI complex induces much smaller perturbations because the structure is less changed by the presence of OR1896-CF$_3$. The second is that the bulky CF$_3$ group clashes with the hydrophobic residues of cTnI thus reducing the OR1896-CF$_3$ binding affinity.

In this report we synthesized a novel analog of the Ca^{2+}-sensitizer, OR1896. We show that OR1896-CF$_3$ binds to both domains of cTnC•3Ca^{2+}. Moreover, OR1896-CF$_3$ binds to the N-domain of cTnC in a similar manner in the full-length and isolated constructs. It is unclear whether OR1896-CF$_3$ competes with cTnI$_{144-163}$ binding to cNTnC•Ca^{2+}; a series of titrations with OR1896-CF$_3$ will need to be completed to answer this question. It would also be interesting to test the activity of this molecule in isolated muscle fibers. A similar series of broad line ^{19}F NMR experiments as described in Appendix E for dfbp-o could be repeated with OR1896-CF$_3$. These experiments may provide insight into how the pyridazinone class of Ca^{2+}-sensitizers target the muscle fiber to modulate contractility.
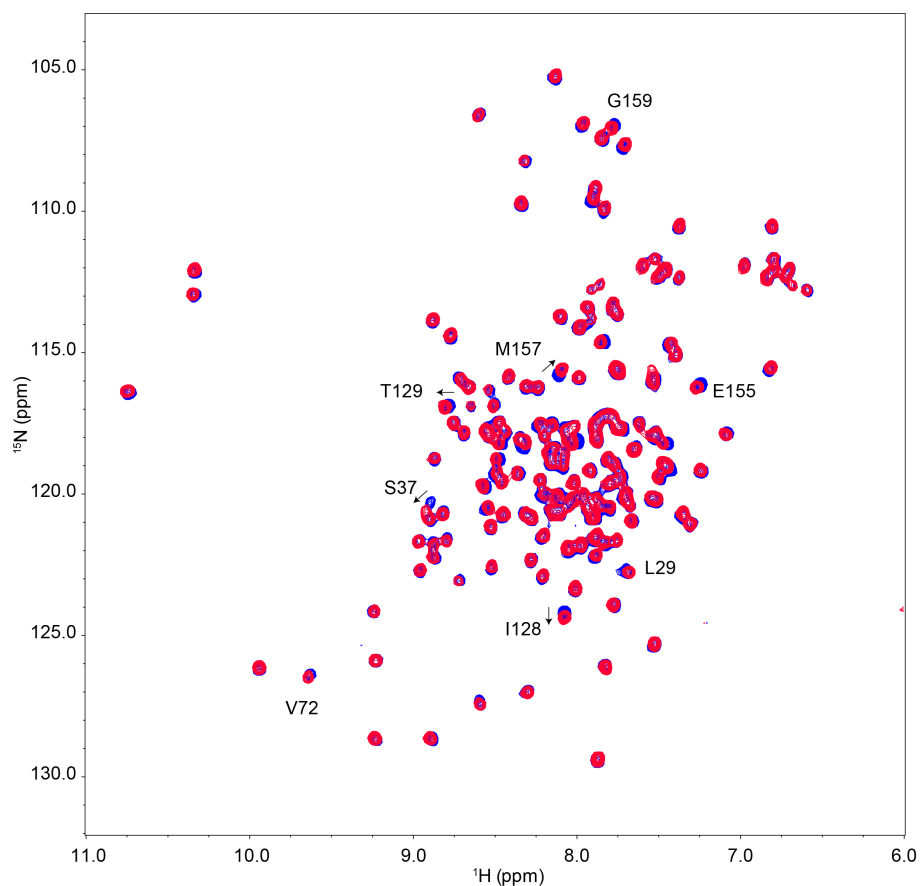
Figure F-4. Overlay of ^{1}H,^{15}N-HSQC NMR spectra acquired during the addition of OR1896-CF$_3$ (~2.5 mM) into cTnC•3Ca^{2+} (~0.35 mM) (no OR1896-CF$_3$: blue peaks, excess OR1896-CF$_3$: red peaks). A few resonances are labeled with arrows indicating the direction of chemical shift perturbation as the ligand bind cTnC•3Ca^{2+}. Residues in both C- and N- terminal domains were perturbed.
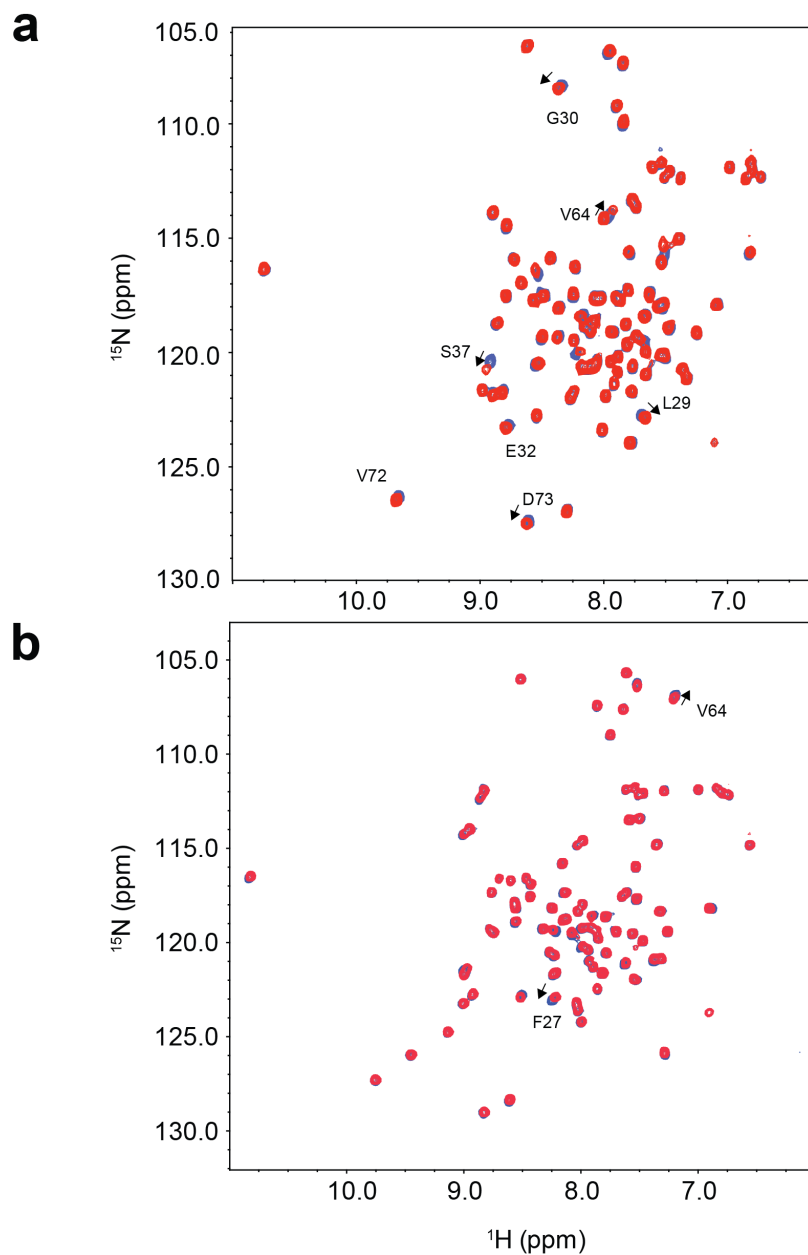
Figure F-5. $^1H,^{15}N$-HSQC NMR spectra of **a**. cNTnC•Ca^{2+} (~0.4 mM) bound to OR1896-CF$_3$ (~1.6 mM) and **b.** cNTnC•Ca^{2+}•cTnI$_{144-163}$ (~0.5 mM) bound to OR1896-CF$_3$ (~2.4 mM) (no OR1896-CF$_3$: blue peaks, excess OR1896-CF$_3$: red peaks). A few resonances are labeled with arrows indicating the direction of chemical shift perturbation as the ligands bind cNTnC•Ca^{2+} or cNTnC•Ca^{2+}•cTnI$_{144-163}$.

References

1.	Szilagyi, S., Pollesello, P., Levijoki, J., Kaheinen, P., Haikala, H., Edes, I., and Papp, Z. (2004) The effects of levosimendan and OR-1896 on isolated hearts, myocyte-sized preparations and phosphodiesterase enzymes of the guinea pig, *Eur. J. Pharmacol. 486*, 67-74.

2.	Takahashi, R., Talukder, M. A., and Endoh, M. (2000) Effects of OR-1896, an active metabolite of levosimendan, on contractile force and aequorin light transients in intact rabbit ventricular myocardium, *J. Cardiovasc. Pharmacol. 36*, 118-125.

3.	Li, M. X., Saude, E. J., Wang, X., Pearlstone, J. R., Smillie, L. B., and Sykes, B. D. (2002) Kinetic studies of calcium and cardiac troponin I peptide binding to human cardiac troponin C using NMR spectroscopy, *Eur. Biophys. J. 31*, 245-256.

4.	Li, M. X., Hoffman, R. M. B., and Sykes, B. D. (2006) Interaction of cardiac troponin C and troponin I with W7 in the presence of three functional regions of cardiac troponin I, *Biochemistry 45*, 9833-9840.

5.	Prashad, M., Hu, B., Har, D., Repic, O., and Blacklock, T. J. (2000) A new, convenient and selective 4-dimethylaminopyridine-catalyzed trifluoroacetylation of anilines with ethyl trifluoroacetate, *Tetrahedron Lett. 41*, 9957-9961.

6.	Delaglio, F., Grzesiek, S., Vuister, G. W., Zhu, G., Pfeifer, J., and Bax, A. (1995) NMRPipe: A multidimensional spectral processing system based on UNIX pipes, *J. Biomol. NMR 6*, 277-293.

7.	Johnson, B. A., and Blevins, R. A. (1994) NMRView: A computer program for teh visualization and analysis of NMR data, *J. Biomol. NMR 4*, 603-614.

8.	Robertson, I. M., Baryshnikova, O. K., Li, M. X., and Sykes, B. D. (2008) Defining the binding site of levosimendan and its analogues in a regulatory cardiac troponin C-troponin I complex, *Biochemistry 47*, 7485-7495.

9.	Sia, S. K., Li, M. X., Spyracopoulos, L., Gagne, S. M., Liu, W., Putkey, J. A., and Sykes, B. D. (1997) Structure of cardiac muscle troponin C unexpectedly reveals a closed regulatory domain, *J. Biol. Chem. 272*, 18216-18221.

10.	Pollesello, P., and Nore, P. (2003) Complete structure analysis of OR-1746, a complex product of cyclocondensation of arylhydrazomalononitriles containing clusters of protonated and unprotonated nitrogens, by pulsed-field-gradient heteronuclear NMR, *J. Pharm. Biomed. Anal. 31*, 125-131.

11.	Sorsa, T., Heikkinen, S., Abbott, M. B., Abusamhadneh, E., Laakso, T., Tilgmann, C., Serimaa, R., Annila, A., Rosevear, P. R., Drakenberg, T., Pollesello, P., and Kilpelainen, I. (2001) Binding of

levosimendan, a calcium sensitizer, to cardiac troponin C, *J. Biol. Chem. 276*, 9337-9343.

12.   Sorsa, T., Pollesello, P., Permi, P., Drakenberg, T., and Kilpelainen, I. (2003) Interaction of levosimendan with cardiac troponin C in the presence of cardiac troponin I peptides, *J. Mol. Cell. Cardiol. 35*, 1055-1061.